

ISSN

Period.

VOL. 548 NOS. 1 + 2 JULY 12, 1

COMPLETE IN ONE ISSUE

10th Int. Symp. on HPLC of proteins,
peptides and polynucleotides
Wiesbaden, October 29-31, 1990

JOURNAL OF

CHROMATOGRAPHY

INCLUDING ELECTROPHORESIS AND OTHER SEPARATION METHODS

SYMPOSIUM VOLUMES

EDITORS

E. Heftmann (Orinda, CA)

Z. Deyl (Prague)

EDITORIAL BOARD

E. Bayer (Tübingen)

S. R. Binder (Hercules, CA)

S. C. Churms (Rondebosch)

J. C. Fetzer (Richmond, CA)

E. Gelpí (Barcelona)

K. M. Gooding (Lafayette, IN)

S. Hara (Tokyo)

P. Helboe (Brønshøj)

W. Lindner (Graz)

T. M. Phillips (Washington, DC)

S. Terabe (Hyogo)

H. F. Walton (Boulder, CO)

M. Wilchek (Rehovot)

ELSEVIER

Scope. The *Journal of Chromatography* publishes papers on all aspects of chromatography, electrophoresis and related methods. Contributions consist mainly of research papers dealing with chromatographic theory, instrumental development and their applications. The section *Biomedical Applications*, which is under separate editorship, deals with the following aspects: developments in and applications of chromatographic and electrophoretic techniques related to clinical diagnosis or alterations during medical treatment; screening and profiling of body fluids or tissues with special reference to metabolic disorders; results from basic medical research with direct consequences in clinical practice; drug level monitoring and pharmacokinetic studies; clinical toxicology; analytical studies in occupational medicine.

Submission of Papers. Manuscripts (in English; four copies are required) should be submitted to: Editorial Office of *Journal of Chromatography*, P.O. Box 681, 1000 AR Amsterdam, The Netherlands, Telefax (+31-20) 5862 304, or to: The Editor of *Journal of Chromatography, Biomedical Applications*, P.O. Box 681, 1000 AR Amsterdam, The Netherlands. Review articles are invited or proposed by letter to the Editors. An outline of the proposed review should first be forwarded to the Editors for preliminary discussion prior to preparation. Submission of an article is understood to imply that the article is original and unpublished and is not being considered for publication elsewhere. For copyright regulations, see below.

Publication. The *Journal of Chromatography* (incl. *Biomedical Applications*) has 38 volumes in 1991. The subscription prices for 1991 are:

J. Chromatogr. (incl. *Cum. Indexes, Vols. 501-550*) + *Biomed. Appl.* (Vols. 535-572):
Dfl. 7220.00 plus Dfl. 1140.00 (p.p.h.) (total ca. US\$ 4519.00)

J. Chromatogr. (incl. *Cum. Indexes, Vols. 501-550*) only (Vols. 535-561):
Dfl. 5859.00 plus Dfl. 810.00 (p.p.h.) (total ca. US\$ 3604.75)

Biomed. Appl. only (Vols. 562-572):

Dfl. 2387.00 plus Dfl. 330.00 (p.p.h.) (total ca. US\$ 1468.75).

Subscription Orders. The Dutch guilder price is definitive. The US\$ price is subject to exchange-rate fluctuations and is given as a guide. Subscriptions are accepted on a prepaid basis only, unless different terms have been previously agreed upon. Subscriptions orders can be entered only by calendar year (Jan.-Dec.) and should be sent to Elsevier Science Publishers, Journal Department, P.O. Box 211, 1000 AE Amsterdam, The Netherlands, Tel. (+31-20) 5803 642, Telefax (+31-20) 5803 598, or to your usual subscription agent. Postage and handling charges include surface delivery except to the following countries where air delivery via SAL (Surface Air Lift) mail is ensured: Argentina, Australia, Brazil, Canada, Hong Kong, India, Israel, Japan*, Malaysia, Mexico, New Zealand, Pakistan, PR China, Singapore, South Africa, South Korea, Taiwan, Thailand, USA. * For Japan air delivery (SAL) requires 50% additional charge of the normal postage and handling charge. For all other countries airmail rates are available upon request. Claims for missing issues must be made within three months of our publication (mailing) date, otherwise such claims cannot be honoured free of charge. Back volumes of the *Journal of Chromatography* (Vols. 1-534) are available at Dfl. 208.00 (plus postage). Customers in the USA and Canada wishing information on this and other Elsevier journals, please contact Journal Information Center, Elsevier Science Publishing Co. Inc., 655 Avenue of the Americas, New York, NY 10010, USA, Tel. (+1-212) 633 3750, Telefax (+1-212) 633 3990.

Abstracts/Contents Lists published in Analytical Abstracts, Biochemical Abstracts, Biological Abstracts, Chemical Abstracts, Chemical Titles, Chromatography Abstracts, Clinical Chemistry Lookout, Current Contents/Life Sciences, Current Contents/Physical, Chemical & Earth Sciences, Deep-Sea Research/Part B: Oceanographic Literature Review, Excerpta Medica, Index Medicus, Mass Spectrometry Bulletin, PASCAL-CNRS, Pharmaceutical Abstracts, Referativnyi Zhurnal, Research Alert, Science Citation Index and Trends in Biotechnology.

See inside back cover for Publication Schedule, Information for Authors and information on Advertisements.

All rights reserved. No part of this publication may be reproduced, stored in a retrieval system or transmitted in any form or by any means, electronic, mechanical, photocopying, recording or otherwise, without the prior written permission of the publisher, Elsevier Science Publishers B.V., P.O. Box 330, 1000 AH Amsterdam, The Netherlands.

Upon acceptance of an article by the journal, the author(s) will be asked to transfer copyright of the article to the publisher. The transfer will ensure the widest possible dissemination of information.

Submission of an article for publication entails the authors' irrevocable and exclusive authorization of the publisher to collect any sums or considerations for copying or reproduction payable by third parties (as mentioned in article 17 paragraph 2 of the Dutch Copyright Act of 1912 and the Royal Decree of June 20, 1974 (S. 351) pursuant to article 16 b of the Dutch Copyright Act of 1912) and/or to act in or out of Court in connection therewith.

Special regulations for readers in the USA. This journal has been registered with the Copyright Clearance Center, Inc. Consent is given for copying of articles for personal or internal use, or for the personal use of specific clients. This consent is given on the condition that the copier pays through the Center the per-copy fee stated in the code on the first page of each article for copying beyond that permitted by Sections 107 or 108 of the US Copyright Law. The appropriate fee should be forwarded with a copy of the first page of the article to the Copyright Clearance Center, Inc., 27 Congress Street, Salem, MA 01970, USA. If no code appears in an article, the author has not given broad consent to copy and permission to copy must be obtained directly from the author. All articles published prior to 1980 may be copied for a per-copy fee of US\$ 2.25, also payable through the Center. This consent does not extend to other kinds of copying, such as for general distribution, resale, advertising and promotion purposes, or for creating new collective works. Special written permission must be obtained from the publisher for such copying.

No responsibility is assumed by the Publisher for any injury and/or damage to persons or property as a matter of products liability, negligence or otherwise, or from any use or operation of any methods, products, instructions or ideas contained in the materials herein. Because of rapid advances in the medical sciences, the Publisher recommends that independent verification of diagnoses and drug dosages should be made.

Although all advertising material is expected to conform to ethical (medical) standards, inclusion in this publication does not constitute a guarantee or endorsement of the quality or value of such product or of the claims made of it by its manufacturer.

This issue is printed on acid-free paper.

JOURNAL OF CHROMATOGRAPHY

VOL. 548 (1991)

JOURNAL of CHROMATOGRAPHY

INCLUDING ELECTROPHORESIS AND OTHER SEPARATION METHODS

SYMPOSIUM VOLUMES

EDITORS

E. HEFTMANN (Orinda, CA), Z. DEYL (Prague)

EDITORIAL BOARD

E. Bayer (Tübingen), S. R. Binder (Hercules, CA), S. C. Churms (Rondebosch), J. C. Fetzer (Richmond, CA), E. Gelpí (Barcelona), K. M. Gooding (Lafayette, IN), S. Hara (Tokyo), P. Helboe (Brønshøj), W. Lindner (Graz), T. M. Phillips (Washington, DC), S. Terabe (Hyogo), H. F. Walton (Boulder, CO), M. Wilchek (Rehovot)



ELSEVIER

AMSTERDAM — OXFORD — NEW YORK — TOKYO

J. Chromatogr., Vol. 548 (1991)

All rights reserved. No part of this publication may be reproduced, stored in a retrieval system or transmitted in any form or by any means, electronic, mechanical, photocopying, recording or otherwise, without the prior written permission of the publisher, Elsevier Science Publishers B.V., P.O. Box 330, 1000 AH Amsterdam, The Netherlands.

Upon acceptance of an article by the journal, the author(s) will be asked to transfer copyright of the article to the publisher. The transfer will ensure the widest possible dissemination of information.

Submission of an article for publication entails the authors' irrevocable and exclusive authorization of the publisher to collect any sums or considerations for copying or reproduction payable by third parties (as mentioned in article 17 paragraph 2 of the Dutch Copyright Act of 1912 and the Royal Decree of June 20, 1974 (S. 351) pursuant to article 16 b of the Dutch Copyright Act of 1912) and/or to act in or out of Court in connection therewith.

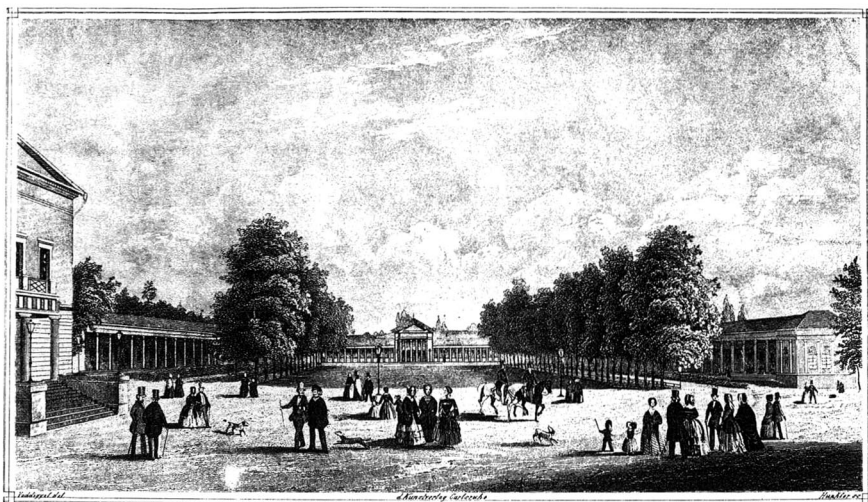
Special regulations for readers in the U.S.A. This journal has been registered with the Copyright Clearance Center, Inc. Consent is given for copying of articles for personal or internal use, or for the personal use of specific clients. This consent is given on the condition that the copier pays through the Center the per-copy fee stated in the code on the first page of each article for copying beyond that permitted by Sections 107 or 108 of the U.S. Copyright Law. The appropriate fee should be forwarded with a copy of the first page of the article to the Copyright Clearance Center, Inc., 27 Congress Street, Salem, MA 01970, U.S.A. If no code appears in an article, the author has not given broad consent to copy and permission to copy must be obtained directly from the author. All articles published prior to 1980 may be copied for a per-copy fee of US\$ 2.25, also payable through the Center. This consent does not extend to other kinds of copying, such as for general distribution, resale, advertising and promotion purposes, or for creating new collective works. Special written permission must be obtained from the publisher for such copying.

No responsibility is assumed by the Publisher for any injury and/or damage to persons or property as a matter of products liability, negligence or otherwise, or from any use or operation of any methods, products, instructions or ideas contained in the materials herein. Because of rapid advances in the medical sciences, the Publisher recommends that independent verification of diagnoses and drug dosages should be made.

Although all advertising material is expected to conform to ethical (medical) standards, inclusion in this publication does not constitute a guarantee or endorsement of the quality or value of such product or of the claims made of it by its manufacturer.

This issue is printed on acid-free paper.

SYMPOSIUM VOLUME



**TENTH INTERNATIONAL SYMPOSIUM
ON
HIGH-PERFORMANCE LIQUID CHROMATOGRAPHY
OF PROTEINS,
PEPTIDES AND POLYNUCLEOTIDES**

Wiesbaden (Germany), October 29–31, 1990

Guest Editors

KLAUS K. UNGER
(Mainz, Germany)

MILTON T. W. HEARN
(Melbourne, Australia)

FRED E. REGNIER
(West Lafayette, IN, USA)

JAN-CHRISTER JANSON
(Uppsala, Sweden)

JOSEPH J. DeSTEFANO
(Wilmington, DE, USA)

CONTENTS

10TH INTERNATIONAL SYMPOSIUM ON HIGH-PERFORMANCE LIQUID CHROMATOGRAPHY OF PROTEINS, PEPTIDES AND POLYNUCLEOTIDES, WIESBADEN, OCTOBER 29-31, 1991

Foreword 1

THEORY

Investigations of liquid-liquid partition chromatography of proteins
by M.-R. Kula, L. Elling and A. Walsdorf (Jülich, Germany) 3

Hydrophilic-interaction chromatography of peptides on hydrophilic and strong cation-exchange columns
by B.-Y. Zhu, C. T. Mant and R. S. Hodges (Edmonton, Canada) 13

Evaluation of kinetic models for biospecific adsorption and its implications for finite bath and column performance
by M. A. McCoy and A. I. Liapis (Rolla, MO, USA) 25

Multivalent ion-exchange model of biopolymer chromatography for mass overload conditions
by P. Cysewski (Bydgoszcz, Poland), A. Jaulmes, R. Lemque, B. Sébille and C. Vidal-Madjar (Thiais, France) and G. Jilge (Mainz, Germany) 61

Application of the split-peak effect to study the adsorption kinetics of human serum albumin on a reversed-phase support
by C. Vidal-Madjar, H. Place, L. Boulkanz and A. Jaulmes (Thiais, France) 81

Solution properties of polyelectrolytes. VII. Non-ideal mechanisms in size-exclusion chromatography of synthetic polyions, peptides and proteins
by E. Perez-Paya, L. Braco, C. Abad, V. Soria and A. Campos (Valencia, Spain) 93

High-performance liquid chromatography of amino acids, peptides and proteins. CX. Principal component analysis of four sets of group retention coefficients derived from reversed-phase high-performance liquid chromatography of peptides
by M. C. J. Wilce, M. I. Aguilar and M. T. W. Hearn (Clayton, Australia) 105

High-performance liquid chromatography of amino acids, peptides and proteins. CXI. Retention behaviour of proteins with macroporous tentacle-type anion exchangers
by M. T. W. Hearn, A. N. Hodder, F. W. Fang and M. I. Aguilar (Clayton, Australia) 117

High-performance liquid chromatography of amino acids, peptides and proteins. CXII. Analysis of operating parameters affecting the breakthrough curves in fixed-bed chromatography of proteins using several mathematical models
by A. Johnston, Q. M. Mao and M. T. W. Hearn (Clayton, Australia) 127

High-performance liquid chromatography of amino acids, peptides and proteins. CXIII. Predicting the performance of non-porous particles in affinity chromatography of proteins
by Q. M. Mao, A. Johnston, I. G. Prince and M. T. W. Hearn (Clayton, Australia) 147

SORBENTS

Characterization of synthetic macroporous ion-exchange resins in low-pressure cartridges and columns. Evaluation of the performance of Macro-Prep 50 S resin in the purification of anti-Klenow antibodies from goat serum
by L. Dunn, M. Abouelezz, L. Cummings, M. Navvab, C. Ordunez, C. J. Siebert and K. W. Talmadge (Richmond, CA, USA) 165

- Comparison of silica-based cyanopropyl and octyl reversed-phase packings for the separation of peptides and proteins
by N. E. Zhou and C. T. Mant (Edmonton, Canada), J. J. Kirkland (Wilmington, DE, USA) and R. S. Hodges (Edmonton, Canada) 179
- Silica *versus* polymer-based stationary phases for reversed-phase high-performance liquid chromatographic analyses of rat insulin biosynthesis. A comparison of resolution and recovery
by S. Linde and B. S. Welinder (Gentofte, Denmark) 195
- Ion-exchange high-performance liquid chromatography of nucleotides and polypeptides on new types of ion-exchange sorbents, based on polystyrene-coated silicas
by A. A. Kurganov and V. A. Davankov (Moscow, USSR) and K. K. Unger (Mainz, Germany) 207
- High-performance liquid chromatography and ultrafiltration of whey proteins with inorganic porous materials coated with polyvinylimidazole derivatives
by B. Chaufer, M. Rollin and B. Sébille (Thiais, France) 215

AFFINITY CHROMATOGRAPHY

- Purification of *Phleum pratense* pollen extract by immunoaffinity chromatography and high-performance ion-exchange chromatography
by E. Bolzacchini, P. Di Gennaro, G. Di Gregorio, B. Rindone, P. Falagiani and G. Mistrello (Milan, Italy) and I. Sondergaard (Copenhagen, Denmark) 229
- A ten-residue fragment of an antibody (mini-antibody) directed against lysozyme as ligand in immunoaffinity chromatography
by G. W. Welling, J. van Gorkum, R. A. Damhof and J. W. Drijfhout (Groningen, Netherlands), W. Bloemhoff (Leiden, Netherlands) and S. Welling-Wester (Groningen, Netherlands) 235
- Effect of antigen size on optimal ligand density of immobilized antibodies for a high-performance liquid chromatographic support
by J. W. Wheatley (Berkeley, CA, USA) 243
- Affinity of trypsin for amidine derivatives immobilized on dextran-coated silica supports
by M. Ellouali, S. Khamlichi, J. Jozefonvicz and D. Muller (Villetaneuse, France) 255

PREPARATIVE CHROMATOGRAPHY

- Multi-column preparative reversed-phase sample displacement chromatography of peptides
by R. S. Hodges, T. W. L. Burke and C. T. Mant (Edmonton, Canada) 267
- Analysis and purification of DNA restriction fragments by high-performance liquid chromatography
by P. L. Mauri, P. G. Pietta and M. Pacé (Milan, Italy) 281
- High-performance liquid chromatographic purification of antiviral components in Neuramide
by S. Giacobbe, N. Miraglia and B. Rindone (Milan, Italy), G. Folchitto (Ariccia, Italy) and G. Antonelli (Rome, Italy) 289

ANALYTICAL APPLICATIONS

- Glycosylation of extracellular superoxide dismutase studied by high-performance liquid chromatography and mass spectrometry
by M. Strömqvist (Umeå, Sweden) and J. Holgersson and B. Samuelsson (Gothenburg, Sweden) 293
- Peptide maps at picomolar levels obtained by reversed-phase high-performance liquid chromatography and pre-column derivatization with phenyl isothiocyanate. Microsequencing of phenylthiocarbamyl peptides
by F. J. Colilla (Madrid, Spain), S. P. Yadav and K. Brew (Miami, FL, USA) and E. Mendez (Madrid, Spain) 303

Fingerprinting of molecular components in individual human cerebrospinal fluid samples with a new micropurification system by F. Nyberg, S. Lyrenäs and Å. Danielsson (Uppsala, Sweden)	311
High-performance liquid chromatographic determination of peptides in biological fluids by automated pre-column fluorescence derivatization with fluorescamine by V. K. Boppana, C. Miller-Stein, J. F. Politowski and G. R. Rhodes (King of Prussia, PA, USA)	319
Separation of acidic peptides by reversed-phase ion-pair chromatography. Analytical application to a series of acidic substrates of casein kinases by A. Calderan, P. Ruzza, O. Marin, M. Secchieri, G. Borin and F. Marchiori (Padova, Italy)	329
Animal test or chromatography? Validated high-performance liquid chromatographic assay as an alternative to the biological assay for ornipressin. by R. H. Buck, M. Cholewinski and F. Maxl (Basle, Switzerland)	335
Non-radioactive detection of MHC class II-peptide antigen complexes in the sub-picomole range by high-performance size-exclusion chromatography with fluorescence detection by H. Kalbacher and H. Kropshofer (Tübingen, Germany)	343
High-performance liquid chromatographic separation of modified and native-melittin following transglutaminase-mediated derivatization with a dansyl fluorescent probe by E. Perez-Paya, L. Bráco and C. Abad (Valencia, Spain) and J. Dufourcq (Pessac, France)	351
Phenotyping of bovine milk proteins by reversed-phase high-performance liquid chromatography by S. Visser, C. J. Slangen and H. S. Rollema (Ede, Netherlands)	361
Separation and quantitation of serum proinsulin and proinsulin intermediates in humans by S. Linde, M. E. Røder, S. G. Hartling, C. Binder and B. S. Welinder (Gentofte, Denmark)	371
OTHER SEPARATION METHODS	
Structure-stability relationship of Immobiline chemicals for isoelectric focusing as monitored by capillary zone electrophoresis by M. Chiari, C. Etori, A. Manzocchi and P. G. Righetti (Milan, Italy)	381
Effects of temperature, carrier composition and sample load in asymmetrical flow field-flow fractionation by A. Litzén (Uppsala, Sweden) and K.-G. Wahlund (Lund, Sweden)	393
<i>Author Index</i>	407

 * In articles with more than one author, the name of the author to whom correspondence should be addressed is indicated in the
 * article heading by a 6-pointed asterisk (*)
 *

FOREWORD

The *10th International Symposium on High-Performance Liquid Chromatography of Proteins, Peptides and Polynucleotides* was held in Wiesbaden, from October 29th–31st, 1990. The symposium attracted over 300 participants and highlighted the most significant achievements in high-resolution techniques for the analysis and purification of biomacromolecules. The format of the meeting followed the successful approach of the previous symposia, with 32 oral and 120 poster presentations spread over ten sessions. The three-day programme focused on the design of surfaces and packings for biochromatography, protein–surface interactions, high-resolution methods in the analysis of biopolymers, particularly in molecular biology, and novel concepts in the isolation, purification and quality assurance of recombinant proteins.

To mark the 10th anniversary of the symposium, a “Festvortrag” was presented by the Nobel Laureate Professor R. Huber, Munich, on serine and cysteine proteases and their natural inhibitors and their structures and implications for function and drug design. For the first time thematic sessions were included in the programme, dealing specifically with new applications in biochromatography using the tentacle type of ion exchangers and micropurification techniques. Two lively discussions centred on the limits of bioanalysis and on alternatives to preparative chromatography. Dialogues and discussions continued into the evening during three receptions with the elegant flavour of the Kurhaus and the mediaeval spirit of the Kloster Eberbach in the Rhine valley.

My Symposium co-Chairmen (J. J. DeStefano, J. C. Janson, M. T. W. Hearn and F. E. Regnier) and myself would like to express our appreciation to all attendees, particularly those who contributed to the oral, poster and discussion sessions. We are particularly indebted to Dr. B. Österlund and his staff for their efforts in organizing and running the meeting. The generous support of Pharmacia LKB Biotechnology, Tosoh and E. Merck is gratefully acknowledged. We would also like to take this opportunity to thank Hewlett-Packard for their donation in supporting the travel of students to this meeting.

Mainz (Germany)

K. K. UNGER

Investigations of liquid–liquid partition chromatography of proteins

MARIA-REGINA KULA*, LOTHAR ELLING and ACHIM WALSDORF

Institut für Enzymtechnologie der Heinrich-Heine-Universität Düsseldorf im Forschungszentrum Jülich, Postfach 2050, W-5170 Jülich (Germany)

ABSTRACT

In the liquid–liquid partition chromatography (LLPC) of proteins, the favourable properties of aqueous two-phase systems are combined with the advantages of column chromatography. An investigation of the basic properties shows that the efficiency of resolution is determined by the same parameters as for liquid chromatography and the same mathematical models can be applied. In affinity LLPC the high sensitivity of the elution volume to small changes of the partition coefficient in the range 0.2–1.5 may be exploited using biospecific ligands. This paper reports the purification of formate dehydrogenase and monoclonal antibody by affinity LLPC. As a result of biospecific interaction in a homogeneous phase, affinity LLPC gives a better utilisation of ligands than conventional affinity chromatography.

INTRODUCTION

Aqueous two-phase polymer systems have been used successfully for the separation of bioactive molecules and viable cells [1]. Phase diagrams for aqueous phase systems consisting of polyethylene glycol (PEG)–dextran (Dx) or PEG–salt have been established for use in partition experiments [1]. The partition of added components such as proteins in aqueous phase systems is mainly determined by size and surface properties, *e.g.* hydrophobicity and charge. The partition coefficient (K) can also be affected by pH, partitioning of the ionic species, and the molecular weight and concentration of the polymers used. To increase the selectivity, Flanagan and Barondes [2] added affinity ligands covalently bound to one of the phase-forming polymers to aqueous two-phase systems [2]. Affinity partition has been used successfully for the purification of enzymes [3–9], nucleic acids and oligonucleotides [10,11] and for separating cells [12,13].

Müller [14] developed matrices for liquid–liquid partition chromatography using aqueous PEG–Dx phase systems. Müller [14] grafted linear polyacrylamide chains of 15–25 monomers to macroporous diol-substituted silica and synthetic polymers (TSK-HW gel), which resulted in a resin that is preferentially wetted by the dextran-rich phase as a result of the incompatibility of PEG and polyacrylamide. Liquid–liquid partition chromatography (LLPC) was performed using the PEG-rich phase as the mobile phase and the dextran-rich phase as the stationary phase [14].

In this way the favourable properties of the aqueous phase systems could be combined with the advantages of column chromatography. This paper reports investigations of the basic chromatographic properties of the support materials and new applications in affinity LLPC.

EXPERIMENTAL

The support materials LiParGel 750 and 650, particle size 25–40 μm , were a gift of E. Merck (Darmstadt, Germany). The company also provided experimental samples of polyacrylated LiChrospher Diol, a porous spherical silica gel with 1000 Å pores and 10 μm particle size. All other materials and methods were as described by Walsdorf and co-workers [15,16]. Ascites fluid with monoclonal antibody (mAb) against horseradish peroxidase (POD) was kindly provided by E. Hadas (Department of Biotechnology, Tel Aviv University, Israel). The mAb was purified as described by Elling *et al.* [17].

RESULTS AND DISCUSSION

General investigations of liquid–liquid partition chromatography

Calibration of the column

According to Martin and Syngé [10], the volume of the stationary phase (V_s), the volume of the mobile phase (V_m), the elution volume of component 1 and 2 (V_{el}) and the partition coefficient ($K_{(n)}$) of component n are related as follows:

$$V_s = (V_{el(2)} - V_{el(1)}) / (1/K_{(2)} - 1/K_{(1)}) \quad (1)$$

$$V_m = V_{el(1)} - V_s(1/K_{(1)}) \quad (2)$$

$$V_{el} = V_s/K + V_m \quad (3)$$

$$K_{(n)} = V_s / (V_{el} - V_m) \quad (4)$$

To calculate V_{el} or K , the volumes of the mobile and stationary phases for a given column must be known. The data for V_{el} and K were obtained by independent LLPC and batch partition experiments, respectively, and were fitted to a hyperbolic function (eqn. 3), which yielded reliable values for V_m and V_s (Fig. 1).

The non-ideal behaviour of proteins in LLPC is related to electrostatic interactions with negatively charged groups on the matrix (*e.g.*, lysozyme in Fig. 1), and size exclusion effects, which limit the access of large proteins ($\geq 100\,000$ dalton, see ferritin in Fig. 1) to the stationary phase inside the LiParGel matrix [15]. Mass transfer effects by film diffusion are not responsible for the observed changes in available V_s for LiParGel 750. The elution volumes of various proteins remain constant over the usual range of linear flow velocities. Mass transport effects are evident in other parameters describing the chromatographic processes, as discussed later. Size exclusion was not observed on polyacrylated LiChrospher Diol columns for proteins at least up to 500 000 dalton molecular weight [15].

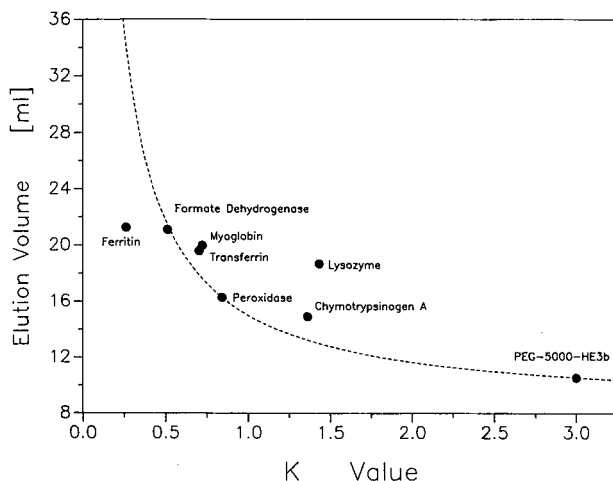


Fig. 1. Relationship between the elution volume and the partition coefficient (K) in liquid-liquid partition chromatography for LiParGel 750. Phase system: 2.7% PEG 20 000-4.5% Dx 500 in 10 mM potassium phosphate buffer (pH 7.0) with 75 mM potassium bromide. Flow-rate, 1 ml/min; column, 30 \times 1 cm. ---- = Calculated elution volume; ● = measured elution volume.

Physical data for the support are available for LiChrospher Diol. From the bead dimensions, density (0.5 g/cm³) and internal surface area (25-30 m²/g), it can be calculated that the dextran-rich stationary phase layer has a thickness of approximately 18 nm, assuming an even distribution over the entire surface. Based on the same assumptions it was calculated that about 98% of the stationary phase is located inside the porous particles. With an average pore size of 1000 Å, the mobile phase is able to enter the beads. Mass transport by diffusion over a large interface of thin layers of the immiscible phases should be sufficiently fast to reach partition equilibrium; diffusion within the pores should therefore represent a major resistance. This resistance may be more pronounced than in adsorption chromatography as the mobile phase has a higher viscosity than aqueous buffers due to the presence of PEG.

Factors influencing resolution in liquid-liquid partition chromatography

The efficiency of LLPC columns, *i.e.*, the resolution of two peaks, can be defined by the column parameters used in liquid chromatography [18].

Influence of linear flow-rate on peak resolution and plate height. Fig. 2 shows the influence of linear flow-rate on the resolution (R_s value) and the plate height for a LiParGel 750 column. The resolution for POD-myoglobin increases with decreasing linear flow-rate until a maximum is reached at 0.02 cm/s. Linear flow-rates lower than 0.02 cm/s gave higher height equivalent to a theoretical plate (HETP) values and a lower resolution. The HETP is related to the molecular weight of the proteins and lower values are observed for myoglobin (molecular weight 17 600 daltons) than for peroxidase (molecular weight 40 000 daltons). This is due to the higher diffusion rate of lower-molecular-weight molecules, which leads to a higher mass transfer rate within the pores. The characteristic curve for the relative resolution of myoglobin and peroxidase can be explained by the Van Deemter equation [18], which described the relationship between the linear flow-rate and plate height.

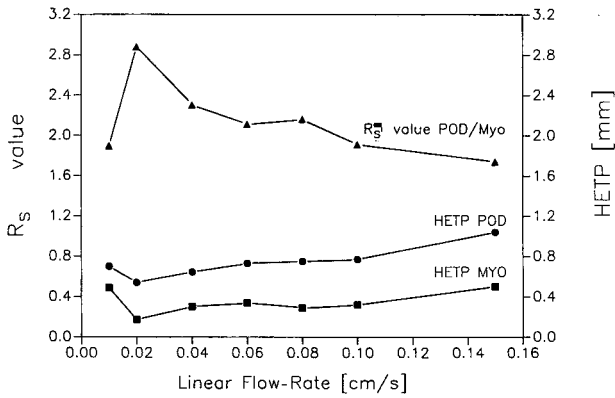


Fig. 2. Influence of the linear flow-rate on peak resolution (R_s) and the height of a theoretical plate (HETP). Support material: LiParGel 750. Phase system 5.4% PEG 6000–9.0% Dx 40 in 100 mM sodium chloride, 50 mM sodium phosphate buffer (pH 7.5). Column dimensions: 30 × 1 cm. The HETP standard deviation ($n = 3$) was 4.8 and 3.1% for myoglobin and peroxidase, respectively.

The influence of the linear flow-rate on the resolution (R_s) for LiParGel 650 is illustrated in Fig. 3. For curves 1–3 in Fig. 3, $R_s > 1$, which means a good resolution of the proteins under investigation. Again, a decrease in the linear flow-rate improves the resolution; the limiting linear flow-rate could not be reached with the chromatographic equipment used. Peak resolution of the proteins in curves 4 and 5 is not reached ($R_s < 1$). Here the partition coefficient must be altered, *e.g.*, by changes in the phase composition, to improve the resolution. The curves presented may be used to assess the maximum flow-rate with good resolution for preparative separations.

Influence of the sample volume on the number of theoretical plates. Fig. 4 shows

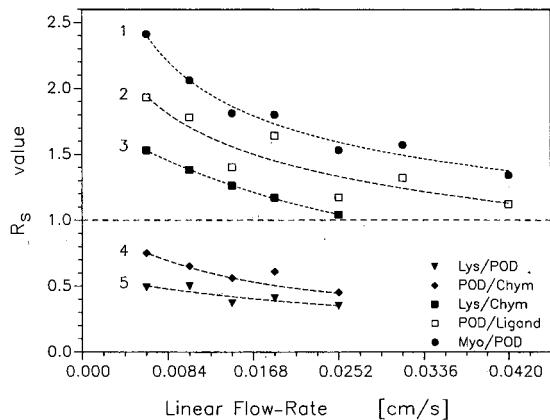


Fig. 3. Influence of the linear flow-rate on peak resolution of different proteins. Lys = lysozyme; POD = horseradish peroxidase; Chym = chymotrypsin; myo = myoglobin; ligand PEG-5000 HE3b. Support material: LiParGel 650. Phase system: 5.4% PEG 6000–9.0% Dx 40; column dimensions: 30 × 0.5 cm; sample volume, 100 μ l. For conditions see Fig. 2.

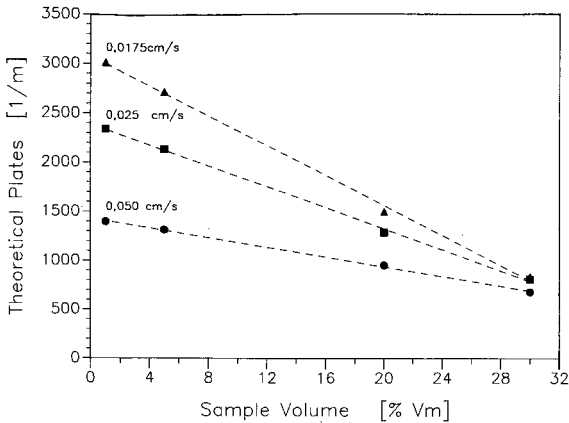


Fig. 4. Number of theoretical plates as a function of sample volume of myoglobin (17 600 dalton; 1 mg/ml). Support material: LiParGel 750; phase system, 2.7% PEG 20 000–4.5% Dx 500 in 12.6 mM potassium phosphate buffer (pH 7.0) with 50 mM sodium chlorate; column dimensions, 30×1 cm; $V_m = 10.6$ ml; $V_s = 5.34$ ml.

the plot of the number of theoretical plates (N) versus sample volume for LiParGel 750.

The chromatographic parameter N is inversely proportional to the sample volume. The sample volume is normalized as a percentage of the mobile phase (V_m) to facilitate comparisons between different column dimensions. The slopes obtained for different linear flow-rates indicate that the loss of theoretical plates is higher at lower linear flow-rates. For an increase in sample size (in this instance myoglobin) from 1 to 30% V_m , the loss of theoretical plates is 72 and 52% for linear flow-rates of 0.0175 and 0.05 cm/s, respectively. When the sample volume is increased to 60% V_m , a linear decrease of the number of theoretical plates is also observed [Fig. 5, with bovine

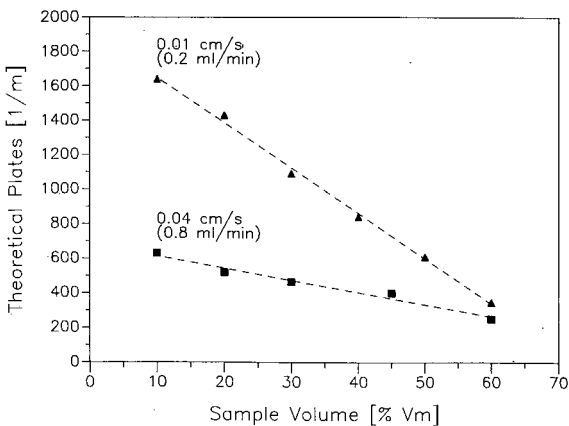


Fig. 5. Number of theoretical plates as a function of sample volume of bovine serum albumin (BSA 68 000 dalton, 1 mg/ml). For conditions see Fig. 4.

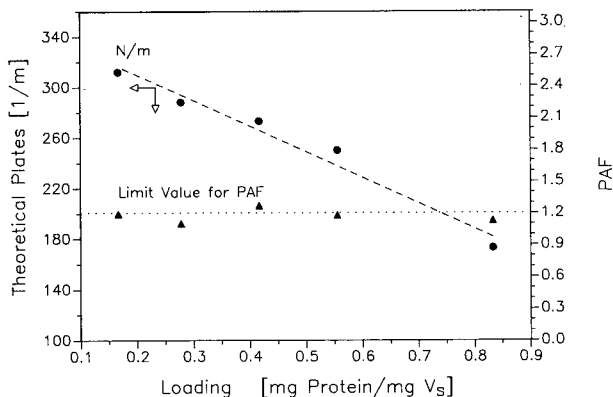


Fig. 6. Influence of column loading on the number of theoretical plates and the peak asymmetry factor (PAF). Support material: LiParGel 650; phase system, 5.4% PEG 6000–9.0% Dx 40; flow velocity, 0.0345 cm/s (0.15 ml/min); sample volume, 4.35% of V_m (100 μ l); $V_m = 2.3$ ml; $V_s = 1.2$ ml. For conditions see Fig. 2. Density of $V_s = 1.1$ mg/ml.

serum albumin (BSA) as an example]. The peaks are still symmetrical under these conditions [peak asymmetry (PAF) ≤ 1.2] and the number of theoretical plates can be calculated from the peak width. Owing to the higher molecular weight of BSA and the lower number of available theoretical plates, the loss in N is not as pronounced as for myoglobin with increasing sample volume.

Influence of sample loading on the column resolution. The influence of increasing protein concentration in the sample on the number of theoretical plates and the PAF was investigated using BSA (Fig. 6).

The number of theoretical plates decreases with higher protein loadings, which are expressed as a percentage of the stationary phase. The symmetry of the peaks is not affected up to 0.85 mg BSA/mg V_s (PAF ≤ 1.2). Protein loadings of more than 0.85 mg/mg V_s resulted in asymmetric multiple peaks, as shown in Fig. 7. Experi-

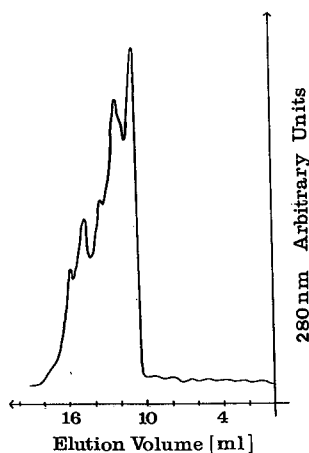


Fig. 7. Peak deformation as a consequence of column overloading (1.875 mg BSA per mg stationary phase). Flow velocity, 0.0345 cm/s (0.15 ml/min). For conditions see Fig. 6.

ments with larger diameter columns (1.6 and 2.6 cm) gave comparable results (data not shown). In a similar manner to liquid chromatography, the capacity of an LLPC column can be increased by increasing the diameter. A limiting factor remains the solubility of the product in the mobile phase, although this was not a problem with BSA.

In conclusion, the results demonstrate that the efficiency of LLPC columns is determined by the same parameters as for liquid chromatography and the same mathematical models can be applied.

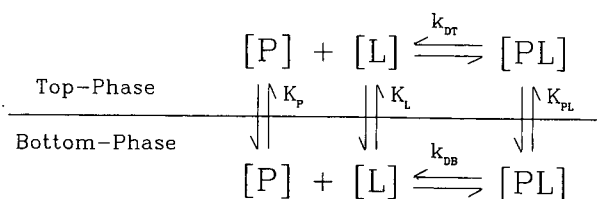
Affinity liquid-liquid partition chromatography

In Fig. 1 the relationship between elution volume V_{el} , and partition coefficient, K , is shown for a given column. The conditions that increase the partition coefficient in the range of 0.2–1.5 for the product of interest will lead to a faster elution. Bio-specific interactions can be utilized to influence selectively the partition coefficient.

Fig. 8 illustrates the linked equilibria of partition and protein–ligand (PL) association for a 1:1 complex. The yield of PL is determined by the partition coefficient of the protein–ligand complex (K_{PL}), the dissociation constant in the top and bottom phase (K_{DT} , K_{DB}) and the ligand concentration [L]. A ligand with a high K_L value will selectively shift the protein–ligand complex to the top phase. High K_L values can be ensured by covalent binding to PEG.

*Affinity liquid-liquid partition chromatography of formate dehydrogenase from *Candida boidinii**

As an example, the interaction of formate dehydrogenase (FDH) with Procion Red HE3b was studied [16]. Fig. 9 shows that increasing the ligand concentration in the mobile phase rapidly decreases the elution volume of FDH. Higher ligand concentrations cause only a minor further decrease of the elution volume as the binding sites of the enzyme are saturated and V_{el} is approaching the void volume for large K .



[P] = Conc. of Protein

[L] = Conc. of Ligand

[PL] = Conc. of Protein/Ligand Complex

k_{DT} = Equilibrium Constant of the Complex in the Top-Phase

k_{DB} = Equilibrium Constant of the Complex in the Bottom-Phase

K_P = Partition Coefficient of the Protein

K_L = Partition Coefficient of the Ligand

K_{PL} = Partition Coefficient of the Complex

Fig. 8. Linked equilibria in affinity partitioning.

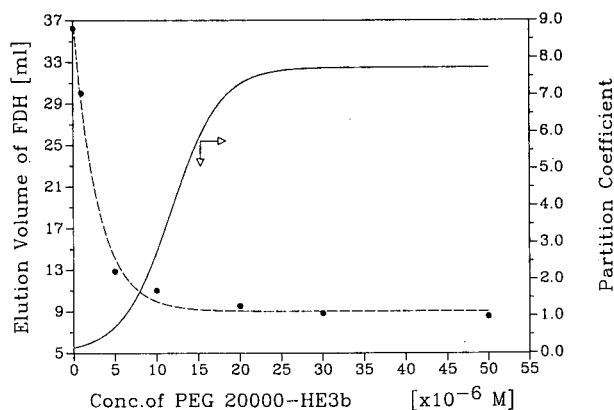


Fig. 9. Elution volume of formate dehydrogenase as a function of ligand concentration (PEG 20 000-HE3b) in the mobile phase. Support material, LiParGel 750; phase system, 4.5% PEG 20 000–6.9% Dx 500; buffer, 5 mM ammonium sulphate in 6.3 mM potassium phosphate (pH 7.0); column dimensions, 30×1 cm.

With $5 \cdot 10^{-5}$ M PEG-Procion Red HE3b in the mobile phase, FDH from a heat conditioned crude extract (10 min at 55°C to denature other dehydrogenases, 2.5 mg/ml protein) could be purified by a factor of 5.8 with 83% activity yield. The concentration of ligand required for purification is lowered by about two orders of magnitude compared to affinity partitioning of FDH ion batch systems [19].

Affinity liquid-liquid partition chromatography of monoclonal antibody

If the antigen (POD, $K = 1.0$) and the mAb ($K = 0.2$) prefer different phases in a PEG-Dx aqueous two-phase system, the characteristic separation profile of the LLPC column (Fig. 1) can be utilized to shift the elution position of mAb with the antigen as the affinity ligand, without prior PEG modification of the ligand. Different concentration ratios of ligand/mAb were prepared for incubation and were subsequently injected onto a small LLPC column (30×0.5 cm) with or without antigen as a ligand in the mobile phase ($V_s = 2.09$ ml, $V_m = 2.42$ ml). Fig. 10 demonstrates that the elution volume of the mAb can be decreased from 12 ml down to 9.0 ml (increase of K from 0.22 to 0.32). Owing to the dissociation of the mAb-antigen complex (1:1 complex), at least a ten fold higher ligand concentration is needed in the absence of ligand in the mobile phase (Fig. 10a) to reach the same K values shown in Fig. 10b. When antigen is present in the mobile phase the maximum decrease of the elution volume is reached at POD/mAb molar concentration ratios where the mAb concentration is even higher than the ligand concentration.

The partition equilibria in affinity partitioning (Fig. 8) are reached very fast. The dissociation constants of the immunocomplex are the limiting factors for separation assuming that they are equal in the top and bottom phases. With the ligand in the mobile phase (Fig. 10b), dissociation is depressed. Owing to the mode of separation, that is a mobile PEG-rich phase moving along a stationary Dx-rich phase with equal concentrations of ligand ($K_{\text{POD}} = 1.0$), a decrease of 2 ml in the elution volume is reached at molar concentration ratios of ligand/mAb < 1 .

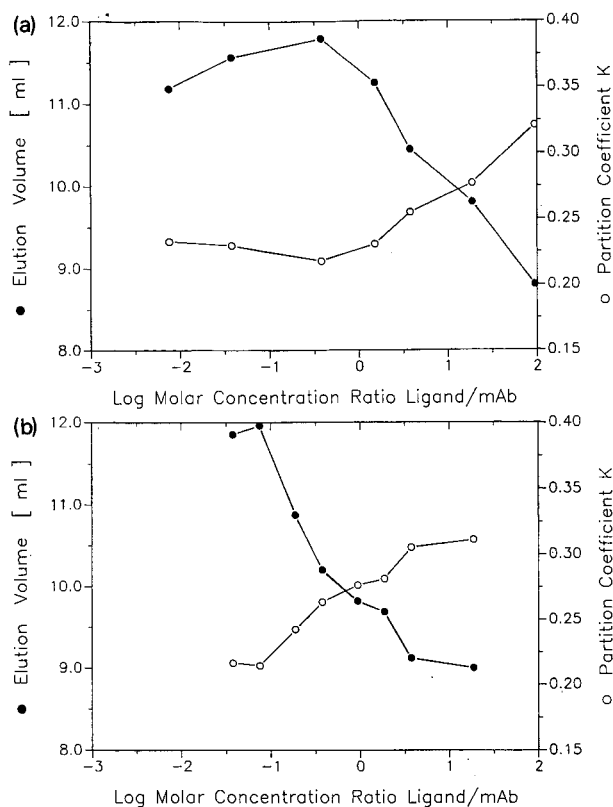


Fig. 10. Elution volume and partition coefficient K of monoclonal antibody as a function of the log of the molar concentration ratio of ligand (horseradish peroxidase) and mAb. (a) Without ligand in the mobile phase; the ligand was only present in the incubation mixture prior to separation. (b) With ligand in the mobile phase. Column: LiChrospher Diol 1000/10 (30×0.5 cm); phase system, 5.4% PEG 6000–9.0% Dx 70 in 50 mM potassium phosphate buffer (pH 7.4) with 150 mM sodium chloride; $V_m = 2.42$ ml; $V_s = 2.09$ ml.

CONCLUSIONS

In conclusion, affinity LLPC is a versatile technique for the purification of proteins. As a result of the high sensitivity of LLPC to small changes of the partition coefficient, affinity based purifications can be achieved as demonstrated for formate dehydrogenase at relatively low concentrations of PEG-bound triazine dye. This sensitivity can also be exploited when the unmodified ligand has a partition coefficient sufficiently different from the molecule (*e.g.* POD–mAb). In addition, size exclusion effects shown with LiParGel 750 (Fig. 1) may be utilized to improve the separation of free antigen and the corresponding immunocomplex. As the interaction of ligand and target molecule takes place in a homogeneous phase involving only liquid–liquid equilibria, but no adsorption or binding on the solid matrix, the utilisation of ligands is much improved compared to affinity chromatography and activity yields are expected to be high.

ACKNOWLEDGEMENTS

L. E. and A. W. were supported by a fellowship within the BMFT program "Angewandte Biologie und Biotechnologie" administered by DECHEMA. The authors thank Dr. E. Hadas for the gift of mAb. The authors are indebted to Professor W. Müller for valuable discussions and to the E. Merck (Darmstadt, Germany) for the supply of support material and special columns.

REFERENCES

- 1 P. A. Albertsson, *Partition of Cell Particles and Macromolecules*, Wiley-Interscience, New York, 3rd ed., 1986.
- 2 S. D. Flanagan and S. H. Barondes, *J. Biol. Chem.*, 250 (1975) 1484.
- 3 G. Kopperschläger and G. Johansson, *Anal. Biochem.*, 124 (1982) 117.
- 4 K. H. Kroner, A. Cordes, A. Schelper, M. Morr, A. F. Bückmann and M.-R. Kula, in T. C. J. Gribnau, J. Visser and R. J. F. Nivard (Editors), *Affinity Chromatography and Related Techniques*, Elsevier, Amsterdam, 1982, p. 491.
- 5 G. Kopperschläger, G. Lorenz and E. Usbeck, *J. Chromatogr.*, 259 (1983) 97.
- 6 G. Johannsson, G. Kopperschläger and P. A. Albertsson, *Eur. J. Biol.*, 131 (1983) 589.
- 7 G. Johannsson and M. Andersson, *J. Chromatogr.*, 303 (1984) 39.
- 8 G. Johannsson, M. Andersson and H. E. Akerlund, *J. Chromatogr.*, 298 (1984) 483.
- 9 G. Johannsson and M. Andersson, *J. Chromatogr.*, 303 (1984) 39.
- 10 A. J. P. Martin and R. L. M. Syge, *Biochem. J.*, 35 (1941) 1358.
- 11 W. Müller, *Kontakte (Darmstadt)*, No. 3 (1986) 3.
- 12 L. J. Karr, J. M. Van Alstine, R. S. Snyder, S. G. Shafer and J. M. Harris, in D. Fisher and I. A. Sutherland (Editors), *Separations Using Aqueous Two-Phase Systems – Applications in Cell Biology and Biotechnology*, Plenum Press, New York, 1989, p. 193.
- 13 S. J. Stocks and D. E. Brooks, in D. Fisher and I. A. Sutherland (Editors), *Separations Using Aqueous Two-Phase Systems – Applications in Cell Biology and Biotechnology*, Plenum Press, New York, 1989, p. 183.
- 14 W. Müller, *Eur. J. Biochem.*, 128 (1986) 213.
- 15 A. Walsdorf and M.-R. Kula, *J. Chromatogr.*, 542 (1991) 55.
- 16 A. Walsdorf, D. Forciniti and M.-R. Kula, *J. Chromatogr.*, 523 (1990) 103.
- 17 L. Elling, M.-R. Kula, E. Hadas and E. Katchalski-Katzir, *Anal. Biochem.*, 192 (1991) 74.
- 18 L. R. Snyder and J. J. Kirkland, *Introduction to Modern Liquid Chromatography*, Wiley-Interscience, New York, 2nd ed., 1979.
- 19 A. Cordes and M.-R. Kula, *J. Chromatogr.*, 376 (1986) 375.

Hydrophilic-interaction chromatography of peptides on hydrophilic and strong cation-exchange columns

BING-YAN ZHU, COLIN T. MANT and ROBERT S. HODGES*

Department of Biochemistry and the Medical Research Council of Canada Group in Protein Structure and Function, University of Alberta, Edmonton, Alberta T6G 2H7 (Canada)

ABSTRACT

Hydrophilic-interaction chromatography (HILIC) was recently introduced as a potentially useful separation mode for the purification of peptides and other polar compounds. The elution order of peptides in HILIC, which separates solutes based on hydrophilic interactions, should be opposite to that obtained in reversed-phase chromatography, which separates solutes based on hydrophobic interactions. Three series of peptides, two of which consisted of positively charged peptides (independent of pH at pH < 7) and one of which consisted of uncharged or negatively charged peptides (dependent on pH), and which varied in overall hydrophilicity/hydrophobicity, were utilized to examine the separation mechanism and efficiency of HILIC on hydrophilic and strong cation-exchange columns.

INTRODUCTION

Hydrophilic-interaction chromatography (HILIC) has recently been promoted as a novel chromatographic mode for application to the separation of a wide range of solutes [1]. Separation by HILIC, in a manner similar to normal-phase chromatography (to which it is related), depends on hydrophilic interactions between the solutes and the hydrophilic stationary phase, *i.e.*, solutes are eluted from a HILIC column in order of increasing hydrophilicity (decreasing hydrophobicity). Thus, elution orders of solutes in HILIC should be opposite to that obtained in reversed-phase high-performance liquid chromatography (RP-HPLC), which separates solutes based on hydrophobic interactions, *i.e.*, solutes are eluted from a RP-HPLC column in order of increasing hydrophobicity (decreasing hydrophilicity). HILIC is characterized by separations being effected by a linear A–B gradient of decreasing organic modifier concentration, *i.e.*, starting from a high concentration of organic modifier (typically, 70–90% aqueous acetonitrile).

In this study, we set out to evaluate the potential of HILIC for peptide separations. To this end, we examined the retention behavior of three series of model synthetic peptides varying in both hydrophobicity/hydrophilicity and charge. From the observed retention behavior of these series of model peptides (encompassing various controlled combinations of peptide characteristics) during HILIC on both HILIC and strong cation-exchange columns, we were able to assess the potential

TABLE I
PROPERTIES OF SYNTHETIC PEPTIDE STANDARDS

Peptide	Peptide sequence ^a	Net charge			Hydrophilicity/hydrophobicity ^b	
		pH 2.0	pH 6.5	pH 7	pH 2	pH 7
S1	*NH ₂ -*Arg-Gly-Ala-Gly-Gly-Leu-Gly-Leu-Gly-*Lys-amide	+3	+3	11.5	19.9	
S2	Ac-*Arg-Gly-Gly-Gly-Leu-Gly-Leu-Gly-*Lys-amide	+2	+2	12.3	17.5	
S3	Ac-*Arg-Gly-Ala-Gly-Gly-Leu-Gly-*Lys-amide	+2	+2	14.5	19.9	
S4	Ac-*Arg-Gly-Val-Gly-Gly-Leu-Gly-*Lys-amide	+2	+2	17.5	23.4	
S5	Ac-*Arg-Gly-Val-Val-Gly-Leu-Gly-*Lys-amide	+2	+2	22.7	29.3	
C1	Ac-Gly-Gly-Gly-Leu-Gly-Gly-Ala-Gly-Gly-Leu-*Lys-amide	+1	+1	14.7	18.6	
C2	Ac-*Lys-Tyr-Gly-Leu-Gly-Gly-Ala-Gly-Gly-Leu-*Lys-amide	+2	+2	17.5	23.4	
C3	Ac-Gly-Gly-Ala-Leu-*Lys-Ala-Leu-*Lys-Gly-Leu-*Lys-amide	+3	+3	21.4	30.2	
C4	Ac-*Lys-Tyr-Ala-Leu-*Lys-Ala-Leu-*Lys-Gly-Leu-*Lys-amide	+4	+4	24.2	35.0	
A1	Ac-†Glu-Tyr-Gly-Ala-Gly-Gly-Ala-Gly-Gly-Leu-†Glu-amide	0	-2	17.8	14.4	
A2	Ac-Gly-Gly-Leu-Gly-Gly-Ala-Gly-Gly-Leu-†Glu-amide	0	-1	17.9	17.5	
A3	Ac-†Glu-Tyr-Ala-Ala-†Glu-Ala-Ala-†Glu-Gly-Leu-†Glu-amide	0	-4	24.8	17.0	
A4	Ac-Gly-Gly-Ala-Leu-†Glu-Ala-Ala-†Glu-Gly-Leu-†Glu-amide	0	-3	24.9	20.1	

^a Ac = N^ε-Acetyl; amide = C^α-amide. Variations in the composition of S1-S5 are shown in bold. Potentially positively charged residues (Lys, Arg) are denoted *; potentially negatively charged residues (Glu) are denoted †.

^b Peptide hydrophilicity/hydrophobicity is expressed as the sum of the hydrophobicity coefficients (ΣR_c) of Guo *et al.* [4].

value of HILIC for peptide separations, and also draw some conclusions concerning the mechanism of such separations.

EXPERIMENTAL

Materials

HPLC-grade water and acetonitrile and reagent-grade potassium chloride were obtained from J. T. Baker (Phillipsburg, NJ, USA), HPLC-grade trifluoroacetic acid (TFA) from Pierce (Rockford, IL, USA), ACS-grade orthophosphoric acid from Anachemia (Toronto, Canada) and synthetic peptide standards for RP-HPLC (S1–S5), cation-exchange chromatography (CEC) (C1–C4) and anion-exchange chromatography (AEC) (A1–A4) from Synthetic Peptides Inc. (University of Alberta, Edmonton, Canada). The sequences of the three series of standards are shown in Table I.

Apparatus

The HPLC instrument consisted of a Spectra-Physics (San Jose, CA, USA) SP8700 solvent-delivery system, SP8750 organizer coupled to an Hewlett-Packard (Avondale, PA, USA) HP 1040A detection system, HP 3390A integrator, HP 85 computer, HP 9121 disc drive and HP 7470 plotter.

Columns

Peptides were separated on four columns: (1) a polyhydroxyethylaspartamide HILIC column, 200 × 4.6 mm I.D., particle size 5 μm, pore size 300 Å (PolyLC, Columbia, MD, USA); (2) a polysulfoethylaspartamide strong cation-exchange column, 200 × 4.6 mm I.D., 5 μm, 200 Å (PolyLC); (3) a Mono S HR 5/5 strong cation-exchange column, 50 × 5 mm I.D., 10 μm (Pharmacia, Dorval, Canada); and (4) a SynChropak RP-P C₁₈ reversed-phase column, 250 × 4.6 mm I.D., 6.5 μm, 300 Å (SynChrom, Lafayette, IN, USA).

Synthetic model peptides

The relevant properties of the model peptides employed are shown in Table I. Peptide standards S1–S5 were originally designed to monitor RP-HPLC column performance (efficiency, selectivity and resolution) [2]. Each of the peptides carries a net positive charge of +3 (S1) or +2 (S2–S5) at pH between 2 and 7, *i.e.*, the pH range over which silica-based columns may be employed. Peptides C1–C4 were designed to monitor cation-exchange column performance [3]. These four peptides contain only basic residues (no acidic residues are present) and the net positive charges on the standards (+1, +2, +3 and +4 for C1, C2, C3 and C4, respectively) remain unaltered over the range pH 2–7. Peptides A1–A4 are monitors of anion-exchange column performance. The net charge on these four peptides is pH dependent (the peptides contain only acidic residues, no basic residues are present: at pH <4.0–4.5 (the pK_a of the side-chain carboxyl group of glutamic acid), the glutamic acid side-chain carboxyl is protonated, *i.e.*, uncharged; at pH >4.0–4.5, the glutamic acid side-chain carboxyl is deprotonated, *i.e.*, negatively charged. Thus, at pH 2, the four peptides are uncharged; at pH 7, peptides A1, A2, A3 and A4 possess net charges of -1, -2, -3 and -4, respectively.

A convenient means of assigning hydrophilicity/hydrophobicity values to the model peptides was required. Guo *et al.* [4] determined a precise set of amino acid side-chain hydrophilicity/hydrophobicity parameters (or coefficients) by examining the effect of different residue side-chains on the RPC retention time, during linear gradient elution at pH 2 and 7, of a synthetic model octapeptide, Ac-Gly-X-X-(Leu)₃-(Lys)₂-amide, where X was substituted by the 20 amino acids found in proteins. The overall hydrophilicity/hydrophobicity of each peptide in Table I was determined by summing the coefficients (ΣR_c) of Guo *et al.* [4] for all of the residues in the peptide.

RESULTS AND DISCUSSION

HPLC of synthetic model peptides

Fig. 1A shows the reversed-phase separation on the C₁₈ column of peptides S1-S5. Aqueous TFA-acetonitrile mobile phases at pH 2 are currently employed for most peptide separations [5,6], and the separation shown in Fig. 1A was achieved by a linear A-B gradient of increasing acetonitrile concentration (1% B/min at a flow-rate of 1 ml/min), where eluent A was 0.05% aqueous TFA and eluent B was 0.05% TFA in acetonitrile. As expected, the elution order of the peptides was in order of increasing peptide hydrophobicity, with the least hydrophobic peptide (S1; $\Sigma R_c = 11.5$)

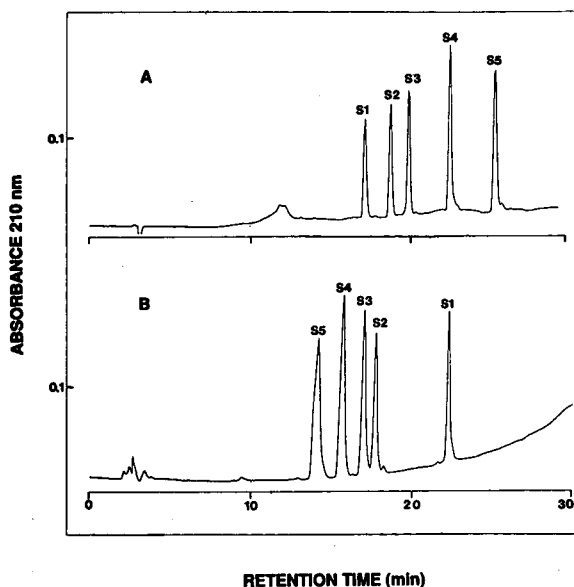


Fig. 1. Separation of a mixture of synthetic positively charged peptides by (A) RP-HPLC and (B) HILIC. (A) Column, SynChropak RP-P C₁₈ (250 × 4.6 mm I.D.); mobile phase, linear A-B increasing acetonitrile gradient (1% B/min) at a flow-rate of 1 ml/min, where A is 0.05% aqueous TFA and B is 0.05% TFA in acetonitrile; temperature, 26°C. (B) Column, Polyhydroxyethylaspartamide HILIC column (200 × 4.6 mm I.D.); mobile phase, linear A-B decreasing acetonitrile gradient (1% B/min) at a flow-rate of 1 ml/min, where A is 0.2% orthophosphoric acid in acetonitrile and B is 0.2% aqueous orthophosphoric acid (starting conditions were 85% A-15% B); temperature, 26°C. The sequences of peptides S1-S5 are shown in Table I.

being eluted first and the most hydrophobic peptide (S5; $\Sigma R_c = 22.7$) being eluted last (Table I).

Fig. 1B shows the separation of the same peptides on the HILIC column. The peptides were subjected to a linear A–B gradient of decreasing acetonitrile concentration (1% B/min, starting from 85% A–15% B, at a flow-rate of 1 ml/min) at pH 2, where eluent A was 0.2% H_3PO_4 –acetonitrile and eluent B was 0.2% aqueous H_3PO_4 . In RP-HPLC, hydrophobic interactions between peptides and the hydrophobic stationary phase are favoured owing to the absence of organic modifier (acetonitrile) in the starting eluent (0.05% aqueous TFA); elution of peptides is then achieved with an increasing concentration of acetonitrile in the mobile phase. In contrast, in HILIC, hydrophilic interactions between peptides and the hydrophilic stationary phase are favoured owing to the presence of a high concentration of acetonitrile in the starting eluent (85% aqueous acetonitrile–0.2% H_3PO_4); elution of peptides is then achieved with a decreasing concentration of acetonitrile in the mobile phase.

It has been observed by others [7–12] that high concentrations of organic modifier or inverse gradients (high concentrations of organic modifier decreasing to lower concentrations) on reversed-phase columns have shown elution order reversals for peptides and proteins compared with standard RP-HPLC conditions (low concentrations of organic modifier increasing to higher concentrations). Silanophilic interactions were deemed responsible for these results. Simpson and Moritz [12] recently showed that inverse gradients only show elution order reversals for some proteins and only on particular reversed-phase columns. The reversals that were observed were explained by silanophilic interactions and/or conformational changes induced in the proteins by the high concentration of organic modifier. In contrast, the results of this study with peptides showing elution order reversal on comparing RP-HPLC and HILIC (Fig. 1) is due to the hydrophobic/hydrophilic interactions of the peptides with the mobile phase/stationary phase. The peptides S2–S5 (Fig. 1) each have the same basic character (one Arg and one Lys residue) and the same net positive charge (+2 at pH 2), which rules out silanophilic interactions as a mechanism for elution order reversal.

TFA is a moderately hydrophobic anionic ion-pairing reagent [5,6,13], *i.e.*, the negatively charged trifluoroacetate ion will ion pair with positively charged groups (such as α -amino groups and the side-chains of basic residues) and, thus, increase the peptide retention time (and apparent hydrophobicity) during RP-HPLC of peptides containing these groups. In HILIC, it is desirable to emphasize peptide hydrophilicity as much as possible. Therefore, orthophosphoric acid was used in place of TFA in the HILIC mobile phase, the phosphate ion being a much more hydrophilic counter ion than trifluoroacetate [13]. From Fig. 1B, the peptides were eluted in opposite order to that obtained during RP-HPLC (Fig. 1A), as would be expected from an HILIC separation. It might be expected that the relative retention time differences between individual peptides would be approximately the same in both RP-HPLC and HILIC. However, the retention time of peptide S1 on the HILIC column was considerably longer than expected, in relation to the other four peptides, based on hydrophilicity considerations alone. This observation suggested that the HILIC column may be exhibiting ionic interactions, *i.e.*, a mixed-mode separation, based on both peptide hydrophilicity and net charge. If the HILIC sorbent possessed some negatively

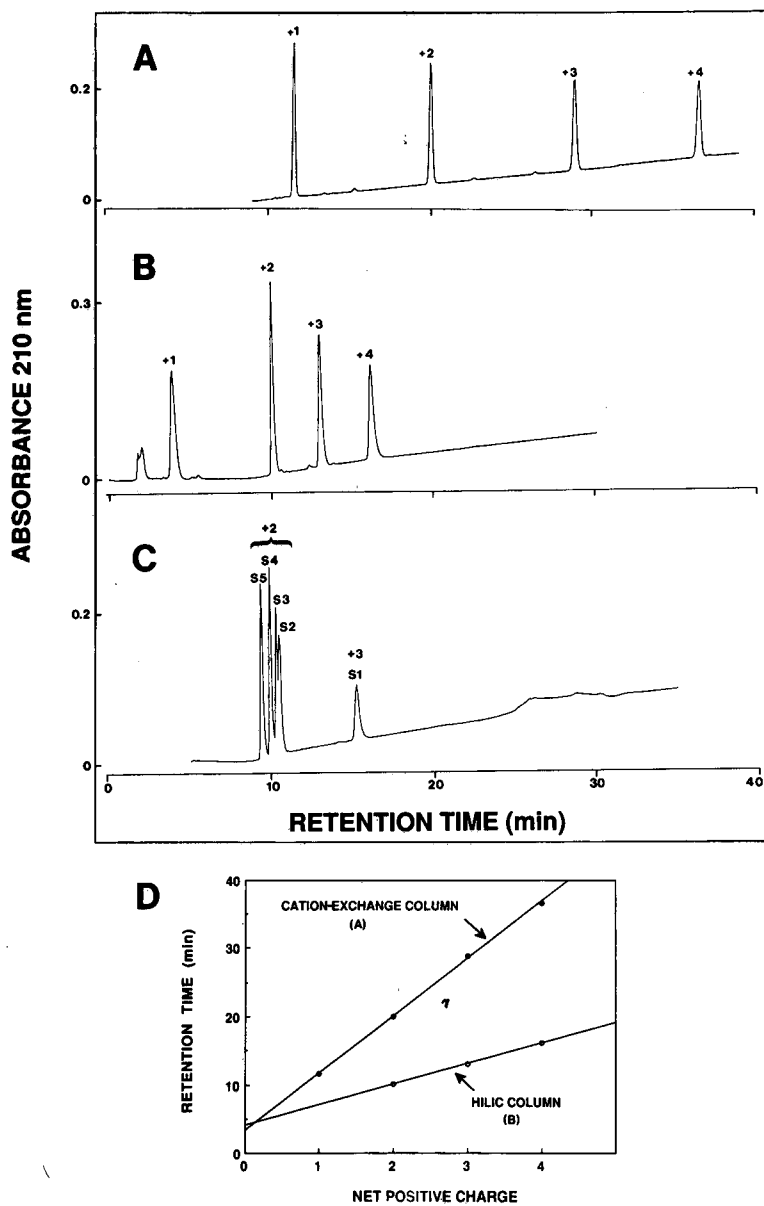


Fig. 2. Separation of a mixture of synthetic positively charged peptides by cation-exchange chromatography on (A) a strong cation-exchange column and (B and C) a HILIC column. (A) Column, Polysulfoethylaspartamide strong cation-exchange column (200×4.6 mm I.D.). (B and C) polyhydroxyethylaspartamide HILIC column (200×4.6 mm I.D.). Mobile phase: linear A–B gradient (2% B/min, equivalent to 5 mM KCl/min) at a flow-rate of 1 ml/min, where buffer A is 5 mM KH_2PO_4 (pH 6.5) and buffer B is buffer A plus 0.25 M KCl, both buffers containing 50% (v/v) acetonitrile; temperature, 26°C. A and B show the separation of the cation-exchange peptide standards C1, C2, C3 and C4 (+1, +2, +3 and +4 net charge, respectively). C shows the separation of peptide standards S1–S5. D shows the relationship between peptide retention time and net positive charge during cation-exchange chromatography of peptides C1–C4 on the (A) cation-exchange and (B) HILIC columns. Peptide C1 (+1 net charge) was eluted prior to the salt gradient on the HILIC column (B) and is not included in the plot in D. The sequences of the peptides are shown in Table I.

charged (*i.e.*, anionic) character, then peptide S1 (+3 net charge) would interact more strongly than peptides S2–S5, all four of which have a net charge of +2. The relative retention time difference between peptides S2, S3, S4 and S5 during HILIC are consistent with those obtained by RP-HPLC, suggesting that peptides with the same net charge exhibit similar relative hydrophilic and hydrophobic effects.

Peptide cation-exchange standards C1–C4 (+1 to +4 net charge, respectively) (Table I) were utilized to verify that the HILIC column was exhibiting ionic interactions. As noted previously, the retention behavior of these peptides should be unaffected in the pH range 2–7.

Fig. 2A and B show the elution profiles of the four peptide standards on a strong cation-exchange column (polysulfoethylaspartamide [1,14,15]) and the HILIC column, respectively. Both columns were run under standard ion-exchange conditions, *i.e.*, increasing salt (KCl) gradient in a phosphate buffer (5 mM aqueous KH_2PO_4 , pH 6.5). Acetonitrile is often added to the mobile phase to suppress hydrophobic interactions with ion-exchange sorbents and to ensure ideal ion-exchange behavior [3]. Both the cation-exchange column (Fig. 2A) and the HILIC column (Fig. 2B) required a salt gradient to elute the peptide standards. In addition, as would be expected with ideal cation-exchange column behaviour [3], the peptides show a linear relationship between retention time and net positive charge [except peptide C1 (+1 net charge), which is eluted prior to the salt gradient on the HILIC column] (Fig. 2D). These results clearly indicated that, under these conditions, the HILIC column was behaving as a cation-exchange column, *i.e.*, the HILIC sorbent must contain negatively charged functionalities as a result of the manufacturing process. The ideal HILIC column (*i.e.*, solute separation based on hydrophilic interactions alone) would not show such ionic interactions. The shorter retention times of the peptides on the HILIC column compared with the cation-exchange column may be explained by the former possessing a smaller ion-exchange capacity.

Fig. 2C shows the elution profile of peptides S1–S5 on the HILIC column, run under the same conditions as in A and B. Peptides S2–S5 (all +2 net charge) were eluted from the column earlier than peptide S1 (+3), as would be expected with a cation-exchange separation. However, it is apparent that peptides S2–S5 were also resolved by a hydrophilic interaction mechanism, as the four peptides were eluted in order of increasing hydrophilicity [S5, the least hydrophilic ($\Sigma R_c = 29.3$) to S2, the most hydrophilic ($\Sigma R_c = 17.5$) (Table I)]. This result indicated that the dominant interactions between the peptides and the HILIC sorbent are ionic in character and that hydrophilic interactions are then additive to provide the mixed-mode separation.

Although Figs. 1 and 2 demonstrated the importance of ionic interactions during separations of basic peptides, hydrophilic interactions were also certainly a major factor influencing their retention behavior. We now wished to determine whether the column could retain peptides with no charge, *i.e.*, whether the HILIC column could retain and separate peptides *via* hydrophilic interactions only. The model peptides selected to clarify this point were the anion-exchange standards A1–A4 (containing one to four acidic residues, respectively; Table I). As stated previously, at pH 2, these peptides are uncharged, as their side-chain carboxyl groups are protonated. Fig. 3A, shows the reversed-phase separation of the four peptides on the C_{18} column. The order of peptide elution is based on increasing peptide hydrophobicity (Table I), with the most hydrophilic peptide, A1 ($\Sigma R_c = 17.8$), being eluted first, followed by A2

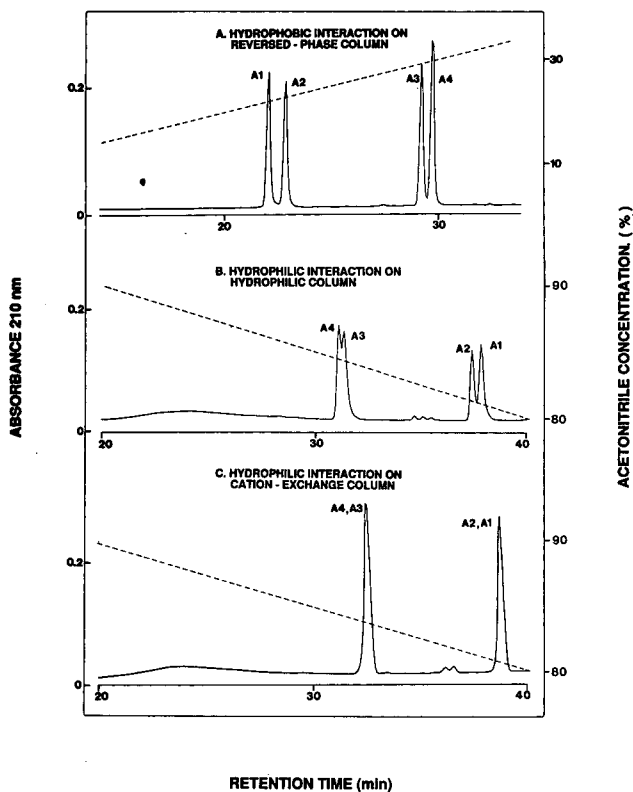


Fig. 3. Separation of a mixture of synthetic neutral peptides by (A) RP-HPLC, (B) HILIC on a HILIC column and (C) HILIC on a strong cation-exchange column. (A) Column, SynChropak RP-P C₁₈ (250 × 4.6 mm I.D.); mobile phase, linear A–B increasing acetonitrile gradient (1% B/min) at a flow-rate of 1 ml/min, where A is 0.05% aqueous TFA and B is 0.05% TFA in acetonitrile. (B) Column, Polyhydroxyethylaspartamide HILIC column (200 × 4.6 mm I.D.); mobile phase, linear A–B decreasing acetonitrile gradient (0.5% B/min, following 10-min isocratic elution with 95% A–5% B), where A is 0.2% orthophosphoric acid in acetonitrile and B is 0.2% aqueous orthophosphoric acid. (C) Column, Polysulfoethylaspartamide strong cation-exchange column (200 × 4.6 mm I.D.); mobile phase as in B; temperature, 26°C. The dotted lines denote the respective acetonitrile gradients. The sequences of peptides A1, A2, A3 and A4 are shown in Table I.

($\Sigma R_c = 17.9$), A3 ($\Sigma R_c = 24.8$) and finally A4 ($\Sigma R_c = 24.9$), the most hydrophobic peptide. In contrast, when HILIC was carried out with these peptides on the HILIC column (Fig. 3B), their retention and separation were clearly based on hydrophilic interactions with a reversal in elution order to that obtained by RP-HPLC (Fig. 3A), *i.e.*, the peptides were now eluted in order of increasing hydrophilicity. The resolution of the four peptides was not as effective on the HILIC column (Fig. 3B) compared with the reversed-phase column (Fig. 3A), even though the decreasing gradient slope of the HILIC run was shallower (0.5% acetonitrile/min) than that of the increasing gradient slope of the RP-HPLC run (1% B/min). However, the HILIC column was still able to resolve partially the two peptide pairs A1–A2 and A3–A4.

It seemed reasonable to assume that, by its nature, the charged character of a cation-exchange sorbent would also possess considerable hydrophilic character. Fig. 3C shows the HILIC separation of peptides A1–A4 on the polysulfoethylaspartamide strong cation-exchange column run under the same conditions as the HILIC column (Fig. 3B). Even though the cation-exchange column could not resolve the two peptide pairs A1–A2 and A3–A4, the column clearly retained the peptides based on hydrophilic interactions, with the least hydrophilic peptide pair, A3–A4, being eluted first and the most hydrophilic pair, A1–A2, being eluted last.

The polysulfoethylaspartamide cation exchanger is an hydrophilic silica-based packing. The Mono S strong cation-exchange column, which contains an organic polyether-based sorbent, was demonstrated to exhibit some hydrophobic character that could be suppressed by the addition of acetonitrile to the mobile phase buffers [3]. Interestingly, Fig. 4A shows that, under conditions where the starting buffer does not contain acetonitrile, and with a combined increasing salt (5 mM KCl/min) and acetonitrile (1% B/min) gradient, peptides S1, S2 and S5 were separated by a mixed-mode mechanism. Thus, peptides S2 and S5 (+2 net charge) were well separated from S1 (+3 net charge) mainly by an ionic mechanism, while S5 was resolved from S2 by an *hydrophobic* interaction mechanism. Thus, S5, which is more hydrophobic than S2 ($\Sigma R_c = 29.3$ and 17.5 , respectively, at neutral pH), was eluted later than the latter peptide. In contrast, under the same run conditions, the polysulfoethylaspartamide column exhibited a mixed ionic and *hydrophilic* separation mechanism (Fig. 4D). Peptide S1 (+3 net charge) was well resolved from peptides S2 and S5 (+2 net charge) mainly by ionic interactions with the column, whilst peptides S2 and S5 were separated through hydrophilic interactions (S2 is eluted later than the less hydrophilic S5). Thus, the separation of S2 and S5 is reversed when comparing the two cation-exchange columns (Fig. 4A and D). This reversal can be readily explained by the difference in hydrophobicity of the two sorbents [*i.e.*, the Mono S sorbent is more hydrophobic (less hydrophilic) than the hydrophilic polysulfoethylaspartamide sorbent].

Fig. 4B demonstrates that hydrophobic interactions between the Mono S column and the peptides can be overcome by the addition of 10% acetonitrile to buffers A and B; ideal cation-exchange chromatography was now observed and no separation of peptides with identical net positive charge was achieved (*i.e.*, S2, S3, S4 and S5, with net charges of +2, were not resolved). In contrast, identical run conditions on the polysulfoethylaspartamide column separated peptides S2–S5 by hydrophilic interaction (Fig. 4E). Acetonitrile does not overcome hydrophilic interactions; on the contrary, it promotes these interactions.

Fig. 4C demonstrates that the Mono S column could separate peptides by a mixed ionic and hydrophilic interaction mechanism by simply increasing the concentration of acetonitrile in the mobile phase to 50% (v/v). Thus, peptides S2–S5 (+2 net charge) were now separated by hydrophilic interactions. Under the same run conditions on the polysulfoethylaspartamide column (Fig. 4F), a similar, albeit improved, separation of peptides S2–S5 was observed. In fact, S2 and S3 (which differ only by a single methyl group; Table I) were not fully resolved on the Mono S column (Fig. 4C); in contrast, they showed baseline resolution on the polysulfoethylaspartamide column (Fig. 4F).

Although the dominating interactions exhibited by both cation-exchange col-

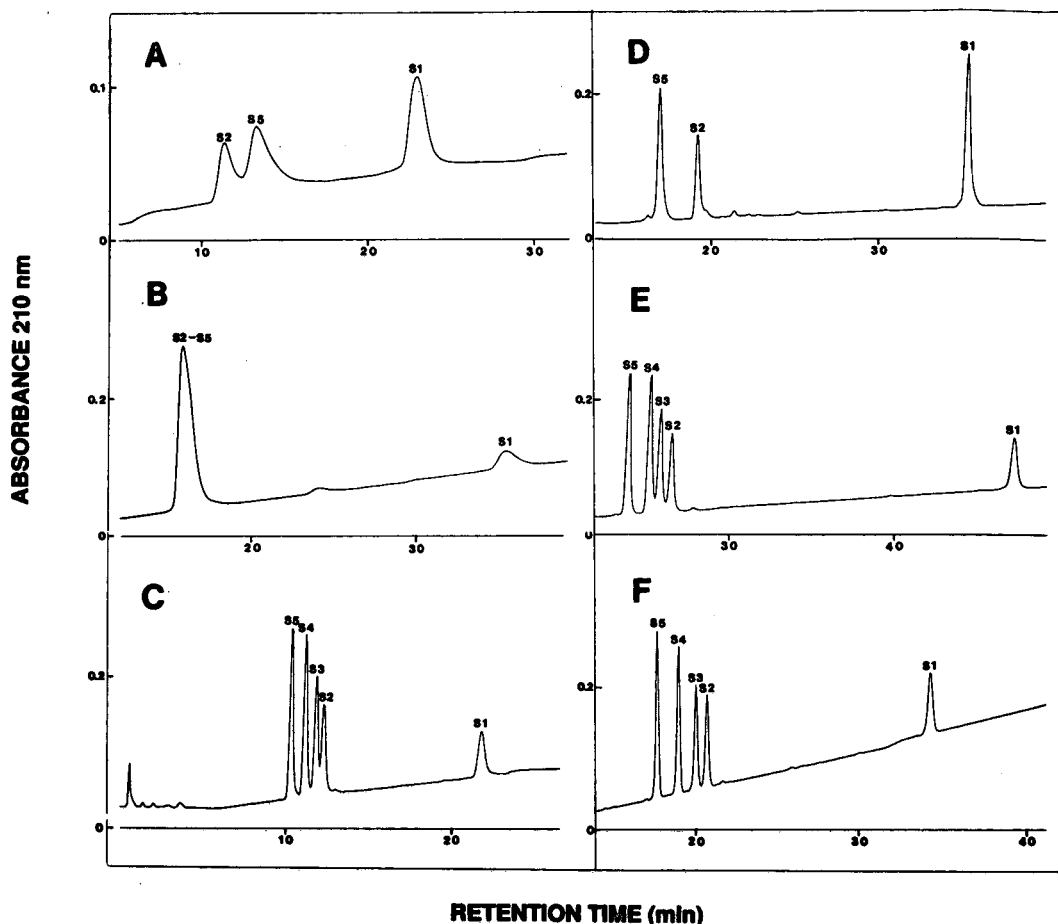


Fig. 4. Comparison of the mixed-mode separation of a mixture of synthetic positively charged peptides on two strong cation-exchange columns. Column: (A, B and C) non-silica-based Mono S HR 5/5 strong cation-exchange column (50×5 mm I.D.); (D, E and F) silica-based polysulfoethylaspartamide strong cation-exchange column (200×4.6 mm I.D.). Mobile phase: (A and D) linear A-B increasing salt and acetonitrile gradient (2% B/min, equivalent to 5 mM KCl/min and 1% acetonitrile/min) at a flow-rate of 1 ml/min, where buffer A is 5 mM aqueous KH_2PO_4 (pH 6.5) containing 50 mM KCl and buffer B is 5 mM aqueous KH_2PO_4 (pH 6.5) containing 0.25 M KCl and 50% (v/v) acetonitrile; (B and E) linear A-B increasing salt gradient (2% B/min, equivalent to 5 mM KCl/min) at a flow-rate of 1 ml/min, where buffer A is 5 mM aqueous KH_2PO_4 (pH 6.5) and buffer B is buffer A plus 0.25 M KCl, both buffers containing 10% (v/v) acetonitrile; (C and F) linear A-B increasing salt gradient (2% B/min, equivalent to 5 mM KCl/min) at a flow-rate of 1 ml/min, where buffer A is 5 mM aqueous KH_2PO_4 (pH 6.5) and buffer B is buffer A plus 0.25 M KCl, both buffers containing 50% (v/v) acetonitrile. Temperature, 26°C. The sequences of peptides S1-S5 are shown in Table I.

umns were ionic, with hydrophilic and hydrophobic interactions secondary, the performance of the polysulfoethylaspartamide column was always superior under the different sets of run conditions employed in Fig. 4. This is evidenced, for example, by the improved separation and peak shape of peptides S2-S5 on this column (Fig. 4D, E and F) compared with the Mono S column (Fig. 4A, B and C) under the same run

conditions. In addition, a good separation of these peptides on the polysulfoethylaspartamide column compared with the Mono S column was achieved with a lower level of acetonitrile in the mobile phase buffers: compare Fig. 4E (where only 10% of acetonitrile was required to produce the illustrated elution profile on the polysulfoethylaspartamide column) with Fig. 4C, where 50% of acetonitrile was required to achieve a similar separation on the Mono S. Low acetonitrile concentrations are advantageous for most peptides, which are more soluble in highly aqueous media. The column capacity of the former column was also considerably greater than that of the Mono S column. Thus, the retention times of the five peptides were considerably longer on the polysulfoethylaspartamide column (Fig. 4F) than on the Mono S column (panel Fig. 4C) under identical run conditions. This increased capacity of ionic groups on the polysulfoethylaspartamide column could also contribute to the improved hydrophilic interaction chromatography observed on this column during mixed-mode operation (Fig. 4). If one must operate a column in a mixed mode, it is preferable to have only two types of interactions, rather than three as observed with the Mono S column (Fig. 4). The hydrophobic interactions on the Mono S column are not advantageous in that they cause peak broadening and must be overcome just to obtain elution of more highly charged peptides [3].

CONCLUSIONS

Even though the ideal hydrophilic interaction sorbent has yet to be developed, it is certainly worthwhile continuing the development of such a sorbent lacking ionic characteristics. At present, the hydrophilic sorbent of the polysulfoethylaspartamide strong cation-exchange column utilized in this study is the most versatile. It provides excellent selectivity during operation in a mixed mode where conditions are selected to promote hydrophilic and ionic interactions, and this selectivity is achievable at a low acetonitrile concentration in the mobile phase. This cation-exchange column could also provide excellent selectivity changes with pH, which result in changes in the net charge on many peptides as the carboxyl groups are ionized with increasing pH. This combined effect of utilizing pH and hydrophilicity in cation-exchange chromatography may well rival reversed-phase chromatography for peptide applications. This mixed-mode separation in cation-exchange columns may also be superior in terms of selectivity to those achieved by capillary zone electrophoresis.

ACKNOWLEDGEMENTS

This work was supported by the Medical Research Council of Canada and equipment grants from the Alberta Heritage Foundation for Medical Research. We also acknowledge T. W. Lorne Burke for skilled technical assistance.

REFERENCES

- 1 A. J. Alpert, *J. Chromatogr.*, 499 (1990) 177.
- 2 C. T. Mant and R. S. Hodges, *LC · GC*, 4 (1986) 250.
- 3 T. W. L. Burke, C. T. Mant, J. A. Black and R. S. Hodges, *J. Chromatogr.*, 476 (1989) 377.
- 4 D. Guo, C. T. Mant, A. K. Taneja, J. M. R. Parker and R. S. Hodges, *J. Chromatogr.*, 359 (1986) 499.

- 5 C. T. Mant and R. S. Hodges, in K. M. Gooding and F. E. Regnier (Editors), *HPLC of Biological Macromolecules: Methods and Applications*, Marcel Dekker, New York, 1990, pp. 301–332.
- 6 C. T. Mant, N. E. Zhou and R. S. Hodges, in E. Heftmann (Editor), *Chromatography, Part B*, Elsevier, Amsterdam, 5th ed., in press.
- 7 K. E. Bij, Cs. Horváth, W. R. Melander and A. Nahum, *J. Chromatogr.*, 203 (1981) 65.
- 8 M. T. W. Hearn and B. Grego, *J. Chromatogr.*, 218 (1981) 497.
- 9 D. W. Armstrong and R. E. Boehm, *J. Chromatogr. Sci.*, 22 (1984) 379.
- 10 R. S. Blanquet, K. H. Bui and D. W. Armstrong, *J. Liq. Chromatogr.*, 9 (1986) 1933.
- 11 R. J. Simpson, R. L. Moritz, E. Nice and B. Grego, *Eur. J. Biochem.*, 165 (1987) 21.
- 12 R. J. Simpson and R. L. Moritz, in C. T. Mant and R. S. Hodges (Editors), *HPLC of Peptides and Proteins: Separation, Analysis and Conformation*, CRC Press, Boca Raton, FL, 1991, pp. 399–408.
- 13 D. Guo, C. T. Mant and R. S. Hodges, *J. Chromatogr.*, 386 (1987) 205.
- 14 D. L. Crimmins, J. Gorka, R. S. Thoma and B. D. Schwartz, *J. Chromatogr.*, 443 (1988) 63.
- 15 A. J. Alpert and P. C. Andrews, *J. Chromatogr.*, 443 (1988) 85.

Evaluation of kinetic models for biospecific adsorption and its implications for finite bath and column performance

M. A. McCOY and A. I. LIAPIS*

Department of Chemical Engineering and Biochemical Processing Institute, University of Missouri-Rolla, Rolla, MO 65401-0249 (USA)

ABSTRACT

Dynamic models that could describe the adsorption of adsorbate onto ligand immobilized on porous or non-porous particles in batch and column systems, are presented and solved.

Two different kinetic models (kinetic models 1 and 2) are used to describe the dynamics of the adsorption mechanism when β -galactosidase is adsorbed onto monoclonal antibody immobilized on porous silica particles. The differences in the theoretical predictions of the concentration of the adsorbate in the fluid of the finite bath obtained from kinetic models 1 and 2, are not significant and the agreement between experiment and theory is good. But the two different kinetic models lead to different estimates for the value of the pore diffusivity, and provide significantly different concentration profiles for the adsorbate in the pore fluid and adsorbed phases of the adsorbent particles of the batch system. The column results indicate that the differences in the breakthrough curves obtained from kinetic models 1 and 2, increase as the column length increases. Also, the concentration profiles of the adsorbate in the adsorbent particles obtained from kinetic models 1 and 2, are significantly different and their differences vary along the axial distance of the column. The results indicate that while it is a necessary condition for a kinetic model to describe properly the experimental overall mass-transfer resistance, this is not also a sufficient condition for the accurate determination of the adsorption mechanism and for the accurate estimation of the values of the rate constants and of the pore diffusivity. Furthermore, the differences in the concentration profiles of the adsorbate in the adsorbent particles, obtained from kinetic models 1 and 2, have important implications on the performance of the adsorption stage, as well as on the performance of the wash and elution stages. Experiments are suggested which could provide information that could significantly improve the model discrimination and parameter estimation studies for the determination of a proper mechanism for the dynamics of the adsorption step and of an accurate estimate for the value of the pore diffusivity. When the estimated value of the pore diffusivity is varied by $\pm 20\%$, the effect on the dynamic behavior of the batch and column systems can be appreciable. The effect on the dynamic behavior of the batch and column systems when the estimated value (from a correlation) of the film mass transfer coefficient is varied by $\pm 20\%$, is not significant.

The batch adsorption of β -galactosidase onto anti- β -galactosidase immobilized on non-porous glass coated beads is found to be controlled by film mass transfer and the dynamics of the adsorption step. The batch model with a second-order reversible interaction mechanism for the adsorption step, provides theoretical predictions such that the agreement between experiment and theory is reasonable. When the estimated value (from a correlation) of the film mass transfer coefficient is varied by $\pm 20\%$, the effect on the dynamic behavior of the batch and column systems (having nonporous adsorbent particles) is not significant. Column experiments are suggested which could provide information, in addition to the information obtained from batch experiments, that could improve the model discrimination and parameter estimation studies for the determination of a proper mechanism for the dynamics of the adsorption step, in affinity adsorption systems involving non-porous adsorbent particles.

INTRODUCTION

Industry has significant interest in the design, optimization, and control of large-scale affinity adsorption systems which are to be employed in the purification of biologically active macromolecules for use as pharmaceuticals or in other applications where the purity of the product is a very important consideration. Certain fundamental mechanisms underlying the affinity adsorption separations have been identified and constitutive expressions which may be used to quantify these mechanisms and their effects, have been suggested and constructed [1-19]. The parameters characterizing the mechanisms involved in the different stages (*i.e.*, adsorption, wash, elution) of affinity adsorption and in the different operational modes [*i.e.*, batch, fixed bed (column), fluidized bed] could be estimated from proper correlations and/or by matching the predictions of appropriate models, which are developed to describe the behavior of affinity adsorption in the different stages and operational modes, with experimental data [1-4,11-20].

It is well established that affinity adsorption experiments are tedious, time consuming, and expensive. The number of experiments at the bench-scale and pilot-scale levels could be significantly reduced by developing and employing mathematical models that would satisfactorily predict the behavior of the affinity adsorption stages under different operational modes. Such models may be used to guide the experiments [1,11-14,16,18-21] in regions of the experimental space where a better scientific understanding of the behavior of affinity adsorption mechanisms may be obtained, and even new and interesting phenomena might be observed. Furthermore, these models could be used in the complex tasks of design, optimization, control, and scale-up of affinity adsorption processes. It should be emphasized that there is nothing more practical than a mathematical model which can accurately predict the dynamic behavior, scale-up, and design of a process of interest, since such a model could obviate many experiments which in the case of affinity chromatography are tedious, time consuming, and expensive.

In this work, the dynamic behavior of the adsorption of β -galactosidase onto monoclonal antibody ligand immobilized on (a) porous silica particles and on (b) non-porous glass coated beads, is studied by two different kinetic models that characterize the dynamics of the interaction (adsorption step) between the adsorbate and ligand. Also, the effects on the dynamic behavior of biospecific adsorption of the parameters that characterize film mass transfer and intraparticle diffusion, are examined. Both finite bath (batch) and column (fixed bed) adsorption systems are considered.

THEORY

Single component adsorption is considered to occur, and the mass transfer and interaction steps are as follows: (i) The transport of adsorbate from the bulk fluid to the external surface of the adsorbent particle (film mass transfer). (ii) The transport of adsorbate within the porous adsorbent particle (intraparticle diffusion); in case that the adsorbent particle is non-porous, intraparticle diffusion does not occur. (iii) The interaction between the adsorbate and the immobilized ligand (adsorption step). The interaction step (iii) may be composed of several substeps, depending on the

complexity of the adsorbate–ligand interaction, and could include the binding of multivalent adsorbates to monovalent ligands [1,4,11]. Yon [11] has shown that in most affinity chromatography systems the partitioning will seem to be monovalent, *i.e.*, interaction between a monovalent adsorbate and a monovalent ligand. In this work, the partitioning is considered as being monovalent.

The most commonly used mode of operation in affinity chromatography separations is the fixed bed mode with axial flow [2,4,10,14,16]. Batch (finite bath) adsorption systems would be appropriate where the fluid to be processed was of high viscosity or contains particulate material. Arve and Liapis [1], Liapis [14–17] and Petropoulos *et al.* [12] have indicated that, for a given affinity adsorption system, the parameters that characterize the intraparticle mass transfer and adsorption mechanisms should be independent of the operational mode (*e.g.*, batch, fixed bed, fluidized bed), and therefore, if these parameters are estimated by utilizing information obtained from finite bath experiments (batch experiments are easier to perform and analyze [1,10,14–20] than column experiments), then their values should characterize the intrinsic mechanisms (intraparticle mass transfer and adsorption mechanisms) in other operational modes. This theoretical approach of Arve and Liapis [1] has been shown to be valid by the data of the affinity chromatography system studied by Horstmann and Chase [22]. Furthermore, Johnston and Hearn [20] compared the experimental dynamic adsorption data of the binding of several proteins (with different molecular geometries) to several ion-exchange and dye-affinity chromatographic resins, with the theoretical predictions of different models. They found [20] that the model of Arve and Liapis [1,4] provided the best agreement between experiment and theory, and furthermore, the values of the kinetic parameters estimated by matching the theoretical predictions of this model with the experimental data, were found [20] to be consistent with enzyme kinetic theory.

Finite bath with porous adsorbent particles

The porous adsorbent particles are suspended in the liquid of the finite bath by agitation so that the liquid has free access, and the bulk concentration of the adsorbate is taken to be uniform throughout the bath except in a thin film (film mass transfer resistance) of liquid surrounding each particle. The adsorption process is considered to be isothermal since the heat of adsorption apparently does not change the temperature [13,14–16,19] of the liquid phase even in large-scale systems; this occurs because the total amount of adsorbed material is small and the heat capacity of the liquid phase is high.

A differential mass balance for the adsorbate in the fluid phase of the finite bath gives

$$\frac{dC_d}{dt} = \left(\frac{1 - \varepsilon}{\varepsilon} \right) \left(\frac{\alpha + 1}{r_0} \right) K_f [C_p(t, r_0) - C_d] \quad (1)$$

Eqn. 1 can be used for particles having geometry of slab, cylinder or sphere by putting $\alpha = 0, 1$ or 2 , respectively. The initial condition of eqn. 1 is given by

$$C_d = C_{d0} \quad \text{at} \quad t = 0 \quad (2)$$

The transport of the adsorbate in the adsorbent particle is considered to be governed by the diffusion [1,12] of the species in the pore fluid (pore diffusion) of the particle. The intraparticle (pore diffusion) transport mechanism is taken to be one-dimensional and in particles that have an axis of symmetry. It is understood that in the case of the slab and the cylinder, the particles are of infinite extent or alternatively one must artificially assume that the ends of a finite cylinder or edges of a finite slab are sealed in order to keep the problem one-dimensional. A differential material balance for the adsorbate in the adsorbent particle is given by

$$\frac{\partial(\varepsilon_p C_p)}{\partial t} + \frac{\partial C_s}{\partial t} = \frac{1}{r^\alpha} \frac{\partial}{\partial r} \left(r^\alpha \varepsilon_p D_p \frac{\partial C_p}{\partial r} \right) \quad (3)$$

The initial and boundary conditions for eqn. 3 are

$$C_p = 0 \quad \text{at} \quad t = 0, \quad 0 \leq r \leq r_0 \quad (4)$$

$$C_s = 0 \quad \text{at} \quad t = 0, \quad 0 \leq r \leq r_0 \quad (5)$$

$$\varepsilon_p D_p \left. \frac{\partial C_p}{\partial r} \right|_{r=r_0} = K_f [C_d - C_p(t, r_0)], \quad t > 0 \quad (6)$$

$$\left. \frac{\partial C_p}{\partial r} \right|_{r=0} = 0, \quad t > 0 \quad (7)$$

If restricted [12,20] pore diffusion occurs, then ε_p and D_p would vary with the loading of the adsorbate in the adsorbed phase, as shown by the restricted pore diffusion mathematical model of Petropoulos *et al.* [12]. If the effect of restricted pore diffusion on the mass flux of the adsorbate is not significant, then the values of ε_p and D_p may be considered to be constant [1,12,20].

It is apparent that eqn. 3 can be solved only if an appropriate expression for the term $\partial C_s / \partial t$ is available. This term represents the accumulation of the adsorbed species on the internal surface of the porous adsorbent particle, and it can be quantified if a mathematical expression could be constructed that would describe the mechanism of the adsorption of the adsorbate onto the immobilized ligand. In this work, two different kinetic models for the adsorption mechanism are considered:

(1) The adsorption is completely reversible and with no interaction between the adsorbed molecules. The interaction between unbound monovalent adsorbate (A_1) in the solution and vacant immobilized monovalent ligand (L_1) may be considered to be of the form [1,5,6,13,14,20,22]



where $A_1 L_1$ represents the non-covalent adsorbate–ligand complex. Then assuming elementary interactions, the rate of the adsorption step may be described by the following second-order reversible interaction:

$$\frac{\partial C_s}{\partial t} = k_{11} C_p (C_T - C_s) - k_{21} C_s \quad (9)$$

The subscript 1 in the rate constants k_{i1} ($i = 1, 2$), indicates that these parameters characterize the forward and reverse rates of the second-order interaction given by kinetic model 1. This model is described by eqn. 8 and its dynamic expression is given by eqn. 9. The accumulation term, $\partial C_s/\partial t$, in eqn. 9 becomes equal to zero when adsorption equilibrium is established, and the following expression for the equilibrium isotherm is obtained:

$$C_s = \frac{C_T K C_p}{1 + K C_p} \quad (10)$$

Eqn. 10 represents the Langmuir equilibrium adsorption model where $K = k_{11}/k_{21}$. It should be noted that at equilibrium the value of C_p in eqn. 10 should be equal to the value of C_d .

The initial condition of eqn. 9 is given by eqn. 5. Eqns 1, 3 and 9 could now be solved simultaneously in order to obtain the dynamic behavior of C_d , C_p and C_s . It should be noted at this point that if the interaction between the adsorbate and ligand occurs infinitely fast, then the adsorbate molecules in the solution and in the adsorbed phase are in equilibrium at every point in the pore and the term $\partial C_s/\partial t$ in eqn. 3 would take the following form (eqn. 10 is employed):

$$\frac{\partial C_s}{\partial t} = \left(\frac{\partial C_s}{\partial C_p} \right) \left(\frac{\partial C_p}{\partial t} \right) = \left[\frac{C_T K}{(1 + K C_p)^2} \right] \left(\frac{\partial C_p}{\partial t} \right) \quad (11)$$

(2) Lundstrom *et al.* [6] have indicated that, in certain systems, macromolecule-induced exchange interactions may occur on the surface of the adsorbent, whereby an already adsorbed molecule is exchanged with a protein molecule from the solution; this process may occur even if the spontaneous desorption of biomolecules is very small. They have suggested a kinetic model for the adsorption step, which may be considered for systems where the volume of the immobilized ligand is smaller than the volume of the adsorbate molecule. It is assumed that a biomolecule adsorbs on the surface forming one type of adsorbate-ligand complex ("form a"), and that after adsorption it may change conformation ("form b"). An adsorbed molecule in "form a" is considered to occupy an area A_a on the surface, while an adsorbed molecule in "form b" is considered to occupy an area A_b . The adsorbed molecules of "form a" and "form b" are competing for the same area on the surface, and it is assumed that both exchange interactions and spontaneous desorption take place on the surface. The exchange interactions are modelled as a desorption, which depends on the concentration of the adsorbate in the pore fluid, $C_p(t,r)$. If C_T now represents the available adsorption sites for molecules of "form a" and δ represents the ratio of A_b to A_a ($\delta = A_b/A_a$), then the interaction rate expressions for this physical model are

$$\frac{\partial C_{sa}}{\partial t} = (k_{12} C_p - k_{32} C_{sa})(C_T - C_{sa} - \delta C_{sb}) - k_{42} C_p C_{sa} - k_{22} C_{sa} \quad (12)$$

$$\frac{\partial C_{sb}}{\partial t} = k_{32} C_{sa}(C_T - C_{sa} - \delta C_{sb}) - k_{62} C_p C_{sb} - k_{52} C_{sb} \quad (13)$$

C_{sa} and C_{sb} represent the concentrations of the adsorbate in the complexes of "form a" and "form b", respectively. The parameters k_{i2} ($i = 1, 2, \dots, 6$) are interaction rate constants. The parameters k_{22} and k_{52} characterize the spontaneous desorption of adsorbate from complexes of "form a" and "form b", respectively. The rate constants k_{42} and k_{62} characterize macromolecule-induced exchange interactions from complexes of "form a" and "form b", respectively. The parameter k_{12} characterizes the rate of formation of the complex of "form a" by the forward interaction between adsorbate in the solution (pore fluid) and immobilized vacant ligand. The rate constant k_{32} characterizes the rate of formation of the complex of "form b" from the complex of "form a". The subscript 2 in the rate constants k_{i2} ($i = 1, 2, 3, \dots, 6$) indicates that these parameters characterize the interactions described by kinetic model 2. This model is described by the dynamic expressions shown in eqns. 12 and 13. The accumulation term, $\partial C_s/\partial t$, in eqn. 3 is obtained from the terms $\partial C_{sa}/\partial t$ and $\partial C_{sb}/\partial t$. It should be noted that the equilibrium expressions for C_{sa} and C_{sb} are obtained from eqns. 12 and 13 by setting the accumulation terms ($\partial C_{sa}/\partial t$, $\partial C_{sb}/\partial t$) equal to zero. Furthermore, at $t = 0$ the concentrations C_{sa} and C_{sb} are considered to be equal to zero, and thus, $C_s = C_{sa} + C_{sb} = 0$ (eqn. 5) at $t = 0$. Eqns. 1, 3 and 12 and 13 could now be solved simultaneously in order to obtain the dynamic behavior of C_d , C_p and C_s . It is also worth noting that when the parameters k_{32} , k_{42} , k_{52} and k_{62} are all set equal to zero, the concentration C_{sb} (because of its initial condition that at $t = 0$, $C_{sb} = 0$) also becomes equal to zero for all times, and thus, kinetic model 1 (where $C_s = C_{sa}$) is obtained from kinetic model 2 under these conditions.

Finite bath with non-porous adsorbent particles

In the previous section porous adsorbents were considered, since it is common to use porous particles in order to obtain high macromolecule adsorption capacities per unit volume. But the porous adsorbent particles, for a given mode of operation, would have a higher overall mass transfer resistance (because of the intraparticle mass transfer resistance) than that encountered in non-porous adsorbent particles of the same dimension. In non-porous adsorbents the ligands are immobilized on the outer surface of the particle.

For single component adsorption in a finite bath with non-porous adsorbent particles, eqn. 1 assumes the following form:

$$\frac{dC_d}{dt} = \left(\frac{1 - \varepsilon}{\varepsilon} \right) \left(\frac{\alpha + 1}{r_0} \right) K_f (C_{dp} - C_d) \quad (14)$$

In eqn. 14, C_{dp} denotes the concentration of the adsorbate in the liquid layer adjacent to the surface of the non-porous adsorbent particle. Since $dC_d/dt = -[(1 - \varepsilon)/\varepsilon](dC_s/dt)$, the term dC_s/dt would be given by eqn. 15

$$\frac{dC_s}{dt} = \left(\frac{\alpha + 1}{r_0} \right) K_f (C_d - C_{dp}) \quad (15)$$

where C_{dp} is related to C_s , as is shown below. The initial conditions for eqns. 14 and 15 are given by eqns. 2 and 5, respectively. The only remaining step is an equation for C_{dp} .

It is apparent that in order to develop an expression for C_{dp} , one has to consider the controlling mechanisms of the adsorption process (of course, only at equilibrium the value of C_{dp} should be equal to the value of C_d). The following two cases may be considered:

(i) It is assumed that adsorption is controlled by film mass transfer, and therefore, C_{dp} is taken to be in equilibrium with the concentration of the adsorbate in the adsorbed phase, C_s , at every point on the surface of the adsorbent particle. If, for example, the equilibrium adsorption data of a given system are described by the Langmuir isotherm given in eqn. 10, then the expression for C_{dp} would have the following form:

$$C_{dp} = \frac{C_s}{K(C_T - C_s)} \quad (16)$$

For this example, the right-hand-side of eqn. 16 should replace C_{dp} in eqns. 14 and 15, and the resulting non-linear ordinary differential equations will have to be integrated simultaneously in order to obtain the variation of C_d and C_s with time. If the equilibrium isotherm of an adsorption system is given by an expression other (*e.g.*, eqns. 12 and 13 with $\partial C_{sa}/\partial t = \partial C_{sb}/\partial t = 0$) than that shown in eqn. 10, then the expression for C_{dp} would have a form other than that given in eqn. 16.

(ii) It is considered that adsorption is controlled by film mass transfer and by the dynamics of the interaction (adsorption step) mechanism between the adsorbate and the ligand. In this case, C_{dp} and C_s are not in equilibrium. If, for example, kinetic model 1 described by eqn. 9 is considered to represent the dynamics of the adsorption step for a given system, then the concentration C_{dp} would be given (by combining eqns. 9 and 15) by the following expression:

$$C_{dp} = \frac{(\gamma C_d + k_{21} C_s)}{[k_{11}(C_T - C_s) + \gamma]} \quad (17)$$

where

$$\gamma = \left(\frac{\alpha + 1}{r_0} \right) K_t \quad (18)$$

For this example, the right-hand-side of eqn. 17 should replace C_{dp} in eqns. 14 and 15, and the resulting non-linear ordinary differential equations will have to be integrated simultaneously in order to obtain the variation of C_d and C_s with time. If the rate of the adsorption step is described by an expression other (*e.g.*, eqns. 12 and 13 of kinetic model 2) than that of kinetic model 1, then the expression for C_{dp} would have a form other than that given in eqn. 17. In this study, all calculations involving non-porous adsorbent particles (finite bath and column systems) have been carried out by considering that adsorption is controlled by film mass transfer and by the dynamics of the adsorption step [*i.e.*, in this study case (ii) has been considered].

The value of the film mass transfer coefficient, K_f , of the adsorbate in eqns. 1, 6, 14, 15 and 18, was calculated from the following expression [23]:

$$K_f = \frac{2D_{mf}}{d_p} + 0.31 \left[\frac{(\Delta\rho)\mu g}{\rho^2} \right]^{1/3} \left(\frac{\mu}{\rho D_{mf}} \right)^{-2/3} \quad (19)$$

where D_{mf} denotes the diffusion coefficient of the adsorbate in free solution; d_p is the mean diameter of the adsorbent particles; $\Delta\rho$ is the density difference between the particulate and continuous phases; ρ is the density of the liquid solution; μ is the viscosity; and $g = 9.80665 \text{ m/s}^2$.

Column with porous adsorbent particles

Single-component adsorption is considered to take place from a flowing liquid stream in a fixed bed of particles under isothermal conditions, and the concentration gradient in the radial direction of the bed is considered to be not significant [4,13,16,24]. A differential mass balance for the adsorbate in the flowing fluid stream gives

$$\frac{\partial C_d}{\partial t} - D_L \frac{\partial^2 C_d}{\partial x^2} + \frac{V_f}{\varepsilon} \frac{\partial C_d}{\partial x} = \left(\frac{1-\varepsilon}{\varepsilon} \right) \left(\frac{\alpha+1}{r_0} \right) K_f [C_p(t,x,r_0) - C_d] \quad (20)$$

In eqn. 20 the velocity of the fluid stream, V_f , is taken to be independent of the space variable x , because the liquid solutions encountered in affinity chromatography systems are very dilute and the main component of the solution is the carrier fluid (for non-dilute solutions a material balance, as shown in ref. 25, would provide the expression for $\partial V_f / \partial x$). The pressure drop through the fixed bed can be determined by the methods reported in pp. 129–134 of the book by Geankoplis [23]. The initial and boundary conditions of eqn. 20 are as follows:

$$C_d = 0 \quad \text{at} \quad t = 0, \quad 0 \leq x \leq L \quad (21)$$

$$\frac{V_f}{\varepsilon} C_d - D_L \frac{\partial C_d}{\partial x} = \frac{V_f}{\varepsilon} C_{d,in} \quad \text{at} \quad x = 0, \quad t > 0 \quad (22)$$

$$\frac{\partial C_d}{\partial x} = 0 \quad \text{at} \quad x = L, \quad t > 0 \quad (23)$$

The value of D_L may be estimated by the methods reported in ref. 26. In certain systems the axial dispersion coefficient, D_L , is so low that by setting its value equal to zero the error introduced in the prediction of the behavior of an affinity adsorption system is not significant [24,26]. When D_L is set equal to zero, the term $D_L(\partial^2 C_d / \partial x^2)$, in eqn. 20, becomes equal to zero, and the boundary condition at $x = 0$ (eqn. 22) becomes as follows:

$$C_d = C_{d,in} \quad \text{at} \quad x = 0, \quad t > 0 \quad (24)$$

The intraparticle diffusion mechanism of the adsorbate and the interaction mechanism between the adsorbate and the ligand for an affinity adsorption system in a column, should be the same as those in a finite bath (these are intrinsic mechanisms, as discussed earlier). For a given kinetic model of the adsorption mechanism (*e.g.*, kinetic model 1 or kinetic model 2) that would provide a satisfactory expression for the term $\partial C_s/\partial t$ in eqn. 3, the resulting equation for $\partial C_s/\partial t$ and eqns. 3 and 20 will have to be solved simultaneously in order to obtain the variation of C_d , C_p and C_s with time and space.

Column with non-porous adsorbent particles

For single-component adsorption in a column with non-porous adsorbent particles, C_{dp} replaces $C_p(t,x,r_0)$ in eqn. 20 and the resulting expression is solved together [13] with eqn. 25

$$\frac{\partial C_s}{\partial t} = \left(\frac{\alpha + 1}{r_0} \right) K_f (C_d - C_{dp}) \quad (25)$$

The initial condition of eqn. 25 is as follows:

$$C_s = 0 \quad \text{at} \quad t = 0, \quad 0 \leq x \leq L \quad (25a)$$

The solution of these equations provides the variation of C_d and C_s with time and space. In this study, an expression for C_{dp} developed under the conditions of case (ii) discussed above, was employed in eqns. 20 and 25.

The value of the film mass transfer coefficient, K_f , of the adsorbate in the column (eqns. 3, 6, 20 and 25) was calculated from the expression given in eqn. 5 of ref. 13. For the column systems studied in this work, the estimated values of D_L were so low that D_L was set equal to zero in eqns. 20 and 22. By setting D_L equal to zero, the error introduced in the calculated dynamic behavior of the column systems was insignificant.

Computational methods

The method of orthogonal collocation [27,28] was applied to the space variable r of the partial differential equation that describes mass transfer in the porous adsorbent particles, while the method of characteristics [28] was applied to the partial differential equation that describes mass transfer in the flowing fluid stream of the column ($D_L = 0$). The ordinary differential equations of the systems having porous adsorbent particles, were numerically integrated by using a third-order semi-implicit Runge-Kutta method (see ref. 28) developed by Michelsen [29]. The ordinary differential equations of the systems having non-porous adsorbent particles, were solved numerically by Gear's method (see ref. 28). The value of the effective pore diffusivity, D_p , as well as the values of the rate constants in kinetic models 1 and 2, were estimated by matching the equilibrium and dynamic (batch) experimental data with the theoretical predictions obtained from the solution of the equations of the models, through the use of a modified (non-linear least squares) Levenberg-Marquardt method (see ref. 30).

RESULTS AND DISCUSSION

The affinity chromatography systems studied in this work, involve (a) the adsorption of β -galactosidase onto monoclonal antibody ligand immobilized on porous silica particles [1], and (b) the adsorption of β -galactosidase onto monoclonal antibody ligand immobilized on non-porous glass coated beads [19,31]. Kinetic model 1 and kinetic model 2 are taken to represent two different dynamic mechanisms for the adsorption of β -galactosidase onto immobilized monoclonal antibody (anti- β -galactosidase) ligand. In our studies with kinetic model 2, spontaneous desorption of adsorbate from the complexes of "form a" and "form b" was not considered, and thus, k_{22} and k_{52} were set equal to zero. The desorption of adsorbate from the complexes of "form a" and "form b" was considered to occur only by macromolecule (β -galactosidase)-induced exchange interactions ($k_{42} \neq 0, k_{62} \neq 0$), and thus, the desorption mechanism of kinetic model 2 was made to be significantly different than that of kinetic model 1 (only spontaneous desorption is considered in kinetic model 1 with $k_{21} \neq 0$).

In Fig. 1, curve 1 represents the equilibrium data (equilibrium isotherm at $T = 293$ K) of the adsorption of β -galactosidase onto anti- β -galactosidase immobilized on porous silica particles [1]. The Langmuir (eqn. 10) expression with $C_T = 2.2$ mg/cm³ and $K = 4.54 \cdot 10^3$ cm³/mg, describes [1] curve 1. Curve 2 represents the best fit for the equilibrium data when kinetic model 2 with $\delta = 1$ and $\partial C_{sa}/\partial t = \partial C_{sb}/\partial t = 0$, is employed. The values of the parameters of the equilibrium expressions that describe curve 2 are as follows: $C_T = 2.2$ mg/cm³; $K_1 = k_{12}/k_{32} = 2.0 \cdot 10^3$; $K_2 = k_{42}/k_{32} = 32.2$; $K_3 = k_{62}/k_{32} = 3.55 \cdot 10^3$; and $k_{22} = k_{52} = 0$. It is worth noting that although curves 1 and 2 are described by significantly different equilibrium adsorption models, the quantitative differences between the two curves are not large. In fact, the quantitative differences are rather very small for all values of the concentration of β -galactosidase greater than $2 \cdot 10^{-4}$ mg/cm³. The data in curve 3 of Fig. 1 have been obtained from the same equilibrium expressions that describe curve 2 (the values of C_T , K_1 , K_2 , K_3 , k_{22} and k_{52} in curve 3, are the same as those used in curve 2), but in curve 3 the value of δ is equal to 2. The quantitative differences between curves 2 and 3 are very small for intermediate and high adsorbate concentrations. At very low concentrations of β -galactosidase, the quantitative differences between curves 2 and 3 are larger (the largest difference of about 20.76% occurs at $C_d = 10^{-4}$ mg/cm³) because at these low C_d values the concentration of the adsorbate in the complex of "form b", C_{sb} , is not insignificant, and thus, $\delta C_{sb} = 2C_{sb}$ (curve 3) is greater than $\delta C_{sb} = 1C_{sb}$ (curve 2), in eqns. 12 and 13. This may explain why the adsorptivity described by curve 2 is higher than that described by curve 3. It should be noted at this point that the agreement between curves 1 and 2 is better than that between curves 1 and 3. For this reason, the value of δ was taken to be equal to one in all subsequent model calculations (Figs. 2-5 and 7-10).

In Fig. 1, curve 4 represents the equilibrium data [19,31] (equilibrium isotherm at $T = 293$ K) of the adsorption of β -galactosidase onto anti- β -galactosidase immobilized on non-porous glass coated beads. The Langmuir equation with $C_T = 0.33490$ mg/cm³ and $K = 19.120$ cm³/mg, describes [19] curve 4. By comparing the values of the parameters (C_T and K) of the equations that describe curves 1 and 4, it is observed that the values of C_T and of the association constant, K , of the adsorption of

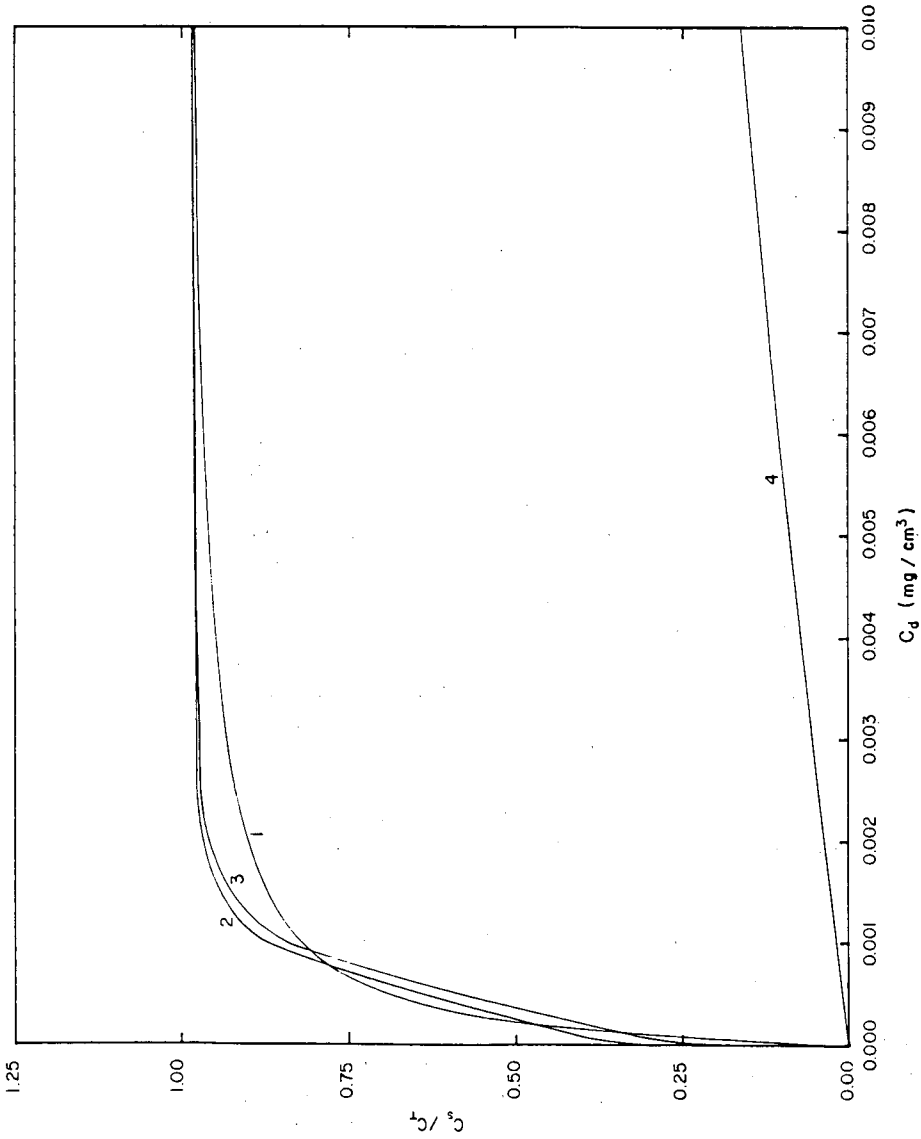


Fig. 1. Equilibrium adsorption isotherms; curves 1, 2 and 3 represent the adsorption of β -galactosidase onto anti- β -galactosidase immobilized on porous silica particles; curve 4 represents the adsorption of β -galactosidase onto anti- β -galactosidase immobilized on non-porous glass coated beads; curves 1 and 4 are obtained from eqn. 10; curves 2 and 3 are obtained from eqns. 12 and 13 when $\partial C_{sb}/\partial t = \partial C_{sb}/\partial t = 0$, and with $\delta = 1$ and $\delta = 2$, respectively; $T = 293$ K.

β -galactosidase onto anti- β -galactosidase immobilized on non-porous glass coated beads, are lower than the values obtained when the monoclonal antibody is immobilized on porous silica particles and the adsorbate interacts with the immobilized anti- β -galactosidase. The difference in the values of C_T may merely reflect differences in the total amounts of anti- β -galactosidase that can be coupled to the two different supports (porous silica particles; non-porous glass coated beads) which have different available surface areas per unit volume of particle. However, the difference in K values may be evidence for various alterations (*e.g.*, conformational changes [14,16]) occurring in the anti- β -galactosidase structure, when the monoclonal antibody is immobilized on different supports. These alterations may effect the ability of anti- β -galactosidase to bind adsorbate to varying extents. Chase [32] has also reported that in the equilibrium adsorption of β -galactosidase onto anti- β -galactosidase immobilized on porous silica particles and on Sepharose 4B, the values of C_T and K depended on which material the monoclonal antibody had been coupled to. The details of the experiments of the adsorption of β -galactosidase onto anti- β -galactosidase immobilized on non-porous glass coated beads as well as to the adsorption of β -galactosidase onto a control adsorbent, are reported in refs. 19 and 30. It is worth mentioning at this point that the equilibrium expressions obtained from kinetic model 2 (with $k_{22} = k_{52} = 0$) could not properly correlate the data represented by curve 4. Thus, kinetic model 2 was not employed in the dynamic calculations (finite bath and column systems) involving the adsorption of β -galactosidase onto anti- β -galactosidase immobilized on non-porous glass coated beads (Figs. 6 and 13–15).

In Fig. 2 the finite bath model predictions are compared with the experimental batch data of the adsorption of β -galactosidase onto monoclonal antibody ligand immobilized on porous silica particles. The dimensionless concentrations, C_d/C_{d0} , of the adsorbate in the fluid of the finite bath represented by curve 1, have been obtained from the batch model by employing kinetic model 1. The C_d/C_{d0} values of curve 2 have been obtained from the batch model when kinetic model 2 is employed. It is observed that the agreement between experiment and theory is satisfactory. Furthermore, the differences in the theoretical predictions of curves 1 and 2 are small although kinetic models 1 and 2 are different. It may also be observed that over the total operational time period, the agreement between curve 1 and the experimental data is slightly better than the agreement between curve 2 and the experimental data. The values of the rate constants that characterize the interaction mechanisms in kinetic models 1 and 2, were estimated by matching the predictions obtained from the expressions of the equilibrium (*i.e.*, eqn. 10, eqns. 12 and 13 with $\partial C_{sa}/\partial t = \partial C_{sb}/\partial t = 0$) and dynamic (batch) adsorption models with the corresponding equilibrium (equilibrium isotherm) and finite bath (dynamic) experimental data. The values of the mass transfer and interaction parameters for curves 1 and 2 are as follows:

$$\text{Curve 1: } r_0 = 7.5 \cdot 10^{-3} \text{ cm, } \varepsilon = 0.985, \varepsilon_p = 0.5, K_f = 5.84 \cdot 10^{-4} \text{ cm/s,} \\ D_p = 6.9 \cdot 10^{-8} \text{ cm}^2/\text{s, } k_{11} = 2.35 \cdot 10^{-2} \text{ cm}^3/(\text{mg})(\text{s}) \text{ and } k_{21} = \\ 5.17 \cdot 10^{-6} \text{ s}^{-1}.$$

$$\text{Curve 2: } r_0 = 7.5 \cdot 10^{-3} \text{ cm, } \varepsilon = 0.985, \varepsilon_p = 0.5, K_f = 5.84 \cdot 10^{-4} \text{ cm/s,} \\ D_p = 5.6 \cdot 10^{-8} \text{ cm}^2/\text{s, } k_{12} = 3.14 \cdot 10^{-2} \text{ cm}^3/(\text{mg})(\text{s}), k_{22} = 0.0, \\ k_{32} = 1.57 \cdot 10^{-5} \text{ cm}^3/(\text{mg})(\text{s}), k_{42} = 5.06 \cdot 10^{-4} \text{ cm}^3/(\text{mg})(\text{s}), k_{52} = \\ 0.0, k_{62} = 5.58 \cdot 10^{-2} \text{ cm}^3/(\text{mg})(\text{s}) \text{ and } \delta = 1.$$

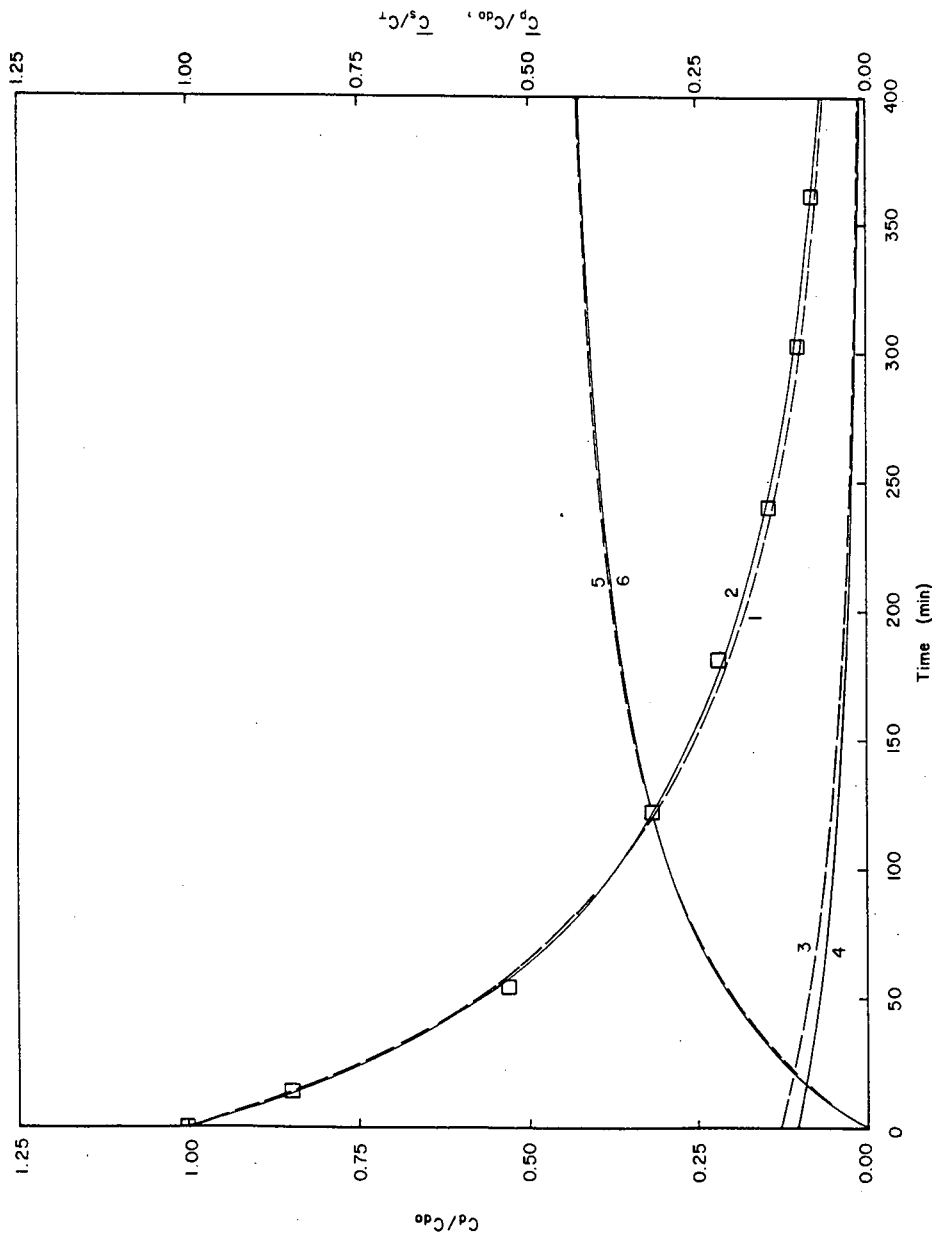


Fig. 2. Finite batch adsorption of β -galactosidase onto anti- β -galactosidase immobilized on porous silica particles; \square = experimental data; curves 1, 3 and 5 = predictions of the batch model employing kinetic model 1; curves 2, 4 and 6 = predictions of the batch model employing kinetic model 2 ($\phi = 1$). $C_{d0} = 1.58 \cdot 10^{-2}$ mg/cm³, $T = 293$ K.

The above data indicate that when kinetic model 2 is employed, the value of D_p , estimated by matching the experimental batch data with the predictions of the finite bath model, is smaller by 18.84% than that obtained when kinetic model 1 is used in the batch model. Furthermore, the value of the parameter k_{12} that characterizes the forward interaction rate for the formation of the complex of "form a" is about 33.62% larger than the value of k_{11} . The above comparisons may suggest that the finite bath model employing kinetic model 2 would provide a higher overall adsorption rate at earlier times (higher values of C_d) than that obtained from the finite bath using kinetic model 1, and the opposite would occur at longer times (lower values of C_d). This appears to be the case by comparing the predictions in curves 1 and 2. The value of the rate constant k_{32} suggests that the rate of formation of the complex of "form b" is very slow by comparison to the rate of formation of the complex of "form a" ($k_{12} \gg k_{32}$). In fact, the concentration C_{sb} is very much smaller than C_{sa} ($C_{sa} \gg C_{sb}$) for most of the operational time, and furthermore, since k_{62} is about 110 times larger than k_{42} the desorption of adsorbate from the complex of "form b" is much faster than that from the complex of "form a". The values of the parameters k_{32} and k_{62} may suggest that a few adsorbed β -galactosidase molecules in "form a" change conformation to "form b", where the complex of "form b" may be considered to represent a complex which significantly facilitates the desorption of the adsorbed adsorbate by macromolecule-induced exchange interactions ($k_{62} \gg k_{42}$). Also, the parameter k_{21} that characterizes the desorption of adsorbed adsorbate in kinetic model 1, is much smaller than the value of k_{11} ($k_{11} \gg k_{21}$). The above data and discussion could suggest that the reason for the very small differences between curves 1 and 2 (although the kinetic models 1 and 2 represent different overall adsorption mechanisms), is that the overall rate of adsorption of β -galactosidase onto anti- β -galactosidase immobilized on porous silica particles appears to be controlled by the forward interaction step of the overall adsorption mechanism (the forward interaction step is characterized by k_{11} in kinetic model 1, and by k_{12} in kinetic model 2) and by the intraparticle diffusion mechanism (characterized by D_p). Numerous simulations have shown that the effect of the film mass transfer resistance (characterized by K_f) on the overall rate of adsorption, is not as significant as the effects of pore diffusion and of the adsorption step. It was found that the variation of the estimated value ($K_f = 5.84 \cdot 10^{-4}$ cm/s) of K_f by $\pm 20\%$, has no significant effect on the dynamic behavior of the batch system. In Fig. 2, curves 3 and 4 represent the dynamic behavior of the dimensionless average concentration (\bar{C}_p/C_{d0}) of β -galactosidase in the pore fluid of the porous silica particles, obtained from the batch model by employing kinetic models 1 and 2, respectively. Curves 5 and 6 represent the dynamic behavior of the dimensionless average concentration of β -galactosidase in the adsorbed phase (\bar{C}_s/C_T) calculated from the finite bath model by using kinetic models 1 and 2, respectively (for kinetic model 2, $\bar{C}_s = \bar{C}_{sa} + \bar{C}_{sb}$). It can be observed that the differences between curves 3 and 4 are very small for most of the operational time. The differences between curves 3 and 4 are larger only at the very early times of the adsorption process, and would appear to have no effect (the use of kinetic model 1 or 2) on the overall dynamic performance of the adsorption process since the adsorption stage would be terminated at longer times where the differences between curves 3 and 4 are insignificant and a considerable amount of β -galactosidase would have been adsorbed. The differences between curves 5 and 6 are very small for all times of operation, and thus, the use of

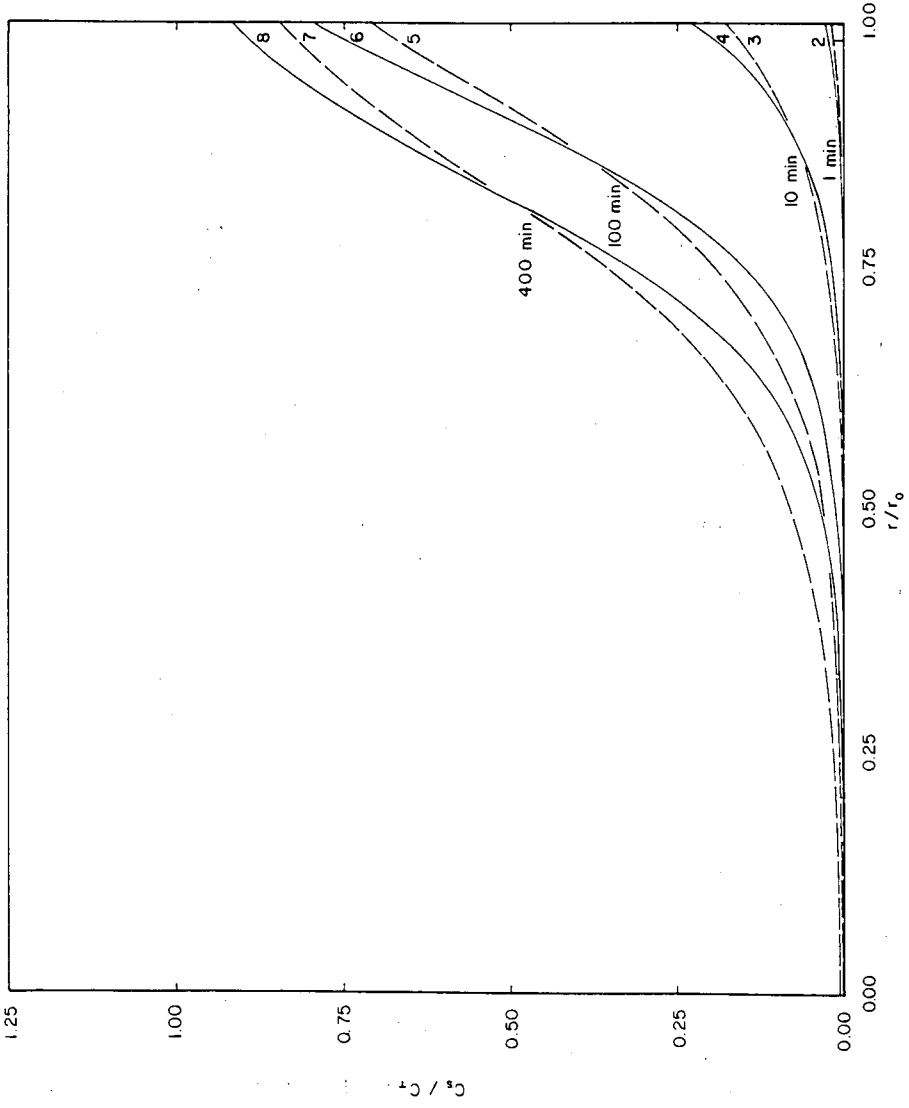


Fig. 3. Concentration profiles of β -galactosidase in the adsorbed phase of the porous adsorbent particles; curves 1, 3, 5 and 7 are obtained from the batch model employing kinetic model 1; curves 2, 4, 6 and 8 are obtained from the batch model employing kinetic model 2 ($\phi = 1$). Batch times: 1 min \equiv curves 1 and 2; 10 min \equiv curves 3 and 4; 100 min \equiv curves 5 and 6; 400 min \equiv curves 7 and 8. $C_{a0} = 1.58 \cdot 10^{-2}$ mg/cm³; $T = 293$ K.

kinetic model 1 or 2 would appear to have no effect on the dynamic performance of the adsorption stage.

In Fig. 3, the dimensionless concentration profiles of adsorbed β -galactosidase in the adsorbent particle are presented at different times. The data obtained by using kinetic model 2 (curves 2, 4, 6 and 8, where $C_s = C_{sa} + C_{sb}$) indicate that the capacity of the immobilized ligands at the outer parts of the adsorbent particle has been used more effectively than in the case where kinetic model 1 is used, and the profiles of curves 2, 4, 6 and 8 are steeper than those represented by curves 1, 3, 5 and 7. This may be due to the fact that $k_{12} > k_{11}$. On the other hand, the data in curves 1, 3, 5 and 7 have been obtained from a model whose pore diffusivity has a higher value than that of the system in curves 2, 4, 6 and 8, and this leads to a faster penetration of β -galactosidase to the interior of the adsorbent particle and to the higher values of C_s/C_T in the interior parts of the particle for the system in curves 1, 3, 5 and 7. The differences in the adsorbed concentration profiles shown in Fig. 3, do not lead to any significant differences for the values of the average adsorbed concentrations (\bar{C}_s/C_T) in the adsorbent particles, as curves 5 and 6 of Fig. 2 indicate. This may occur because it appears that, in the adsorption of β -galactosidase onto anti- β -galactosidase immobilized on porous silica particles, the effect of restricted pore diffusion [12] is negligible and the phenomenon of percolation threshold [12] does not occur. The results may have been very different if an affinity chromatography system exhibiting restricted pore diffusion [12] had been considered, and it may be possible that in such a system kinetic model 2 may represent an adsorption mechanism which may be more appropriate than that of kinetic model 1, or the opposite may be the case (kinetic model 1 may be more appropriate than kinetic model 2).

But the results in Fig. 3 clearly show that different kinetic models (kinetic models 1 and 2) employed to describe the adsorption mechanism, can lead to significantly different concentration profiles for the adsorbate in the adsorbed phase; of course, they also lead to different concentration profiles for the adsorbate in the pore fluid (these concentration profiles in the pore fluid are not shown in Fig. 3). These differences in the concentration profiles within the adsorbent particles, may have important implications with regard to the operation of the wash and elution stages, since the wash and elution rates depend [1-4] on the concentration profiles of the adsorbate (in the pore fluid and adsorbed phase) that were established at the end of the adsorption stage. Thus, while the results in Fig. 2 indicate that kinetic models 1 and 2 do not lead to significant differences in the average concentrations of the adsorbate in the pore fluid and adsorbed phases of the adsorbent particles, the data in Fig. 3 strongly show that the two different kinetic models can lead to significant differences in the concentration profiles and this can have important implications [1-4] on the operation and performance of the wash and elution stages. This finding indicates that it is important in kinetic model discrimination studies [14,16,18] to identify the kinetic model that would provide an appropriate physical description of the adsorption mechanism of the finite bath model.

In Figs. 4 and 5, the effect of varying the estimated value of the pore diffusivity, D_p , by $\pm 20\%$ is examined. In Fig. 4 the finite bath model uses kinetic model 1, while in Fig. 5 kinetic model 2 is employed. It can be observed that, at the earlier times of the adsorption process, the differences between curves 1, 2 and 3 and between curves 4, 5 and 6, are not significant because at those earlier times the concentration gradient in

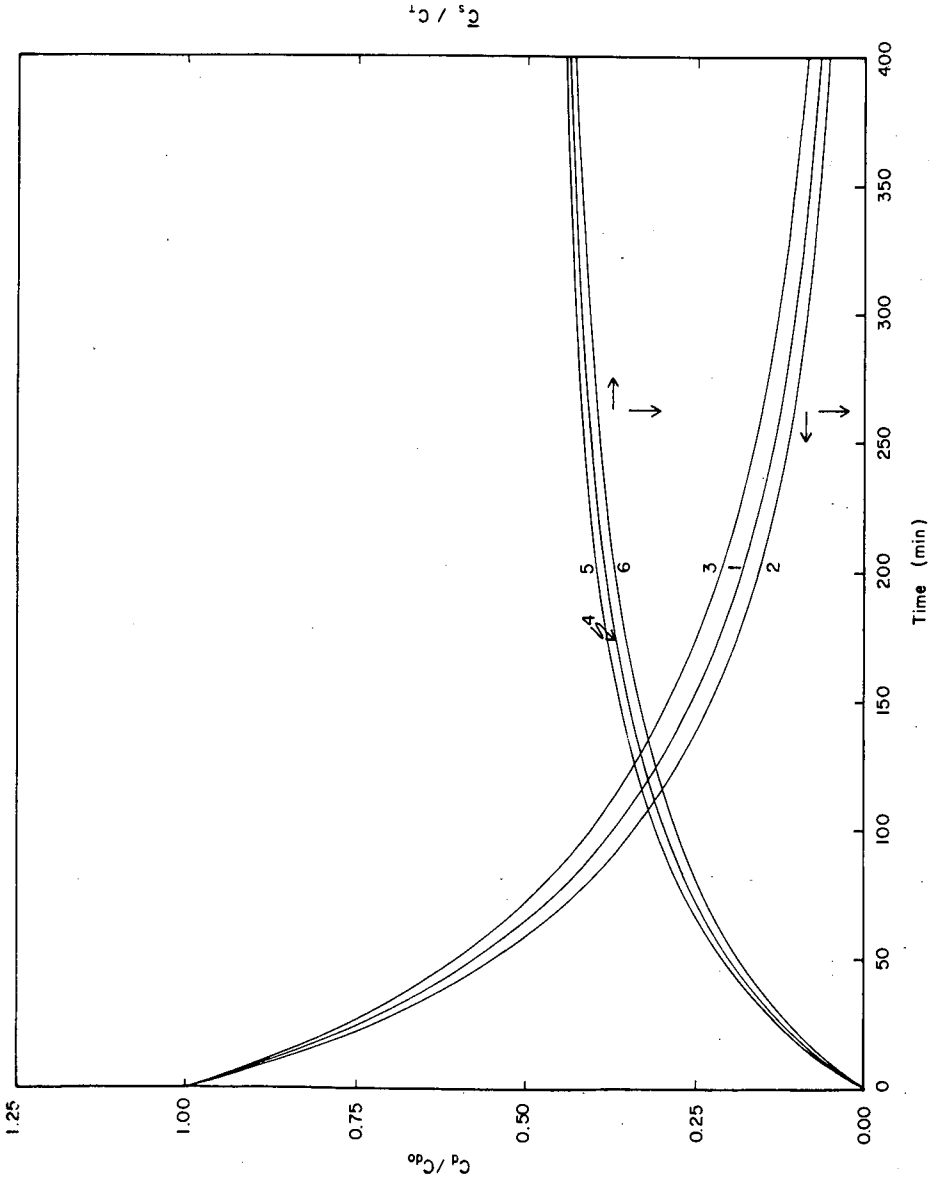


Fig. 4. The effect of the variation of the estimated value of D_p by $\pm 20\%$, on the dynamic behavior of C_d/C_{d0} and C_s/C_{s0} . The results are obtained from the batch model employing kinetic model 1. $D_p = 6.9 \cdot 10^{-8} \text{ cm}^2/\text{s}$ in curves 1 and 4; $D_p = 1.2 (6.9 \cdot 10^{-8}) \text{ cm}^2/\text{s}$ in curves 2 and 5; $D_p = 0.8 (6.9 \cdot 10^{-8}) \text{ cm}^2/\text{s}$ in curves 3 and 6. $C_{d0} = 1.58 \cdot 10^{-2} \text{ mg/cm}^3$, $T = 293 \text{ K}$.

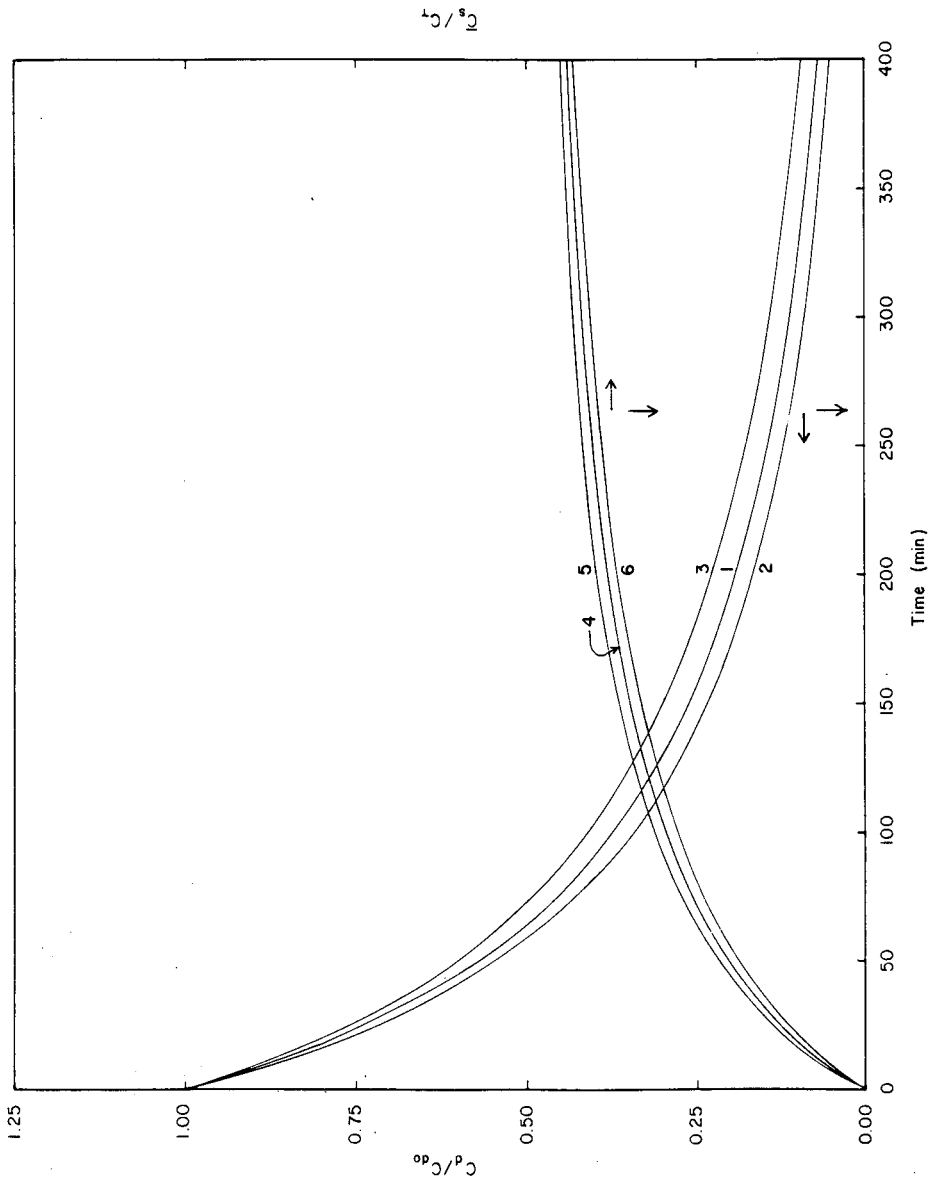


Fig. 5. The effect of the variation of the estimated value of D_p by $\pm 20\%$, on the dynamic behavior of C_d/C_{d0} and \bar{C}_s/C_T . The results are obtained from the batch model employing kinetic model 2 ($\delta = 1$). $D_p = 5.6 \cdot 10^{-8}$ cm²/s in curves 1 and 4; $D_p = 1.2 (5.6 \cdot 10^{-8})$ cm²/s in curves 2 and 5; $D_p = 0.8 (5.6 \cdot 10^{-8})$ cm²/s in curves 3 and 6. $C_{d0} = 1.58 \cdot 10^{-2}$ mg/cm³; $T = 293$ K.

the pore fluid ($\partial C_p/\partial r$) is high, and the mass transfer rate of the adsorbate in the porous particle is high and less sensitive to the value of D_p . At large times, the concentration gradient in the pore fluid is small and this leads to a significantly decreased mass transfer rate, which is slightly more sensitive (for the affinity chromatography system and the operational times presented in Figs. 4 and 5) to the value of D_p when compared with the effect at earlier times. The largest effect of D_p on C_d/C_{d0} and \bar{C}_s/C_T occurs at intermediate times, where the concentration gradient, $\partial C_p/\partial r$, has moderate values and the sensitivity of the mass transfer rate on the value of D_p could increase significantly, as it can be observed for the systems in Figs. 4 and 5. Also, while the change in the estimated value of D_p is symmetric ($\pm 20\%$) the effect of this change on C_d/C_{d0} and \bar{C}_s/C_T is asymmetrical. Furthermore, it appears that the variation of the estimated value of D_p affects the dynamic behavior of C_d/C_{d0} more than the dynamic behavior of \bar{C}_s/C_T . For the system in Fig. 5 the effect of the variation of the value of D_p on C_d/C_{d0} and \bar{C}_s/C_T appears to be larger than the corresponding effect on the system in Fig. 4; it should be noted that the concentration gradient in the pore fluid is higher when kinetic model 2 is used (also the concentration gradient in the adsorbed phase is higher when kinetic model 2 is used, at it can be observed in Fig. 3). The above discussion and results in Figs. 4 and 5 suggest that (i) it is important to have an accurate value for the pore diffusivity, and (ii) if the value of D_p is estimated by matching the experimental finite bath data with the predictions of the batch model, it is important to use a proper kinetic model for the adsorption mechanism and emphasize in the estimation procedure the importance of the experimental data obtained at times after the initial adsorption rate period (the data at intermediate operational times).

In Fig. 6 the experimental batch data of the adsorption of β -galactosidase onto anti- β -galactosidase immobilized on non-porous glass coated beads, are presented. The results in curve 1 represent the theoretical predictions of the finite bath model when kinetic model 1 is taken to represent the adsorption mechanism. The agreement between the experimental results and curve 1 is considered to be reasonable. The parameters k_{11} and k_{21} were estimated by matching the predictions of the batch model with the experimental data. The values of the parameters of the batch model that provides the results of curve 1, are as follows: $\varepsilon = 0.895$, $r_0 = 0.86 \cdot 10^{-2}$ cm, $K_f = 2.64 \cdot 10^{-4}$ cm/s, $k_{11} = 6.19 \cdot 10^{-2}$ cm³/(mg)(s), and $k_{21} = 0.32 \cdot 10^{-2}$ s⁻¹. The experimental methods and procedures used to obtain the experimental data in Fig. 6, are reported in refs. 19 and 31. Curve 2 describes the variation of the dimensionless concentration C_s/C_T with time. The effect of changing the estimated value ($K_f = 2.64 \cdot 10^{-4}$ cm/s) of K_f by $\pm 20\%$, has negligible effect on the dynamic behavior of C_d/C_{d0} and C_s/C_T for all operational times. The results in Fig. 6 suggest that if an appropriate estimate of the value of K_f can be obtained [1,18], then the dynamics of the kinetic model developed to represent the adsorption mechanism would play the most significant role in determining the adsorption rate in batch systems involving non-porous adsorbent particles. It is worth noting again that kinetic model 2 was not used to describe the adsorption mechanism of the affinity chromatography system in Fig. 6, because of the reason reported in the discussion of curve 4 of Fig. 1.

In Fig. 7 the breakthrough curves of the adsorption of β -galactosidase onto anti- β -galactosidase immobilized on porous silica particles, are presented for six different column lengths. Curves 1, 3, 5, 7, 9 and 11 represent the results obtained from the column model employing kinetic model 2 whose parameter values were taken to be

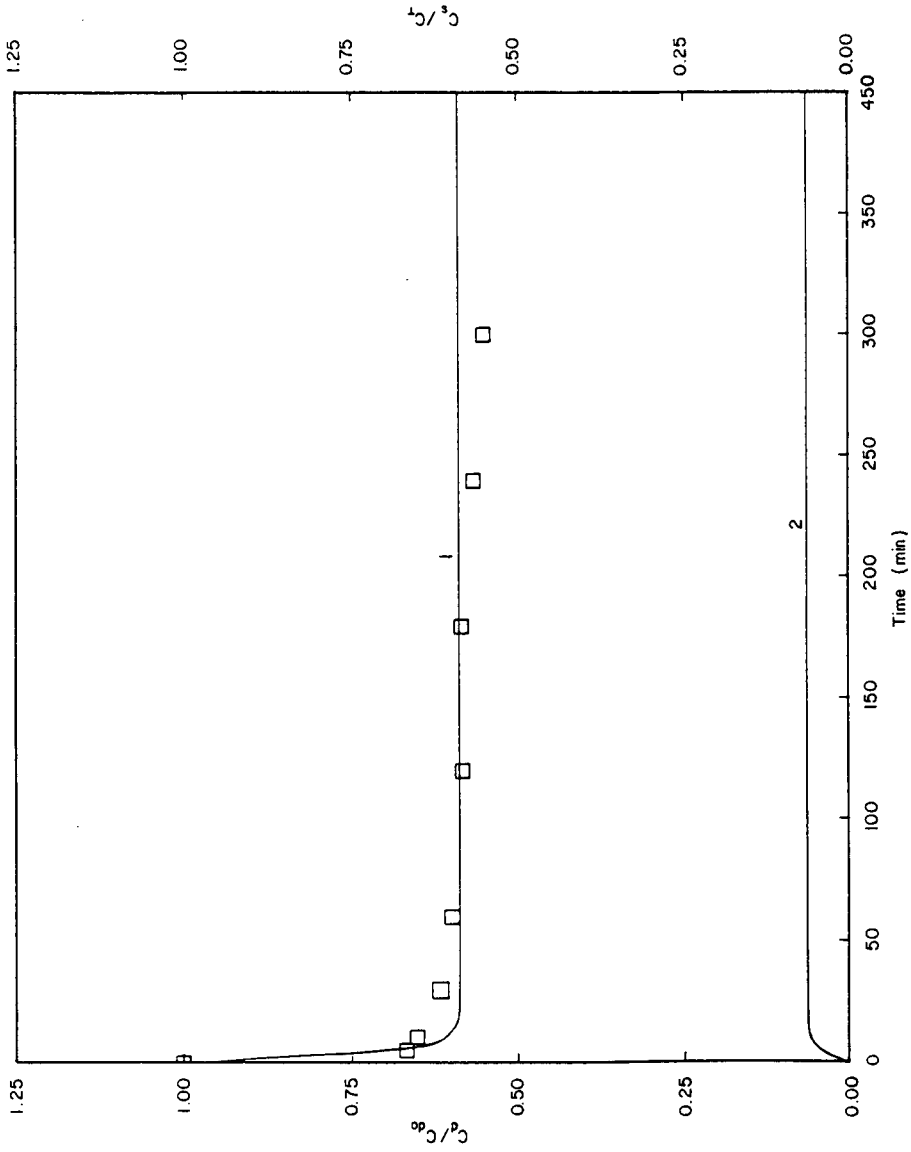


Fig. 6. Finite bath adsorption of β -galactosidase onto anti- β -galactosidase immobilized on non-porous glass coated beads; \square = experimental data; curves 1 (C_d/C_{d0} versus time) and 2 (C_s/C_T versus time) have been obtained from the batch model employing kinetic model 1; $C_{d0} = 6.0 \cdot 10^{-3}$ mg/cm³; $T = 293$ K. When the estimated value of K_f ($K_f = 2.64 \cdot 10^{-4}$ cm/s) is varied by $\pm 20\%$, the results of C_d/C_{d0} coincide with curve 1 and those of C_s/C_T coincide with curve 2.

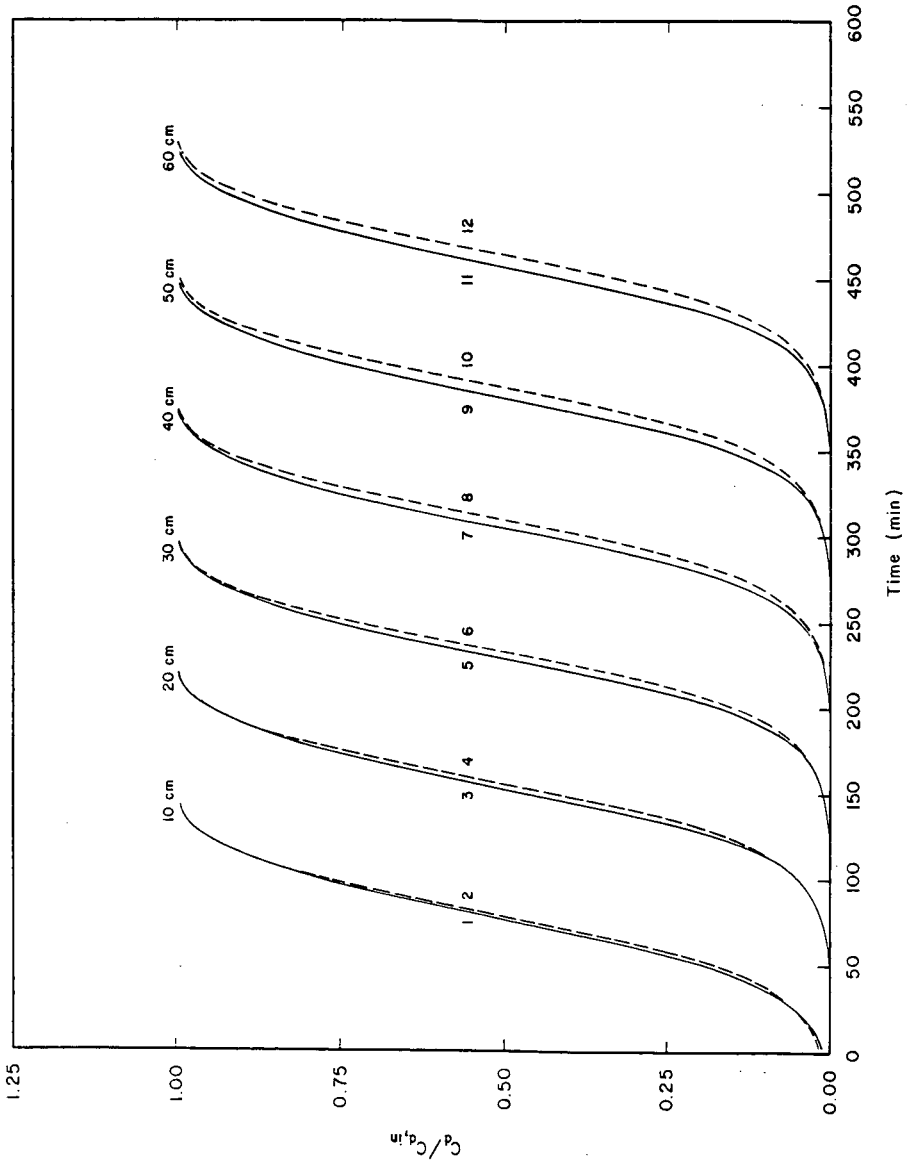


Fig. 7. Breakthrough curves of the adsorption of β -galactosidase onto anti- β -galactosidase immobilized on porous silica particles, for different column lengths; kinetic model 2 ($\delta = 1$) is used for curves 1, 3, 5, 7, 9 and 11; kinetic model 1 is used for curves 2, 4, 6, 8, 10 and 12. $C_{d,in} = 0.1 \text{ mg/cm}^3$; $T = 293 \text{ K}$.

the same as those estimated from the finite bath data; the value of the pore diffusivity was also taken to be the same as that estimated from the batch data, and thus, $D_p = 5.6 \cdot 10^{-8} \text{ cm}^2/\text{s}$. Curves 2, 4, 6, 8, 10 and 12 represent the results when kinetic model 1 is used to describe the adsorption mechanism in the column model, and the values of the rate constants k_{11} and k_{21} were taken to be the same as those estimated from the finite bath data; the value of the pore diffusivity was estimated from the batch data (curve 1 of Fig. 2) and its value is $D_p = 6.9 \cdot 10^{-8} \text{ cm}^2/\text{s}$. The values of other parameters used in the column model to obtain the results in Figs. 7–12 are as follows: $C_{d,\text{in}} = 0.1 \text{ mg/cm}^3$, $r_0 = 5 \cdot 10^{-3} \text{ cm}$, $\varepsilon = 0.4$, $V_f = 3 \cdot 10^{-2} \text{ cm/s}$, $\varepsilon_p = 0.5$, $K_f = 8.93 \cdot 10^{-4} \text{ cm/s}$. For each column length, the results in Fig. 7 indicate that kinetic models 1 and 2 provide almost identical starting times of breakthrough. It is also observed that kinetic model 2 provides, for a given time, higher breakthrough values ($C_d/C_{d,\text{in}}$) than those obtained from kinetic model 1, except for the early phase of the breakthrough of the 10-cm column. The differences between the breakthrough curves obtained from the column model by employing kinetic models 1 and 2, increase as the column length increases. Furthermore, it is found that the largest difference, for a given column length, occurs in the neighborhood of 50% breakthrough. Of course, in practical operations it is most often the case that it is the earlier part of the breakthrough curve that is of most interest as the adsorption stage of an actual process would be terminated at less than 50% breakthrough. The results in Fig. 7 suggest that the performance of the adsorption stage can be influenced by the differences in the mechanisms of the kinetic models (kinetic models 1 and 2), and the differences in the mechanisms affect more the performance of longer columns. Furthermore, the effect on the performance of the adsorption stage will have implications on the operation and performance of the wash and elution stages [2,4]. The operation and performance of the wash and elution stages will also be influenced from the fact that the two kinetic models provide different concentration profiles (pore fluid and adsorbed phase) for the adsorbate in the adsorbent particles and along the length of the fixed bed, at the end of the adsorption stage. In Figs. 8 and 9 the concentration profiles of the adsorbate in the pore fluid and the adsorbed phase of the adsorbent particles, are presented at different positions along the column length and at the time of 10% breakthrough. Curves 1, 3, 5 and 7 in Figs. 8 and 9 have been obtained when kinetic model 1 is used in the column model, while curves 2, 4, 6 and 8 have been obtained by employing kinetic model 2. It can be observed that the concentration profiles obtained from kinetic models 1 and 2 are different for a given dimensionless axial position (x/L), and this could have significant implications [2,4] on the performance and operation of the elution and wash stages.

In Fig. 10 the time required to reach a certain level of breakthrough is plotted *versus* column length. It can be observed that lines 1, 3, 5 and 7 are essentially having the same slope; also lines 2, 4, 6 and 8 have essentially the same slope. The results in Figs. 7 and 10 suggest that constant-pattern behavior appears to occur for this adsorption system. In the initial region the mass transfer front spreads as it progresses, but some distance from the inlet it reaches an asymptotic form and after this asymptotic form has been established it progresses as a stable mass transfer zone with no further change in shape.

In Figs. 11 and 12 the effect on the breakthrough curve of the column having a length of 30 cm is presented when the estimated value of D_p is changed by $\pm 20\%$. It is observed that in the neighborhood of 50% breakthrough the effect is insignificant. The

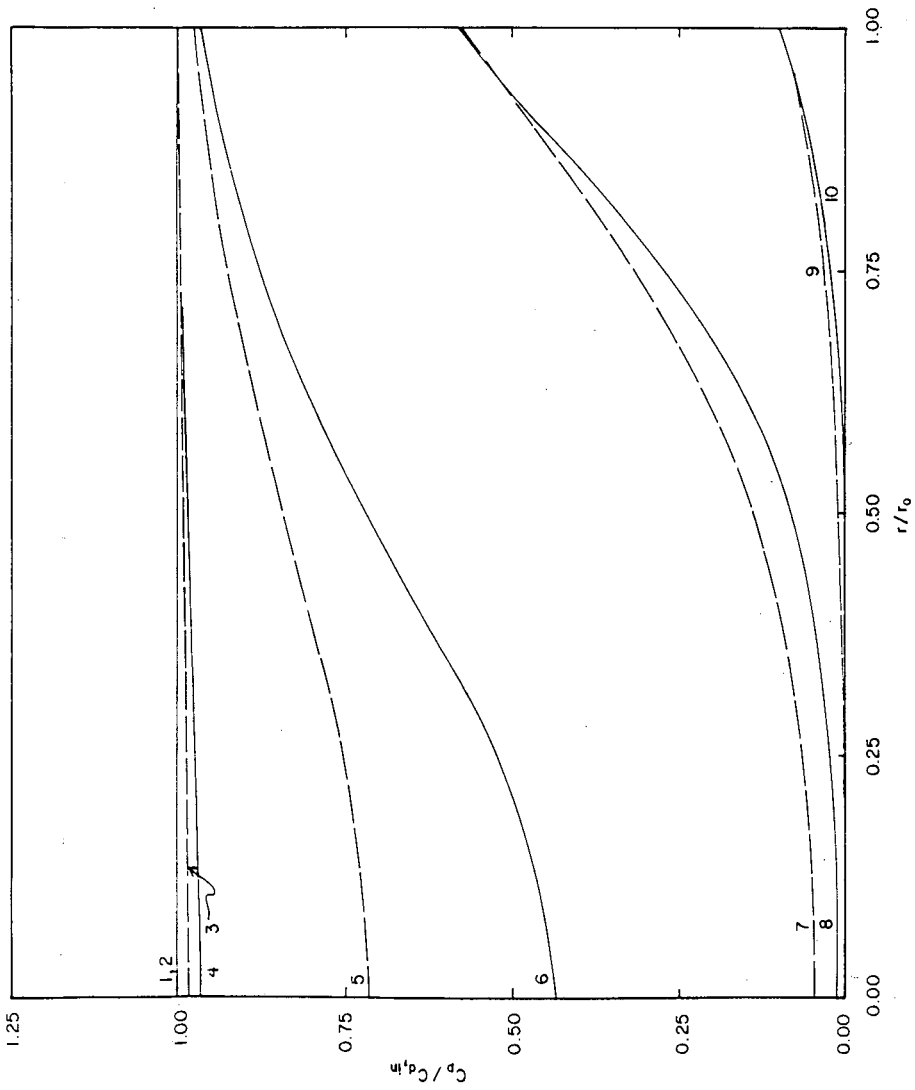


Fig. 8. Concentration profiles of β -galactosidase in the pore fluid of the adsorbent particles, at different positions along the length of a column of 30 cm; kinetic model 1 is used for curves 1, 3, 5, 7 and 9; kinetic model 2 ($\delta = 1$) is used for curves 2, 4, 6, 8 and 10. Dimensionless axial positions, x/L : 0.0 \equiv curves 1 and 2; 0.5 \equiv curves 3 and 4; 0.6 \equiv curves 5 and 6; 0.8 \equiv curves 7 and 8; 1.0 \equiv curves 9 and 10. $C_{d,in} = 0.1 \text{ mg/cm}^3$, $T = 293 \text{ K}$.

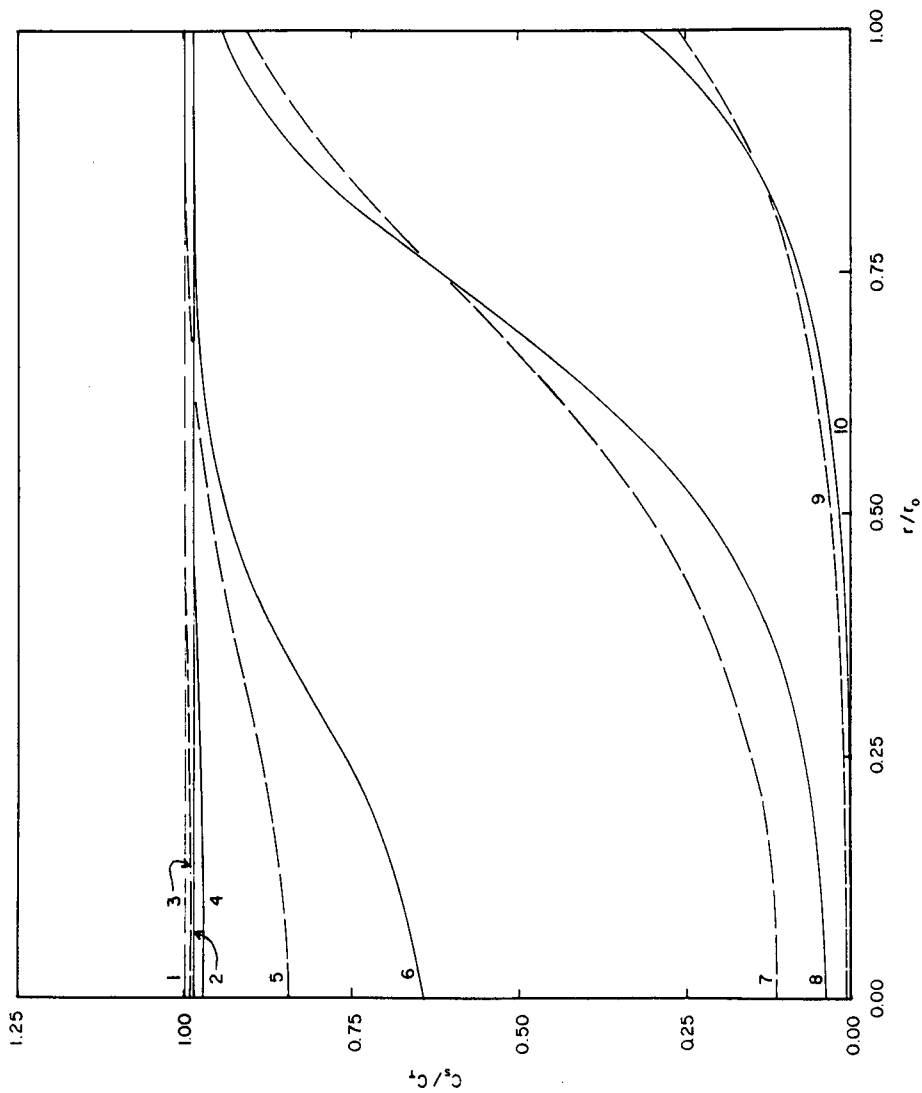


Fig. 9. Concentration profiles of β -galactosidase in the adsorbed phase of the adsorbent particles, at different positions along the length of a column of 30 cm; kinetic model 1 is used for curves 1, 3, 5, 7 and 9; kinetic model 2 ($\delta = 1$) is used for curves 2, 4, 6, 8 and 10. Dimensionless axial positions, x/L : 0.0 \equiv curves 1 and 2; 0.5 \equiv curves 3 and 4; 0.6 \equiv curves 5 and 6; 0.8 \equiv curves 7 and 8; 1.0 \equiv curves 9 and 10. $C_{d,in} = 0.1 \text{ mg/cm}^3$; $T = 293 \text{ K}$.

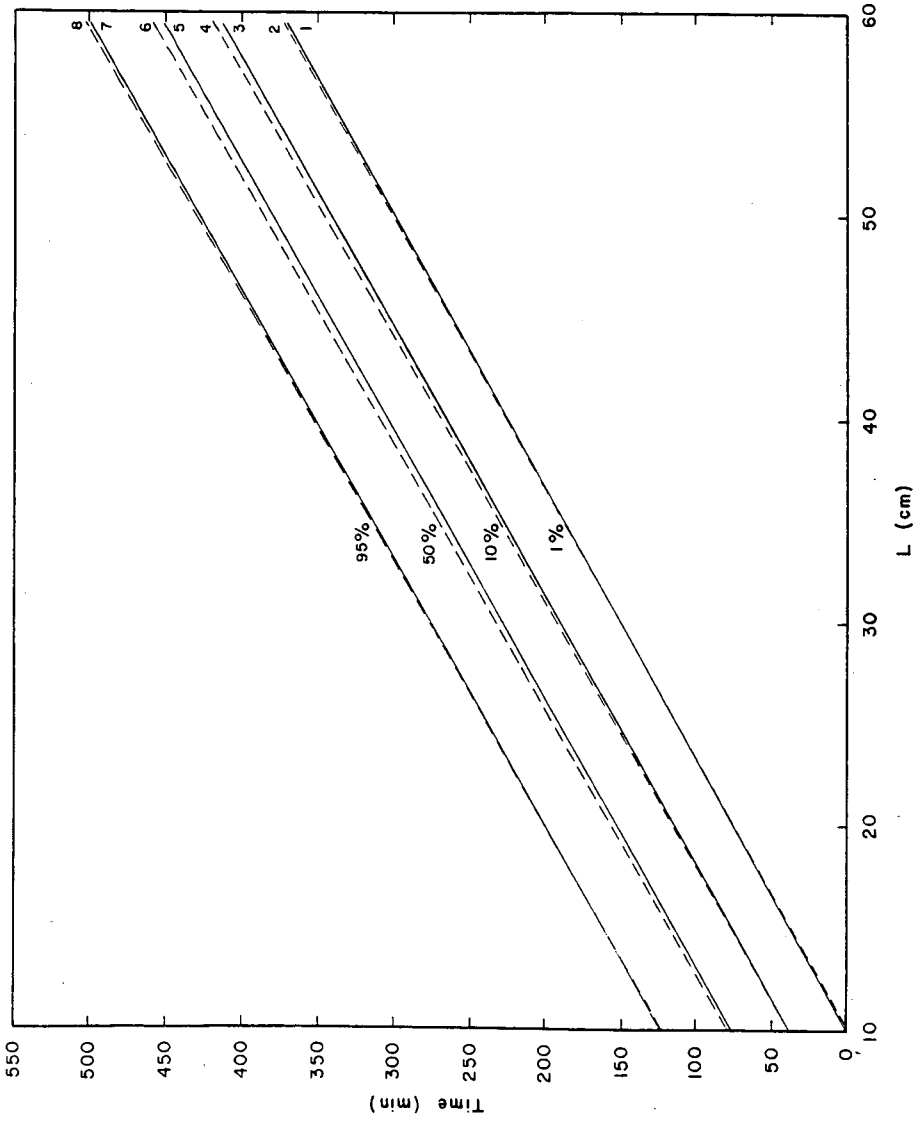


Fig. 10. Time required to reach a certain percentage of breakthrough for a given column length, in the adsorption of β -galactosidase onto anti- β -galactosidase immobilized on porous silica particles; kinetic model 2 ($\delta = 1$) is used for lines 1, 3, 5 and 7; kinetic model 1 is used for lines 2, 4, 6 and 8. $C_{a,in} = 0.1 \text{ mg/cm}^3$; $T = 293 \text{ K}$.

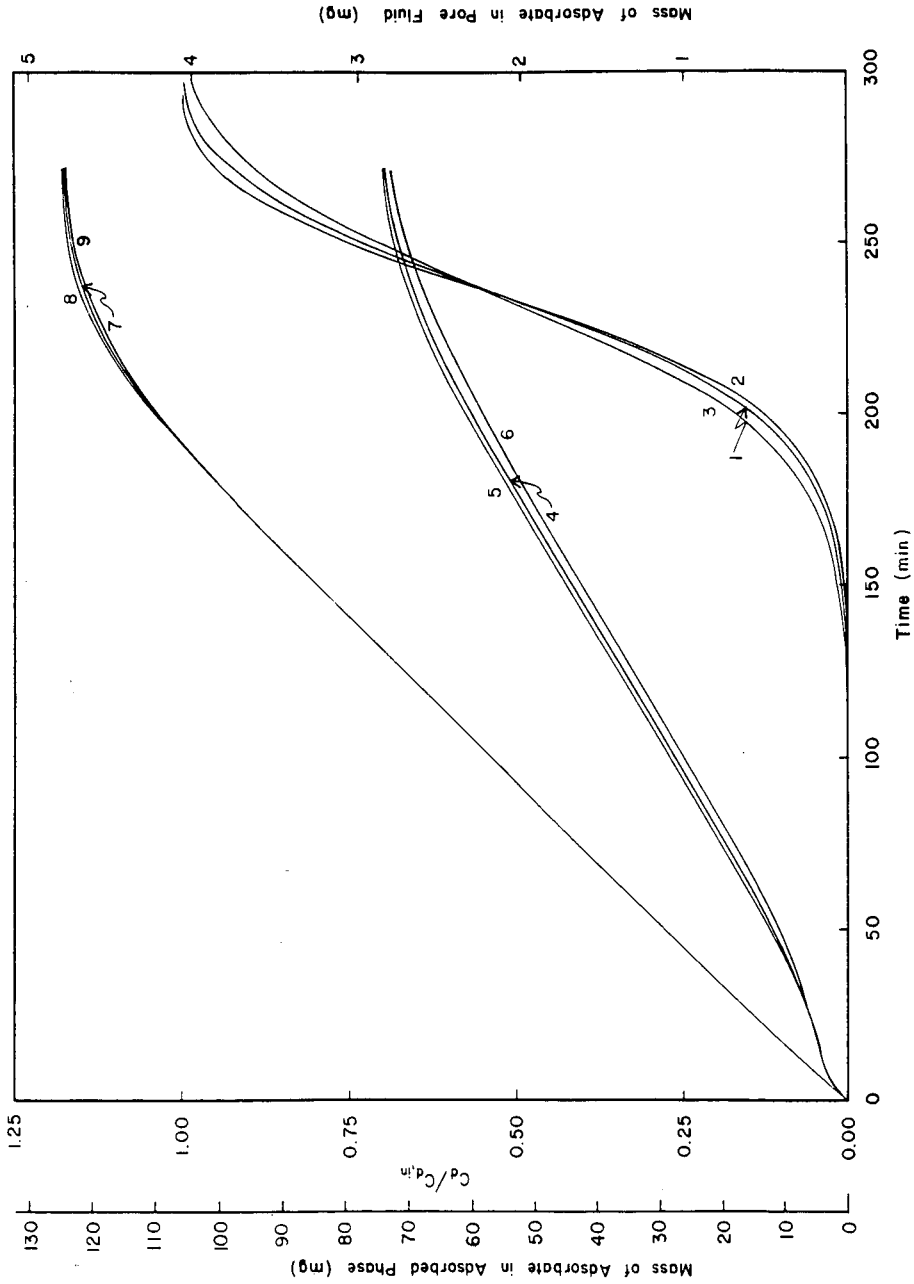


Fig. 11. The effect of the variation of the estimated value of D_p by $\pm 20\%$, on the dynamic behavior of $C_d/C_{d,in}$ and on the dynamic behavior of the mass of β -galactosidase in the pore fluid and adsorbed phases of the adsorbent particles, in a column of 30 cm; kinetic model 1 is used; curves 1, 2, 3 are for $C_d/C_{d,in}$; curves 4, 5, 6 are for the mass in the pore fluid; curves 7, 8, 9 are for the mass in the adsorbed phase; $D_p = 6.9 \cdot 10^{-8} \text{ cm}^2/\text{s}$ in curves 1, 4 and 7; $D_p = 1.2 \cdot 10^{-8} \text{ cm}^2/\text{s}$ in curves 2, 5 and 8; $D_p = 0.8 \cdot 10^{-8} \text{ cm}^2/\text{s}$ in curves 3, 6 and 9. $C_{d,in} = 0.1 \text{ mg}/\text{cm}^3$; $T = 293 \text{ K}$.

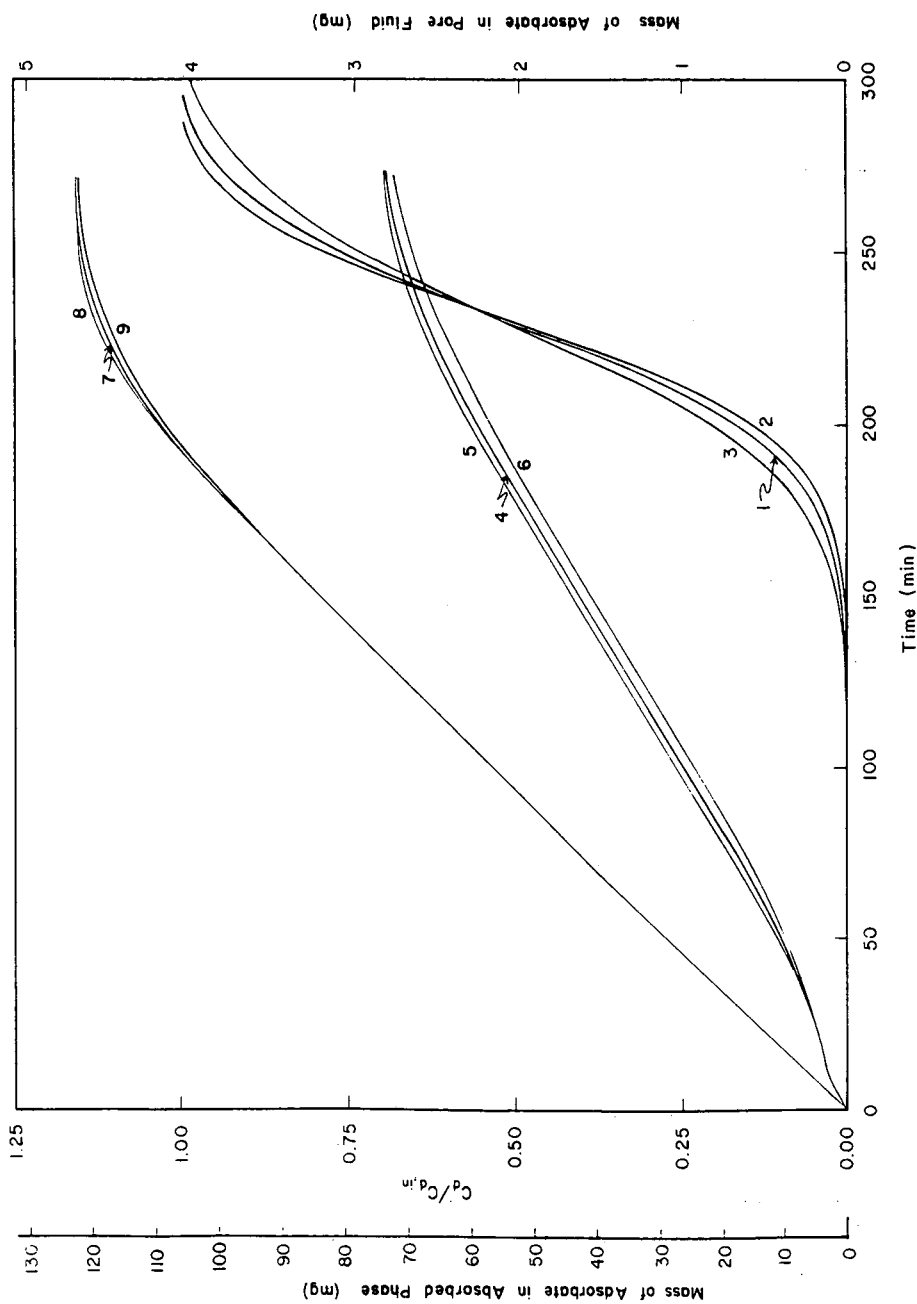


Fig. 12. The effect of the variation of the estimated value of D_p by $\pm 20\%$, on the dynamic behavior of $C_d/C_{d,in}$ and on the dynamic behavior of the mass of β -galactosidase in the pore fluid and adsorbed phases of the adsorbent particles, in a column of 30 cm; kinetic model 2 ($\beta = 1$) is used; curves 1, 2, 3 are for $C_d/C_{d,in}$; curves 4, 5, 6 are for the mass in the pore fluid; curves 7, 8, 9 are for the mass in the adsorbed phase; $D_p = 5.6 \cdot 10^{-8} \text{ cm}^2/\text{s}$ in curves 1, 4 and 7; $D_p = 1.2 (5.6 \cdot 10^{-8}) \text{ cm}^2/\text{s}$ in curves 2, 5 and 8; $D_p = 0.8 (5.6 \cdot 10^{-8}) \text{ cm}^2/\text{s}$ in curves 3, 6 and 9. $C_{d,in} = 0.1 \text{ mg}/\text{cm}^3$, $T = 293 \text{ K}$.

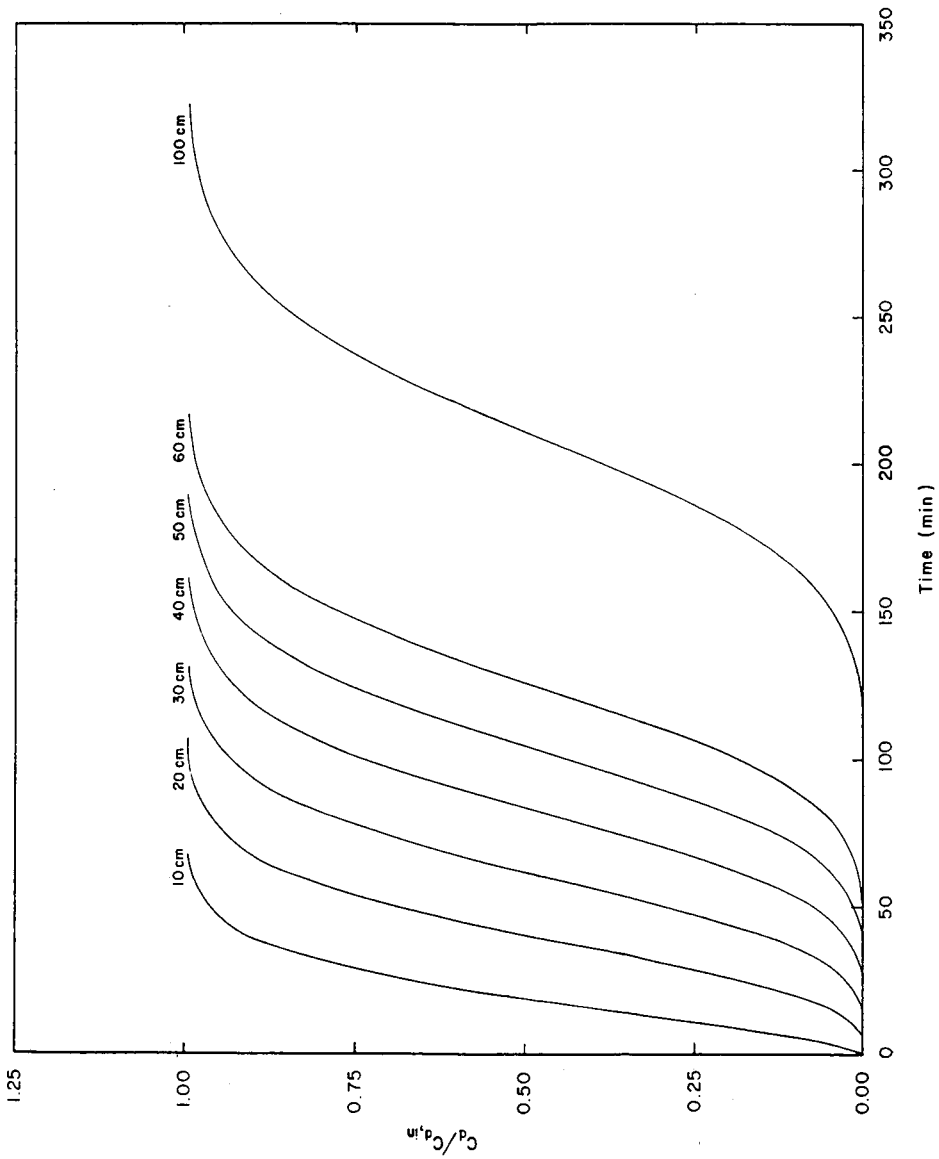


Fig. 13. Breakthrough curves of the adsorption of β -galactosidase onto anti- β -galactosidase immobilized on non-porous glass coated beads, for different column lengths. $C_{d,in} = 6.2 \cdot 10^{-3}$ mg/cm³; $T = 293$ K.

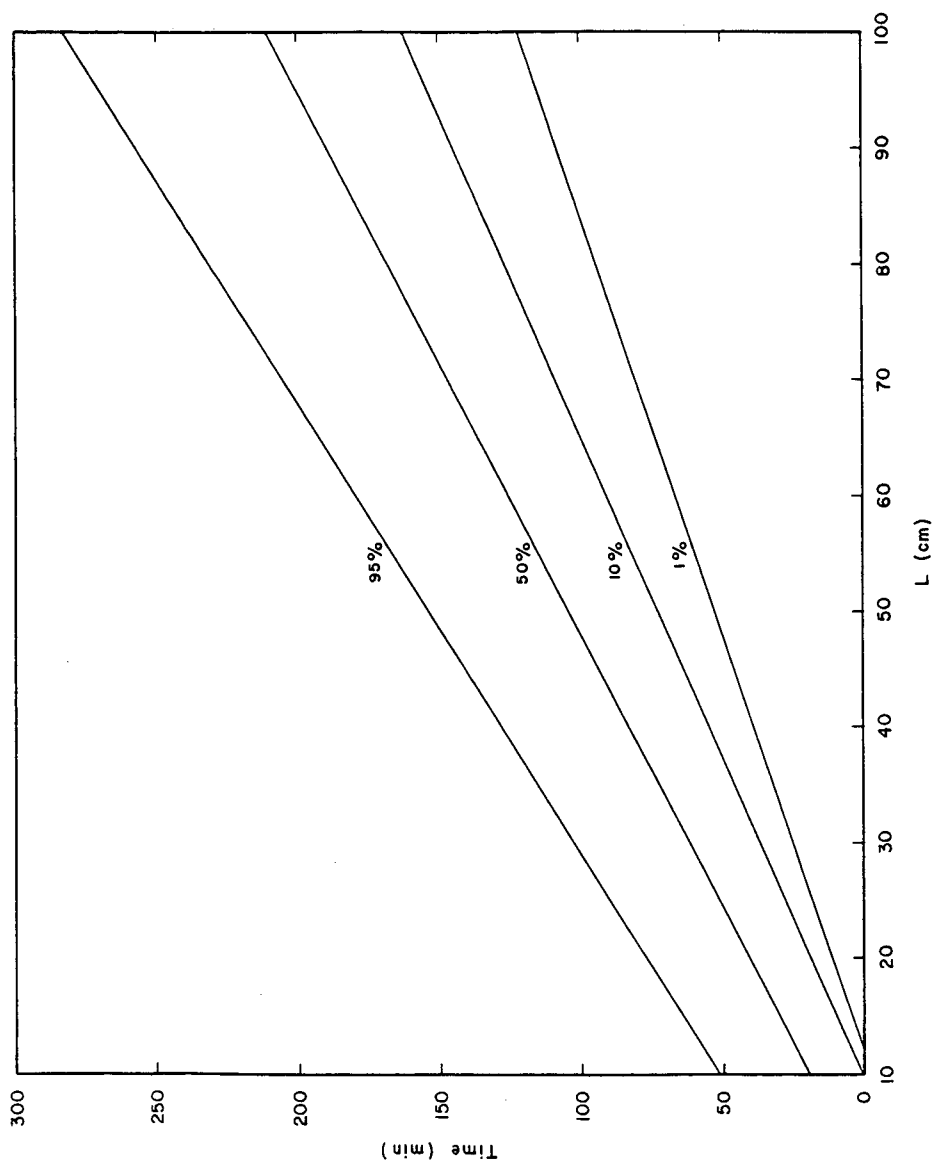


Fig. 14. Time required to reach a certain percentage of breakthrough for a given column length, in the adsorption of β -galactosidase onto anti- β -galactosidase immobilized on non-porous glass coated beads. $C_{d,in} = 6.2 \cdot 10^{-3} \text{ mg/cm}^3$; $T = 293 \text{ K}$.

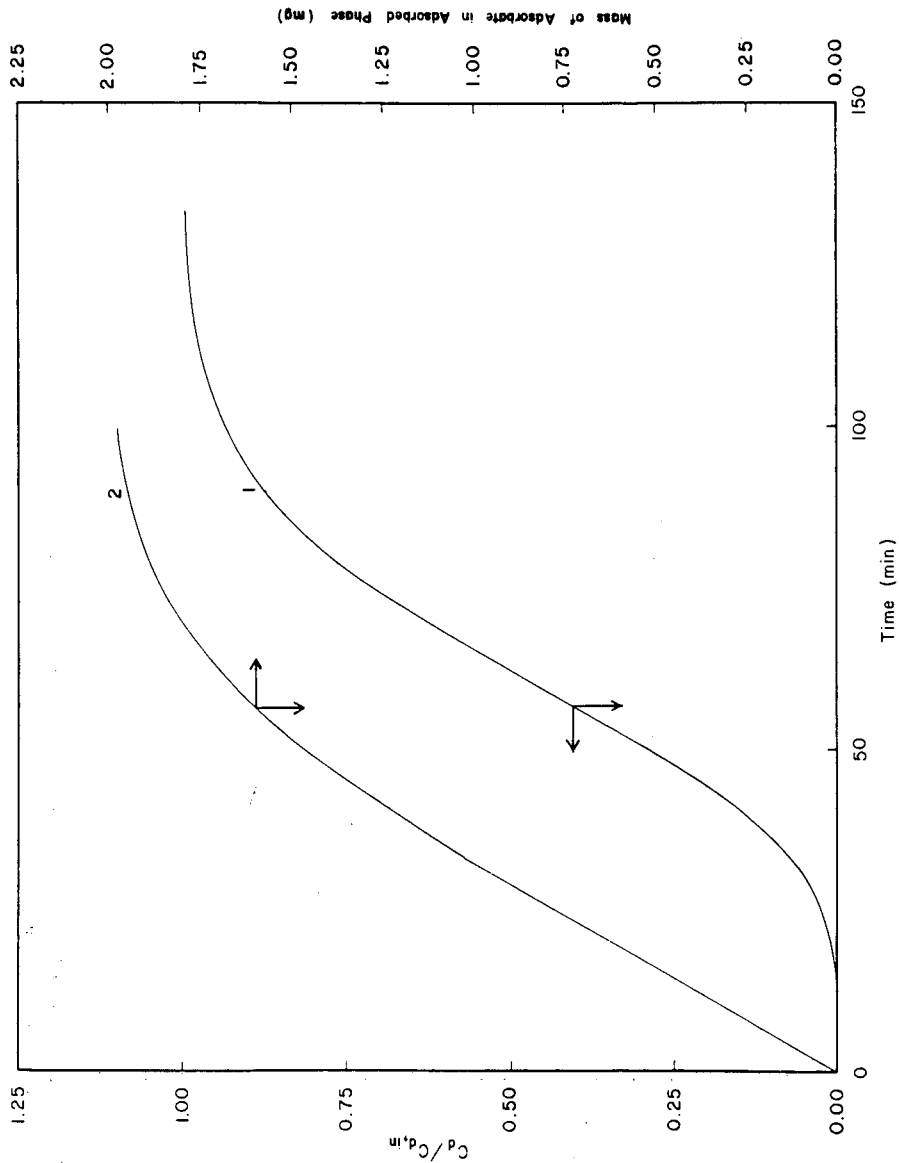


Fig. 15. The effect of the variation of the estimated value of K_r ($K_r = 4.38 \cdot 10^{-4}$ cm/s) by $\pm 20\%$, on the dynamic behavior of $C_d/C_{d,in}$ and on the dynamic behavior of the mass of β -galactosidase in the adsorbed phase of the non-porous adsorbent particles, in a column of 30 cm. The dynamic results obtained with $K_r = 1.2 (4.38 \cdot 10^{-4})$ cm/s, and with $K_r = 0.8 (4.38 \cdot 10^{-4})$ cm/s, coincide with the results obtained when $K_r = 4.38 \cdot 10^{-4}$ cm/s.

effect is also very small for the initial part and up to about 5% breakthrough. The effect increases after 5% breakthrough and starts decreasing again at about 25% breakthrough. These results suggest that if column switch occurs between 5% and 25% breakthrough, it is important to have an accurate value for D_p in order to predict properly the breakthrough curve, and thus, the column switch time. While the results in curves 7, 8 and 9 of Figs. 11 and 12 indicate that the effect of the variation of the estimated value of D_p on the total mass of adsorbed adsorbate is insignificant for most time after the start of breakthrough, the data in curves 4, 5 and 6 of Figs. 11 and 12 show that the variation of the value of D_p has a moderate effect on the total mass of the adsorbate in the pore fluid, and this effect could influence the operation and performance of the wash and elution [2,4] stages.

In Fig. 13 the theoretical breakthrough curves of the adsorption of β -galactosidase onto anti- β -galactosidase immobilized on non-porous glass coated beads, are presented for different column lengths. Kinetic model 1 was taken to represent the adsorption mechanism and the values of its parameters were the same as those used in the finite bath calculations with the non-porous adsorbent particles. The values of other parameters used in the column model that provided the results in Figs. 13–15, are as follows: $C_{d,in} = 6.2 \cdot 10^{-3} \text{ mg/cm}^3$, $\varepsilon = 0.4$, $V_f = 3 \cdot 10^{-2} \text{ cm/s}$, $r_0 = 0.86 \cdot 10^{-2} \text{ cm}$, and $K_f = 4.38 \cdot 10^{-4} \text{ cm/s}$. In Fig. 14 the times for different levels of breakthrough are plotted *versus* column length. The lines in Fig. 14 have different slopes, and this result is different than that obtained for the system in Fig. 10. The results in Figs. 13 and 14 indicate that the column length influences significantly the level of utilization [4] of the immobilized ligands, and this would have an effect on the performance of the wash and elution stages. In Fig. 15, the effect of the variation of the estimated value of K_f by $\pm 20\%$ is presented for a column of 30 cm. It is observed that the effect on the breakthrough curve and on the total amount of adsorbate in the adsorbed phase of the column, is insignificant; similar results were obtained for other column lengths.

CONCLUSIONS AND RECOMMENDATIONS

Finite bath and column models that could describe the adsorption of a single adsorbate onto ligand immobilized on porous or non-porous particles, were presented and solved.

Two different kinetic models were used to describe the dynamics of the adsorption mechanism (adsorption step) of the overall mass-transfer resistance of the adsorption of β -galactosidase onto monoclonal antibody immobilized on porous silica particles. The values of the ratios of certain parameters of the two kinetic models were estimated by matching the experimental equilibrium adsorption data with the predictions of the equilibrium expressions of the two kinetic models. The values of the remaining kinetic rate constants, as well as the value of the pore diffusivity, were estimated by matching the experimental batch (dynamic) data with the dynamic predictions of the finite bath model employing either kinetic model 1 or kinetic model 2. The agreement between the dynamic experimental data and the predictions of the finite bath model obtained by using kinetic model 1 or 2, was found to be satisfactory. The calculations show that the concentrations of the adsorbate in the fluid of the finite bath, as well as the average concentrations of the adsorbate in the pore fluid and in the adsorbed phase obtained from the batch model when kinetic

model 1 is employed, are not significantly different (quantitatively) than those obtained from the finite bath model when kinetic model 2 is used. But it was found that the two different kinetic models of the adsorption mechanism, lead to the estimation of different values for the pore diffusivity, D_p . These different values for the pore diffusivity, as well as the differences in the expressions describing the two different kinetic models of the adsorption mechanism, make the dynamic predictions of the concentration profiles of the adsorbate in the pore fluid and the adsorbed phase obtained by the batch model (or the column model) employing kinetic model 1, to be significantly different than those concentration profiles obtained when kinetic model 2 is used. The results in this study indicate that the two different kinetic models describe properly (quantitatively) the experimental overall mass-transfer resistance (the dynamic behavior of C_d/C_{d0} in the finite bath) of the batch adsorption system, but these two different kinetic models provide significantly different concentration profiles for the adsorbate in the pore fluid and adsorbed phases. These findings suggest that while proper (in quantitative terms) description of the experimental overall mass-transfer resistance may represent a necessary condition in model discrimination studies [14,16,18,21] for the determination of an appropriate kinetic model for the adsorption mechanism, this condition may not also be sufficient for proper kinetic model discrimination. The results suggest that the experimental concentration profiles of the adsorbate in the pore fluid and the adsorbed phase of the adsorbent particles would provide, if measured at different batch operational times, additional very useful information, so that proper discrimination studies between different kinetic models of the adsorption mechanism could be performed. The availability of the experimental concentration profiles in the adsorbent particles, would not only contribute in the determination of the appropriate physical kinetic mechanism, but it would also lead to better estimates for the value of the pore diffusivity and for the values of the rate constants of the kinetic model determined to represent the adsorption mechanism. In practice, it may be difficult to measure the concentration profiles of the adsorbate in the pore fluid, but one might develop an experimental technique to measure the concentration profiles of the adsorbate in the adsorbed phase. For example, it might be possible, in certain affinity adsorption systems, to label the adsorbate molecules. The adsorption process could be terminated at a certain operational time, and the adsorbent particles may be embedded in gelatin and sliced quickly (so that the adsorbed concentration profiles do not change appreciably) into very small (e.g., 10 μm) sections using a microtome. Examination of the sections using an appropriate sensor might provide information with regard to the concentration profile of the adsorbate in the adsorbed phase. Experts in experimental analytical methods may perhaps devise different experimental techniques for measuring the concentration profiles of the adsorbate in the adsorbent particles. It should be noted at this point that even if only experimental information about the concentration profiles of the adsorbate in the adsorbed phase may be obtained, this information together with the experimental batch data of the adsorbate concentration in the fluid of the finite bath, could (i) significantly increase the information base for the construction of models describing the pore diffusion and interaction (adsorption) mechanisms, and (ii) could also increase the accuracy of the parameter estimation and model discrimination strategies, so that the proper kinetic model for the adsorption mechanism is determined, and accurate values for the pore diffusivity and the rate constants of the

adsorption mechanism may be estimated. The above approach could also be applicable to affinity adsorption systems exhibiting restricted [12] pore diffusion; of course, it should be noted that such systems would involve more complex parameter estimation and model discrimination studies.

The results obtained from the column simulations (with porous adsorbents) indicate that the differences in the breakthrough curves obtained from kinetic models 1 and 2, increase as the column length increases. Furthermore, for a given time, the concentration profiles in the pore fluid and the adsorbed phase obtained from kinetic models 1 and 2, are very different, and they also differ with the position along the axial distance. These column results suggest that experimental breakthrough curves obtained from relatively long columns, as well as measured concentration profiles within the adsorbent particles along the axial distance of relatively long columns, would provide additional very useful information for kinetic model discrimination and parameter estimation studies that would involve column (model) calculations. The kinetic model and parameter values determined from the column calculations, should be compared with those determined from the batch (finite bath) calculations involving the experimental batch data. It should be noted that parameter estimation and kinetic model discrimination studies involving column systems with porous adsorbent particles, may not be practical [1-4,14,16,18] because the column calculations are much more tedious, complex, and time consuming (with respect to computational time) than the batch calculations; furthermore, the column experiments are more difficult, time consuming, and expensive than the finite bath experiments. Thus, it is easier to determine the kinetic model of the adsorption mechanism and to estimate the value of D_p and the values of the kinetic rate constants from batch systems, as discussed above. But after the kinetic model has been determined, it should be used in the column model to predict the breakthrough curve for a relatively long column. The theoretical breakthrough curve should then be compared with the experimental breakthrough curve of the same relatively long column; also the theoretical concentration profiles in the adsorbent particles at different positions along the axial distance should be compared with the experimental, if available, concentration profiles. If the differences between the experimental and theoretical column data are not significant, this could indicate that a proper kinetic model for the adsorption mechanism and a proper value for D_p were determined from the studies involving the batch experimental data and batch model (it is assumed here that the non-intrinsic mass-transfer mechanisms in the finite bath and column systems, are described accurately by appropriate [1-4,13,16,18] expressions in the batch and column models). It should be noted that the batch and column experiments suggested above, they should preferably be carried out at different temperatures and with different initial (C_{d0}) and inlet ($C_{d,in}$) adsorbate concentrations.

In the affinity adsorption systems with the porous silica particles, the variation of the estimated value of the film mass-transfer coefficient K_f by $\pm 20\%$, has no significant effect on the dynamic behavior of the batch and column systems. The effect of the variation of the estimated value of the pore diffusivity D_p by $\pm 20\%$ on the dynamic behavior of the batch and column systems, can be appreciable. Furthermore, the variation of the estimated value of D_p affects the dynamic behavior of the concentration profiles of the adsorbate within the adsorbent particles. As we discussed above, different kinetic models of the adsorption mechanism also provide different

concentration profiles for the adsorbate within the adsorbent particles. Since the performance and operation of the wash and elution stages depend [1–4] significantly on the concentration profiles of the adsorbate (in the adsorbent particles) established at the end of the adsorption stage, it is very important to estimate accurately the value of the pore diffusivity and to determine a proper kinetic model for the adsorption mechanism of the affinity chromatography system under consideration. This could allow the accurate estimation of the performance of the adsorption stage, and could provide accurate initial conditions [1–4] for estimating the performance of the wash and elution stages.

The adsorption of β -galactosidase onto anti- β -galactosidase immobilized on non-porous glass coated beads, was described by kinetic model 1. It was found that when the adsorption rate is considered to be controlled by film mass-transfer and the interaction mechanism (kinetic model 1), a reasonable agreement between the experimental batch data and the predictions of the batch model is obtained. The variation of the estimated value of the film mass-transfer coefficient by $\pm 20\%$, has no significant effect on the dynamic behavior of the batch and column systems. Thus, if an accurate estimate of the film mass-transfer coefficient can be obtained from an appropriate correlation [1–4,13,16,18,23] (for batch or column operation) then the kinetic model that describes the adsorption mechanism could be determined from parameter estimation and model discrimination studies involving experimental batch data and the predictions of the batch model. For these affinity adsorption systems (systems having non-porous adsorbent particles), the calculations involving the column model are not much more complex and time consuming than the finite bath calculations (this is not the case for the systems having porous adsorbent particles), and thus, the kinetic model of the adsorption mechanism could also be determined from parameter estimation and model discrimination studies involving the predictions of the column model and the experimental breakthrough curves obtained from (i) different inlet concentrations of the adsorbate, (ii) different column lengths, and (iii) different temperatures of operation.

NOTATION

A_1	molecule of adsorbate
A_a	area occupied by adsorbed molecule in "form a"
A_b	area occupied by adsorbed molecule in "form b"
A_1L_1	non-covalent adsorbate-ligand complex
C_d	concentration of adsorbate in the bulk fluid phase (finite bath), or in the flowing fluid stream (column), mg/cm^3
$C_{d,\text{in}}$	concentration of adsorbate at $x < 0$ when $D_L \neq 0$, or at $x = 0$ when $D_L = 0$, mg/cm^3
C_{d0}	initial concentration of adsorbate in bulk fluid phase of finite bath, mg/cm^3
C_{dp}	concentration of adsorbate in the liquid layer adjacent to the surface of a non-porous adsorbent particle, mg/cm^3
C_p	concentration of adsorbate in pore fluid, mg/cm^3
\bar{C}_p	average concentration of adsorbate in pore fluid, mg/cm^3
C_s	concentration of adsorbate in adsorbed phase, mg/cm^3
\bar{C}_s	average concentration of adsorbate in adsorbed phase, mg/cm^3

C_{sa}	concentration of adsorbed adsorbate in "form a", mg/cm ³
C_{sb}	concentration of adsorbed adsorbate in "form b", mg/cm ³
\bar{C}_{sa}	average concentration of adsorbed adsorbate in "form a", mg/cm ³
\bar{C}_{sb}	average concentration of adsorbed adsorbate in "form b", mg/cm ³
C_T	maximum concentration of adsorbate in adsorbed phase when all available (accessible) ligand is utilized, mg/cm ³
D_L	axial dispersion coefficient of adsorbate, cm ² /s
D_p	pore diffusion coefficient of adsorbate (in adsorbent particle), cm ² /s
K_f	film mass transfer coefficient of adsorbate, cm/s
K	k_{11}/k_{21} , cm ³ /mg
K_1	k_{12}/k_{32} , dimensionless
K_2	k_{42}/k_{32} , dimensionless
K_3	k_{62}/k_{32} , dimensionless
k_{11}	rate constant in eqn. 9, cm ³ /(mg)(s)
k_{21}	rate constant in eqn. 9, s ⁻¹
k_{12}	rate constant in eqn. 12, cm ³ /(mg)(s)
k_{22}	rate constant in eqn. 12, s ⁻¹
k_{32}	rate constant in eqns. 12 and 13, cm ³ /(mg)(s)
k_{42}	rate constant in eqn. 12, cm ³ /(mg)(s)
k_{52}	rate constant in eqn. 13, s ⁻¹
k_{62}	rate constant in eqn. 13, cm ³ /(mg)(s)
L	column length, cm
L_1	vacant immobilized ligand
r	radial distance in adsorbent particle, cm
r_0	radius of adsorbent particle, cm
t	time, s
T	temperature, K
V_f	superficial fluid velocity, cm/s
x	axial distance, cm

Greek letters

α	form factor; 0, 1 and 2 for slab, cylinder and sphere, respectively
γ	given by eqn. 18
δ	A_b/A_a
ε	void fraction in finite bath, or column
ε_p	void fraction in porous adsorbent particle

ACKNOWLEDGEMENTS

The authors gratefully acknowledge that this work was supported by the Monsanto Company and the NATO Scientific Affairs Division under Grant No. 0770/88.

REFERENCES

- 1 B. H. Arve and A. I. Liapis, *AIChE J.*, 33 (1987) 179.
- 2 B. H. Arve and A. I. Liapis, *Biotechnol. Bioeng.*, 30 (1987) 638.

- 3 B. H. Arve and A. I. Liapis, *Biotechnol. Bioeng.*, 31 (1988) 240.
- 4 B. H. Arve and A. I. Liapis, *Biotechnol. Bioeng.*, 32 (1988) 616.
- 5 W. Norde, *Adv. Colloid Interface Sci.*, 25 (1986) 267.
- 6 I. Lundstrom, B. Ivarsson, U. Jonsson and H. Elwing, in W. J. Feast and H. S. Munro (Editors), *Polymer Surfaces and Interfaces*, Wiley, New York, 1987, pp. 201-230.
- 7 A. A. Gorbunov, A. Ye. Lukyanov, V. A. Pasechnik and A. V. Vakhrushev, *J. Chromatogr.*, 365 (1986) 205.
- 8 J. Hubble, *Biotechnol. Bioeng.*, 30 (1987) 208.
- 9 A. E. Mark, P. D. Jeffrey and L. W. Nichol, *J. Theor. Biol.*, 131 (1988) 137.
- 10 E. N. Lightfoot, M. C. M. Cockrem, S. J. Gibbs and A. M. Athalye, in N. N. Li and H. Strathmann (Editors), *Separation Technology*, Engineering Foundation, New York, 1988, pp. 122-154.
- 11 R. J. Yon, *J. Chromatogr.*, 457 (1988) 13.
- 12 J. H. Petropoulos, A. I. Liapis, N. P. Kolliopoulos, J. K. Petrou and N. K. Kanellopoulos, *Bioseparation*, 1 (1990) 69.
- 13 A. I. Liapis, A. B. Anspach, M. E. Findley, J. Davies, M. T. W. Hearn and K. K. Unger, *Biotechnol. Bioeng.*, 34 (1989) 467.
- 14 A. I. Liapis, *J. Biotechnol.*, 11 (1989) 143.
- 15 A. I. Liapis, in N. N. Li and H. Strathmann (Editors), *Separation Technology*, Engineering Foundation, New York, 1988, pp. 420-487.
- 16 A. I. Liapis, in A. B. Mersmann and S. E. Scholl (Editors), *Fundamentals of Adsorption (Proceedings of the Third International Conference on Fundamentals of Adsorption, Sonthofen, May 7-12, 1989)*, Engineering Foundation, New York, 1990.
- 17 B. H. Arve and A. I. Liapis, in A. I. Liapis (Editor), *Fundamentals of Adsorption*, Engineering Foundation, New York, 1987, pp. 73-87.
- 18 A. I. Liapis, *Sep. Purif. Methods*, 19 (1990) 133.
- 19 M. A. McCoy, B. J. Hearn and A. I. Liapis, *Chem. Eng. Commun.*, (1991) in press.
- 20 A. Johnston and M. T. W. Hearn, *J. Chromatogr.*, 512 (1990) 101.
- 21 D. M. Bates and D. G. Watts, *Non-Linear Regression Analysis and Its Implications*, Wiley-Interscience, New York, 1988.
- 22 B. J. Horstmann and H. A. Chase, *Chem. Eng. Res. Des.*, 67 (1989) 243.
- 23 C. J. Geankoplis, *Transport Processes and Unit Operations*, Allyn and Bacon, Boston, MA, 1983.
- 24 F. H. Arnold, H. W. Blanch and C. R. Wilke, *Chem. Eng. J.*, 30 (1985) B9.
- 25 J. H. Harwell, A. I. Liapis, R. Litchfield and D. T. Hanson, *Chem. Eng. Sci.*, 35 (1980) 2287.
- 26 F. H. Arnold, H. W. Blanch and C. R. Wilke, *Chem. Eng. J.*, 30 (1985) B25.
- 27 J. Villadsen and M. L. Michelsen, *Solution of Differential Equation Models by Polynomial Approximation*, Prentice-Hall, Englewood Cliffs, NJ, 1978.
- 28 C. D. Holland and A. I. Liapis, *Computer Methods for Solving Dynamic Separation Problems*, McGraw-Hill, New York, 1983.
- 29 M. L. Michelsen, *AIChE J.*, 22 (1976) 594.
- 30 J. J. Moré, B. S. Garbow and K. E. Hillstrom, *User Guide for MINPACK-1, Report ANL-80-74*, Argonne National Labs., Argonne, IL, 1980.
- 31 B. J. Hearn, *M.S. Thesis*, Department of Chemical Engineering, University of Missouri-Rolla, Rolla, MO, 1989.
- 32 H. A. Chase, *J. Chromatogr.*, 297 (1984) 179.

CHROMSYMP. 2319

Multivalent ion-exchange model of biopolymer chromatography for mass overload conditions

PIOTR CYSEWSKI

Akademia Medyczna w Bydgoszczy, Zakład Chemii Fizycznej, M. Skłodowskiej-Curie 9, 85-094 Bydgoszcz (Poland)

ALAIN JAULMES, RAMONA LEMQUE, BERNARD SÉBILLE and CLAIRE VIDAL-MADJAR*

Laboratoire de Physico-Chimie des Biopolymères, C.N.R.S., Université Paris-Val-de-Marne, 2 Rue Henry Dunant, 94320 Thiais (France)

and

GERD JILGE^a

Institut für Anorganische Chemie und Analytische Chemie, Johannes Gutenberg-Universität, W-6500 Mainz (Germany)

ABSTRACT

The simple model of multivalent ion-exchange biopolymer chromatography is analyzed on the basis of classical quasi-chemical treatments. The rigorous isotherm equation deduced from the stoichiometric displacement model (SDM) was used to simulate the migration of a solute through the chromatographic column in the isocratic and gradient elution modes. The peak profiles generated for various sample sizes were compared with those obtained on the basis of a Langmuir isotherm. Peak tailing increases with the value of the exponent Z , defined as the ratio of the protein valency to the displacing counter-ion valency. For large Z the asymmetries due to the non-linearity of the isotherm are still present for small sample sizes, but may be reduced by using a displacing counter ion of higher valency. To illustrate the theoretical results, the ion-exchange model was applied to analyse the zonal elution behaviour of bovine serum albumin on a polymeric anion-exchange stationary phase deposited on silica. The effective charge of the protein ($m = 8$) was determined at infinite dilution with mono- and a divalent counter-ions. This value was introduced into the SDM isotherm to predict the elution behaviours in mass-overload conditions and the maximum loading capacity of the protein was determined. Good agreement between theory and experiment was obtained: for about the same capacity factor at infinite dilution, a larger peak asymmetry due to non-linear effects is found with a monovalent counter ion.

INTRODUCTION

High-performance ion-exchange chromatography (HPIEC) is being increasingly used for protein separations on both analytical and preparative scales. The stoichiometric displacement model (SDM) was successfully applied to predict the HPIEC retention behaviour at infinite dilution of a wide variety of biopolymers [1–3].

^a Present address: Boehringer Ingelheim GmbH, W-6507 Ingelheim, Germany.

It considers electrostatic interactions and is derived from the simple laws of mass action expressing the chemical equilibria between the interacting species [4].

Although the most important interactions involved in ion-exchange chromatography are electrostatic interactions between charged centres ruled by the simple Coulomb law, the retention behaviour is much more complex [5,6]. The complicated three-dimensional biopolymer structure, the unknown charge distribution, the amphoteric character of the protein and the heterogeneity of the support are the main reasons for difficulties in acquiring a proper understanding of the retention and binding behaviour of proteins. However, the SDM has been tested for a large number of HPIEC systems at infinite solute dilution and accounts well for retention volume variations with the displacer salt concentration. The model was recently improved to take hydrophobic interactions into account and to explain why the retentions observed at high salt concentrations deviate from those predicted by the SDM theory [7].

Starting from the simple SDM hypothesis, the adsorption of proteins on ion-exchange supports was explained by the multivalent ion-exchange scheme of Velayudhan and Horváth [8] and by the mass-action model of Whitley and co-workers [9,10]. The adsorption isotherms show strong curvature depending on the valency of the studied protein or the charge of the counter ion of the displacing salt. As retention volumes and peak shapes in non-linear chromatography are mainly governed by the adsorption isotherm [11], strong retention shifts and peak distortions are to be expected in the HPIEC of proteins at finite solute concentrations.

As HPIEC is being increasingly used for preparative purposes [12], it is useful to be able to predict the elution behaviour of proteins in mass-overload conditions to optimize separations [13–15]. The aim of this paper is to give an explicit presentation of the ion-exchange adsorption model and to apply it to numerical simulations of the ion-exchange chromatographic process.

Although the SDM model has been successfully applied to predict the retention of proteins on ion-exchange supports at infinite dilution, the simulations for mass-overload conditions were all limited to a Langmuir isotherm [10,13,14] or a two-site Langmuir-type isotherm [15]. Until now the rigorous form of the ion-exchange isotherm has not been used because it has the drawback of being an explicit form of the solute concentration as a function of the amount adsorbed. A Langmuir model was often found to fit well the adsorption protein data on ion exchangers [9], but it is unable to describe the dependence on salt concentration.

Therefore, simulations based on the rigorous SDM isotherm are useful for a better understanding of the HPIEC behaviour of proteins and for optimizing separations in mass-overload conditions using linear or gradient elution. To illustrate the theoretical results obtained with an SDM isotherm, the ion-exchange model was applied to analyse the zonal elution behaviour of bovine serum albumin (BSA) on a weak anion-exchange HPIEC support, *viz.*, a copolymer of vinylimidazole and vinylpyrrolidone (PVP–PVI) deposited on silica.

THEORETICAL

Let us consider the equilibrium of the system consisting of a liquid biopolymer solution and a solid ion-exchange particle. We assume the following:
the deviations from ideality of the protein solutions are small and concentration

is a sufficient measure of their activity, which means that activity coefficients are equal to unity in the whole concentration range; this fairly crude assumption is extensively accepted [1-10];

protein adsorption has a multi-point nature, which has been shown experimentally, for example, by Jennissen [16];

the properties of biopolymer molecules (charge, valency, structure, size, etc.) do not change during the ion-exchange process;

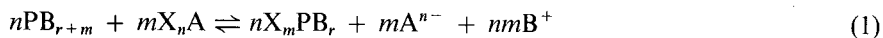
solid adsorbents must have a wide-pore and homogeneous nature although significant deviations from such an ideal model are observed in experimental investigations;

the particle adsorption properties are represented by active adsorption centres which are entirely covered by co-ions; and

the adsorption of proteins has a competitive character and their binding to the surface is accompanied by simultaneous desorption of an equivalent amount of salt counter ions.

Ion-exchange adsorption isotherm

The process of ion-exchange adsorption-desorption equilibria may be represented by the following expression

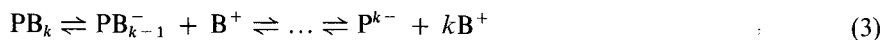


where P symbolizes the protein molecule, X the part of the solid surface containing one adsorption site and A and B are ions with charges of opposite signs relative to particle and protein, respectively. The numbers of bonds in all complexes are indicated by appropriate subscripts, as in usual chemical formulae. The salt counter ion is n -valent, the protein molecule is m -valent towards particles and has a total charge $r + m$. The chemical equilibria are given for anion-exchange chromatography, but may easily be adapted, as well as all further developments, for cation-exchange chromatography.

The law of mass action for the ion-exchange process may be given as

$$K' = \frac{\{X_mPB_r\}^n [A^{n-}]^m [B^+]^{mn}}{[PB_{r+m}]^n \{X_nA\}^m} \quad (2)$$

where K' is given in terms of volumetric and surface concentrations and brackets [] and braces { } represent the concentrations of the given species in bulk-phase solutions (mol/l) and in the adsorbed state (mol/m²), respectively. In general, the protein molecule is a poly-ion interacting with a given number of co-ions in solution and must undergo the multivalent dissociation process. It is possible to write the set of chemical equations for the equilibrium state



where k is the maximum number of ions interacting with protein and is equal to the total surface charge of protein. Of course, the probabilities of the various complexes

are not identical. The given equilibrium conditions determine all the concentrations. The set 3 can be written in a simple way (for $k = r + m$)



the equilibrium constant of which is as follows

$$K'' = \frac{[\text{PB}_r^{m-}][\text{B}^+]^m}{[\text{PB}_{r+m}]} \quad (5)$$

If we combine eqns. 2 and 5, we obtain

$$K = \frac{\{X_m\text{PB}_r\}^n [\text{A}^{n-}]^m}{[\text{PB}_r^{m-}]^n \{X_n\text{A}\}^m} \quad (6)$$

where $K = K'/(K'')^n$ is related to the equilibrium



The total number of available sites for adsorption, Q_x , may be expressed as the sum of the sites taken by protein, mQ_p , and those taken by the salt counter ions

$$Q_x = nS\{X_n\text{A}\} + mQ_p \quad (8)$$

where S is the total interfacial surface area and $Q_p = S\{X_m\text{PB}_r\}$ is the amount of adsorbed protein.

We may now write the isotherm equation by substituting eqn. 8 into eqn. 6 and simple rearrangement

$$[\text{PB}_r^{m-}] = \frac{Q_p}{L} \left(\frac{[\text{A}^{n-}]}{Q_x - mQ_p} \right)^Z \quad (9)$$

where $Z = m/n$, $L = SK^{1/n}/(nS)^Z$ and Q_x/m is the maximum protein loading capacity. The above isotherm is a complex expression of the concentration as a function of the adsorbed amount. In general, the adsorbed amount cannot be expressed as a function of solute concentration but, of course, may be calculated by numerical means.

In the case of equal valencies for the protein and salt counter ion, Z is equal to unity and the isotherm is of the Langmuir type

$$Q_p = \frac{Q_x}{m} \cdot \frac{K_1[\text{PB}_r^{m-}]}{[\text{A}^{n-}] + K_1[\text{PB}_r^{m-}]} \quad (10)$$

where $K_1 = K^{1/n}$. For some given experimental conditions, m may be equal to the valency of the displacing salt, n , as the charge of the protein is usually ruled by the pH of the medium. However, with the experimental conditions used for ion-exchange separations, this situation is unrealistic, the number Z determined with monovalent displacing counter ions generally being larger than 3 [7].

For extremely low concentrations, eqn. 9 becomes of the Henry isotherm type

$$Q_P = LQ_X^Z \cdot \frac{[PB_r^{n-}]}{[A^{n-}]^Z} \quad (11)$$

The retention volume may be related to the isotherm parameters by the well known relationship

$$k' = V_{(C \rightarrow 0)}^R / V_0 - 1 = \frac{1}{V_0} \left(\frac{dQ_P}{dC} \right)_{C=0} \quad (12)$$

where C is the protein concentration and V_0 the volume of the mobile phase. Using eqn. 9 leads to

$$k' = \frac{Q_X^Z}{V_0 R} \quad (13)$$

where $R = [A^{n-}]^Z/L$. One obtains here the same expression as that found for the SDM of Regnier and co-workers [1-3], which relates the retention volume at infinite dilution to the displacing-salt concentration.

Numerical simulation method

The theoretical propagation differential equation describing the solute mass balance may be written as

$$\frac{\partial C}{\partial t} + u \cdot \frac{\partial C}{\partial z} + \frac{1}{\Delta v_0} \cdot \frac{\partial q}{\partial t} = D' \cdot \frac{\partial^2 C}{\partial z^2} \quad (14)$$

where q is the amount of solute adsorbed in an infinitesimal cross-slice of column and Δv_0 is the corresponding mobile phase volume. One uses the abscissa, z , along the column length, the time, t , elapsed from the moment of injection, the mobile phase velocity, u , and the solute concentration, C . D' is a global dispersion coefficient accounting for all the contributions to the dispersive effect.

The equilibrium is assumed to be reached at any time, so that C is a function of q according to eqn. 9, which may be written in the form

$$C = \Omega \cdot \frac{q}{(q_X - mq)^Z} \quad (15)$$

where q_X is the number of binding sites on the solid phase for the infinitesimal cross-slice and Ω is a function of $[A^{n-}]$

$$\Omega = \frac{(n\Delta S)^Z}{\Delta SK^{1/n}} \quad (16)$$

ΔS is the adsorbing surface area in the slice. A stepwise numerical method was used to solve the system given by eqns. 14 and 15.

Mobile phase progression and Fick's law. The band broadening is due to various terms such as the diffusion in the mobile phase, the flow non-uniformity and the kinetic mass-transfers. As a first approximation we assume that all these effects are included in the global dispersion coefficient D' . In HPLC experiments the axial diffusion in the mobile phase and the eddy diffusion can usually be neglected, but slow mass-transfer kinetics are the main contribution to the large theoretical plate heights often observed for the elution of proteins in the isocratic mode. A rigorous numerical procedure should account for slow mass-transfer kinetics separately [10,17]. However, for the column efficiencies generally used in protein separations, one may approximate the kinetic contribution with the global dispersive term. We have shown [17] that the limit for this approximation is close to a theoretical plate number of 15; the approximation leads to a 5% deviation for the retention time at the peak maximum and a 10% deviation for the peak width.

Several methods for solving the differential equation (eqn. 14) in the presence of a Langmuir-type isotherm and axial dispersion have been described: algorithms were supplied as standard subroutines to simulate isocratic elution [18,19] and linear gradient elution [13]; Lin *et al.* [20] suggested the Lax-Wendroff scheme; Phillips *et al.* [19] employed a finite difference technique where a global first-order law includes mass-transfer kinetics.

The approach adopted here combines the Craig method [14,15], which divides the column into a series of discrete stages, and the finite difference technique. As shown previously [17], this more versatile algorithm enables one to combine axial dispersive effects with any kinetic law for solute mass-transfers. Moreover, the method is not limited to the simulation of peak profiles with linear solvent gradients but permits gradients of arbitrary shape to be considered.

The column is assumed to be divided into slices of thickness Δz . Fick's law, expressed as

$$\Phi = -\Sigma D' \cdot \frac{\partial C}{\partial z} \quad (17)$$

is approximated by

$$\Phi = -\Sigma D' \cdot \frac{\Delta C}{\Delta z} \quad (18)$$

where Σ is the cross-sectional area of the liquid phase and Φ is the molar rate of solute "exchanged" by dispersion between two adjacent slices. It can be defined by the equation

$$\Phi = -\Delta v_0 \cdot \frac{\Delta_r C}{\Delta t} \quad (19)$$

where $\Delta_r C$ is the resulting partial concentration change in a slice during the time interval Δt necessary to the liquid phase to flow from one slice to the following one

$$\Delta z / \Delta t = u \quad (20)$$

We calculate $\Delta_f C = -\Phi \Delta t / \Delta v_0 = -\Phi / u \Sigma$. Here $\Delta_f C = (D'/u)(\Delta C / \Delta z) = \Delta C F$, where $F = D'/u \Delta z$ is a factor independent of z or t .

Thus Fick's law can be written for the extreme slices

$$\left. \begin{aligned} \Delta_f C(\Delta z, t) &\approx F[C(2\Delta z, t) - C(\Delta z, t)] \\ \Delta_f C(L, t) &\approx F[C(L - \Delta z, t) - C(L, t)] \end{aligned} \right\} \quad (21)$$

and for the inner slices

$$\left. \begin{aligned} \Delta_f C(z, t) &= \Delta_f C(z, t) - \Delta_f C(z - \Delta z, t) \\ &= F\{C(z + \Delta z, t) - C(z, t) - [C(z, t) - C(z - \Delta z, t)]\} \\ &= F[C(z + \Delta z, t) - 2C(z, t) + C(z - \Delta z, t)] \end{aligned} \right\} \quad (22)$$

To ensure the convergence of the numerical procedure, Δt may be subdivided into fractions and the changes subsequently added for every slice.

The mobile phase progression is rendered by a mere index shift of the mobile phase concentrations in the slices.

Sorption equilibrium inside a given slice. We assume that the equilibrium takes place as soon as the two new fractions meet in a given slice: thus $q(z, t)$ and $C(z - \Delta z, t)$ will originate the new values $q(z, t + \Delta t)$ and $C(z, t + \Delta t)$.

The initial values q_0 and C_0 give the total amount of solute in the slice: $s = q_0 + \Delta v_0 C_0$, which will be equal to the final amount, $\bar{q} + \Delta v_0 \bar{C}$, at equilibrium.

As

$$\bar{C} = \Omega \cdot \frac{\bar{q}}{(q_x - m\bar{q})^2} \quad (23)$$

one can write

$$\bar{q} + \frac{\Delta v_0}{R} \cdot \frac{\bar{q}}{(q_x - m\bar{q})^2} - q_0 - \Delta v_0 C_0 = 0 \quad (24)$$

A step interpolation will yield the value of \bar{q} , from which one can deduce \bar{C} according to the equation

$$\bar{C} = C_0 + \frac{q_0 - \bar{q}}{\Delta v_0} \quad (25)$$

The method described above has two interesting features: it is built to ensure mass conservation all through the simulated chromatographic process and the thickness of the slices may be chosen as low as desirable to approach close to the actual physical phenomena.

Case of gradient elution. The concentration of counter ions, $[A^{n-}]$, is an arbitrary function of the quantity $y = z - ut$. For example it may be either:

(1) a linear function

$$\left. \begin{aligned} [A^{n-}] &= C_c^0 + Gy \quad (\text{for } y \geq 0) \\ [A^{n-}] &= C_c^0 \quad (\text{for } y \leq 0) \end{aligned} \right\} \quad (26)$$

with which assumption, at any point of the column,

$$[A^{n-}] = C_c^0 + GyY(y) \quad (27)$$

where the step Dirac function Y is 1 for $y > 0$ and 0 for $y \leq 0$,

(2) or a parabolic function

$$\left. \begin{aligned} [A^{n-}] &= C_c^0 + Gy + \frac{B}{2}y^2 \quad (\text{for } y \geq 0) \\ [A^{n-}] &= C_c^0 \quad (\text{for } y \leq 0) \end{aligned} \right\} \quad (28)$$

EXPERIMENTAL

Materials

The reagents used for the stationary phase synthesis were N-vinylimidazole, vinylpyrrolidone and 1,4-butanediol diglycidyl ether, purchased from Janseen Chimica (Beerse, Belgium).

The silica support (LiChrospher Si-300) (particle diameter $d_p = 10 \mu\text{m}$ and pore size 300 Å) was purchased from Merck (Darmstadt, Germany).

The protein used for the chromatographic study, BSA monomer, was obtained from Sigma (St. Louis, MO, USA). The buffer was Tris, obtained from Aldrich-Chemie (Steinheim, Germany).

Chromatography

The chromatographic system consisted of a pump (HPLC PUMP 420, Kontron Instruments, Zurich, Switzerland) and a UV detector (Model SPD-6A, Shimadzu, Kyoto, Japan) operating at 280 nm. A sample injector (Model 7125, Rheodyne, Berkeley, CA, USA) with a 20- μl sample loop was used. To determine the ion-exchange capacity, frontal loading was performed with a 2-ml sample loop and the displacing salt elution was monitored at 256 nm.

The chromatographic packing was a polymeric anion-exchange stationary phase deposited on silica. The polymer used was a PVP-PVI copolymer (75:25) cross-linked with 1,4-butanediol diglycidyl ether (BUDGE). It was synthesized using the one-step polymer-coating method developed by Sébille and co-workers [21,22].

The specific anion-exchange capacity of the adsorbent per unit volume of mobile phase was 0.15 mequiv./ml. It was determined by frontal loading with sodium chloride as the eluent and sodium nitrate as the displacing agent.

The chromatographic column (100 \times 41 mm I.D.) was slurry packed. The column temperature was maintained at 10°C during the experiments using a thermostated water-bath. The eluent used was 20 mM Tris buffer (pH 7.5). For the isocratic elution, the ionic strength was imposed by a monovalent (NaCl) or a divalent salt

(Na_2SO_4). The capacity factor for infinite dilution, k' , was calculated by reference to the retention volume of an unretained protein, α -chymotrypsinogen A.

Computer system

The analogue output of the detector was connected to a digital voltmeter (Model 3497; Hewlett-Packard, Palo Alto, CA, USA). The data (4 digits precision) were stored on floppy disk and analysed with a personal computer (Compaq Deskpro, Model 386/20e) equipped with an arithmetic coprocessor.

The simulations were performed in Pascal language. The step Δz used for calculations was 0.05 cm. A numerical dispersion contributed to the broadening of the elution peak [23]; its contribution to the plate height was $H_N = 0.05$ cm.

RESULTS AND DISCUSSION

Numerical simulations

For comparison with a Langmuir-type isotherm, various isotherms generated with eqn. 9 and increasing values of $Z = m$ are given in Fig. 1. All the isotherms have the same slope at the origin ($k' = 10$). The solute maximum loading capacity (dashed line for each Z value) is equal to the ion-exchange capacity available for adsorption divided by m . The curvature of the isotherm at the origin increases with increasing $Z = m$ value and the derivative of the isotherm reaches zero for lower solute concentrations

$$k'' = \frac{1}{V_0} \left(\frac{d^2 Q_P}{dC^2} \right)_{C=0} = - \frac{2 m z k'^2 V_0}{Q_x} \quad (29)$$

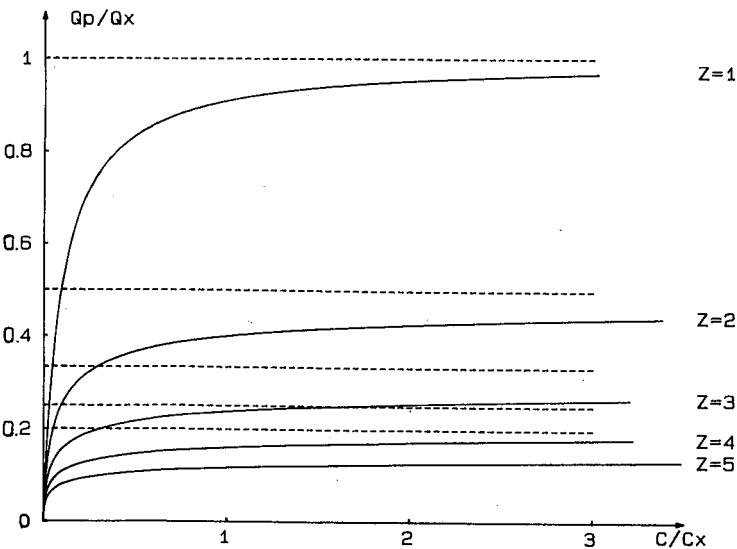


Fig. 1. Influence of exponent Z on the shape of SDM adsorption isotherm ($Z = m$), with equal slopes at the origin ($k' = 10$).

It may therefore be predicted, on the basis of the SDM theory, that the range for linear chromatography will be limited at large m values and strongly tailing peaks will be observed in the isocratic elution mode at much lower concentrations than with a Langmuir isotherm.

The isotherms of Fig. 1 were used to simulate the chromatographic behaviour with isocratic elution with a monovalent displacing ion. In Fig. 2 the theoretical profiles generated with increasing sample size and $m = Z = 5$ are compared with those obtained on the basis of a Langmuir isotherm ($Z = 1$). The simulations were performed with a fixed value of the solute capacity factor ($k' = 10$). This can be related to experiments where k' is kept constant by changing the displacing salt concentration. The results of the simulation are presented as a plot of the outlet solute concentration divided by the active site concentration ($C_x = Q_x/V_0$) vs. the reduced elution volume, $V_r(V)/V_0$. In this instance the dispersive coefficient was kept at a negligible value, but a dispersive effect arises from the numerical steps chosen for the calculation [23]. The corresponding contribution to the plate height is $H_N = 0.05$ cm.

For solute concentrations larger than $C_x/10$ the retention volume at the peak maximum is already close to V_0 when $m = Z = 5$. In agreement with theory [24], the

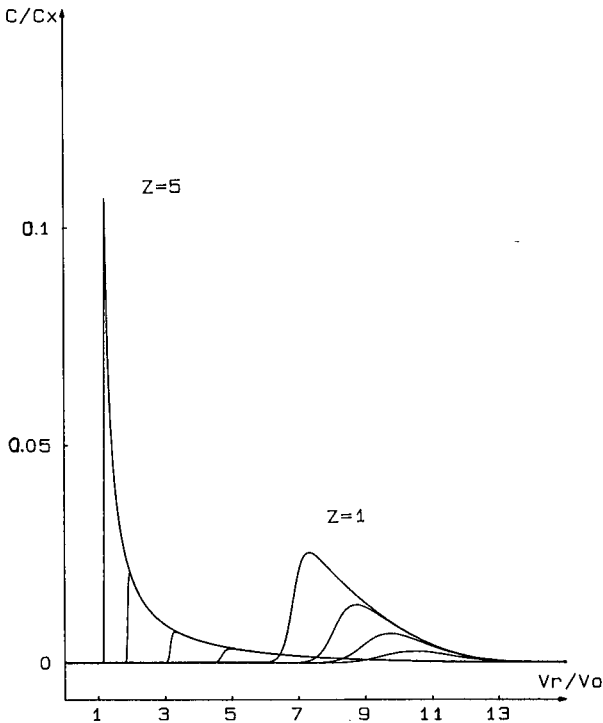


Fig. 2. Isocratic elution with a monovalent displacing salt. Comparison of the peak profiles simulated with a Langmuir isotherm and an SDM isotherm ($Z = 5$). Column length, 5 cm; flow-rate, 1 ml/min; sample volume, 0.020 ml; isocratic elution with $k' = 10$. Sample size: $Q_x/15$, $Q_x/30$, $Q_x/60$, $Q_x/120$.

rear part of the peak coincides with the derivative of a convex adsorption isotherm if the dispersive effects can be neglected

$$V(C) = V_0 + \frac{dQ_P}{dC} \tag{30}$$

The influence of the dispersive effect on the elution peaks generated with $m = Z = 5$ is shown in Fig. 3. In spite of the larger dispersion coefficients used for the simulations, corresponding to the plate-height contributions $H_D = 0.12$ cm and $H_D = 0.6$ cm (Fig. 3a and b), the retention volume at the peak maximum is still well predicted by the first derivative of the adsorption isotherm (dotted line).

These results show that, with isocratic elution and under mass-overload conditions, non-linear effects dramatically control the retention process of solutes with large effective charge number. With larger values of the charge of the solute, m , the curvature at the origin increases (eqn. 29) and generates strong tailings with a shift towards lower retention volumes [11].

For a solute with a given charge number ($m = 6$), Fig. 4 illustrates the influence of non-linear effects with counter ions of various valencies. The capacity factor at

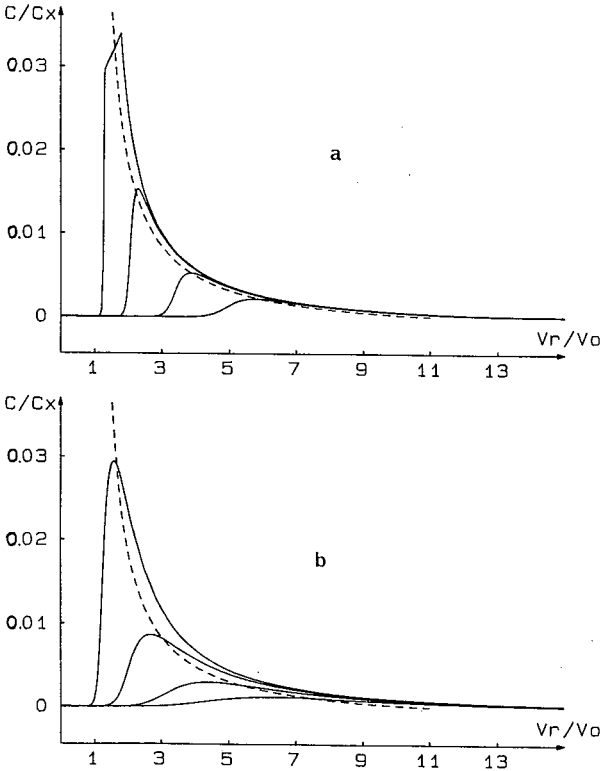


Fig. 3. Influence of the dispersive effects on the peak shapes generated with $Z = 5$ (SDM isotherm). Same conditions as in Fig. 2 and (a) $D' = 0.010$ cm²/s, $H_D = 0.12$ cm; (b) $D' = 0.050$ cm²/s, $H_D = 0.60$ cm. Dashed lines, first derivative of the adsorption isotherm.

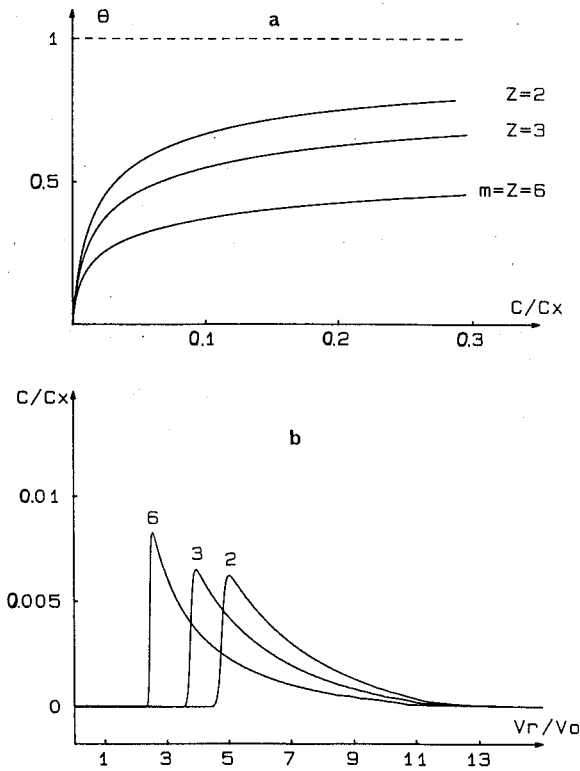


Fig. 4. Influence of the valency of the counter ion on the isocratic elution of a solute with six effective charges. (a) SDM isotherm; (b) peak profiles simulated with an SDM isotherm. Exponent $Z = 2, 3, 6$. Same conditions as in Fig. 2 with sample size $Q_x/60$.

infinite dilution remained constant for the simulated profiles ($k' = 10$). As predicted from eqn. 29, the tailing due to the overload effects increases with increasing valency of the displacer ion used in the eluent. This result shows that a displacing counter ion of larger valency should be used in order to reduce mass-overload effects in the isocratic elution mode.

This conclusion is of limited application in practice, however: because of the high selectivity of the supports, linear gradient elution is most commonly used for protein separations by HPIEC, in order to reduce band broadening. A model was described [25] that predicts the separation of proteins at infinite dilution, with a linear salt gradient. Antia and Horváth [13] studied the effect of gradient elution and column overload on the separation of a binary mixture with a numerical procedure, but their simulations were limited to isotherms of the Langmuir type.

Because of the significant differences observed between the simulations performed with isocratic elution in the cases of an SDM isotherm and a Langmuir isotherm (Fig. 2), it is interesting to examine the influence of the valency of the counter ion in gradient elution on the elution profile of a solute with a given value of the charge, m . To compare with the simulations in the isocratic mode in Fig. 4, the solute charge is

6 and for each Z the slope of the gradients was selected so as to obtain the end of the rear edge of the peak at $V_r/V_0 \approx 11$ (Fig. 5). The initial value of k' at the gradient beginning is 100: this would correspond to experiments where the initial concentration of the displacing salt is adjusted to give $k' = 100$. As already shown with simulations assuming a Langmuir isotherm [13], gradients strongly reduce the asymmetry owing to the non-linearity of the isotherm. With a linear salt gradient (Fig. 5a), the mass-overload effects increase with displacing counter ions of lower valency.

Although not very realistic, but for illustrating the versatility of the present algorithm, Fig. 5b shows the profiles obtained with a parabolic gradient simulating salt concentrations increasing with time. For comparison with the peaks in Fig. 5a, the initial slope at the origin was set to a value equal to the slope of the linear gradient. The front of the peak is eluted at a slightly lower retention volume, and the peak tailing is much reduced, especially when a monovalent displacing ion is assumed for the simulations. Of course, other types of gradient functions could have been used, such as a linear one ending with a plateau.

These simulations based on the rigorous SDM isotherm predict, for a pure

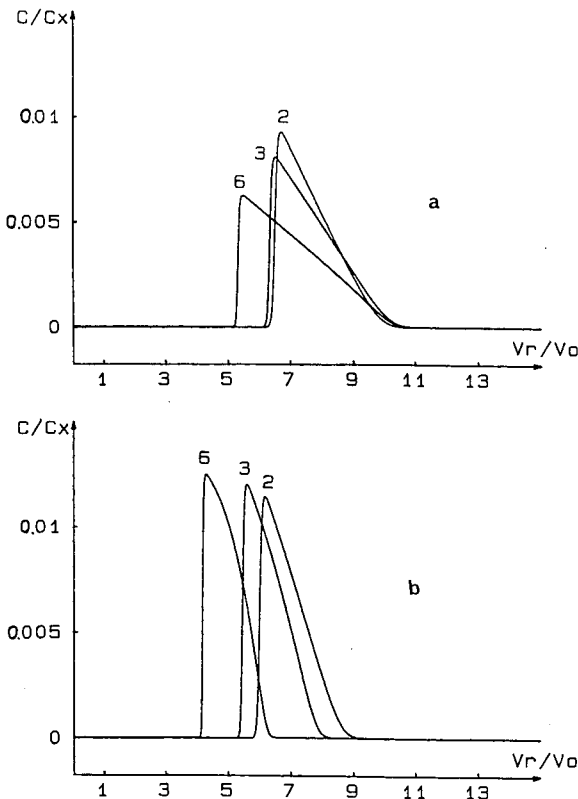


Fig. 5. Influence of the valency of the counter ion on the gradient elution of a solute with six effective charges. (a) Linear gradient; (b) parabolic gradient ($B/C_x = 2.10^{-5} \text{ s}^{-2}$). $Z = 2$, $G/C_x = 0.017 \text{ s}^{-1}$; $Z = 3$, $G/C_x = 0.008 \text{ s}^{-1}$; $Z = 6$, $G/C_x = 0.003 \text{ s}^{-1}$. Same conditions as in Fig. 2 with sample size $Q_x/60$. Initial value of $k' = 100$.

ion-exchange mechanism, more important non-linearity effects with proteins of larger effective charge, but a decrease in mass-overload effects is to be expected with a displacing counter ion of higher valency.

HPIEC study of BSA with isocratic elution

To illustrate the previous theoretical simulations, we studied the chromatographic behaviour of BSA eluted from an anion-exchange column under mass-overload conditions. This protein was selected to test the model as the adsorption of BSA on the anion-exchange support, a PVP-PVI (75:25) copolymer deposited on silica, is described by an isotherm of convex shape.

In order to determine the exponent, Z , retention studies were first performed in the linear range of the adsorption isotherm and analysed with the SDM model for infinite dilution [1-3]. The capacity factor, k' , extrapolated to zero sample size is related to the displacing counter ion concentration C_C , according to the equation

$$\log k' = a - Z \log C_C \quad (31)$$

Fig. 6 shows the variations of k' with the concentration of a mono- or a divalent salt. The values of Z were calculated by a linear regression analysis of plots of $\log k'$ vs. $\log C_C$. The Z value determined with sodium chloride as the displacing salt is 7.9 ± 0.4 . With sodium sulphate the Z value is 4.1 ± 0.4 . The errors are given for a 95% confidence interval. This result is in agreement with theory, the ratio Z being twice as large with chloride ions as that measured with sulphate ions.

The apparent Z values are generally considered to be mean values over all orientations of molecules on the surface [6]. Moreover, Z measurements may be affected by hydrophobic interactions [7] and its value may be non-integral when

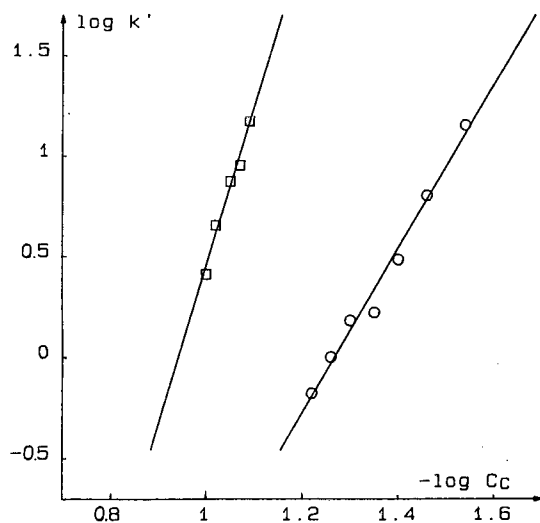


Fig. 6. Dependence of $\log k'$ on the \log (salt concentration) for BSA on an anion exchanger, PVP-PVI on silica; flow-rate, 1 ml/min; eluent, 0.020 M Tris buffer (pH 7.5). (\square) NaCl; (\circ) Na_2SO_4 .

determined with a monovalent salt. With experimental conditions close to those used in this work, Melander *et al.* [7] measured values of Z of 3.55 and 2.99 for BSA eluted from a weak and a strong anion exchanger, respectively, with ammonium sulphate as the displacing salt. The value for the weak anion exchanger is close to that determined on PVP-PVI at pH 7.5 by varying the sodium sulphate concentration. The good agreement of the effective charge of the protein ($m = 8$) deduced from Z measurements with mono- and divalent displacing ions show that, with both salts, the retention is mainly governed by an ion-exchange mechanism. This value of m was selected to simulate the elution peaks under mass-overload conditions.

Fig. 7 illustrates the experimental profile of the BSA (dotted lines) with a displacing salt with a monovalent counter ion (sodium chloride) and a divalent counter ion (sodium sulphate). An impurity (about 10% of the total sample) is eluted on the tailing end of the main peak. For comparing peak shapes, we tried to fix the salt concentration so as to obtain k' values as close as possible for both displacing salts. This can only be partially achieved, as small variations in salt concentration induce

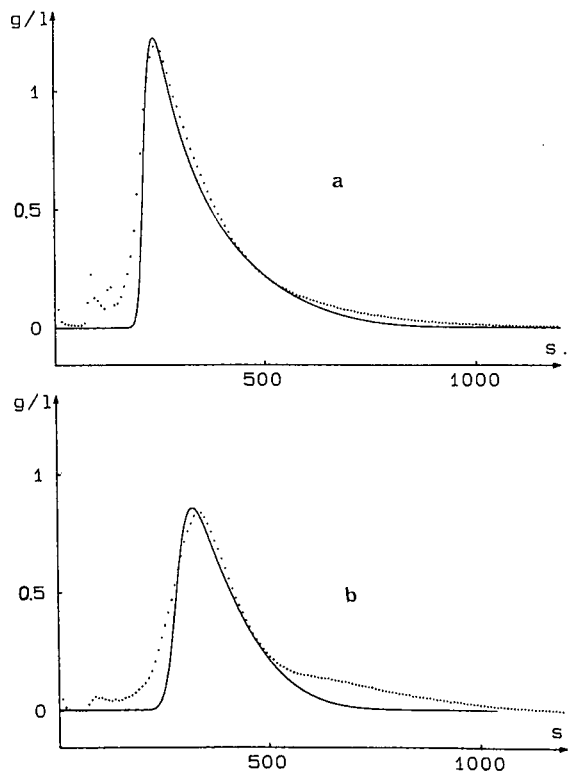


Fig. 7. Comparison of non-linear effects for BSA eluted with a mono- or a divalent counter ion from a PVP-PVI anion-exchange column. Eluent, 0.020 M Tris buffer (pH 7.5); flow-rate, 1 ml/min; column length, 10 cm; $V_0 = 1.2$ ml. Dotted lines, experimental values stored by computer data acquisition; solid lines, best fit of the simulated peak. $Q_x = 5.7$ mg; $D' = 0.015$ cm²/s; $H_D = 0.22$ cm; $H_N = 0.05$ cm. (a) 80 mM NaCl, sample size 0.025 mg, $k' = 8$, $m = Z = 8$; (b) 35 mM Na₂SO₄, sample size 0.035 mg, $k' = 6.2$, $m = 8$, $Z = 4$.

large variations in the retention volume. The value of k' is 8 with sodium chloride (80 mM) and 6.2 with sodium sulphate (35 mM).

The theoretical profiles were fitted to the experimental profiles by fixing three parameters of the adsorption isotherm: k' , m and Z . The plate height measured at infinite dilution is $H = 0.27$ cm. Taking into account the contribution to the plate height due to the numerical dispersion, H_N , the H value determines the contribution of the global dispersive effects, H_D , to be used in the simulations ($H = H_D + H_N$): simulations were performed with a global dispersive coefficient $D' = 0.015$ cm²/s. As usual with protein elution in the isocratic mode [5,22], the reduced plate height is large ($H/d_p = 270$). This poor efficiency is mainly due to slow mass-transfer kinetics such as the slow adsorption-desorption chemical exchanges and the restricted diffusion of BSA into the 300-Å pores of the support used.

The maximum loading capacity for the protein, Q_x/m , is the only parameter to be calculated from the best fit to the experimental profiles observed with a monovalent (Fig. 7a) and a divalent displacing ion (Fig. 7b). The maximum loading capacity per unit volume of mobile phase used in the simulations with both counter ions is $Q_x/mV_0 = 0.59$ mg/ml.

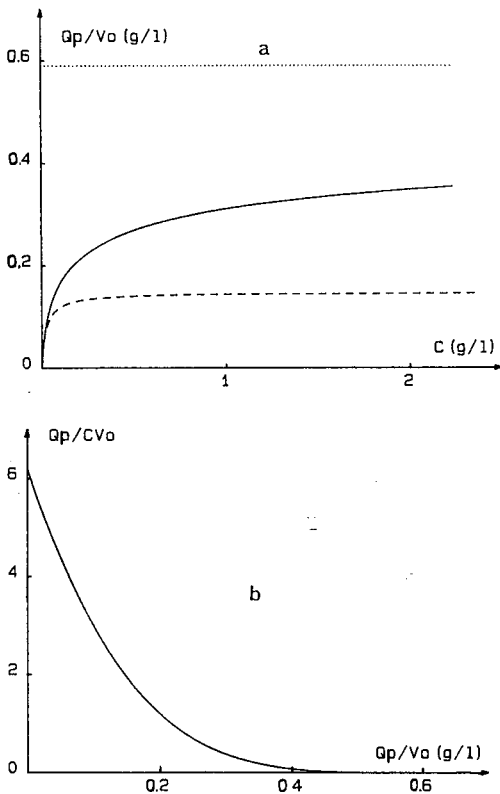


Fig. 8. Adsorption isotherm of BSA adsorbed on the PVP-PVI anion-exchange support in the presence of a divalent counter ion. Same experiment as in Fig. 7b ($k' = 6.2$; $k'' = -521$ l/g). (a) Solid line, SDM isotherm; dashed line, Langmuir isotherm; dotted line, $Q_x/mV_0 = 0.6$ mg/ml (protein loading capacity). (b) Scatchard plot corresponding to the SDM isotherm.

The experimental asymmetries determined from the ratio of half-widths measured at 20% of the peak height are 4.7 with sodium chloride (Fig. 7a) and 2.4 with sodium sulphate (Fig. 7b) in the mobile phase. The comparison of peak asymmetry may roughly be predicted by expanding $V(C)$ in first order near the origin (eqn. 30)

$$V(C) \approx V_0(1 + k' + k''C) \quad (32)$$

In the absence of dispersive effects and for small concentrations, the slope of the straight line defining the peak diffuse edge as $C = f(V)$ is equal to $1/(k''V_0)$. Therefore, a comparison of the asymmetries of the peaks in Fig. 7a and b could approximately be calculated from the ratio of these slopes, which for the present example is 3.3. This value is larger than the experimental value (2), which was determined from the ratio of the asymmetries measured at 20% of the peak maximum. The theoretical ratio would correspond to asymmetries measured near the baseline, but peak width determinations too close to the baseline would interfere with impurities. The comparison of the experimental asymmetries of BSA eluted with sodium chloride or sodium sulphate in the buffer is in good agreement with theory, which predicts an increase in peak tailing for mass-overload conditions when a monovalent ion is used as a displacer.

Fig. 8a shows the adsorption isotherm of BSA on the anion-exchange polymeric stationary phase in the presence of 35 mM sodium sulphate. The simulations in Fig. 7b were performed on the basis of this isotherm, with $m = 8$ and $Z = 4$. For comparison, the Langmuir isotherm (dotted line) with the same slope and curvature at the origin is given. Its protein maximum capacity is 32 times lower than that for the SDM isotherm, illustrated in Fig. 8a by a dotted line parallel to the concentration axis. Therefore, a Langmuir isotherm cannot be used to describe at the same time the adsorption behaviours at low and high protein concentrations in the solvent: the low concentration range determines the slope of the isotherm at the origin of the capacity factor. At high concentrations, the maximum loading capacity is reached very progressively in the case of an SDM isotherm with a large Z exponent and this is related to the overload effects observed in chromatography.

Fitting a Langmuir or a sum of two Langmuir isotherms to the experimental data for proteins adsorbed on an ion exchanger may lead to erroneous conclusions, as shown from the Scatchard plot in Fig. 8b. From this plot, one may conclude that the support is heterogeneous with adsorption on two different kinds of sites. The corresponding model, a sum of two Langmuir isotherms, is of course a wrong interpretation: the isotherm is of the SDM type (eqn. 9) and an exponent Z different from unity is responsible of the curvature of the Scatchard plot.

CONCLUSIONS

This study has shown that the rigorous isotherm derived from the law of mass action should be used to analyse the experimental adsorption data by an ion-exchange mechanism. For experiments determining directly the amount adsorbed as a function of concentration, such as frontal elution, the Scatchard plot may lead to the misinterpretation of results such as the existence of two kinds of sites. In contrast, a plot of $(Q_P/CV_0)^{1/Z}$ vs. Q_P should be used, the exponent Z being determined independently with the SDM model, extrapolated to zero surface coverage (eqn. 31).

Similarly, the parameter Z and the charge of the protein determined at infinite dilution should be introduced into the SDM isotherm equation to analyse or simulate non-linear effects in zonal elution on an ion-exchange support. This approach was used in this work and led to the prediction that peak tailing due to column overloading may be reduced by using a counter ion of higher valency. This conclusion may be useful for optimizing separations in preparative chromatography.

The theoretical results are in good agreement with experiments to analyse the non-linear elution behaviour of BSA on an anion exchanger. The above conclusions are not necessarily valid with other experimental systems, however: a pure ion-exchange mechanism is not often encountered in practice. Although the SDM theory predicts well the HPIEC retentions of many proteins at infinite dilution in most instances, it does not describe the elution behaviours of proteins at finite solute concentrations, because the model does not account for hydrophobic or self-association effects.

The multivalent ion-exchange theory is a first step in studying the adsorption mechanism of proteins on ion-exchange supports. It gives a simple tool for understanding the nature of the protein adsorption behaviour: a comparison of the elution profiles predicted on the basis of the SDM theory and the experimental profiles will give information about the nature of the adsorption process.

We are still far from a reliable explanation of all the characteristics of HPIEC and further investigations are necessary. The following aspects of the properties of HPIEC should be taken into account:

- the association–dissociation equilibria between protein molecules in both bulk and surface phases;

- the non-homogeneous character of the charge distribution both on the support surface and on the biopolymer molecule;

- the three dimensional structure of the protein, which may be changed during the binding process, and also the changes in the number of sites occupied by one biopolymer molecule, which means that the change in the value of m as a function of concentration must be considered;

- irreversible adsorption and the presence of pores of various sizes and shapes;

and

- the modification of the support charge characterized by the adsorption–desorption of protein.

These are only a few features which should be considered in subsequent models to account for the complexity of HPIEC phenomena. Finally, the generalization to the multi-component case could be useful for optimizing the experimental conditions for the separation of proteins by preparative HPIEC.

ACKNOWLEDGEMENT

We gratefully thank the University of Paris-Val de Marne for the financial support, which allowed P.C. to collaborate with the CNRS Laboratory in Thiais.

REFERENCES

- 1 M. A. Rounds and F. E. Regnier, *J. Chromatogr.*, 283 (1984) 37.
- 2 W. Kopaciewicz, M. A. Rounds, J. Fausnaugh and F. E. Regnier, *J. Chromatogr.*, 266 (1983) 3.
- 3 R. R. Drager and F. E. Regnier, *J. Chromatogr.*, 359 (1986) 147.
- 4 A. Velayudhan and Cs. Horváth, *J. Chromatogr.*, 367 (1986) 160.
- 5 M. T. W. Hearn, A. N. Hodder and M. I. Aguilar, *J. Chromatogr.*, 443 (1987) 97.
- 6 M. T. W. Hearn, A. N. Hodder and M. I. Aguilar, *J. Chromatogr.*, 458 (1988) 45.
- 7 W. R. Melander, Z. El Rassi and Cs. Horváth, *J. Chromatogr.*, 469 (1989) 3.
- 8 A. Velayudhan and Cs. Horváth, *J. Chromatogr.*, 443 (1988) 13.
- 9 R. D. Whitley, R. Wachter, F. Liu and N. H. L. Wang, *J. Chromatogr.*, 465 (1989) 137.
- 10 R. D. Whitley, J. M. Brown, N. P. Karajgikar and N. H. L. Wang, *J. Chromatogr.*, 483 (1989) 263.
- 11 A. Jaulmes, C. Vidal-Madjar, H. Colin and G. Guiochon, *J. Phys. Chem.*, 90 (1986) 207.
- 12 F. E. Regnier and I. Mazsaroff, *Biotechnol. Prog.*, 3 (1987) 22.
- 13 F. D. Antia and Cs. Horváth, *J. Chromatogr.*, 484 (1989) 1.
- 14 L. R. Snyder, G. B. Cox and P. E. Antle, *J. Chromatogr.*, 444 (1988) 303.
- 15 G. B. Cox, P. E. Antle and L. R. Snyder, *J. Chromatogr.*, 444 (1988) 325.
- 16 H. P. Jennissen, *Biochemistry*, 15 (1976) 5683.
- 17 A. Jaulmes and C. Vidal-Madjar, *Anal. Chem.*, 63 (1991) 1165.
- 18 J. A. Jönsson and P. Lövkqvist, *J. Chromatogr.*, 408 (1987) 1.
- 19 M. W. Phillips, G. Subramanian and S. M. Cramer, *J. Chromatogr.*, 454 (1988) 1.
- 20 B. Lin, Z. Ma, S. Golshan-Shirazi and G. Guiochon, *J. Chromatogr.*, 500 (1990) 185.
- 21 B. Sébille, J. Piquion and B. Boussouira, *Eur. Pat. Appl.*, EP225829, 1987.
- 22 R. Lemque, C. Vidal-Madjar, M. Racine, J. Piquion and B. Sébille, *J. Chromatogr.*, 553 (1991) in press.
- 23 M. Czok and G. Guiochon, *Anal. Chem.*, 62 (1990) 189.
- 24 J. F. K. Huber and R. G. Gerritse, *J. Chromatogr.*, 58 (1971) 137.
- 25 R. W. Stout, S. I. Sivakoff, R. D. Ricker and L. R. Snyder, *J. Chromatogr.*, 353 (1986) 439.

CHROMSYMP. 2356

Application of the split-peak effect to study the adsorption kinetics of human serum albumin on a reversed-phase support

CLAIRE VIDAL-MADJAR*, HÉLÈNE PLACE, LAHOUSSINE BOULKANZ and ALAIN JAULMES

Laboratoire de Physico-Chimie des Biopolymères, CNRS, Université Paris Val de Marne, UM 27, 2 Rue Henry Dunant, 94320 Thiais (France)

ABSTRACT

The adsorption step of human serum albumin on a reversed-phase support was analyzed by studying the "split-peak" effect in mass-overload conditions. This behavior is characterized by the occurrence of a first non-retained fraction and is described by an analytical expression in the case of a Langmuirian adsorption isotherm. The method was applied to determine the column loading capacity, the number of mass-transfer units and the apparent adsorption rate constant measured at a given flow-rate.

The nature of the organic modifier influences the split-peak effect: it increases with the eluotropic strength of the organic solvent added to the buffer. Compared to the results with pure buffer, it is the association of two effects, the decrease of the column loading capacity and that of the apparent adsorption rate constant, which increases the split-peak effects observed when methanol and 2-propanol are added to the eluent. These results allow us to gain a better understanding of the role of the organic solvent in the elution behavior of proteins in reversed-phase high-performance liquid chromatography.

INTRODUCTION

Reversed-phase high-performance liquid chromatography (RP-HPLC) is widely used for separating proteins and peptides. A stoichiometric displacement model [1] was developed that accounts for protein elution and the importance of the role of the organic solvent was demonstrated.

However, some behaviors are not always well understood: for example, two or more peaks are sometimes observed from a single species [2], their occurrence and shape depending on mobile phase gradient conditions and column temperature. To describe the mechanism, two steps were suggested [3]: the first one is related to the adsorption kinetics of the protein, while the other one concerns all further conformational events occurring on the surface until elution.

Until now, kinetic studies have mainly focused on the conformational changes of the protein occurring after adsorption on the surface. However, examination of the first adsorption kinetic step is important for a better understanding of the elution behavior of proteins in RP-HPLC. Since slow adsorption kinetics are related to the

split-peak effect [4,5], a possible approach is to investigate the occurrence of a non-retained peak in isocratic elution. Adsorption kinetics are usually analyzed from breakthrough curves or elution peak shapes [6], but the study of the split-peak phenomenon remains close to the conditions used in analytical chromatography.

The split-peak effect was first described theoretically many years ago by Giddings and Eyring [7], but was revealed experimentally for the HPLC of proteins due to their slow adsorption kinetics and because of the short columns and high flow-rates used. Nevertheless, the potentialities of the method were not fully exploited because kinetic measurements were limited to the linear range [4,5].

We described a kinetic model for irreversible adsorption [8], one which predicts the occurrence of the elution peak splitting in mass-overload conditions and irreversible adsorption: a solute fraction elutes at the void volume while the other one is irreversibly retained in the column. The unretained fraction increases with the sample size and an analytical expression relates this fraction to the number of mass-transfer units and to the column loading capacity.

On the basis of this model, the goal of the present work is to analyze the kinetic adsorption step of human serum albumin (HSA) on a reversed-phase support in the presence of various organic solvents in the mobile phase. In a preceding paper [9] we have studied the influence of increasing concentrations of acetonitrile on the split-peak effect. An important decrease in the number of transfer units characterizing the adsorption kinetic process was observed when increasing amounts of acetonitrile were added to the eluent. A similar trend was observed when other organic modifiers were used. In this paper we shall study the influence of the nature of solvents with an hydroxyl group (methanol and 2-propanol). Since these solvents are often used to elute peptides or proteins on reversed-phase supports, this approach is useful in order to understand better the role of the organic modifier in the RP-HPLC of proteins.

THEORY

The adsorption kinetic model starts from the differential equation describing the solute migration through the column:

$$\frac{\partial C}{\partial t} + u \cdot \frac{\partial C}{\partial z} + \frac{1}{V_0} \cdot \frac{\partial Q}{\partial t} = D' \cdot \frac{\partial^2 C}{\partial z^2} \quad (1)$$

and the second order Langmuir kinetic law:

$$\frac{\partial Q}{\partial t} = k_a C(Q_x - Q) - k_d Q \quad (2)$$

where C is the concentration of solute in the mobile phase, z the abscissa in the column length, t the time and u the mobile phase velocity. Q is the amount of adsorbed solute, Q_x the maximum loading capacity and V_0 the mobile phase volume. D' is a global dispersion coefficient accounting for axial and eddy diffusion; k_a and k_d are the adsorption and desorption rate constants. The equilibrium constant is $K = k_a/k_d$.

Solutions of the above system of differential equations exist for the ideal case

($D' = 0$) and the analytical expressions depend on the boundary conditions: breakthrough curves in frontal elution [10] or peak profiles with a finite pulse injection [11] or a Dirac injection function [12].

As shown by Goldstein [11], the solution for a rectangular injection of time duration t_i and solute concentration C_i , is given by two separate expressions according to the time elapsed after the time t_0 necessary to elute a non-retained compound. The concentration at the column outlet is given by the ratio:

$$C = C_i P/E \quad (4)$$

For $t > t_0 + t_i$, P and E are given by:

$$P = J(nr, nT) - J(nr, nT - nT_i) \quad (5a)$$

$$E = J(nr, nT) - J(nr, nT - nT_i) + [1 - J(n, rnT)] \cdot \exp[(1 - r)(n - nT)] + \\ + J(n, rnT - rnT_i) \cdot \exp[(1 - r)(n - nT + nT_i)] \quad (5b)$$

For $t < t_0 + t_i$, P and E are given by

$$P = J(nr, \alpha T) \quad (6a)$$

$$E = J(nr, \alpha T) + [1 - J(n, r\alpha T)] \cdot \exp[(1 - r)(n - nT)] \quad (6b)$$

where the J function is given by:

$$J(x, y) = 1 - e^{-y} \int_0^x I_0(2\sqrt{\tau y}) \cdot e^{-\tau} d\tau \quad (7)$$

where I_0 is the Bessel function of zeroth order and

$$n = \frac{Q_x k_a}{\delta} \quad (8)$$

$$r = \frac{1}{1 + KC_i} \quad (9)$$

$$T = (t - t_0) \cdot \frac{\delta}{KQ_x r} \quad T_i = t_i \cdot \frac{\delta}{KQ_x r} \quad (10)$$

Q_x is the column loading capacity and δ is the flow-rate. The parameter n is the number of transfer units characteristic of the adsorptive exchange. It is related to the plate height kinetic contribution [13] according to:

$$H_K = \frac{2Lk'^2}{n(1 + k')^2} \quad (11)$$

where L is the column length and k' is the solute capacity factor at infinite dilution ($k' = KQ_x/V_0$).

The split-peak effect is characterized from the ratio of the non-retained amount on the amount injected ($Q_i = C_i\delta$). The amount eluted as a first peak is given by integrating the elution peak expression for $t < t_i$ (eqns. 4 and 6).

In the case of irreversible adsorption ($k_d = 0$) and in the absence of dispersive effects ($D' = 0$), we have shown in a previous paper [8] that this ratio f is given by the expression:

$$f = \frac{Q_x}{nQ_i} \text{Ln}[1 + (e^{nQ_i/Q_x} - 1)e^{-n}] \quad (12)$$

When f is extrapolated to zero amount injected, the unretained fraction is f_0 :

$$f_0 = e^{-n} = e^{-k_x Q_x/\delta} \quad (13)$$

The limit of eqn. 12 for zero flow-rate is the trivial expression of f : $f_\infty = 1 - Q_x/Q_i$, for $Q_i > Q_x$, and $f_\infty = 0$ for $Q_i < Q_x$.

A simulation algorithm was used [8] to solve numerically the set of differential eqns. 1 and 2. It is based on a numerical step procedure and describes the solute migration through the column accounting for adsorption kinetic effects in mass-overload conditions and for solute dispersion in the mobile phase. The simulations of the chromatographic process in non-linear elution have shown that the split-peak expression given by eqn. 12, can still be applied in the presence of dispersive effects and does not depend on the shape of the injection signal.

The parameters of eqn. 12, namely the number of mass-transfer units n and the maximum loading capacity Q_x , were determined by fitting the model to the variations of f as a function of sample size. Instead of desorbing the adsorbed protein by using another eluent after every injection, we determined the experimental variation of f as a function of the cumulated amounts injected: the validity of the method was previously demonstrated from numerical simulations [8]. The non-linear regression was performed with a Fortran program that uses the partial derivatives *versus* n and Q_x in eqn. 12 to converge to the best fit parameters.

MATERIALS AND METHODS

The chromatographic experiments were performed on an HPLC system: a pump (2150; LKB, Bromma, Sweden), a sample injector (7125; Rheodyne, Berkeley, CA, USA) with a 20- μ l loop and a UV detector (Spectra-100; Spectra-Physics, San Jose, CA, USA), set at 280 nm.

The reversed-phase support (Spherisorb RP-C₆) of particle diameter 10 μ m, pore size 80 Å and specific surface area 220 m²/g, was packed into 50 × 4.6 mm stainless-steel columns, kindly supplied by S.F.C.C.-Shandon (Eragny sur Oise, France). The temperature of the column and that of the eluent was kept constant within 0.1°C using a thermostated-cryostated water-bath.

The mobile phase was a 0.067-M potassium phosphate buffer at pH 7.4 modified

with organic solvents, HPLC grade: acetonitrile, methanol and 2-propanol. The HSA samples (Sigma, A1887, St. Louis, MO, USA) were dissolved in the same eluent as that used for the mobile phase.

The data acquisition of the chromatographic signal was performed with a micro-computer (Apple IIe, Cupertino, CA, USA) equipped with a 12-bit analog-to-digital converter, and an instrumentation amplifier (Analog Devices, Norwood, MA, USA). The speed for data acquisition was selected so as to obtain a minimum of fifteen data per peak width and peak integrations were performed with the same computer. An integrator with a sampling rate high enough to define the width of the non-retained peak, can be used as well for peak area measurements.

RESULTS

Split-peak effect

Adsorption kinetics are revealed when a part of the solute injected is eluted as the first peak at the column void volume (0.4 ml) while the other part is irreversibly adsorbed on the support. As shown in Fig. 1, with an eluent containing 40% methanol, the successive injections of HSA (0.08 mg) lead to increasing amounts of the non-retained fraction. The saturation of the column is reached when the protein is totally eluted as the first peak.

The increase of the unretained fraction is related to the maximum loading capacity and to the rate of adsorption of the protein. The pattern of Fig. 1 changes with the nature of the eluent and more generally with the experimental conditions used. For example, Fig. 2 shows that the split-peak behavior increases when the same experiment is carried out at a lower temperature. With 20% acetonitrile [9] or 2-propanol in the buffer, the appearance of the first peak can already be noticed at the first injections. In

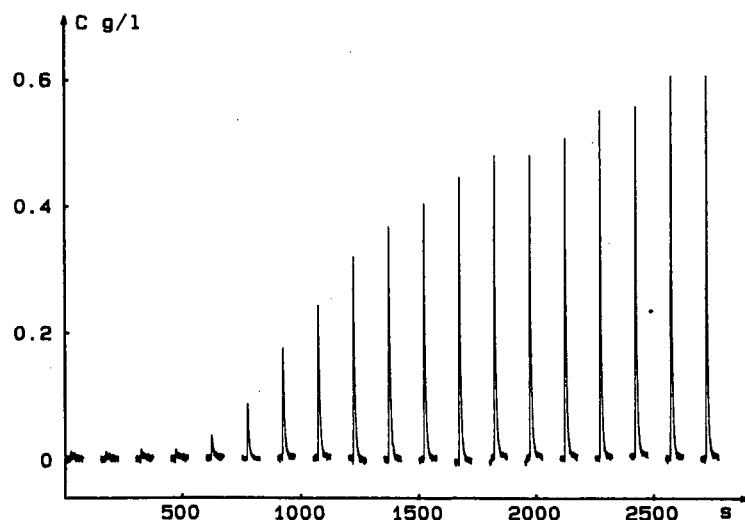


Fig. 1. Successive injections of HSA on a reversed-phase support at 20°C. Eluent: 0.067 M phosphate buffer pH 7.4 + 40% methanol. HSA sample size: 80 μ g; $L = 5$ cm; $V_0 = 0.4$ ml; $\delta = 1$ ml/min.

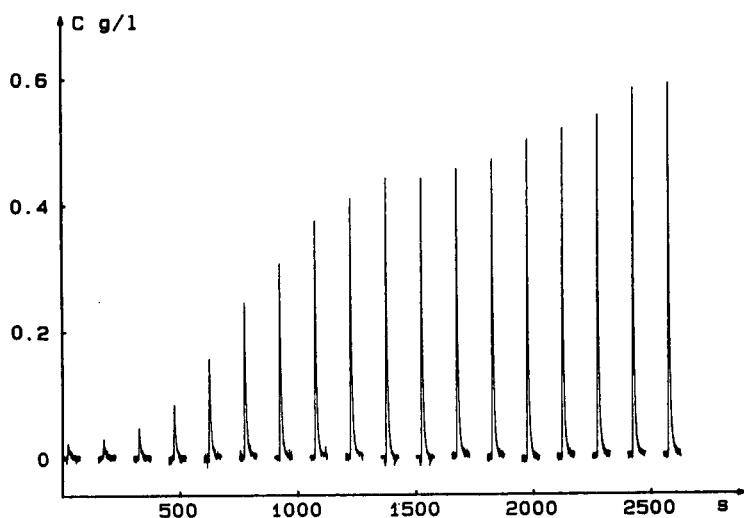


Fig. 2. Successive injections of HSA on a reversed-phase support at 10°C. Same experimental conditions as in Fig. 1.

contrast, with pure buffer or with solutions of methanol in the buffer, the occurrence of the first peak is observed only when the total amount injected is close to the saturation value.

HSA is desorbed with 40% acetonitrile after every experiment. The method permits the regeneration of the column for another split-peak study. However, reproducible experiments are only achieved when a first HSA adsorption had saturated the most active sites of the surface because the washing step with 40% acetonitrile does not permit the regeneration of high-affinity sites. The experiments are therefore performed on a surface which is not uniform, since some HSA still remains adsorbed on the surface. This is not a serious drawback with HSA, because protein-protein interactions are negligible: HSA is not retained on a column packed with a diol-support where the protein is covalently bound [14].

The amounts of non-retained solute are calculated from peak areas after calibration of the detector. The ratio of the cumulated unretained amounts to the total amounts injected gives the fraction f of unretained solute. The plot of $1/f$ as a function of the sample size provides a good display when split-peak effects are small, since important variations are observed at low f ratio before reaching the asymptotic value of 1 at large sample sizes.

The influence of the nature of the organic solvent on the split-peak effect is illustrated by the plot $1/f$ versus Q_i at 20°C (Fig. 3): at low sample sizes an important splitting of the HSA elution peak is observed with 20% 2-propanol (f_0 ca. 0.5). In contrast, with 40% methanol or with pure buffer, one can only observe the split-peak effect if the total amount injected is close to the column capacity. An important increase of the split-peak effect is observed at 10°C, by adding methanol to the eluent (Fig. 4).

As previously noticed when acetonitrile was used as a modifier [9], the split-peak

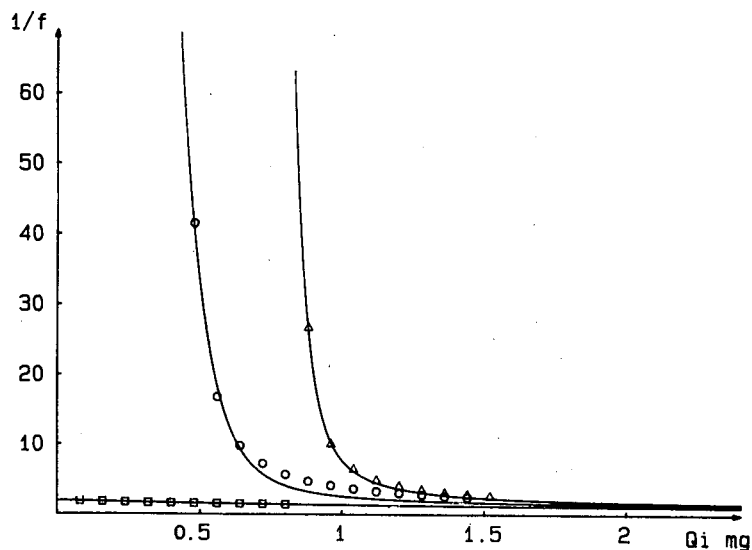


Fig. 3. Variation of the non-retained fraction f with the amount of HSA injected at 20°C. Eluent: 0.067 M phosphate buffer + organic solvent. — = Best fit of the theoretical model (eqn. 12). Δ = Buffer; \circ = buffer + 40% methanol; \square = buffer + 20% isopropanol. HSA sample size: 80 μg ; $L = 5$ cm; $V_0 = 0.4$ ml; $\delta = 1$ ml/min.

effect increases with the amount of organic modifier added. This effect is more important with 2-propanol than with methanol. In the latter case 40% of organic modifier were necessary to observe a split-peak effect that differs significantly from that of the pure buffer. For this study we selected the concentration of the organic solvent added in a range which was convenient to study the split-peak effect.

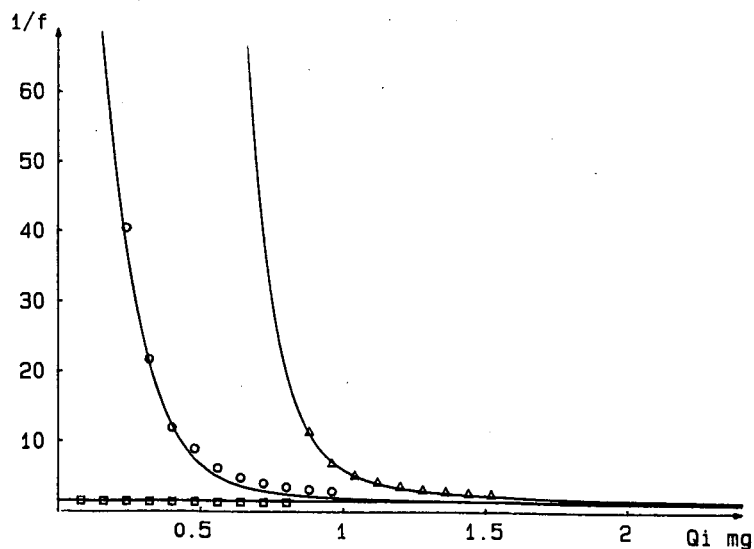


Fig. 4. Variation of the non-retained fraction f with the amount of HSA injected at 10°C. Same conditions as in Fig. 3.

TABLE I
KINETIC MEASUREMENTS FROM THE SPLIT-PEAK EFFECT

Eluent	Temperature (°C)	δ (ml/min)	n	Q_x/V_0 (g/l)	k_a ($l\ g^{-1}s^{-1}$)	t_0/n (s)	f_0 (%)
Buffer	10	1.0	10.0 ± 0.5	2.00 ± 0.05	0.20 ± 0.02	2.5	$4.5 \cdot 10^{-3}$
	20	0.5	14.0 ± 0.5	1.90 ± 0.05	0.15 ± 0.01	3.6	$8.3 \cdot 10^{-5}$
	20	1.0	21.0 ± 0.5	2.05 ± 0.05	0.41 ± 0.01	1.2	$7.6 \cdot 10^{-8}$
	20	1.5	14.0 ± 0.5	1.90 ± 0.02	0.43 ± 0.02	1.2	$8.3 \cdot 10^{-5}$
Methanol (40%) in buffer	10	1.0	5.2 ± 0.1	1.2 ± 0.1	0.17 ± 0.02	4.6	0.55
	20	0.5	5.8 ± 0.1	1.4 ± 0.05	0.08 ± 0.01	8.7	0.30
	20	1.0	8.3 ± 0.2	1.5 ± 0.05	0.22 ± 0.02	3.0	0.025
	20	1.5	6.6 ± 0.2	1.2 ± 0.05	0.33 ± 0.03	2.5	0.14
	20	1.75	6.4 ± 0.1	1.3 ± 0.05	0.34 ± 0.03	2.3	0.17
2-Propanol (20%) in buffer	10	1.0	0.47 ± 0.01	0.65 ± 0.05	0.030 ± 0.005	54	62.5
	20	0.5	0.85 ± 0.05	0.60 ± 0.05	0.030 ± 0.005	59	42.7
	20	1.0	0.65 ± 0.05	0.80 ± 0.1	0.035 ± 0.005	38	52.2
	20	1.5	0.66 ± 0.01	0.80 ± 0.1	0.049 ± 0.005	25	51.7

Kinetic measurements

Table I gives the values of the parameters n and Q_x determined from the least-square fit of eqn. 12 to experimental data. The errors on the estimated parameters for a 95%-confidence interval are given. The precision of the measurements depends on the value of the unretained fraction at infinite dilution (f_0). To visualize the time for protein adsorption the quantities $V_0/n \cdot \delta = t_0/n$ are listed in the same table: t_0/n is the simplified expression of the adsorption rate constant for a first-order kinetic mechanism. Fig. 3 and 4 show that good agreement is obtained between the theoretical model (full line) and the experimental data.

The precision on the Q_x determination is good (*ca.* 5%) when the kinetics of HSA adsorption are fast as with pure buffer or buffer plus methanol ($n > 3$): steep curves are observed, converging to the saturation value. The precision on the n determination is between 2 and 5%, but the optimal range for achieving kinetic measurements, is between 1 and 50%.

The variations of the unretained fraction with the sample size were studied at different flow-rates. Some dispersions in the maximum loading capacity determination are due to the poor reproducibility of the surface available for adsorption after every column regeneration. As with the theoretical plate height, the reciprocal of the number of transfer units increases with flow-rate. According to eqn. 8 a plot of $1/n$ versus δ should intercept the origin. This is not the case since a significant increase of k_a calculated from the n and Q_x values (eqn. 8) is observed with increasing flow-rates (Table I).

DISCUSSION

The split-peak model for mass-overload conditions is based on several assumptions: the irreversibility of the adsorption process, a Langmuir-type adsorption

isotherm, and no diffusion in the pores or in the stagnant mobile phase volume. It can therefore be applied to analyze experiments if these criteria are fulfilled.

The irreversibility of the adsorption process is shown from the absence of tailing in the shape of the non-retained peak: Giddings and Eyring [7] have shown that slow desorption originates important tailings: their expression is given by the product of a Bessel function and an exponential one decreasing with time. Moreover, no base-line drift was observed even at higher UV detector sensitivities.

The adsorption isotherm can not be determined in the case of irreversible adsorption (infinite Henry adsorption constant), but the adsorption of HSA was often found to be of the Langmuirian type and the maximum loading capacity was used to determine the surface available for protein adsorption.

The model does not account for the diffusion in the pores but the choice of an 80-Å support allows us to assume that HSA is mainly adsorbed on the external surface of the particles. Schmidt *et al.* [15] have shown that albumin is almost totally excluded from a 100-Å LiChrosorb diol-support. Moreover, as discussed in a previous paper [9], the maximum loading capacity in pure buffer corresponds to the adsorption of HSA as a monolayer on the external surface of the particles. The capacity of the support measured in the presence of methanol or 2-propanol in the buffer is even lower and this is in good agreement with the assumption that there is no diffusion of the protein into the pores.

The kinetic model accounts for the dispersion effects but not for the mass-transfer at the particle boundary or in the stagnant fluid between the particles [16]. Its importance is considerable since a variation of k_a calculated from n and Q_x values was observed with flow-rate (Table I). The experiments were performed only for a limited range of flow-rates but a general trend was observed within experimental errors: a decrease of k_a with increasing mobile phase velocities with an asymptotic value reached at the larger flow-rates studied. The important increase in k_a at low flow-rates reveals the contribution of diffusion in the stagnant fluid film. Therefore the adsorption rate constants measured in this work are not simply the rate constants for the adsorption chemical step, but must also be considered as apparent ones for the adsorption on the whole system particle plus the boundary layer.

The approach used in this work for measuring adsorption kinetics is similar to that used by Chase [6] to analyze frontal experiments, on the basis of Thomas' solution [10]: because of the difficulties in considering kinetic models based on a rigorous approach, the adsorption process is described by an apparent adsorption rate constant k_a , which is experimentally measurable and enables us to make a comparison between the various systems studied.

The split-peak effect is characterized by the f_0 value (Table I). When the splitting is important as with 2-propanol, the limiting value of f for infinite dilution, f_0 , and therefore the number of mass-transfer units n , can be determined by extrapolation from the plot of f versus Q_i ; but, in the case of fast adsorption kinetics or low split-peak effects, as with pure buffer or buffer modified with methanol ($f_0 < 0.01$), the model must be fitted to the experimental data in order to determine n .

The association of two effects, namely the lower adsorption rate constant and the lower loading capacity, is responsible for the increase in the split-peak observed in the presence of an organic solvent (Table I). Compared to the results with pure buffer, adsorption kinetics are roughly twice as slow with 40% methanol in the buffer and

twenty times as slow with 2-propanol. This may be related to a decrease of the interfacial energy in the presence of an organic modifier. Van Oss [17] has shown that the electron-acceptor parameter of the solvent and its decrease with additions of the organic modifier should explain the retention behaviors of proteins in reversed-phase liquid chromatography.

The slower kinetics observed with an organic solvent in the buffer may also be due to a restricted diffusion in the stationary-phase layer formed by the solvation of the alkyl chains of the reversed-phase support [18]. The lower capacities for HSA adsorption observed in the presence of organic modifiers can not be explained by the displacement retention model of proteins in RP-HPLC [1]. This could be due to an alteration of the native conformation of the protein in the presence of an organic solvent or to the restricted diffusion in the stationary-phase layer that prevents HSA from adsorption on the whole available surface.

With all the solvents studied and for a given flow-rate of 1 ml/min, the number of transfer units and therefore the k_a values measured at 10°C are smaller than those measured at 20°C (Table I). This is in good agreement with the usual kinetic variations with temperature.

The variations of the split-peak effect with sample size are related to the loading capacity of HSA. We did not study the split-peak effects with other proteins, but this variation will only be observed if the saturation of the support is achieved. This is not the case with all proteins because of possible self-association. Moreover, this type of study is easier with columns of low capacity.

CONCLUSIONS

The ability of the model to predict the occurrence of the split-peak phenomenon is satisfactory: its importance increases with increasing flow-rates, lower loading capacities or slower adsorption kinetics. HSA adsorption on the reversed-phase support is highly dependent of the nature of the eluent. The apparent adsorption rate constants are of the same order of magnitude with pure buffer as with a buffer modified with methanol. Slower adsorption kinetics are found with an eluent containing 2-propanol.

Because of the dispersion of the experimental measurements as a function of flow-rate, it is not possible to distinguish between kinetic mass transfers due to chemical adsorptive exchange and those due to diffusion in a stagnant fluid, but the determination of the apparent adsorption rate at a given flow-rate is useful in order to gain a better understanding of the role of the solvent in the first adsorption step of proteins.

Kinetic studies can be carried out by frontal elution but the split-peak method presents several advantages: experiments are quick, easy to perform, and are more precise because they are based on peak area measurements and not on the analysis of band broadenings, where dispersive effects may interfere. The amount of solute required is small, since the loading capacity can be determined from several injections and complete column saturation is not necessary. The method is however limited to adsorption studies on low capacity supports such as non-porous ones or those with pores small enough to exclude the protein. Moreover, as with the frontal technique, the analysis of the experimental data is based on a model assuming a Langmuir kinetic law

and this limits the applicability of the method to systems with a Langmuirian adsorption isotherm.

REFERENCES

- 1 X. Geng and F. E. Regnier, *J. Chromatogr.*, 296 (1984) 15.
- 2 K. Benedek, S. Dong and B. L. Karger, *J. Chromatogr.*, 317 (1984) 227.
- 3 K. Benedek, *J. Chromatogr.*, 458 (1988) 93.
- 4 D. S. Hage, R. R. Walters and H. W. Hethcote, *Anal. Chem.*, 58 (1986) 274.
- 5 L. A. Larew and R. R. Walters, *Anal. Biochem.*, 164 (1987) 537.
- 6 A. Jaulmes and C. Vidal-Madjar, *Adv. Chromatogr.*, 28 (1989) 1.
- 7 J. C. Giddings and H. Eyring, *J. Phys. Chem.*, 59 (1955) 416.
- 8 A. Jaulmes and C. Vidal-Madjar, *Anal. Chem.*, 63 (1991) 1165.
- 9 H. Place, B. Sébille and C. Vidal-Madjar, *Anal. Chem.*, in press.
- 10 H. Thomas, *J. Am. Chem. Soc.*, 66 (1944) 1664.
- 11 S. Goldstein, *Proc. Royal Soc. London, Ser. A*, 219 (1953) 151.
- 12 J. L. Wade, A. F. Bergold and P. W. Carr, *Anal. Chem.*, 59 (1987) 1286.
- 13 C. Horvath and H. J. Lin, *J. Chromatogr.*, 149 (1978) 43.
- 14 C. Vidal-Madjar, A. Jaulmes, M. Racine and B. Sébille, *J. Chromatogr.*, 458 (1988) 13.
- 15 D. E. Schmidt, R. W. Giese, D. Conron and B. L. Karger, *Anal. Chem.*, 52 (1980) 177.
- 16 Cs. Horváth and H. J. Lin, *J. Chromatogr.*, 126 (1976) 401.
- 17 C. J. van Oss, *Isr. J. Chem.*, 30 (1990) 251.
- 18 C. A. Lucy, J. L. Wade and P. W. Carr, *J. Chromatogr.*, 484 (1989) 61.

CHROMSYMP. 2310

Solution properties of polyelectrolytes

VII^a. Non-ideal mechanisms in size-exclusion chromatography of synthetic polyions, peptides and proteins

ENRIQUE PEREZ-PAYA, LORENZO BRACO and CONCEPCION ABAD*

Departamento de Bioquímica y Biología Molecular, Universidad de Valencia, Burjassot, E-46100 Valencia (Spain)

and

VICENTE SORIA and AGUSTIN CAMPOS

Departamento de Química Física, Universidad de Valencia, Burjassot, E-46100 Valencia (Spain)

ABSTRACT

Chromatographic data for sodium polystyrene sulphonate were obtained on both silica- and polymer-based size-exclusion supports using mobile phases of various pH and ionic strength. Deviations of the elution volume were observed towards both lower and higher values relative to the reference calibration graph obtained with uncharged standards. An empirical correlation is proposed in order to account for all the secondary effects observed. The general applicability of this correlation was further tested for chromatographic data obtained for a series of peptides and proteins on a silica-based support under very different eluent conditions. Deviations from ideal elution behaviour such as ion-exclusion and hydrophobic effects were analysed in the light of this approach.

INTRODUCTION

High-performance aqueous size-exclusion chromatography (HPASEC) has attracted increasing attention in recent years because of the possibilities it offers both in basic biochemistry and for biotechnological applications. It has proved to be a powerful tool in the separation of biopolymers (peptides, proteins, polynucleotides, etc.) [1] and macromolecular assemblies (viral particles, liposomes, etc.) [2,3] using typically mild, non-aggressive mobile phase conditions which preserve the native structure and functionality of the solute. However, considerable experimental evidence has shown that the elution mechanism of most biopolymers on HPASEC supports deviates from a pure size-exclusion mechanism, mainly owing to a number of secondary effects, including ion exclusion and ion exchange, hydrophobic interaction and hydrogen bonding, originating from specific solute-matrix interactions [4].

* For Part VI, see ref. 14.

Although these effects have turned out to be advantageous in some instances and have been exploited to improve the separation of macromolecules of similar hydrodynamic volume, it is in general desirable to minimize (if not cancel) them, particularly for characterization purposes. Considerable efforts have been made in this direction in the last decade by both manufacturers, to design supports as inert as possible without a decrease in gel performance, and by chromatographers, to manipulate the mobile phase conditions rationally to any given separation. At the same time, different theoretical approaches have been elaborated attempting to quantitate the aforementioned secondary effects. At present, however, it seems that the total suppression of these effects has not yet been achieved and that there is no theory capable of predicting them in a completely satisfactory manner, especially for biological macromolecules, characterized by widely differing geometry and spatial configuration, surface topology and charge distribution. For this reason, most attempts to account for secondary effects are based on experimental evidence obtained on packing materials of very different nature with model charged macromolecules, *e.g.*, linear polyelectrolytes such as sodium polystyrene sulphonate (NaPSS) or poly(sodium acrylate).

Dubin and co-workers [5–7] proposed a model to predict ion-exclusion effect based on the reduction in the pore volume accessible for polyions, calculating a repulsion volume as a function of an electrostatic potential of the stationary phase. The same group also recently proposed [8] the use of a hydrophobicity index related to the hydrophobic effect. Mori [9] established an empirical correlation between the repulsion volume and eluent ionic strength. Other attempts have been made to obtain a parameter representative of the size and shape of a biopolymer (or macromolecular assembly). Thus, the product $M[\eta]$, where M and $[\eta]$ are the macromolecule molecular weight and intrinsic viscosity, respectively, and a number of modifications of this product [5,6,9–14] and other macromolecular dimensions representative of a variety of geometries have been suggested [15–18]. Finally, some theoretical models for ion exclusion have been presented, most of them based on the Poisson–Boltzmann equation to calculate the electrostatic interaction for a charged polymer near a charged wall [19,20].

In this paper, we propose an empirical correlation for analysing in a general manner secondary effects in the HPASEC of both model polyelectrolytes and biopolymers. This approach interprets solute–matrix attractive–repulsive interactions in terms of (bio)polymer–support compatibility, making use of a thermodynamic formalism previously developed for uncharged polymers [21,22]. In order to evaluate the general applicability of this correlation, we first analysed the chromatographic behaviour of NaPSS on silica- and polymer-based supports using different mobile phase compositions, and then the same treatment was extended to the chromatographic data reported by Irvine [23] on the elution of a series of peptides and proteins.

EXPERIMENTAL

Chemical and reagents

Dextran samples obtained from Pharmacia (Uppsala, Sweden) of molecular weight 10 000, 40 000, 83 000, 177 000 and 500 000 g mol^{-1} were used as standards for uncharged polymers. The chromatographic low-molecular-weight range was covered

using poly(ethylene oxide) (PEO) standards of molecular weight 2000 and 4000 g mol⁻¹, purchased from Fluka (Darmstadt, Germany). NaPSS samples were dialysed fractions of commercial standards from Pressure Chemical (Pittsburgh, PA, USA) of molecular weight 1600, 4000, 16 000, 31 000, 88 000, 177 000 and 354 000 g mol⁻¹ with polydispersity lower than 1.1. All reagents used in the preparation of buffers were of analytical-reagent grade from Merck (Darmstadt, Germany). High-performance liquid chromatographic grade water (Merck) was tested conductimetrically daily as reported elsewhere [13].

Viscosity

Viscosity values for uncharged polymers in pure water at 25.0°C were obtained using the following viscosimetric equations: $[\eta] = 97.8 \cdot 10^{-3} M^{0.50} \text{ ml g}^{-1}$ for dextrans [24] and $[\eta] = 2.0 + 0.016 M^{0.76} \text{ ml g}^{-1}$ for PEO [25], where M = molecular weight. The effect of ionic strength and pH on the viscosity of non-ionic polymers was neglected [6, 13, 14]. Concerning NaPSS, the intrinsic viscosities of the polyion p at finite salt (c_s) and polyion (c_p) concentrations, denoted by $[\eta]_{p,c_p,c_s}$ were calculated using a recently proposed general equation whose validity has been demonstrated for a wide range of solvent compositions, [13, 14, 26, 27].

Chromatographic measurements

The Waters Assoc. liquid chromatographic equipment used has been described elsewhere [13]. Ultrahydrogel-250 (U-250) column packed with hydroxylated polymethacrylate-based gel of 250 Å nominal pore size and a silica-based Protein I-250 column were used. The interstitial packing volume and total pore volume were 5.5 and 5.1 ml for the U-250 and 5.9 and 6.1 ml for the I-250 column, as measured with high-molecular-weight dextran and ²H₂O, respectively.

Buffers of pH 7.0 and 5.9 (phosphate) and 4.0 (acetate) were used as eluents, in all instances following degassing and filtration through regenerated cellulose 0.45-μm pore diameter filters from Micro Filtration Systems (Dublin, CA, USA).

The column was equilibrated overnight prior to starting any experiment. Polymer solutions were always prepared using the corresponding mobile phase as solvent. The volume injected was 100 μl in all instances, covering an NaPSS concentration range from 0.1 to 10 g l⁻¹. The calibration graphs for uncharged standards were obtained by extrapolation to zero concentration of peak elution volumes obtained for at least three injected concentrations.

RESULTS AND DISCUSSION

The most common approach used to analyse secondary effects in HPASEC of polyelectrolytes is based on the comparison of calibration graphs obtained under the same experimental conditions for both the polyion under study and uncharged polymers as a reference. The choice of an appropriate quantity for the hydrodynamic volume of the charged macromolecule is, however, the subject of some controversy, as has been mentioned previously [16–18]. In this work, we used for this purpose the product $M[\eta]_{p,c_p,c_s}$ as a useful representative polyelectrolyte size parameter under any experimental conditions at finite concentration of polyion and salt, c_p and c_s . We have recently reported on the chromatographic behaviour of NaPSS independently on

polymer-based [13] and silica-based [14] supports as a function of a number of chromatographic variables.

We next present a direct comparison of the elution of NaPSS on both types of supports for the same mobile phase compositions. Fig. 1 depicts the calibration graphs obtained for this polyelectrolyte on either a I-250 or a U-250 column using (A) 0.02 *M* and (B) 0.05 *M* acetate buffer (pH 4.0) as eluent; Fig. 1. also includes the calibration graphs for uncharged polymers (dextrans and PEO) as a reference for ideal SEC. This comparison may be of particular interest taking into account that I-250 has been a commonly used silica-based column for biopolymer separation [28,29] whereas U-250 is a relatively recent soft, polymer-based support [2,13,30,31] with the advantages of a wide range of pH stability and a higher inertness as far as residual charge density is concerned [32].

Fig. 1A shows that at $c_s = 0.02 M$ the polyion-matrix electrostatic repulsion is indeed stronger for I-250 than for U-250, as deduced from the divergence between the calibration graphs for NaPSS and the uncharged standards. At moderately higher eluent ionic strength, $c_s = 0.05 M$ (Fig. 1B), ion exclusion is cancelled in the case of U-250 whereas a substantial divergence still remains for I-250. Note that for the polymer-based support polyion and reference calibrations are not completely congruent, probably owing the appearance of a salt-induced matrix-solute hydrophobic interaction, shifting the elution volume to higher values than those expected for ideal behaviour. In this regard, Mori [9] has recently reported some hydrophobic retention of NaPSS on derivatized silica supports using mobile phases with relatively high ionic strength. On the other hand, the resolution observed for I-250 is higher than that for

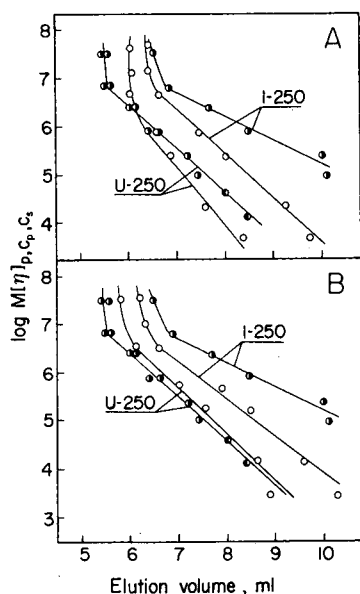


Fig. 1. Comparison of calibration graphs obtained for (○) NaPSS and standard uncharged polymers (●, dextrans; ●, PEO) on a silica-based column (I-250) and a polymer-based column (U-250) at $c_p = 10 \text{ g l}^{-1}$ using (A) 0.02 *M* and (B) 0.05 *M* acetate buffer (pH 4.0) as eluents.

U-250, so that the former could be more suitable for compromised separations of either polyelectrolytes of close molecular weight or ionomers. It is also worth commenting that in the limit of total exclusion different elution volumes can be obtained for the same value of $M[\eta]_{p,c_p,c_s}$ depending on the mobile phase composition. In this regard, it has been pointed out [33] that for the elution of uncharged polymers in organic media, different polymer-solvent interactions (represented by either the exponent a in the viscometric equation or the second virial coefficient) determine different polymer-gel interactions and, consequently, different elution volumes may correspond to similar hydrodynamic volumes.

As can be observed in the different calibration graphs in Fig. 1, the elution volume of NaPSS can be shifted, depending on c_p and on mobile phase ionic strength and pH, towards either higher or lower values relative to the reference calibration. The same behaviour has been widely observed experimentally in the past for uncharged polymers in organic binary mixed eluents [34]. In both instances, *i.e.*, aqueous SEC of polyions and SEC of synthetic polymers using organic mobile phases, the deviations (to higher or lower elution volumes) from the reference calibration graph (assumed to correspond to a pure size-exclusion mechanism) can be attributed to polymer-matrix interactions, although it is evident that the molecular causes for these secondary effects must be different.

Based on this phenomenological similarity between both types of systems, we next derive an expression which affords a new approach to the analysis of secondary effects in the SEC of charged (bio)polymers.

The elution volume of an uncharged polymer on a SEC support can be expressed through the basic equation

$$V_e = V_0 + K_{\text{SEC}} V_p \quad (1)$$

where V_e is the experimental elution volume of the sample, V_0 and V_p are the dead volume and the total pore volume of the column, respectively and K_{SEC} is the distribution coefficient for pure SEC. The elution behaviour of a polyelectrolyte on the same support when secondary effects take place can be described by

$$V'_e = V_0 + K'_{\text{SEC}} V_p \quad (2)$$

where V'_e is the experimental elution volume of the polyion and K'_{SEC} is a new distribution coefficient accounting for the different contributions to the separation mechanism. If we assume that V_e and V'_e correspond to the elution volume of an uncharged polymer and a polyelectrolyte having the same $M[\eta]_{p,c_p,c_s}$, then K'_{SEC} can be divided into two contributions and expressed as

$$K'_{\text{SEC}} = K_{\text{SEC}} K_p \quad (3)$$

where K_p is a partition coefficient for secondary effects. It must be noted that in this context K_p can be higher, equal to or lower than unity, therefore accounting for any type of deviation (to higher or lower elution volumes) from the reference calibration (see Fig. 1). In other words, $K_p > 1$ means that the polyion is eluted at a higher elution volume than a reference uncharged polymer of the same $M[\eta]_{p,c_p,c_s}$, this sec-

ondary effect being based on polyelectrolyte–support net favourable interactions (*e.g.*, hydrogen bonding, hydrophobic interactions). On the other hand, $K_p < 1$ implies a situation where unfavourable interactions between the polyion and the matrix (essentially electrostatic repulsion) take place and, consequently, the polyelectrolyte is eluted at a lower elution volume than the reference polymer. Obviously, $K_p = 1$ is considered as pure size exclusion, *i.e.*, when no secondary effect is observed.

Substitution of K'_{SEC} from eqn. 3 into eqn. 2 yields

$$V'_e = V_0 + K_{SEC}K_pV_p \quad (4)$$

Alternatively, the experimental elution volume of the polyelectrolyte can be expressed as

$$V'_e = V_0 + K_{SEC}V_p^* \quad (5)$$

where

$$V_p^* = K_pV_p \quad (6)$$

is a variable denoting a virtual pore volume, *i.e.*, a corrected V_p “effectively seen” by the macromolecule because of the secondary effects taking place. Some comments deserve to be made on this parameter, which can be regarded as a descriptor of the elution behaviour of (bio)polymers. Although V_p and V_p^* have the same units, the former corresponds to the geometrical volume of the pores whereas the latter, rather than having a strictly geometrical meaning, should be correlated with the time of residence of the sample inside the pores. In other words, V_p^* will be higher than V_p when the polyion residence time in the stationary phase is longer than that for an uncharged reference polymer of the same hydrodynamic volume, owing to polyelectrolyte–support attractive interactions. In contrast, V_p^* will be lower than V_p when the polyion resides inside the stationary phase for a shorter time than a reference polymer of the same hydrodynamic volume, owing to repulsive interactions with the matrix. In this regard, and only for the deviations towards lower elution volumes relative to the reference calibration, V_p^* could be considered equivalent to the effective pore volume reported by Dubin and Tecklenburg [5], V'_p which is a measure of the portion of the pore available to the polyion.

Concerning the procedure for the calculation of V_p^* values, assuming that V'_e and V_e values connected through a horizontal line in the calibration plots are compared, rearrangement of eqns. 1 and 5 yields

$$V_p^* = (V'_e - V_0)(V_e - V_0)^{-1}V_p \quad (7)$$

where V'_e corresponds to the experimental polyion elution volume and V_e to the elution volume obtained for a hypothetical uncharged standard of the same $M[\eta]_{p,c_p,c_s}$. As an example, Table I summarizes the V_p^* values together with the related parameters V'_e , K'_{SEC} and V_e calculated for NaPSS samples of different molecular weight on U-250 at $c_p = 10 \text{ g l}^{-1}$ with 0.02 M phosphate buffer (pH 5.9) as eluent. It can be observed that V_p^* varies with the molecular weight of the polyion. In order to attempt to find an empirical correlation accounting for this variation, we used an

TABLE I

MOLECULAR WEIGHT DEPENDENCE OF V_p^* FOR NaPSS AND RELATED PARAMETERS INVOLVED IN ITS CALCULATIONChromatographic conditions: phosphate buffer (pH 5.9, $c_s = 0.02 M$) as eluent; $c_p = 10 g l^{-1}$.

M (kilodalton)	V_c' (ml)	K'_{SEC}	V_c (ml)	V_p^* (ml)
1.6	8.02	0.497	9.03	3.62
4.0	7.03	0.302	8.23	2.84
16.0	6.46	0.189	7.25	2.78
31.0	6.07	0.112	6.65	2.51
88.0	5.74	0.047	6.05	2.22

approach which regards the chromatographic secondary effects as the result of a competition between polymer-eluent and matrix-eluent interactions. This competition can be described by the preferential adsorption coefficient, λ , widely used in polymer solution thermodynamics and recently applied to SEC of uncharged polymers [21,22]. As (i) the variation of λ with the molecular weight of the solvated polymer is experimentally given by [35]

$$\lambda M^{1/2} = \lambda_{\infty} M^{1/2} + C \quad (8)$$

where λ_{∞} denotes the preferential solvation coefficient at infinite molecular mass and C is a constant, and (ii) λ is proportional to $\ln K_p$ [21], and taking eqn. 6 into account, the following expression is obtained:

$$M^{1/2} \ln(V_p^*/V_p) = AM^{1/2} + B \quad (9)$$

where A and B are proportionality constants. This empirical correlation relating the virtual pore volume, V_p^* , with the polyion molecular weight, will be used to test secondary effects for NaPSS and also peptide and protein chromatographic data.

A plot of the first member of eqn. 9 vs. $M^{1/2}$ should yield a straight line, for a given mobile phase composition and injected polyion concentration, whose slope reflects the extent of secondary effects. Thus, negative slopes can be attributed to matrix-polyion electrostatic repulsion and positive slopes would indicate favourable interactions (mainly hydrophobic effects and/or hydrogen bonding); if a slope near zero is obtained, secondary effects are counterbalanced and the elution behaviour approaches ideal SEC.

Fig. 2 shows the plots for NaPSS on U-250 obtained under different experimental conditions by varying c_p and pH at constant $c_s = 0.02 M$. V_p^* values were evaluated as mentioned above. As can be seen, at this ionic strength all slopes are negative. A good correlation was observed in all instances, which supports eqn. 9. Note, however, that some deviations appear corresponding to elution volumes outside the linear portion of the calibration graphs. For a given pH, ion exclusion is attenuated as the polyion concentration increases up to $c_p = 10 g l^{-1}$, a value that was considered as an upper limit to prevent the appearance of viscous fingering [13].

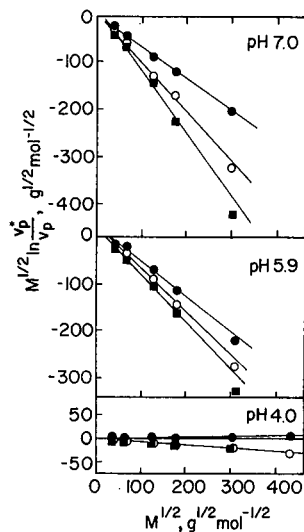


Fig. 2. Plot of eqn. 9 for the chromatographic data obtained for NaPSS on U-250 at c_p values of (■) 0.1, (○) 1.0 and (●) 10 g l^{-1} using 0.02 M phosphate (pH 7.0 and 5.9) and acetate (pH 4.0) buffers as eluents.

On the other hand, a decrease in pH causes a diminution in polymer-support electrostatic repulsion, which has been previously explained on the basis of protonation of residual carboxyl groups on the matrix. Thus, at pH 4.0, for $c_p = 10 \text{ g l}^{-1}$, a slope near zero is obtained even at this low ionic strength, which allows operation under quasi-ideal SEC conditions. This confirms the low activity of this gel, especially when compared with other commercially available hydrophilic supports.

In order to test eqn. 9 in the zone of the plot corresponding to positive slopes (hydrophobic and other effects), the ionic strength of the mobile phase was increased to 0.2 M . Fig. 3 shows a comparison of the chromatographic behaviour of NaPSS (analysed through eqn. 9) on U-250 and I-250 using 0.2 M acetate buffer (pH 4.0) as eluent. A good fit was observed for the different c_p values applied. Note that under these conditions the behaviour on the polymer-based support was quasi-ideal, a slight

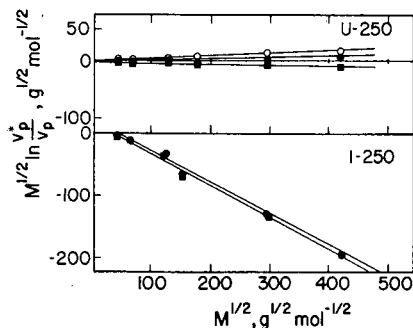


Fig. 3. Comparison of the plots of eqn. 9 obtained for NaPSS at different concentrations on U-250 and I-250 using 0.2 M acetate buffer (pH 4.0) as eluent. Symbols as in Fig. 2.

concentration effect being apparent. It must be pointed out that although this plot plausibly offers a more precise way to analyse deviations from ideal SEC under any given experimental conditions than conventional $\log M[\eta]$ vs. elution volume plots, in the region of positive slopes it does not allow an assignment of the specific contributions of operating individual secondary effects, and for this reason it is difficult to establish unambiguously a trend for the variation of the slope with c_p at this ionic strength. On the other hand, it must be noted that under these experimental conditions significant ion exclusion still remains when using I-250, which corroborates a surface residual charge density markedly higher than that for U-250.

Concerning the meaning of the variation of V_p^* (or its equivalent K_p) with the polyion molecular weight, the results in Figs. 2 and 3 show that as a general trend throughout the plot, the lower is M the closer is the value of K_p to unity (ideal SEC). This is reflected in the negative slope zone by a decrease in V_p^* (or K_p) as M increases, *i.e.*, the ion-exclusion effect is largest for the largest polyelectrolytes. In contrast, in the positive slope region V_p^* (or K_p) increases when M increases, *i.e.*, the secondary effects (hydrophobic and other interactions) are more pronounced for the largest molecules. It is worth mentioning in this regard that a similar qualitative dependence of K_p on M for synthetic polymers in organic media has been reported for $K_p > 1$ for polystyrene [36] and for $K_p < 1$ for poly(N-vinyl-3,6-dibromocarbazole) [37], both with tetrahydrofuran as eluent.

The results presented so far have been obtained for NaPSS, conventionally used as a model chain-like polyelectrolyte. It has been shown that for this polyion the expression proposed is valid when using two kinds of supports under very different experimental conditions. However, the interest of most chromatographers using aqueous SEC is increasingly focusing on biopolymers, particularly peptides and proteins. In order to test the general applicability of eqn. 9 for the analysis of secondary effects in the elution behaviour of these biomolecules, we selected from the literature the set of chromatographic data reported by Irvine [23]. That study can be considered as a suitable framework to check eqn. 9, because a wide variety of peptides and proteins covering a molecular weight range from 574 to 66 000 g mol⁻¹ were eluted with mobile phases of widely varying composition. Briefly, the author reported on the elution of the biopolymers on a TSK G2000SW column with eluents of low pH containing different concentrations of phosphoric, trifluoroacetic or heptafluorobutyric acid as ion-pairing agents.

In order to test eqn. 9, two approximations were made. First, $\log M$ instead of $\log M[\eta]$ was used in the calculation of V_p^* , obtained in a similar way to that mentioned above. Second, as absolute uncharged standards (*e.g.*, dextrans, PEO) were not employed in Irvine's work, we were obliged to select one calibration graph (among the reported) as a relative reference system, namely, 0.1 M phosphoric acid as mobile phase (see Fig. 2C in ref. 23). This eluent composition presumably permitted a minimization of secondary effects because of both an effective charge screening of the biopolymer (owing to the moderately high ionic strength) and the low hydrophobicity of this ion-pairing agent relative to the other acids used.

Fig. 4. depicts the fitting of the data from Irvine's paper (see Fig. 2 in ref. 23) taking the above assumptions into account. Inspection of Fig. 4 reveals that as both the ionic strength and hydrophobicity of the ion-pairing acid increase, the slope shifts from negative towards positive values. Some considerations can be made in relation

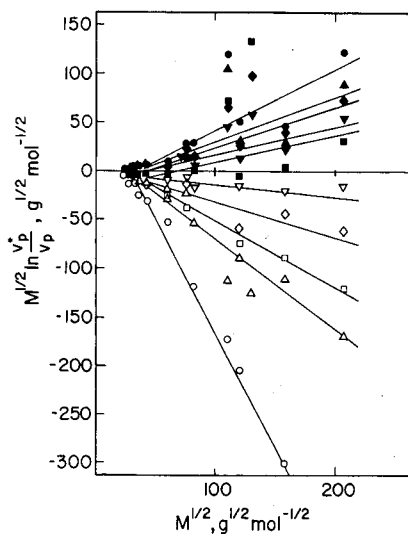


Fig. 4. Plot of eqn. 9 for a series of different peptides and proteins eluted on TSK G2000SW with eluents of low pH containing different concentrations of phosphoric acid ($\circ = 0.005 M$; $\triangle = 0.02 M$), trifluoroacetic acid ($\square = 0.005 M$; $\nabla = 0.01 M$; $\blacktriangledown = 0.015 M$; $\blacklozenge = 0.02 M$) or heptafluorobutyric acid ($\diamond = 0.005 M$; $\blacksquare = 0.01 M$; $\blacktriangle = 0.015 M$; $\bullet = 0.02 M$) as ion-pairing agents. A mobile phase consisting of $0.1 M$ phosphoric acid was taken as a reference corresponding to the horizontal line in the plot. Primary chromatographic data were taken from ref. 23.

to the secondary effects taking place under each particular chromatographic condition. First, the fits are in general good in the negative slope zone, where the predominant interaction induced by the very low pH of the mobile phase is likely to be an electrostatic repulsion between the positively charged silica-based support (as suggested by the author) and the peptides and proteins exhibiting net positive charge. Second, in the positive slope zone hydrophobic interaction is likely to be the main secondary effect taking place. However, the fits in this instance are in general not as good. A possible explanation for this behaviour could be that the biopolymers under these conditions exhibit at least two kinds of hydrophobic sites on the surface: on the one hand the non-polar chains of the ion-paired acid molecules, and on the other specific surface hydrophobic patches which can vary widely both in nature and topological distribution from one protein or peptide to another. It can be easily understood that the physico-chemical processes underlying surface recognition and interaction of different ion-paired proteins with the chromatographic matrix are complex and that deviations from linearity due to intrinsic biopolymer heterogeneities are not surprising. Anyway, a general trend is clearly observed in the plot in the positive slope region, so that an increase in ion-pairing acid concentration and replacement of trifluoroacetic by heptafluorobutyric acid give rise to an increase in the slope.

Finally, it is worth mentioning that a functionality similar to that in eqn. 9 has been reported [38] for the elution behaviour on a size-exclusion support of another type of biopolymer, namely double-stranded DNA restriction fragments, of great interest for biotechnologists and molecular biologists. In particular, for large DNA fragments, an anomalous retention behaviour of unknown mechanism was observed

where the retention parameter increased as a function of $L^{1/2}$, L being the chain length of the DNA fragment. Again, it is apparent that the interpretation of non-ideal SEC elution behaviour of biopolymers, including peptides, proteins and polynucleotides, is particularly complicated when the mobile phase composition strongly favours compatibility between the support and the solute and that more sophisticated treatments are needed to quantitatively account for the different interactions involved in deviations from pure size exclusion.

ACKNOWLEDGEMENTS

This work was partially supported by Grant No. PB87-0996 from DGICYT (Spain). One of the authors (E.P.-P.) was the recipient of a long-term fellowship from the Generalitat Valenciana.

REFERENCES

- 1 K. M. Gooding and F. E. Regnier, in K. M. Gooding and F. E. Regnier (Editors), *HPLC of Biological Macromolecules (Chromatographic Science Series, Vol. 51)*, Marcel Dekker, New York, 1990, Ch. 3.
- 2 A. Foriers, B. Rombaut and A. Boeyé, *J. Chromatogr.*, 498 (1990) 105.
- 3 M. Ollivon, A. Walter and R. Blumenthal, *Anal. Biochem.*, 152 (1986) 262.
- 4 M. Janado and P. L. Dubin, in P. L. Dubin (Editor), *Aqueous Size-Exclusion Chromatography (Journal of Chromatography Library, Vol. 40)*, Elsevier, Amsterdam, 1988, Ch. 2 and 3.
- 5 P. L. Dubin and M. M. Tecklenburg, *Anal. Chem.*, 57 (1985) 275.
- 6 P. L. Dubin, C. M. Speck and J. I. Kaplan, *Anal. Chem.*, 60 (1988) 895.
- 7 P. L. Dubin, R. M. Larter, C. J. Wu and J. I. Kaplan, *J. Phys. Chem.*, 94 (1990) 7243.
- 8 P. L. Dubin and J. M. Principi, *Anal. Chem.*, 61 (1989) 780.
- 9 S. Mori, *Anal. Chem.*, 61 (1989) 530.
- 10 M. G. Styring, H. H. Teo, C. Price and C. Booth, *Eur. Polym. J.*, 24 (1988) 333.
- 11 A. Bose, J. E. Rollings, J. M. Caruthers, M. R. Okos and G. T. Tsao, *J. Appl. Polym. Sci.*, 27 (1982) 795.
- 12 A. E. Hamielec and M. G. Styring, *Pure Appl. Chem.*, 57 (1985) 955.
- 13 E. Perez-Payá, L. Braco, A. Campos, V. Soria and C. Abad, *J. Chromatogr.* 461 (1989) 229.
- 14 V. Soria, A. Campos, R. García, M. J. Parets, L. Braco and C. Abad, *J. Liq. Chromatogr.*, 13 (1990) 1785.
- 15 M. Potschka, *Anal. Biochem.*, 162 (1987) 47.
- 16 M. Potschka, *J. Chromatogr.*, 441 (1988) 239.
- 17 M. le Maire, A. Viel and J. V. Møller, *Anal. Biochem.*, 177 (1989) 50.
- 18 P. L. Dubin, J. I. Kaplan, B.-S. Tian and M. Mehta, *J. Chromatogr.*, 515 (1990) 37.
- 19 G. F. Smith and W. N. Dean, *J. Colloid Interface Sci.*, 91 (1983) 571.
- 20 D. A. Hoagland, *Macromolecules*, 23 (1990) 2781; and refs. 37 and 41-45 cited therein.
- 21 R. Tejero, R. Gavara, C. Gomez, B. Celda and A. Campos, *Polymer*, 28 (1987) 1455.
- 22 R. García, B. Celda, V. Soria, R. Tejero and A. Campos, *Polymer*, 28 (1990) 1694.
- 23 G. B. Irvine, *J. Chromatogr.*, 404 (1987) 215.
- 24 F. R. Senti, N. N. Hellmann, N. H. Ludwig, G. E. Babcock, R. Tobin, C. A. Class and B. Lamberts, *J. Polym. Sci.*, 17 (1955) 527.
- 25 H. G. Elias, *Kunst.-Plast.*, 4 (1961) 1.
- 26 V. Soria, R. García, A. Campos, L. Braco and C. Abad, *Br. Polym. J.*, 20 (1988) 115.
- 27 M. J. Parets, R. García, V. Soria and A. Campos, *Eur. Polym. J.*, 26 (1990) 767.
- 28 J. L. Hodge and E. F. Rossomando, *Anal. Biochem.*, 100 (1979) 179.
- 29 H. G. Barth, *J. Chromatogr. Sci.*, 18 (1980) 409.
- 30 T. Malfait, D. Sloopmaekers and F. Van Cauwelaert, *J. Appl. Polym. Sci.*, 39 (1990) 571.
- 31 B. Rombaut, A. Foriers and A. Boeyé, *J. Virol. Methods*, 29 (1990) 303.
- 32 Waters Chromatography Division, Millipore, *Polym. Notes*, 2, No. 1, July (1987) 31.
- 33 A. Campos, V. Soria and J. E. Figueruelo, *Makromol. Chem.*, 180 (1979) 1961.

- 34 J. E. Figueruelo, V. Soria and A. Campos, in J. Cazes and X. Delamare (Editors), *Liquid Chromatography of Polymers and Related Materials II (Chromatographic Science Series, Vol. 13)*, Marcel Dekker, New York, 1980, pp. 49–71.
- 35 C. Strazielle and H. Benoit, *Makromol. Chem.*, 172 (1973) 169.
- 36 S. Mori and T. Suzuki, *Anal. Chem.*, 52 (1980) 1625.
- 37 J. M. Barrales-Rienda, P. A. Galera, A. Horta and E. Sainz, *Macromolecules*, 18 (1985) 2572.
- 38 B. E. Boyes, D. G. Walker and P. L. McGeer, *Anal. Biochem.*, 170 (1988) 127.

CHROMSYMP. 2320

High-performance liquid chromatography of amino acids, peptides and proteins

CX^a. Principal component analysis of four sets of group retention coefficients derived from reversed-phase high-performance liquid chromatography of peptides

M. C. J. WILCE, M. I. AGUILAR and M. T. W. HEARN*

Department of Biochemistry and Centre for Bioprocess and Technology, Monash University, Clayton, Victoria 3168 (Australia)

ABSTRACT

Principal component analysis procedures have been used to further characterise peptide retention behaviour in reversed-phase (RP) high-performance liquid chromatography. In particular, the analysis was performed with four new scales of group retention coefficients (GRCs) in conjunction with fourteen physicochemical descriptors of the side chain functionalities of the twenty naturally occurring amino acids. The results demonstrate a negative correlation between GRCs derived from peptide retention data with RP-C18 or RP-C8 stationary phases and aqueous trifluoroacetic acid–acetonitrile solvents and amino acid parameters which describe electronic characteristics. Conversely, there was a positive correlation between GRCs derived from peptide retention data with a RP-C18 stationary phase and aqueous trifluoroacetic acid–acetonitrile–2-propanol mixtures and amino acid parameters related to steric and volume characteristics. These results are interpreted in terms of the solvophobic theory. The relevance of quantitative structure–retention relationships to the mechanistic basis of peptide and protein interactions with chromatographic surfaces is discussed.

INTRODUCTION

Reversed-phase high-performance liquid chromatography (RP-HPLC) has in recent times become the most widely used technique for the purification of peptides and polypeptides. In addition, the use of RP-HPLC has enabled various physicochemical parameters associated with peptide and protein surface interactions and folding hierarchies to be evaluated rapidly and quantitatively [1].

Despite the ever increasing usage of RP-HPLC for the separation and analysis of peptide and proteins fully developed mechanistic models are not yet available to describe the interactive processes that occur between the non-polar stationary phase,

* For part CIX, see ref. 23.

the mobile phase and the peptide or protein solute. The development of such physical models would provide the basis for significant improvement in the practical application of optimisation protocols. In addition their development would enable elucidation of the key parameters that control the physicochemical basis of peptide and protein binding to hydrocarbonaceous surfaces.

Solvophobic theory, as developed by Sinanoglu and co-workers [2–6] and adapted by Horváth and co-workers [7,8] for isocratic reversed-phase chromatography, endeavours to provide a mechanistic and thermodynamic basis for the interpretation of solute, solvent and stationary phase interactions in reversed-phase chromatographic systems. While providing insight into the overall free energy, ΔG^0 , considerations that control the RP-HPLC retention process, the practical implementation of solvophobic theory can present difficulties. For example, full evaluation of solvophobic parameters requires *inter alia* knowledge of the values of the microthermodynamic surface tension and dielectric constant of the mobile phase. For multicomponent eluents such values are not generally available from literature sources. The lack of practical and accessible mechanistic models has forced most investigators to rely upon non-mechanistic, empirical models to describe peptide or protein retention behaviour with non-porous and porous, chemically modified *n*-alkylsilicas. The most fully developed and available of these models is the Linear Solvent Strength (LSS) gradient model as originally developed by Snyder [9,10]. This model provides a quantitative basis for the evaluation of peptide and protein retention behaviour under ideal reversed-phase conditions and allows a rational selection of chromatographic parameters in order to achieve a set of optimal chromatographic conditions. While the LSS retention model provides a useful basis for the optimisation of peptide or protein separation it does not allow the assessment of the fundamental physicochemical and structural parameters of the biosolute which underlie the retention process.

One approach that can be employed to elucidate the biosolute parameters which control the interaction of peptides and proteins with the reversed-phase chromatographic environment is to examine chromatographically derived amino acid retention coefficients. We have previously developed four new sets of chromatographically derived retention coefficients [11] which allow a more detailed analysis of reversed-phase retention processes involving peptide or protein interactions than previously reported hydrophobicity coefficients. Central to the development of these new group retention coefficients (GRCs) were a number of important considerations, including: (1) each of the four sets of retention coefficients were derived from peptides eluted from different chromatographic systems with well defined aquo-organic mobile phase conditions and *n*-alkylsilica stationary phases, (2) they were derived from the reversed-phase retention data of more than 1300 peptides which in effect produce coefficients that represent the RP-HPLC retention characteristics of each amino acid in a wide range of peptide environments, (3) the retention data used to calculate the coefficients are measures of the dynamic interaction of the peptide with the alkyl chains of the stationary phase, and (4) the large number of peptide examples were required to provide a high level of statistical significance.

The various chromatographic systems included in the development of these new GRCs included three different chemically bonded *n*-alkylsilica reversed-phase stationary phases, namely, RP-C18, RP-C8 and RP-C4, and two different organic solvents in

the aquo-organic mobile phase, acetonitrile (ACN) and 2-propanol-ACN. The range of experimental conditions used to derive the GRCs thus allows the influence of these different mobile and stationary phases on the GRCs to be assessed. The derivation and implications of these coefficients have been described in detail previously [11].

This study explores the fundamental physicochemical parameters that underlie the retention process with peptides in each of the four chromatographic systems. Each of the four sets of GRCs were examined with principal component analysis in conjunction with a range of fundamental parameters that describe the various characteristics of the amino acid side chains. This detailed analysis allows the retention coefficients to be resolved down to fundamental parameters that can be related to overall properties of the amino acid side chains in a peptidic environment and a specific chromatographic condition.

MATERIALS AND METHODS

The GRCs used in this study were derived from the retention data of over 1300 peptides, as described previously [11]. In this study, four sets of GRCs are considered. Each of the four sets of GRCs has been generated from peptides eluted from different chromatographic conditions (as shown in Table I).

These four sets of GRCs were subjected to principal component analysis in conjunction with the parameters described by Fauchere *et al.* [12]. The principal component analysis was performed with use of the SPSS[®] program upon the Monash University Vax computer.

RESULTS AND DISCUSSION

Theoretical considerations

According to the solvophobic theory, the physicochemical basis of the retention processes in RP-HPLC phase is largely a result of incremental changes in the microscopic surface tension. More specifically, the binding process can be visualised in terms of the preferential interaction of the solute with the non-polar surface as a result of its expulsion from the polar mobile phase of higher surface tension. A number of factors such as size and composition of the peptide solute and the precise composition of the mobile phase will therefore impinge upon the binding process.

TABLE I
THE FOUR DIFFERENT CHROMATOGRAPHIC CONDITIONS FROM WHICH PEPTIDES WERE ELUTED TO DERIVE THE GROUP RETENTION COEFFICIENTS AND THEIR ABBREVIATED NAMES

Abbreviated name	Chromatographic conditions
C18	RP-C18 stationary phase; aqueous trifluoroacetic acid (TFA)-ACN mobile phase
C8	RP-C8 stationary phase; aqueous TFA-ACN mobile phase
C4	RP-C4 stationary phase; aqueous TFA-ACN mobile phase
TPA	RP-C18 stationary phase; aqueous TFA-ACN-2-propanol mobile phase

The retention of a solute in a reversed-phase chromatographic system can be described by the isocratic retention factor, k' , such that under near equilibrium conditions:

$$\ln k' = -\frac{1}{RT} \Delta G^0 + \ln \left(\frac{RT}{PV} \right) + \Phi \quad (1)$$

where ΔG^0 is the overall difference in free energy of the solute between the mobile phase and the stationary phase, V is the mean molar volume of the solvent, P is the operating pressure, T the temperature, R the molar gas constant and Φ is a constant related to the density of the accessible ligands. The ΔG^0 term can be further represented as:

$$\Delta G^0 = \Delta G_{\text{cav}}^0 + \Delta G_{\text{es}}^0 + \Delta G_{\text{vdw}}^0 + \Delta G_{\text{assoc}}^0 + \Delta G_{\text{red}}^0 \quad (2)$$

where ΔG_{cav}^0 is the difference between the mobile phase and stationary phase in free energy associated with cavity formation, ΔG_{es}^0 is the free energy change derived from any electrostatic interactions, ΔG_{vdw}^0 is the free energy change caused by Van der Waals interactions, $\Delta G_{\text{assoc}}^0$ is the free energy change from ligate-eluite association and ΔG_{red}^0 is essentially a correction term for non-ideal behaviour that accounts for any other change in the difference in the free energy of the solute moving between the mobile phase and stationary phase.

According to solvophobic theory, the capacity factor of a solute eluted with a particular column and eluent composition can be related to physical and chemical properties of the solute and the mobile phase according to the following expression:

$$\ln k' = A' + B' \left(\frac{1 - \lambda}{2\lambda} \right) \frac{\mu_s^2}{v_s} \frac{1}{1 - (\alpha_s/v_s)} + C' \Delta A \quad (3)$$

where the constants A' , B' and C' are given by

$$A' = \Phi - \frac{\Delta G_{\text{vdw.assoc}}}{RT} + \frac{\Delta G_{\text{vdw.s}}}{RT} + \frac{4.836N^{1/3}(\kappa^e - 1)V^{2/3}\gamma}{RT} + \ln \frac{RT}{PV} \quad (4)$$

$$B' = ND/RT \quad (5)$$

where N is Avagadro's number, and

$$C' = N\gamma/RT \quad (6)$$

The parameter λ is defined as:

$$v_{\text{SL}} = \lambda v_s \quad (7)$$

where v_{SL} and v_s are the molecular volumes of the solute-ligand complex and the unbound solute, respectively. The term D is the dielectric constant of the medium,

while μ_s and α_s refer to the static dipole moment and the polarisability of the solute, respectively.

Experimentally it has been shown that the solvophobic forces which have the greatest influence on k' are those which are dependent on surface tension, γ [7]. Eqn. 3 can therefore be simplified to

$$\ln k' = A'' + B''\gamma \quad (8)$$

where A'' is the sum of all the terms present in eqn. 3 which do not contain the surface parameter and

$$B'' = \frac{N\Delta A_h + 4.836N^{1/3}(\kappa^e - 1)V^{2/3}}{RT} \quad (9)$$

The parameter κ^e is defined as the ratio of the energy required for the formation of a cavity with a surface area equal to solute areas and the energy required to extend the planar surface of the liquid by the same area. The dependency of k' on the surface tension, γ and hydrophobic contact area, ΔA_h , as described by the solvophobic theory has been experimentally validated for low-molecular-weight solutes [7] and small peptides [13]. In the case of small peptides, each constituent amino acid will contribute to the overall retention according to intrinsic physical properties such as hydrophobicity, charge and/or polarity, size and shape. The relative magnitude of the contribution of each residue within a peptide which is intrinsic to the experimental retention data of a peptide solute has been derived in our previous studies from multiple linear regression analysis of a retention data base of over 1300 peptide retention times. These chromatographically derived retention coefficients were therefore subjected to factor analysis to identify the underlying parameters which control the interactive properties of each amino acid residue within a peptidic environment. A summary of the various chromatographic conditions and the abbreviations used to describe these conditions are listed in Table I.

Statistical analysis of the group retention coefficients

Principal component analysis is a statistical technique used to identify a relatively small number of factors that can be used to represent relationships among sets of many interrelated variables. The aim of the present study was to derive insight into the molecular and atomic forces behind peptide retention processes in RP-HPLC. Each of the four sets of GRCs were therefore subjected to principal component analysis in conjunction with a range of independently determined amino acid parameters.

Fourteen physicochemical descriptors of the side chains of the 20 naturally occurring amino acids were used and are listed in Table II. It has been shown previously that these parameters describe either steric, volume or electronic characteristics of the amino acid side chains [12]. The first of these steric parameters, Ξ , listed in Table II describes the steric influence of the side chain in terms of complexity, branching and symmetry, while ν and ν_{reg} are a function of the minimal Van der Waals radius. The next five parameters characterise the volume rather than the shape of the side chain. These include values for the length of the amino acid side chain, L , the

TABLE II

PARAMETERS DESCRIBED BY FAUCHERE *ET AL.* [12] THAT WERE USED IN THE PRINCIPAL COMPONENT ANALYSIS

Parameter	Description	Factor
\mathcal{E}	Measure of steric influence, including three attributes: complexity, branching and symmetry	Steric
v	A function of the minimum Van der Waals radius	Steric
v_{reg}	Smoothed steric parameter	Steric
L	Length of the amino acid side chain	Volume
$B1$	Minimum width of the amino acid chain	Volume
$B5$	Maximum width of the amino acid chain	Volume
α	Polarisability of the amino acid side chain	Volume
V_v	Normalised Van der Waals volume	Volume
σ	Inductive field effects	Electronic
n_H	Number of hydrogen bond donors	Electronic
n_N	Number of full non-bonding orbitals on oxygen and nitrogen	Electronic
i_A	Number of positive charges	Electronic
i_B	Number of negative charges	Electronic
pK_a	Dissociation of hydrogens from side chains	Electronic

minimum and maximum width of the side chain, $B1$ and $B5$, respectively, the polarisability, α , which is related to molar refractivity and is a function of the molecular volume, and V_v which is the normalised Van der Waals volume. The remaining six parameters represent descriptors of the electronic properties of the side chains. These include σ , which describes inductive field effects, n_H , the number of OH and NH bonds, n_N , the number of full non-bonding orbitals on O and N atoms, i_A and i_B , the number of positive and negative charges, respectively and the pK_a of each amino acid side chain. As noted by Fauchere *et al.* [12] these parameters probably do not describe all the possible components of amino acid side chains, and redundancy between individual parameters cannot be ruled out. However, these categories are sufficient to give a reasonable indication of the major parameters that control the chromatographic retention process and to explain the differences between the four sets of retention coefficients.

The initial statistics of the principal component analysis indicated that five factors described approximately 85% of the total variance of the fourteen parameters plus the four sets of retention coefficients. The pattern of factor loading is displayed in Fig. 1. Factor loadings in the rotated factor matrix of less than 0.35 were set to zero. The first factor (factor 1) which includes the TPA set of retention coefficients, also contains parameters that are related to steric and volume parameters of the amino acid side chains. Factors 2 and 4 do not contain any of the retention coefficient sets. However, these factors validate the analysis in that factor 2 represents four of five volume related parameters while factor 4 includes four of the six electronic-related parameters. Factor 3, contains both the C18 and C8 sets of retention coefficients. This factor has a predominantly electronic character including the number of full non-bonding orbitals on oxygen, n_H , and the number of positive charges, i_A . The results of linear correlation analysis of the four GRC scales are shown in Table III. The C18 and C8 sets of GRCs have a high correlation coefficient and were expected to be

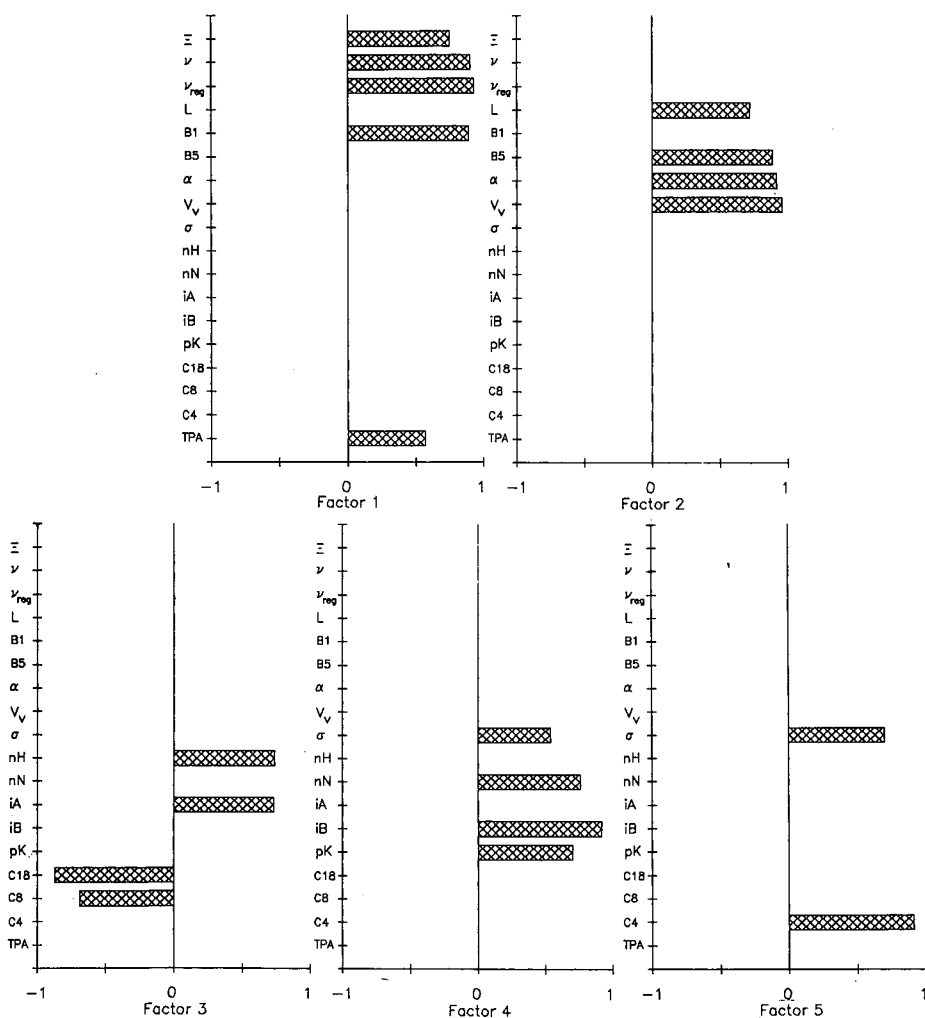


Fig. 1. Pattern of factor loading for each of the five factors.

part of the same factor. The fifth factor, (factor 5) contains two parameters, the C4 set of retention coefficients and σ , the parameter that describes the inductive field effects of the amino acid side chains. Table IV lists the percentage of the total variance accounted for by each of the 5 factors. Five factors were chosen because they accounted for all four of the group retention coefficient scales and further, each of these five factors provided a significant contribution of the total variance of the analysis [14], Table IV.

The effect of the organic modifier in the mobile phase on the group retention coefficients

The role of the organic modifier in the retention process can be analysed through comparison of the correlation results for the C18 and TPA GRCs sets. The results of

TABLE III

CORRELATION COEFFICIENTS FROM LINEAR REGRESSION ANALYSIS OF THE FOUR GROUP RETENTION COEFFICIENT SCALES

	C18	C8	C4
C8	0.80		
C4	-0.05	-0.05	
TPA	0.44	0.30	0.15

linear regression analysis are shown in Table III. The data indicated that while the C18 and C8 coefficient sets had a high degree of linearity, both the C4 and TPA showed no linearity with any of the other coefficient sets. The only difference between the C18 and TPA retention coefficient sets (Table I), is that the peptides used to generate these two sets of retention coefficients were eluted with a different mobile phase. The C18 retention coefficients were calculated from peptides eluted with a gradient of TFA-ACN-water with a RP-C18 stationary phase, while the TPA coefficients were generated from peptides eluted with a gradient of TFA-2-propanol-ACN-water and with the same RP-C18 stationary phase. Even though the TPA coefficients were not generated from peptides eluted in 2-propanol but a mixture of 2-propanol-ACN any differences in the retention process as reflected in the GRCs must be due to the presence of 2-propanol. It is therefore the effect of 2-propanol in the mobile phase that is controlling the differing RP-HPLC retention processes.

Table V lists the dielectric constant and solvent polarity of 2-propanol, ACN and water for comparison. Since 2-propanol has a lower dielectric constant and solvent polarity than ACN, charge interactions therefore appear to play a limited role in the solute-solvent component of the retention process in the TPA chromatographic environment. Furthermore, it is apparent from the principal component analysis that the parameters which are related to the TPA retention coefficient set are steric or volume measures. Thus, these facets of the size of the amino acid side chains control the region of the peptidic solute that can interact with the alkylsilica stationary phase in RP-HPLC systems when 2-propanol is used in part as a co-organic modifier in the mobile phase.

TABLE IV

THE PERCENTAGE OF TOTAL VARIANCE ACCOUNTED FOR BY EACH OF THE FIVE FACTORS DERIVED FROM PRINCIPAL COMPONENT ANALYSIS

Factor	Percentage of total variance
1	31.9
2	21.9
3	14.1
4	10.2
5	6.7
Total	84.8

TABLE V

DIELECTRIC CONSTANT AND SOLVENT POLARITY OF 2-PROPANOL, ACN AND WATER

Solvent	Dielectric constant	Solvent polarity
2-Propanol	20.3	4.0
ACN	37.5	5.8
Water	80.0	10.2

The C18 and C8 coefficients sets were generated from peptides eluted with a mobile phase gradient of TFA-ACN-water and, stationary phases of 18 and 8 carbon alkyl chains, respectively. Fig. 1 indicates that the coefficients of the two GRCs sets correspond in an opposing way to the electronic parameters, that is, the C18 and C8 sets have a negative correlation with the electronic parameters. In other words, the analysis indicates that as the electronic characteristics of an amino acid side chain increase, then the smaller will be its retention coefficient.

In terms of the solvophobic theory, the parameters which will be directly affected by changes in the organic modifier include, D , the dielectric constant and γ , the surface tension. It is evident from the data listed in Table V that 2-propanol-ACN-water mixtures will have a lower dielectric constant and polarity than ACN-water mixtures. This will in turn influence the ability of the peptide solutes to interact with the solvent molecules which will then directly impinge upon the resultant retention coefficients for each amino acid residue. For small solutes such as amines or individual amino acids, the dominant force behind solute-surface interactions can be related to the surface tension of the mobile phase and the hydrophobic surface area of the solute [7]. In addition, the parameters related to the dipole moment, μ_s , the polarisability, α_s , and the molecular volume, v_s , of each constituent amino acid residue within a particular peptide sequence will be closely dependent on the properties of the mobile phase and the neighbouring amino acids within the peptide. As a consequence, there is a fine balance between the relative contribution of all the possible factors involved in the retention process. The results of principal component analysis reveal that for peptides eluted with TFA-water-ACN mixtures, there is a negative correlation between the amino acid GRCs and the electronic properties of each residue. This can be contrasted with the positive correlation between the GRCs and the steric and volume properties of amino acids with peptides eluted with TFA-water-ACN-2-propanol mixtures. Thus in relative terms, the residues with high dipolar characteristics contribute less to retention as they can interact more easily with the relatively polar solvent molecules. In contrast, in the presence of 2-propanol, the larger residues interact more strongly with the stationary phase rather than the mobile phase. This behaviour can be understood in terms of the solvophobic theory if one considers the solvent cavity created about the solute. Because 2-propanol has a low dielectric constant, D , charge or dipole interactions between the solute and solvent will be minimised. Therefore, the solvent forming the wall of the cavity will become more ordered than the bulk solvent, thus reducing the entropy, ΔS^0 , of the system. The change in free energy of any system is related to the change in entropy as follows:

$$\Delta G^0 = \Delta H^0 - T\Delta S^0 \quad (10)$$

where ΔH^0 is the change in enthalpy. Any decrease in entropy is energetically unfavourable. Thus, it is energetically unfavourable in terms of entropy for a cavity to be formed around larger amino acid side chains. As a consequence a favourable decrease in ΔG^0 will occur upon binding to the stationary phase sorbent. Our findings are in accord with the results predicted by the solvophobic theory since eqns. 3–6 show that there should be a linear relationship between the solvent dielectric constant and $\log k'$. Moreover, similar conclusions have been reached by Horváth *et al.* [7], and, Fausnaugh *et al.* [15] from studies of proteins eluted from reversed-phase and hydrophobic interaction chromatographic sorbents.

The effect of alkyl chain length on the group retention coefficients

Further examination of the results of the principal component analysis indicated that the C18 and C8 retention coefficients are negatively correlated to two electronic parameters in factor 3, while the C4 coefficients are positively correlated with the electronic parameter σ , inductive field affect, factor 5, Fig. 1. These three coefficient sets were generated from peptides eluted with the same mobile phase, a gradient of TFA–ACN–water. It is therefore the differing length of the *n*-alkyl chain (*i.e.*, C4 versus C18 or C8) of the stationary phase ligands that is controlling the retention processes observed between C18 and C8 retention coefficients, and the C4 coefficients. Since the C18 and C8 coefficients show a strong linear relationship with each other the solute retention processes are very likely to be similar.

The similarity of the C18 and C8 retention coefficients and their differences with the C4 coefficients have been previously observed with retention behaviour of peptides [11]. For example, the retention behaviour of a family of paracelsin peptide analogues were examined under isocratic conditions on a series of reversed-phase sorbents which varied in alkyl chain length from C1 to C18. Plots of k' versus chain length showed a retention maxima between $n = 2$ and 4, which was followed by a significant decrease for $n \leq 5$ carbon atoms [16]. In addition, nuclear magnetic resonance studies have documented differences in the dynamic structure of the C18 (or C8) and C4 *n*-alkyl ligands [17]. From measurement of the spin lattice relaxation times of reversed-phase ligands with a range of alkyl chain lengths it was found that the RP-C4 alkyl ligands had a far more rigid conformation than the 18- and 8-carbon alkyl ligands. The extreme rigidity of the RP-C4 alkyl ligands could mean that this stationary phase provides an essentially planar surface for the interaction of the solute with the stationary phase. However, since the RP-C4 retention coefficients only account for 6.7% of the total variance of the principal component analysis and because these coefficients were correlated with only one other parameter, it is difficult from these data to draw more specific conclusions on the factors which are important in the interactions of peptide solutes with C4 stationary phases.

CONCLUSIONS

A large number of chromatographically derived amino acid hydrophobicity coefficients have been published in recent years (for compendia see refs. 11 and 18). The main use for these scales has been associated with the prediction of the retention position of peptides of known amino acid composition or alternatively for the prediction of internal and external areas within a protein structure through the

analysis of hydrophathy profiles [11,18,19]. However, there has been no detailed analysis of the precise physicochemical basis of the retention coefficients in terms of the underlying forces which control the peptide-stationary phase interaction. It is evident from the present study that the relative interactive potential of peptides is intimately dependent on the specific nature of both the stationary phase ligand and the mobile phase composition. While this result is anticipated on the basis of the large body of literature on the empirical separation of peptides by RP-HPLC and solvophobic theory, the present study characterises more completely the complex nature of peptide-surface interactions in more quantitative terms. Furthermore, it has been assumed previously that a single coefficient value will represent the binding contribution capacity of an individual amino acid in all possible sequence arrangements. This assumption is clearly untenable in view of the results of the present study as well as examples [18,20] which demonstrate chromatographic resolution between peptides of identical amino acid composition but different sequences. These experimental observations simply reflect that the interaction of peptides with chromatographic surfaces is orientation specific. The results of the present study will thus underpin further investigations to unravel the physicochemical factors which determine the ability of amino acid residues within a particular peptide sequence to participate in the binding process. Such studies on the atomic and molecular forces which determine the contact region(s) of peptides and proteins in the adsorptive modes of HPLC [21,22], including RP-HPLC are currently underway in these laboratories.

ACKNOWLEDGEMENTS

These investigations were supported by grants from the National Health and Medical Research Council of Australia, the Australian Research Council, the Potter Foundation and the Buckland Foundation.

REFERENCES

- 1 M. T. W. Hearn and M. I. Aguilar, *J. Chromatogr.*, 359 (1986) 31.
- 2 O. Sinanoglu, in B. Pullman (Editor), *Molecular Associations in Biology*, Academic Press, New York, 1968, pp. 427-445.
- 3 O. Sinanoglu and S. Abdunur, *Fed. Proc.*, 24 (1965) 12.
- 4 O. Sinanoglu, *Adv. Chem. Phys.*, 12 (1967) 283.
- 5 T. Halicioğlu and O. Sinanoglu, *Ann. N.Y. Acad. Sci.*, 158 (1969) 308.
- 6 O. Sinanoglu, *Theor. Chim. Acta*, 33 (1974) 279.
- 7 Cs. Horváth, W. Melander and I. Molnár, *J. Chromatogr.*, 125 (1976) 129.
- 8 Cs. Horváth, W. Melander and I. Molnár, *Anal. Chem.*, 49 (1977) 142.
- 9 M. A. Stadalius, H. S. Gold and L. R. Snyder, *J. Chromatogr.*, 296 (1984) 31.
- 10 L. R. Snyder, in Cs. Horváth (Editor), *High-Performance Liquid Chromatography — Advances and Perspectives*, Vol. 3, Academic Press, New York, 1983, p. 157.
- 11 M. C. J. Wilce, M. I. Aguilar and M. T. W. Hearn, *J. Chromatogr.*, 536 (1991) 165.
- 12 J.-L. Fauchere, M. Charton, L. B. Kier, A. Verloop and V. Pliska, *J. Peptide Res.*, 32 (1988) 269.
- 13 M. T. W. Hearn and B. Grego, *J. Chromatogr.*, 203 (1981) 349.
- 14 R. A. Johnson and D. W. Wichern, *Applied Multivariate Statistical Analysis*, Prentice-Hall, Englewood Cliffs, NJ, 1982, pp. 359-457.
- 15 J. L. Fausnaugh, L. A. Kennedy and F. E. Regnier, *J. Chromatogr.*, 317 (1984) 141.
- 16 K. D. Lork, K. K. Unger, H. Bruckner and M. T. W. Hearn, *J. Chromatogr.*, 476 (1989) 135.
- 17 B. Pfeleiderer, K. Albert, K. D. Lork, K. K. Unger, H. Bruckner and E. Bayer, *Angew. Chem., Int. Ed. Engl.*, 28 (1989) 327.

- 18 M. T. W. Hearn and M. I. Aguilar, in A. Neugerger and L. L. M. van Deenen (Editors), *Modern Physical Methods in Biochemistry*, Part B, Elsevier, Amsterdam, 1988, pp. 107–142.
- 19 J. M. R. Parker, D. Guo and R. S. Hodges, *Biochemistry*, 25 (1986) 5425.
- 20 R. Houghten and S. T. DeGraw, *J. Chromatogr.*, 386 (1987) 223.
- 21 A. N. Hodder, K. J. Machin, M. I. Aguilar and M. T. W. Hearn, *J. Chromatogr.*, 517 (1990) 317–331.
- 22 A. N. Hodder, K. J. Machin, M. I. Aguilar and M. T. W. Hearn, *J. Chromatogr.*, 507 (1990) 33–44.
- 23 A. J. Wirth, K. K. Unger and M. T. W. Hearn, *J. Chromatogr.*, (1991) in press.

CHROMSYMP. 2321

High-performance liquid chromatography of amino acids, peptides and proteins

CXI^a. Retention behaviour of proteins with macroporous tentacle-type anion exchangers

M. T. W. HEARN*, A. N. HODDER^b, F. W. FANG and M. I. AGUILAR

Department of Biochemistry and Centre for Bioprocess Technology, Monash University, Clayton, Victoria 3168 (Australia)

ABSTRACT

The chromatographic behaviour of various proteins with Fractogel-TMAE and LiChrospher-TMAE tentacle-type strong anion-exchange sorbents has been investigated. In particular, the $\log \bar{k}$ versus $\log 1/\bar{c}$ (where \bar{k} is the median capacity factor and \bar{c} is the corresponding salt concentration) dependencies for two salt systems (NaCl and KBr) have been documented. The Fractogel-TMAE sorbent exhibited retention characteristics in terms of relative protein charge dependencies (slope Z_c) and affinity values ($\log K_c$, which is $\log \bar{k}$ at $c = 10^{-6} M$, where c is the concentration of the displacer ion) which were similar to the more conventional anion-exchange sorbents such as the Mono-Q sorbent. However, the Z_c and $\log K_c$ values obtained with the LiChrospher-TMAE sorbent were significantly decreased for most proteins. Furthermore, proteins such as carbonic anhydrase and myoglobin were not retained at pH values up to 4 and 2 units above their pI values, respectively. These results illustrate the different adsorptive properties of the tentacle-type sorbents compared to other monolayer or polymer layer ion exchangers in terms of accessibility of the charged ligand and the underlying retention mechanism.

INTRODUCTION

Over the past several years, research interest in the development of specially designed macroporous ion-exchangers with enhanced features for the analysis and purification of proteins has been stimulated by two conceptual considerations. The first consideration, epitomised by the work of Afeyan and co-workers [1,2], has led to considerable interest with micro- and mesoparticulate porous support materials of very large nominal pore diameters, *e.g.* with pore diameters typically in the range 250–500 nm. Ion-exchange sorbents, developed from such macroporous support ma-

^a For Part CX, see ref. 10.

^b Present address: CSIRO Australian Animal Health Laboratory, P.O. Bag 24, Geelong, Victoria 3220, Australia.

terials, exhibit adsorption characteristics with proteins which are typified by convective rather than diffusive control processes. With this class of high-performance ion-exchangers, high rates of protein adsorption have been reported at very high linear flow velocities [2].

Advancements in the second consideration, namely the evaluation of new criteria for the design and localisation of ligands in particular chemical environments at the surface of macroporous support materials, has led to significant improvements in biomimetic affinity chromatography, immobilised metal chelate chromatography, and ion-exchange chromatography. Arising from research in this area has been the emergence of the so-called tentacle-type sorbents [3,4]. With this class of sorbent, linear polyelectrolyte chains are initially introduced to the surface of a hydrophilic support material, followed where necessary by subsequent chemical derivatisation reactions. In a previous study, we examined the protein adsorption characteristics of pretreated glass beads and LiChrospher Si 1000 derivatised with N-trimethylamino-methylacrylamide (TMAE-acrylamide) according to the three-step procedure of Müller *et al.* [3,4]. With these tentacle type sorbents, the adsorption data corresponded to Hill-type isotherms, with the Hill coefficients indicating an approximately Gaussian affinity distribution of the binding sites for the protein. The present study extends these investigations through evaluation of the retention dependencies of several proteins chromatographed under gradient conditions on TMAE-Fractogel HW65 (Fractogel-TMAE) and TMAE-LiChrospher Si 1000 (LiChrospher-TMAE) sorbents with two different displacing salt systems.

MATERIALS AND METHODS

Chemicals and reagents

Bovine erythrocyte carbonic anhydrase, sperm whale muscle myoglobin (type III), hen egg white lysozyme (grade 1), bovine ribonuclease A (type III A), bovine insulin and piperazine were obtained from Sigma (St. Louis, MO, USA). The recombinant pig growth hormone (pGH) was available in highly purified form from associated studies carried out in these laboratories. The proteins were purified and characterised as described previously [5]. Sodium chloride and potassium bromide (AnalaR grade) were obtained from BDH (Port Fairy, Australia).

Quartz-distilled water was further purified on a Milli-Q system (Millipore, Bedford, MA, U.S.A.). Buffers were adjusted to pH 9.60 using either hydrochloric acid (specific gravity 1.16, AnalaR grade) or hydrogen bromide (specific gravity 1.46–1.49, AnalaR grade) all of which were purchased from BDH.

Apparatus

All chromatographic procedures were performed with a Pharmacia (Uppsala, Sweden) FPLC system consisting of two P-500 pumps, a V-7 injector and 278-nm fixed wavelength UV monitor coupled to a Perkin Elmer LC1-100 integrator via a Norton digital processor. Isocratic and gradient elution were controlled with a Pharmacia GP-250 solvent programmer. The Fractogel-TMAE and the LiChrospher-TMAE sorbents were obtained as prepacked columns (150 × 10 mm I.D. and 50 × 10 mm I.D., respectively) from E. Merck, Darmstadt, Germany. The Mono-Q sorbent, as prepacked columns, (50 × 5 mm I.D.) was obtained from Pharmacia. The

prepacked LiChrospher- and Fractogel-TMAE and Mono-Q columns were interfaced with the UV detector by zero dead volume connectors. Samples were injected using Scientific Glass Engineering glass syringes at a protein concentration of 5 mg/ml, typically as 10–100 μ l injections. The protein solutions were prepared in the elution buffer and prefiltered through 0.22- μ m ACRO LC13 Gelman filters.

Chromatographic procedures

The composition of the eluent was 20 mM piperazine, pH 9.60 (eluent A), containing up to 300 mM displacer salt (eluent B). All eluents were filtered through Millipore 0.45- μ m cellulose acetate HAWP04700 filters and degassed. Eluents were used for a maximum of two days before replacement. Protein solutions were prepared by dissolving the purified protein in eluent A at a concentration of 5 mg/ml, and filtered through 0.22- μ m ACRO LC13 filters (Gelman Sciences, Sydney, Australia). All chromatographic measurements were replicates ($n > 5$). With the gradient elution experiments, the gradient time was varied between 17.1 and 171 min with a constant flow-rate of 1 ml/min. The column dead time was obtained from the retention time of a salt breakthrough peak whilst the gradient elapse time for the different columns was also determined from plots of the conductivity *versus* time. Column effluent conductivity was measured with a Radiometer Cdm3 conductivity meter equipped with a CDC304 glass electrode. All chromatographic measurements were carried out at ambient temperature (*ca.* 20°C). At the start of each day, columns were equilibrated using a step elution protocol with the relevant eluent combination for at least 60 min. The gradient retention parameters b , $\log \bar{k}$ and $\log (1/\bar{c})$ (where b is the gradient steepness parameter, \bar{k} is the median capacity factor and \bar{c} is the corresponding salt concentration) were calculated using the Chromcalc program, developed in this laboratory and written in BASIC for IBM XT or AT computers as previously described [5]. Retention data ($\log \bar{k}$ and $\log 1/\bar{c}$) were subjected to iterative regression analysis to determine the slope (Z_c) and the $\log \bar{k}$ value at \bar{c} (concentration of the displacer ion) = 10^{-6} M ($\log K_c$).

RESULTS AND DISCUSSION

It is well known that a large variety of mobile phase parameters can be used to influence the retention behaviour of proteins in high-performance ion-exchange chromatography (HPIEC). In particular, variation in the pH and the nature and concentration of the displacing salt are widely used to affect improvement in resolution and recovery. Studies over many years have documented the importance of choosing the most appropriate displacing ion and co-ion in HPIEC. Important aspects of this selection relate not only to the relative affinity of the ion/co-ion for binding to the sorbent, but also what kosmotropic or chaotropic characteristics the individual ions manifest with regard to the water structure associated with the protein [5,6]. In the present study, we were thus interested to compare the influence of KBr as a displacing salt with the more conventional, and popular, choice, NaCl, on the retention behaviour of several proteins eluted from the Fractogel-TMAE sorbent and the LiChrospher-TMAE sorbent. Further, we wished to compare the behaviour of these so called 'tentacle' sorbents with the widely used microparticulate sorbent, Mono-Q. The physical characteristics of these columns are summarised in Table I. The proteins

TABLE I
ANION-EXCHANGE RESIN COLUMN CONFIGURATIONS

Sorbent	Column length (mm)	Column diameter (mm)	Particle diameter (μm) ^a	Pore size (Å)
Fractogel-TMAE	150	10	25-40	650
LiChrospher-TMAE	50	10	5	1000
Mono-Q	50	5	10	800

^a Nominal particle diameter as indicated by the manufacturer.

listed in Table II were eluted from the two 'tentacle-type' anion exchangers by gradient elution from 0-300 mM of displacing salt, using gradient times ranging from 17.1 to 171 min at a constant flow-rate of 1 ml/min. Similar conditions were used for the Mono-Q experiments. The retention data were evaluated according to the dependency of $\log \bar{k}$ on $\log 1/\bar{c}$ according to the relationships derived [5,6] from the Linear Solvent Strength Model, namely,

$$\log \bar{k} = \log K + Z_c \log 1/\bar{c}$$

where \bar{k} is the median capacity factor of the biosolute, *i.e.* the capacity factor of the biosolute at the mid-point of the column under gradient elution and \bar{c} is the median concentration of the displacing salt. The slope parameter (Z_c) can be taken as a measure of the average number of charges located in the contact area (ionotope) established between the protein and the sorbent surface. Tables III and IV summarise the results of this evaluation using NaCl and KBr, respectively. These Tables also include comparative data from the published literature for several of the proteins eluted with the same salts and gradient system from the Mono-Q sorbent. Values of

TABLE II
PHYSICAL PROPERTIES OF PROTEINS

Protein (source)	Abbreviation	pI	Molecular weight
Ovalbumin (hen egg white)	OV	4.70	43 000
Insulin (bovine pancreas)	INS	5.32	5 700
Carbonic anhydrase (bovine erythrocytes)	CA	5.89	30 000
Growth hormone (porcine recombinant)	GH	6.70	22 100
Myoglobin (sperm whale muscle)	MYO	7.68	17 500
Ribonuclease A (bovine pancreas)	RIB	9.60	12 640
Lysozyme (hen egg white)	LYS	11.00	14 300

TABLE III
RETENTION PARAMETERS FOR PROTEINS ELUTED WITH NaCl

Protein	Mono-Q		Fractogel-TMAE		LiChrospher-TMAE	
	Z_c	$\log K_c$	Z_c	$\log K_c$	Z_c	$\log K_c$
OV	9.4	51.3	7.0	37.4	1.4	6.7
INS	5.4	28.8	3.2	17.1	1.3	5.7
CA	3.1	17.3	2.4	11.8		Not retained
GH	3.1	16.0	4.6	23.5	0.8	3.5
MYO	4.6	17.0	3.3	16.1		Not retained
RIB	1.6	7.7	2.7	12.8	0.7	2.1
LYS	1.5	6.0		Not retained	4.9	24.3

$\log K_c$, which were determined by extrapolation of the $\log \bar{k}$ versus $\log (1/\bar{c})$ plots to the limit case of $\bar{c} \rightarrow 10^{-6} M$, are also included in Tables III and IV. $\log K_c$ values also provide some indication of the relative influence of experimental conditions on the affinities of protein solutes for the particular sorbent. Figs. 1-4 show the results of the elution behaviour of the test proteins over a range of ionic strengths for the Fractogel-TMAE and LiChrospher-TMAE sorbents.

Several observations can be made on the basis of the results shown in these figures and the derived values of Z_c and $\log K_c$ shown in Tables III and IV, about the retention behaviour of the selected proteins with these sorbents. The net-charge concept [7] has been widely used as a basis to predict the retention properties of proteins in both anion- and cation-exchange chromatography. According to this model, for strong anion-exchange systems, a protein will be retained when the solvent pH is greater than the pI of the protein. Inspection of the data, listed in Table III with NaCl as the displacer salt, reveals that this concept is not universally followed, with anomalous results observed for this group of proteins with the Mono-Q resin. For example, both the Z_c and $\log K_c$ values of the proteins decreased as the pI of the protein solute approached the pH of the solvent (pH 9.60). However, RIB and LYS, which have pI values equal to 9.60 and 11.00 respectively, exhibited significant retention on the Mono-Q sorbent. These results are in accord with the non-uniform distribution of

TABLE IV
RETENTION PARAMETERS FOR PROTEINS ELUTED WITH KBr

Protein	Mono-Q		Fractogel-TMAE		LiChrospher-TMAE	
	Z_c	$\log K_c$	Z_c	$\log K_c$	Z_c	$\log K_c$
OV	9.5	48.9	7.2	37.7	1.6	7.2
INS	3.9	20.9	2.8	14.8	1.6	6.5
CA	5.6	28.4	2.4	7.0		Not retained
GH	3.9	20.2	4.0	20.6	0.7	2.8
MYO	4.8	24.2	1.9	8.5		Not retained
RIB	0.8	3.5	1.6	7.1	0.4	1.7
LYS	3.3, 1.0	10.2, 5.3		Not retained	1.9	10.1

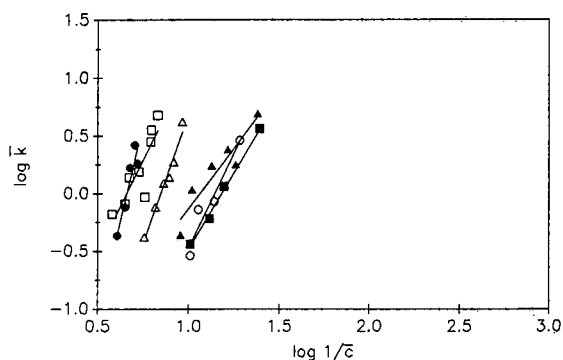


Fig. 1. Plots of $\log \bar{k}$ versus $\log 1/\bar{c}$ for proteins eluted on the Fractogel-TMAE column with NaCl as the displacer salt. The plots were derived from gradient elution data at pH 9.60, a flow-rate of 1 ml/min, with gradient times between 17.1 and 171.1 min. See Table II for code to protein solutes, and Table III for the Z_c and $\log K_c$ values obtained from these plots. \circ = MYO; \bullet = OV; \triangle = GH; \blacktriangle = CA; \square = INS; \blacksquare = RIB.

negatively charged amino acids on the protein surface which generate patches of negative charge through which binding of the protein to the stationary phase surface may occur.

Comparison of retention properties of the test proteins on the Fractogel-TMAE and LiChrospher-TMAE sorbents reveals several interesting behavioural features. Firstly, OV shows similar retention behaviour on the Fractogel-TMAE and Mono-Q sorbents, but the Z_c and $\log K_c$ values for OV diminished significantly with the LiChrospher-TMAE sorbent. This finding is surprising considering the pI of OV (4.70) is almost 5 pI units lower than the solvent pH. Similar behaviour was also observed with GH, and also for CA and MYO which were both unretained on the LiChrospher-TMAE sorbent. In contrast, the more basic proteins RIB and LYS were still retained on the LiChrospher-TMAE sorbent. Clearly, the density and/or the accessibility of the positively charged ligands on the silica based LiChrospher-TMAE tentacle support differ from that on the Fractogel-TMAE sorbent. These differences

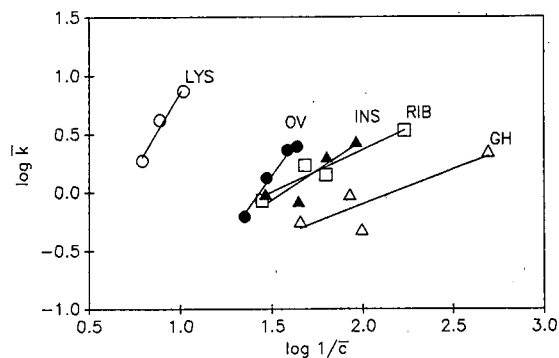


Fig. 2. Plots of $\log \bar{k}$ versus $\log 1/\bar{c}$ for proteins eluted on the LiChrospher-TMAE column with NaCl as the displacer salt. See legend to Fig. 1 for other details.

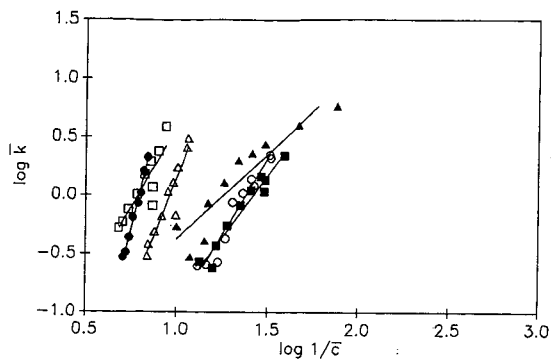


Fig. 3. Plots of $\log \bar{k}$ versus $\log 1/\bar{c}$ for proteins eluted on the Fractogel-TMAE column with KBr as the displacer salt. See legend to Fig. 1 for other details and Table IV for the Z_c and $\log K_c$ values obtained from these plots.

in retention behaviour observed for these tentacle sorbents reflect the composite effect of the ligand environment. In the case of the LiChrospher-TMAE sorbent, the N-trimethylaminomethylacrylamide chains are introduced via a pre-existing glyceridyl-propylsilane coverage of the silica surface, which will clearly represent a different chemical environment of hydroxyl groups to that occurring with the polydisperse hydroxy environment of the Fractogel HW65. In addition, the polymer characteristics of the silica or Fractogel matrix itself will engender secondary effects. A possible consequence of these effects is that other forces such as hydrophobic interactions may contribute to the interactive process. Depending on the quality of the glyceridyl-propylsilane coverage of the silica surface, residual silanol groups could also influence the retention behaviour, particularly with basic proteins such as LYS. In an associated study [3] we have shown that high coverage glyceridylpropyl silicas similar to those used in the present investigation do not however exhibit significant adsorption of proteins attributable to free silanols under elution conditions commonly used for ion exchange.

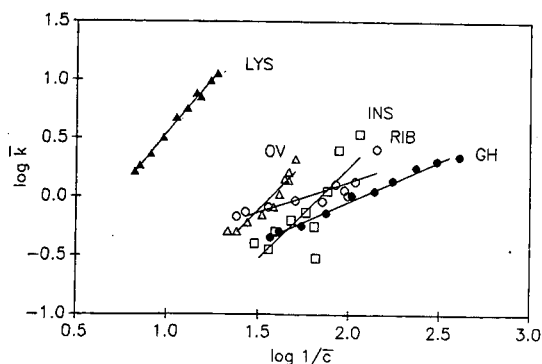


Fig. 4. Plots of $\log \bar{k}$ versus $\log 1/\bar{c}$ for proteins eluted on the LiChrospher-TMAE column with KBr as the displacer salt. See legend to Fig. 3 for other details.

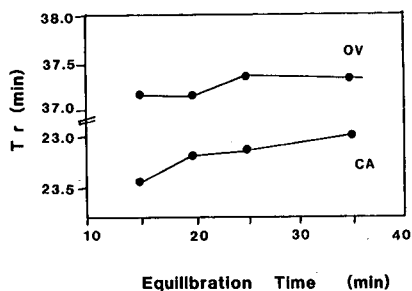


Fig. 5. Plots of retention time (T_r) versus equilibration time for OV and CA eluted on the Fractogel-TMAE column. The data were derived with a gradient time of 34.5 min and flow-rate of 1.0 ml/min and NaCl as the displacer salt.

The influence of the chaotropic salt KBr on the Z_c and $\log K_c$ values of the test proteins is listed in Table IV. According to the stoichiometric displacement model, the displacement of a protein solute from the charged surface is accompanied by the adsorption of a stoichiometric amount of displacer counter-ion. As a consequence, Z_c values should be independent of the chemical nature of the displacer ion and differences in $\log K_c$ should reflect the relative affinity of the counter-ion for the anion-exchange sorbent. Comparison of the Z_c and $\log K_c$ values for Fractogel-TMAE with both displacer salts reveals that similar behaviour was observed for all proteins on this resin. Similar Z_c and $\log K_c$ values were also observed for all proteins except LYS when eluted from the LiChrospher-TMAE sorbent. Once again, this result would not be anticipated for these proteins on the basis of their respective pI values *i.e.* their retention behaviour is not in accord with the classical Boardman-Partridge model. The Z_c and $\log K_c$ values for LYS decreased by a factor of 2 when KBr was employed as displacer salt. Similar results were also observed previously for LYS with the Mono-Q sorbent, and have been suggested [8] to be related to the conformational changes associated with the interaction of KBr with the lysozyme molecule.

After 250 h of continuous chromatographic elution under isocratic low or high salt conditions at 1 ml/min at pH 9.6, the LiChrospher-TMAE sorbent did not show

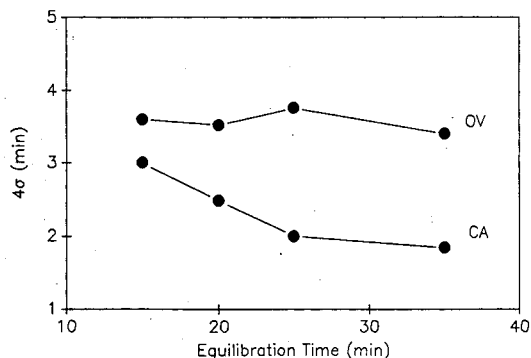


Fig. 6. Plots of solute bandwidth (4σ) versus equilibration time for OV and CA eluted on the Fractogel-TMAE column. See legend to Fig. 5 for other details.

any significant change in performance in terms of retention or peak shape variation. Similar stability of retention and peak shape was noted with continuous elution at pH 9.6 with the Fractogel-TMAE sorbent. However, changes in peak shape, which were protein specific, were noted as a consequence of the choice of re-equilibration time following a gradient experiment. Figs. 5 and 6 show examples of the effect of re-equilibration time with OV and CA as test proteins with the Fractogel-TMAE sorbent. In these experiments, a constant linear gradient time of 34.5 min at a flow-rate of 1 ml/min was used with a mixture of OV and CA injected at the same concentration. Following each gradient run, the time taken to re-equilibrate the column from the 100% buffer B conditions was varied from 15 to 35 min. As is evident from Figs. 5 and 6, no significant change in the retention time for either protein occurred following re-equilibration irrespective of the re-equilibration time. However, a change in peak width (as $4\sigma_v$) was evident for CA whilst the $4\sigma_v$ for OV showed more limited variation although the trend towards smaller $4\sigma_v$ values with longer re-equilibration times also occurred. It can be concluded from these results that re-equilibration volumes of approximately two-times the column volume will permit adequate re-conditioning. Such behaviour is consistent with the flexible nature of the tentacle surface but clearly the origin of this phenomenon requires further characterisation. However, it can be noted that similar kinetic variations have been noted with other fuzzy surface ion-exchange adsorption systems following regeneration, *e.g.* polymeric membranes following removal of fouling components [9].

CONCLUSIONS

The experimental data obtained in this study provides the first documentation of the retention dependencies, as revealed from the $\log \bar{k}$ versus $\log 1/\bar{c}$ plots, of several proteins with the so called 'tentacle-type' sorbents Fractogel-TMAE and LiChrospher-TMAE. As also noted in our earlier studies on the batch adsorption and kinetics of protein adsorption with similar tentacle-type sorbents [3], the surface properties and mode of chemical modification of the support material can strongly influence the chromatographic performance. The LiChrospher-TMAE is derived from the corresponding glycidylpropoxy-bonded silica with the oxirane ring opened by acidic hydrolysis. The matrix used for the Fractogel-TMAE sorbent is, in contrast, derived from polymerisation of various methacrylate esters with vinyl alcohol emulsifiers. These two hydrophilic support materials would thus be expected to generate two discrete classes of 'tentacle-type' sorbents following introduction of the individual, linear polyelectrolyte chains of N-trimethylaminomethyl acrylamide by radical grafting polymerisation initiated by Ce^{4+} ions. Differences in the chemical characteristics of the surface of the support material, including the hydroxyl group distribution, the effect of acrylamide monomer to hydroxyl group ratio, and the permeation of the monomer and Ce^{4+} initiator to the inner interstices of the porous particle will all affect the 'tentacle' polymer chain length, and ultimately the sorbent characteristics. Besides confirming that these new classes of anion-exchange sorbents exhibit $\log \bar{k}$ versus $\log 1/\bar{c}$ dependencies compatible with other microparticulate sorbents in current use for the analysis and purification of proteins and polypeptides, these studies also highlight the need for additional, detailed investigations on protein adsorption behaviour with chromatographic sorbents in order to allow further improvements in sorbent design to be affected.

ACKNOWLEDGEMENTS

These investigations were supported by grants from the Australian Research Council and Monash University Research Grants Committee.

REFERENCES

- 1 N. Afeyan, S. Fulton, N. Gordon, I. Mazsaroff, L. Varady and F. Regnier, *9th International Symposium on HPLC of Proteins, Peptides and Polynucleotides, Philadelphia, PA, Nov. 6-8*, Abstract 101.
- 2 N. Afeyan, D. Whitney, L. Varady, I. Mazsaroff, N. Gordon and S. Fulton, *Abstract 10th International Symposium on HPLC of Proteins, Peptides and Polynucleotides, Wiesbaden, Nov. 1990*.
- 3 R. Janzen, K. K. Unger, W. Müller and M. T. W. Hearn, *J. Chromatogr.*, 522, (1990) 77.
- 4 W. Müller, *J. Chromatogr.*, 510 (1990) 133.
- 5 A. N. Hodder, M. I. Aguilar and M. T. W. Hearn, *J. Chromatogr.*, 476 (1989) 391.
- 6 A. N. Hodder, M. I. Aguilar and M. T. W. Hearn, *J. Chromatogr.*, 512 (1990) 41.
- 7 N. K. Boardman and S. M. Partridge, *Biochem. J.*, 59 (1955) 543.
- 8 A. N. Hodder, K. J. Machin, M. I. Aguilar and M. T. W. Hearn, *J. Chromatogr.*, 517 (1990) 317.
- 9 A. G. Fane and J. M. Radovich in J. A. Asenjo (Editor), *Separation Processes In Biotechnology*, Marcel Dekker, New York, 1990, pp. 236.
- 10 M. C. J. Wilce, M. I. Aguilar and M. T. W. Hearn, *J. Chromatogr.*, 548 (1991) 105.

CHROMSYMP. 2315

High-performance liquid chromatography of amino acids, peptides and proteins

CXII^a. Analysis of operating parameters affecting the breakthrough curves in fixed-bed chromatography of proteins using several mathematical models

A. JOHNSTON, Q. M. MAO and M. T. W. HEARN*

Department of Biochemistry and Centre for Bioprocess Technology, Monash University, Clayton, Victoria 3168 (Australia)

ABSTRACT

Performance of a packed bed, in terms of adsorbent utilization and kinetic characteristics, was studied for the adsorption of HSA to the ion-exchange resins, DEAE Trisacryl M and DEAE Sepharose FF. The influence of column length, temperature and feed concentration on the shape of the breakthrough curve has been investigated and the resulting operating capacities, q^* measured by graphical integration. Mathematical models prevalent in the literature have been used to extract out the kinetic parameters, the effective diffusivity, D_p , and the interaction rate constant, k_1 , from the experimental breakthrough curves, and these parameters have been used to evaluate the performance of the columns and to validate the models selected. The effect of protein size on the adsorption behaviour was also investigated using the proteins HSA, transferrin and ferritin, determining q^* , k_1 , and D_p from the breakthrough curves.

INTRODUCTION

Chromatographic separation of proteins relies upon the differential rates of solute migration encompassing relative retention characteristics throughout a packed bed. In such systems, complex mixture of proteins can be separated on the basis of biophysical differences, such as apparent ionic charge (ion-exchange chromatography), hydrodynamic size (gel filtration), hydrophobicity (reversed-phase chromatography, hydrophobic interaction chromatography), as well as on the basis of functional differences, utilizing their preferential affinities for biospecific and biomimetic adsorbents (affinity chromatography).

On a preparative scale, large volumes of a fermentation broth or a biological fluid are required to be processed to extract the protein of interest. In process

* For Part CXI, see ref. 36.

applications, the feed is often continually loaded down a packed chromatographic bed, the upper part of the bed, at the feed entrance, selectively adsorbing the proteins in order of their respected affinities and diffusivities. Protein left in the bulk solution is substantially removed by the lower layers of the adsorbent, near the exit, and the effluent becomes essentially protein depleted, as illustrated by the curve shown in Fig. 1 (position a). At some time later the bed becomes saturated, the proteins appear in the effluent (position b) and the bed is then said to have reached the breakthrough point. Protein concentration in the effluent continues to rise until the outlet concentration reaches the value of the inlet concentration (see Fig. 1, position c). The concentration profile emerging from the bed is termed the breakthrough curve. This type of

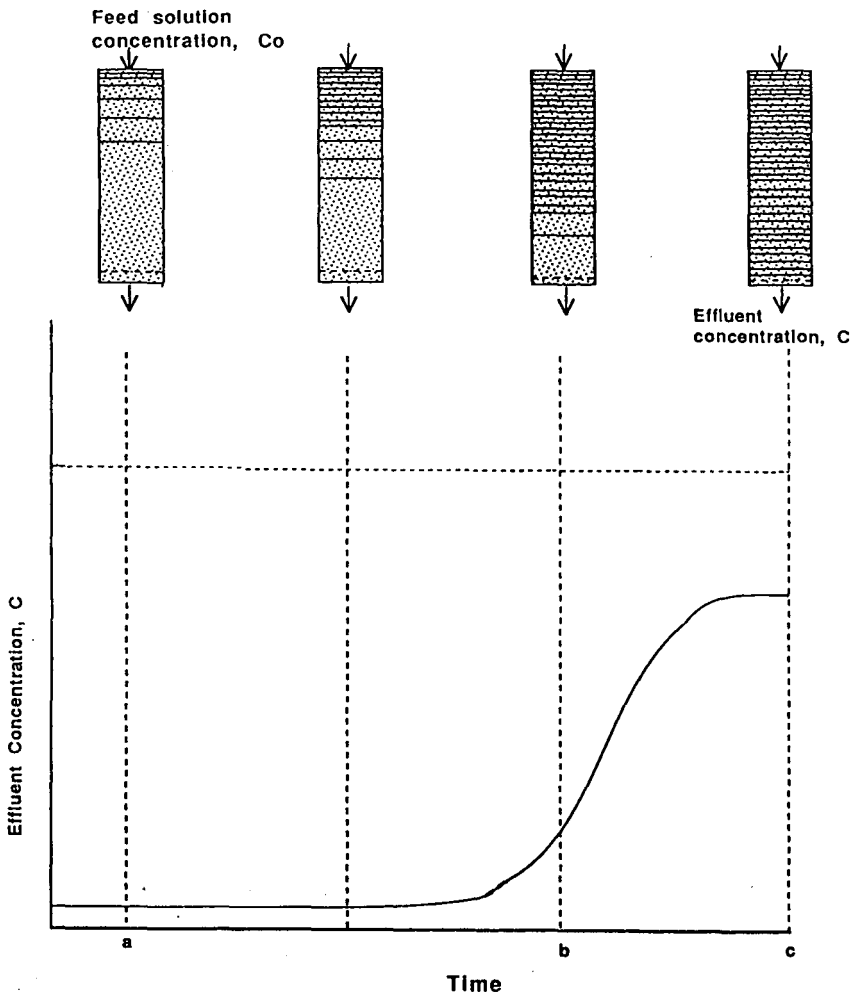


Fig. 1. Schematic representation of the adsorption of a protein solution to a resin in a packed bed, progressing as bands, or adsorption zones, with the effluent concentration profile (breakthrough curve) emerging from the packed bed.

preparative loading (frontal chromatography) is in direct contrast to analytical zonal chromatography, where the sample to be separated is injected in small quantities as a pulse onto the top of the column.

Breakthrough curves represent important profiles of the processes which are occurring down the chromatographic bed. Two characteristics of these breakthrough curves are important in assessing the performance of the bed: firstly, the position of the breakthrough curve which depends *inter alia* on the operating capacity of the adsorbent, and secondly the shape, which can be indicative of the interaction kinetics of the protein. In preparative chromatography, feed loading is usually terminated when the protein concentration in the effluent exceeds a certain amount. This choice is made to maximize the capacity of the adsorbent and minimize the amount of protein lost in the effluent. A steep breakthrough curve is therefore desirable. Thus, with knowledge of the adsorbent's capacity and its adsorption kinetics, the operating performance of the system can be optimized. This optimization becomes increasingly more important in preparative biochromatography where high productivity and high yield of product are paramount.

This study then represents an initial cross-examination of some of the factors thought to influence adsorption behaviour of ion-exchange adsorbents in process biochromatography. The parameters studied include the column length, temperature and feed concentration, as well as the effect of the size of the protein, and were selected to assess their effects on the breakthrough curves. Graphical integration and mathematical models found in the literature were also used to extract out physico-chemical parameters governing the adsorption process, from the experimental profiles emerging from the operation of packed bed chromatographic systems.

THEORY

Equilibrium parameters of an ion-exchange resin

For a packed bed, operating at constant flow-rate, the operating capacity can be calculated by graphical integration as seen by the relationship,

$$q^* = \int_{V=0}^{V_f} \frac{[C_0 - C(t)]dV}{V_c} \quad (1)$$

where q^* = protein concentration bound to the resin in equilibrium with C_0 ; C_0 = feed concentration, inlet concentration; $C(t)$ = protein concentration in the effluent at any time, t ; V = volume of feed passed through the column; V_c = volume of the chromatographic bed; V_f = total volume passed. This graphical treatment is applicable to high interaction rates, and is based on the concept that interaction occurs within an adsorption zone that descends through the packed bed, see Fig. 1.

Analysis of the shape of the curve can be initially based on visual examination. If the adsorption process was infinitely rapid, the curve would appear as a sharp rectangular front. However, in many situations a sigmoidal shape is commonly seen which is the result of a complex interplay of equilibrium and non-equilibrium processes occurring during adsorption. The curve may be steep or relatively flat or in some cases

considerably distorted [1] as a consequence of inadequate fluid mixing along the bed, slow kinetics of adsorption, slow diffusion of the protein, non-specific adsorption or conformational changes of the protein. The steepness, or slope, of the profile can be estimated from measurements of the "spread" of the curve, which is determined by the difference between the volume throughput at 10% saturation (V_{10}) and the volume throughput at 90% saturation (V_{90}). For ideal, infinitely fast adsorption, the breakthrough curve is a sharp front, the spread is minimal, and thus the difference between V_{10} and V_{90} is zero.

Mathematical models

A quantitative analysis of the non-equilibrium effects contributing to the shape of the breakthrough curves is only possible if the chromatographic process can be described in physical terms based on mathematical solutions. In this context, the concept of a theoretical model (from the word "modus", a measure) implies that the process can be described by a set of equations which reflect the physical reality of the adsorption and mass transport events. Mathematical descriptions of adsorption processes in biochromatography first gained prominence in the 1940's, when the local equilibrium model was developed. The adsorption behaviour was derived from purely thermodynamic considerations, yielding equilibrium isotherms that were based on either a constant separation factor (for example the Freundlich isotherm), the Langmuir equation or simply empirical relationships. Martin and Synge [2] put forward the plate theory, directly relating adsorption chromatography in a fixed bed to fractional distillation and extraction processes. According to the plate theory, the chromatographic bed consists of a number of theoretical plates, and within each plate local equilibrium was established between the mobile and stationary phases. Diffusion between the plates was assumed negligible. The equilibrium relationship between the two phases was a linear one, with the distribution ratio being independent of the concentration of the solutes. The plate theory has been widely used in analytical zonal chromatography to predict peak positions and widths [3,4] but has limited application in preparative chromatography, where the interaction between the solutes and the phases is no longer a simple linear first order process, that is, overloaded conditions may apply.

Although simple in concept and computation, these numerical solutions derived from the plate theory also provide little insight to the understanding of the dynamics of adsorption. It must be remembered that the adsorption of a protein to an adsorbent is a dynamic process: local equilibrium will rarely be achieved in this flowing system, partly because it takes time for the protein to reach the surface of the adsorbent, and partly because diffusion inside a porous adsorbent can be comparatively slow. Obviously, the slower the fluid flow and the larger the pores of the adsorbent, the more complete the process approaches the near-equilibrium criterion.

If the process is seen then, as a series of mass transfer mechanisms operating at or near equilibrium, the mathematical equations become a complex set of partial differential equations, too complex as yet to solve analytically. Other approaches to modelling this dynamic process have therefore been concerned with simplifying the equations, by assuming that one mass transfer mechanism predominantly controls the adsorption, see Golshan-Shirazi and Guiochon [5] for an extensive review. For example, Hubble [6] describes a simple model in which all the mass transfer resistances

except the rate of interaction have been neglected, and the mathematical equations are solved in discrete stages down the column bed. Applying it here to ion-exchange adsorption of protein, the model of Hubble gives the concentration of protein adsorbed to the resin as,

$$q = \frac{(b - \sqrt{x})(2k_1q_0 + b + \sqrt{x}) - (b + \sqrt{x})(2k_1q_0 + b - \sqrt{x})e^{(t\sqrt{x})}}{2k_1[e^{(t\sqrt{x})}(2k_1q_0 + b - \sqrt{x}) - (2k_1q_0 + b + \sqrt{x})]} \quad (2)$$

where $x = (b^2 - 4k_1^2C_{0i}q_m)$; $b = -(k_1C_{0i} + k_1q_m + k_2)$; C_{0i} = inlet concentration of stage i ; k_1 = forward rate constant; k_2 = reverse rate constant; q = concentration of adsorbed protein at any time, t ; q_m = maximum protein capacity of the adsorbent; q_0 = initial concentration of protein adsorbed at each stage.

Thomas [7] devised an analytical solution to the mass balance equations that describe fixed bed ion-exchange adsorption for small solutes and fixed bed gas adsorption. The solution is based on a second order rate of exchange, assuming all other mass transport resistances are negligible. When applied to protein adsorption to ion-exchange sorbents, the concentration emerging from the column can be calculated from the sigmoidal relationship,

$$\frac{C(t)}{C_0} = \frac{J(n/r, nT)}{J(n/r, nT) + [1 - J(n, nT/r)] \exp[(1 - 1/r)(n - nT)]} \quad (3)$$

where $r = 1 + C_0/K_d$; $n = q_m k_1 z / u_0$; $T = [u_0(K_d + C_0) / (z q_m)](t - z\varepsilon / u_0)$; $K_d = k_2/k_1 = 1/K_a$; ε = bed voidage; J = the integral of the Bessel function; u_0 = superficial velocity; z = column length, bed height.

Arnold *et al.* [8] have argued that with porous particles the rate at which protein diffuses into the interior is likely to be significant. In fact, it is conceivable that if the protein to be purified has a large hydrodynamic radius and the pore openings of the sorbent are small, mass transfer of the protein will be reduced due to the geometric restraints placed upon its movement into the pores. Arnold *et al.* in development of their model equations, have visualized the mass transfer steps as a number of transfer units each acting in series. Their simplified solution is based on the assumption that the effect of axial dispersion is small and that the rate of adsorption is infinitely fast compared to the effects of pore diffusion. The equation for the breakthrough curve takes the form,

$$T-1 = \left(\frac{1}{N_{\text{pore}}} + \frac{1}{N_f} \right) \left[\phi(X) + \frac{N_{\text{pore}}}{N_f} (\ln X + 1) \right] \left(\frac{N_{\text{pore}}}{N_f} + 1 \right)^{-1} \quad (4)$$

where $\phi(X) = 2.44 - 3.66\sqrt{1-X}$; $X = C(t)/C_0$; $T = (V - \varepsilon v) / (\rho_b q^* v / C_0)$; $N_{\text{pore}} = 15D_p(1 - \varepsilon)z / r_p^2 u_0$; $N_f = K_f a_p z / u_0$; a_p = external surface area of the adsorbent per unit volume of the bed; $C(t)$ = concentration of protein in solution at any time; t ; D_p = effective (pore) diffusivity; K_f = film mass transfer coefficient; q^* = equilibrium concentration of protein adsorbed; ρ_b = bulk density of the adsorbent; v = volume of the adsorbent.

For cases where the equilibrium relationship is no longer a linear one, and more than one mechanism is proposed to operate, the interrelated equations become too complex for an exact, analytical solution, and numerical computation offers the only practical solution. Vermeulen [9] has outlined a solution to the mass balance equations using an empirical approximation to the finite series arising from the equations. Fleck *et al.* [10] used the finite difference method of Crank and Nicholson, basing their solution on a constant flow pattern, and assuming a dominantly slow interaction rate of mass transfer within the adsorbent. Katoh *et al.* [11] use this same technique to evaluate the breakthrough curve from the adsorption of trypsin to the affinity adsorbent, Sepharose 4B-STI. Garg and Ruthven [12] also used this technique for describing the micro-diffusion during molecular sieving. Orthogonal collocation techniques are also gaining popularity, despite the fact that the large grid system necessary for an accurate solution often renders long computational times. Some investigators have solved the equations by collocation techniques using various equilibrium relationships. For example, Tien and Thodos [13] have derived solutions for favourable Freundlich isotherm, Morton and Murni [14] for an empirical non-linear relationship, whilst Antonson and Dranoff [15] have applied these techniques to the Langmuir isotherm. These investigators [13–15] have all assumed that intraparticle diffusion is the rate controlling mechanism, thus reducing the complexity of their numerical solutions. Also using orthogonal collocation techniques, Arve and Liapis [16] have incorporated three rate controlling mechanisms, that is, resistances due to pore diffusion, film diffusion and the dynamics of the interaction step, into a computational solution for the breakthrough profile. The fundamental mass balance equation from which their solution is derived takes the form.

$$D_a \frac{\partial^2 C(t)}{\partial x^2} - \frac{u_0}{\varepsilon} \frac{\partial C(t)}{\partial x} = \frac{\partial C(t)}{\partial t} + \left(\frac{1 - \varepsilon}{\varepsilon} \right) \frac{\partial q}{\partial t} \quad (5)$$

where D_a = axial diffusivity; x = distance down the bed. The overall rate of change of the amount of protein adsorbed to the sorbent, $(\partial q / \partial t)$, is dictated by various mass transfer coefficients and surface interaction rates. As yet there is no exact solution to eqn. 5. There are, however, conditional solutions provided that certain terms are neglected or that fixed values (sometimes unreasonable) are chosen for the boundary conditions. Eqns. 2–4 represent these conditional solutions. Unconditional solutions arise from numerical techniques, such as those developed by Arve and Liapis. Despite the inherent pitfalls of numerical, brute-force solutions, particularly with respect to numerical instability, and lengthy computational time, the solution of Arve and Liapis, represents the most advanced treatment yet available for the quantification or prediction of the adsorption behaviour of proteins. Neglecting the axial diffusion term, D_a , in eqn. 5, the numerical solution is described by Arve and Liapis [16] and is referred to hereafter in conjunction with eqn. 5.

It is important to recognise that each mass transfer resistance may affect the efficiency of the adsorption process to a different extent, and thus subtle differences may be evident in the pattern of the breakthrough curves emerging from the packed bed. This can be seen most clearly in a pictorial representation, as shown in Fig. 2, which compares theoretical profiles for the chemical adsorption process of small solutes under non-linear conditions, taken from mathematical model solutions

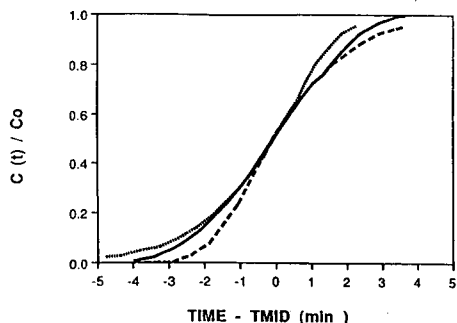


Fig. 2. Theoretical breakthrough curves for a Langmuir equilibrium equation, for different rate controlling mechanisms. The time is taken from the moment when enough liquid has passed through to displace the column dead volume and TMID corresponds to the time at 50% breakthrough, the midpoint. = Fluid film; ——— = pore diffusion and - - - = solid film.

outlined in the literature [17]. For a particular set of operating conditions, the differences between the curves generated from either a pore diffusion model, a solid film resistance model or a liquid film resistance model are significant, and the greatest difference is seen at the initial time region. Thus, if a film diffusion model were to be used when pore diffusion restrictions were significant, large errors in predicting the dynamic capacity could occur. To further emphasize the differences in the theoretical predictions of the breakthrough curves incurred from different models, Fig. 3 compares the breakthrough curves derived from the models used in this investigation and outlined above. The models of Hubble [6] and Thomas [7] assume that the adsorption is controlled by the rate of interaction, Arnold *et al.* [8] assume the rate limiting step is pore diffusion, whilst Arve and Liapis [16] include three rates; an interaction rate, pore diffusion and a film coefficient. The curves of Fig. 3 were derived for a given set of conditions, $k_1 = 0.01$ mg/ml s and $D_p = 6.1 \cdot 10^{-11}$ m²/s, and for these conditions the models of Hubble and Thomas give nearly identical curves as expected. For the same k_1 , the model of Arve and Liapis predicts a shallower curve. This is because the model

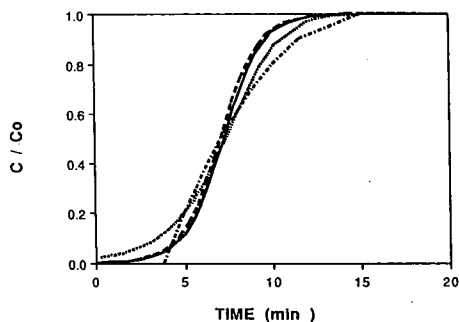


Fig. 3. Comparison of the theoretical solutions based on the adsorption of human serum albumin to DEAE Trisacryl M. ——— = Hubble [6]; - - - = Thomas [7]; = Arnold *et al.* [8] and - · - · - = Arve and Liapis [16]. $C_0 = 1.5$ mg/ml, $q_m = 20$ mg/ml resin, $K_a = 56$ ml/mg, $u_0 = 0.042$ cm/s, $z = 1.3$ cm, $K_f = 8 \cdot 10^{-6}$ m/s, $k_1 = 0.01$ ml/mg s.

of Arve and Liapis includes not one but three independent rate constants, and thus the overall resistance, which is proportional to the sum of the reciprocal of each of these constants, will be higher. A higher overall resistance will therefore render a shallower breakthrough curve. In other words, if one were to fit a particular experimental curve, the best correlated value of k_1 , computed from the model of Hubble or Thomas, will be low or a slow rate. The model of Arve and Liapis, will give a higher k_1 value, or a faster rate, which will be a closer approximation to the true rate of interaction.

When simplifying assumptions are used to reduce the mass balance equations from an intractable, complex form into something more manipulative, the question then should be raised as to what the physical consequences are. Have these assumptions any relation to the treatment of the experimental data? Are the assumptions physically valid?

In spite of the limitations of the models outlined above, each has contributed further towards understanding the adsorption process with biopolymers. Which model to select to adequately characterise the process at hand depends on the complexity of the feed stock, the integrity of the target protein and the homogeneity of the adsorbent's micro- and macro-structure. Moreover, the model may satisfy the necessary conditions to provide an adequate description of the overall experimental mass transfer resistances but not provide a sufficient condition to allow discrimination of the individual kinetic events [5,18]. However, most important is whether the selected model provides practical guidelines for the scale-up of the purification at the plant level. Such a selection may in fact use a model which does not precisely reflect the physical realities of the adsorption process. Equally relevant is the need for more precise physical models with extensive data bases which simulate more adequately the experimental measurements. Even with the sophisticated mathematical processing packages which are currently available, long computational times are often required and these theoretical methods cannot as yet accommodate the simplest error function in process chromatography as practiced today—the inadvertent foibles of the plant operator.

The development of the heuristic and physical criteria which will allow the choice of a particular model remains an important and challenging task. The aim of this work was thus twofold. Experimental data has been generated to provide an examination of the parameters influencing the breakthrough curve, and hence the efficiency of the chromatographic column, with specific reference to the effect of column length, temperature, concentration and the pore to protein size ratio. These data have then been used to test the efficacy of four of the models discussed above. The solutions of Hubble (eqn. 2), Thomas (eqn. 3) and Arve and Liapis (eqn. 5) have been adapted to obtain the interaction rate constant, k_1 , for several proteins to an anion-exchange sorbent, whilst the values for effective diffusivity, D_p , were extracted from the solutions of Arnold (eqn. 4) and Arve and Liapis (eqn. 5) for human serum albumin (HSA) with two different anion-exchange sorbents.

The effect of operating parameters

Van Deemter plots, showing the dependence of column efficiency, measured in terms of height equivalent to a theoretical plate (HETP) on the flow velocity are abundant in the literature [19,20]. The adverse effects of operating packed bed chromatographic systems at high flow velocities are clearly evident from such plots. To

obtain a small HETP and therefore an efficient separation process, uniform packing of the sorbent is essential with polydisperse particles. A significant loss of efficiency can incur through uneven size distribution of the adsorbent causing local variation in the bed voidage. Due to current limitations in packing technology, the problem of uneven packing becomes increasingly severe as the bed length and diameter increases, and this can then lead to maldistribution of the feed flow. These limitations result in shallow and distorted breakthrough curves. The length of the column has therefore been recognised as an important and influential parameter, and its effect on the breakthrough curve, and hence column efficiency has been addressed here.

Another parameter thought to influence process performance is temperature. It is known that an increase in temperature leads to a decrease in fluid viscosity, which will render an increase in the mobility, and hence diffusivity, D_m , of protein in solution (according to the correlation developed by Young *et al.* [21], $D_m \propto 1/(MW T^{1/3})$). High diffusivities will in turn lead to better mixing and faster mass transfer. Yamamoto *et al.* [4] have shown that an increase in temperature decreases the HETP of an analytical chromatographic column. Davies *et al.* [22] have shown a greater capacity in the separation of bilirubin from albumin in ion-exchange chromatography, when the system is operated at high temperature. From a thermodynamic point of view, this observation is not surprising. If the process of protein adsorption to an ion-exchange resin is exothermic, an increase in temperature will favour an increase in capacity, q^* . Indeed, the Van't Hoff equation predicts an increase in the association constant reflecting the change in the strength of interaction.

The effect of feed concentration on the adsorption performance is also of interest. Chromatographic operation in the overload mode, that is, at high solute concentrations, has been demonstrated to improve the productivity of mass transport in a separation process [23,24]. Why this occurs has not yet been elucidated. On the other hand, it has been suggested that there is a dependency of protein diffusivity on concentration. At high solution concentrations (> 1 mg/ml) the protein may have less freedom to move about by Brownian motion because of the increased number of molecules in solution and because of possible lateral interactions with increasing amounts of protein bound to the resin. Lundstrom and Elwing [25] and Petropoulos *et al.* [26] have viewed the interaction of protein-protein and protein-adsorbent in terms of surface coverage. Petropoulos *et al.* illustrated that the binding capacity depends on the availability and the probability of a protein in solution finding an adsorbed protein without any nearest neighbours, and at high coverages the availability and the probability will be low and thus the lateral interactions will become more significant. Thus high feed concentrations may influence the adsorption behaviour and hence alter the shape of the breakthrough curve.

Restricted diffusion is also believed to affect the performance of an adsorbent, and result in elongated breakthrough curves. A protein of large molecular dimensions is therefore anticipated to experience geometric constraint as it adsorbs to the porous resin. Furthermore, the effective aperture of the pore openings will diminish very quickly as the large protein molecules bind. Because of these influences the effect of protein size on the physicochemical parameters, k_1 and D_p , has also been addressed here as part of the present investigations.

MATERIALS AND METHODS

HSA was supplied as a 21% solution from Commonwealth Serum Laboratories (C.S.L.) (Melbourne, Australia), human apotransferrin, and ferritin isolated from horse liver, were purchased from Sigma (St. Louis, MO, USA). Fresh protein solutions were prepared with buffer the day of experimentation. For HSA and ferritin a 20 mM sodium acetate-acetic acid, pH 5.2 buffer, was chosen, unless stated otherwise, whilst 20 mM Tris-HCl, pH 7.0 was needed to affect adsorption of apotransferrin. Buffer salts were obtained from Aldrich (Milwaukee, WI, USA). Two weak anion-exchange resins were used in the experiments. Pharmacia DEAE Sepharose Fast Flow (FF) was selected as being a resin widely used in industry and therefore likely to be subjected to the variation in operating parameters investigated in this work. DEAE Trisacryl M, purchased from Australia Chemical Company (Melbourne, Australia) was selected for studying the effects of pore-to-protein size because (i) of its high molecular cut-off (according to the manufacturer), (ii) of its narrow particle size distribution and (iii) it has been used with our previous results with good reproducibility.

Pharmacia 5/5 HR columns (0.5 cm I.D., 5 cm maximum column length) were packed with the ion-exchange resins, DEAE Sepharose FF and DEAE Trisacryl M, to a bed height of 1.1–4.5 cm. When studying the temperature effects the columns were immersed in a water bath, maintained at a constant temperature. The other

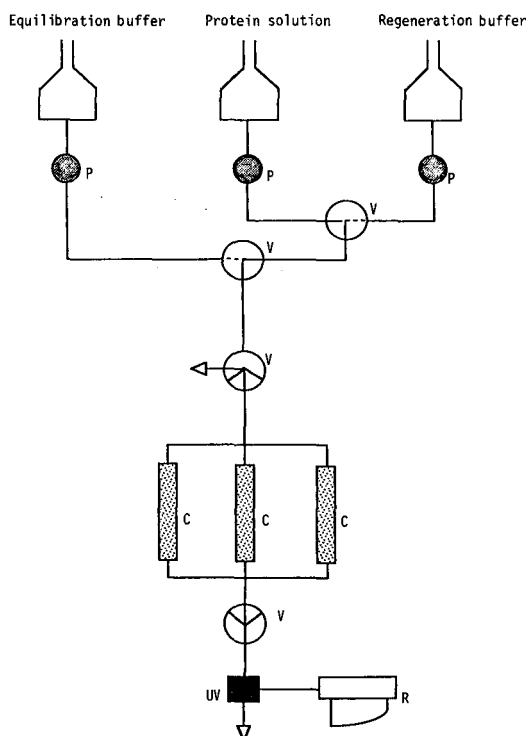


Fig. 4. Experimental set-up for fixed-bed configuration. P = Pump; UV = UV detector; V = valve; C = FPLC column and R = chart recorder.

experiments were carried out at room temperature. The columns were connected to a fast performance liquid chromatograph (FPLC) LC-500, from Pharmacia, that enabled automated and sequential loading, washing and elution of three identical columns. The effluent passed through a Model 1 UV Spectrophotometer, from Pharmacia (Uppsala, Sweden), which measured protein concentration at 280 nm, and this was linked to a two-pen chart recorder from Pharmacia for tracing the breakthrough curve. The experimental set-up is given in Fig. 4.

The protein concentrations were selected to ensure that the maximum capacity of the resin was attained so that overloaded conditions were maintained. These concentration levels were determined from the isotherms generated from batch experiments derived from our previous experiments [27,28]. Unless stated, a feed concentration of 1.5 mg/ml for HSA and transferrin and 0.1 mg/ml for ferritin was loaded onto the columns at a rate of 0.5 ml/min ($u_0 = 0.042$ cm/s).

The theoretical solutions of eqns. 2-5 were generated by computer programs written in PASCAL or FORTRAN on an IBM PC linked to a VAX mainframe. Graphical integration of the experimental breakthrough curves were also performed using the IBM PC.

Values for the film mass transfer coefficient, K_f , were taken from the correlation of Ohashi *et al.* [29] whilst the value for the mobile free diffusivity was calculated from the correlation given by Young *et al.* [21].

RESULTS AND DISCUSSION

Influence of column length, temperature, feed concentration and protein size on the capacity of the adsorbent and the shape of the breakthrough curve

Fig. 5 illustrates the change in the shape of the breakthrough curve for the adsorption of HSA to DEAE Trisacryl M with decreasing column length. Here it is clearly evident that the shorter the column, the sharper the profiles at the initial stages of adsorption. This observation concurs with the concept that in practical terms, with short columns consisting of preparative sorbents of broader particle diameter, the

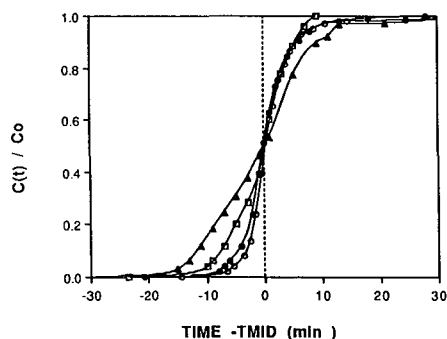


Fig. 5. Experimental breakthrough curves for the adsorption of HSA to DEAE Trisacryl M, showing the influence of bed length. The time is taken from the moment when enough liquid has passed through to displace the column dead volume and TMID corresponds to the time at 50% breakthrough, the midpoint. \circ = 1.4 cm; \bullet = 2.3 cm; \square = 2.7 cm; \blacktriangle = 4.5 cm; --- = ideal.

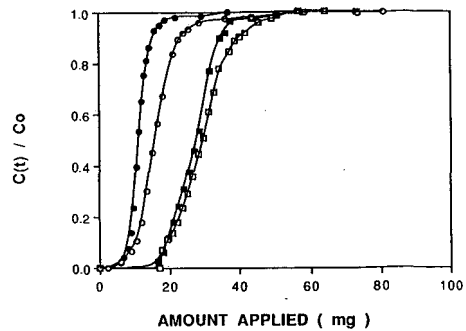
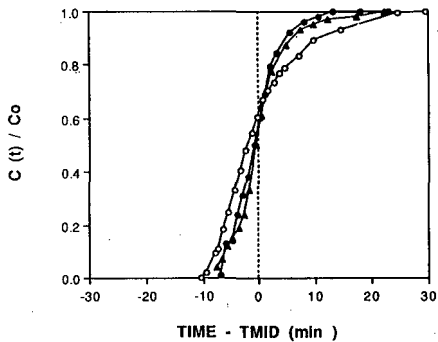


Fig. 6. Experimental breakthrough curves for the adsorption of HSA to DEAE Trisacryl M, showing the influence of temperature. $z = 1.3$ cm. $\circ = 4^\circ\text{C}$; $\bullet = 25^\circ\text{C}$; $\blacktriangle = 60^\circ\text{C}$ and $---$ = ideal.

Fig. 7. Experimental breakthrough curves for the adsorption of HSA to DEAE Trisacryl M, showing the influence of concentration at two different lengths. $\blacksquare = 1.5$ mg/ml and 4.5 cm; $\square = 3.0$ mg/ml and 4.5 cm; $\bullet = 1.5$ mg/ml and 1.4 cm; $\circ = 3.0$ mg/ml and 1.4 cm.

greater the likelihood that the column is better packed and an even flow established throughout the bed, allowing a better performance. Further experiments with non-interactive low molecular solutes acting as probes could have been used to confirm this result.

A sharper breakthrough at the initial stage is also obtained at higher temperatures as illustrated by the profiles for the adsorption of HSA to DEAE Trisacryl M in Fig. 6. At high temperatures the protein solution is less viscous so that fluid mixing within the bed is superior. A similar trend with temperature was found when HSA was loaded onto a column packed with DEAE Sepharose FF (results not shown). The influence of the feed concentration is illustrated in Fig. 7, using the adsorption of HSA to DEAE Trisacryl M as an example. Slightly more distortion of the breakthrough curve is evident at higher concentrations, and this might be attributed to a decrease in the diffusion of the protein in solution. Mathematical simulations [30] of the adsorption of protein solution onto non-porous particles, using

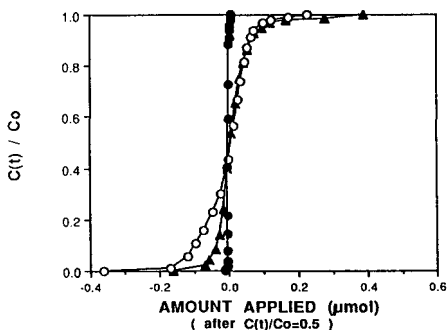


Fig. 8. Experimental breakthrough curves for the adsorption of different proteins to DEAE Trisacryl M, showing the influence of protein size. $C_0 = 1.5$ mg/ml for HSA (\blacktriangle) and transferrin (\circ) ($\text{pH} = 7.0$), $C_0 = 0.1$ mg/ml for ferritin (\bullet), $z = 1.8$ cm.

modifications of eqns. 1 and 3, have demonstrated that with this type of sorbent there is no change in the shape of the breakthrough curve for increasing protein concentration. From these simulations and the experimental results it can be concluded that the trend shown in Fig. 7 may be due to an increase in the restriction of movement of protein into the pores. This result was investigated further in terms of the model equation of Arnold *et al.* [8] and Arve and Liapis [16], as discussed later.

The effect of the protein size on packed bed adsorption was investigated using HSA, transferrin and ferritin and DEAE Trisacryl M. The experimental profiles in Fig. 8 represent the effluent concentration of the three proteins with respect to the amount of protein applied to the column. The curves were matched at the midpoint ($C(t)/C_0 = 0.5$) to standardize the different concentration used. ($C_0 = 1.5$ mg/ml for HSA and transferrin, whilst $C_0 = 0.1$ mg/ml for ferritin). A comparison of the curves of Fig. 8 leads to the conclusion that the largest protein, ferritin has the sharpest front, which is contrary to what one would expect, since one might anticipate that the slow diffusion of the large protein would render slow kinetics and a shallow curve. In addition, high values of the rate constants obtained for the experimental breakthrough curves of ferritin adsorbing to DEAE Trisacryl M were calculated, see Table IV, which corresponds to the sharp front of Fig. 8. The extremely small value for the capacity, $q_m = 0.003$ μ mol/ml, suggests that ferritin may only bind to the external surface of the

TABLE I

COMPARISON OF LENGTH, TEMPERATURE AND CONCENTRATION ON THE SPREAD OF THE BREAKTHROUGH CURVE, ($V_{10}-V_{90}$) AND THE AMOUNT BOUND (OPERATING CAPACITY, q^*)

Resin ^a	Length (cm)	Temperature (°C)	Concentration (mg/ml)	$V_{10}-V_{90}$ (ml)	Capacity, q^* (mg/ml)
Trisacryl M	1.1			5.3	34
	1.3			6.8	45
	1.6			4.4	36
	2.3			5.3	36
	2.7			6.6	32
	4.5			10.5	31
Trisacryl M		4		9.4 ^b	31 ^c
		25		6.1	35
		60		6.1	39
Sephacryl FF		4		8.8	36
		10		9.6	38
		25		6.4	43
		38		6.9	45
Trisacryl M			1.5 ^d	4.4	36
			3.0	4.3	50
			1.5 ^e	10.5	32
			3.0	13.0	33

^a HSA adsorption.

^b Standard deviation 20–30%.

^c Standard deviation 5–17%.

^d 1.4 cm column length.

^e 4.5 cm column length.

sorbent particles. If this is the case, there is no slow diffusion into the pores, so that the overall rate, reflected in the value of k_1 , becomes fast.

The change in the sigmoidal pattern of the breakthrough curves of Figs. 5–8 has been assessed from the values of $V_{10} - V_{90}$. As noted in the Introduction, large $V_{10} - V_{90}$ values represent large deviations from ideal, equilibrium behaviour. Table I, compares the $V_{10} - V_{90}$ values obtained from the breakthrough curves of HSA adsorbing to DEAE Sepharose FF for different bed lengths, temperatures and feed concentration. Although there is some experimental scatter amongst the values, it is clearly evident that short columns (1–2 cm bed heights) have low $V_{10} - V_{90}$ values whilst those for long columns (4–5 cm bed heights) are two-fold higher. This trend was also seen for the DEAE Sepharose FF studied (data not shown). Similarly, the $V_{10} - V_{90}$ values for adsorption to DEAE Trisacryl at 4°C is higher than at 60°C, and the $V_{10} - V_{90}$ values for the adsorption to DEAE Sepharose FF at 4°C is higher than at 38°C. These results emphasize what can be seen visually, that short columns and high operating temperatures exhibit relatively sharper breakthrough curves and hence have smaller $V_{10} - V_{90}$ values. A useful evaluation of the sigmoidal characteristic of a profile can therefore be carried out using this type of measurement.

The operating capacities, q^* , represented in the curves of Figs. 5–7 were derived using eqn. 1, and these capacities are also listed in Table I. There was found to be a general decline in capacity with increasing column length and decreasing temperature for both the DEAE Trisacryl M and the DEAE Sepharose FF. Again, these results for the capacities concur with the conclusions drawn from visual examination and the $V_{10} - V_{90}$ values. The more efficient short columns bind more protein possibly due to better bed packing ensuring superior flow patterns within the bed, and less channeling. In addition, the short columns are less likely to undergo bed compression, which invariably leads to a loss in operating capacity. High operating temperatures also exhibit a higher efficiency and greater capacity, because of an inherently lower fluid viscosity, better mixing and mass transfer.

Kinetic parameter evaluation

To use the model equations of Arve and Liapis [16], it is necessary to know *a priori* the association constant, K_a , since this value is directly related to the forward rate of interaction through the dynamic relationship, $K_a = k_1/k_2$. The K_a values used for the purpose of these investigations were those obtained from batch experiments previously reported [28]. It was found that the value of K_a could be changed by 20% without affecting the shape or position of the breakthrough curves obtained from theoretical simulations. (This was also the case with the film mass transfer coefficient, K_f). Thus the values for K_a obtained from the batch experiments were assumed to be adequate estimates of the appropriate values of K_a for the column experiments. Note however, that the maximum capacities given in Tables I and IV are lower than those reported in our earlier studies on batch adsorption [28] because the pH of the buffer used in the column experiments was 2 pH units less than in the batch experiments. This may have an effect on the overall charge of the protein which may affect how much binds to the sorbent. It has also been well established that there is a reduction in capacity when fixed bed chromatography is used as opposed to batch adsorption [31,32]. This loss could be attributed to bed compression and an increase in the film layer surrounding the resin. Both these effects will lead to a decrease in the transfer of the protein from solution to the adsorbent.

Using the models of Hubble [6], Thomas [7] and Arve and Liapis [16], the interaction rate constant, k_1 , and the maximum capacity, q_m , were obtained by fitting iteratively the theoretical curve to the experimental breakthrough curve. Because of long computational times, the number of curves analysed using the model of Arve and Liapis was limited. In all cases, the maximum capacity for use in the theoretical solutions was changed to align the theoretical curve with the experimental one at the midpoint [$C(t)/C_0 = 0.5$]. In all cases it was necessary to change the value of k_1 or D_p from initial estimates to give curves of best fit, as determined by a least squares determination. A typical comparison of the theoretically determined profile and the experimental one is given in Fig. 9. The models of Hubble and Thomas yield very similar curves that correlate well with the experimental curve, and the resultant rate constants are similar. This result is to be expected since the assumptions inherent in the models of Hubble and Thomas are the same, although the method of numerical solution is different. The theoretical curve of Arve and Liapis fits the experimental curve well up to 50% breakthrough, and then the theoretical and experimental curves diverge towards the saturation point. This discrepancy between the theoretical and experimental curve at the later stages of the breakthrough curve has been shown to occur for several other model simulations [30,33]. It has been suggested that this divergence is due to the presence of non-specific binding on the adsorbent or conformational changes of the protein, two non-ideal occurrences that have not been accommodated in the models developed to date [16,18]. The worst curve fit of our experimental data was obtained with the model of Arnold *et al.*, the theoretical curve being a square root function, rather than a sigmoid (again see Fig. 9). This suggests that this model is not suitable for predicting the adsorption process of the proteins ferritin, HSA and transferrin to the weak ion-exchange resins, Trisacryl M and Sepharose FF, although it has gained some success in amino acid adsorption studies [8].

Fig. 10 shows the rate constants obtained from the models of Hubble and

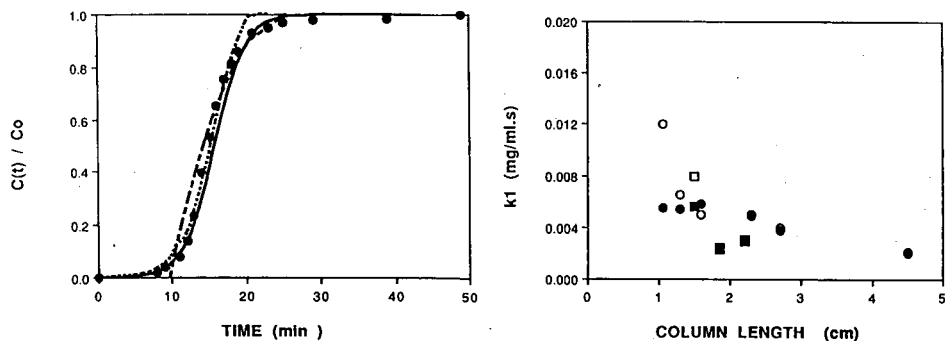


Fig. 9. Typical curve fit of the theoretical curves generated from Thomas (eqn. 3) (—), Arnold *et al.* (eqn. 4) (---) and Arve and Liapis (eqn. 5) (-----) to the experimental curve (●) of HSA adsorbing to DEAE Trisacryl M. $C_0 = 1.5$ mg/ml, $q_m = 42$ mg/ml resin, $K_a = 56$ ml/mg, $u_0 = 0.042$ cm/s, $z = 1.3$ cm, $K_f = 8 \cdot 10^{-6}$ m/s.

Fig. 10. Variation of the rate constant with the bed length, from the experiments with HSA adsorbing to DEAE Trisacryl M or DEAE Sepharose FF. The values for k_1 were obtained from the models of Hubble and Thomas. ○ = Hubble, Trisacryl; ● = Thomas, Trisacryl; □ = Hubble, Sepharose and ■ = Thomas, Sepharose.

TABLE II

THE EFFECT OF THE LENGTH OF THE PACKED BED AND OPERATING TEMPERATURE ON THE INTERACTION RATE CONSTANT, k_1 , AS CALCULATED FROM THE THEORETICAL MODELS

Resin ^a	Length (cm)	Temperature (°C)	k_1^b	k_1^c (ml/mg s)	k_1^d
Trisacryl M	1.3	20	0.010	0.005	0.040
	4.5	20	0.002	0.002	0.005
Trisacryl M	1.3	4	— ^e	0.004 ^f	— ^e
	1.3	60	— ^e	0.006	— ^e

^a HSA adsorption.

^b Eqn. 2 (Hubble).

^c Eqn. 3 (Thomas).

^d Eqn. 5 (Arve and Liapis).

^e Not determined.

^f Relative standard deviation 17%.

Thomas for the various column lengths. Other results of k_1 are given in Table II. The values of these rate constants are within the same order of magnitude as those calculated in our previous batch experiments [28], for example, $k_1 = 0.007$ – 0.012 ml/mg s for HSA adsorbing to DEAE Trisacryl M, pH 6.0. These results obtained from the Hubble or Thomas models indicate a trend of increasing k_1 , with decreasing column length, for example, when $z = 1.3$ cm $k_1 = 0.012$ ml/mg s, whilst at $z = 4.5$ cm $k_1 = 0.002$ ml/mg s. The interaction rate, k_1 , is indicative of the interaction of a particular protein with the functional groups on the resin, and should therefore remain constant for increasing column lengths. These observations suggest that the rate constants, k_1 , derived from the Hubble and Thomas models are lumped constants, which incorporate but not discriminate other mass transfer resistances such as protein diffusivities, or pore resistances. Table II also shows that there is a slight increase of k_1 with temperature, and when considering the form of the Arrhenius relationship, $k_1 = Ae^{-Ea/RT}$, which suggests that at higher temperatures the likelihood of interaction is

TABLE III

THE EFFECT OF THE LENGTH OF THE PACKED BED AND OPERATING TEMPERATURE ON THE EFFECTIVE DIFFUSIVITY, D_p , AS CALCULATED FROM THE THEORETICAL MODELS

Resin ^a	Length (cm)	Temperature (°C)	D_p^b ($\times 10^{-11}$ m/s)	D_p^c
Trisacryl M	1.3	20	1.10	6.1
	4.5	20	0.28	6.1
Trisacryl M	1.3	4	0.39	6.1
	1.3	60	0.91	6.1

^a HSA adsorption.

^b Eqn. 4 (Arnold *et al.*).

^c Eqn. 5 (Arve and Liapis).

TABLE IV

THE INFLUENCE OF PROTEIN SIZE ON THE INTERACTION RATE, AS CALCULATED FROM THE THEORETICAL MODELS

Protein ^a	q_m ($\mu\text{mol/ml}$)	k_1^b ($\text{ml}/\mu\text{mol s}$)	k_1^c	D_p^d ($\cdot 10^{-11} \text{ m}^2/\text{s}$)
Human Serum Albumin	1.49 ^e	0.12	0.10	0.7
Transferrin	0.98	0.13	0.25	1.1
Ferritin	0.003	4.51	5.14	1.1

^a Adsorption to DEAE Trisacryl M.^b Eqn. 2 (Hubble).^c Eqn. 3 (Thomas).^d Eqn. 4 (Arnold *et al.*).^e Buffer pH 7.0.

greater since more molecules will have higher energy, this increase is not surprising. Table III shows the effect of column length and operating temperature on the effective diffusivity, D_p , as calculated from theoretical models. The results obtained from the model of Arnold *et al.* [8] show a trend of increasing D_p with decreasing column length, and increasing operating temperature, which is similar to the effect on k_1 in the model values in Table II. The fact that D_p is actually a lumped parameter of Arnold *et al.* may explain this similarity.

In order to determine the effect of pore-to-protein size on the breakthrough curves, the adsorption of ferritin, transferrin and HSA to the DEAE Trisacryl M were examined in independent experiments. Table IV lists the operating capacities, q_m , the interaction rates, k_1 (from eqns. 2 and 3) and the effective diffusivities (from eqn. 4) for the three proteins adsorbing to DEAE Trisacryl M. Considering the differences in the hydrodynamic radii of the three proteins (diameter of ferritin is about 110 Å, whilst that of HSA is 45 Å) according to the correlation of Young *et al.* [21], the diffusion of ferritin into the pores of the DEAE Trisacryl M is anticipated to be significantly slower than transferrin or HSA. This behaviour in fact was observed with the capacity of DEAE Trisacryl M for ferritin being small, 0.003 $\mu\text{mol/ml}$, compared to HSA, 1.49 $\mu\text{mol/ml}$, due to these geometric constraints. Moreover, it is conceivable that adsorption of ferritin is limited to the surface of the adsorbent. Experimental capacities for the adsorption of several other proteins, varying in molecular weights onto the cation-exchange resin, Whatman Cellulose CM52, have also shown that capacity decreases with increasing molecular weight of a protein [34].

Note however, that the effective diffusivities shown in Tables III and IV are not significantly smaller than the correlated diffusivities of the proteins in free solution [35] although the model of Arnold *et al.* which has been used to calculate these values for D_p , neglects all the other mass transfer resistances associated with adsorption. Furthermore, the correlation between the theoretical curves of eqn. 4 and the experimental curves was very poor, so that the values obtained should be treated with certain scepticism.

The values for k_1 , from eqn. 2, also appear protein dependent, see Table IV, with the highest value being for the largest protein ferritin. As k_1 is protein specific, this difference is not surprising, and similar high values were calculated in our bath

experiments. Furthermore, this concurs with the relative steepness of the breakthrough curves of Fig. 8, where the largest protein appeared to have the sharpest front.

These results highlight the necessity for theoretical models to reflect the physical features of the adsorption process if the derived rate constants are to have physical significance.

CONCLUSIONS

In this investigation, the column length, temperature, protein concentration and protein size have been varied to assess their influence on the capacity of ion-exchange resins and on the kinetic parameters associated with an ion-exchange adsorption interaction. Improved performance, in terms of a higher operating capacity and sharper breakthrough curves, was seen on shorter columns. This observation has been well known [20] in large-scale process chromatography where difficulties in packing have been overcome by the design and implementation of “stacked” bed columns. An increase in the temperature of the operation was also found to improve the performance. Whilst many proteins are heat-sensitive, restricting the temperature of the purification steps to 4–10°C, there are proteins, for example HSA, which are stable at temperatures of up to 60°C. Operation at higher temperatures thus looks promising in terms of increased adsorbent capacity and better fluid characteristics. A two-fold increase in the protein concentration of the feed had little influence on the shape of the breakthrough curve. This observation is important from a process aspect, because it implies that a variation on the feedstock concentration, for example the HSA content in plasma, will not unduly affect the performance. As an added bonus, an increase in the feedstock concentration will reduce the processing time. The results from the breakthrough curves of different proteins, reveal that the capacity of the ion-exchange resin, DEAE Trisacryl M is smallest for the largest protein, ferritin, although the large values obtained from the mathematical models for the diffusivities suggests that this diffusion is surface related, and in fact ferritin adsorption is limited to the exterior of the adsorbent.

The application of the mathematical models used in these investigations has shown that there are still shortcomings in these models as projected in the Theory section. That there is a need to develop further the concept of a “modus”, a physical model that reflects the realities of the adsorption process is undoubtable. Evidence of non-idealities are apparent in the experimental breakthrough curves and these deviations from ideal behaviour are as yet unquantifiable using the mathematical solutions available today.

ACKNOWLEDGEMENTS

The support of the Australian Research Grants Committee and Monash University Research Committee is gratefully acknowledged.

REFERENCES

- 1 F. B. Anspach, A. Johnston, H.-J. Wirth, K. K. Unger and M. T. W. Hearn, *J. Chromatogr.*, 499 (1990) 103.
- 2 A. J. P. Martin and R. L. M. Synge, *Biochem. J.*, 35 (1941) 1351.
- 3 E. Gleukauf, *Trans. Faraday Soc.*, 51 (1955) 34.
- 4 S. Yamamoto, M. Nomura and Y. Sano, *AIChE. J.*, 33 (1987) 1427.
- 5 S. Golshan-Shirazi and G. Guiochon, *J. Chromatogr.*, 506 (1990) 495.
- 6 J. Hubble, *Biotech. Tech.*, 3 (1989) 113.
- 7 H. C. Thomas, *Am. Phys. Chem. Soc. J.*, 66 (1944) 1664.
- 8 F. H. Arnold, H. W. Blanche and C. R. Wilke, *Chem. Eng. J.*, 30 (1985) B9.
- 9 T. Vermeulen, *Ind. Eng. Chem.*, 45 (1953) 1664.
- 10 R. D. Jr. Fleck, D. J. Kirwan and K. R. Hall, *Ind. Eng. Chem. Fundam.*, 12 (1) (1973) 95.
- 11 S. Katoh, T. Kambayashi, T. R. Deguchi and F. Yoshida, *Biotechnol. Bioeng.*, 20 (1978) 267.
- 12 D. R. Garg and D. M. Ruthven, *Chem. Eng. Sci.*, 28 (1973) 791.
- 13 C. Tien and G. Thodos, *AIChE. J.*, 5 (1959) 373.
- 14 E. L. Morton and P. W. Murni, *AIChE. J.*, 13 (1967) 965.
- 15 C. R. Antonson and J. S. Dranoff, *Chem. Eng. Progr. Symp. Ser.*, 96 (1969) 65.
- 16 B. H. Arve and A. I. Liapis, *Biotechnol. Bioeng.*, 32 (1988) 616.
- 17 D. M. Ruthven, *Principles of Adsorption and Adsorption Process*, Wiley, New York, 1984, pp. 261-268.
- 18 M. A. McCoy and A. I. Liapis, *J. Chromatogr.*, 548 (1991) 25.
- 19 J. R. Sportsmann, J. D. Liddell and G. S. Wilson, *Anal. Chem.*, 55 (1983) 771.
- 20 J.-Ch. Janson and P. Hedman, *Adv. Biochem. Eng.*, 25 (1982) 45.
- 21 M. E. Young, P. A. Carroad and R. L. Bell, *Biotechnol. Bioeng.*, 12 (1980) 947.
- 22 C. R. Davies, P. S. Malchesky and G. M. Saidel, *Artificial Organs*, 14 (1990) 14.
- 23 S. Ghodbane and G. Guiochon, *J. Chromatogr.*, 452 (1988) 209.
- 24 J. H. Know and H. M. Pyper, *J. Chromatogr.*, 363 (1986) 1.
- 25 I. Lundstrom and H. Elwing, *J. Theor. Biol.*, 110 (1984) 195.
- 26 J. H. Petropoulos, A. I. Liapis, N. P. Kolliopoulos, J. K. Petrou and N. K. Kanellopoulos, *Bioseparations*, 1 (1990) 69.
- 27 A. Johnston and M. T. W. Hearn, *J. Chromatogr.*, 512 (1990) 101.
- 28 A. Johnston and M. T. W. Hearn, *J. Chromatogr.*, 556 (1991) in press.
- 29 H. Ohashi, T. Sugawar, K. Kikuchi and K. Konno, *J. Chem. Eng. Japan*, 14 (1981) 433.
- 30 Q. M. Mao, A. Johnston, I. G. Prince and M. T. W. Hearn, *J. Chromatogr.*, 548 (1991) 147.
- 31 A. Johnston, *M.Sc. Thesis*, Monash University, Melbourne, 1988.
- 32 K. K. Unger and R. Janzen, *J. Chromatogr.*, 373 (1986) 227.
- 33 B. J. Horstmann and H. A. Chase, *Chem. Eng. Res. Des.*, 67 (1989) 243.
- 34 R. K. Scopes, *Anal. Biochem.*, 114 (1981) 8.
- 35 P. A. Davies, *J. Chromatogr.*, 483 (1989) 221.
- 36 M. T. W. Hearn, A. H. Hodder, F. W. Fang and M. I. Aguilar, *J. Chromatogr.*, 548 (1991) 117.

High-performance liquid chromatography of amino acids, peptides and proteins

CXIII.^a Predicting the performance of non-porous particles in affinity chromatography of proteins

Q. M. MAO, A. JOHNSTON, I. G. PRINCE and M. T. W. HEARN*

Department of Biochemistry and Centre for Bioprocess Technology, Monash University, Clayton, Victoria, 3168 (Australia)

ABSTRACT

A mathematical model, based on the Langmuir adsorption isotherm, has been developed to predict the performance of bioaffinity chromatography columns, packed with non-porous particles, in protein purification at the laboratory and preparative scales. Both the surface kinetics and the external film resistance as the rate controlling steps have been taken into account. The effects of particle size, fluid flow-rate and adsorbate concentration are examined. The model has been used to determine the forward interaction rate constant (k_f) for different adsorbate–ligand systems. Examples of the comparison between predicted and experimental breakthrough curves of a lysozyme–Cibacron Blue F3GA biomimetic affinity system are given. The influence of ionic strength and ligand density have also been evaluated.

INTRODUCTION

In recent years, non-porous monodisperse silica beads used as matrix supports in biochromatography (*e.g.* in biomimetic, hydrophobic and biospecific adsorption modes) have gained interest [1]. The main practical advantage of the non-porous packings in analytical and laboratory scale biochromatography with zonal elution systems is fast separation with high efficiency due to the absence of restrictive pore diffusion process with the adsorbates. Theoretical analyses on the behaviour of non-porous particles in biospecific adsorption processes, on the other hand, are largely lacking.

The literature on packed-bed adsorption theories and their applications to affinity chromatography has been reviewed extensively, see for example by Yang and Tsao [2] and Liapis [3]. In the concluding remarks of their review, Yang and Tsao pointed out that the lack of theoretical analysis on affinity chromatography was partly due to the difficulties encountered in solving the rigorous mathematical models.

^a For part CXII, see ref. 20

Certain simplifications must be made in order to obtain solutions. However, as most affinity chromatography systems display non-linear adsorption isotherm characteristics, the most important simplification of assuming a linear adsorption isotherm, which is often used as the basis of adsorption models, may be inappropriate. The models developed for affinity chromatography found in the literature [4–8] typically fall into two groups. In the first group a single mechanism is assumed to be the rate limiting step, either pore diffusion [5] or surface interaction [4], from which analytical solutions can be obtained. In the second group, the models are more rigorous as all of the possibly important rate limiting steps are considered [6–9]. Various numerical methods have been employed to solve these latter equations which concurrently result in excessive computation time.

The most important rate limiting steps in the biospecific adsorption processes have been identified as: external liquid film mass transfer; internal pore diffusion; and surface interaction [3,6]. For porous particles, pore diffusion resistance has been often considered as the rate controlling step [2,5]. There is no model explicitly developed for non-porous particles for which only the external film mass transfer resistance and the surface interaction rate are the rate limiting steps. The shortcoming of the non-porous particles is their limited surface area. Hence very small particles are preferred [1], subject to the pressure drop permitted in the system. Evidence exists that both the film mass transfer and the surface interaction can be important in determining the overall adsorption rate in systems with small particles [2,3,5].

Group two models attempt to interpret the physical basis of the mass transfer phenomenon by theoretical analysis, but the numerical procedures require special software packages [8] which are not always available. On the other hand, group one models have been found simple to use in preliminary evaluation of the column performance, but fail to address important parameters such as particle size and external film mass transfer coefficients. Hence a model, preferably capable of an analytical solution, yet which addresses both the external mass transfer and surface interaction would be desirable.

The central purpose of this work is to describe the development and method of analytical solution of a mathematical model for non-porous particle systems which satisfies the above criteria. The straightforward nature of the resulting software allows utilization of the model on readily accessible equipment. The applicability of the model is demonstrated with a set of small scale experimental data generated in our laboratory, but the scope of the model and its intended application are directed towards predicting behaviour in preparative systems. Studies to confirm the suitability of the model in large scale equipment are currently underway.

THEORY

Non-porous particle adsorption model (NPPAM)

The non-porous particle adsorption model (NPPAM) has been developed to describe biospecific adsorption behaviour of non-porous particles in a packed bed. The basic assumptions of NPPAM are summarised as follows: (a) The effect of axial diffusion is negligible [3,9], and the fluid velocity is uniform over the cross-section of the column (eqn. 1). (b) The transport of adsorbate from the bulk fluid to the surface of the particle can be described by a film resistance mechanism (eqn. 2). (c) The

interaction between the adsorbate and the immobilized ligand at the particle surface is described by a Langmuir type model (eqn. 3). (d) The mass transfer and surface interaction steps are considered to occur in series (eqn. 4).

The continuity equation linking concentration, axial distance and time takes essentially the same form as those presented in the literature [10-12]:

$$\frac{U \partial C}{\varepsilon \partial x} + \frac{\partial C}{\partial t} + \frac{1 - \varepsilon}{\varepsilon} \frac{\partial q}{\partial t} = 0 \quad (1)$$

where U is the superficial liquid velocity, ε is the interstitial void fraction of the packed bed, x is the axial distance, t is time, C is the adsorbate concentration in the bulk of the liquid phase, and q is the adsorbate concentration in the solid phase.

The rate of mass transfer in the liquid film at the particle surface is described by

$$\frac{\partial C^*}{\partial t} = \frac{3}{R_0} \frac{1 - \varepsilon}{\varepsilon} K_f (C - C^*) \quad (2)$$

where R_0 is the radius of the particle, K_f is the liquid film mass transfer coefficient, and C^* is the intermediate concentration of the adsorbate in the liquid phase at the surface of the particles. The term $(3/R_0)(1 - \varepsilon)/\varepsilon$ is the interface area per unit interstitial void volume of the packed bed.

The surface interaction rate is described by the second-order reversible equation

$$\frac{\partial q}{\partial t} = k_1 [(q_m - q)C^* - K_d q] \quad (3)$$

where k_1 is the forward interaction rate constant, q_m is the maximum adsorption capacity of the immobilized ligand, and K_d is the adsorption equilibrium constant.

As the film mass transfer and the surface interaction steps are considered to occur in series, the mass balance between the liquid concentration at the particle surface and the solid concentration can be written.

$$\varepsilon \frac{\partial C^*}{\partial t} = (1 - \varepsilon) \frac{\partial q}{\partial t} \quad (4)$$

Eliminating C^* and its derivative from eqns. 2, 3 and 4 we get

$$\frac{\partial q}{\partial t} = \frac{A k_1 [(q_m - q)C - K_d q]}{A + k_1 (q_m - q)} \quad (5)$$

where $A = \frac{3}{R_0} K_f$

Eqns. 1 and 5 are the basic equations of NPPAM in which both the film mass transfer and surface interaction rates are considered finite. Simplified cases may be derived from these two equations. In eqn. 5, if $K_f \rightarrow \infty$ then the surface interaction

(second-order kinetics) is considered as the rate controlling step. As a result, $A \gg k_1 (q_m - q)$ and the denominator on the right-hand side of eqn. 5 then can be put equal to A . Hence, when $K_f \rightarrow \infty$ eqn. 5 becomes

$$\frac{\partial q}{\partial t} = k_1[(q_m - q)C - K_d q] \quad (6)$$

On the other hand, if $k_1 \rightarrow \infty$ then the external mass transfer becomes the rate controlling step. As a result, $A \ll k_1 (q_m - q)$ and the denominator on the right-hand side of eqn. 5 can be put equal to $k_1 (q_m - q)$. Hence when $k_1 \rightarrow \infty$ eqn. 5 becomes

$$\frac{\partial q}{\partial t} = A \left(C - \frac{K_d q}{q_m - q} \right) \quad (7)$$

The solutions of these two simplified cases where a single mechanism was the rate limiting step have already been reported in the literature. The case of second-order kinetics controlling adsorption (eqn. 6) has been solved by Thomas [13]. The solution with external film resistance controlling adsorption (eqn. 7) has been presented by Hiester and Vermeulen [14].

The Thomas solution

The Thomas solution on fixed bed performance was originally developed for application to ion-exchange columns [13]. It has been shown [11,14] that the Thomas solution can be applied to the adsorption processes in general where the equilibrium relationship can be expressed by the Langmuir isotherm. At equilibrium, $q = q^*$, the attainable adsorption capacity of the adsorbent, and $C = C_0$, whilst $\partial q / \partial t$ in eqn. 6 can be put equal to zero since q is now constant. When such conditions apply, then the relationship between q^* and C_0 takes the familiar form

$$q^* = \frac{q_m C_0}{K_d + C_0} \quad (8)$$

By introducing the dimensionless terms:

$$X = \frac{C}{C_0}, \quad Y = \frac{q}{q^*},$$

and

$$r^* = \frac{K_d}{K_d + C_0} \quad (9)$$

eqn. 6 can be rewritten as

$$\frac{\partial Y}{\partial t} = \Delta_a [X(1 - Y) - r^* Y(1 - X)] \quad (10)$$

where

$$\Delta_a = k_1(K_d + C_0) = -\frac{k_1 C_0}{r^* - 1} \quad (11)$$

By defining the dimensionless time parameter τ and dimensionless distance parameter ζ such that

$$\zeta = \frac{x(1 - \varepsilon)q^* \Delta_a}{UC_0} \quad (12)$$

$$\tau = \Delta_a \left(t - \frac{x\varepsilon}{U} \right) \quad (13)$$

the continuity eqn. 1 simplifies to

$$\frac{\partial X}{\partial \zeta} + \frac{\partial Y}{\partial \tau} = 0 \quad (14)$$

and eqn. 10 becomes

$$\frac{\partial Y}{\partial \tau} = [X(1 - Y) - r^* Y(1 - X)] \quad (15)$$

By appropriate substitution $\partial X/\partial \zeta$ can then be written as

$$\frac{\partial X}{\partial \zeta} = -[X(1 - Y) + r^* Y(1 - X)] \quad (16)$$

Assuming the bed is initially free of adsorbate, the boundary conditions are given by

$$\begin{array}{ll} X = 1 & \text{at } \zeta = 0 \text{ for all } \tau \\ Y = 0 & \text{at } \tau = 0 \text{ for all } \zeta \end{array}$$

Thomas solved eqns. 15 and 16 and obtained a solution for the breakthrough curve which can be expressed in the following form [10,12,14]

$$\frac{C}{C_0} = \frac{J(r^* \zeta, \tau)}{J(r^* \zeta, \tau) + [1 - J(\zeta, r^* \tau)] \exp[(r^* - 1)(\tau - \zeta)]} \quad (17)$$

The Hiester and Vermeulen approach

Hiester and Vermeulen [14] adapted the Thomas solution to solve the case where external film resistance is the rate controlling step. Introducing the dimensionless terms defined in the Thomas solution, eqn. 7 became

$$\frac{\partial Y}{\partial t} = \Delta_E [X(1 - Y) - r^* Y(1 - X)] \quad (18)$$

where

$$\Delta_E = \frac{AC_0}{q^*[1 + Y^*(r^* - 1)]} \quad (19)$$

Y^* was defined as an average value of q/q^* . As was suggested by Hiester and Vermeulen [14], Y^* has been given the numerical value $Y^* = 0.5$.

Here the time and distance parameters are defined as

$$\zeta = \frac{x(1 - \varepsilon)q^*\Delta_E}{UC_0} \quad (20)$$

$$\tau = \Delta_E \left(t - \frac{x\varepsilon}{U} \right) \quad (21)$$

so that eqn. 18 takes the form of eqn. 15 and the continuity eqn. 1 takes the form of eqn. 14. The boundary conditions remained unchanged. Therefore the solution given by eqn. 17 is applicable for the case where film resistance is controlling.

The solution for NPPAM

A similar method to that outlined above was adopted to obtain the solutions of the present model.

Introducing dimensionless terms, eqn. 5 becomes:

$$\frac{\partial Y}{\partial t} = \Delta_{aE}[X(1 - Y) - r^*Y(1 - X)] \quad (22)$$

where

$$\Delta_{aE} = \frac{AC_0}{q^*[1 + Y^*(r^* - 1)] - (A/k_1)(r^* - 1)} \quad (23)$$

The time and distance parameters are

$$\zeta = \frac{x(1 - \varepsilon)q^*\Delta_{aE}}{UC_0} \quad (24)$$

$$\tau = \Delta_{aE} \left(t - \frac{x\varepsilon}{U} \right) \quad (25)$$

Therefore eqns. 1 and 22 can be written in exactly the same dimensionless form as in the Thomas solution, *i.e.* eqns. 14, 15 and 16. The boundary conditions are still the same as in the Thomas solution. Hence the breakthrough curves can be calculated with eqns. 8, 9, 23–25, and 17.

It can be noted that the only difference in the three cases discussed is in the expressions of the terms Δ_a , Δ_E and Δ_{aE} , and

$$\frac{1}{\Delta_{aE}} = \frac{q^*[1 + Y^*(r^* - 1)]}{AC_0} - \frac{r^* - 1}{k_1 C_0} = \frac{1}{\Delta_E} + \frac{1}{\Delta_a} \quad (26)$$

Eqn. 26 is similar in form to that describing the total resistance of an electrical circuit with single resistances acting in series. This equation, therefore suggests that the rate limiting steps are also occurring in series.

The solution given by eqn. 17 contains the J function which is a complex function used in the solutions of many heat and mass transfer problems [10,14,16]. Numerical values of J function have been tabulated [10,15] and methods for calculating its value are also available [10,12,14,16]. A detailed procedure for evaluating the values of the J function is given in the Appendix. In these investigations, the NPPAM approach has been applied only to frontal chromatographic data. The application of NPPAM to a finite bath will be discussed in a separate paper.

EXPERIMENTAL

Packed bed adsorption data of a lysozyme-Cibacron Blue F3GA affinity system with non-porous particles was used in this work for evaluating the model predictions. The non-porous silica with a particle size of 1.5 μm was made as described in our previous publications [1,17,18] and is commercially available from Merck (Darmstadt, Germany). The non-porous silica was chemically modified with 3-mercaptopropyltrimethoxysilane (MPS) as described in ref. 17. The immobilization of Cibacron Blue F3GA on MPS-activated silica was performed as described in ref. 1. The dye affinity sorbent was packed into columns (19 \times 4 mm I.D.). The mobile phase used was 0.1 M phosphate buffer with 1 M sodium chloride except for some cases where phosphate buffer only was used. The flow-rate was 0.5 ml/min. Details on materials, methods, equipment setup and operating procedures have been published previously [17,18].

RESULTS AND DISCUSSION

The NPPAM has been programmed in FORTRAN for easy transfer between PC and mainframe computers. As the computer code is short and simple, it is readily convertible to the different programming languages. Simulations of the adsorption process of proteins in fixed bed packed with non-porous particles have been carried out on an IBM PC/AT compatible machine. The effect of varying the rate constant, particle size, flow-rate and inlet concentration of protein in the liquid on the breakthrough curves are presented in Figs. 1–8. The dimensionless outlet concentrations were plotted against both the time and the amount of adsorbate applied to the column in cases with varying flow-rate and inlet concentration. The effect of varying both the adsorption equilibrium constant and the rate constant on the shape of the breakthrough curves are shown in Figs. 5–8. The maximum adsorption capacity of the particles (q_m) used in the model simulation was 1.6 mg/ml solid. The liquid film mass transfer coefficient (K_f) used was $3.5 \cdot 10^{-4}$ m/s except in Fig. 2 where K_f was estimated for different particle sizes using correlations discussed previously [9]. Other parameters

TABLE I
PARAMETERS USED IN MODEL SIMULATION

$q_m = 1.6$ mg/ml solid.

Fig. No.	d_p (μm)	C_0 (mg/ml)	Flow (ml/min)	k_1 (ml/mg s)	K_d (mg/ml)
1	1.5	0.1	0.5	0.25–1.0	0.08
2	1.5–200	0.1	0.5	2.0	0.08
3, 4	1.5	0.1	0.25–1.0	0.4	0.08
5, 6	1.5	0.1–0.4	0.5	0.4	0.08
7, 8	1.5	0.1–0.4	0.5	2.0	0.008

used are listed in Table I. Because the data available for the model evaluation was from laboratory scale columns, the parameters used in the model simulations largely correspond to these experimental conditions. However, there is no restriction for the NPPAM to be applied in the parameter range appropriate to the preparative scale.

For a saturated column, the amount of the adsorbate retained in the column, which is equal to the area behind the breakthrough curve [5,12] corresponds to the attainable adsorption capacity of the adsorbent q^* , as given in eqn. 8. In preparative affinity chromatography, however, the actual process would be terminated when the level of adsorbate in the effluent rises above a certain level, normally at less than 50% of the feed concentration [4,5,8]. In this case, a system with a sharp breakthrough curve would be much more efficient in utilising the column capacity than a system with a shallow one, as the amount of adsorbate retained when the process was terminated at the set concentration of the effluent, say *e.g.* 10% of that in the feed, is larger in the case with a sharper curve. Therefore, the breakthrough curves generated from the model simulation can be used to extract the performance information needed to optimize the process, such as the percentage utilisation of the column capacity, the amount of adsorbate lost in the effluent, and the processing time, etc. under various operating conditions. When comparing the sharpness of the breakthrough curves generated from different parameters, the appropriate variable for the abscissa corresponding to the parameter examined should be used, so that the area behind each curve is proportional to the amount adsorbed for every curve in the same graph. Hence, in evaluating the

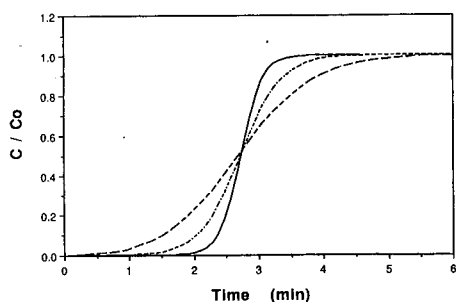


Fig. 1. Breakthrough curves simulated by NPPAM on the effect of forward interaction rate constant. [$k_1 = 0.25$ (---), 0.5 (-·-·-), 1.0 (—) ml/mg s].

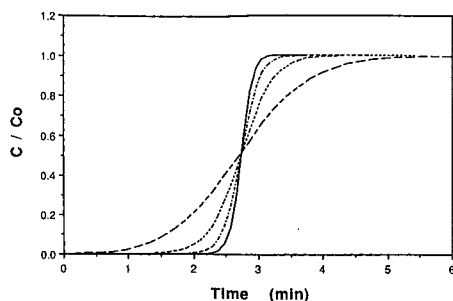


Fig. 2. Breakthrough curves simulated by NPPAM on the effect of particle diameter. — = 1.5; - · - · - = 50; - - - = 100 and - - - - = 200 μm .

effect of flow-rate, the abscissa should be either the volume of the solution or the amount of the adsorbate applied, and in evaluating the effect of feed concentration the abscissa should be the amount of adsorbate applied.

Fig. 1 shows that a higher value of the surface interaction rate constant will lead to a sharper breakthrough curve and hence a more efficient system. However, the rate constant may not be adjustable as it is largely determined by the chosen protein–ligand system. In that case, the efficiency of the system can be improved by employing smaller particles as shown in Fig. 2. The sharper breakthrough curve of smaller particles is due to the increased mass transfer rate which is caused not only by the increased particle surface area, but also by the larger film mass transfer coefficient ($3.4 \cdot 10^{-4}$ for 1.5- μm particle compared with $1.2 \cdot 10^{-5}$ for 200- μm particle) as predicted from the literature correlation [9]. Fig. 3 shows the effect of flow-rate on processing time. As expected the lower flow-rate requires longer processing time. However, when the same curves were plotted against the amount of the adsorbate applied to the column, as shown in Fig. 4 it can be seen that lower flow-rate gives a sharper breakthrough curve. Hence, depending on the operating requirement (*e.g.* effluent concentration), an optimum flow-rate can be worked out from these model simulations which will not give the highest but the optimum percentage utilization of the column capacity that results in the highest processing rate.

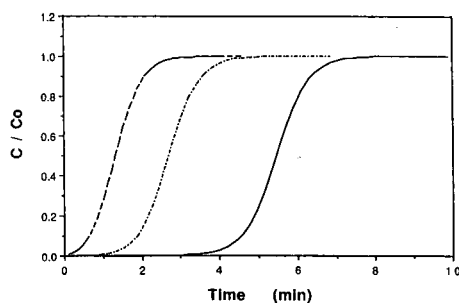


Fig. 3. Breakthrough curves simulated by NPPAM on the effect of flow-rate (— = 0.25, - · - · - = 0.5, - - - = 1.0 ml/min) as a function of time.

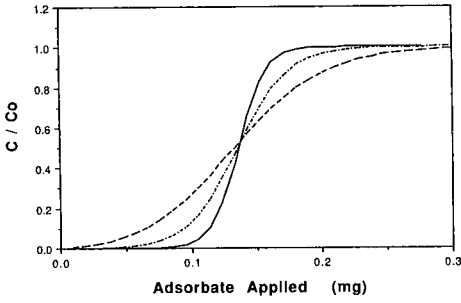


Fig. 4. Breakthrough curves simulated by NPPAM on the effect of flow-rate (— = 0.25, - · - · - = 0.5, - - - = 1.0 ml/min), as a function of the amount of adsorbate applied.

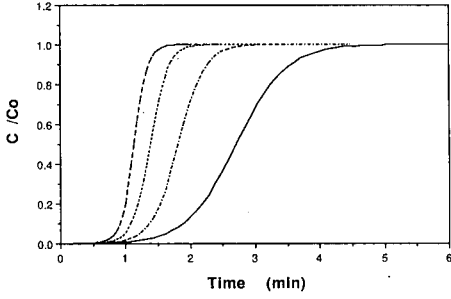


Fig. 5. Breakthrough curves simulated by NPPAM on the effect of inlet concentration, as a function of time for high value of K_d (0.08 mg/ml) and low value of k_1 (0.4). — = 0.1 mg/ml; - · - · - = 0.2 mg/ml; - - - = 0.3 mg/ml and - - - - = 0.4 mg/ml.

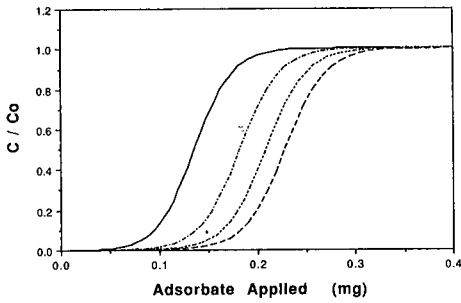


Fig. 6. Breakthrough curves simulated by NPPAM on the effect of inlet concentration, as a function of the amount of adsorbate applied for high value of K_d (0.08 mg/ml) and low value of k_1 (0.4). Denotation of lines as in Fig. 5.

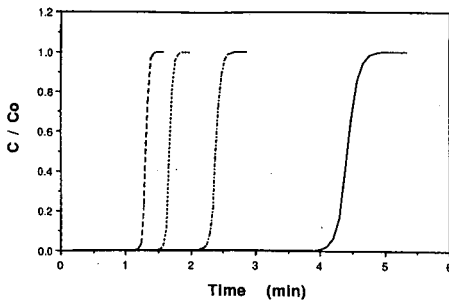


Fig. 7. Breakthrough curves simulated by NPPAM on the effect of inlet concentration, as a function of time for low value of K_d (0.008 mg/ml) and high value of k_1 (2.0). Denotation of lines as in Fig. 5.

The effect of varying the inlet concentration of the adsorbate on the predicted breakthrough curves is shown in Figs. 5 to 8. Figs. 5 and 7 show the effect on the processing time, and Figs. 6 and 8 show the effect on the column efficiency. From eqn. 8 it can be seen that the amount of adsorbate retained in the column is a function of both the feed concentration C_0 and the adsorption equilibrium constant K_d provided that the maximum adsorption capacity q_m is held constant. Increasing C_0 will increase the amount of protein adsorbed and cause the breakthrough curves to shift to the right as is the case in Figs. 6 and 8. The sharpness of the curves, on the other hand, was not influenced by the change in C_0 . The improved column efficiency at higher C_0 is mainly due to the increased amount of the adsorbate retained. As listed in Table I, higher value of k_1 and lower value of K_d were used to generate the breakthrough curves presented in Figs. 7 and 8. More adsorbate was retained in the column for this system compared with the system illustrated in Figs. 5 and 6 at the same values of C_0 . However, the change of the amount adsorbed on the column to the variation of C_0 in Fig. 8 is not as sensitive as for the system shown in Fig. 6.

From the model simulations shown in Figs. 1 to 8 it can be seen that NPPAM is a useful tool in evaluating the binding performance of affinity adsorption columns with non-porous particles. It takes only seconds to generate a breakthrough curve on

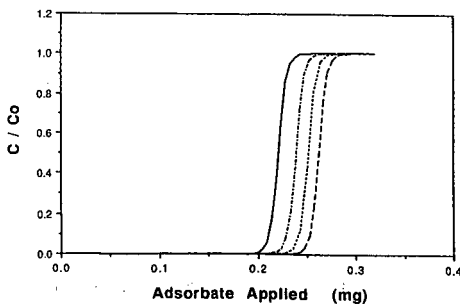


Fig. 8. Breakthrough curves simulated by NPPAM on the effect of inlet concentration, as a function of the amount of adsorbate applied for low value of K_d (0.008 mg/ml) and high value of k_1 (2.0). Denotation of lines as in Fig. 5.

a normal PC, which is particularly useful in fitting experimental curves where hundreds of iterations may be necessary. As discussed above, the amount of the adsorbate retained in the column is equal to the area behind the breakthrough curve. Therefore, numerical integration of the breakthrough curves generated from the model simulation may serve as a check of the accuracy of the model prediction. Calculation shows that the difference between the amount adsorbed calculated from eqn. 8 and the integrated result is always less than 0.01%.

One point requiring discussion on the NPPAM is that in its solution there is an approximation of Y^* , inherited from the Hiester and Vermeulen's method [12,14]. Although $Y^* = q/q^*$ is a variable since q varies with time, it was necessary to assign to Y^* a constant value in order to use the Thomas solution. $Y^* = 0.5$ was used in the model simulation throughout this paper, as suggested by Hiester and Vermeulen [14]. Therefore, the effect of the value of Y^* on the shape of the breakthrough curves and the area behind the curves predicted by the model should be closely monitored. Calculations were carried out using $Y^* = 0.1, 0.5$ and 0.9 . It was found that the value of Y^* has no influence on the area behind the breakthrough curves. For most conditions used in the present model simulation, the effect of varying Y^* on the shape of the breakthrough curve is also negligible in the range of $Y^* = 0.1$ to 0.9 . In some extreme cases, the curve with $Y^* = 0.9$ is slightly sharper than the one with $Y^* = 0.1$. The method to calculate breakthrough curves in cases where the effect of the Y^* value can not be neglected has been discussed by Hiester and Vermeulen [14].

Beside predicting the performance of a packed bed for given operating conditions and system parameters, the model can also be used for fitting parameters to packed bed experimental results to derive system kinetic data such as the surface interaction rate constant and the mass transfer coefficient, as well as to verify thermodynamic data. Figs. 9–12 show the comparison between the predicted and the experimental breakthrough curves for lysozyme adsorption to a biomimetic dye affinity sorbent. In Figs. 9–12 the points are the experimental data and the lines are the model predictions. The ligand used was Cibacron Blue F3GA and the mobile phase used was 0.1 M phosphate buffer with 1 M sodium chloride except for the case in Fig. 12 where phosphate buffer only was used. The reason for using sodium chloride in the

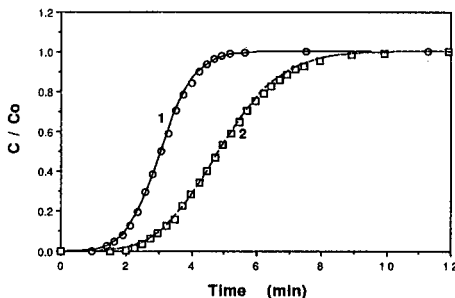


Fig. 9. Predicted (lines) and experimental (points) breakthrough curves for the adsorption of lysozyme on Cibacron Blue F3GA immobilized on 1.5 μm diameter non-porous silica particles. Mobile phase: 0.1 M phosphate buffer with 1 M sodium chloride. Flow-rate = 0.5 ml/min. Column: 19 mm long and 4 mm I.D. $K_d = 0.073$ mg/ml, $C_0 = 0.013$ (\square) and 0.075 (\circ) mg/ml. For other parameters related to predicted curves (1 and 2) see Table II.

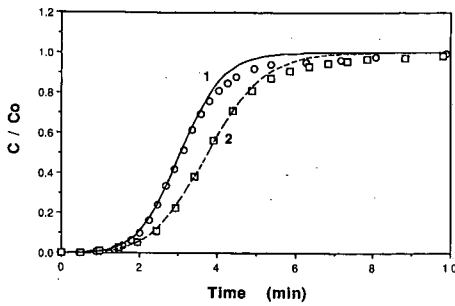


Fig. 10. Predicted (lines) and experimental (points) breakthrough curves for lysozyme adsorption. Mobile phase: 0.1 M phosphate buffer with 1 M sodium chloride. $K_d = 0.073$ mg/ml, $C_0 = 0.036$ (\square) and 0.057 (\circ) mg/ml. For other experimental parameters see legend of Fig. 9.

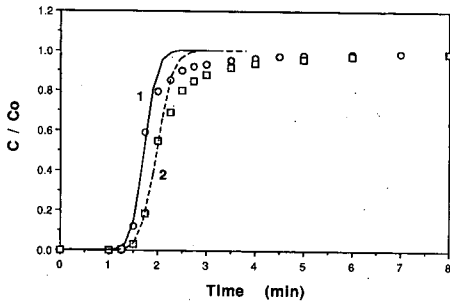


Fig. 11. Predicted (lines) and experimental (points) breakthrough curves for lysozyme adsorption. Mobile phase: 0.1 M phosphate buffer with 1 M sodium chloride. $K_d = 0.23$ mg/ml, $C_0 = 0.04$ (\square) and 0.1 (\circ) mg/ml. For other experimental parameters see legend of Fig. 9.

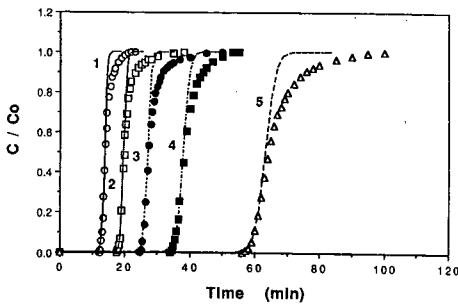


Fig. 12. Predicted (lines) and experimental (points) breakthrough curves for lysozyme adsorption with high ligand density. Mobile phase: 0.1 M phosphate buffer. $C_0 = 0.100$ (\circ); 0.065 (\square); 0.045 (\bullet); 0.030 (\blacksquare) and 0.018 (\triangle) mg/ml. For other experimental parameters see legend of Fig. 9 and Table II. For other parameters related to predicted curves (1-5) see Table II.

TABLE II
RESULTS OF MODEL PREDICTION

Fig. No.	Curve No.	C_0 (mg/ml)	q_m (mg/ml solid)	K_d (mg/ml)	k_1 (ml/mg s)
9	1	0.075	1.503	0.073	0.375
	2	0.013	1.430		0.596
10	1	0.057	1.326	0.073	0.456
	2	0.036	1.385		0.467
11	1	0.100	1.781	0.230	1.218
	2	0.040	1.700		1.753
12	1	0.100	5.030	0.0055	0.448
	2	0.065	4.825		0.565
	3	0.045	4.722		0.648
	4	0.030	4.671		0.605
	5	0.018	5.082		0.648

mobile phase was to suppress non-specific binding phenomena. The film mass transfer coefficient was predicted from correlations in the literature [9] and a value of $3.4 \cdot 10^{-4}$ m/s was used. The maximum adsorption capacity q_m and the equilibrium constant K_d were derived from the experimental data.

A subroutine was written to find the appropriate value of the forward surface interaction rate constant k_1 which would give a satisfactory fit to the experimental curve. The objective function chosen to be minimized is the sum of the squares of the percentage deviation between predicted and experimental values of C/C_0 , over the range of $C/C_0 = 0.01$ to 0.95 on the experimental breakthrough curve. This practice gave a much greater weight to the initial part of the curve in the minimization process. Therefore, in cases where a good fit to the whole breakthrough curve is not possible, the initial part of the curve would have a close fit, as in an actual process the adsorption phase would be terminated at less than 50% breakthrough [5]. In order to obtain the best fit, q_m has also been adjusted. The rate constant (k_1) obtained and the parameters used are listed in Table II.

The agreement between model prediction and experimental data is quite good in Fig. 9. However, the model could only fit the initial part of the experimental breakthrough curves well in most cases in Figs. 10, 11 and 12. In every case where deviation from the experimental data occurred, the model always predicted that the column approached saturation faster than that indicated by the experiment. This phenomenon has been reported in the literature for both porous [8] and non-porous [9] particles. In their adsorption study of lysozyme-anti-lysozyme system with non-porous silica particles, Liapis *et al.* [9] suggested that non-specific interaction between lysozyme and the silica may be responsible for the disagreement between model prediction and experimental data. Initially most of lysozyme molecules would interact with anti-lysozyme which was fast, hence specific adsorption was dominant. As time progressed, the dominant adsorption mechanism switched to non-specific adsorption which was slower, hence the overall adsorption rate decreased. This point was supported by the experimental data for a system with a higher ligand density which

showed better agreement between measured and predicted breakthrough curves. These workers proposed that the amount of non-specific surface area compared to the area of the particles covered by the ligand was lower in the system with the antibody immobilized to high (average) density. However, the trend was reversed in the present study where the system with higher ligand density showed poorer agreement between predicted and measured breakthrough curves, as shown in Table II and Figs. 9–12. In this case, heterogeneity in the ligand distribution and the resulting steric hindrance might be the main cause of the slow adsorption when the column approaches protein saturation.

CONCLUSIONS

It can be concluded that NPPAM in its present form has already shown promising features in predicting the performance of non-porous particles in affinity chromatography for both laboratory and preparative systems. As the model allows independent evaluation of the factors affecting the protein–ligand interaction, as well as the factors affecting the mass transfer behaviour of the proteins, the model is compatible to those more sophisticated models [7,8]. The simplicity of the model not only allows shorter running time, but also makes the modification and adaptation of the model easier. The model simulations have shown that for the affinity chromatography columns employing non-porous particles, column efficiency can be improved by using smaller particles, moderate flow-rate, and employing a protein–ligand system with reasonably fast interaction rates. The deviation of the experimental data from the model prediction may be due to the effect of heterogeneity in the ligand distribution and other mass transfer process, as well as different adsorption mechanisms.

APPENDIX

The J function

The solution of the models requires the knowledge of the J function which took the form of [10,12,14]

$$J(\alpha, \beta) = 1 - \int_0^\alpha e^{-(\alpha+\lambda)} I_0(2\sqrt{\beta\lambda}) d\lambda \quad (\text{A1})$$

where I_0 is a modified Bessel function of the first kind. The numerical value of the J function lies between zero and one, and where $J(0, \beta) = 1.0$ and $J(\alpha, 0) = e^{-\alpha}$.

When both α and β are large (>10), Thomas suggested the following approximation [14]

$$J(\alpha, \beta) = \frac{1}{2} \left[1 - \operatorname{erf}(\sqrt{\alpha} - \sqrt{\beta}) + \frac{e^{-(\sqrt{\alpha}-\sqrt{\beta})^2}}{\sqrt{\pi(\sqrt{\beta} + \sqrt[4]{\alpha\beta})}} \right] \quad (\text{A2})$$

According to Hiester and Vermeulen [14], eqn. A2 is accurate to within 1% when $\alpha\beta \geq 36$. The error function in the equation can be calculated from [19]

$$\operatorname{erf}(x) = \frac{2}{\sqrt{\pi}} \left[x + \sum_{k=1}^n (-1)^k \frac{x^{(2k+1)}}{k!(2k+1)} \right] \quad (\text{A3})$$

It was found when $n \geq 30$, the difference between calculated value and the tabulated value of the error function in the literature [12,19] is less than 0.0001.

For smaller value of α and β , a formula used by Tan [16] gives a better approximation.

$$J(\alpha, \beta) = 1 - e^{-\beta} \sum_{k=0}^n \frac{\beta^k A_k(\alpha)}{k!k!} \quad (\text{A4})$$

where

$$A_0(\alpha) = 1 - e^{-\alpha}$$

$$A_k(\alpha) = kA_{k-1}(\alpha) - \frac{\alpha^k}{e^\alpha} \quad \text{for } k \geq 1$$

Calculation has shown that for $(\alpha + \beta) \leq 75$ and $\alpha \leq 35$, the difference between the result of eqn. A4 and the tabulated value of the J function [10,15] is less than 0.00002. For $(\alpha + \beta) > 75$ or $\alpha > 35$, eqn. A2 is accurate to within 0.0001 compared with tabulated data.

SYMBOLS

C	Liquid phase concentration.
C_0	Inlet liquid concentration.
C^*	Intermediate liquid concentration.
k_1	Forward interaction rate constant.
K_d	Adsorption equilibrium constant.
K_f	Liquid film mass transfer coefficient.
q	Solid phase concentration.
q_m	Maximum solid adsorption capacity.
q^*	Attainable adsorption capacity of the adsorbent (eqn. 8).
R_0	Particle radius.
r^*	Equilibrium parameter (eqn. 9).
t	Time.
U	Superficial liquid velocity.
X	$= C/C_0$.
Y	$= q/q^*$.
x	Axial distance.
ϵ	Adsorption column void fraction.
τ	Dimensionless time parameter.
ζ	Dimensionless distance parameter.

ACKNOWLEDGEMENT

This project was supported by a grant provided by the Australian Research Council. The assistance provided by Mr. H.-J. Wirth in obtaining experimental data is greatly appreciated.

REFERENCES

- 1 F. B. Anspach, K. K. Unger, J. Davies and M. T. W. Hearn, *J. Chromatogr.*, 457 (1988) 195.
- 2 C. Yang and G. T. Tsao, *Adv. Biochem. Eng.*, 25 (1982) 1.
- 3 A. I. Liapis, *J. Biotechnol.*, 11 (1989) 143.
- 4 H. A. Chase, *J. Chromatogr.*, 297 (1984) 179.
- 5 F. H. Arnold, H. W. Blanch and C. R. Wilke, *Chem. Eng. J.*, 30 (1985) B9.
- 6 B. H. Arve and A. I. Liapis, *AIChE J.*, 33 (1987) 179.
- 7 B. H. Arve and A. I. Liapis, *Biotechnol. Bioeng.*, 32 (1988) 616.
- 8 B. J. Horstmann and H. A. Chase, *Chem. Eng. Res. Des.*, 67 (1989) 243.
- 9 A. I. Liapis, B. Anspach, M. E. Findley, J. Davies, M. T. W. Hearn and K. K. Unger, *Biotechnol. Bioeng.*, 34 (1989) 467.
- 10 T. K. Sherwood, R. L. Pigford and C. R. Wilke, *Mass Transfer*, McGraw-Hill, New York, 1975.
- 11 J. M. Coulson and J. F. Richardson, *Chemical Engineering*, Vol. 3, Pergamon Press, Oxford, 2nd ed., 1979.
- 12 A. L. Hines and R. N. Maddox, *Mass Transfer, Fundamentals and Applications*, Prentice-Hall, Englewood Cliffs, NJ, 1985.
- 13 H. G. Thomas, *J. Am. Chem. Soc.*, 66 (1944) 1664.
- 14 N. K. Hiester and T. Vermeulen, *Chem. Eng. Prog.*, 48 (1952) 505.
- 15 F. Helfferich, *Ion Exchange*, McGraw-Hill, New York, 1962.
- 16 H. Tan, *Chem. Eng.*, Oct. 24. (1977) 158.
- 17 F. B. Anspach, A. Johnston, H.-J. Wirth, K. K. Unger and M. T. W. Hearn, *J. Chromatogr.*, 476 (1989) 205.
- 18 F. B. Anspach, A. Johnston, H.-J. Wirth, K. K. Unger and M. T. W. Hearn, *J. Chromatogr.*, 499 (1990) 103.
- 19 E. Kreyszig, *Advanced Engineering Mathematics*, John Wiley & Sons, New York, 6th ed., 1988.
- 20 A. Johnston, Q. M. Mao and M. T. W. Hearn, *J. Chromatogr.*, 548 (1991) 127.

CHROMSYMP. 2353

Characterization of synthetic macroporous ion-exchange resins in low-pressure cartridges and columns

Evaluation of the performance of Macro-Prep 50 S resin in the purification of anti-Klenow antibodies from goat serum

LEE DUNN*, MOHAMED ABOUELEZZ, LARRY CUMMINGS, MOHSEN NAVVAB, CHERYL ORDUNEZ, CHRISTOPHER J. SIEBERT and KENNETH W. TALMADGE

Bio-Rad Laboratories, CBU Research and Development, Chemical Division, 3300 Regatta Blvd., Richmond, CA 94804 (USA)

ABSTRACT

Three ion-exchange materials and one hydrophobic-interaction chromatography packing, based on a rigid macroporous polymer with large, relatively uniform pores, have been evaluated for low-pressure liquid chromatography of antibodies. These sorbents have high capacities for both small and large proteins and are mechanically, chemically, and thermally stable. Macro-Prep 50 S, CM and Q ion-exchange materials are strongly acidic, weakly acidic, and strongly basic, respectively. Protein binding and recovery, pressure-flow properties, and chemical and thermal stability were determined for each sorbent. A rapid, two-step method for the purification of anti-Klenow antibodies from goat serum was developed, based on the Macro-PrepTM 50 S strong-acid cation-exchange material and the Econo-Pac[®] HIC prepacked hydrophobic-interaction cartridge.

INTRODUCTION

The introduction of ion-exchange cellulose particles as a column packing material was a significant event in the history of protein purification [1,2]. Although physically weak and unstable, ion-exchange cellulose particles were very effective packings, because proteins could be freely bound and released from the complex outer surface regions of the particles, and non-specific adsorption was relatively low. Over the next three decades, improvements in the physical and chemical properties of ion exchangers led to the current, highly efficient materials, suitable for ion-exchange high-performance liquid chromatography (HPLC) of biopolymers [3,4]. The generally accepted use of particles $\leq 10 \mu\text{m}$ to achieve high performance requires expensive high-pressure equipment. The need for reducing costs and increasing the scale of high-performance separations in processing techniques for biological products has placed new demands on chromatographic materials. This necessitates a better understanding of the physical and chemical properties of porous packing materials. The

pharmaceutical and biotechnology industries need chromatographic materials with high chemical stability to withstand harsh sanitation conditions, with high mechanical strength to hold up under the pressures and flow-rates needed for large-scale separations, and high dynamic load capacities, giving high recoveries of biological activity.

This report describes a new macroporous methacrylate polymer (Macro-Prep™ 50) that meets the above-mentioned requirements. Three ion-exchange resins, as well as a hydrophobic-interaction packing, are discussed. All of these materials are characterized by a high percentage of pores in the range of 1000–1500 Å. To test this macroporous material, goat antibodies against the Klenow fragment of DNA polymerase from *Escherichia coli* [5] were purified on the Macro-Prep 50 S and Econo-Pac® HIC 5-ml cartridges.

MATERIALS AND METHODS

Materials

All chemicals used were of analytical-reagent grade. Guanidine-HCl was obtained from Aldrich (Milwaukee, WI, USA). Monobasic sodium phosphate, dibasic sodium phosphate, sodium acetate, thimerosal, 4-morpholinepropanesulfonic acid (MOPS), 4-morpholineethanesulfonic acid (MES) and 4-(2-hydroxyethyl)-1-piperazineethanesulfonic acid (HEPES) buffers, bovine serum albumin (BSA), bovine carbonic anhydrase B, cytochrome *c*, human hemoglobin, human immunoglobulin (IgG), human transferrin, lysozyme, myoglobin, and ribonuclease A were purchased from Sigma (St. Louis, MO, USA). Macro-Prep 50 CM, Q, and S packings, Econo-Pac HIC cartridges, ammonium sulfate, protein assay standard I (bovine γ -globulin) and II (BSA), sodium dodecyl sulfate (SDS), Tris-HCl, Coomassie Blue, Tween 20, horseradish peroxidase-conjugated protein G, Klenow DNA polymerase, and 3,3',5,5'-tetramethylbenzidine (TMB) were obtained from Bio-Rad (Richmond, CA, USA). Goat serum (Bethyl Labs., Montgomery, TX, USA) was obtained from goats inoculated with Klenow DNA polymerase.

Polymer characterization

The pore structure analysis of the ion-exchange sorbents was carried out by mercury intrusion porosimetry, using the pore sizer, Model 9310 (Micromeritics Instruments, Norcross, GA, USA). In mercury porosimetry the volume of mercury intruded into the pores in a sample is measured as a function of pressure. From these measurements a variety of physical properties can be calculated, including pore diameter, pore volume, and total pore surface area. Particle-size distributions were determined by electrozone sensing, using an Elzone 80XY analyzer (Particle Data, Elmhurst, IL, USA) and by visual examination, using a light microscope.

The mechanical rigidity of the Macro-Prep 50 ion-exchange material was examined by measuring the backpressure (p.s.i.) as a function of the linear flow-rate (cm/h). Backpressure was measured with a 0–1000 p.s.i. electronic transducer (Sensym, Sunnyvale, CA, USA). Macro-Prep 50 CM, Q, and S resins were packed into Bio-Rex® MP columns (10 × 1 cm I.D.) under gravity and equilibrated with deionized water for 24 h at 1.0 ml/min, using a Model 1350 pump (Bio-Rad). The flow-rate was increased to 5.0 ml/min and maintained at this rate for 30 min before measuring

the backpressure. Subsequently, the flow-rate was increased in 5.0 ml/min increments and maintained for 30 min at each new flow-rate before measuring the backpressure.

The swelling and shrinking properties of the resins were determined by measuring changes in bed volume due to changes in pH (4.0–10.0), salt concentration (0–1.0 *M* NaCl), and organic solvents. Columns, 60 × 1.5 cm I.D., were filled to a height of approximately 11 cm with Macro-Prep resins. The bed height was determined before and after equilibration in the test solutions for 24 h, at a flow-rate of 1.0 ml/min.

The three Macro-Prep 50 ion-exchangers were submitted to an independent laboratory for a series of standard biological tests designed to detect potentially toxic contaminants leaching from the resins. The tests included; (a) USP systemic and intracutaneous injections of saline and cottonseed oil extracts of the resins into rabbits, (b) intraperitoneal injections of saline and cottonseed oil extracts of the resins into mice and guinea pigs, (c) cytotoxicity of extracts to L-929 mouse fibroblast cells in tissue culture, (d) Ames mutagenicity test.

Determination of ion-exchange capacity

Ionic capacities of the ion exchangers were determined by conductometric titrations with a YSI Model 32 Conductance Meter (Yellow Springs Instrument, Yellow Springs, OH, USA) and Model 3403 microcell ($K = 1.0/\text{cm}$). Using the Macro-Prep 50 S material as an example, 5.0 ml of resin was washed with deionized water, equilibrated with 0.5 *M* HCl for 1 h, and washed with deionized water until the conductivity was $\leq 2.0 \mu\text{S}/\text{cm}$. Macro-Prep 50 S and CM packings were then titrated with 0.1 *M* NaOH. The Macro-Prep 50 Q packing was converted to the hydroxide form and titrated with 0.1 *M* HCl.

Determination of protein binding capacity

Static protein binding capacities for Macro-Prep 50 CM, Q, and S materials were determined by using an excess of protein. The conditions for the Macro-Prep 50 S resin are given as an example for these determinations. The Macro-Prep 50 S packing (0.5–1.0 ml) was washed with water, followed by 20 *mM* sodium acetate buffer, pH 5.0 (binding buffer). Next, the material was equilibrated for 24 h with 100 mg human IgG, dissolved in *ca.* 35 ml of binding buffer. The sorbent was washed with binding buffer to remove unbound material, and the bound protein was eluted with 20 *mM* Tris-HCl (pH 9.0), containing 1.0 *M* NaCl. The protein was quantitated using one of the following methods; absorbance at 280 nm, Bradford [6] reagent (Bio-Rad), BCA assay [7] (Pierce, Rockford, IL, USA). Protein-binding capacity, in mg IgG/ml resin, and percent recovery were calculated. The static protein-binding capacities for the Macro-Prep 50 CM and Q materials were performed similarly. For the CM packing, the proteins (100 mg) were bound in 15 ml of 10 *mM* sodium acetate buffer (pH 5.0), and eluted with 100 *mM* Tris-HCl buffer (pH 8.0). For the Q packing, the proteins (100 mg) were bound in 5.0 ml of 10 *mM* Tris-HCl buffer (pH 8.3), and eluted with 50 *mM* Tris-HCl buffer (pH 8.3), containing 1.0 *M* NaCl.

Chromatography

High-performance liquid chromatography was carried out on a HRLC® Model 800 chromatography system (Bio-Rad). Low-pressure liquid chromatography was

performed on an Econo System, consisting of a Model EP-1 Econo Pump, Model EM-1 Econo UV Monitor, and a Model ES-1 Econo System controller (Bio-Rad). Fractions were collected with a Model 2110 fraction collector (Bio-Rad). All buffers were filtered through 0.2- μm membrane filters (Gelman Sciences, Ann Arbor, MI, USA).

Column lifetime of the resins was determined by running 100 gradient cycles on a HRLC 800 gradient system, equipped with a Model AS-100 automatic sampler (Bio-Rad). Using the Macro-Prep 50 S support (10×1.0 cm I.D.) as an example, each cycle consisted of a 10-min gradient from 0–100% B, where buffer A was 10 mM sodium phosphate (pH 6.9), and buffer B was buffer A plus 1.0 M NaCl. Every tenth cycle, a Cationic Protein Standard (Bio-Rad) containing myoglobin, ribonuclease A, and cytochrome *c* was injected onto the column.

Enzyme-linked immunosorbent assay (ELISA)

Determination of specific antibody activity against the Klenow DNA polymerase was performed by ELISA. Wells of microtiter plates were coated overnight at 4°C with 50 μl of Klenow DNA polymerase at a concentration of 1.0 $\mu\text{g}/\text{ml}$ in 50 mM sodium carbonate buffer (pH 9.6). Plates were washed one time with 200 μl of a solution consisting of 20 mM sodium phosphate (pH 7.2), 120 mM sodium chloride, 0.05% Tween 20, and 0.01% thimerosal (PTT). Wells were incubated for 2 h at room temperature with 200 μl PTT, containing 0.5% BSA (referred to as PTTB) to block non-specific binding sites on the plates. The plates were then washed once with 200 μl of PTT, blotted dry and sealed with parafilm before being stored at 4°C. Column fractions were assayed for antibody binding activity by adding 50–100 μl aliquots of the samples, diluted with PTTB, to the coated plates for 1–3 h at room temperature. The plates were washed twice with PTT and then incubated for 1 h at room temperature with 100 μl of horseradish peroxidase-conjugated protein G, diluted 1/10 000 with PTTB. The plates were then washed three times with PTT, and the enzyme activity was measured by adding 100 μl of TMB substrate for 5–10 min at room temperature before stopping the reactions with 100 μl of 0.5 M sulfuric acid. The plates were read at 450 nm, using a Model 3550 Microplate Reader (Bio-Rad).

SDS-polyacrylamide gel electrophoresis (SDS-PAGE)

Electrophoretic separations were carried out under reducing conditions by the method of Laemmli [8] on 12% pre-cast Mini-PROTEAN II® ready gels (Bio-Rad), 12% single percentage gel, 0.376 M Tris-HCl (pH 10), using the Mini-PROTEAN II cell and a Model 500/200 power supply (Bio-Rad). Staining was performed with Coomassie Blue.

RESULTS

Physical properties

Three macroporous ion-exchange derivatives were evaluated, a carboxylate weak-cation exchanger, a sulfopropyl strong-cation exchanger, and a quaternary ammonium strong-anion exchanger. The macroporous nature of the beads was confirmed by scanning-electron microscopy, as shown in Fig. 1. The bead shown is approximately 20 μm in size.

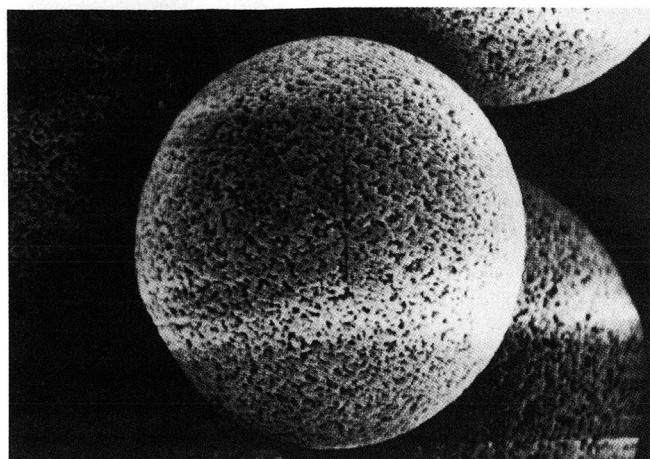


Fig. 1. Scanning.-electron micrograph of Macro-Prep 50 Q resin, obtained with an International Scientific Instrument, Model ISI SX-40. Magnification 2400 \times .

The surface and pore structure of the beads were characterized (Table I) by mercury intrusion porosimetry for pore size, pore volume, and surface area. The pore-volume distribution of the beads was plotted as a function of pore diameter for the Macro-Prep 50 Q packing. The results in Fig. 2 illustrate that most of the pore volumes were between 1000 and 1500 Å with only a low percentage of small pores.

The swelling and shrinking properties of the ion-exchange materials were different in aqueous and organic liquids. Macro-Prep 50 CM and Q packings exhibited less than 1% shrinkage or swelling in the pH range from 4–10, while the Macro-Prep 50 S packing exhibited less than 3% (Table I). In the range of 0.1–1.0 M NaCl, the Macro-Prep 50 CM and Q materials exhibited less than 5% shrinkage or swelling, and the Macro-Prep 50 S packing exhibited less than 9% (Table I). In organic solvents, such as acetonitrile and methanol, the packings swell 20–30% (unpublished results).

TABLE I
PHYSICAL AND CHEMICAL PROPERTIES OF MACRO-PREP 50 RESINS

	Macro-Prep 50 CM	Macro-Prep 50 Q	Macro-Prep 50 S
Type of exchanger	Weak cation	Strong anion	Strong cation
Functional group	$-\text{COO}^-$	$-\text{N}^+(\text{CH}_3)_3$	$-\text{SO}_3^-$
Ionic capacity	210 ± 30 $\mu\text{equiv./ml}$	190 ± 40 $\mu\text{equiv./ml}$	160 ± 40 $\mu\text{equiv./ml}$
Counter ion	Na^+	Cl^-	Na^+
Protein capacity	≥ 25 mg hemoglobin/ml	≥ 15 mg ferritin/ml	≥ 35 mg IgG/ml
Mean particle size	50 μm	50 μm	50 μm
Pore size (nominal)	1200 Å	1200 Å	1200 Å
Surface area	18–22 m^2/g	18–22 m^2/g	18–22 m^2/g
Pore volume	≥ 0.5 ml/g	≥ 0.5 ml/g	≥ 0.5 ml/g
Swell/shrink			
pH 4–10	<1%	<1%	<3%
0.1–1.0 M NaCl	<4%	<5%	<9%

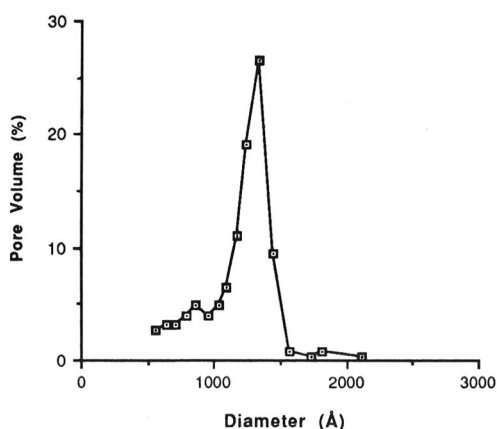


Fig. 2. Macro-Prep 50 Q material analyzed by mercury porosimetry, as described under Materials and Methods. Percent total pore volume is plotted as a function of the pore diameter.

The beads were mechanically strong in aqueous solutions, based on measurements of the backpressures at increasing flow-rates. The results of the pressure-flow-rate experiments for the three ion-exchange resins are shown in Fig. 3. The maximum linear velocity that could be reached was 3800 cm/h for the Macro-Prep CM material, 5700 cm/h for the Q material, and 4560 cm/h for the S material.

Ion-exchange properties

Ion-exchange capacity, static protein binding capacities, and protein recoveries for the three ion exchange materials are listed in Table II. Ion-exchange capacities of several lots of Macro-Prep ion exchangers were analyzed and the range for each is shown. The ionic capacities were found to vary by as much as 25% from the average value, determined for each material (data not shown).

The static protein capacity varied for each of the ion-exchange resins, depending upon the protein tested. Macro-Prep 50 CM material exhibited static protein-

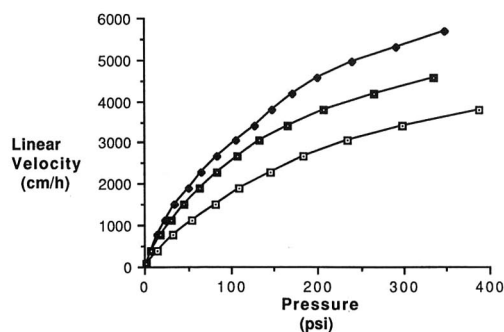


Fig. 3. Macro-Prep 50 CM (\square), Macro-Prep 50 Q (\blacklozenge) and Macro-Prep 50 S (\blacksquare) materials were packed into 10×1.0 cm Bio-Rex MP columns. The backpressure, in p.s.i. was measured at increasing flow-rate, as described under Materials and Methods. The flow-rates (ml/min) have been converted to linear velocity (cm/h).

TABLE II

IONIC CAPACITY, PROTEIN-BINDING CAPACITY, AND RECOVERY

The ionic and static protein binding capacities were performed as described in the Materials and Methods. The percent recoveries were performed at loadings of 25% of the maximum capacity.

Materials	Ionic capacity (μ equiv./ml resin)	Binding capacity (mg/ml resin)	Recovery (%)
<i>Macro-Prep 50 CM</i>	210 \pm 40		
BSA		20	84
Cytochrome <i>c</i>		15	95
Ribonuclease A		15	108
Transferrin		26	108
Hemoglobin, human		35	79
<i>Macro-Prep 50 Q</i>	190 \pm 40		
BSA		17	98
Ferritin		23	94
Thyroglobulin		24	88
<i>Macro-Prep 50 S</i>	160 \pm 40		
Cytochrome <i>c</i>		35	103
IgG, human		57	102
Lysozyme		51	97
Ribonuclease A		62	102

binding capacities ranging from 15 to 35 mg/ml resin for five proteins examined. Similarly, static binding capacities of 17 to 24 mg/ml resin were observed of the Q material. The Macro-Prep 50 S material exhibited higher static protein-binding capacities, 35 to 62 mg/ml resin, depending upon the protein tested.

Protein recovery was good for all the proteins tested, as seen in Table II. Macro-Prep 50 S and Q resins showed 94 to 108% recoveries of the proteins tested, while the recoveries from the CM sorbent were also high, except for BSA (84%) and hemoglobin (79%).

TABLE III

CHEMICAL AND THERMAL STABILITY OF IONIC CAPACITY

The Macro-Prep 50 materials were suspended in the solutions and assayed at the indicated times for ionic capacity, as described under Materials and Methods.

Exposure	Ionic capacity (μ equiv./ml resin)		
	Macro-Prep 50 CM	Macro-Prep 50 Q	Macro-Prep 50 S
Control	238	190	184
1% SDS, 24 h	241	168	194
8 M Guanidine-HCl, 24 h	234	195	189
1 M HCl, 7 days	249	189	192 (3 days)
1 M NaOH, 7 days	239	186	191 (3 days)
Autoclave, 121°C, 30 min	205	193	194

TABLE IV

CHEMICAL AND THERMAL STABILITY OF PROTEIN-BINDING CAPACITY

The Macro-Prep 50 materials were suspended in the solutions and assayed at the indicated times for the static protein-binding capacity, as described under Materials and Methods.

Exposure	Protein capacity (mg/ml resin)			
	Macro-Prep 50 CM ^a	Macro-Prep 50 Q ^b	Macro-Prep 50 Q ^c	Macro-Prep 50 S ^d
Control	40	20	17	40
1% SDS, 24 h	40	19	—	43
8 M Guanidine-HCl, 24 h	36	20	—	42
1 M HCl, 72 h	40	—	20	43
1 M NaOH, 72 h	40	—	16	41
Autoclave, 121°C, 30 min	40	—	17	45

^a Hemoglobin (human).

^b Ferritin.

^c Different resin sample used for control.

^d IgG (human).

Chemical properties

Treatment of Macro-Prep 50 packings with 1.0 M HCl, 1.0 M NaOH, 1% SDS, and 8 M guanidine-HCl can be carried out without substantial loss in ionic (Table III) or static protein-binding capacity (Table IV). Sanitization can be achieved with 1.0 M NaOH and sterilization by autoclaving at 121°C for 30 min. Except for losses in ionic capacities of the CM material after autoclaving (14%) and the Q material after treatment with SDS (11%), all materials were virtually unaffected by these treatments.

A major concern of the pharmaceutical and biotechnology industries is contamination of biological products by toxic materials coming from chromatographic resins. To address this concern a series of standard biological tests, including USP systemic and intracutaneous injections, tissue culture cytotoxicity, and the Ames mutagenicity test were performed on extracts of the three Macro-Prep 50 ion-exchange materials. All results were negative; no extract showed signs of toxicity, cytotoxicity, or mutagenicity in any of the tests.

Separation of standard proteins

The chromatographic performance of the Macro-Prep 50 ion-exchange packings was demonstrated by separating mixtures of proteins under gradient elution conditions (Fig. 4). Carbonic anhydrase, transferrin, and BSA are well resolved on the Macro-Prep 50 Q column (Fig. 4a) as are myoglobin, ribonuclease A, and cytochrome *c* on the Macro-Prep 50 S column (Fig. 4b). With the Macro-Prep 50 CM material (Fig. 4c), myoglobin, ribonuclease A, and cytochrome *c* are resolved. Cytochrome *c* was split into two peaks (presumably due to the oxidized and reduced forms of the protein) under the gradient conditions used.

Column lifetime studies over 100 gradient cycles on 10 × 1.0 cm columns indicated that the resins were robust. After 100 gradient cycles, with every tenth cycle

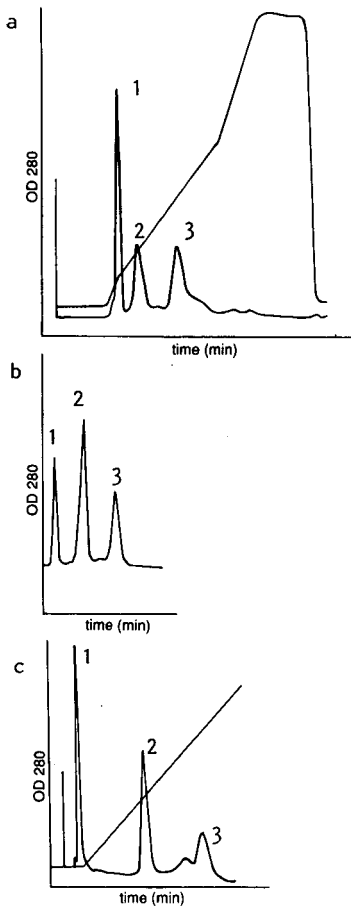


Fig. 4. Chromatography of standard protein mixtures on Macro-Prep 50 Q, S, and CM ion-exchange columns. (a) Separation of (1) bovine carbonic anhydrase B, (2) human transferrin and (3) BSA on a column (30×2.5 cm I.D.) of Macro-Prep 50 Q with mobile phase buffers of (A) 50 mM Tris-HCl (pH 8.6) and (B) 50 mM Tris-HCl (pH 8.6), containing 500 mM NaCl at a flow-rate of 4.0 ml/min. The proteins were eluted by a linear gradient of 0 to 50% B over 45 min, followed by a 30 min linear gradient to 100% B. (b) Separation of (1) myoglobin, (2) ribonuclease A, and (3) cytochrome *c* on a column (30×1.0 cm I.D.) of Macro-Prep 50 S with mobile-phase buffers of (A) 20 mM phosphate (pH 8.0) and (B) 20 mM phosphate (pH 8.0), containing 1.0 M NaCl. The proteins were eluted by a linear gradient of 0 to 70% B over 20 min at a flow-rate of 3.0 ml/min. (c) Separation of (1) myoglobin, (2) ribonuclease A and (3) cytochrome *c* on a column (20×1.0 cm I.D.) of Macro-Prep 50 CM with mobile-phase buffers of (A) 20 mM HEPES (pH 8.2) and (B) 20 mM HEPES (pH 8.2), containing 1.0 M NaCl. The proteins were eluted by a linear gradient of 0 to 60% B over 25 min at a flow-rate of 3.0 ml/min.

including an injection of a protein mixture, the performance was unchanged. The chromatograms in Fig. 5 for the first and hundredth cycle on the Macro-Prep 50 S column depict very similar profiles, demonstrating that the resin is stable under these conditions. Similar results, not shown, have been obtained for the Macro-Prep 50 Q and CM supports.

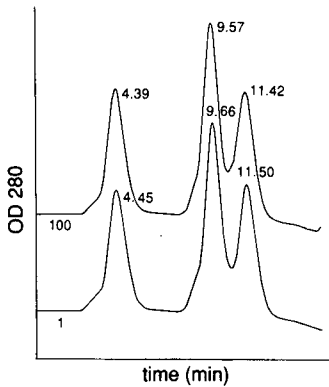


Fig. 5. A Macro-Prep 50 S column (10×1.0 cm I.D.) was subjected to 100 gradient cycles. Every tenth cycle, the protein standard (myoglobin, ribonuclease A, and cytochrome *c*) was injected onto the column. The chromatograms are shown for injection during the first and hundredth cycle.

Antibody purification from serum

The utility of these new chromatographic materials was demonstrated by the purification of antibodies against Klenow DNA polymerase from goat serum, using Macro-Prep 50 S, a strong-acid cation exchanger, as a first chromatographic step. Buffer and pH conditions were optimized for the purification of IgG on the Macro-Prep 50 S resin. In data not shown, similar separations were observed with several different buffers, including HEPES, MES, MOPS, and sodium phosphate.

The Macro-Prep 50 S material in 5.0 ml prepacked Econo-Pac cartridges provided a convenient way for separating IgG from goat serum, as shown in Fig. 6a. For

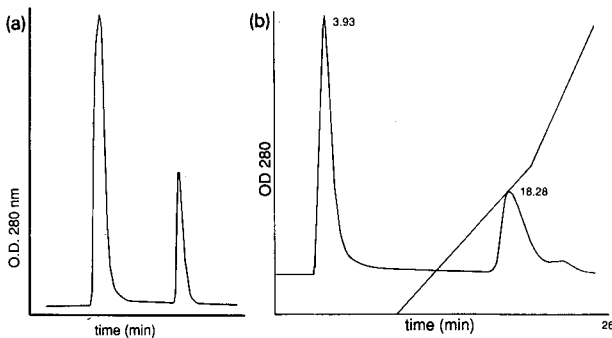


Fig. 6. Fractionation of goat serum on Macro-Prep 50S. (a) Dialyzed goat serum (2.0 ml) was fractionated on an Econo-Pac S cartridge, containing 5.0 ml of the Macro-Prep S material, equilibrated in 20 mM MOPS buffer (pH 6.8). The proteins were eluted by a 0–100% gradient over 20 min, using 20 mM MOPS buffer (pH 6.8), containing 1.0 M NaCl, at a flow-rate of 1.0 ml/min. (b) Goat serum, dialyzed against 20 mM MOPS (pH 6.8), was fractionated on a Macro-Prep 50 S column (10×1.0 cm I.D.), equilibrated in 20 mM MOPS buffer (pH 6.8). The column was washed for 10 min with the equilibration buffer, followed by a 0–50% gradient over 10 min with 20 mM MOPS buffer (pH 6.8), containing 1.0 M NaCl at a flow-rate of 1.0 ml/min.

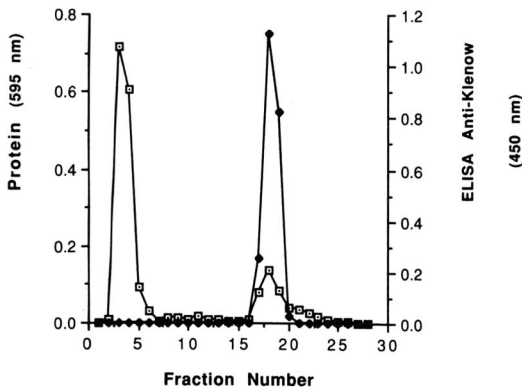


Fig. 7. Anti-Klenow activity from goat serum fractionation on Macro-Prep 50 S material. Fractions were collected from the separation shown in Fig. 6b and analyzed for Klenow binding activity (◆), as described under Materials and Methods. Protein (□) was determined on aliquots in microtiter plates with the Bio-Rad Protein Assay, using a Model 3550 Microplate Reader at 595 nm.

comparison, the same sample was chromatographed on a 10 × 1.0 cm column of the Macro-Prep 50 S packing (Fig. 6b). Identity of the two major peaks was confirmed with a Bio-Sil® SEC-250 gel filtration column (data not shown) and by SDS-PAGE (Fig. 8). Under these chromatographic conditions, most of the albumin is eluted in the first peak with 20 mM MOPS buffer (pH 6.8) while the IgG is bound and subsequently eluted with a salt gradient. Up to 10 ml of dialyzed goat serum was processed on the column (Fig. 6b) without loss in IgG purity; however, with higher loads some loss in recovery of IgG was noted. This step has been scaled up to purify

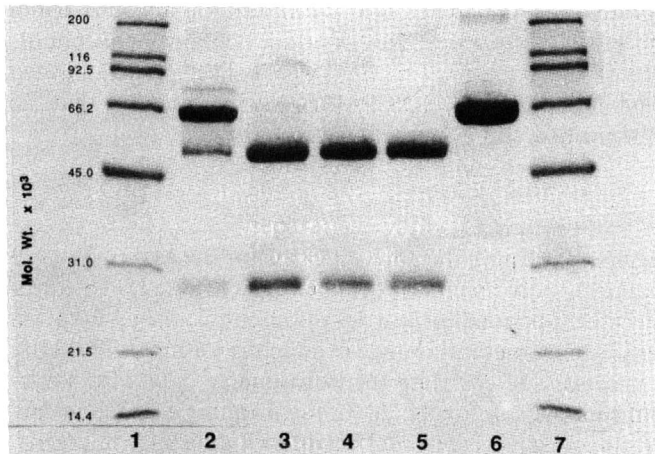


Fig. 8. SDS-PAGE analyses of goat serum fractions. SDS-PAGE on 12% gels under reducing conditions: low-molecular-weight Bio-Rad standard (lanes 1 and 7); dialyzed goat serum, (lane 2); IgG pool from Macro-Prep S column (lane 3); IgG pool from Econo-Pac HIC cartridge (lane 4); goat IgG standard (lane 5); goat albumin standard (lane 6).

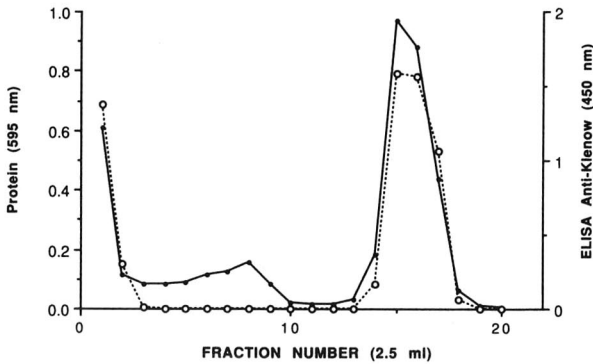


Fig. 9. Purification of IgG pool on Econo-Pack HIC cartridge. The IgG pool (1.5 ml) from the Macro-Prep 50 S chromatography was mixed with 1.5 ml of buffer A [20 mM phosphate (pH 6.8), containing 2.4 M $(\text{NH}_4)_2\text{SO}_4$] and added to an Econo-Pac HIC cartridge (5.0 ml), equilibrated in buffer A. The column was eluted at 1.0 ml/min for 8 min with 25% buffer B [20 mM phosphate (pH 6.8)], followed by a 20-min gradient from 25 to 100% B. Fractions were assayed for Klenow binding activity (○) and protein (●).

0.9 g of antibody, following chromatography of 100 ml of the dialyzed goat serum on a 20×2.5 -cm column of Macro-Prep 50 S material. The profile obtained with this column was similar to those seen with the 5-ml cartridge and smaller column.

Fractions were collected from the Macro-Prep S column (Fig. 6b) and assayed for protein and specific anti-Klenow antibodies (Fig. 7). Klenow binding activity was present only in the second peak containing the IgG. The SDS-PAGE results in Fig. 8 show that the pooled IgG fraction from the Macro-Prep S column was relatively pure, with minor contaminants of albumin and other (unidentified) components. To purify the IgG from the Macro-Prep 50 S column further, a second step consisting of hydrophobic-interaction chromatography (HIC) was performed. The antibody fraction from the Macro-Prep S step was diluted 1:1 with 2.4 M ammonium sulfate and injected onto a 5.0-ml Econo-Pac HIC cartridge. This cartridge contains hydrophobic methoxy groups on the Macro-Prep 50 matrix. Fractions were collected and analyzed for protein and anti-Klenow binding (Fig. 9). SDS-PAGE (Fig. 8) indicated that the antibody fraction was highly purified and essentially free of albumin.

DISCUSSION

The geometric parameters concerning the pore structure for the Macro-Prep 50 resins were determined by mercury porosimetry of the dry beads (Table I). To correlate the porosimetry data with the functional properties of the resins, the assumption is made that the resins undergo little structural change in aqueous solutions. To verify this assumption, it will be necessary to correlate the porosimetry data with steric-exclusion chromatography in aqueous solution [9,10]. In the scanning electron micrograph, the Macro-Prep 50 resin appears as spherical beads with a distinctive macroporous structure on their surface and interior. The rigidity and mechanical strength of the resins were demonstrated by the minimal swelling and shrinking in aqueous solution between pH 4 and 10 and at salt concentrations up to 1.0 M (Table I), and the pressure-flow-rate study shown in Fig. 3. Linear flow-rates up to 3800 cm/h could be

obtained without collapse of the chromatographic bed. The column lifetime studies of the ion exchangers (Fig. 5) indicated no deformation or increase in backpressure, that would be indicative of collapse of the resin.

In protein separations, two important geometric parameters of a resin are the mean pore size and pore-size distribution. These determine the accessibility of the internal pore surface to different proteins. Unger *et al.* [11] have stated that the pore diameter must be a least five times the protein diameter to permit access of the protein to the total internal surface. They concluded that the pore diameters should be large and the particle diameters should be small to minimize the deleterious effects of pores on resolution. It has been estimated that a 1000-Å pore size would allow almost complete access to the internal surface for molecules of $> 10^5$ MW [12]. Sorbents with increasingly larger pore sizes have been developed for ion-exchange chromatography of proteins. However, beads with large pores typically exhibit broad pore-size distributions, including a significant fraction with small pores. Ritchie *et al.* [13] have demonstrated that in size-exclusion chromatography, resolution can be increased with a very narrow pore size distribution. This ensures that the sample is loaded in the minimum column volume. With large pore macroporous beads, more than 95% of the surface area occurs within the pore [3,13], placing significant performance requirements on the pore structure. In these macroporous packings the detailed structure and its effects on the microenvironment of the ionic groups is largely unknown, with uncertainties for the solute access being greatest for the smallest pores [10].

The Macro-Prep 50 beads exhibit an unimodal pore size distribution (Fig. 2) with an unusually high percentage of large pores of an average of 1200 Å. Only a minor fraction of small pores are present. In practical terms, this means that a large percentage of the functional groups on the internal surface is accessible for binding a wide molecular weight range of proteins. The experimental data to support this supposition are the relative independence of molecular weight of the static protein binding capacities for each of the ion-exchange resins (Table II). For example, the Macro-Prep 50 Q material exhibited a binding capacity of 24 mg/ml for thyroglobulin (660 000 MW), 23 mg/ml for ferritin (450 000 MW), and 17 mg/ml for BSA (68 000 MW).

The Macro-Prep 50 packings appear to be biologically safe for pharmaceutical applications. Extracts from the three ion-exchangers showed no sign of animal toxicity, tissue culture cytotoxicity, or mutagenicity in the Ames test. These ion-exchange resins show excellent chemical and thermal stability, as no decrease in protein-binding capacity was observed after 3 days with 1.0 M sodium hydroxide or 1.0 M hydrochloric acid. HIC resins are less chemically stable to base, but they can tolerate 0.1 M sodium hydroxide (data not shown). The resins can be autoclaved without loss in protein binding capacity. These results suggest that the materials can be easily and safely sanitized. The mechanical stability was further demonstrated in column lifetime studies. For example, the Macro-Prep 50 S material exhibited no change in the retention time or peak shape of injected protein standards after 100 gradient cycles (Fig. 5).

Macro-Prep 50 resins have been utilized in the purification of antibodies to Klenow DNA polymerase from goat serum. This purification was monitored by SDS-PAGE and ELISA for specific binding to the Klenow DNA polymerase. The initial evaluation was performed on 5.0-ml prepacked cartridges of Macro-Prep 50 S

(Econo-Pac S cartridge) with subsequent scale-up to 8- and 100-ml columns of Macro-Prep 50 S. The antibody fraction collected from the S resin was relatively pure as determined by SDS-PAGE. Further purification was achieved using a 5.0 ml Econo-Pac HIC prepacked cartridge to yield a highly purified IgG.

ACKNOWLEDGEMENTS

We would like to acknowledge the following individuals who contributed significantly to this investigation: David Cacciatore, Chris Moran, Harvard Morehead, Ted Tisch, Dr. Eberhardt Kuhn and Dr. Curt Munson.

REFERENCES

- 1 E. A. Peterson and H. A. Sober *J. Am. Chem. Soc.*, 78 (1956) 751.
- 2 S. R. Himmelhoch and E. A. Peterson *Anal. Biochem.*, 17 (1966) 383.
- 3 F. E. Regnier, *Anal. Biochem.*, 126 (1982) 1.
- 4 Y. Kato, K. Nakamura and T. Hashimoto, *J. Chromatogr.*, 245 (1982) 193.
- 5 C. M. Joyce and N. D. F. Grindley, *Proc. Natl. Acad. Sci. U.S.A.*, 80 (1983) 1830.
- 6 M. M. Bradford, *Anal. Biochem.*, 72 (1976) 248.
- 7 P. K. Smith, R. I. Krohn, G. T. Hermanson, A. K. Mallia, F. H. Gartner, M. D. Provenzano, E. K. Fujimoto, N. M. Goetze, B. J. Olson and D. C. Klenk, *Anal. Biochem.*, 150 (1985) 76.
- 8 U. Laemmli, *Nature (London)*, 227 (1970) 680.
- 9 K. Jerabek, *Anal. Chem.*, 57 (1985) 1595.
- 10 A. Guyot, *Reactive Polymers*, 10 (1989) 113.
- 11 K. K. Unger, R. Janzen and G. Jilge, *Chromatographia*, 24 (1987) 144.
- 12 G. Vanecek and F. E. Regnier, *Anal. Biochem.*, 121 (1982) 156.
- 13 H. J. Ritchie, P. Ross and D. R. Woodward, *Chromatography and Analysis*, October (1990) 9.

CHROMSYMP. 2265

Comparison of silica-based cyanopropyl and octyl reversed-phase packings for the separation of peptides and proteins

NIAN E. ZHOU and COLIN T. MANT

Department of Biochemistry and the Medical Research Council of Canada Group in Protein Structure and Function, University of Alberta, Edmonton, Alberta T6G 2H7 (Canada)

J. JACK KIRKLAND

Central Research and Development, E.I. du Pont de Nemours and Company, Experimental Station, B-228, P.O. Box 80228, Wilmington, DE 19880-0228 (USA)

and

ROBERT S. HODGES*

Department of Biochemistry and the Medical Research Council of Canada Group in Protein Structure and Function, University of Alberta, Edmonton, Alberta T6G 2H7 (Canada)

ABSTRACT

The performance of a silica-based C_8 packing was compared with that of a less hydrophobic, silica-based cyanopropyl (CN) packing during their application to reversed-phase high-performance liquid chromatography (linear trifluoroacetic acid–water to trifluoroacetic acid–acetonitrile gradients) of peptides and proteins. It was found that: (1) the CN column showed excellent selectivity for peptides which varied widely in hydrophobicity and peptide chain length; (2) peptides which could not be resolved easily on the C_8 column were widely separated on the CN column; (3) certain mixtures of peptides and small organic molecules which could not be resolved on the C_8 column were completely separated on the CN column; (4) impurities arising from solid-phase peptide synthesis were resolved by a wide margin on the CN column, unlike on the C_8 column, where these compounds were eluted very close to the peptide product of interest; and (5) specific protein mixtures exhibited superior resolution and peak shape on the CN column compared with the C_8 column. The results clearly demonstrate the effectiveness of employing stationary phases of different selectivities (as opposed to the more common optimization protocol of manipulating the mobile phase) for specific peptide and protein applications, an approach underestimated in the past.

INTRODUCTION

The excellent resolving power of the reversed-phase (RP) mode has resulted in its becoming the predominant high-performance liquid chromatographic (HPLC) technique for peptide separations [1,2]. In addition, many protein separations are also effected through this HPLC mode [3,4]. Optimization of peptide and protein separations during RP-HPLC may generally be approached in two ways, mobile phase manipulation on a given reversed-phase column or employment of different stationary phases with complementary selectivities, the former approach being more commonly employed. With the wide choice of variables (*e.g.*, ion-pairing reagent, pH,

organic modifier, other additives) available to the researcher when manipulating mobile phase conditions, in addition to the option of changing the gradient-rate and flow-rate, it is perhaps not surprising that this approach to optimization of peptide and protein separations has become dominant. However, this dominance has tended to obscure the effectiveness of employing stationary phases of different selectivities for specific applications.

Although RP-HPLC on stationary phases containing alkyl chains (*e.g.*, C₈, C₁₈) as the functional ligand is still the method of choice for most peptide [1,2] and many protein separations [3,4], less hydrophobic [5] cyanopropyl (CN) packings have been applied during RP-HPLC of both peptides and proteins [5–12]. One of the reasons why these packings have not seen more use may be due to problems of stationary phase instability [6,9,12,13], with significant and rapid loss of stationary phase ligands often observed when employing acidic mobile phases, such as the frequently used aqueous trifluoroacetic acid (TFA)–acetonitrile system (pH 2). Kirkland and co-workers [13,14] recently reported the development of stable silica-based bonded phases, based on protecting the siloxane bond between the silica and the functional ligand with bulky side groups. Monofunctional alkyl- and cyanopropylsilanes containing two isopropyl groups (instead of the usual methyl groups) were found to produce exceptionally stable alkyl and CN reversed-phase packings.

This paper compares the performances of such highly stable C₈ and CN columns during their application to RP-HPLC of a range of peptides (with varying chain length and hydrophobicity), proteins and small organic molecules. The advantages for specific applications of employing a cyanopropyl stationary phase with characteristics (in terms of hydrophobicity and selectivity) markedly different to those of the commonly used C₈ packing are clearly demonstrated.

EXPERIMENTAL

Materials

HPLC-grade water and acetonitrile were obtained from J. T. Baker (Philipsburg, NJ, USA) and HPLC-grade TFA from Pierce (Rockford, IL, USA). Alkylphenone standards were obtained from Pierce, thioanisole from Aldrich (Milwaukee, WI, USA), dithiothreitol (DTT) from Schwarz-Mann Biotech (Cleveland, OH, USA) and bovine ribonuclease A, equine cytochrome *c*, chicken lysozyme, papain, bovine serum albumin, bovine α -lactalbumin, sperm whale myoglobin, bovine α -chymotrypsinogen A and baker's yeast enolase from Sigma (St. Louis, MO, USA). Rabbit skeletal troponin T, troponin I and troponin C and rabbit cardiac tropomyosin were prepared from tissue extracts.

Peptide synthesis

The peptides described were synthesized either on a Beckman (Berkeley, CA, USA) Model 990 peptide synthesizer or an Applied Biosystems (Foster City, CA, USA) Model 430A peptide synthesizer, using the general procedure for solid-phase peptide synthesis described by Hodges and co-workers [15,16].

Apparatus

The HPLC instrument consisted of an HP1090 liquid chromatograph (Hewlett-

Packard, Avondale, PA, USA), coupled to an HP1040A detection system, HP9000 Series 300 computer, HP9133 disc drive, HP2225A Thinkjet printer and HP7440A plotter.

Columns

Three columns were employed: (1) silica-based C₈ packing (150 × 4.6 mm I.D. column) containing a monomeric stationary phase of diisopropyl-*n*-octyl groups (5-μm particle size, 94-Å pore size, 5.78% carbon loading) from DuPont (Wilmington, DE, USA) (this packing is equivalent to the commercial 25-cm Zorbax-Rx columns available from MacMod Analytical, Chadds Ford, PA, USA); (2) silica-based CN packing (Zorbax SB-300CN) (150 × 4.6 mm I.D. column) containing a monomeric stationary phase of diisopropyl-3-cyanopropyl groups (6 μm, 250 Å) from Rockland Technologies (West Chester, PA, USA); and (3) Aquapore RP-300 C₈ (220 × 4.6 mm I.D. column) (7 μm, 300 Å) from Chromatographic Specialties (Brockville, Ontario, Canada). All packings and columns were new to ensure a fair comparison.

RESULTS AND DISCUSSION

Comparison of C₈ and CN column performance in RP-HPLC of peptides

Although CN packings have been employed for RP-HPLC of peptides [5–9,11,12], it has been reported [6,8,17] that hydrophilic/moderately hydrophobic and/or small peptides are generally not retained well by such packings. In contrast, such packings have proved useful for the separation of hydrophobic peptides [10,12].

The peptides shown in Table I were subjected to a linear A–B gradient (1%

TABLE I
PEPTIDES USED IN THIS STUDY

Peptides	Sequence ^a
10G–40G	Ac-(Gly-Lys-Gly-Leu-Gly) _n -amide, where <i>n</i> = 2,4,6,8; 10G, 20G, 30G, 40G, respectively
5A–50A	Ac-(Leu-Gly-Leu-Lys-Ala) _n -amide, where <i>n</i> = 1,2,4,6,8,10; 5A, 10A, 20A, 30A, 40A, 50A, respectively
5L–50L	Ac-(Leu-Gly-Leu-Lys-Leu) _n -amide, where <i>n</i> = 1,2,4,6,8,10; 5L, 10L, 20L, 30L, 40L, 50L, respectively
7A–35A	Ac-Lys-Cys-Ala-Glu-Gly-Glu-Leu-(Lys-Leu-Glu-Ala-Gly-Glu-Leu) _n -amide, where <i>n</i> = 0,1,2,3,4; 7A, 14A, 21A, 28A, 35A, respectively
7B–35B	Ac-Lys-Cys-Ala-Glu-Leu-Glu-Gly-(Lys-Leu-Glu-Ala-Leu-Glu-Gly) _n -amide, where <i>n</i> = 0,1,2,3,4; 7B, 14B, 21B, 28B, 35B, respectively
8W–8Y	Ac-Gly-X-X-(Leu) ₃ -(Lys) ₂ -amide, where X = Trp,Phe,Leu,Ile,Val,Tyr; 8W, 8F, 8L, 8I, 8V, 8Y, respectively
S1	Arg-Gly-Ala-Gly-Gly-Leu-Gly-Leu-Gly-Lys-amide
S2–S5	Ac-Arg-Gly-X-Y-Gly-Leu-Gly-Leu-Gly-Lys-amide, where X–Y = Gly-Gly, Ala-Gly, Val-Gly, Val-Val; S2, S3, S4, S5, respectively
E1	Ac-Glu-Tyr-Gly-Ala-Gly-Gly-Ala-Gly-Gly-Leu-Glu-amide
E2	Ac-Gly-Gly-Gly-Leu-Gly-Gly-Ala-Gly-Gly-Leu-Glu-amide
E3	Ac-Glu-Tyr-Ala-Ala-Glu-Ala-Ala-Glu-Gly-Leu-Glu-amide
E4	Ac-Gly-Gly-Ala-Leu-Glu-Ala-Ala-Glu-Gly-Leu-Glu-amide

^a Ac denotes N^α-acetyl; amide denotes C^α-amide.

B/min at a flow-rate of 1 ml/min, where solvent A is 0.05% aqueous TFA and solvent B is 0.05% TFA in acetonitrile; pH 2) on the CN packings. As a comparison, the peptides were also chromatographed on the DuPont C₈ column. These peptides exhibit a wide range of both peptide size and hydrophobicity.

The retention data (Table II) obtained from three sets of peptides shown in Table I (the G, A and L series of peptide polymers) serve to summarize the general trend of RP-HPLC retention behaviour exhibited by all of the peptides used. For the purpose of this study, each peptide in these three series is referred to by a number and letter which denote, respectively, the number of residues it contains and to which polymer series it belongs. Thus, 10G refers to the ten-residue G series peptide, 30A refers to the 30-residue A series peptide, etc. These three sets of peptide polymers cover a similar range of chain length but differ in overall hydrophobicity; the hydrophobicity of these series of peptides increases in the order G < A < L. From Table II, each peptide was consistently eluted earlier from the CN column than from the C₈ column. Interestingly, the CN column provided greater selectivity for earlier eluted peptides. For instance, the difference in retention times (Δt) for G10 and G20 on the column was 7.4 min; in contrast, Δt for these peptides was only 3.5 min on the C₈ column. Similarly, for other peptide pairs, Δt between A5 and A10 was 14.6 min (CN) or 8.3 min (C₈), Δt between A10 and A20 was 7.9 min (CN) and 5.2 min (C₈), Δt

TABLE II

COMPARISON OF PEPTIDE RETENTION TIMES AND PEAK WIDTHS ON C₈ AND CN COLUMNS IN RP-HPLC

Peptide	C ₈ ^a		CN ^a	
	<i>t_R</i> (min) ^b	<i>W</i> (min) ^c	<i>t_R</i> (min)	<i>W</i> (min)
G10	20.4	0.14	7.9	0.26
G20	23.9	0.17	15.3	0.25
G30	25.4	0.14	18.5	0.20
G40	27.1	0.12	21.2	0.17
A5	24.0	0.15	8.6	0.38
A10	32.3	0.15	23.2	0.27
A20	37.5	0.15	31.1	0.22
A30	40.8	0.15	34.3	0.18
A40	43.9	0.14	37.8	0.17
A50	49.6	0.24	43.4	0.19
L5	30.8	0.16	18.1	0.24
L10	39.8	0.15	32.2	0.17
L20	45.7	0.13	39.5	0.14
L30	49.3	0.15	43.1	0.14
L40	52.2	0.20	45.8	0.15
L50	53.7	0.25	47.4	0.13

^a C₈ denotes DuPont sterically protected C₈ column (150 × 4.6 mm I.D.); CN denotes sterically protected Zorbax SB-300CN column (150 × 4.6 mm I.D.).

^b *t_R* denotes retention time; the data were obtained by linear A-B gradient elution (1% B/min and 1 ml/min), where eluent A was 0.05% aqueous TFA and eluent B was 0.05% TFA in acetonitrile (pH 2). Absorbance at 210 nm.

^c *W* denotes peak width at half-height.

between L5 and L10 was 14.1 min (CN) and 9.0 min (C_8) and Δt between G20 and A5 was 6.7 min (CN) and 0.1 min (C_8).

The improvement in separation of the more hydrophilic peptides on the CN column compared with the C_8 column was achieved at the expense of some peak broadening of these peptides on the former column compared with the latter. In fact, this points to an interesting difference between the two column packings. Thus, on the less hydrophobic CN packing, peak widths are decreased, up to a point, with increasing peptide retention time, *e.g.*, the peak widths of the G series peptides decreased from 0.26 min (G10) to 0.17 min (G40) as the peptide retention time increased from 7.9 min (G10) to 21.2 min (G40). Table II shows similar results for the earlier eluted ($< ca.$ 35 min) A and L series peptides. In contrast to the CN column, the C_8 column exhibited the opposite peak width *vs.* retention time relationship, *i.e.*, the later eluted peaks ($> ca.$ 40 min) on the C_8 column exhibited some peak broadening; *e.g.*, the peak widths of L30, L40 and L50 (retention times of 49.3, 52.2 and 53.7 min, respectively) were 0.15, 0.2 and 0.25 min, respectively. Finally, it should be noted that the minimum peak widths on both columns were essentially identical, *i.e.*, *ca.* 0.12–0.15 min.

The possibility that gradient delay time (the time for the gradient to reach the top of the column from the solvent mixer) may have played a role in the observed retention behaviour of early eluted peptides on the CN column (improved separation over that observed on the C_8 column with concomitant peak broadening) was investigated. A large gradient delay time may potentially cause the separation of more hydrophilic solutes initially to be essentially isocratic. For instance, a delay time of 5 min with a mobile phase flow-rate of 1 ml/min means that 5 ml (*i.e.*, *ca.* two column volumes for a column of 150×4.6 mm I.D.) of starting eluent will have passed through the column, following sample injection, prior to the start of the gradient. Fig. 1 demonstrates the effect of increasing gradient delay time on the elution profile of four eleven-residue peptides, E1–E4 (Table I) on the CN column (A, B and C) and the Zorbax C_8 column (D). These N-terminal acetylated peptides contain only acidic residues (Glu) with no basic residues present, *i.e.*, the peptides are uncharged at pH 2.0, thus avoiding the complication of any potential ionic interactions with the column packings. Fig. 1A shows the elution profile of the peptides on the CN column, where the acetonitrile gradient was started immediately following sample injection. As observed previously for the earlier eluted G, A and L series peptides (Table II), the peak width decreased with increasing peptide retention time (from a peak width of 0.21 min for E1 at a retention time of 12.5 min to a peak width of 0.15 min at a retention time of 19.7 min for E4). The gradient delay time for the HP instrumentation employed in this study is low (*ca.* 2 min at a flow-rate of 1 ml/min, *i.e.*, less than one column volume for a 150×4.6 mm I.D. column), suggesting any potential effects of such a delay would be minimal. Fig. 1B and C show the effect of increasing the gradient delay times by a further 10 and 20 min, respectively, by employing an isocratic hold prior to the start of the gradient. These delay times translate into *ca.* five and nine column volumes (10- and 20-min isocratic holds, respectively; Fig. 1B and C, respectively) of starting eluent prior to the start of the gradient. It is immediately apparent that the increasing delay time resulted in increasing peak broadening of the earliest eluted peptide, E1. Thus, the peak width of this peptide increased from 0.21 min in the absence of an isocratic hold (Fig. 1A) to 0.34 min and, finally, 0.43 min

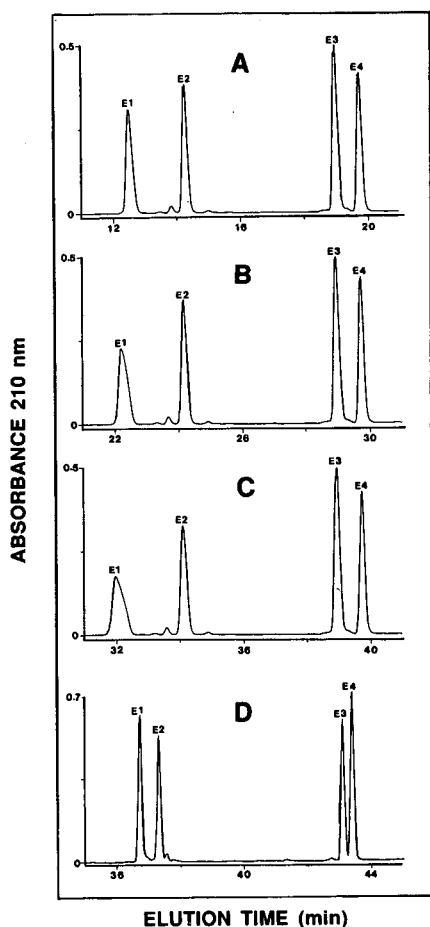


Fig. 1. Effect of gradient delay time on performance of C_8 and CN columns during RP-HPLC of peptides. Columns: sterically protected C_8 column from DuPont (150×4.6 mm I.D., particle size $5 \mu\text{m}$, pore size 94 \AA) and sterically protected Zorbax CN column (150×4.6 mm I.D.; $6 \mu\text{m}$, 250 \AA). Conditions: linear A–B gradient (1% B/min) at a flow-rate of 1 ml/min, where eluent A is 0.05% aqueous TFA and eluent B is 0.05% TFA in acetonitrile (pH 2); 26°C . Absorbance at 210 nm. Sample volume: $20 \mu\text{l}$ of eluent A. (A, B and C) separation of peptides on CN column with isocratic holds (prior to the start of the acetonitrile gradient) of 0, 10 and 20 min, respectively; (D) separation of peptides on C_8 column with a 20-min isocratic hold. The sequences of peptides E1–E4 are shown in Table I.

following the employment of isocratic holds of 10 and 20 min, respectively (Fig. 1B and C, respectively). Some minor peak broadening with increasing delay time is also apparent for peptide E2, with peptides E3 and E4 unaffected. However, although Fig. 1 demonstrates that large gradient delays affected the peak broadening of the relatively hydrophilic peptide, E1, it also clearly shows that the relative separation of the four peptides was unaffected, *i.e.*, the concentration of acetonitrile required to elute each peptide remained identical in the absence or presence of an isocratic hold. Hence, the initial isocratic elution prior to the gradient affected only the peak width and not column selectivity.

Fig. 1D shows the elution profile of the four peptides on the Zorbax C₈ column following a 20-min isocratic hold. This profile was identical with that obtained in the absence of an isocratic hold, indicating that the initial isocratic elution prior to the gradient has no effect on peak broadening on this column. In a similar manner to that observed above (Table II) for the earlier eluted G, A and L series peptides, the selectivity of the CN column for peptides E1–E4 (Fig. 1A) is superior to that of the C₈ column (Fig. 1D).

Overall, the peak broadening observed on the CN column for earlier eluted peptides is no more a significant disadvantage of the column than the similar peak broadening observed for later eluted peptides on the C₈ column.

Application of the CN column to the analysis and purification of synthetic peptides

Fig. 2 compares the separation of two peptides, 8W and 8F, on (A) the C₈ and (B) the CN columns. These two peptides differ by only two residues: two phenylalanine residues in 8F are replaced by two tryptophan residues in 8W. Fig. 2 demonstrates a marked difference in their retention behaviour on the CN and C₈ columns. Thus, from a poor separation on the C₈ column ($\Delta t = 0.3$ min only) (A), the peptides were separated by a much wider margin of 4.7 min on the CN column (B). This dramatic change in the separation of the two peptides between the C₈ and CN columns implies significant selectivity differences between the dipolar cyanopropyl and the octyl functionalities. This selectivity difference may be very useful in multiple peptide synthesis [18], a method to synthesize, cleave and purify several peptides simultaneously in a single batch. Up to now, the limiting factor in the success of this technique has been the resolving power of HPLC for resolving complex peptide mix-

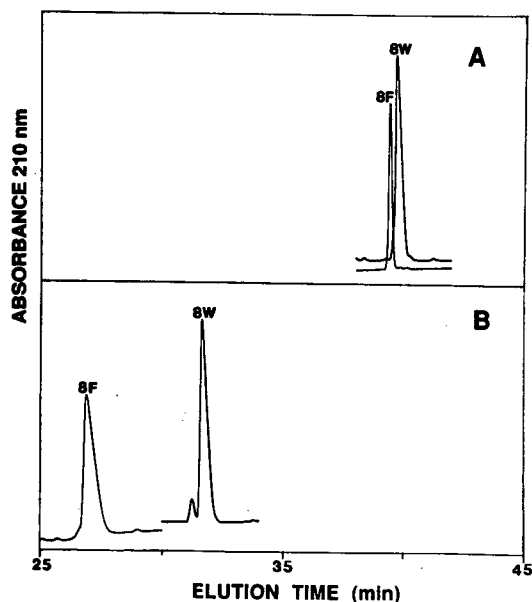


Fig. 2. RP-HPLC of synthetic peptides on (A) C₈ and (B) CN columns. Columns and conditions as in Fig. 1. The sequences of peptides 8F and 8W are shown in Table I.

tures quickly and efficiently [18]. An important practical feature of the sterically protected CN column in such applications is the outstanding stability of this ligand in aggressive environments. It should also be noted that peptides which are eluted together on the CN column may be separated on the C₈ column.

Fig. 3 compares the chromatographic behaviour of peptides with that of a series of three alkylphenones (propiophenone, butyrophenone and valerophenone; A2, A3 and A4, respectively) on (A) the C₈ and (B) the CN columns. The alkylphenones, commonly used as internal standards for RP-HPLC, were chosen to represent typical small organic molecules.

All of the four peptides shown in Fig. 3 exhibited similar elution behaviour on the two columns in terms of both retention time and satisfactory peak shape. In contrast, the alkylphenones showed a dramatic difference in their retention behaviour on the two columns. On the C₈ column (Fig. 3A), the alkylphenones were retained to an extent similar to that of the four peptides, making the resolution of these two classes of compounds difficult. In contrast, on the CN column (Fig. 3B), the alkylphenones were barely retained, greatly simplifying their separation from the peptides. In addition, it should be noted that peptides 21B and 35A were much better resolved on the CN column (Fig. 3B) than on the C₈ column (Fig. 3A) (there was, in fact, a reversal of elution order), again implying selectivity differences between the two types of functional groups. DTT (dithiothreitol) was added to the sample mixture to keep peptides 35A, 21B and 35B (Table I) in their reduced form and, hence, prevent inter-chain disulphide bond formation between peptides.

As noted above (Table II, Figs. 1–3), the wide variation in retention behaviour

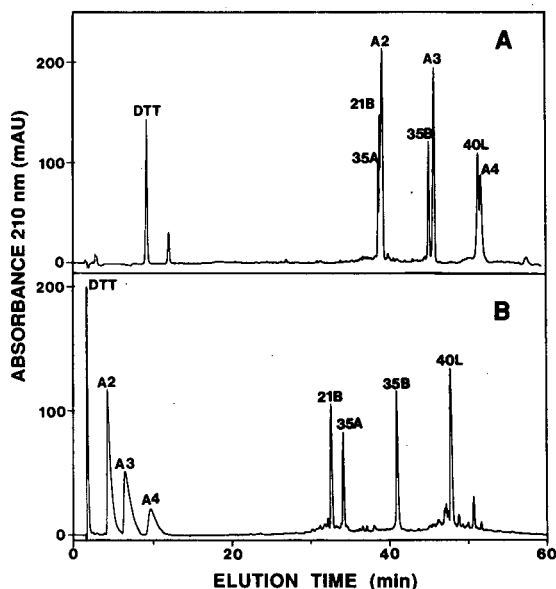


Fig. 3. RP-HPLC of mixtures of synthetic peptides and small organic molecules on (A) C₈ and (B) CN columns. Columns and conditions as in Fig. 1. The sequences of peptides 35A, 21B, 35B and 40L are shown in Table I. A2, A3 and A4 denote propiophenone, butyrophenone and valerophenone, respectively; DTT denotes dithiothreitol.

for alkylphenones and peptides on the C_8 and CN columns is illustrative of the different selectivities associated with these ligands. This selectivity difference is a function of two properties. First, the more polar CN phase itself can exhibit significantly different interactions with solutes, relative to those with the highly hydrophobic, less polar C_8 phase. Second, the level of organic modifier needed for solute elution is significantly less for the CN phase than the C_8 phase; the CN phase is much weaker [19]. It is well known that the selectivity of reversed-phase separations often is strongly affected by the percentage of organic component or the concentration of water associated with elution [20]. Stated otherwise, the $\log k'$ versus percentage organic component plots for different solutes often show different slopes. For weaker phases such as CN, lower concentrations of organic component (higher concentrations of water) are required, compared with C_8 phases, creating an environment for significant potential changes in band spacing. This is especially the case for mixtures of small and large molecules that also exhibit profound differences in the intercepts of $\log k'$ versus percentage organic component plots (plots for peptides are much steeper than those for alkylphenones). Therefore, striking differences in the $\log k'$ versus percentage organic component relationships often lead to large differences in band spacing, such as exhibited for the alkylphenone/peptide data in Fig. 3. Changing from the strongly hydrophobic C_8 phase to CN creates an environment whereby such selectivity differences are greatest. The band-spacing differences seen in Fig. 3 are further enhanced as a result of the lower surface area of the CN column (wider pores) compared with the C_8 column. This magnifies the effect of column strength, as even less organic component (more water) is required to elute the same components.

The results shown in Fig. 3 suggested a role for the CN column in purifying organic contaminants, such as those encountered in solid-phase peptide synthesis. These contaminants, including side-chain protecting groups, coupling reagents, cleavage reagents and scavengers, are often difficult to separate from the desired peptide product during RP-HPLC on C_8 and C_{18} columns. For example, thioanisole is a good scavenger and accelerator of the reaction cleaving the synthesized peptide from the resin support [21,22]. In many cases, this scavenger is eluted with the peptide product of interest from an alkyl-bonded reversed-phase column. An example of this can be seen in Fig. 4A, where thioanisole (T) was not separated from synthetic peptide 35B on the C_8 column (the DTT is again present to prevent interchain disulphide bond formation between peptide molecules). In contrast, on the CN column (Fig. 4B), whereas the retention time of the peptide was similar to that exhibited on the C_8 column (Fig. 4A), thioanisole was now barely retained, thus achieving an easy separation.

Purification of extremely hydrophobic peptides on the CN column

Very hydrophobic peptides, such as membrane-associated peptides, often pose special problems during RP-HPLC owing to their limited solubility and tendency to aggregate. In addition, they may be adsorbed irreversibly to some reversed-phase sorbents [23]. Gerber *et al.* [24] and Takagaki *et al.* [25] successfully separated hydrophobic peptides by RP-HPLC with a mobile phase consisting of formic acid, water and ethanol. The difficulty with this system is that peptide detection by UV absorbance is only possible at relatively insensitive wavelengths such as 280 nm, owing to the presence of formic acid. Knighton *et al.* [12] employed RP-HPLC with a mobile

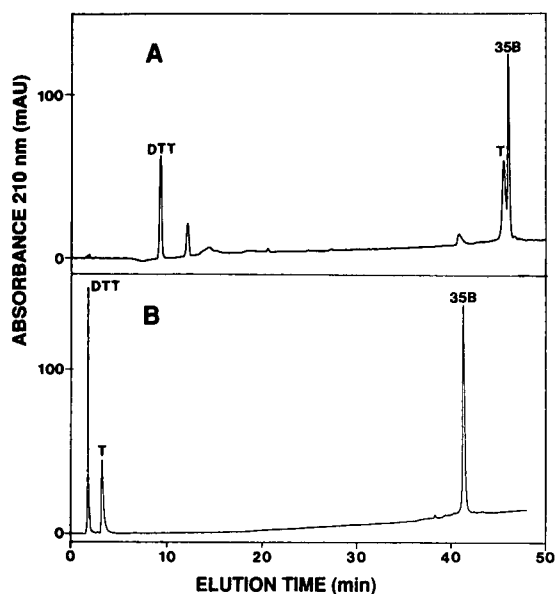


Fig. 4. RP-HPLC of synthetic peptide and thioanisole (T) on (A) C_8 and (B) CN columns. Columns and conditions as in Fig. 1. The sequence of peptide 35B is shown in Table I. DTT denotes dithiothreitol.

phase containing ammonium hydrogencarbonate to purify lipid-associated peptides successfully. However, it was very difficult to work with this mobile phase owing to the formation of carbon dioxide bubbles in the detector flow cell [12]. Tomich *et al.* [26] recently reported that the addition of the non-ionic detergent *n*-octyl- β -D-glucopyranoside to the mobile phase can prevent membrane-spanning peptides from binding irreversibly to a reversed-phase packing. This detergent binds to the stationary phase, reducing the potential sites of interaction on the solid matrix [26]. When employing this mobile phase, a subsequent dialysis step is required to remove the detergent from the eluted peptides. Taneja *et al.* [27] reported the separation of hydrophobic peptide polymers on a C_3 column through employment of 2-propanol as the organic modifier. Despite these reports of successful RP-HPLC purification of exceptionally hydrophobic peptides, routine methods for such purifications are not yet well established.

The major problem limiting routine successful purification of very hydrophobic peptides by RP-HPLC is the excessive strength of hydrophobic interaction between the peptides and alkyl-bonded stationary phases such as C_8 and C_{18} sorbents. It seemed reasonable, therefore, that a less hydrophobic stationary phase, such as the CN stationary phase, may be more promising for this kind of application. Fig. 5 compares the elution profile of a hydrophobic synthetic peptide P22 [Ac-(Lys) $_2$ -Gly-(Leu) $_{16}$ -(Lys) $_2$ -Ala-amide] on the C_8 (Fig. 5A) and CN (Fig. 5B) columns. About 12% less acetonitrile in the mobile phase was required to elute P22 from the CN column compared with the C_8 column. In addition, a greater separation of P22 from impurities (I) was achieved on the CN column. Finally, the peak width of P22 on the CN column was less than that on the C_8 column (0.32 and 0.50 min, respectively). Similar results were obtained with synthetic peptide P26 [Ac-(Lys) $_2$ -Gly-(Leu) $_{20}$ -

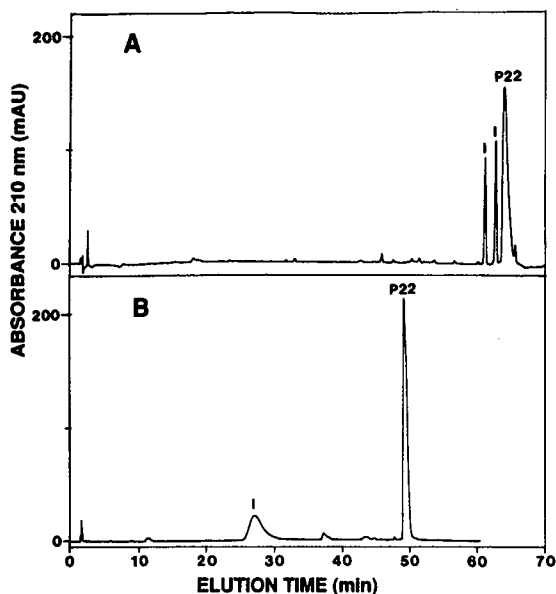


Fig. 5. RP-HPLC of a synthetic hydrophobic peptide on (A) C_8 and (B) CN columns. Columns and conditions as in Fig. 1, except sample volume is $20 \mu\text{l}$ in 70% eluent A–30% eluent B. The sequence of peptide P22 is shown in the text. I denotes impurity.

(Lys)₂–Ala–amide], with peak widths of 0.52 and 0.38 min on the C_8 and CN columns, respectively. These results, coupled with those presented in Fig. 1, suggest that the employment of a CN column with an aqueous TFA–acetonitrile mobile phase is a simple and effective method for purification of very hydrophobic peptides.

RP-HPLC of proteins on the C_8 and CN columns

There has been a significant increase in recent years in the application of RP-HPLC to the analysis and separation of proteins [4,28]. The best recovery and overall resolution of proteins has generally been demonstrated on large-pore, silica-based stationary phases containing relatively short alkyl chains (*e.g.*, C_3) [29,30]. The trade-off has been that such short-chain stationary phases (and, indeed, cyano phases) are generally less stable than those with longer alkyl ligands, which shield more effectively the underlying siloxane bonds from hydrolysis by the mobile phase. However, this problem is minimized or even eliminated with such sterically protected packings as those employed in the present study and described previously [13].

Table III compares the performances of the sterically protected C_8 (C_8 -2 in Table III) and CN columns during the RP-HPLC of thirteen proteins with that of a conventional C_8 packing containing dimethyloctyl groups (C_8 -1 in Table III). The latter C_8 column was chosen because in our hands it has proved to be one of the better commercially available packings. The peak width at half-height was again used as an index of column performance. All three columns were run under identical linear A–B gradient elution conditions (1%B/min and 1 ml/min), where eluent A was 0.05% aqueous TFA and eluent B was 0.05% TFA in acetonitrile (pH 2).

From Table III, it is clearly apparent that the peak widths of all thirteen proteins were significantly less on the sterically protected C₈ packing (C₈-2) than on the conventional C₈ column (C₈-1), even though the pore size of the former column is only 94 Å compared with 300 Å for the latter. The smaller particle size of the sterically protected packing (5 μm) compared with the conventional packing (7 μm) may partly explain the narrower peptide peak widths on the former column, although the relatively small difference in these particle sizes probably had no major effect. With the exception of ribonuclease A, the peak widths of the proteins were even smaller on the sterically protected CN column compared with the DuPont C₈ column (C₈-2).

The CN column also exhibited the best column performance of the three in terms of protein resolution. Based on the data shown in Table III, the resolution (*R_s*) of any two peaks was calculated according to the equation

$$R_s = \frac{1.176\Delta t}{W_1 + W_2}$$

where Δt is the difference in retention time between two protein peaks (1 and 2) and W_1 and W_2 are their peak widths at half-height. The resolution of every possible combination of protein pairs within the thirteen proteins was calculated for all three columns. Out of a total of 78 possible combinations of protein pairs, only five calculated resolutions were less on the CN column than on the DuPont C₈ column (C₈-2).

TABLE III
COMPARISON OF PROTEIN RETENTION TIMES AND PEAK WIDTHS ON C₈ AND CN COLUMNS IN RP-HPLC

No.	Protein	<i>N</i> ^a	C ₈ -1 ^b		C ₈ -2 ^b		CN ^b	
			<i>t_R</i> (min) ^c	<i>W</i> (min) ^d	<i>t_R</i> (min)	<i>W</i> (min)	<i>t_R</i> (min)	<i>W</i> (min)
1	Ribonuclease	124	32.4	0.44	28.7	0.30	24.0	0.38
2	Troponin T	259	39.3	0.78	33.7	0.34	31.1	0.15
3	Cytochrome <i>c</i>	104	37.8	0.50	34.0	0.32	30.4	0.23
4	Lysozyme	129	40.8	0.42	36.8	0.30	33.3	0.25
5	Troponin I	178	42.2	0.68	37.2	0.39	34.9	0.19
6	Bovine serum albumin	582	44.5	0.81	40.4	0.60	36.1	0.50
7	Papain	212	45.9	1.12	40.6	0.65	37.6	0.29
8	α-Lactalbumin	123	45.0	0.46	41.0	0.44	35.9	0.18
9	Tropomyosin	284	46.9	1.12	41.7	0.79	39.3	0.46
10	Myoglobin	153	48.0	0.77	42.5	0.38	38.4	0.17
11	α-Chymotrypsinogen A	245	48.4	0.58	42.7	0.38	39.7	0.19
12	Enolase	436	52.1	0.77	45.5	0.35	42.4	0.29
13	Troponin C	159	52.6	0.49	47.8	0.39	44.3	0.19

^a *N* denotes number of amino acid residues.

^b C₈-1 denotes Aquapore RP-300 C₈ column (220 × 4.6 mm I.D.); C₈-2 denotes DuPont sterically protected C₈ column (150 × 4.6 mm I.D.); CN denotes Zorbax sterically protected cyanopropyl column (150 × 4.6 mm I.D.) (see Experimental).

^c *t_R* denotes retention time; the data were obtained by linear A-B gradient elution (1% B/min and 1 ml/min), where eluent A was 0.05% aqueous TFA and eluent B was 0.05% TFA in acetonitrile (pH 2). Absorbance at 210 nm.

^d *W* denotes peak width at half-height.

In addition, 24 out of the possible 78 combinations showed an increase in protein resolution of $> 100\%$ compared with this C_8 column (C_8-2).

Fig. 6 demonstrates the elution profiles of selected mixtures of proteins on (A and C) the DuPont C_8 and (B and D) the Zorbax CN columns. It is apparent from Fig. 6A and B that the columns exhibited considerable selectivity differences for some proteins. Thus, on the C_8 column (Fig. 6A), protein pairs of bovine serum albumin and papain (proteins 6 and 7 in Table III) and myoglobin and α -chymotrypsinogen A (proteins 10 and 11) were completely unresolved. In contrast, all four proteins were resolved on the CN column (Fig. 6B). Ferris *et al.* [31] made a similar observation concerning selectivity differences between C_3 , diphenyl and CN columns during RP-HPLC of ribosomal proteins.

From Fig. 6C and D, the CN column performance (D) is clearly superior to that of the C_8 column (C) for the mixture of five proteins (troponin T, troponin I, α -lactalbumin, myoglobin and troponin C; proteins 2, 5, 8, 10 and 13, respectively), although the separation of specific proteins may be superior on the C_8 column, *e.g.*, note the improved separation of troponin I (protein 5) from α -lactalbumin (protein 8) on the C_8 column (Fig. 6C) compared with the CN column (Fig. 6D). The overall superior performance of the CN column is exemplified by both narrower peak widths and milder elution conditions (*i.e.*, less organic solvent) required to elute the proteins from this less hydrophobic packing. Milder elution conditions frequently translate into better recoveries of purified proteins compared with those obtained from more hydrophobic hydrocarbon stationary phases [32].

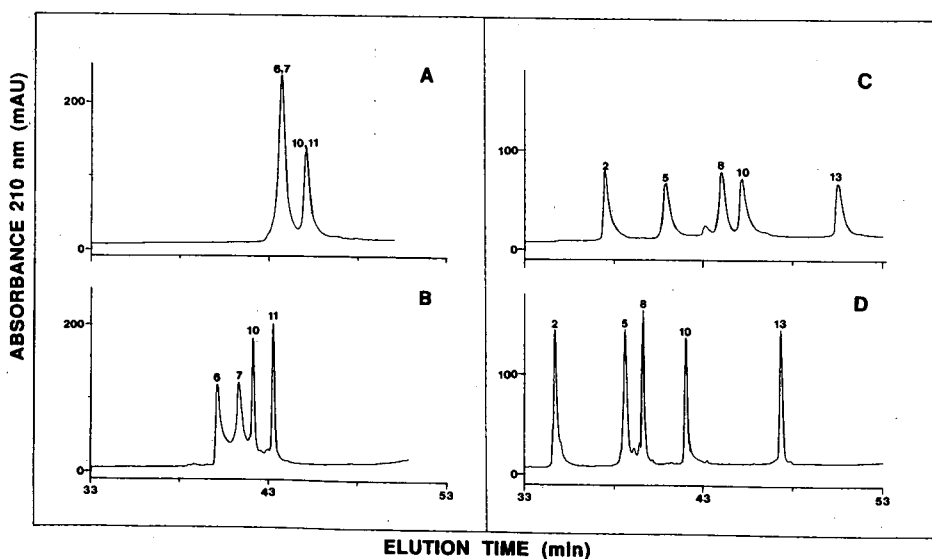


Fig. 6. RP-HPLC of proteins on (A and C) C_8 and (B and D) CN columns. Columns and conditions as in Fig. 1. Peak numbers denotes proteins shown in Table III.

CONCLUSIONS

Comparison of C₈ and CN column performance during peptide and protein separations clearly show how stationary phases of different hydrophobicities and selectivities may complement each other for specific applications. In addition, the results suggest that optimization of peptide and protein separations through employment of different RP-HPLC stationary phases (as opposed to the more common optimization protocol of manipulating the mobile phase) is an approach underestimated in the past.

ACKNOWLEDGEMENTS

This work was supported by the Medical Research Council of Canada and by equipment grants, a postdoctoral fellowship (N.E.Z.) and a research allowance from the Alberta Heritage Foundation for Medical Research.

REFERENCES

- 1 C. T. Mant and R. S. Hodges, in K. Gooding and F. E. Regnier (Editors), *HPLC of Biological Macromolecules: Methods and Applications*, Marcel Dekker, New York, 1990, p. 301.
- 2 C. T. Mant, N. E. Zhou and R. S. Hodges, in E. Heftmann (Editor), *Chromatography, Part B*, Elsevier Amsterdam, 5th ed., in press.
- 3 F. E. Regnier, *Methods Enzymol.*, 91 (1983) 137.
- 4 K. Gooding and F. E. Regnier (Editors), *HPLC of Biological Macromolecules: Methods and Applications*, Marcel Dekker, New York, 1990.
- 5 C. T. Wehr, L. Correia and S. R. Abbott, *J. Chromatogr. Sci.*, 20 (1982) 114.
- 6 I. M. Chaiken and C. J. Hough, *Anal. Biochem.*, 107 (1980) 11.
- 7 M. A. Anzano, A. B. Roberts, J. M. Smith, L. C. Lamb and M. B. Sporn, *Anal. Biochem.*, 125 (1982) 217.
- 8 D. M. Abercrombie, C. J. Hough, J. R. Seeman, M. J. Brownstein, H. Gainer, J. T. Russell and I. M. Chaiken, *Anal. Biochem.*, 125 (1982) 395.
- 9 D. R. Knighton, D. R. K. Harding, J. R. Napier and W. S. Hancock, *J. Chromatogr.*, 249 (1982) 193.
- 10 G. E. Tarr and J. W. Crabb, *Anal. Biochem.*, 131 (1983) 99.
- 11 P. Tempst, M. W. Hunkapiller and L. E. Hood, *Anal. Biochem.*, 137 (1984) 188.
- 12 D. R. Knighton, D. R. K. Harding, J. R. Napier and W. S. Hancock, *J. Chromatogr.*, 347 (1985) 237.
- 13 J. J. Kirkland, J. L. Glajch and R. D. Farlee, *Anal. Chem.*, 61 (1988) 2.
- 14 J. L. Glajch and J. J. Kirkland, *US Pat.*, 4 705 725, (1988).
- 15 J. M. R. Parker and R. S. Hodges, *J. Protein Chem.*, 3 (1985) 465.
- 16 R. S. Hodges, P. D. Semchuk, A. K. Taneja, C. M. Kay, J. M. R. Parker and C. T. Mant, *Pept. Res.*, 1 (1988) 19.
- 17 B. Fransson, *J. Chromatogr.*, 361 (1986) 161.
- 18 F. S. Tjoeng, D. S. Towery, J. W. Bullock, D. E. Whipple, K. F. Fok, M. H. Williams, M. E. Zupc and S. P. Adams, *Int. J. Pept. Protein Res.*, 35 (1990) 141.
- 19 P. E. Antle, A. P. Goldberg and L. R. Snyder, *J. Chromatogr.*, 321 (1985) 1.
- 20 L. R. Snyder and P. E. Antle, *LC · GC*, 3 (1985) 98.
- 21 H. Yajima, N. Fujii, S. Funakoshi, T. Watanabe, E. Murayama and A. Otaka, *Tetrahedron*, 44 (1988) 805.
- 22 J. M. Stewart and J. D. Young, *Solid Phase Peptide Synthesis*, Pierce, Rockford, IL, 1985, p. 38.
- 23 C. Edelstein and A. M. Scanu, in W. S. Hancock (Editor), *Handbook of HPLC for the Separation of Amino Acids, Peptides and Proteins*, Vol. II, CRC Press, Boca Raton, FL, 1984, p. 405.
- 24 G. E. Gerber, R. J. Anderegg, W. C. Herlihy, C. P. Gray, K. Biemann and H. G. Khorana, *Proc. Natl. Acad. Sci. U.S.A.*, 76 (1979) 227.
- 25 Y. Takagaki, G. E. Gerber, K. Nihei and H. G. Khorana, *J. Biol. Chem.*, 255 (1980) 1536.

- 26 J. M. Tomich, L. W. Carson, K. J. Kanes, N. J. Vogelaar, M. R. Emerling and J. M. Richards, *Anal. Biochem.*, 174 (1988) 197.
- 27 A. K. Taneja, S. Y. M. Lau and R. S. Hodges, *J. Chromatogr.*, 317 (1984) 1.
- 28 C. T. Mant and R. S. Hodges (Editors), *HPLC of Peptides and Proteins: Separation, Analysis and Conformation*, CRC Press, Boca Raton, FL, 1991.
- 29 J. D. Pearson and F. E. Regnier, *J. Liq. Chromatogr.*, 6 (1983) 497.
- 30 J. A. Bietz, in K. Gooding and F. E. Regnier (Editors), *HPLC of Biological Macromolecules: Methods and Applications*, Marcel Dekker, New York, 1990, p. 429.
- 31 R. J. Ferris, C. A. Cowgill and R. R. Traut, *Biochemistry*, 23 (1984) 3434.
- 32 M. Hermodson and W. C. Mahoney, *Methods Enzymol.*, 91 (1983) 352.

CHROMSYMP. 2323

Silica versus polymer-based stationary phases for reversed-phase high-performance liquid chromatographic analyses of rat insulin biosynthesis

A comparison of resolution and recovery

S. LINDE* and B. S. WELINDER

Hagedorn Research Laboratory, Niels Steensens Vej 6, DK-2820 Gentofte (Denmark)

ABSTRACT

Because of the problems caused by the irreversible binding of insulins and proinsulins to several silica-based reversed-phase columns, the use of polymeric reversed-phase columns was investigated for the analysis of rat islet polypeptides involved in insulin biosynthesis. No irreversible binding of insulins and proinsulins was observed for the polymeric reversed-phase columns, probably due to the absence of silanol groups. The six polypeptides involved in insulin biosynthesis in rat islets were equally well resolved in shallow trifluoroacetic acid–acetonitrile gradients on the silica-based Nucleosil 300-5C₄ column (45°C), the polymer-based Asahipak C4P-50 (25 and 45°C), and ODP-50 columns (45°C). In shallow triethylammonium phosphate–acetonitrile gradients (25°C) satisfactory resolution of the two rat proinsulins was only obtained on the polymer-based Asahipak C4P-50 and C8P-50 columns. Increasing the separation temperature to 45°C improved the separation of the two insulins and the two proinsulins in all cases. The shifts in retention times for the individual islet polypeptides observed in relation to the increased separation temperature were found to be different for the silica C₄ and the polymer C₄ columns. Recoveries of rat islet polypeptides were comparably high from the silica- and the polymer-based C₄ columns and linear load-response curves were obtained in the microgram to picogram mass range on both columns.

INTRODUCTION

Proinsulin is synthesized in the β -cells, one of the four cell types in the islets of Langerhans in the endocrine pancreas. The enzymatic cleavage of proinsulin at two positions with paired basic amino acid residues results in the formation of equimolar amounts of insulin and C-peptide. Most mammals produce a single insulin, but in the rat (and other rodents) two different non-allelic insulin genes are expressed, resulting in the formation of two sets of closely related proinsulins, insulins and C-peptides, differing in 4 out of 86 amino acids, 2 out of 51 amino acids, and 2 out of 31 amino acids, respectively.

We have recently described the successful separation of all these β -cell specific polypeptides by reversed-phase high-performance liquid chromatography (RP-HPLC) utilising carefully selected silica-based stationary phases eluted with very

shallow trifluoroacetic acid (TFA)–acetonitrile gradients [1,2]. However, several of the stationary phases examined during this evaluation suffered from severely non-ideal behaviour (pronounced non-specific binding and lack of column-to-column reproducibility) [2]. Consequently, we have evaluated the use of polymeric RP columns for this type of analysis. Three different Asahipak columns with C₁₈, C₈ and C₄ anchored to the same polymer skeleton (polyvinylalcohol) were eluted with TFA or triethylammonium phosphate in acetonitrile, and the separation and recoveries of the rat C-peptides, insulins and proinsulins at ambient or elevated temperatures were optimized and compared to similar separations using selected silica-based stationary phases.

MATERIALS AND METHODS

HPLC equipment

The HPLC system consisted of two M6000A pumps, a WISP 710A, a 660 solvent programmer, a 730 data module (all from Waters), and a Pye Unicam LC-UV detector.

Silica-based columns

LiChrosorb RP-18 (5 μm) and LiChrosorb RP-8 (5 μm), both 250 \times 4.0 mm I.D. were obtained from Merck, Nucleosil 120-5C₁₈ (5 μm) and 300-5C₄ (5 μm), both 250 \times 4.0 mm I.D. were obtained from Macherey-Nagel, Zorbax Protein Plus (6 μm), 250 \times 4.6 mm I.D. was obtained from DuPont, and Bakerbond WP Butyl (5 μm), 250 \times 4.6 mm I.D. was obtained from J. T. Baker.

Polymer-based columns

Asahipak ODP-50 (5 μm) 150 \times 4.6 mm I.D. and Asahipak C8P-50 (5 μm) and C4P-50 (5 μm), both 250 \times 4.6 mm I.D., were obtained from Asahi Chemical Industry Co.

Reagents

Phosphoric acid (p.a.) was from Merck, TFA (peptide synthesis grade) was from Applied Biosystems, triethylamine (99%) was from Janssen Chimica and acetonitrile (HPLC grade S) was from Rathburn Chemicals. All other chemicals were of analytical reagent grade. Distilled water was drawn from a Millipore Milli-Q plant, and all buffers were filtered (0.45 μm , Millipore), and vacuum-ultrasound degassed before use.

Samples

Human insulin (HI), human proinsulin (HPI) and mono-[¹²⁵I]-(TyrA14)-porcine insulin (200–300 mCi/mg) were obtained from Novo-Nordisk. Rat pancreatic polypeptide and porcine glucagon were from Sigma. Medium from cultured newborn rat islet cells was used as a source of rat insulins. This medium contained 63 $\mu\text{g}/\text{ml}$ insulin I + II and equimolar amounts of C-peptide I and II. Biosynthetically labelled rat islet polypeptides, including rat proinsulin I and II (nanogram amounts), were prepared by the incubation of rat islets with [³H]leucine and [³⁵S]methionine as described [1].

HPLC conditions

The columns were eluted with linear acetonitrile gradients in 0.1% TFA (6% during 60 min) or in 0.125 M triethylammonium phosphate (TEAP), pH 4.0 (5% during 60 min). Flow-rate: 1.0 ml/min for the silica-based columns and 0.5–1.0 ml/min for the polymer-based columns (pressure limit, 150 bar). Separation temperature: ambient or 45°C. The column eluate was monitored at 210 nm. In experiments with labelled polypeptides the eluate was collected in 0.5-min fractions and counted in a Packard Tri-Carb liquid scintillation counter (Model 460 C) after the addition of 4 ml Optiphase "HiSafe" (LKB).

Resolution

The resolution (R_s) was calculated as $2 \cdot (t_2 - t_1)/(w_1 + w_2)$, where t_2 and t_1 are the retention times of two adjacent peaks, and w_1 and w_2 their base widths. A baseline separation results in $R_s = 1$, a 12.5%-overlap in $R_s = 0.5$ assuming Gaussian peaks.

Recovery

The recoveries of microgram amounts of polypeptides were calculated from UV areas (rat insulin I and II), nanogram amounts from [^3H]leucine counts (rat proinsulin I and II), and picogram amounts from [^{125}I]counts (A14-monoiodoinsulin) after the HPLC separations in comparison with identical samples either injected into a loop (10 m \times 0.2 mm I.D.) or counted directly.

Dose-response curves were determined for all three mass ranges on a silica-based (Nucleosil 300-5C₄), and a polymer-based column (Asahipak C4P-50).

RESULTS

Resolution

The separation of rat insulins (I and II), C-peptides (I and II), and proinsulins (I and II) from islets biosynthetically labelled with [^3H]leucine and [^{35}S]methionine (this amino acid being present in insulin II and proinsulin II, only) for 60 min [1] was attempted on several silica- and polymer-based RP columns. As can be seen from Table I the resolution (R_s) obtained for the two C-peptides and the two insulins were satisfactory (> 0.5) for all columns eluted with TEAP-acetonitrile, whereas the two proinsulins in most cases would not be resolved. Only two polymeric columns, Asahipak C₈ and C₄, were able to separate the proinsulins satisfactorily.

When the same columns were eluted with shallow acetonitrile gradients in TFA at room temperature (Table II), all the columns were able to separate the C-peptides, the silica-based C₄ and C₃ columns as well as all the polymer-based columns separated the insulins satisfactorily, but none of the silica-based columns, and only one of the polymer-based columns (Asahipak C₄), were able to separate the two proinsulins.

Temperature effect

The RP-HPLC separation of rat islet polypeptides in TFA-acetonitrile was furthermore performed at 45°C (see Table II).

Chromatograms of two optimized separations on the silica-based Nucleosil C₄ and the polymer-based, Asahipak C₄ column performed at room temperature and at 45°C are shown in Fig. 1. The identity of the individual peaks was based upon amino

TABLE I
RESOLUTION (R_s) OF BIOSYNTHETICALLY LABELLED RAT ISLET POLYPEPTIDES
Mobile phase: 0.125 M TEAP, pH 4.0 in acetonitrile, linear gradient 0.08% acetonitrile/min, 25°C.

	Bonded phase	Stationary phase	R_s^a	Comments		
				C-peptides	Insulins	Proinsulins
Silica-based	C_{18}	LiChrosorb RP-18	0.8	1.0	0	Incipient separation of the proinsulins at 45°C ($R_s=0.4$)
	C_{18}	Nucleosil 120-5C ₁₈	1.6	1.2	0.4	
	C_8	LiChrosorb RP-8	1.1	1.3	0	Inverse elution of the proinsulins
	C_4	Nucleosil 300-5C ₄	1.2	0.5	0.4	
	$C_{4'}$	Bakerbond WP Butyl	1.1	1.1	0	
	C_3	Zorbax Protein Plus	1.3	1.0	0	
Polymer-based	C_{18}	Asahipak ODP-50	1.1	1.3	0	Non-ideal peak shapes for the proinsulins
	C_8	Asahipak C8P-50	0.8	1.2	0.5	Baseline separation of the proinsulins
	C_4	Asahipak C4P-50	0.6	1.8	1.3	

^a An R_s value of 0.5 or higher is required for satisfactory separation.

TABLE II
RESOLUTION (R_s) OF BIOSYNTHETICALLY LABELLED RAT ISLET POLYPEPTIDES AT DIFFERENT TEMPERATURES
 Mobile phase: 0.1% TFA-acetonitrile, linear gradient 0.1% acetonitrile/min.

	Bonded phase	Stationary phase	R_s						Comments
			C-peptides		Insulins		Proinsulins		
			25°C	45°C	25°C	45°C	25°C	45°C	
Silica-based	C ₁₈	LiChrosorb RP-18	0.6	n.e. ^a	n.e. ^a	n.e.	n.e.	Irreversible binding of insulins and proinsulins (see ref. 2)	
	C ₁₈	Nucleosil 120-5C ₁₈	1.2	n.e.	n.e.	n.e.	n.e.		
	C ₈	LiChrosorb RP-8	1.8	n.e.	n.e.	n.e.	n.e.		
	C ₄	Nucleosil 300-5C ₄	1.2	0.8	1.1	1.8	0.4	0.8	See Fig. 1, left panels
	C ₄	Bakerbond WP Butyl	1.2	1.0	1.1	2.9	0	0.9	
	C ₃	Zorbax Protein Plus	1.3	0.8	1.0	1.5	0	0.8	
Polymer-based	C ₁₈	Asahipak ODP-50	0.7	0.8	1.4	2.2	0.4	0.8	
	C ₈	Asahipak C8P-50	0.7	0.4	1.2	3.0	0	0.6	
	C ₄	Asahipak C4P-50	0.6	0.6	1.9	2.9	0.7	1.3 ^b	See Fig. 1, right panels.
	C ₄								

^a n.e. = Not eluted.

^b Flow-rate 0.8 ml/min. (At 0.5 ml/min rat insulin II coeluted with rat proinsulin I, see Fig. 2).

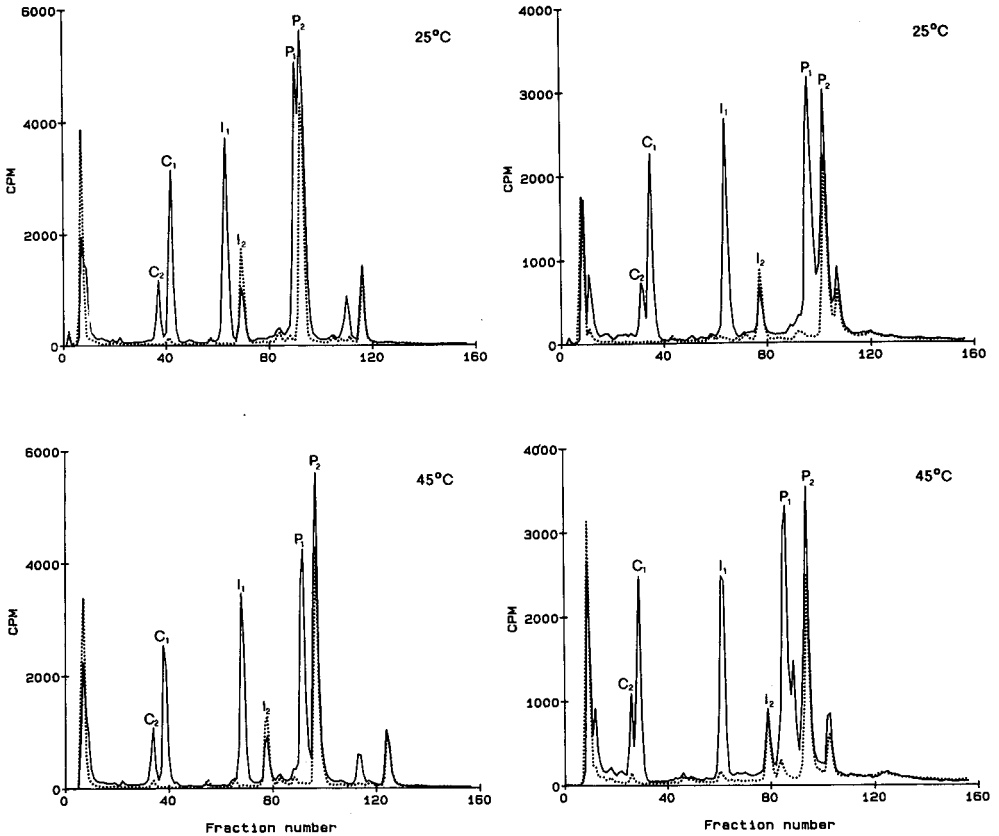


Fig. 1. RP-HPLC separation of a 3 M acetic acid extract of 50 rat islets labelled for 60 min with 2.5 μCi [^3H]leucine and 2.5 μCi [^{35}S]methionine, using a Nucleosil 300-5C₄ column, eluted at 1.0 ml/min with a linear acetonitrile gradient (27–33%) in 0.1% TFA during 60 min (left panels); and an Asahipak C4P-50 column eluted at 0.8 ml/min with a linear acetonitrile gradient (26–32%) in 0.1% TFA during 60 min (right panels). Fractions at 0.5-min intervals were collected and counted for [^3H]- and [^{35}S]radioactivity. The separations shown in the upper panels were performed at ambient temperature (25°C), the separations in the lower panels at 45°C. The solid line represents [^3H]-radioactivity, the dotted line [^{35}S]radioactivity. The peaks are C₁ (C-peptide I), C₂ (C-peptide II), I₁ (insulin I), I₂ (insulin II), P₁ (proinsulin I) and P₂ (proinsulin II).

acid analysis and amino acid sequencing as described in ref. 1. The effect of temperature on the retention times of several pancreatic islet polypeptides was further examined on the same two columns and are depicted in Fig. 2.

Recovery

Load-response curves of pancreatic islet polypeptides were determined for three mass ranges using either the areas of the UV curves (microgram amounts of insulin) or radioactivity [^3H]leucine proinsulin for the nanogram range, [^{125}I]insulin for the picogram range), as shown in Fig. 3.

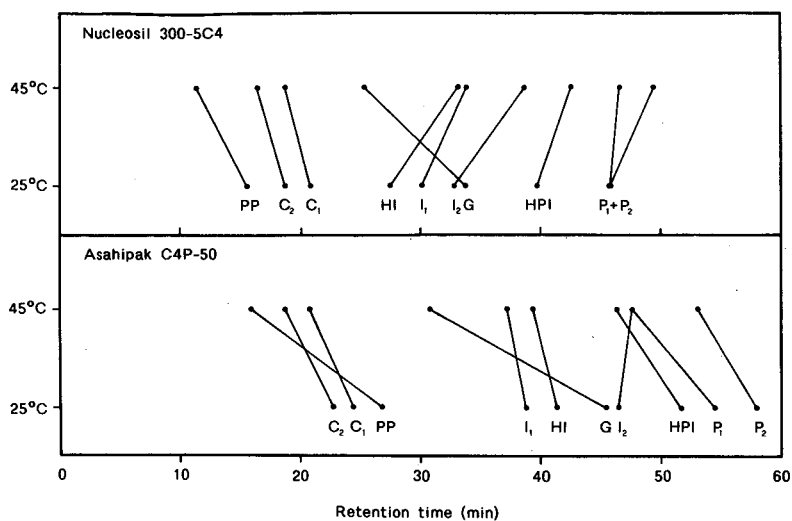


Fig. 2. The retention times of individual pancreatic polypeptides were measured after RP-HPLC of 1 μg of each polypeptide (except for the rat proinsulins, where only nanogram amounts were available) on a Nucleosil 300-5C₄ column (upper panel) and on an Asahipak C4P-50 (lower panel). The separations were performed at 25 and 45°C on both columns. The Nucleosil column was eluted at 1.0 ml/min, the Asahipak column at 0.5 ml/min. The gradients were the same as described in the legend to Fig. 1. The peak identities are, besides those described in the legend to Fig. 1, PP (rat pancreatic polypeptide), HI (human insulin), G (glucagon) and HPI (human proinsulin).

The ratios between individual rat islet polypeptides in identical samples (extracts of 50 rat islets) eluted from the silica-based Nucleosil C₄ column and the polymer-based Asahipak C₄ column are compared in Table III.

All major individual rat islet polypeptides were isolated after a preparative RP-HPLC separation of 500 biosynthetically labelled rat islets. After speed-vac concentration of the individual compounds, these samples were used for the measurement of the absolute recoveries (as described in Materials and Methods). The results are summarized in Table IV.

TABLE III

RATIOS BETWEEN INDIVIDUAL RAT ISLET POLYPEPTIDES AFTER RP-HPLC CALCULATED FROM [³H]LEUCINE COUNTS

	Nucleosil 300-5C ₄	Asahipak C4P-50
C-peptide I/C-peptide II	1.83 ± 0.06 ^a	1.57 ± 0.20
Insulin I/insulin II	2.22 ± 0.07	2.20 ± 0.07
Proinsulin I/proinsulin II	0.88 ± 0.03	1.25 ± 0.11
C-peptides/insulins	0.75 ± 0.01	0.80 ± 0.03
C-peptides/proinsulins	1.05 ± 0.01	1.08 ± 0.03
Insulins/proinsulins	1.39 ± 0.02	1.34 ± 0.05

^a Mean ± S.D., *n* = 5.

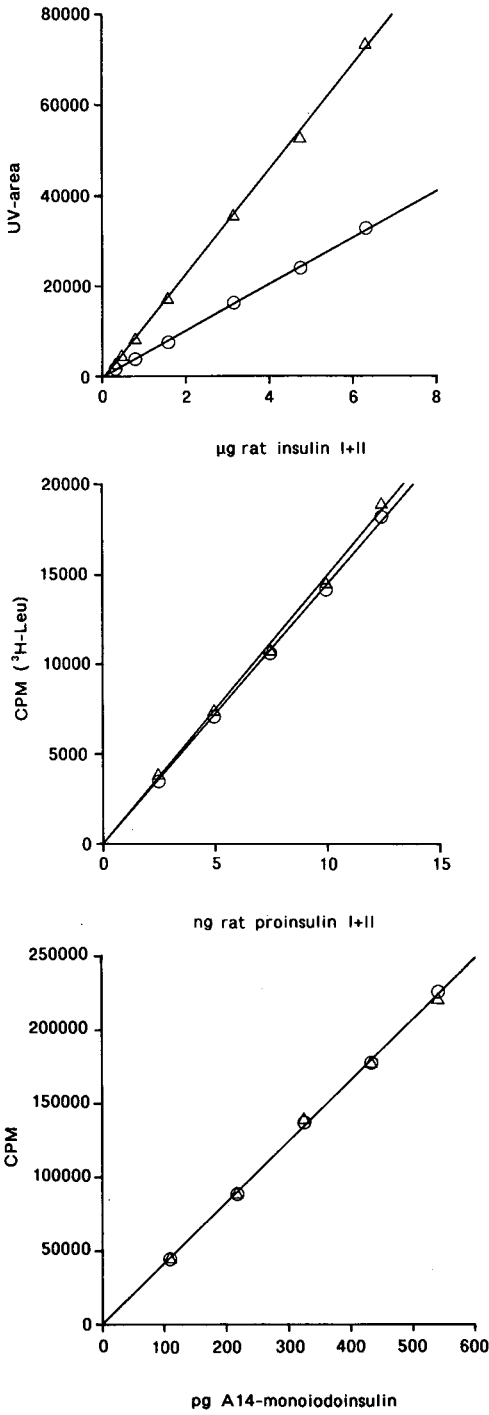


Fig. 3.

TABLE IV

ABSOLUTE RECOVERY (%) OF INDIVIDUAL PANCREATIC ISLET POLYPEPTIDES AFTER RP-HPLC

Polypeptides ^a	Mass range	Nucleosil 300-5C ₄	Asahipak C4P-50
Rat C-peptide I	μg-ng	88.5 ± 1.8 ^b	94.2 ± 8.2
Rat C-peptide II	μg-ng	99.2 ± 3.7	122.8 ± 6.2
Rat insulin I	μg-ng	97.8 ± 2.3	100.7 ± 2.5
Rat insulin II	μg-ng	88.7 ± 4.1	90.9 ± 7.6
Rat proinsulins	ng	105.3 ± 2.5	109.9 ± 4.6
Porcine insulin	pg	98.8 ± 2.3	99.2 ± 2.3
Mean recovery		96.4	102.9

^a The polypeptide samples are described in the legend to Fig. 3.^b Mean ± S.D., *n* = 5.

DISCUSSION

RP-HPLC is the obvious method to use for the study of insulin biosynthesis due to its extremely high resolving power of closely related insulins and insulin-related polypeptides [3]. Optimization of the separation of the pairs of rat insulins I and II, C-peptides I and II, and proinsulins I and II resulted in the satisfactory separation of all these polypeptides which are involved in insulin biosynthesis in the rat [1,2].

The use of a silica-based C₁₈ column (LiChrosorb RP-18) in combination with TFA-acetonitrile as mobile phase (room temperature) was the preferred system in our initial studies [1] until certain batch-to-batch variations (resulting in irreversible binding of insulins and proinsulins) necessitated further investigations. These binding phenomena were also observed for other C₁₈ and C₈ columns in combination with TFA-acetonitrile, but were absent for C₄ and C₃ silica-based columns [2].

However, the selectivities for these columns were reduced to a level where no separation of rat proinsulin I and II was possible, in accordance with the finding that C₁₈ and C₈ columns are more resolute than C₄ columns [4].

Since no irreversible binding was ever observed when all these columns were

Fig. 3. Load-response curves for rat insulin I and II (upper curve), rat proinsulin I and II (middle curve) and A14 monoiodoinsulin (lower curve) after RP-HPLC on a Nucleosil 300-5C₄ column (○), and on an Asahipak C4P-50 column (△) eluted at 45 and 25°C, respectively, as described in the legend to Fig. 1. The samples were dilutions in 3 M acetic acid, 0.1% human serum albumin of medium from cultured newborn rat islet cells containing from 0.3 μg to 6.3 μg insulin I+II (upper curve), of rat islets biosynthetically labelled as described in the legend to Fig. 1; containing from 2.5 ng to 12.4 ng of proinsulin I+II (middle curve) and of carrier-free mono-[¹²⁵I]-(Tyr A14)-porcine insulin containing from 100–500 pg of monoiodoinsulin. The column eluates were registered at 210 nm, and the peak areas integrated (Waters 730 data module) in the case of insulin or counted in the collected 0.5-min fractions for [³H]leucine radioactivity (specific radioactivity approximately 1500 cpm/ng of proinsulin) or for [¹²⁵I]radioactivity (specific radioactivity approximately 400 cpm/pg of monoiodoinsulin).

eluted with TEAP–acetonitrile, the observations were ascribed to the presence of silanol groups, not being effectively masked by poor ion-pairing reagents (such as TFA) [2].

The logical conclusion of these observations was an evaluation of the use of polymer-based RP-columns and in contrast to the silica-based C_{18} - and C_8 columns, no irreversible binding was observed for the polymer-based C_{18} -, C_8 - and C_4 columns eluted with TFA–acetonitrile, probably due to the absence of silanol groups in the polyvinylalcohol skeleton [5].

The two different types of stationary phases were further evaluated after elution with TEAP–acetonitrile, another popular mobile phase for the separation of insulin and insulin-like compounds [3,4]. None of the silica-based columns were able to resolve the two rat proinsulins (Table I), whereas this separation could be performed at room temperature on the polymer-based C_4 column in both mobile phases (Table I and II) and on the polymer C_8 column in TEAP–acetonitrile (Table I).

Increasing the separation temperature to 45°C, (previously noticed to improve the proinsulin separation under similar experimental conditions [2]) resulted in increased R_s values for the proinsulins on the silica-based C_3 - and C_4 - columns as well as on all polymer-based columns eluted with TFA–acetonitrile (Table II). The resolution of the two insulins was increased as well, whereas that of the two C-peptides was decreased. A similar temperature effect was also noticed for the LiChrosorb RP-18–TEAP–acetonitrile system (Table I), but with this stationary–mobile phase the improvement was not sufficient to obtain a satisfactory proinsulin separation.

In order to extend the examination of the influence of temperature on the retention times after RP-HPLC, several pancreatic islet polypeptides were analyzed at 25 and 45°C using the silica-based and polymer-based C_4 column, as shown in Fig. 2. Interestingly, the retention times of individual islet polypeptides were affected differently on the silica- and polymer-based columns. On the silica C_4 columns polypeptides with mol. wt. < 5000 (C-peptides, pancreatic polypeptide, glucagon) eluted earlier when the temperature was increased to 45°C, whereas polypeptides with mol. wt. > 5000 (insulins, proinsulins) eluted later. Especially, the retention time of glucagon was influenced by temperature. On the polymer C_4 column the retention times for both glucagon and pancreatic polypeptides were markedly lowered by increasing the temperature, in fact all the polypeptides, except insulin II, were eluted earlier at 45°C indicating that the selectivities of the two columns are different. These results suggest that the effect of the temperature can not apparently be described as a general effect, but depends upon several chromatographic parameters (the actual stationary and mobile phase) and the nature of the sample polypeptide. It is therefore not surprising that literature reports have described major [6–10] as well as minor improvements [11] and even negative effects [12] of the separation temperature upon the resolution of polypeptides after RP-HPLC.

Precise and quantitative calculations of the insulin biosynthesis (based on the measurement of the [3 H]leucine radioactivity of the individual polypeptides eluted from the RP-HPLC column) can only be performed if the recoveries of the individual components are known for all potential mass ranges.

Load–response curves for insulins and proinsulins (mass ranges from microgram to picogram amounts) are shown in Fig. 3. For microgram amounts of insulins the UV area is an accurate measure of the mass, but it should be noticed that due to

differences in the elution rate the areas were not comparable. In the nanogram and picogram range the UV areas could not be used for quantitation. [^3H]Leucine radioactivity was used for nanogram amounts and [^{125}I]radioactivity for picogram amounts, the measured radioactivity being unaffected by the elution rate. In all three mass ranges, a linear relation between the amount of polypeptide applied and that recovered after RP-HPLC was obtained (correlation coefficients from 0.9983 to 0.9996). Further, these relations were comparable for the two types of columns, suggesting identical recoveries over the whole mass range.

Further elucidation of the recoveries may be gained from the ratios between the individual rat islet polypeptides after RP-HPLC (Table III). These ratios were comparable for the silica- and the polymer-based C_4 columns examined, except for that of the two proinsulins. An additional peak eluting between rat proinsulin I and II was observed after separation on the Asahipak C_4 column at 45°C (Fig. 1, lower panel right). This peak coeluted with proinsulin I at 25°C (Fig. 1, upper panel right). On the Nucleosil C_4 column we have observed a similar peak between the two proinsulins, when using a more shallow acetonitrile gradient (data not shown). In this case the peak coeluted with proinsulin II under the conditions shown in Fig. 1. This might explain the discrepancy of the ratios between the proinsulins after separation on the two column types. This component was not identified, but consists presumably of an intermediate form of proinsulin, as also is the case for the later eluting minor peaks seen in the chromatograms in Fig. 1. It has been shown that on the Nucleosil C_4 column the human proinsulin intermediates cleaved at the B-C junction elute earlier than human proinsulin, whereas the proinsulin intermediates cleaved at the A-C junction eluate later [13].

Furthermore, the ratios between the individual rat islet polypeptides after RP-HPLC on an Asahipak ODP-50 column (TFA-acetonitrile) were not changed when compared to a separation performed on two identical columns in series (data not shown) another demonstration of identical recoveries of the individual polypeptides.

In order to determine the absolute recoveries of the individual polypeptides, it was attempted to collect all the polypeptides from a separation of biosynthetically labelled rat islets on Nucleosil C_4 (60 min *ca.* 60 ml eluate), speed-vac concentrate and reinject the sample, but the resulting chromatogram was obscured by the occurrence of oxidized forms of the methionine containing insulin II and proinsulin II partly overlapping insulin I and proinsulin I, respectively (data not shown). This oxidation has been shown to occur during the sample concentration [14].

The absolute recoveries were therefore measured for the individually isolated polypeptides injected on the HPLC column and compared to injections bypassing the RP-HPLC column with a loop (or counting the sample before analysis), as shown in Table IV. The methionine sulphoxide forms of rat insulin II and proinsulin II (originated during speed-vac concentration) were added to the respective native forms. The recoveries were comparably high on both types of C_4 columns, with a slight tendency to higher recoveries from the polymer-based C_4 column (only significant for the C-peptide II).

From the literature it is well-known that the recoveries of polypeptides are not always quantitative, especially if small amounts are applied [15,16]. Reduced recoveries of larger polypeptides, *e.g.* greater than 20–30 amino acid residues have been described, even after injection of microgram amounts [17], but quantitative recoveries have been reported as well [12,18,19], even down to femtogram amounts [20].

It has been reported that insulin recovery from a silica-based C₁₈ column eluted with shallow acetonitrile gradients in TEAP or ammonium sulphate is close to 100%, whereas the recovery of proinsulin (and related compounds) are substantially lower (60–80%) [3]. The reason for the higher recovery of proinsulin found in our study could be due to the use of the less hydrophobic C₄ columns.

In conclusion, we have shown that polymeric C₁₈, C₈ and C₄ columns eluted with shallow TFA–acetonitrile gradients were free of the irreversible binding of insulins and proinsulins previously noticed for certain silica C₁₈- and C₈ columns, probably due to the absence of silanol groups in the polymeric skeleton. At ambient temperature (25°C) only one polymeric RP column (C₄) was able to separate all polypeptides involved in the rat insulin biosynthesis whereas at 45°C all the polymeric RP columns (C₁₈, C₈ and C₄) and several silica RP columns (C₄ and C₃) were able to perform this separation satisfactorily. The recoveries were comparably high, and the ratios between the individual polypeptides recovered after RP-HPLC on the two C₄ columns were virtually identical, as was the case after separation on one compared to two columns connected in series (polymer C₁₈ column). These results are a prerequisite for the quantitative calculations of the rat insulin biosynthesis.

ACKNOWLEDGEMENTS

We greatly appreciate the excellent technical assistance of Ragna Jørgensen.

REFERENCES

- 1 S. Linde, J. H. Nielsen, B. Hansen and B. S. Welinder, *J. Chromatogr.*, 462 (1989) 243.
- 2 S. Linde and B. S. Welinder, *J. Chromatogr.*, 536 (1991) 43.
- 3 B. S. Welinder, H. H. Sørensen and B. Hansen, *J. Chromatogr.*, 361 (1986) 357.
- 4 J. Rivier and McClintock, in A. R. Kerlavage (Editor), *The Use of HPLC in Receptor Biochemistry*, Alan R. Liss, New York, 1989, p. 77.
- 5 C. T. Wehr, in W. S. Hancock (Editor), *CRC Handbook for the HPLC Separation of Amino Acids, Peptides and Proteins*, CRC Press, Boca Raton, FL, 1984, p. 31.
- 6 J. L. DiCesare, *Chromatogr. Newsl.*, 9 (1981) 16.
- 7 T. P. Davis, H. Schoemaker, A. Chen and H. I. Yamamura, *Life Sci.*, 30 (1982) 971.
- 8 H. Schoemaker, T. P. Davis, N. W. Pedigo, A. Chen, E. S. Berens, P. Ragan, N. C. Ling and H. I. Yamamura, *Eur. J. Pharmacol.*, 81 (1982) 459.
- 9 L. F. Lloyd and P. H. Corran, *J. Chromatogr.*, 240 (1982) 445.
- 10 D. J. Smith, R. M. Venable and J. Collins, *J. Chromatogr. Sci.*, 23 (1985) 81.
- 11 M. Abrahamsson and K. Grönningsson, *J. Liq. Chromatogr.*, 3 (1980) 495.
- 12 J. E. Rivier, *J. Liq. Chromatogr.*, 1 (1978) 343.
- 13 S. Linde, M. E. Røder, S. G. Hartling, C. Binder and B. S. Welinder, *J. Chromatogr.*, 548 (1991) 371.
- 14 S. Linde, J. H. Nielsen, B. Hansen and B. S. Welinder, *J. Chromatogr. Biomed. Appl.*, 530 (1990) 29.
- 15 C. T. Wehr, L. Correia and S. R. Abbott, *J. Chromatogr. Sci.*, 20 (1982) 114.
- 16 D. M. Desiderio, S. Yamada, F. S. Tanzer, J. Horton and J. Trimble, *J. Chromatogr.*, 217 (1981) 437.
- 17 M. T. W. Hearn, in Cs. Horváth (Editor), *High-Performance Liquid Chromatography*, Vol. 3, Academic Press, New York, 1983, p. 87.
- 18 H. P. J. Bennett, C. A. Browne and S. Solomon, *Biochemistry*, 20 (1981) 4530.
- 19 P. Böhlen, F. Castillo and R. Guillemin, *Int. J. Pept. Protein Res.*, 16 (1980) 306.
- 20 R. L. Emanuel, G. H. Williams and R. W. Giese, *J. Chromatogr.*, 312 (1984) 285.

CHROMSYMP. 2338

Ion-exchange high-performance liquid chromatography of nucleotides and polypeptides on new types of ion-exchange sorbents, based on polystyrene-coated silicas

A. A. KURGANOV and V. A. DAVANKOV

Nesmeyanov Institute of Organo-Element Compounds, Academy of Sciences of USSR, Moscow (USSR)
and

K. K. UNGER*

Institut für Anorganische Chemie und Analytische Chemie, Johannes Gutenberg-Universität, D-6500 Mainz (Germany)

ABSTRACT

A novel type of ion exchanger was prepared by multipoint covalent binding of polystyrene chains onto the surface of porous silica followed by polymer-analogous modification of the bonded layer. Both anion and cation exchangers were synthesized and examined in the separation of nucleotides and proteins. Rapid and efficient separation of basic polypeptides on strong anion exchangers and that of acidic polypeptides on strong cation exchangers could be achieved. For the separation of complete mixtures of polypeptides the application of zwitter-ionic ion exchangers can be recommended.

INTRODUCTION

Ion-exchange high-performance liquid chromatography (HPLC) proved to be a powerful chromatographic method for separating ionic inorganic and organic compounds. This method was found to be especially useful for the separation of biologically active materials and several review papers on this topic have been published [1,2]. In this kind of separation, various types of polymer-based ion exchangers are commonly used as adsorbents, whereas the application of silica-based exchangers is limited by the hydrolytic stability of the latter. Many attempts have been made to overcome this disadvantage of the silica packing. One of the most promising approaches was introduced by Alpert and Regnier [3], who first adsorbed polyethylene imine on the surface of macroporous silicas and then cross-linked the polymer by various cross-linking agents. In this manner, a fully insoluble and hydrolytically stable polymeric layer was formed on the surface of the silica. Another type of silica-based ion exchanger with a polymeric modifying layer was introduced by Schomburg and co-workers [4,5]. Using chemical modification of polybutadiene which was cross-linked on the surface of silica they succeeded in preparing both anion and cation exchangers. In this article, we report on the synthesis and use of new ion exchangers

which are based on polystyrene-coated silica. We were the first to describe the chemical binding of polystyrene chains onto the surface of silica as the initial step in the preparation of chiral polymeric bonded ligand-exchanging phases [6]. Other types of chemical transformations of the bonded polystyrene-coated silica easily produce cation or anion exchanging phases which are of excellent chromatographic performance and enhanced hydrolytic stability when compared to monomeric phases.

EXPERIMENTAL

Materials

Base silicas, Zorbax PSM-500 and PSM-1000, both of particle diameter (d_p) = 5 μm , were purchased from Du Pont de Nemours (Wilmington, DE, USA). All solvents used in the chromatographic experiments were of HPLC grade and were a gift of E. Merck (Darmstadt, Germany). Other materials were laboratory grade and were used as purchased.

The proteins used in the chromatographic experiments included ribonuclease A from bovine pancreas, myoglobin from horse skeletal muscle, hen egg albumin, chicken egg white lysozyme and human transferrin, (all from Serva, Heidelberg, Germany), trypsin inhibitor from soy-beans, conalbumin, ferritin, and cytochrome *c* (all from Boehringer, Mannheim, Germany). Nucleotides were purchased from Sigma Chemie, Deisenhofen, Germany.

Equipment

The chromatograph employed consisted of two LKB 2150 pumps, the LKB controller 2152, the variable-wavelength detector BT 3030 (Biotronik, Maintal, Germany) operated at 220 nm and a potentiometric recorder 2210 (LKB, Bromma, Sweden)^a. Columns were 125 \times 4.6 mm I.D. (Hyperchrom, Bischoff, Leonberg, Germany).

Preparation of ion exchangers

The coating procedure for polystyrene-vinylsilane copolymers onto silica was described elsewhere in detail [7]. The characteristic data of the polymer-modified silicas were as follows: carbon content: PSM-500 2.4% (w/w), PSM-1000 1.4% (w/w). On the basis of the specific surface area of the native silica (PSM-500 25 m^2/g , PSM-1000 15 m^2/g), the ligand density of the average polymer unit was estimated to be 9.4 $\mu\text{mol}/\text{m}^2$ for PSM-500 and 9.8 $\mu\text{mol}/\text{m}^2$ for PSM-1000. Such high values of ligand density are rather common for polymer-modified macroporous silicas [7].

The subsequent chemical modification of polystyrene-coated silicas was performed by a method quite similar to that known for pure polystyrene. An aliquot of the modified PSM-500 was sulphonated by using chlorosulphonic acid in dichloroethane at room temperature yielding a cation exchanger with a capacity of 0.21 mmol SO_3H groups per gram based on the sulphur content. Another aliquot of polymer-coated PSM-500 was chloromethylated by monochloromethyl ether in dichloromethane in the presence of SnCl_4 and then aminated by the action of an alco-

^a The sensitivity of the detector was 0.1 a.u.f.s.

holic solution of trimethylamine thus producing an anion exchanger with a capacity of 0.17 mmol $N(CH_3)_3$ groups per gram.

On the bases of polymer-coated PSM-1000, a zwitter-ionic exchanger was synthesized. For this purpose, the chloromethylated product was sulphonated and then aminated. Because of the low surface area of this silica, it was not possible to determine analytical capacities. The content of sulphur and nitrogen were $< 0.2\%$ and thus below the limit of determination. However, the chromatographic experiments clearly demonstrated their anion and cation exchange capabilities.

RESULTS AND DISCUSSION

The method for the synthesis of anion exchangers suggested by Alpert and Regnier [3] appeared to be very attractive because of its chemical background: The adsorption of the polymer (polyethylene imine) on the surface of silica. This kind of polymer-surface interaction results from the electrostatic attraction between the deprotonated silanol groups of silica and the protonated positively charged amino groups of the poly-ethylene amine. This prevents the formation of a thick, polymolecular adsorption layer and, at the same time, allows a dense coating of the surface. It is difficult to achieve this type of interaction for a broader series of polymers. In the method postulated by Schomburg [5], the nature of the polymer is not that critical, because it is placed on the silica surface by means of the evaporation of the polymer solution. In this particular case, however, problems arise with regard to the homogeneity of the polymer layer on the surface, which may affect the pore structure of the silica and the reproducibility of the coating process.

In our procedure, the adsorption of the polymer is the result of the chemical reaction of silanol groups at the silica surface with the ethoxysilane units of the styrene-vinylsilane copolymer. Vinylsilane copolymers can be synthesized with different vinylic monomers. Styrene is the most attractive one since styrene-based packings are very common in classical ion-exchange chromatography and many kinds of well-known ion exchangers can currently be produced on polystyrene-coated silicas. Since the aim of this work was to separate biological substances, macroporous silicas with average pore diameters of 50 and 100 nm were chosen as base silicas. The specific surface area of the macroporous silicas was low, corresponding to the large pore size. However, the polymeric coating approximately exhibited a doubled ligand density, calculated on the basis of monomer units, as is the usual observation for silicas with bonded monomeric silanes. This meant that the polymeric-bonded ion exchangers exhibited a higher capacity than those obtained from the modification of monomeric bonded silicas. The polymeric layer did not impair the mass-transfer kinetics and hence the performance of the ion exchanger and also provided an improved shielding of the silica surface. As demonstrated in Fig. 1 a fast and complete separation of 11 nucleotides on an anion exchanger could be achieved in 10 min in a neutral phosphate buffer with a linear salt gradient. Two nucleotides co-elute in peak 9. Anion-exchange chromatography of proteins of the same exchanger is shown in Fig. 2. In this case, a double gradient is used: a linear salt gradient and an exponential proton gradient. Again, an excellent peak shape is observed for the proteins resolved under these conditions.

Fig. 3a shows a separation of a more complex mixture, and, as it often happens

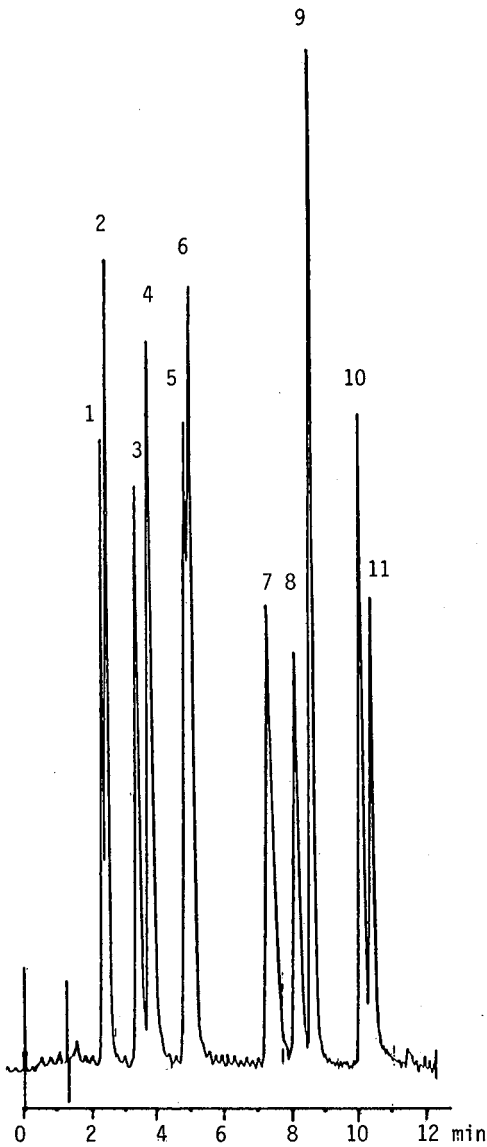


Fig. 1. Separation of a synthetic mixture of nucleotides on a strong anion exchanger made from polystyrene-coated PSM-500. Column: 125×4.6 mm; flow-rate 1 ml/min; gradient elution: from 0 to 14% B in 1 min, from 14 to 20% B in 5 min, from 20 to 50% B in 5 min A: 10 mM phosphate buffer, pH 7.0; B: 10 mM phosphate buffer, pH 7.0, 0.1 M KCl. Components: 1 = uridine monophosphate, 2 = cytidine monophosphate, 3 = adenosine monophosphate, 4 = guanosine monophosphate, 5 = uridine diphosphate, 6 = citidine diphosphate, 7 = adenosine diphosphate, 8 = guanosine diphosphate, 9 = uridine triphosphate + cytidine triphosphate, 10 = adenosine triphosphate, 11 = guanosine triphosphate.

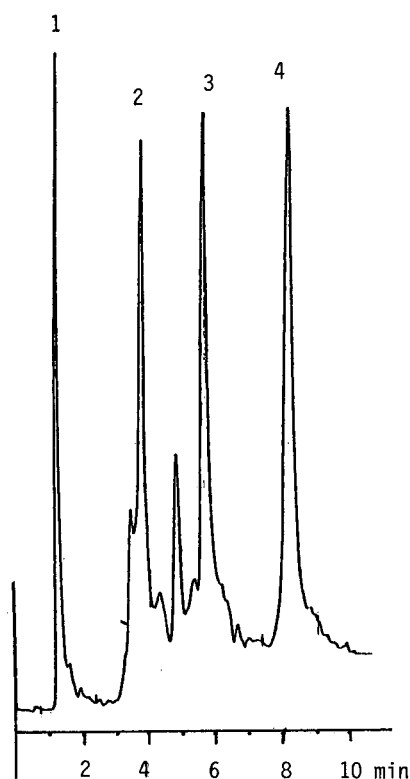


Fig. 2. Separation of a protein mixture on a strong anion exchanger made from polystyrene-coated Zorbax PSM-500. Column: 125 × 4.6 mm; flow-rate: 1 ml/min; gradient elution: from 0 to 50% B in 10 min. A: 10 mM phosphate buffer, pH 8.5; B: 10 mM phosphate buffer, pH 5.5, 1 mM KCl. Components: 1 = myoglobin, 2 = transferrin, 3 = ovalbumin, 4 = trypsin inhibitor.

in the separation of proteins, the general shape of the chromatogram depends on the gradient time. At a gradient time of 40 min (Fig. 3b) the peak of ferritin splits into three, one of which co-elutes with the conalbumin. The changes are well-reproducible, and on a second run of the gradient in 10 min; the shape of the chromatogram fully recovers (compare Fig. 3a and c).

The cation-exchange chromatography of proteins of the synthesized cation exchanger is illustrated in Fig. 4. As above mentioned, a double gradient was applied to achieve a better separation and to improve the peak shape. As is quite common with ion-exchange chromatography, only the appropriate species of a sample mixture can be resolved on a given type of exchanger: acidic proteins on cation exchanger and basic proteins on anion exchangers. For example, strongly basic proteins such as lysozyme elute with the void volume from the anion-exchange column, but are extremely strongly retained on the cation-exchange column. This unfavourable situation initiated the synthesis of a zwitter-ionic packing which has both sulphonic and quaternary ammonium groups. The silica packing was PSM-1000. The results shown

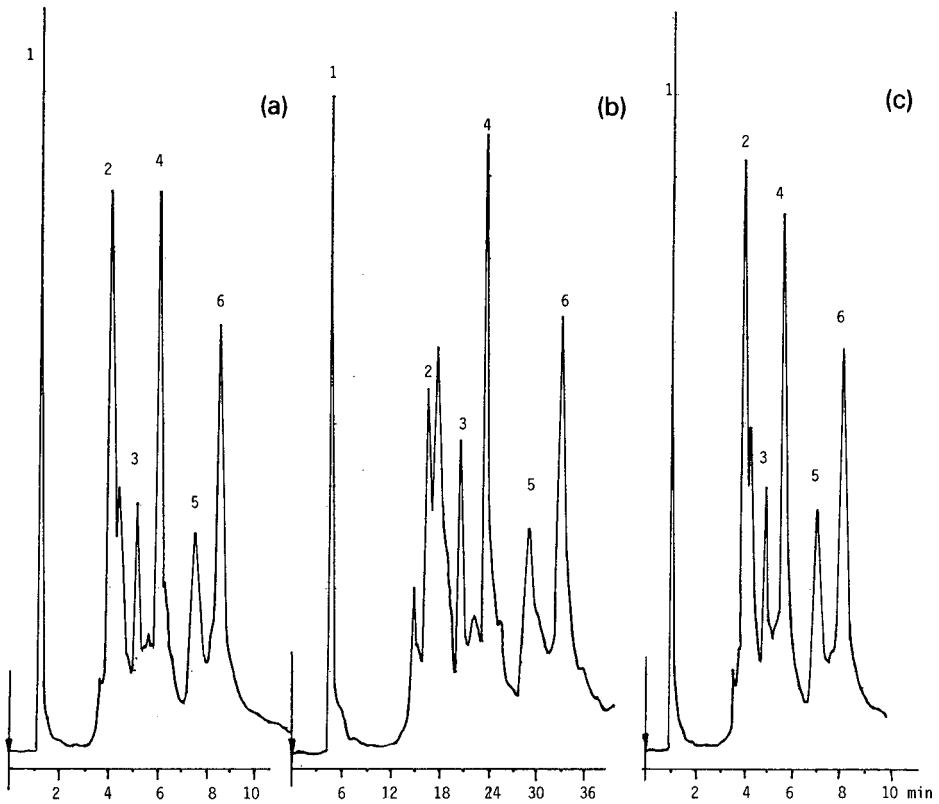


Fig. 3. Separation of a protein mixture on a strong anion exchanger made from polystyrene-coated Zorbax PSM-500. Column: 125×4.6 mm; gradient elution: from 5 to 50% B. Eluents A and B are described in the caption to Fig. 2. Gradient time and flow-rate: (a) 10 min, 1 ml/min; (b) 40 min, 0.25 ml/min; (c) 10 min, 1 ml/min. Components: 1 = myoglobin, 2 = ferritin, 3 = conalbumin, 4 = ovalbumin, 5 = albumin, 6 = trypsin inhibitor.

in Fig. 5 clearly show the ion-exchange properties of the packing. Myoglobin is seen to be eluted later than ovalbumin. Myoglobin is not retained on anion exchangers, ovalbumin is not retained on cation exchangers. The peak of lysozyme (last eluting peak) is relatively broad, even at the high flow-rate used for elution. It seems that this broadening is due to the mixed-mode interactions between lysozyme and the exchanger.

The results also reveal that the ion exchanger contains cationic groups in excess of anionic groups. In spite of this fact, the zwitter-ionic exchanger is well-suited to resolve different types of peptides and proteins and even lysozyme residues in about 10 min.

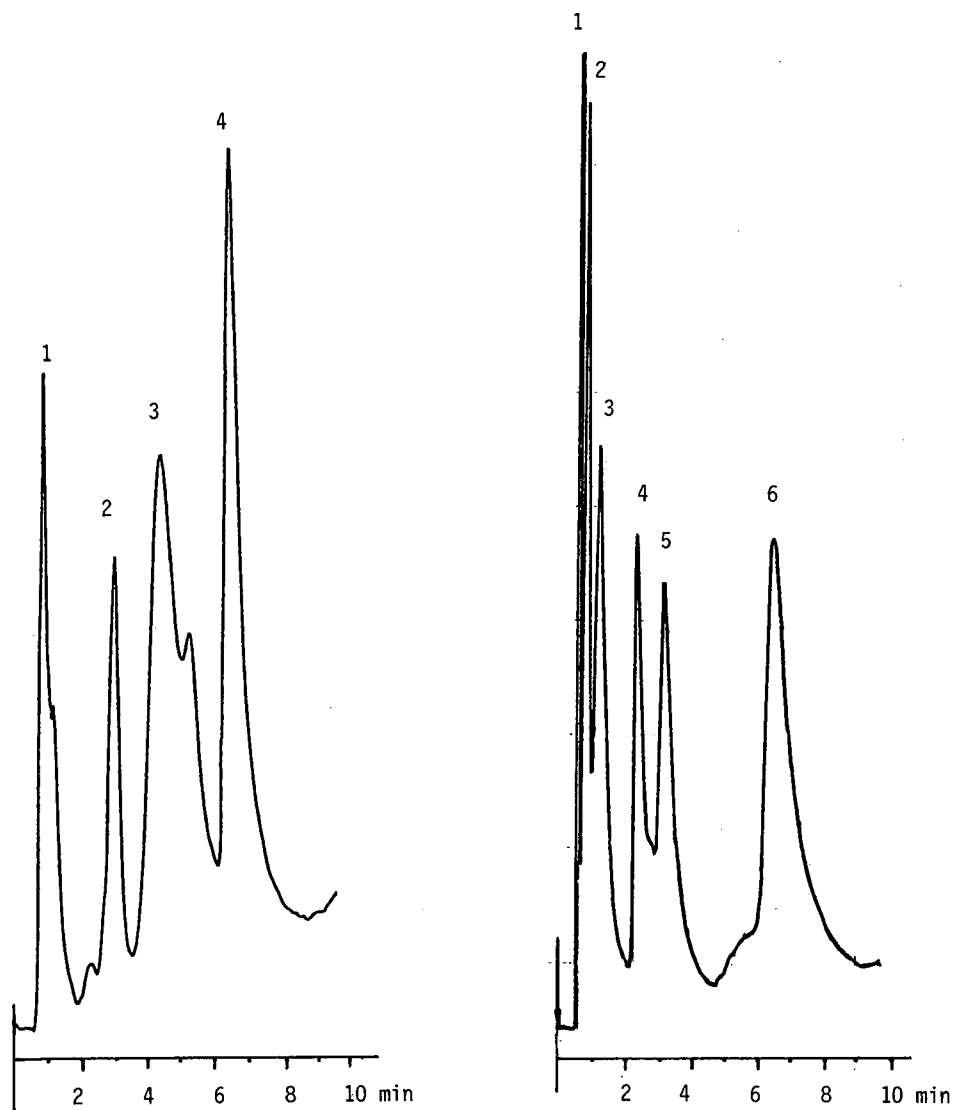


Fig. 4. Separation of a protein mixture on a strong cation exchanger made from polystyrene-coated Zorbax PSM-500. Column: 125×4.6 mm; flow-rate: 1 ml/min; gradient elution: from 30 to 100% B in 10 min. A: 10 mM phosphate buffer, pH 5.0; B: 10 mM phosphate buffer, pH 8.5, 1 M KCl. Components: 1 = ovalbumin, 2 = ribonuclease, 3 = conalbumin, 4 = cytochrome *c*.

Fig. 5. Separation of a protein mixture on a zwitter-ionic exchanger made from Zorbax PSM-1000. Column: 125×4.6 mm; gradient elution: from 16 to 50% B in 4 min at 2 ml/min, from 50 to 100% B in 1 min at 4 ml/min. A: 10 mM phosphate buffer, pH 5.0; B: 10 mM phosphate buffer, pH 8.0, 1 M KCl. Components: 1 = ovalbumin, 2 = myoglobin, 3 = transferrin, 4 = ribonuclease, 5 = cytochrome *c*, 6 = lysozyme.

CONCLUSIONS

A simple method for the preparation of both cation and anion exchangers as well as zwitter-ionic bonded phases was developed for ion-exchange HPLC of proteins and nucleotides. The synthesis is based on polymer-analogous transformations of polystyrene-coated macroporous silicas. The polymer coating permits the attainment of a dense shielding of the silica surface and a higher capacity compared to ion exchangers modified with monomeric silanes. The ion exchanger columns showed excellent performance for proteins and nucleotides. Especially interesting was the application of the zwitter-ionic exchanger which allowed us to resolve both acidic and basic proteins in one run with one buffered mobile phase.

REFERENCES

- 1 B. S. Welinder and S. Linde in W. S. Hancock (Editor), *Handbook of HPLC for the Separation of Amino Acids, Peptides and Proteins*, Vol. II, CRC Press, Boca Raton, FL, 1985, p. 357.
- 2 L. R. Snyder and J. J. Kirkland, *Introduction to Modern Liquid Chromatography*, Wiley, New York, 1979.
- 3 A. J. Alpert and F. E. Regnier, *J. Chromatogr.*, 185 (1974) 375.
- 4 G. Schomburg, A. Deege, U. Bien-Vogelsang and J. Köhler, *J. Chromatogr.*, 282 (1983) 27.
- 5 G. Schomburg, *LC · GC Int.*, (1988) 34.
- 6 A. A. Kurganov, A. B. Tevlin and V. A. Davankov, *J. Chromatogr.*, 261 (1983) 223.
- 7 A. A. Kurganov, O. Kuzmenko, V. A. Davankov, B. Eray, K. K. Unger and U. Trüdinger, *J. Chromatogr.*, 506 (1990) 391.
- 8 V. A. Davankov, A. A. Kurganov and K. K. Unger, *J. Chromatogr.*, 500 (1990) 519.

CHROMSYMP. 2213

High-performance liquid chromatography and ultrafiltration of whey proteins with inorganic porous materials coated with polyvinylimidazole derivatives

BERNARD CHAUFER*, MARIANNE ROLLIN and BERNARD SÉBILLE

Laboratoire de Physico-Chimie des Biopolymères, CNRS-Université Paris XII (UM 27), 2-8 Rue Henry Dunant, 94320 Thiais (France)

ABSTRACT

A coated ultrafiltration membrane was developed which allows the highly selective extraction of lactalbumin from a whey protein mixture. A permeate containing only lactalbumin was obtained using inorganic membranes coated with polyvinylimidazole derivatives containing both ionic and hydrophobic groups. The phenomena involved were analysed with high-performance liquid chromatographic supports bearing similar coatings. With the hydrophobic layer, the selectivity enhancement can be explained through mixed interactions with whey proteins; increasing fouling is due to both lactoglobulin and lactalbumin contributions to the build-up of the boundary layer at the wall of the derivatized membrane.

INTRODUCTION

Ultrafiltration is a pressure-driven membrane process by which macromolecular solutes may be separated or concentrated. A decline in membrane permeability is usually observed; many phenomena are involved (for reviews, see refs. 1–3). In the first few seconds of the run, concentration polarization at the membrane interface is apparent, owing to solute accumulation. The chief result is fouling, which is almost or completely irreversible and which occurs in less than 1 h (sometimes in a few minutes). Owing to protein–membrane interactions, solute adsorption modifies the performance of all membranes with regard to both retention and permeation [4–10]. In fact, the retention of a given protein by an ultrafiltration membrane is dramatically increased if other components of the mixture are so retained, resulting in poor selectivity [4,11–14]. Contrary to common opinion, the selectivity or retention of an ultrafiltration membrane is not based chiefly on its pore size but on the physico-chemical environment of the solute and the chemical nature of the membrane.

The objective here was a highly selective extraction of the smallest component from a concentrated whey protein mixture. To improve the selective extraction of lactalbumin (LA, MW 15 500) *versus* the other main protein, lactoglobulin (LG, MW 35 600), inorganic ultrafiltration membranes of high molecular weight cut-off (100 000) were coated with polyvinylimidazole (PVI) derivatives in order to induce strong interactions between the membrane and the proteins to be concentrated.

To elucidate the protein-membrane interactions involved, high-performance liquid chromatography (HPLC) of the mixture was performed using supports with the same coatings as the membranes. Both ionic and hydrophobic interactions were studied, using standard and whey proteins. The results were compared with those obtained with unmodified and modified membranes.

EXPERIMENTAL

Products

Standard proteins used in HPLC were α -lactalbumin (LA), β -lactoglobulin (LG) and lysozyme (LYS) and were purchased from Sigma (La Verpilliere, France). Bovine serum albumin (BSA, fraction V) was obtained from Fluka (Interchim, Montluçon, France). A concentrated whey protein mixture (90%, w/w; Eurial, Herbignac, France) was produced by ultrafiltration concentration and spray drying. This commercially available product contained 46% (w/w) LG and 14% (w/w) LA.

Reagents

PVI was synthesized by radical polymerization of N-vinylimidazole (Polysciences, Saint Goar, Germany) using azobisisobutyronitrile (AIBN) as initiator [15]. The molecular weight, determined by viscosimetry, was 13 300 [16]. Quaternization and cross-linking of the coated polymer were then performed with agents such as epichlorohydrin (ECl; Prolabo, Paris, France) or the diglycidyl ether of bisphenol A (DGEBA; Epikote 828) kindly provided by Shell (Rueil-Malmaison, France). All organic compounds were of reagent grade and used as received.

Potassium phosphate and chloride were of analytical-reagent grade. Acetonitrile (ACN) of spectroscopic grade was used for HPLC experiments.

Water was deionized and filtered with a 0.2- μ m filter (Eau et Industrie, Le Perreux, France) for ultrafiltration runs. All HPLC eluents were filtered with a 0.45- μ m filter (Sartorius, Palaiseau, France).

Inorganic porous materials

In order to compare HPLC and ultrafiltration experiments, we developed a similar reaction scheme for preparing coatings of PVI derivatives.

Preparation of HPLC materials

Vydac 101TP and Nucleosil 300-10 silica (10 μ m; 300 Å pore diameter) were used as stationary phases. Silica was coated with a PVI solution in methanol (4%, w/v) [17,18]. Cross-linking of vinylimidazole was achieved through a tertiary amine group or adjacent carbon [19,20]. Quaternization and cross-linking of the coated polymer were then performed with agents such as ECl or DGEBA. With ECl, a second quaternization step was effected by the use of methyl iodide [18]. The route is similar to that in previous work described by Régnier and co-workers [21,22] for polyethyleneimine-coated silica.

All characteristics of the columns are listed in Table I.

Preparation of modified inorganic membranes

Ultrafiltration membranes (Carbosep, Tech-Sep, Miribel, France) of molecular

TABLE I
 ADSORPTION OF PVI AND IONIC CAPACITY ON POROUS SILICA

For abbreviations see text and List of Symbols.

Silica	A_s (m^2/g) ^a	PVI (mmol/g) ^b	Cross- linker	Capacity (mmol/g) ^c	Ref.	Column	
						I.D. (mm)	Length (cm)
Vydac 101TP	90	0.56	ECl	0.45 ^d	QPVI	4.6	7.5
Nucleosil 300-10	100	0.66	DGEBA	0.16	KPVI	4.6	15

^a Manufacturer's data.

^b From nitrogen analysis.

^c Ionic capacity (see text).

^d From ref. 18.

weight cut-off 100 000 (M_1 type) were used. The separation layer was mainly composed of zirconium oxide, deposited on the internal wall of a tube of porous carbon (O.D. and I.D. 1.0 and 0.6 cm, respectively, length 60 cm). Membranes were modified with PVI by the same process as described above. One-step quaternization and cross-linking of the polymer coating were achieved with the difunctional reagents ECl or DGEBA. The ammonium content was determined by argentimetric back-titration; a potassium iodide solution ($2 \cdot 10^{-2} M$) was recirculated against the membrane without any pressure so that mainly membrane surface charges were involved. The ionic capacity was found to be in the range 10–20 mmol m^{-2} membrane area.

HPLC apparatus

All HPLC runs performed with PVI silica derivatives (see Table I) included a pump (Waters Model 6000 A), a valve (Rheodyne Model 7125), a UV detector (Varian Model VUV 10, 280 nm) and a potentiometric recorder (Séfram, PE type). The flow-rate was adjusted to 1 ml/min and 50- μ l samples were injected.

Size-exclusion chromatography with a TSK 3000 SW column (30 cm \times 0.72 cm I.D.) was used for analysis of UF samples. An automatic sample injector (Gilson Model 231-401, 50 μ l) and an integrator (Shimadzu Model CR3A) were added to the HPLC line. The flow-rate was 0.7 ml/min.

Ultrafiltration module

The ultrafiltration module was developed at the Centre de l'Énergie Atomique (CEA-Cadarache, St. Paul-Lez-Durance, France). The principles and operating conditions have been described elsewhere [23,24]. Accurate measurements of the pressure drop over the membrane length allowed the determination of τ_w , the wall shear stress.

Experimental procedures

Standard proteins ($1 g l^{-1}$) or whey proteins ($5 g l^{-1}$) were dissolved in phosphate buffer or triethanolamine (TEA) buffer (0.05 M). The pH was adjusted to the appropriate value with either dilute KOH or HCl. For the sake of clarity, ionic strength is expressed as KCl content, the relevant variable here.

HPLC procedure. Between two buffers (isocratic mode), each column was equilibrated with at least five column volumes. Sample injections were repeated until a 2% reproducibility of the capacity factors (k') was obtained. Each reported value is the average of at least three runs. A protein was considered to be not eluted (N.E.) if elution required over 30 column volumes.

Ultrafiltration procedure. Prior to ultrafiltration runs, water and buffer permeation (J_o and J_b , respectively) were determined as reference fluxes.

A whey protein solution (5 g l^{-1}) was then ultrafiltered for 3 h under pressure ($\Delta P = 2 \cdot 10^5 \text{ Pa}$) and with a tangential flow-rate ($V_L = 4.4 \text{ m s}^{-1}$) and a wall shear stress ($\tau_w = 75 \text{ Pa}$) resulting in a hydrodynamically turbulent regime to minimize fouling [23,24]. For all experiments, the concentration of the feed solution was kept constant by permeate remixing in the feed tank. The experimental temperature of the solution was controlled (20°C). Permeate was sampled during the run.

At the end of each run, the membrane was rinsed with water and the water permeation flux was then measured (J_a). The following membrane-cleaning procedure was applied: NaOH (0.1 M , 40°C , 40 min) with a final addition of NaOCl (300 ppm of active chlorine) for 3 min; rinsing with tap water (20 min); HNO_3 (0.05 M , 30°C , 10 min); rinsing with tap water until the permeate pH was neutral; and water permeation flux measurement (J_f); the cleaning procedure was repeated if the ratio J_f/J_o was lower than 0.95.

RESULTS AND DISCUSSION

HPLC results

Capacity factor determination. The capacity factor (k') was obtained from the equation

$$k' = (V_e - V_m)/V_m \quad (1)$$

where V_e and V_m are, respectively, the elution volume of the solute and the mobile phase volume, which was determined by injection of water. In fact, water injection resulted in a positive UV peak followed by a negative peak. For V_m determination, we selected the positive peak which results from phosphate displacement by water, as this peak was little affected by the eluent conditions (pH, ionic strength).

The k' value of a protein should be negative from eqn. 1 if the protein elution is based on a size-exclusion mode; the more negative k' is, the more excluded from the pores the protein is. Moreover, this definition allows the comparison of the elution volumes of proteins which are of different size without using the theoretical SEC volume of each protein.

Strong anion-exchange chromatography with QPVI silica. Supports based on silica coated with epichlorohydrin PVI derivative (QPVI) have been evaluated as protein sorbents by HPLC [18]. The results obtained with a QPVI silica in TEA buffer (50 mM , pH 7) are shown in Table II. The k' of LYS is negative owing to its positive net charge ($pI = 11$) at pH 7; at low ionic strength, negatively charged LG ($pI = 5.1\text{--}5.3$) and BSA ($pI = 4.9$) were not eluted. At high ionic strength, all negatively charged proteins display k' values close to zero but not reaching the theoretical negative SEC k' values. Hence, the elution of BSA and LG with QPVI support in

TABLE II

INFLUENCE OF IONIC STRENGTH ON CAPACITY FACTORS (k') OF PROTEINS WITH QPVI SILICA UNDER ISOCRATIC CONDITIONS: TEA BUFFER (0.05 M), $[KCl]$ AS I

pH	I	k'			
		LA	LG	BSA	LYS
7	0.1	5.92	N.E. ^a	N.E.	-0.11
	1	0.03	0.08	-0.03	0.02

^a N.E. = Not eluted.

TEA buffer is governed by ionic interactions. On the other hand, increasing ionic strength induced a higher retention of LYS owing to enhanced hydrophobic interactions.

As phosphate occurs naturally in milk and whey, the influence of phosphate ions on the mechanism of fouling in whey ultrafiltration has been explored [25–27]. Therefore, in chromatographic runs we used phosphate buffer instead of TEA buffer as the eluent. The influence of the pH, at fixed ionic strength (0.1 M), on the elution of whey proteins (LA, LG) is shown in Fig. 1. The elution volumes decrease as the pH is close to the protein isoelectric point. The retention and the band width of the LA ($pI = 4.8$) peak decrease with increase in pH, as is predictable from the protein charge. On the other hand, a higher retention of LG is observed in this pH range (7–5); no elution is observed from pH 7 until a separation in two subunits appears at pH 5.

For the sake of comparison, Fig. 2 shows the chromatograms of LYS and BSA eluted with QPVI silica under isocratic conditions in phosphate buffer at pH 7 and at low ionic strength (0.1 M). A broad peak of BSA ($pI = 4.9$) is observed owing to its negative net charge at pH 7. On the other hand, LYS is not retained (negative k').

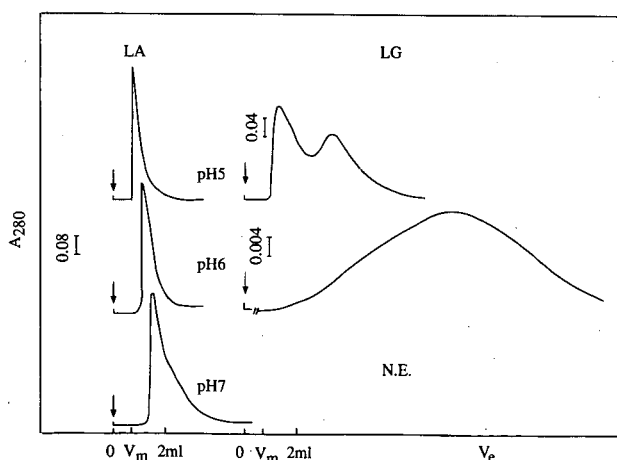


Fig. 1. Influence of pH on chromatograms of LA and LG with QPVI silica under isocratic conditions. Phosphate buffer (0.05 M), KCl (0.1 M); flow-rate, 1 ml/min; V_{inj} , 50 μ l.

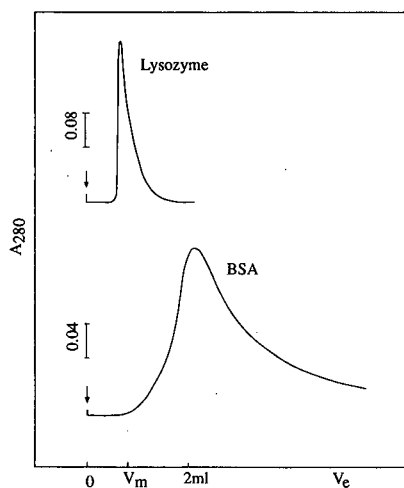


Fig. 2. Chromatograms of LYS and BSA with QPVI silica under isocratic conditions. Phosphate buffer (0.05 *M*, pH 7), KCl (0.1 *M*); flow-rate, 1 ml/min; V_{inj} , 50 μ l.

The k' values of all proteins *versus* pH at low and high ionic strength are given in Table III. At high ionic strength, all k' values became negative or close to zero. Phosphate buffer is a better displacer than TEA (Table II), as a pure size-exclusion mode is never reached with this latter buffer at pH 7. Particular attention must be paid to the k' values at pH 5, where enhanced hydrophobic interactions arise at high salt content. It has been reported previously that ion-exchange packings with PEI coatings exhibit significant hydrophobic interactions, resulting in mixed-mode chromatography for protein separations [28–31]. On the other hand, the increase in k' for lysozyme in the SEC mode at high salt content is in agreement with previous studies [32–35].

TABLE III

INFLUENCE OF pH AND IONIC STRENGTH (*I*) ON CAPACITY FACTORS (k') OF PROTEINS WITH QPVI SILICA

Phosphate buffer (0.05 *M*), [KCl] as *I*.

pH	<i>I</i>	k'			
		LA	LG	BSA	LYS
7	0.1	1.26	N.E. ^a	1.78	-0.08
6	0.1	0.72	18.8	1.29	-0.10
5	0.1	0.18	0.88 ^b 3.42 ^b	0.51	-0.15
7	1	-0.01	-0.01	-0.04	-0.08
6	1	-0.08	-0.10	-0.10	-0.10
5	1	0.03	-0.03	0.00	-0.01

^a N.E. = Not eluted.

^b Two subunits.

Mixed-mode chromatography with KPVI silica. In order to obtain a mixed-mode material, another coated silica was developed by using PVI and a hydrophobic cross-linking agent (DGEBA) (hereafter called KPVI silica).

Experimental results *versus* ionic strength, at fixed pH (pH 7), are given in Table IV. These results are different from the QPVI results. At low ionic strength, any protein is adsorbed on the KPVI coating except LYS, which is strongly retained. The hydrophobic character of the polymer coating is indicated by the high k' value (about 26) of LYS, for which no ionic interactions can be invoked, as both stationary phase and LYS are positively charged. Similar results were obtained with TEA buffer (not shown).

A weakly polar organic solvent (acetonitrile) was added to the mobile phase buffer to suppress hydrophobic interactions. The acetonitrile content lies in the range 0–30% (v/v) because of the poor solubility of proteins in this buffered eluent at high salt concentration.

Fig. 3 shows LA and LG peak profiles in a mobile phase including 30% acetonitrile, phosphate buffer and a high ionic strength. LG appears as a double peak of 2 subunits, not well resolved; LA, which is a more hydrophobic protein than LG, is not entirely displaced from the KPVI phase by this eluent. Table IV gives the capacity factors of all proteins, depending on acetonitrile content, ionic strength and pH. For clarity, Table IV does not include k' values corresponding to 10 and 20% acetonitrile contents; elution, if any, is indicated in the text. The ionic part of the retention mechanism of these proteins is clearly shown as these proteins are not eluted at low ionic strength in acetonitrile-containing eluents. Nevertheless, mixed (ionic and hydrophobic) interactions between negatively charged proteins and the KPVI support still remained ($k' > 2$) at high ionic strength in acetonitrile media. On the other hand, BSA is eluted according to a size-exclusion mode with the KPVI column, at high ionic strength only, revealing that ionic BSA-support interactions are involved in the adsorption of this protein in a low-salt medium. From Table IV, it appears that the

TABLE IV

INFLUENCE OF ACN CONTENT AND IONIC STRENGTH ON PROTEIN CAPACITY FACTORS (k') WITH KPVI SILICA

Phosphate buffer (0.05 M, pH 7), [KCl] as I .

ACN (%)	I	Phase	k'			
			LA	LG	BSA	LYS
0	0.1	KPVI	N.E. ^a	N.E.	N.E.	26.4
	1		N.E.	N.E.	N.E.	N.E.
	1 ^b		N.E.	N.E.	—	—
30	0.1	KPVI	N.E.	N.E.	N.E.	—0.13
	1		2.54	2.02 ^c	—0.26	—0.12
	1 ^b		2.95	2.96 ^c	—0.26	—0.14

^a N.E. = Not eluted.

^b pH 6.

^c Two subunits.

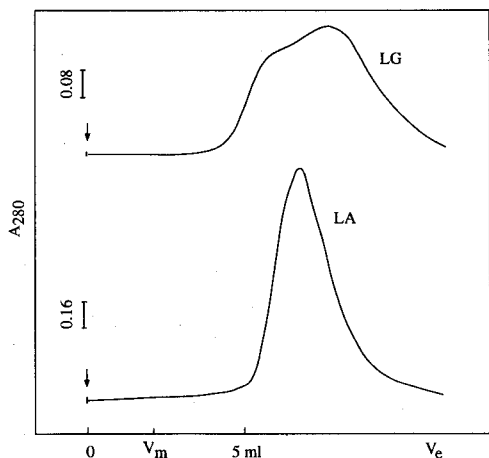


Fig. 3. Chromatograms of LA and LG with KPVI silica under isocratic conditions. Phosphate buffer (0.05 M, pH 7), KCl (1 M), ACN 30% (v/v); flow-rate, 1 ml/min; V_{inj} , 50 μ l.

behaviour of BSA is less hydrophobic than that of whey protein towards the KPVI phase. Finally, the LYS capacity factor becomes negative whatever the ionic strength if the eluting buffer includes acetonitrile.

Ultrafiltration results

Ultrafiltration performances. The permeation flux of pure solvent passing through the membrane can be related to the applied pressure (ΔP) by Darcy's law:

$$J = \Delta P / \mu R_M \quad (2)$$

where μ is the solvent viscosity (Pa s) and R_M is the hydraulic resistance (m^{-1}) of the membrane before use.

Fouling could be introduced as an apparent serial of hydraulic resistances opposite to the mass transfer, so that Darcy's law becomes

$$J = \Delta P / \mu_t (R_M + R_{BL}) \quad (3)$$

where μ_t is the feed solution viscosity (Pa s) and R_{BL} the hydraulic resistance of the boundary layer (m^{-1}).

During ultrafiltration runs, the permeation flux decline (J_t) can be analysed through hydraulic resistance ratios with the following relationship:

$$R_{BL} / R_M = (\mu_b / \mu_t) (J_b / J_t) - 1 \quad (4)$$

where J_b and J_t are the buffer flux and the permeation flux during ultrafiltration at time t , respectively ($l h^{-1} m^{-2}$). Eqn. 4 is a convenient way to define an overall fouling index without any assumption as to cause.

Retention ratios are defined by the following relationship:

$$R(\%) = 100(1 - c_p/c_o) \quad (5)$$

where c is the concentration and subscripts p and o refer to permeate and feed solution, respectively.

Permeate concentrations were determined by SEC (1% accuracy; see Experimental).

Ultrafiltration with M_1 -QPVI and unmodified membranes. Three inorganic Carbosep membranes were tested: an unmodified M_1 -type membrane and two functionalized membranes, hereafter called M_1 -QPVI and M_1 -KPVI, where the PVI coating was cross-linked with ECl or DGEBA, respectively.

In a first step, we compared the ultrafiltration performances of unmodified M_1 and M_1 -QPVI membranes. Ultrafiltration of LYS and BSA solutions by these membranes has been reported previously [13,36]. The physico-chemical conditions (pH 7; 0.2 M KCl) were derived from Table III in order to suppress ionic interactions between LA and QPVI and to achieve a selective extraction of LA from the whey protein mixture. Retention ratios and fouling indexes (R_{BL}/R_M) versus time are shown in Fig. 4. The LG retention ratio is higher with the M_1 -QPVI than with the unmodified M_1 membrane, but complete retention of LG was expected in 0.2 M medium based on HPLC data. Moreover, ionic interactions between LG and the M_1 -QPVI membrane also induce an increase in the LA retention ratio (from 52.5 to 66.2%). On the other hand, the fouling index, R_{BL}/R_M , is reduced with the M_1 -QPVI membrane.

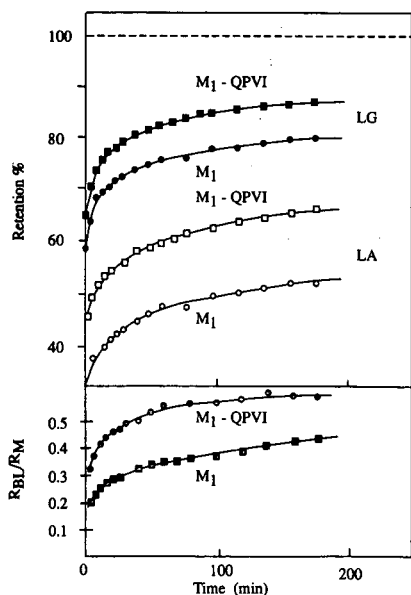


Fig. 4. LA and LG retention ratios (top) and fouling indexes (bottom) with an unmodified M_1 membrane and with an M_1 -QPVI membrane. Phosphate buffer (0.05 M, pH 7); KCl (0.2 M). $\Delta P = 2 \cdot 10^5$ Pa; $V_L = 4.4 \text{ m s}^{-1}$; $\tau_w = 75$ Pa; $T = 20^\circ\text{C}$.

Table V shows the influence of the ionic strength and pH on the properties of UF membranes. Retention ratios of whey proteins with an unmodified membrane are not sensitive to ionic strength. It should be noted that ZrO_2 has a pH of zero electric charge of about 5.7 [37], so that the membrane interface is negative at pH 7. In contrast to the chromatographic results, the LA and LG retention ratios with a functionalized M_1 -QPVI membrane were only slightly dependent on ionic strength. This emphasizes the minor effect of ionic strength on the retention properties of this type of inorganic membrane; nevertheless, the fouling index was significantly decreased when the ionic strength was raised to 1 *M*.

At lower pH and ionic strength (0.1 *M*), the retention ratios of LA and LG increase by over 80% and 90%, respectively. A marked rise in the fouling index ($R_{BL}/R_M = 1.0$) of the M_1 -QPVI membrane is noted at pH 5, very close to the *pI* values of whey proteins. This result agrees with other work [6,10,38,39] which correlates an increase in fouling with the amount of adsorbed protein, which is maximum at a pH close to the *pI*. This long-term fouling can be related to hydrophobic interactions, which are predominant under these pH conditions.

The whey protein retention ratios are enhanced at pH close to protein *pI* whereas HPLC *k'* data (Table III) suggest only weak ionic interactions. Ultrafiltration, with various hydrodynamic conditions not discussed here, is based on a more complicated retention mechanism than HPLC zonal elution.

Ultrafiltration with M_1 -KPVI membrane. A functionalized M_1 membrane with enhanced hydrophobic character (Bisphenol A moiety) was then developed in order to obtain complete retention of LG and to improve the selectivity. Fig. 5 shows that the LG retention ratio is 100% during the entire run at low ionic strength (0.2 *M*) and pH 7. There is a time lag of nearly 30 min before LA appears in the permeate, owing to an adsorption step. The LA retention ratio at the steady state (87%) depends on the complete retention of LG. The hydrophobic moieties of KPVI induce complete retention of LG, an increasing fouling index (1.19) and an increase in LA retention. Table V reports M_1 -KPVI membrane performances *versus* pH and ionic strength. A

TABLE V

INFLUENCE OF pH AND IONIC STRENGTH ON THE ULTRAFILTRATION OF WHEY PROTEINS WITH AN UNMODIFIED M_1 AND TWO FUNCTIONALIZED M_1 MEMBRANES

Phosphate buffer (0.05 *M*), [KCl] as *I*.

pH	<i>I</i>	Membrane	R_{LA}	R_{LG}	R_{BL}/R_M
7	0.2	M_1	52.5	79.5	0.61
	1		52.8	78.9	0.42
7	0.2	M_1 -QPVI	66.2	86.7	0.45
	0.4		63.4	86.7	0.37
	1		59.0	84.5	0.33
6	0.1	M_1 -QPVI	80.6	92.4	0.67
5	0.1		83.7	93.2	1.0
7	0.2	M_1 -KPVI	87.0	100.0	1.19
	1		83.4	97.2	0.84
5	0.2	M_1 -KPVI	93.6	>98	1.24

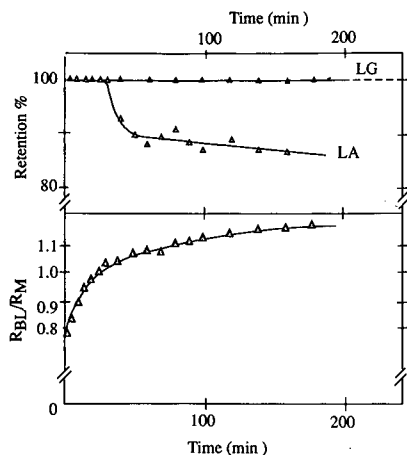


Fig. 5. LA and LG retention ratios (top) and fouling index with an M_1 -KPVI membrane (bottom). Phosphate buffer (0.05 M); KCl (0.2 M); pH 7. $\Delta P = 2 \cdot 10^5$ Pa; $V_L = 4.4 \text{ m s}^{-1}$; $\tau_w = 75$ Pa; $T = 20^\circ\text{C}$.

high ionic strength decreases the fouling index again but is not a basic parameter for retention properties. When the pH is close to the pI , the LA retention ratio is increased owing to its increased hydrophobic character and consequently the fouling index increases; the contribution of LA to the build-up of the boundary layer is thus demonstrated.

This new type of membrane involving mixed interactions appears to be promising for the separation of protein mixtures in the most difficult case, *i.e.*, to separate proteins of the same charge.

CONCLUSIONS

The chromatographic experiments with a quaternized hydrophilic polymer coating (QPVI) show that lactalbumin is not retained at pH 7 and at low salt content (0.1 M) whereas lactoglobulin is not eluted. Ultrafiltration of these proteins from concentrated whey proteins with this functionalized membrane demonstrates enhanced retention compared with an unmodified membrane. However, the separation selectivity is not improved. The main difference between these two types of experiments is due to the large excess of protein with respect to the membrane sites compared with the low protein/ionic sites ratio in zonal chromatographic elution [40]. Further, in UF, the LA retention is dependent on the LG retention, which agrees with previous conclusions regarding the selectivity of protein separations [4,11–14]. The separation properties of an ultrafiltration membrane are dependent on both protein–membrane and protein–protein interactions. An M_1 -QPVI membrane had previously achieved a highly selective extraction of lysozyme with a complete retention of ovalbumin [13,41]. A highly selective extraction can be achieved with strong ionic interactions between the membrane and the proteins to be concentrated, but in the case of the whey protein mixture the difference in interactions is too weak to obtain a highly selective separation.

With a more hydrophobic coating (KPVI), a mixed mode governs the chroma-

tography of LA and LG, as high acetonitrile and salt contents are necessary for eluting these proteins. Ultrafiltration results with this membrane, using aqueous media, show the complete retention of LG and a permeate containing only lactalbumin. Hence, no correlation can be established between UF retention and HPLC capacity factors. Nevertheless, these UF results are more comprehensive judging from the HPLC data. Strong ionic and hydrophobic interactions between proteins (LA and LG) and a modified KPVI membrane are involved in such a way that LA contributes both to complete LG retention and to fouling; the build-up of the boundary layer, composed of protein multilayers, depends on interactions between membrane sites and proteins and/or on the salt used. The boundary layer at the wall of the functionalized membrane is composed of completely retained LG and partially retained LA. The reason for the difference in protein retention is not clear, but perhaps is due to differences in mixed interactions with the KPVI membrane. It should be remembered that the hydrodynamic conditions (not developed here) of the UF process are optimized for this highly selective extraction [23–24]. More detailed HPLC studies with overloaded conditions must be made in order to obtain a better correlation between HPLC and UF runs.

ACKNOWLEDGEMENTS

The authors thank Tech-Sep (Groupe Rhône-Poulenc, Miribel, France) for financial support.

ABBREVIATIONS AND SYMBOLS

ACN	Acetonitrile
BSA	Bovine serum albumin
<i>c</i>	Concentration
DGEBA	Diglycidyl ether of bisphenol A
ECl	Epichlorohydrin
<i>I</i>	Ionic strength
<i>J</i>	Flux ($l\ h^{-1}\ m^{-2}$)
J_0	water flux before use
<i>k'</i>	Capacity factor
KPVI	Quaternized PVI with DGEBA
LA	Lactalbumin
LG	Lactoglobulin
LYS	Lysozyme
QPVI	Quaternized PVI with ECl
<i>pI</i>	Isoelectric point
PVI	Polyvinylimidazole
<i>R</i>	Membrane hydraulic resistance (m^{-1})
<i>R</i> (%)	Retention ratio
TEA	Triethanolamine
V_L	Tangential velocity of the feed solution ($m\ s^{-1}$)

Greek letters

ΔP	Applied pressure (Pa)
μ	Viscosity (Pa s)
τ	Shear stress (Pa)

Subscripts

a	After ultrafiltration
b	Buffer
BL	Boundary layer
f	After the cleaning procedure
M	Membrane
o	Feed solution
p	Permeate
t	Time
w	Wall

REFERENCES

- 1 J. L. Nilsson, *J. Membr. Sci.*, 52 (1990) 121.
- 2 G. B. Van den Berg and C. A. Smolders, *Filtr. Sep.*, March/April (1988) 115.
- 3 G. B. Van den Berg and C. A. Smolders, *Desalination*, 77 (1990) 101.
- 4 K. C. Ingham, T. F. Busby, Y. Sahleström and F. Castino, in A. R. Cooper (Editor), *Polymer Science and Technology, Ultrafiltration Membranes and Applications*, Plenum Press, New York, Vol. 13, 1980, p. 141.
- 5 J. A. Howell, O. Velicangil, M. S. Le and A. L. Herrera Zeppelin, *Ann. N.Y. Acad. Sci.*, 369 (1981) 355.
- 6 L. J. Zeman, *J. Membr. Sci.*, 15 (1983) 23.
- 7 E. Matthiasson, *J. Membr. Sci.*, 16 (1983) 23.
- 8 A. G. Fane, C. J. D. Fell and A. G. Waters, *J. Membr. Sci.*, 16 (1983) 211.
- 9 P. Aimar, S. Baklouti and V. Sanchez, *J. Membr. Sci.*, 29 (1986) 207.
- 10 M. Nyström, *J. Membr. Sci.*, 44 (1989) 183.
- 11 S. Nakao, H. Osada, M. Kuramata, T. Tsuru and S. Kimura, *Desalination*, 70 (1988) 191.
- 12 P. Aimar, C. Taddéi, J. P. Lafaille and V. Sanchez, *J. Membr. Sci.*, 38 (1988) 203.
- 13 B. Chaufer, A. Grangeon, J. Dulieu and B. Sébille, in *Filtra 88*, Société Française de Filtration, Cachan, 1988, p. 302.
- 14 J. H. Hanemaaijer, T. Robbertsen, Th. Van den Boomgaard and J. W. Gunnink, *J. Membr. Sci.*, 40 (1989) 199.
- 15 C. H. Bamford and E. Schofield, *Polymer*, 22 (1981) 1227.
- 16 J. S. Tan and A. R. Sochor, *Macromolecules*, 14 (1981) 1700.
- 17 B. Sébille, B. Boussouira and J. Piquion, *Eur. Pat.*, 86 402 633 (1986).
- 18 B. Boussouira, *Thesis*, Université Paris Val de Marne, Créteil, 1987.
- 19 M. Ito, H. Hatá and K. Kamagata, *J. Appl. Polym. Sci.*, 33 (1987) 1843.
- 20 F. Ricciardi, W. A. Romanchick and M. M. Joullié, *J. Polym. Sci., Polym. Lett. Ed.*, 21 (1983) 1475.
- 21 A. J. Alpert and F. E. Régner, *J. Chromatogr.*, 185 (1979) 375.
- 22 W. Kopaciewicz, M. A. Rounds and F. E. Régner, *J. Chromatogr.*, 318 (1985) 157.
- 23 B. Chaufer, M. Rollin, H. Barnier, A. Grangeon and B. Sébille, in Ch. Eyraud and P. Schaegis (Editors), *Proceedings of the 5th World Filtration Congress, Nice, June 5-8, 1990*, Vol. 1, Société Française de Filtration, Cachan, 1990, p. 458.
- 24 M. Rollin, B. Chaufer, H. Barnier and A. Grangeon, *J. Membr. Sci.*, in preparation.
- 25 C. B. Van den Berg, J. H. Hanemaaijer and C. A. Smolders, *J. Membr. Sci.*, 31 (1987) 307.
- 26 J. P. Labbé, A. Quémarais, F. Michel and G. Daufin, *J. Membr. Sci.*, 51 (1990) 293.
- 27 M. Cheryan, *Ultrafiltration Handbook*, Technomic, Lancaster, PA, 1986, Ch. 4, p. 171.
- 28 W. Kopaciewicz, M. A. Rounds, J. Fausnaugh and F. E. Régner, *J. Chromatogr.*, 266 (1983) 3.
- 29 L. A. Kennedy, W. Kopaciewicz and F. E. Régner, *J. Chromatogr.*, 359 (1986) 73.

- 30 M. A. Rounds, W. D. Rounds and F. E. Regnier, *J. Chromatogr.*, 397 (1987) 25.
- 31 R. R. Drager and F. E. Regnier, *Anal. Biochem.*, 145 (1985) 47.
- 32 E. Pfannkoch, K. C. Lu, F. E. Regnier and H. G. Barth, *J. Chromatogr. Sci.*, 18 (1980) 430.
- 33 B. Sébille, B. Boussouira, V. Housse-Ferrari, B. Chaufer and J. Piquion, presented at the 7th International Symposium on the HPLC of Proteins, Peptides and Polynucleotides, Washington, DC, November 2-4, 1987.
- 34 V. Housse-Ferrari, *Thesis*, Université Pierre et Marie Curie, Paris, 1990.
- 35 V. Housse-Ferrari, B. Chaufer and B. Sébille, *J. Chromatogr.*, in preparation.
- 36 B. Chaufer, J. Dulieu and B. Sébille, in L. Cot and J. Charpin (Editors), *Proceedings of the 1st International Conference on Inorganic Membranes, Montpellier, July 3-6, 1989*, 1989, p. 135.
- 37 M. A. Blesa, A. J. G. Maroto, S. I. Passaggio, N. E. Figliolia and G. Rigotti, *J. Mater. Sci.*, 20 (1985) 4601.
- 38 A. G. Fane, C. J. D. Fell and A. Suki, *J. Membr. Sci.*, 16 (1983) 195.
- 39 A. Suki, A. G. Fane and C. J. D. Fell, *J. Membr. Sci.*, 27 (1986) 181.
- 40 B. Chaufer, M. Rollin and B. Sébille, in A. Faure et al. (Editors), *Proceedings of the 4th Symposium on Protein Purification Technologies, Clermont-Ferrand, March 14-16, 1990*, Vol. 4, Groupement Recherches Biotechnologies Proteins, Villebon/Yvette, 1990, p. 43.
- 41 B. Chaufer, A. Grangeon, J. Dulieu; M. Rollin and B. Sébille, in L. Cot and J. Charpin (Editors), *Proceedings of the 1st International Conference on Inorganic Membranes, Montpellier, July 3-6, 1989*, 1989, p. 475.

CHROMSYMP. 2346

Purification of *Phleum pratense* pollen extract by immunoaffinity chromatography and high-performance ion-exchange chromatography

EZIO BOLZACCHINI, PATRIZIA DI GENNARO, GIUSEPPINA DI GREGORIO and BRUNO RINDONE*

Dipartimento di Chimica Organica e Industriale, Università di Milano, Via Venezian 21, I-20133 Milan (Italy)

PAOLO FALAGIANI and GIOVANNI MISTRELLO

Lofarma Allergeni, Reparto Ricerche, Viale Cassala 40, I-20146 Milan (Italy)

and

IB SONDERGAARD

Royal Veterinary and Agricultural University, 40 Thorvaldsenvej, DK-1871 Frederiksberg C, Copenhagen (Denmark)

ABSTRACT

Basic allergens of *Phleum pratense* pollen extract have been purified by either sequence gel filtration-ion-exchange high-performance liquid chromatography (HPIEX) and size-exclusion HPLC or sequence gel filtration-immunoaffinity chromatography and HPIEX. The second procedure seems to be suitable for preparative purposes.

INTRODUCTION

Phleum pratense (Graminaceae) pollen allergenic extracts are used in the immunotherapy of allergic diseases. Since these extracts are constituted by a mixture of heterogenous proteins, studies aimed at improving their standardisation and knowledge of their chemical composition are needed. An early attempt to characterise phleum allergens was performed using combinations of electrophoretic and immunoelectrophoretic methods [1] and 28 antigens were thus shown to be present, some of them being allergens.

A preparative approach was performed in a sequence of conventional anion-exchange chromatography followed by conventional cation-exchange chromatography [2] and four allergens were isolated. They were the acidic antigens 3 (molecular weight, MW = 10 000; isoelectric point, pI = 3.9), 19 (MW = 15 000; pI = 4.9) and 25 (MW = 15 000; pI = 4.5) and the basic antigen 30 (MW = 34 000; pI = 9.4).

Other purification sequences were gel chromatography-ion-exchange chromatography [3,4] and, more recently, gel filtration-high-performance ion-exchange high-

performance liquid chromatography (HPIEX) and high-performance size-exclusion chromatography (HPSEC) [5]. Some immunochemical characterisation of the basic allergen [6] and analyses of its carbohydrates content [7,8] were also performed.

The uncertainty in the comparison of phleum allergens obtained with different procedures stimulated a recent attempt of better definition of *Phleum pratense* pollen extract composition [9]. However, a preparative-scale multi-step procedure for the separation of phleum components was needed. The preparative work experienced in our laboratory in the purification of *Parietaria judaica* allergens [10–15] using multi-step procedures based essentially on high-performance liquid chromatography (HPLC) stimulated us to use a similar approach for *Phleum pratense* pollen extracts.

EXPERIMENTAL

Phleum pollen extract and gel filtration

A 10-g sample of dry pollen obtained from Allergon (Engelholm, Sweden) was extracted with 200 ml of 0.15 M phosphate buffer (pH 7.2) for 24 h at 4°C. The supernatant obtained after centrifugation at 43 000 g for 40 min was gel-filtered on Sephadex G-25, and phosphate buffer 20 mM pH 6.8, was used as eluent. The exclusion peak corresponding to blue dextran was collected and lyophilised.

HPLC analyses

HPSEC was performed by dissolving lyophilised pollen extracts in 0.15 M phosphate buffer, pH 6.8, 0.5 M potassium chloride and injecting the sample through a Rheodyne 50- μ l loop. The instrument was a Varian 5500 HPLC gradient (Varian Palo Alto, CA, USA), equipped with a Synchronpack 100 (30 \times 10 mm O.D. \times 8 mm I.D.) SEC column, eluted with 0.15 M phosphate buffer, pH 6.8, 0.5 M potassium chloride, at a flow-rate of 1 ml/min. The detectors were a Varian UV 50 instrument at 280 nm and a Hewlett-Packard 1040 diode array detector (Hewlett-Packard, Palo Alto, CA, USA).

HPIEX with an ionic strength gradient was performed by dissolving the material in 10 mM Tris-acetic acid buffer, pH 7.0, 20 mM sodium acetate, and injecting the sample through a Rheodyne 5-ml loop. A Waters Delta Prep 3000 HPLC instrument equipped with a TSK DEAE-5 PW ion-exchange column (15 cm \times 21.5 mm I.D.) was used, eluting with a 40-min gradient of A to B (A: 10 mM Tris-acetic acid buffer, pH 7.0, sodium acetate of the required molarity; B: 10 mM Tris-acetic acid buffer, pH 7.0, containing 500 mM sodium acetate). The flow-rate was 6 ml/min. The fraction was then analysed by radio allergosorbent test (RAST) and RAST-Inhibition (RAST-I).

Immunoabsorbent preparation for affinity chromatography

Purified immunoglobulin fraction from serum of rabbit immunised against *Phleum pratense* pollen extract was coupled to Minileak medium gel (Kem Entek, Copenhagen, Denmark). The mixture constituted 1 g of gel in 10 ml of water containing 1 mg of antibodies and 3 ml of a 3% PEG solution and was left at room temperature for one night. The gel was then transferred into a Pharmacia column and washed with 0.1 M phosphate buffer, pH 7.0 and 0.5 M NaCl.

Affinity chromatography

The immunoabsorbent column was loaded with 10 ml of gelfiltered *Phleum pratense* with protein content 1.2 mg/ml. After 24 h of recycling, specific fractions were eluted with glycine-HCl buffer, pH 2.5, and collected into two samples (A and B) which were neutralised with 0.1 M phosphate buffer pH 6.8, containing 0.5 M KCl, dialysed against water and lyophilised.

Radioallergo sorbent test

The fractions were bound to cyanogen bromide-activated paper discs, and direct RAST or RAST-I was performed according to the method of Yman *et al.* [16] using a pool of sera from 95 patients with high sensitivity to *Phleum pratense* pollen.

Isoelectric focusing (IEF)

A 5% polyacrylamide gel (18 × 9 cm) containing 2 M urea, 0.5 mm thick, was used. Ampholine (LKB, Bromma, Sweden), pH 3–10, was used. The anodic solution was 1 M phosphoric acid and the cathodic solution was 1 M sodium hydroxide. The samples were allowed to migrate at 15°C for 1.5 h at 2500 V and 7 W. Detection was performed by silver staining [17–18].

Fused rocket immunoelectrophoresis (FRIE)

A 1% (w/v) agarose gel (10 cm × 1.5 mm) containing 11 $\mu\text{l}/\text{cm}^2$ Lofarma anti-phleum rabbit antibody (Lofarma Allergeni, Milano, Italy), was used. The buffer was Tris-tricine (pH 8.6, ionic strength 0.1 M). Electrophoresis was performed at 2 V/cm for 18 h at 15°C [19]. Detection was performed by the Coomassie brilliant blue R-250 method (0.5% in water-ethanol-acetic acid, 45:45:10).

Crossed immunoelectrophoresis (CIE)

A 1% (w/v) agarose gel (10 cm × 10 cm × 1.5 mm) was used. The buffer was Tris-tricine (pH 8.6, ionic strength 0.1 M). Electrophoresis in the first dimension was performed at 10 V/cm for 25 min and in the second dimension using 3.75 ml of a 1% agarose gel containing 14 $\mu\text{l}/\text{cm}^2$ Lofarma anti-phleum rabbit antibody and operating at 15°C and 2 V/cm for 18 h [20]. Detection was performed by the Coomassie brilliant blue R-250 method (0.5% in water-ethanol-acetic acid, 45:45:10).

RESULTS AND DISCUSSION

The first purification procedure tested was performed with the gel-filtered extract in a preparative HPIEX experiment at pH 7.0 using an ionic strength gradient with an anion-exchange column. The result is shown in Fig. 1. Most basic and neutral protein components were eluted first in the basic exchanger used. Direct RAST of the fractions showed that the biological activity was spread over the whole chromatogram, and that much activity was present in the first chromatographic fractions, *i.e.* the basic and neutral part of the chromatogram. This was confirmed by RAST-I experiments.

The individual fractions were analysed by electrophoretic and immunochemical methods. Two families of antigens were apparent in FRIE analysis, the first occurring in fractions 1–15 (*i.e.* in the region containing basic and neutral components) and the other in fractions 20–30 (*i.e.* in the region containing acidic components).

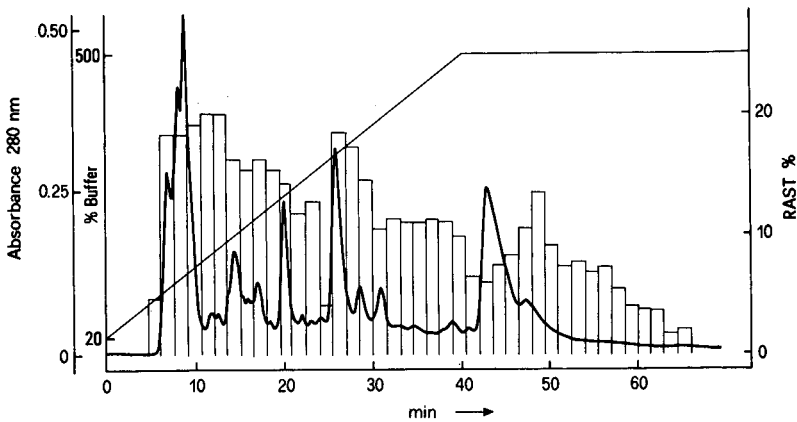


Fig. 1. HPIEX separation of *Phleum pratense* pollen extract and RAST analysis of the fractions.

IEF analysis of the chromatographic fractions showed that most fractions contained complex mixtures of components. Fraction 3 essentially constituted a single component, having an pI value of *ca.* 9.0. The HPSEC analysis of this fraction showed a peak at 11 min retention time which was positive to RAST.

The amount of allergenic material recovered was very low, and this sequence of HPIEX-HPSEC seemed to be unsuitable for preparative purposes.

As an alternative procedure we chose affinity chromatography followed by HPIEX. Polyclonal immunoglobulins were used in order to purify all the antigenic material. The gel-filtered extract was loaded into the affinity column where it was recycled for 24 h to maximise specific interaction. The antigens were then eluted using a pH 2.5 buffer. Two peaks (A and B) were eluted (Fig. 2) and were positive to RAST.

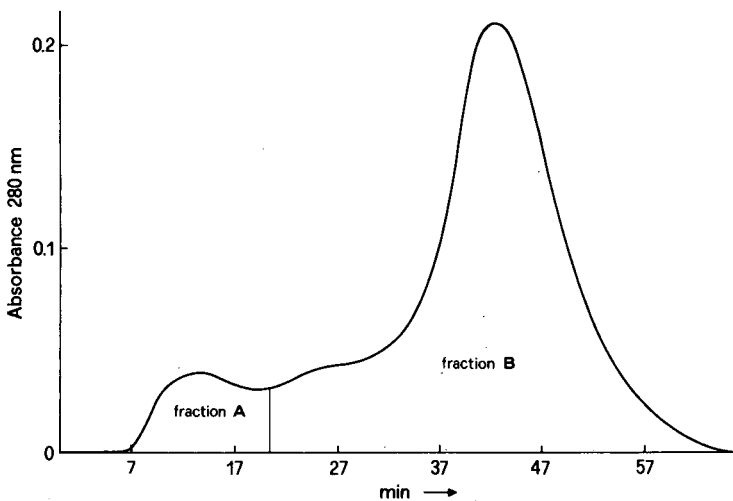


Fig. 2. Immunoaffinity separation of *Phleum pratense* pollen extract.

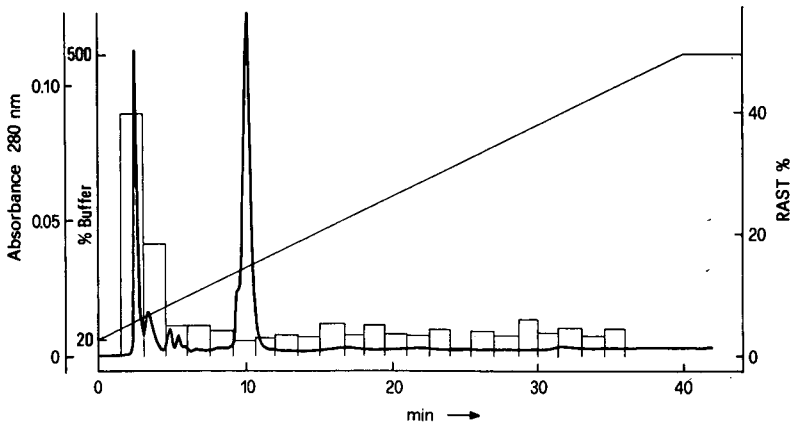


Fig. 3. HPIEX separation of fraction B of *Phleum pratense* pollen extract purified by immunoaffinity chromatography and RAST analysis of the fractions.

The HPIEX analysis of the major fraction (fraction B) using the same anion-exchange column is shown in Fig. 3. Three peaks constituted the fraction, and RAST and RAST-I analysis showed that the two peaks eluted first were allergens. HPIEX showed that these two peaks were the sole components of fraction B.

IEF analysis showed that peak A contained basic proteins and peak B contained both basic and acidic proteins. This is in accord with the elution time of the peaks in the HPIEX column. CIE showed that peak A gave only one precipitation arch and peak B showed two.

The conclusion is that, providing that the antibodies used have affinity against all the antigens in the extract, affinity chromatography of *Phleum pratense* pollen extract is a tool for the first purification step of its allergenic content. HPIEX may be the final purification step of the allergens.

ACKNOWLEDGEMENTS

We thank our students Sonia Poli, Francesca Farina and Monica Odiardo. This work was supported by a CNR grant, Progetto Finalizzato Chimica Fine II, by the Danish Natural Science Research Council and the Danish Agricultural and Veterinary Research Council.

REFERENCES

- 1 B. Weeke, H. Lowenstein and L. Nielsen, *Acta Allergol.*, 29 (1974) 402.
- 2 H. Lowenstein, *Allergy*, 33 (1978) 30.
- 3 E. Puttonen and H. J. Maasch, *J. Chromatogr.*, 242 (1982) 153.
- 4 D. Meineke, R. Wahl and H. J. Maasch, *Allergopharma*, 25 (1988) 242.
- 5 S. Haavik, B. Smestad Paulsen and J. K. Wold, *J. Chromatogr.*, 321 (1985) 199.
- 6 S. Haavik, A. Bryhni Frostad, B. Smestad Paulsen and J. K. Wold, *Int. Arch. Allergy Appl. Immunol.*, 83 (1987) 182.
- 7 S. Haavik, B. Smestad Paulsen and J. K. Wold, *Int. Arch. Allergy Appl. Immunol.*, 78 (1985) 197.
- 8 S. Haavik, B. Smestad Paulsen and J. K. Wold, *Int. Arch. Allergy Appl. Immunol.*, 83 (1987) 225.

- 9 D. G. Marsh, L. Goodfriend, T. P. King, H. Lowenstein and T. Platts-Mills, *Int. Arch. Allergy Appl. Immunol.*, 85 (1988) 194.
- 10 P. Falagiani, E. Cavallone, M. Nali, B. Rindone, S. Tollari, G. Riva and G. Crespi, *J. Chromatogr.*, 328 (1985) 425.
- 11 E. Bolzacchini, G. Di Gregorio, M. Nali, B. Rindone, S. Tollari, P. Falagiani, G. Riva and G. Crespi, *J. Chromatogr.*, 397 (1987) 299.
- 12 E. Bolzacchini, G. Di Gregorio, M. Nali, B. Rindone, S. Tollari, P. Falagiani, G. Riva and G. Crespi, *Allergy*, 42 (1988) 743.
- 13 A. Bassoli, F. Chioccaro, G. Di Gregorio, B. Rindone, S. Tollari, P. Falagiani, G. Riva and E. Bolzacchini, *J. Chromatogr.*, 444 (1988) 209.
- 14 A. Bassoli, E. Bolzacchini, F. Chioccaro, G. Di Gregorio, B. Rindone, S. Tollari, P. Falagiani and G. Riva, *J. Chromatogr.*, 446 (1988) 179.
- 15 I. Sondergaard, P. Falagiani, E. Bolzacchini, P. Civaroli, G. Di Gregorio, V. Madonini, A. Morelli and B. Rindone, *J. Chromatogr.*, 512 (1990) 115.
- 16 L. Yman, G. Ponterius and R. Brand, *Dev. Biol. Standards*, 29 (1975) 171.
- 17 C. R. Merrill, D. Goldman, S. A. Sedman and M. H. Ebert, *Science (Washington D.C.)*, 211 (1981) 1438.
- 18 J. Guevara Jr., D. Johnston, L. S. Rawagali, B. A. Martin, S. Capetillo and L. K. Rodriguez, *Electrophoresis*, 3 (1982) 197.
- 19 N. M. G. Harboe and P. J. Svendsen, *Scand. J. Immunol.*, 17 (Suppl. 10) (1983) 107.
- 20 P. J. Svendsen, B. Weeke and B. G. Johansson, *Scand. J. Immunol. Methods*, 62 (1983) 283.

CHROMSYMP. 2222

A ten-residue fragment of an antibody (mini-antibody) directed against lysozyme as ligand in immunoaffinity chromatography

GAJAL W. WELLING*, JUDITH VAN GORKUM, RIA A. DAMHOF and JAN WOUTER DRIJFHOUT

Laboratorium voor Medische Microbiologie, Rijksuniversiteit Groningen, Oostersingel 59, 9713 EZ Groningen (Netherlands)

W. BLOEMHOFF

Organische Chemie, Gorlaeus Laboratoria, Rijksuniversiteit Leiden, P.O. Box 9502, 2300 RA Leiden (Netherlands)

and

SYTSKE WELLING-WESTER

Laboratorium voor Medische Microbiologie, Rijksuniversiteit Groningen, Oostersingel 59, 9713 EZ Groningen (Netherlands)

ABSTRACT

The interaction between an antibody molecule and a protein antigen is an example of “natural” protein modelling. Amino acids of the antigen-binding site consisting of three hypervariable segments (L1, L2, L3) of the light (L) and three (H1, H2, H3) of the heavy (H) chain of an antibody molecule interact with amino acids present in an epitope of a protein. A ten-residue peptide was synthesized with an amino acid sequence analogous to the hypervariable L3 segment of a monoclonal antibody directed against lysozyme. The peptide was immobilized on CH-Sepharose 4B and the affinity adsorbent was used to purify lysozyme added to a detergent extract of insect cells infected with a recombinant baculovirus. This methodology may also be applicable to other antigen–antibody combinations, in immunoaffinity chromatography for selective purification of a protein or in an immunosensor for detection of a protein.

INTRODUCTION

Multiple non-covalent forces, hydrogen bonding, electrostatic, hydrophobic and van der Waals forces play a role in the binding between a protein antigen and an antibody directed against this protein. The antigen is bound by the antigen-binding site of an antibody, which consists of three hypervariable segments of the light chain (L1, L2, L3) and three of the heavy chain (H1, H2, H3) (Fig. 1).

Antibodies can be raised against a fragment of a protein (a peptide) and these antibodies may react with the intact protein [1]. Apparently, the conformation of the peptide is, at least partly, similar to that of the intact protein. Recently, the tertiary structure of a complex of a nineteen-residue peptide and a monoclonal antibody

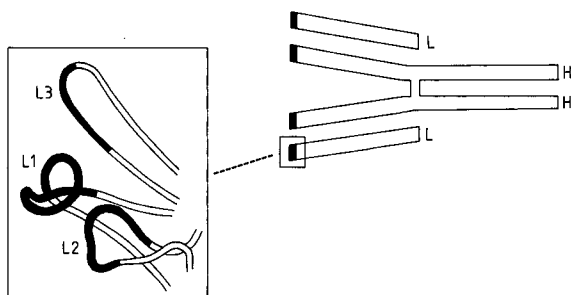


Fig. 1. Schematic representation of an immunoglobulin G molecule. One antigen-binding site (indicated in black) is composed of three hypervariable polypeptide segments of the light chain (L) and three of the heavy chain (H). Inset, spatial location of hypervariable segments (L1, L2, L3) in the L chain.

directed against this peptide was determined [2]. The interaction between the peptide and, in this instance, five of the hypervariable segments is governed by the above-mentioned non-covalent forces. We assume that selected fragments of an antibody may bind a protein antigen by the same forces. In an earlier study [3], it was shown that a synthetic thirteen-residue peptide with an amino acid sequence analogous to that of the H2 segment of a monoclonal antibody (Gloop2) raised against loop peptide (residues 57–83) of lysozyme [4–6] was able to bind lysozyme. In this study, the binding properties of a synthetic ten-residue peptide from the L3 segment of this anti-lysozyme monoclonal antibody were investigated.

EXPERIMENTAL

Peptide selection, synthesis and characterization

Using the modelling studies of complexes of monoclonal antibodies and lysozyme [5,6], a ten-residue peptide of the L3 segment was selected for synthesis, *viz.*, Tyr–Leu–Ser–Tyr–Pro–Leu–Thr–Phe–Gly–Ala. The peptide was synthesized by the semi-automatic solid-phase method with α -amino groups protected with the 9-fluorenylmethoxycarbonyl (Fmoc) group [7,8].

The purity of the peptide was verified by reversed-phase (RP)-high-performance liquid chromatography (HPLC), by amino acid analysis and by determination of the N-terminal amino acid by dansylation [9].

Affinity chromatography

The immunoaffinity adsorbent was prepared by coupling of the synthetic L3 peptide (2 mg) to 0.5 g of activated CH-Sepharose 4B obtained from Pharmacia–LKB (Uppsala, Sweden) in 0.1 M NaHCO₃–Na₂CO₃ (pH 8.2) containing 0.5 M sodium chloride according to the instructions of the manufacturer. The percentage coupling was determined by RP-HPLC of the peptide solution before coupling and the eluate after coupling. More than 99% of the peptide was coupled to the activated column material, resulting in 1.8 μ mol of peptide per gram of dry gel. Excess active groups were blocked by washing with 0.1 M Tris–HCl (pH 8.0). A control column was prepared by blocking active groups with 0.1 M Tris–HCl (pH 8.0). Affinity

chromatography was carried out at room temperature at a flow-rate of 10 ml/h during application of samples and 20 ml/h during chromatography. Columns were eluted with 0.05 M sodium thiocyanate in 20 mM Tris-HCl (pH 7.4), followed by 1 M sodium thiocyanate in the same buffer. The absorbance was measured at 280 nm.

Complex mixture of proteins

Insect cells (sf21) were infected with recombinant baculovirus (AcgD) expressing glycoprotein D of herpes simplex virus. Cells were harvested 50 h after infection and washed twice with Hanks balanced salt solution. After resuspending the cell pellet (10^7 cells per ml) in 10 mM Tris-HCl (pH 7.4), containing 2 mM phenylmethylsulphonyl fluoride (PMSF) and 1 mM N α -p-tosyl-L-lysine chloromethyl ketone (TLCK), the same volume of a buffer consisting of 4% decyl polyethylene glycol 300 (Kwant-Hoog Vacolie Recycling and Synthese, Bedum, Netherlands), 10 mM Tris-HCl (pH 7.4), 2 mM PMSF and 1 mM TLCK was added and the mixture incubated for 30 min at 0°C. Cell debris was removed by low-speed centrifugation, followed by ultracentrifugation at 100 000 g for 1 h. The supernatant containing the extracted proteins was stored in aliquots at -80°C until used. Prior to immunoaffinity chromatography, lysozyme (250 μ g in 100 μ l of water) was added to 500 μ l of an extract of insect cells containing 1.2 mg protein per ml.

RP-HPLC

RP-HPLC was performed with a Pharmacia-LKB system consisting of a Model 2150 HPLC pump, Model 2152 LC controller, Model 11300 Ultrograd mixer driver, a Rheodyne Model 7125 injector, Model 2151 variable-wavelength monitor and a Model 2210 recorder. The column (25 \times 4.6 mm I.D.) contained Nucleosil 10 C₁₈ (Macherey, Nagel, & Co., Düren, Germany). Proteins and peptides were eluted with a gradient from 10% acetonitrile in 0.1% trifluoroacetic acid (TFA) to 40% acetonitrile in 0.09% TFA (30 min) and then 66% acetonitrile in 0.09% TFA (5 min). The absorbance was monitored at 214 nm.

Sodium dodecyl sulphate-polyacrylamide gel electrophoresis (SDS-PAGE)

Samples of 50 μ l of the eluate fractions were analysed on 13.5% SDS polyacrylamide gels [10]. Polypeptide bands were revealed with a silver-staining method [11].

RESULTS AND DISCUSSION

It was shown previously [3] that an immobilized synthetic thirteen-residue peptide from the antigen-binding H2 region of a monoclonal antibody (raised against lysozyme loop peptide residues 57-83 and also reactive with intact lysozyme) could be used to purify lysozyme from a mixture of proteins. Three other unrelated synthetic peptides with charges ranging -6 to +2 did not bind lysozyme [3]. In the present study, another, smaller part of the antigen-binding site of the same monoclonal antibody was investigated. A ten-residue peptide with an amino acid sequence analogous to that of the L3 segment was synthesized.

In Fig. 2a a space-filling model of the antigen binding site is shown in which the surface residues present in the thirteen-residue H2 peptide and the ten-residue L3 peptide are indicated [6]. In addition, the residues of the epitope on lysozyme with

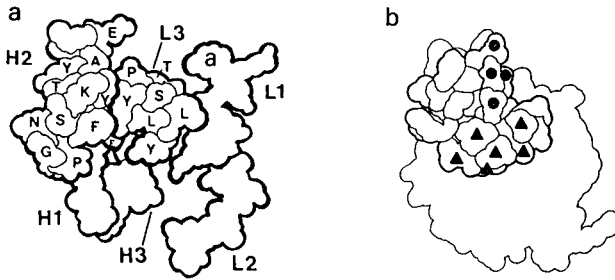


Fig. 2. (a) All-atom space-filling representation of the antigen-binding site perpendicular to the view in Fig. 1 of monoclonal antibody Gloop2 directed against hen egg-white lysozyme. Only the surface amino acid residues present in the synthetic versions of H2 and L3 are indicated by the one-letter code for amino acids. From ref. 6, by permission of Oxford University Press. (b) Space-filling model of lysozyme in which the epitope interaction with Gloop2 is indicated. (▲) Residues interacting with H2; (●) residues interacting with L3. From ref. 5, by permission of Oxford University Press.

which H2 and L3 interact are shown [5] (Fig. 2b). As the L3 peptide does not contain a lysine it could be attached to activated gels via its N-terminal amino acid. However, initial experiments showed that coupling of this peptide to tressyl-activated Sepharose resulted in material that could not bind lysozyme. One of the reasons might be the lack of spatial freedom owing to the close proximity of the gel matrix. This might limit the number of conformations of the peptide and hence the possibility that the peptide may exist in the optimum conformation to interact with the relatively large protein antigen. Therefore, the peptide was coupled to activated CH-Sepharose 4B which contains a six-carbon atom spacer between the activated group and the gel matrix. This material was used for affinity chromatography.

Fig. 3 shows that lysozyme was bound to the column material with the ten-residue peptide as ligand whereas it was not bound by a control column deactivated

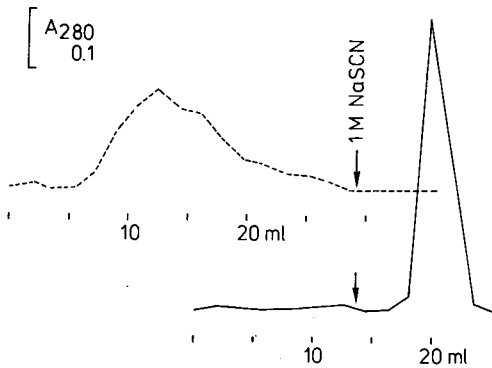


Fig. 3. Affinity chromatography of lysozyme. A ten-residue peptide from the L3 segment of a monoclonal antibody against lysozyme was coupled to activated CH Sepharose 4B. A control adsorbent was prepared by washing with 0.1 *M* Tris-HCl (pH 8.0). Lysozyme (1.6 mg) was applied to each adsorbent. The columns were eluted with 0.05 *M* sodium thiocyanate in 20 *mM* Tris-HCl (pH 7.4). The arrow indicates the start of elution with 1 *M* sodium thiocyanate in the same buffer. The flow-rate was 10 ml/h during application of the sample and 20 ml/h during chromatography. The absorbance was measured at 280 nm. Solid line, anti-lysozyme column; dashed line, control column.

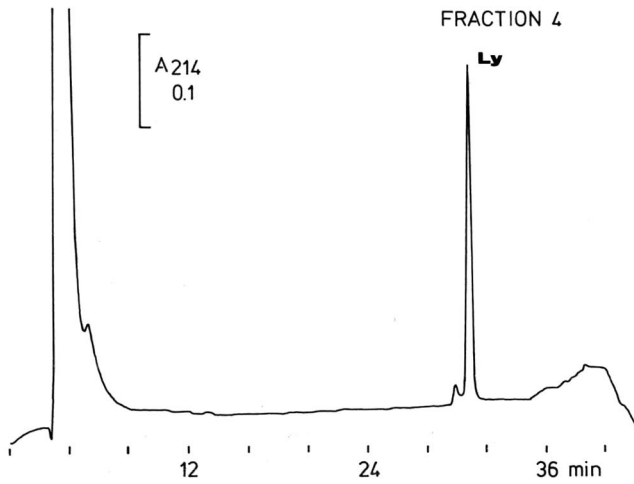
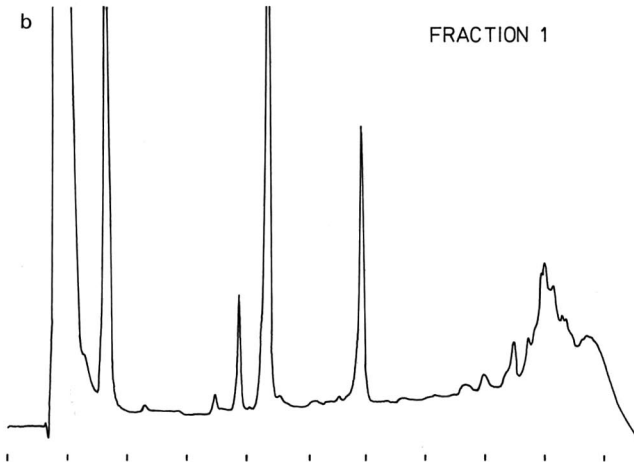
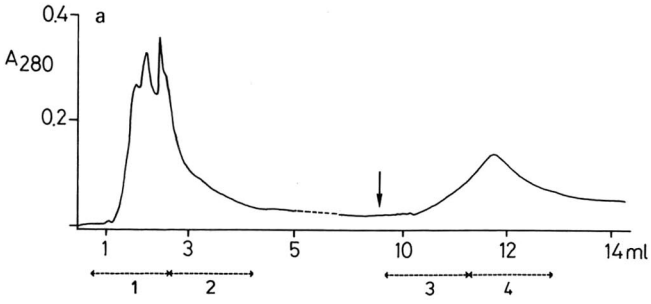


Fig. 4.

(Continued on p. 240)

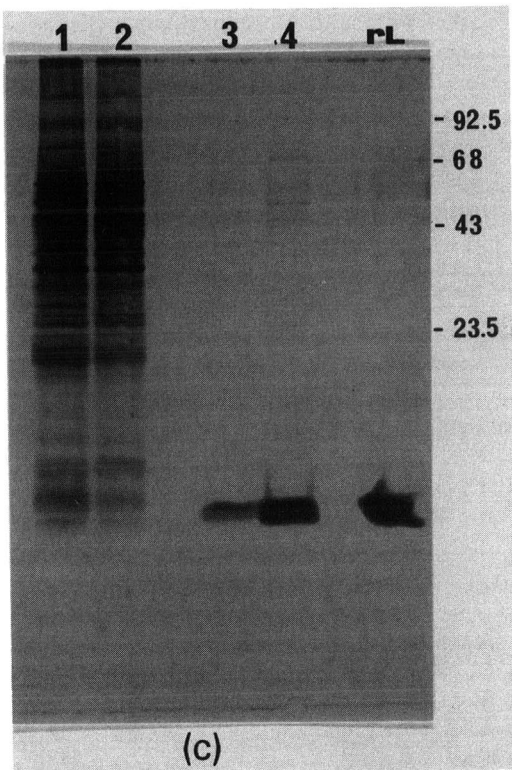


Fig. 4. (a) Affinity chromatography with the anti-lysozyme adsorbent. A 600- μ l volume of a detergent extract of insect cells infected with a recombinant baculovirus (1.2 mg protein per ml) containing 250 μ g of lysozyme was applied to the column. Elution conditions as in Fig. 3. Aliquots of the indicated fractions were analysed by (b) RP-HPLC (300- and 100- μ l of fractions 1 and 4, respectively); the large peaks at 4 min contain sodium thiocyanate and the small peak in front of the lysozyme peak is also present in a reference sample; Ly, lysozyme; (c) SDS-PAGE (50- μ l of fractions 1-4); rL, reference solution of lysozyme. The molecular weights of reference proteins are indicated in kilodaltons.

with Tris-HCl. Binding constants were not determined but further affinity chromatographic experiments showed that lysozyme was eluted slowly from the anti-lysozyme column between 0.1 and 0.2 *M* sodium thiocyanate.

It was then investigated whether the binding was sufficiently selective to purify lysozyme from a complex mixture of proteins. Lysozyme (250 μ g) was added to a detergent extract of insect cells infected with a recombinant baculovirus. This extract contains 1.2 mg protein per ml, 1.7% of the non-ionic detergent decyl polyethylene glycol and protease inhibitors. This mixture was applied to the anti-lysozyme column and the elution pattern is shown in Fig. 4a. Fractions were analysed by RP-HPLC and SDS-PAGE (Fig. 4b and c). This showed that the proteins present in the original cell extract were almost exclusively present in fractions 1 and 2 whereas lysozyme was absent and that a minor amount of these proteins (molecular weights of 40-70 kilodalton) and lysozyme were present in the peak eluted by 1 *M* sodium thiocyanate.

The response of the immune system on contact with a foreign compound, *e.g.*, a protein, is the production of antibodies. The interaction between an antibody molecule and a protein antigen is an example of 'natural' protein modelling. Binding constants are often high and in immunoaffinity chromatography severe conditions are often required for elution of proteins. As a consequence, the native structure of both antibody and protein may be affected. By reducing the immunoligand to its smallest possible size, binding constants will be considerably lower and thus elution of proteins may occur under relatively mild conditions. In general, elution may probably be achieved at concentrations less than in 1 M sodium isothiocyanate used in our study, but under such conditions the peak will be broader. Although peptides are more temperature stable than proteins, they are generally more susceptible to proteolytic degradation. Therefore, depending on the sample, the addition of protease inhibitors or a lower temperature (4°C) would be advisable during immunoaffinity chromatography.

So far only anti-lysozyme peptides have been studied and the selection of peptides was facilitated by the availability of a predicted model of the tertiary structure of an anti-lysozyme monoclonal antibody [6]. We suggest that mini-antibodies (antigen-binding fragments of an antibody) may be constructed either by organic synthesis or by recombinant DNA techniques [12-14]. Tailor-made mini-antibodies might be produced, *i.e.*, against a particular protein according to the following scenario. In hybridoma cells the concentration of immunoglobulin mRNA is relatively high. After hybridization the the RNA of the L or H chain with an oligonucleotide complementary to the constant region, elongation will be possible in the direction of the variable region, *i.e.*, synthesis of cDNA, which then can be sequenced. The amino acid sequence can be deduced from the DNA sequence and the hypervariable segments can be located. In the absence of tertiary structure information, it is then necessary to investigate the binding properties of all six antigen-binding segments. The optimum fragment or combination of fragments can then be used in immunoaffinity chromatography for selective purification of a protein or in immunosensors for detection of a protein.

REFERENCES

- 1 R. A. Lerner, *Nature (London)*, 299 (1982) 592.
- 2 R. L. Stanfield, T. M. Fieser, R. A. Lerner and I. A. Wilson, *Science (Washington, D.C.)*, 248 (1990) 712.
- 3 G. W. Welling, T. Geurts, J. van Gorkum, R. A. Damhof, J. W. Drijfhout, W. Bloemhoff and S. Welling-Wester, *J. Chromatogr.*, 512 (1990) 337.
- 4 M. J. Darsley and A. R. Rees, *EMBO J.*, 4 (1985) 393.
- 5 M. J. Darsley and A. R. Rees, *EMBO J.*, 4 (1985) 383.
- 6 P. de la Paz, B. J. Sutton, M. J. Darsley and A. R. Rees, *EMBO J.*, 5 (1986) 415.
- 7 E. Atherton and R. C. Sheppard, *J. Chem. Soc., Chem. Commun.*, (1985) 165.
- 8 W. J. Weijer, J. W. Drijfhout, H. J. Geerligs, W. Bloemhoff, M. Feijlbrief, C. A. Bos, P. Hoogerhout, K. E. T. Kerling, T. Popken-Boer, K. Slopsema, J. B. Wilterdink, G. W. Welling and S. Welling-Wester, *J. Virol.*, 62 (1988) 501.
- 9 J. C. Wootton, J. G. Taylor, A. A. Jackson, G. K. Chambers and J. R. S. Fincham, *Biochem. J.*, 149 (1975) 739.
- 10 U. K. Laemmli, *Nature (London)*, 227 (1970) 680.
- 11 W. Wray, T. Boulikas, V. P. Wray and R. Hancock, *Anal. Biochem.*, 118 (1981) 197.

- 12 J. S. Huston, D. Levinson, M. Mudgett-Hunter, M.-S. Tai, J. Novotny, M. N. Margolies, R. J. Ridge, R. E. Bruccoleri, E. Haber, R. Crea and H. Oppermann, *Proc. Natl. Acad. Sci. USA*, 85 (1988) 5879.
- 13 R. E. Bird, K. D. Hardman, J. W. Jacobson, S. Johnson, B. M. Kaufman, S.-M. Lee, T. Lee, S. H. Pope, G.S. Riordan and M. Withlow, *Science (Washington, D.C.)*, 242 (1988) 423.
- 14 E. S. Ward, D. Güssow, A. D. Griffiths, P. T. Jones and G. Winter, *Nature (London)*, 341 (1989) 544.

CHROMSYMP. 2144

Effect of antigen size on optimal ligand density of immobilized antibodies for a high-performance liquid chromatographic support

JEFFREY B. WHEATLEY

Rainin Instrument Company, 1780 Fourth Street, Berkeley, CA 94710 (USA)

ABSTRACT

The antigen binding capacities for purified polyclonal antibodies immobilized onto a silica-based high-performance liquid chromatographic (HPLC) affinity support are described for three serum proteins over a range of antibody ligand densities. The rate of decline in the specific activity of the immobilized antibodies with respect to increasing ligand density was found to increase with the molecular weights of the antigens. The antibodies used were purified from whole antiserum using high-performance affinity chromatography and were examined using HPLC on an SCX stationary phase. Conditions are also described for efficient coupling of the ligand to the support.

INTRODUCTION

The binding capacity of an immunoaffinity support is related to the amount of antibody immobilized per gram or milliliter of support. Increasing the specific surface area of the support (area per gram) while maintaining a constant antibody ligand density can result in an increased antigen binding capacity. However, for highly porous particles an increase in surface area is often accompanied by smaller pore diameter. As the pore diameter decreases below certain limits, access to the surface becomes restricted for large molecules. Consequently, maximizing the capacity of a support through an increase in specific surface area must be balanced against the selection of a pore size large enough to permit both sufficient immobilization of antibody and reception of the antigen [1,2]. For a particular immunoaffinity support of defined particle dimensions, optimization of the binding capacity depends considerably on access of the antigen to the binding regions of the immobilized antibodies. Access to the binding sites is influenced by such factors as the molecular orientation of the immobilized antibody molecules and the antibody ligand density in relation to antigen size and pore diameter [3,4]. Also of fundamental importance are the association constants intrinsic to the native antibodies and conditions encountered by the antibodies that can lead to denaturation and loss of binding integrity. These factors arise during the initial purification of the antibody and in the procedures under which the antibody is immobilized onto the support. Denaturation can also result from conditions under which the affinity column is used and stored over time.

It has been shown that the specific activity of immobilized antibodies, expressed as the mole ratio of bound antigen to theoretical antibody binding sites, decreases with increasing ligand density. Eveleigh and Levy [4] found that the mole to mole ratio of bound albumin to antibody decreased with increases in the ligand density of polyclonal anti-human albumin antibody immobilized on cyanogen bromide-activated Sepharose 4B. In a study using a monoclonal antibody for lysozyme, Hearn and Davies [3] reported finding no difference in the specific activities for two antibody ligand densities on cyanogen bromide-activated Sepharose 4B. However, they did observe significant differences for the same antigen-antibody pair on two other porous polymeric supports.

In this study, the effects of increasing ligand density and antigen size on binding capacity were examined for three serum proteins: human IgG immunoglobulin, albumin and α_1 -acid glycoprotein. The binding capacities were measured for polyclonal antibodies immobilized onto Hydropore-EP, a silica-based HPLC affinity support. Conditions are also described for the efficient immobilization of proteins and for the examination of purified antibodies by HPLC on an SCX stationary phase.

EXPERIMENTAL

Materials

Proteins and antisera were obtained from Sigma (St. Louis, MO, USA) and serine methyl ester from Aldrich (Milwaukee, WI, USA). Hydropore-EP (12 μm , 300 Å) and Hydropore-5-SCX (5 μm , 300 Å) are products of Rainin Instrument Co. (Woburn, MA, USA).

Apparatus

Chromatographic and affinity purifications were done using Rainin Rabbit HPLC pumps and Knauer Model 71 and 87 UV detectors from Rainin Instrument Co. Control of pumps, HPLC methods, data acquisition and treatment were accomplished with the Macintosh-based Dynamax HPLC Method Manager from Rainin Instrument Co. Spectrophotometric measurements were made on a Hitachi (San Jose, CA, USA) Model U-2000 scanning spectrophotometer.

Preparation of antigen columns

The antibodies used were purified from whole goat antiserum using high-performance affinity chromatography. Antigen columns were prepared for this purpose by immobilizing the protein, either human IgG immunoglobulin, albumin or α_1 -acid glycoprotein, onto the Hydropore-EP affinity support packed into a 50 \times 4.6 mm I.D. stainless-steel column. This was achieved by recirculating 5–10 mg of protein dissolved at about 1 mg/ml in an ammonium sulfate solution buffered in 0.020 M potassium phosphate (pH 7.0). The solutions were recirculated through the columns at 0.2 ml/min for 16–20 h. Coupling of human IgG and albumin was carried out in 0.75 M ammonium sulfate whereas α_1 -acid glycoprotein was coupled in 2.0 M ammonium sulfate.

Hydropore-EP is derived from porous, spherical silica possessing an average particle diameter of 12 μm and an average pore diameter of 300 Å. The surface of the silica is chemically modified to produce a covalently bound hydrophilic monolayer

possessing epoxide functional groups. The epoxide reacts with nucleophilic groups found in proteins, resulting in covalent immobilization of the protein onto the surface of the support.

Purification of antibodies

The antiserum, diluted 50% in loading buffer, was applied at 0.5 ml/min to the antigen column, which had been pre-equilibrated in 0.15 *M* sodium chloride in 0.010 *M* potassium phosphate (pH 7.0) (loading buffer). The loaded column was washed with loading buffer at 2.0 ml/min until the detector output (at 280 nm) returned to a steady baseline near zero absorbance. The column was then washed at 2.0 ml/min with about 20 column volumes of 0.020 *M* potassium phosphate (pH 7.0). This step, which was performed in order to remove most of the salt, was required for examination of the product by cation-exchange HPLC. After the desalting step, the bound antibodies were eluted with 0.050 *M* potassium phosphate (pH 2.5) at 0.5 ml/min. The product was collected in three fractions, with the middle, concentrated fraction consisting of eluate collected at an absorbance > 1.0 at 280 nm. The pH of the eluate fractions was measured and a sample of the middle fraction was injected onto the cation-exchange column. The pH of the eluate fractions was then adjusted to 6.9–7.2 with 5% sodium hydroxide.

After storage for at least several hours the eluate was centrifuged to remove the small amount of precipitate that invariably appeared. A sample of the middle fraction was then injected onto the antigen column and the concentrations of the eluate fractions were determined from the absorbance at 280 or 230 nm. The middle fraction, typically containing 85% of the eluate protein, was used for binding capacity determinations in all three antigen–antibody systems. The pH of this fraction prior to neutralization ranged from 5.3–5.7 and the protein concentration was between 5 and 10 mg/ml. In Fig. 1 a chromatogram is shown for the injection of goat anti-human

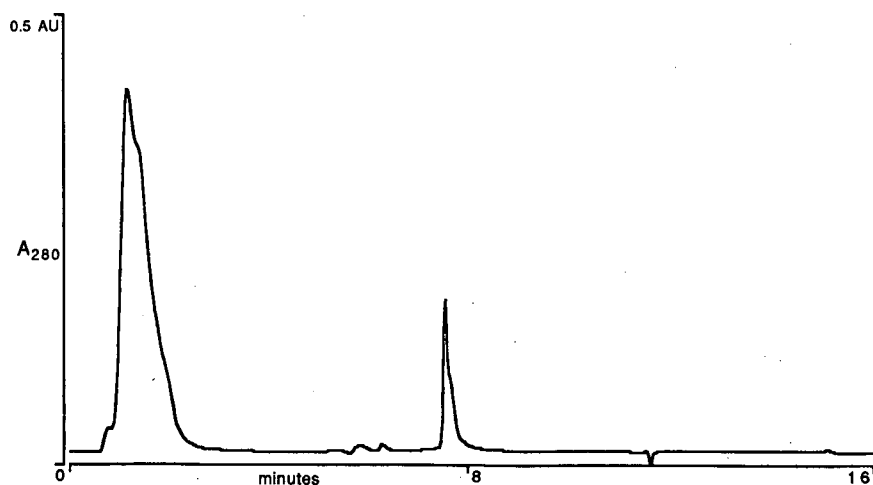


Fig. 1. Goat anti-human albumin antiserum on albumin antigen column. Albumin-specific antibodies are found in the retained band. Column: human albumin immobilized on Rainin Hydropore-EP, 50 × 4.6 mm I.D. Conditions as described in text.

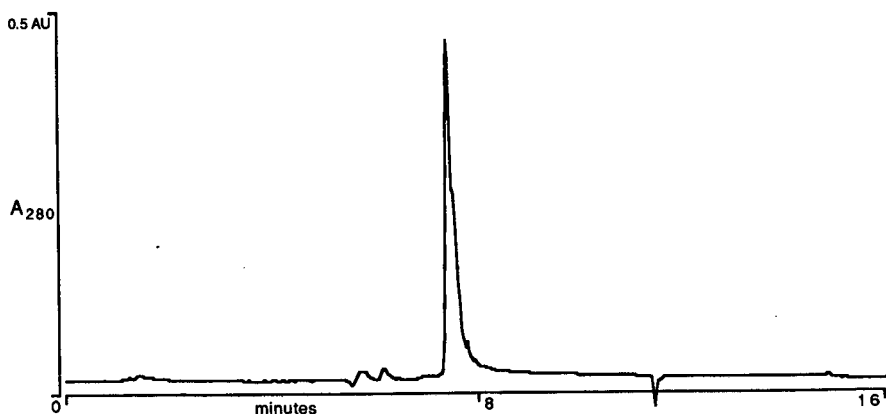


Fig. 2. Purified goat anti-human albumin antibodies injected onto albumin antigen column. Conditions as in Fig. 1.

albumin onto the albumin antigen column. The small retained peak corresponds to antibodies specific for albumin. In Fig. 2 a chromatogram is shown for the injection of the middle fraction of eluate onto the same column, indicating the near absence of the unretained components found in the chromatogram for the whole antiserum.

Measurement of binding capacities and calculations

Purified antibodies were coupled to Hydropore-EP in 0.75 *M* ammonium sulfate buffered in 0.020 *M* potassium phosphate, pH (7.0) according to the following procedure. The antibodies (250–2800 μg) were diluted in 0.020 *M* potassium phosphate; 3.0 *M* ammonium sulfate in 0.020 *M* potassium phosphate was then added to give a concentration of 0.75 *M*. A weighed amount of Hydropore-EP was added to the solution and the mixture was mixed overnight by orbital rotation at room temperature. Most mixtures contained 25 mg of support in a volume of 400 μl . For some samples possessing higher levels of immobilized antibody, the coupling mixture contained either 10 or 25 mg of support in volumes up to 2.5 ml.

The derivatized support was thoroughly washed in phosphate-buffered saline (PBS) (pH 7.0) and mixed overnight in 0.20 *M* serine methyl ester (pH 8.5) to deactivate any unreacted epoxide groups. After thoroughly washing with PBS (pH 7.0), the support was then mixed with an excess of the appropriate antigen for 2 h in PBS (pH 7.0), washed thoroughly with PBS and eluted with 0.10 *M* glycine (pH 2.5). In separate experiments, highly derivatized support was washed in 0.10 *M* sodium acetate containing 0.40 *M* sodium chloride (pH 4.8). Examination of this wash and the serine methyl ester solution following deactivation revealed the presence of only insignificant amounts of IgG.

The amount of antibody bound to the support in the coupling step was determined from the difference between the amount of antibody initially added and that recovered in the post-coupling wash. This and the antigen in the eluate were calculated from their absorbance at either 280 or 230 nm. Absorptivities for 280 nm were taken from the literature, and those for 230 nm were calculated from A_{230}/A_{280} ratios. Molar amounts for antigens and antibodies were based on reported molecular weight values.

The fraction of the theoretical capacity was calculated according to the equation

$$S.A. = \text{mol Ag}/2(\text{mol Ab})$$

where *S.A.* is the specific activity and Ag and Ab refer to antigen bound and antibody immobilized, respectively. If each antibody molecule is assumed to possess two binding sites, a specific activity of 1.0 would indicate that all binding sites are occupied. The purified antibodies used in this study were assumed to be exclusively IgG for the purposes of the study. In point of fact they may have contained small amounts of other immunoglobulin classes.

RESULTS

Immobilization of proteins onto the support

In Fig. 3, the plot of percentage protein coupling *versus* ammonium sulfate concentration determined under static conditions for goat IgG and human α_1 -acid glycoprotein shows that the percentage coupling increases with increasing salt concentration. Virtually complete immobilization was achieved for both proteins, occurring at 0.8 M for goat IgG and at 2.0 M for α_1 -acid glycoprotein. In the preparation of the human IgG and α_1 -acid glycoprotein antigen columns, which was carried out by recirculating the protein in salt concentrations of 0.75 and 2.0 M, respectively, >95% immobilization of protein occurred. The coupling efficiency for the albumin immobilization was found to be 42% at 0.75 M ammonium sulfate. Based on the trend seen in Fig. 3, the efficiency of albumin immobilization would probably have benefitted from the use of a higher concentration.

Immobilization of purified goat anti-human serum protein antibodies in 0.75–0.85 M ammonium sulfate routinely resulted in coupling efficiencies >90% for antibody ligand densities up to *ca.* 50–60 mg/g support. At higher densities the coupling efficiency decreased. For the most highly derivatized support (114 mg/g), 71% coupling was found (data not shown).

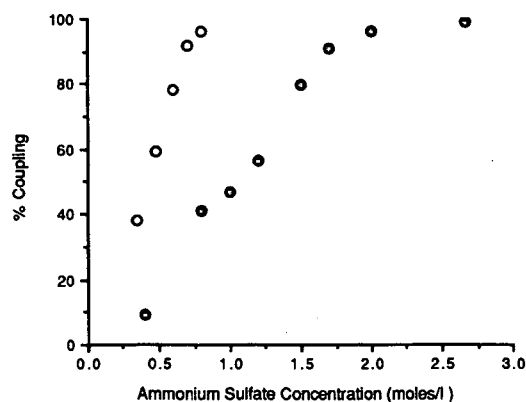


Fig. 3. Percentage protein coupling to Hydropore-EP vs. ammonium sulfate concentration. \circ = Goat IgG; \bullet = human α_1 -acid glycoprotein.

Examination of purified antibody on the SCX stationary phase

In Fig. 4 a chromatogram is shown for the injection of whole goat anti-human albumin antiserum onto the sulfopropyl cation-exchange column, using conditions under which IgG is retained and most proteins show early elution. Fig. 5 shows a chromatogram for the injection of goat IgG and in Fig. 6 a chromatogram is shown for the injection of eluate obtained from the purification of anti-albumin antibodies from the antiserum. The chromatogram for the purified eluate indicates a near absence of the early eluting bands seen in the whole antiserum. Although the possibility cannot be excluded that some serum components could be co-eluting in the retained (antibody) band, the absence of early eluting bands and the minimal presence of unretained components in the chromatogram for the injection of the purified eluate onto the antigen column (Fig. 3) suggest that the eluate consists of antigen-specific antibodies. The chromatograms included here are typical of those obtained for other purifications.

Antibody binding capacities and specific activity

The binding capacities for albumin and α_1 -acid glycoprotein, expressed as milligrams of antigen bound per milligram of immobilized antibody per gram of support, are shown in Fig. 7 and those for IgG in Fig. 8. The antigen binding capacity is linear for all three proteins at low ligand densities. However, as the ligand density increases, the increases in capacity fall off for albumin and IgG. The capacity for α_1 -acid glycoprotein appears to be linear through the highest ligand density examined in this study. The increases in capacity for albumin fall off gradually, and the IgG binding capacity appears to change suddenly, from a linear increase to an actual decline in capacity.

Fig. 9 shows the antigen binding capacities for the three proteins, expressed as micromoles of antigen bound per micromole of immobilized antibody per gram of

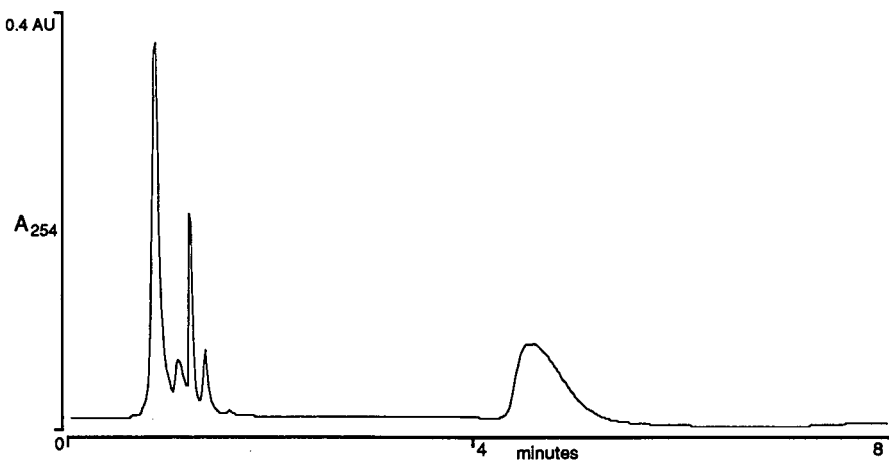


Fig. 4. Goat anti-human albumin antiserum on SCX. The retained peak corresponds to goat IgG as seen in Fig. 5. Column: Hydropore-5-SCX, 100 × 4.6 mm I.D. Conditions: 0–3 min, 0% B, 1 ml/min; 3–6 min, 0–100% B, 2 ml/min; A = 0.02 M potassium phosphate (pH 5.9) and B = 1.0 M sodium chloride in A; detection at 254 nm, 0.4 a.u.f.s.

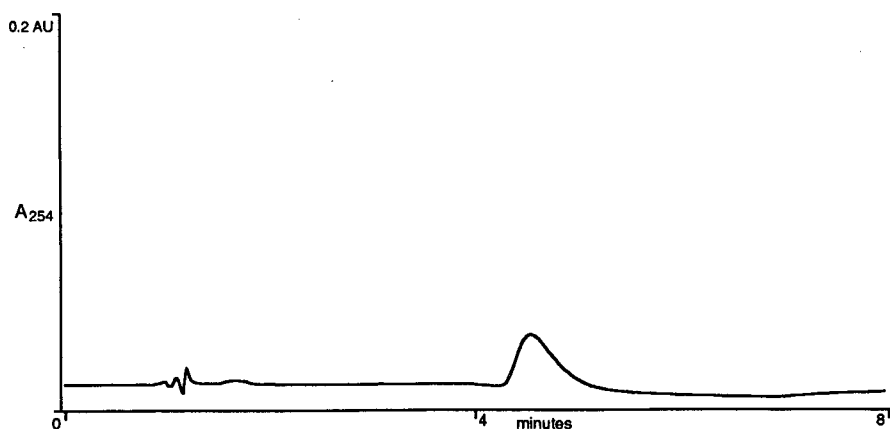


Fig. 5. Goat IgG on SCX. Column and conditions as in Fig. 4.

support, and provides a comparison of antigen binding efficiencies with increasing antibody ligand density. The three antigens show comparable binding efficiencies at low ligand densities. The efficiencies appear to remain fairly linear for both albumin and α_1 -acid glycoprotein throughout the range of ligand densities examined. IgG reflects the trend seen in the previous figures, with the efficiency falling off relatively early and suddenly.

Fig. 10 is derived from the data in Fig. 9 and provides a more sensitive indication of individual and comparative efficiencies. In this graph binding of antigen is expressed as a fraction of the theoretical maximum, where 1.0 would indicate that all antibody binding sites are occupied. The efficiency of α_1 -acid glycoprotein appears to be steady at *ca.* 27% of the theoretical value; for albumin it decreases from about

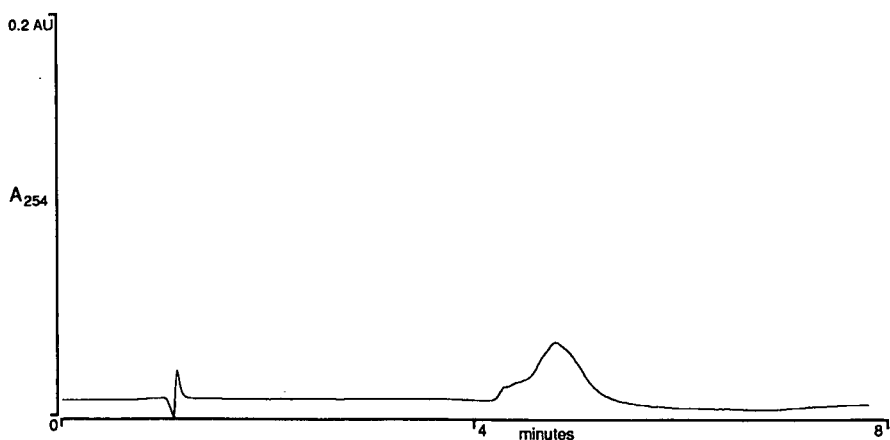


Fig. 6. Purified anti-human albumin antibodies on SCX. The retained band corresponds to goat IgG as seen in Fig. 5. The refractive index peak seen at the void volume is due to differences in the salt content between the sample and mobile phase. Column and conditions as in Fig. 4.

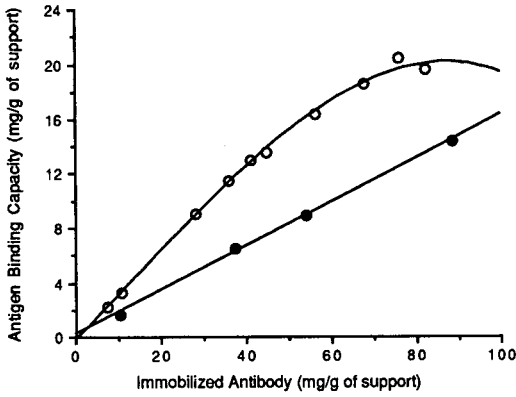


Fig. 7. Binding capacity of albumin and α_1 -acid glycoprotein vs. immobilized antibody density in mg per gram of support. \circ = Human albumin; \bullet = human α_1 -acid glycoprotein.

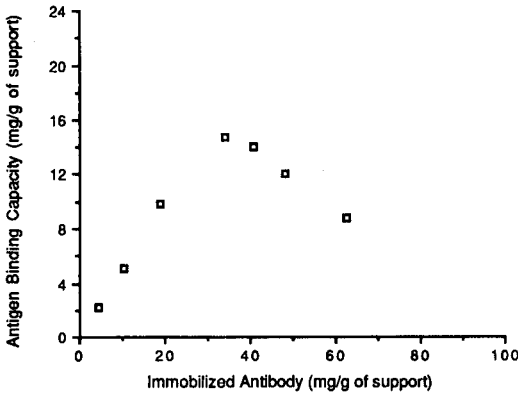


Fig. 8. Binding capacity of human IgG vs. immobilized antibody density in mg per gram of support.

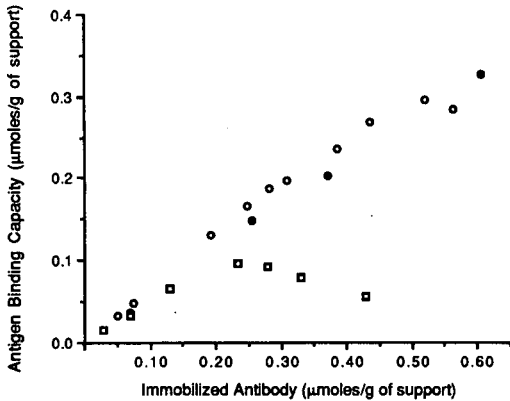


Fig. 9. Binding capacity vs. immobilized antibody density in μ mol per gram of support. \circ = Human albumin; \square = human IgG; \bullet = human α_1 -acid glycoprotein.

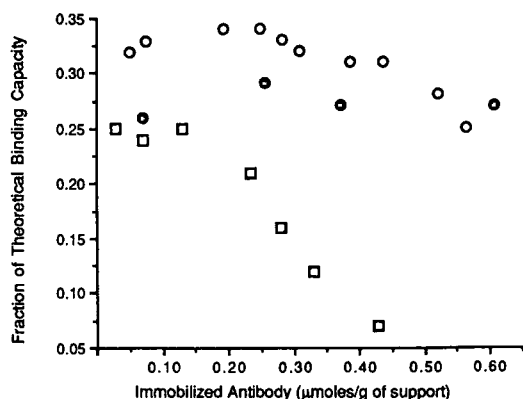


Fig. 10. Fraction of theoretical binding capacity vs. antibody ligand density. ○ = Human albumin; □ = human IgG; ● = human α_1 -acid glycoprotein.

33% to 25% and for IgG it falls from 25% to only 7% at high ligand densities. Overall, albumin appears to experience the highest efficiency, but it can be seen to decrease, beginning about half-way along the ligand density range. Binding of α_1 -acid glycoprotein shows a lower efficiency than that of albumin, but it remains steady throughout the range. The IgG binding efficiency appears to be no greater than that of α_1 -acid glycoprotein at any ligand density, and rapidly falls to low levels.

DISCUSSION

It was found that the efficiency with which antibodies, and proteins in general, couple with the epoxide groups of Hydropore-EP is favored at relatively high salt concentrations. This has been observed both with ammonium sulfate and potassium phosphate and probably results from an improved proximity of the reactive groups due to salt-induced association between the protein and support surface. This effect is similar to that seen for hydrophobic interaction chromatography (HIC) [5-8]. It has been shown [9] that for injections of human albumin and human γ -globulin onto a polyether stationary phase under HIC conditions γ -globulin is strongly retained whereas albumin exhibits early elution. This indicates that γ -globulin is more susceptible to salt-induced surface associations, which is consistent with the coupling results obtained here for human IgG and albumin, in which immobilization of IgG was nearly complete at 0.75 M whereas only 42% of albumin was immobilized. The salt concentration required for efficient immobilization of albumin would probably be similar to that needed for α_1 -acid glycoprotein, which required about 1.9 M ammonium sulfate for 95% coupling (Fig. 3). Although it has been reported that epoxide-type affinity supports exhibit low reactivity at neutral pH [10], the measurements described in this study and performed in other contexts indicate that the utilization of a sufficiently high salt concentration will result in highly efficient immobilization of proteins to this support.

The increased coupling efficiency found at high salt concentrations could result from several factors. Salt-induced partitioning of the protein along the surface of the support would lead to localized concentration of the protein near epoxide groups,

possibly resulting in an increased reaction rate between nucleophilic residues and the epoxide. A downward shift in the pK of nucleophilic side-chains, resulting from a salt-induced hydrophobic association between the protein and support surface, would also increase the reaction rate by increasing the concentration of the unprotonated, reactive form of the nucleophile. Shifts in dissociation constants, thought to result from effects of the local environment of the side-chains, have been reported to occur in some proteins [11,12]. In one study a pK of 5.9 was assigned to a lysine residue in acetoacetate decarboxylase [11], representing a downward shift of more than four units from the value usually associated with the ϵ -amino group. Finally, proteins localized on the surface could provide a proton source for general acid catalysis of the epoxide.

The gradual decrease in specific activity observed for binding of albumin (mol.wt. 69 000) and the absence of any change for α_1 -acid glycoprotein (mol.wt. 44 000) can be compared with the stronger decline seen for IgG (mol.wt. 153 000). The relative rates of decline in specific activity with molecular weight suggest that the approach to ligand binding sites is more restricted for larger antigens. This is further supported by the observation that the specific activity first begins to decline at a lower ligand density for IgG than for albumin. These results suggest that as the molecular weight (size) of the antigen is increased, the ligand density at which the initial drop in specific activity is observed should decrease. An increase in the pore size would be expected to shift this threshold to a higher ligand density. However, as increasing pore size is accompanied by reductions in specific surface area, the absolute capacity could be expected to fall. This kind of trade-off was discussed by Narayanan *et al.* [1] for the immobilization of proteins on silica-based supports of increasing pore diameter. It would be interesting to measure the threshold and rate of decline in specific activity for the binding of a wider (molecular weight) range of antigens in order to examine the correlation of these factors. Although it is tempting to contrast the binding efficiencies for IgG and albumin at the lower ligand densities (25% versus 33%, respectively), the fact that the antibodies for the two systems were derived from different sources precludes comparisons, as has been pointed out by Eveleigh and Levy [4].

The most dramatic effect of antibody ligand density on capacity was seen for IgG, which showed not only early changes in linearity but also significant declines in absolute capacity for the higher ligand densities. The capacity per gram of support dropped from a maximum of about 15 mg for 34 mg of immobilized antibody to 9 mg for 62 mg of ligand, a decline of 40%. Similar observations have been reported by other investigators for an immobilized monoclonal antibody to tissue plasminogen activator [13]. In this study, actual declines in capacity were not observed for α_1 -acid glycoprotein. At the highest ligand density examined for albumin a slight drop in capacity was seen, but more data are required for confirmation. The question arises of whether decreases would occur for albumin and α_1 -acid glycoprotein capacities at ligand densities beyond those examined in this study and how steeply such declines might be in comparison with that seen for IgG. Although the maximum ligand density for IgG on Hydropore-EP was not measured, the moderate decline in coupling efficiency observed at the highest density examined (71% for 116 mg/g) suggests that a limit is being approached.

In conclusion, these findings suggest that in optimizing conditions for immu-

noaffinity applications, the size of the antigen should be considered in selecting the ligand density. The protocol used for the preparation of an immunoaffinity support for one kind of application may not be appropriate for another. Whereas in some instances ligand densities resulting in less than maximum binding efficiency might be acceptable in order to increase absolute capacities, in no event should the ligand densities exceed values that result in a decrease in capacity.

ACKNOWLEDGEMENT

Dr. Donald E. Schmidt is thanked for valuable suggestions on the preparation of the manuscript.

REFERENCES

- 1 S. R. Narayanan, S. Knochs, Jr., and L. J. Crane, *J. Chromatogr.*, 503 (1990) 93–102.
- 2 D. Wu and R. R. Walters, *J. Chromatogr.*, 458 (1988) 169–174.
- 3 M. W. Hearn and J. R. Davies, *J. Chromatogr.*, 512 (1990) 23–39.
- 4 J. W. Eveleigh and D. E. Levy, *J. Solid Phase Biochem.*, 2 (1977) 67–80.
- 5 W. R. Melander, D. Corradini and Cs. Horvath, *J. Chromatogr.*, 317 (1984) 67–85.
- 6 J. L. Fausnaugh, L. A. Kennedy and F. E. Regnier, *J. Chromatogr.*, 317 (1984) 141–155.
- 7 S. Wu, K. Benedek and B. L. Karger, *J. Chromatogr.*, 359 (1986) 3–17.
- 8 R. Hatch, *J. Chromatogr. Sci.*, 28 (1990) 210–214.
- 9 N. T. Miller, B. Feibush and B. L. Karger, *J. Chromatogr.*, 316 (1985) 519–536.
- 10 K. Ernst-Cabrera and M. Wilchek, *Trends Anal. Chem.*, 7 (1988) 58–63.
- 11 D. E. Schmidt and F. H. Westheimer, *Biochemistry*, 10 (1971) 249–253.
- 12 J. R. Knowles, *CRC Crit. Rev. Biochem.*, 4 (1976) 165–173.
- 13 R. S. Matson and M. C. Little, *J. Chromatogr.*, 458 (1988) 67–77.

CHROMSYMP. 2215

Affinity of trypsin for amidine derivatives immobilized on dextran-coated silica supports

M. ELLOUALI, S. KHAMLICH, J. JOZEFONVICZ and D. MULLER*

L.R.M., C.N.R.S.-URA 502, Université Paris-Nord, Avenue J. B. Clément, 93430 Villetaneuse (France)

ABSTRACT

The pancreas contains two very analogous enzymes: trypsin and chymotrypsin. These two enzymes are very similar in their physicochemical characteristics and are therefore quite difficult to separate by classical purification procedures. They constitute a good model for affinity chromatography. It was previously demonstrated that amidine derivatives are able to interact strongly and specifically with these serine proteases and are often used as ligand in affinity chromatography. To understand the trypsin interaction mechanism, we synthesized different amidines and immobilised them with or without spacer arm on silica beads previously coated by dextran substituted with a calculated amount of positively charged diethylaminoethyl functions, in order to minimize the non-specific interactions of silanol groups of the silica material. First the affinity constant and the adsorption capacity of these supports for trypsin were determined in batch procedures, then they were used in affinity chromatography. The effects of ionic strength, pH and competitive inhibitors on proteins desorption were also studied. Last, to demonstrate the importance of passivation, the chromatographic performances of dextran-coated silica phases and a commercial support grafted with the same amidine were compared.

INTRODUCTION

The purification of biomolecules and proteins of therapeutic or commercial interest generally involves a combination of different steps, in particular, precipitation steps using solvents, salts or pH and chromatographic procedures. Each step has a relatively low specificity. Affinity chromatography could be used on a large scale in order to remove the remaining impurities. As well as its technological interest, it is also a good tool for a better understanding of the interaction mechanism between proteins and the active phase.

Benzamidine derivatives are strong and specific serine protease inhibitors [1,2]. It is claimed that the amidine group mimics the cationic side-chain of arginine and lysine binding sites of the protein substrates. Previously, Hixon and Nishikawa [2] used *m*-aminobenzamidine linked via a monosuccinylated-1,6-diaminohexane spacer to cyanogen bromide (CNBr)-Sepharose to purify bovine trypsin. Jameson and Elmore [3] prepared affinity adsorbents for bovine trypsin by covalently coupling *p*-(*p*'-aminophenoxypropoxy)benzamidine to cellulose and agarose and used these supports to separate α - and β -trypsins. The trypsin interaction mechanism with these amidine derivatives is still unknown. Trypsin is obtained in crystalline form from beef

pancreas by the method of Northrop and Kunitz [4]. Further work [5] has improved methods of preparation and has established that the transformation of trypsinogen into trypsin is a proteolytic process and may be accomplished either by autocatalysis or by enterokinase, or by the kinase from a mould of the genus *Penicillium*. The primary structure of bovine trypsin has not yet been completely established [6]. It is a single-chain structure of 226 amino acid residues, cross-linked by six disulphide bridges [7]. Many studies [8,9] have demonstrated that Ser 195, His 57 and Asp 102 residues are important in the trypsin catalytic site and represent a charge relay system in which the serine hydroxyl is acylated by the substrate. The binding site is presumably in the form of a crevice which binds the carbon side-chains or rings of substrates and inhibitors by hydrophobic interactions. The bottom of this crevice contains a negatively charged aspartic acid (Asp 189) which binds electrostatically to the positively charged groups of substrates or inhibitors [6,10].

In this paper, we describe the preparation of coated silica supports bearing different types of trypsin inhibitors. First, affinity constants and binding capacities from adsorption isotherms of these supports for trypsin were determined using batch procedures. Then, the active supports were used in affinity chromatography to study the specific interactions between the amidine function and the trypsin in solution. Finally, in order to demonstrate the importance of passivation, the chromatographic performances of a dextran-coated silica phase and of a commercial support grafted with the same amidine were compared.

EXPERIMENTAL

Reagents

Silica beads provided by IBF Bio-technics (Villeneuve la Garenne, France) were in the range of 40–100 μm and the pore diameter was about 1250 Å. *p*-Aminobenzamidine (pABA) and L-arginine monohydrochloride were provided by Fluka (Buchs, Switzerland). Guanidium carbonate was purchased from Prolabo (Paris, France). 1,1'-Carbonyldiimidazole (CDI) used as coupling agent, was provided by Sigma (St. Louis, MO, USA). 1,4-Butanediol diglycidyl ether (BDGE) was provided by Polysciences (Warrington, PA, USA). Dextran T40 [weight-average molecular weight (\bar{M}_w) 42 000; number-average molecular weight \bar{M}_n 24 700; $I = \bar{M}_w/\bar{M}_n = 1.70$] was obtained from Pharmacia-France (Bois d'Arcy, France).

The commercial support was Nugel Benzamidine (Si-pABA) obtained from Separation Industries Diagnostic Specialties (Metuchen, NJ, USA). The particle size was in the range 40–60 μm and the porosity of the support was 500 Å. The pABA was coupled to the activated support Nugel-polyhydroxyl via an hydrophic spacer arm of eight carbons [2].

N-Benzoyl-L-arginine-4-nitroanilid hydrochloride (L-BAPA) as trypsin substrate was purchased from Merck-Clevenot (Nogent-sur-Marne, France).

Bovine trypsin (type I), with a specific activity of 13.8 U BAEE per mg of protein [one unit of BAEE producing a ΔA_{253} of 0.001 per min at pH 7.6 at 25°C using N-benzoyl-L-arginine ethyl ester (BAEE) as substrate, reaction volume 3.2 ml] was obtained from Sigma.

Preparation of affinity supports

Passivated silica beads (SiD). Silica beads were coated with dextran polymers substituted with a calculated amount of DEAE to minimize the non-specific interactions due to silanol groups of the silica surface as previously described [11].

The percentage of dextran units substituted by diethylaminoethyl (DEAE) functions is 4%. Passivated silica beads were coupled with different types of amidine or guanidine as follows.

Coated silica functionalized by L-arginine (SiD-Arg) (Fig. 1). SiD (2 g) was suspended in 20 ml of 1,4-dioxane and mixed with 1 g of CDI. The gel suspension was gently shaken at room temperature for 3 h. The activated support was then washed successively with 200 ml of 1,4-dioxane and 200 ml of 0.1 M carbonate buffer (pH 10.5), and then resuspended in 20 ml of carbonate buffer containing 500 mg of L-arginine monohydrochloride. The mixture was gently stirred at room temperature for 48 h and the support obtained was filtered and washed successively with 200 ml of 0.1 M carbonate buffer, 0.1 M NaCl (pH 10.5) and 200 ml of 0.05 M phosphate buffer (pH 7.5). The excess of activated groups was neutralized by suspending the support in 0.1 M ethanolamine solution for 3 h. The final support was washed with 200 ml of phosphate buffer (pH 7.5), filtered and dried under vacuum at 40°C.

Coated silica functionalized by pABA (SiD-pABA) (Fig. 1). The coupling procedure was realised in conditions similar to SiD-Arg: 500 mg of pABA were left to react with the activated support.

Coated silica functionalized by pABA using a spacer arm (SiD-B-pABA) (Fig. 1). The synthesis of this support was described previously [12]. Briefly, 2 g of SiD were suspended in 20 ml of diethyl ether and 2 ml of BDGE were added. The suspension was gently stirred for 15 h at room temperature and the activated support was washed successively with 200 ml of diethyl ether, and 200 ml of 0.1 M carbonate buffer (pH 10.5). After filtration, it was suspended in 20 ml of 0.1 M carbonate buffer

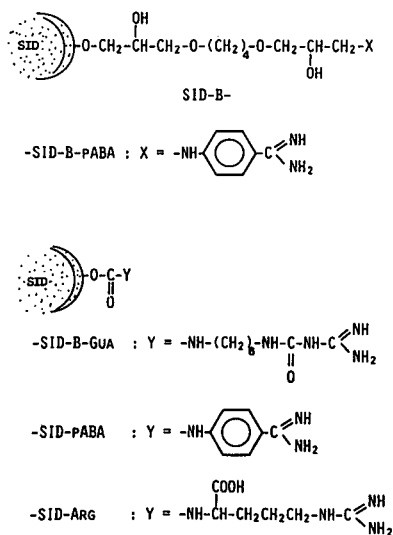


Fig. 1. Structures of the active supports.

(pH 10.5) containing 256 mg of pABA in solution. The mixture was stirred at room temperature for 48 h and the final support was washed and filtered according to the method used for the activated support SiD-Arg.

Coated silica functionalized by guanidine (SiD-B-Gua) (Fig. 1). The coupling reaction of guanidine to the SiD support was described previously [12]. The step of support activation was similar to that already described for the SiD-Arg support. The activated support was then suspended in 20 ml of 0.1 M carbonate buffer solution (pH 10.5) containing 1.5 g of hexamethyldiamine (HMD). The mixture was gently stirred at room temperature for 48 h and then, the support was washed successively with carbonate buffer and 1,4-dioxane. The amine functions of HMD fixed on the support were activated by CDI (1 g of CDI per 2 g of support) and the activated support was then suspended with 1 g of guanidinium carbonate dissolved in 20 ml of 0.1 M carbonate buffer (pH 10.5). The mixture was stirred at room temperature for 48 h. Finally, the support was washed with 0.05 M phosphate buffer and dried under vacuum at 60°C.

Characterization of the functionalized coated silica beads. For each support, the substitution rate of amidine derivatives was determined by acidimetric titration and by elemental analysis (Service Central d'Analyse, CNRS, Vernaison, France). The preparation technique of these derivatisable supports is easy in comparison with the coupling reactions previously reported [2,13] and provides silica supports with a minimum non-specific adsorption of proteins in high-performance liquid affinity chromatography (HPLAC). The passivation of the silica phases is observed by the determination of elution conditions of several proteins with different *pI* values at low ionic strength (phosphate buffer 0.05 M, pH 7.5, NaCl 0.15 M) in high-performance size-exclusion chromatography [14].

Adsorption isotherms procedure of trypsin

Adsorption experiments were performed at room temperature. Isotherms are generated from measurements of trypsin adsorption after 20 min incubation with the active support using the following procedure.

The trypsin concentration varied from 5 to 60 µg/ml; 100 µl of support suspension (20–100 mg/ml) were incubated with 500 µl of bovine trypsin solution at various concentrations in a polystyrene tube for 20 min. After decantating, the amount of residual trypsin in the supernatant was determined by taking 100 µl of this supernatant and adding 700 µl of 0.05 M phosphate buffer containing 0.1 M NaCl (pH 7.5) and 100 µl of the trypsin chromogenic substrate L-BAPA. After adding trypsin, the reaction was stopped after 10 min at 37°C by addition of 100 µl of pure acetic acid. The difference between the control and the remaining concentration of active trypsin in the supernatant corresponds to the amount of trypsin adsorbed. Concentrations of trypsin were determined by reading the absorbance at 405 nm. Isotherms were established and affinity constants were determined using a computer program on the basis of the Langmuir and Tempkin equations [15].

In order to determine the adsorption enthalpy of trypsin on these supports, we established adsorption isotherms at two supplementary temperatures, 37 and 4°C.

Chromatographic assay.

Chromatographic assays were performed on the two supports, SiD-pABA and

the commercial Si-pABA support grafted with the same amidine. These two supports were used in HPLAC according to the following procedure.

The column (12.5 cm \times 0.4 cm I.D) was packed using a slurry method with a suspension of 1 g of resin in the eluent. The liquid chromatographic apparatus consists of a three-head (120°C) chromatographic pump (Merck LC 21B), connected to a Rheodyne 7126 injection valve (sample loop 100 μ l). A Merck-IC 313 variable-wavelength UV-visible detector and the gradient system are connected to a Epson QX-10 computer. The chromatographic signal details are monitored, integrated and stored by the computer. All the equipment was provided by Merck-Clevenot. (Nogent-sur-Marne, France).

All eluents were prepared from high-purity water (ELGA, Villeurbanne, France), degassed and filtered through a Millipore HA 0.22- μ m membrane (Velizy, France).

Trypsin (2 mg) was dissolved in 1 ml of 0.05 M phosphate buffer containing 0.1 M sodium chloride (pH 7.5) (buffer 1) and 100 μ l of this solution were applied to a column of immobilized pABA support equilibrated with buffer 1. The column was washed with buffer 1 and adsorbed trypsin was eluted with 0.05 M phosphate buffer containing 0.1 M sodium chloride (pH 2) (buffer 2) or using buffer 1 containing arginine or guanidine as competitive inhibitors at varying concentrations. Assays were also performed using buffer 1 containing various concentrations of NaCl (buffer 3). The amount of trypsin desorbed was determined from the surface area of the peak given by the computer.

RESULTS AND DISCUSSION

Trypsin adsorption isotherms

In preliminary experiments it was ascertained that steady-state trypsin adsorption was achieved in about 10 min at room temperature. Therefore a time of 20 min was chosen for the determination of the isotherms, which are presented in Figs. 2 and 3. The affinity of these supports was studied by determining the affinity constants from Langmuir or Tempkin adsorption isotherms. The affinity constants of these supports are about $10^6 M^{-1}$ (Table I). These values demonstrate a strong affinity of all these supports for bovine trypsin. SiD-pABA and SiD-B-pABA supports exhibit affinity constants in the same range. This indicates that the spacer arm has no real influence on the bovine trypsin adsorption process. SiD-Arg and SiD-B-Gua supports also show a similar affinity for trypsin. All the supports functionalized with amidine or guanidine groups possess similar affinity constant values. Among synthesized supports, SiD-pABA demonstrates the highest binding capacity, which is probably due to the suitable coupling reaction. The binding capacity of the commercial support is higher than that observed for the SiD-pABA support. This may be explained by the presence of non-specific trypsin adsorption on this commercial support or by a lower availability of the ligand on the SiD-pABA support. This demonstrates the importance of passivation of the inorganic material by the polysaccharide coating, which minimizes the non-specific adsorption of proteins. The other supports, SiD-B-pABA, SiD-Arg and SiD-B-Gua, show a lower binding capacity. This could be due to the lower amount of ligand coupled on these supports or to the fact that ligands fixed on these supports are not really available for interaction with the enzyme in solution.

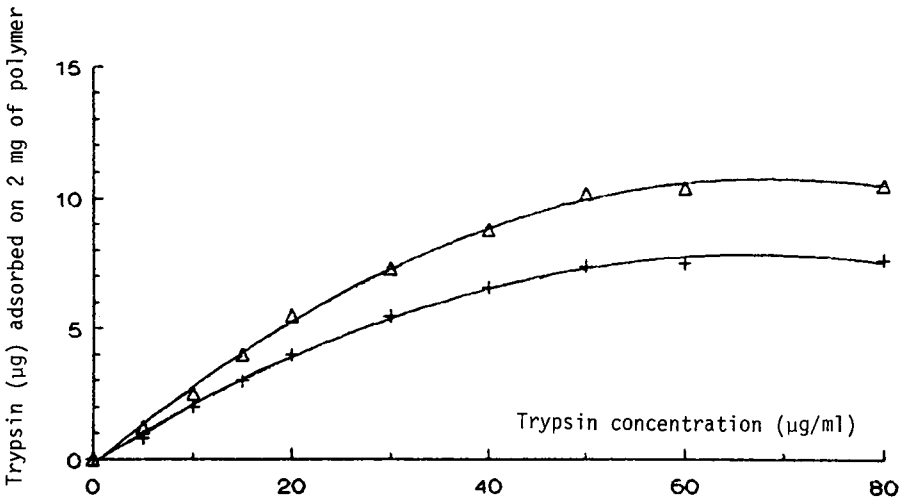


Fig. 2. Adsorption isotherms of bovine trypsin on SiD-pABA (+) and commercial support Si-pABA (Δ).

The affinity constants decrease with temperature (Table II). If we assume that trypsin does not present any structural changes which affect adsorption in the temperature range 4–37°C, we can estimate the trypsin adsorption enthalpy using the relation $\ln K_{\text{Aff}}/dT = \Delta H_{\text{ads}}^0/RT^2$ where K_{aff} is the affinity constant, ΔH_{ads}^0 is the enthalpy of adsorption and T is the temperature. The overall binding process for each support is endothermic with ΔH_{ads}^0 around 4.5 kcal/mol for all the supports except SiD-B-pABA, which presents a higher ΔH_{ads}^0 value. This higher ΔH_{ads}^0 value may be explained by the presence of a spacer arm which facilitates the access of the ligand to the binding site of the enzyme.

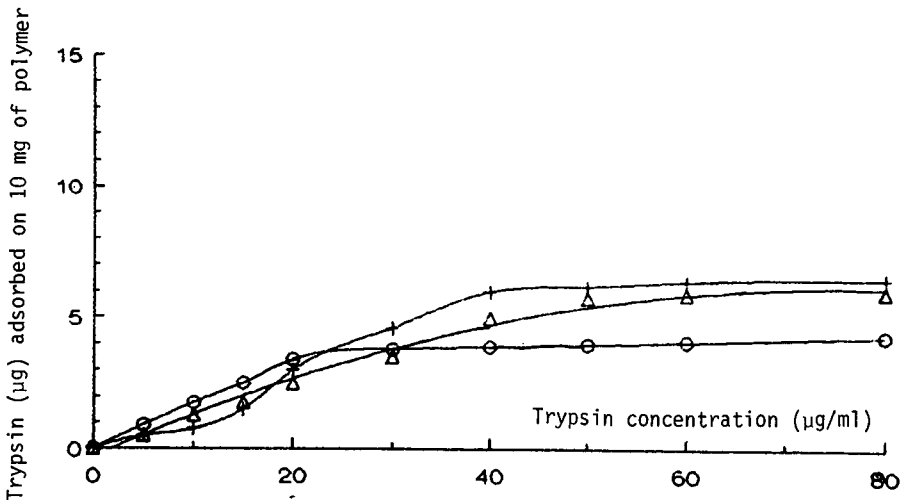


Fig. 3. Adsorption isotherms of bovine trypsin on SiD-B-pABA (+), SiD-Arg (Δ) and SiD-B-Gua (O).

TABLE I

AFFINITY CONSTANTS AND BINDING CAPACITIES OF PASSIVATED SILICA BEADS FUNCTIONALIZED BY AMIDINE DERIVATIVES TO BOVINE TRYPSIN

T = Tempkin isotherm; L = Langmuir isotherm.

Material	Isotherm	Affinity constant (M^{-1})	Binding capacity	
			$\mu\text{g/g}$	mol/g
Si-p-ABA	T	$1.5 \cdot 10^6$	810	$35 \cdot 10^{-9}$
SiD-pABA	T	$3.7 \cdot 10^6$	550	$23 \cdot 10^{-9}$
SiD-B-pABA	T	$2.6 \cdot 10^6$	73	$3.1 \cdot 10^{-9}$
SiD-Arg	T	$1.1 \cdot 10^6$	65	$2.8 \cdot 10^{-9}$
SiD-B-Gua	L	$1.2 \cdot 10^6$	40	$2.5 \cdot 10^{-9}$

HPLAC

The SiD-pABA support presents a high binding capacity for trypsin and can easily be used in affinity chromatography to study the trypsin adsorption process. The chromatographic performances of this support were compared to those of the commercial one. In order to understand the trypsin interaction mechanism with these supports, the enzyme was eluted with solutions of different physicochemical characteristics, and the influence of ionic strength, competitive effects and pH was studied.

Influence of arginine and guanidine. The elution of trypsin with arginine and guanidine in solution at different molarities is presented in Fig. 4. Trypsin desorption from the stationary phase is allowed by the competition between arginine or guanidine and the coupled amidine derivatives. As shown in this figure all the trypsin adsorbed on SiD-pABA is eluted with a 0.5 M arginine or guanidine solution. The same profile is obtained with these two substances. This indicates that probably the same type of interactions occur between trypsin and the two competing substances.

TABLE II

ENTHALPY OF ADSORPTION FOR TRYPSIN BINDING TO AMIDINE DERIVATIVES COUPLED ON PASSIVATED SILICA BEADS DETERMINED FROM ADSORPTION ISOTHERMS AT 4, 21 AND 37°C

Material	Temperature (°C)	Affinity constant (M^{-1})	Enthalpy of adsorption (kcal/mol)
Si-pABA	37	$1.7 \cdot 10^6$	4.5
	21	$1.5 \cdot 10^6$	
	4	$0.7 \cdot 10^6$	
SiD-pABA	37	$4.1 \cdot 10^6$	4.7
	21	$3.7 \cdot 10^6$	
	4	$1.8 \cdot 10^6$	
SiD-B-pABA	37	$4.1 \cdot 10^6$	7.7
	21	$2.6 \cdot 10^6$	
	4	$1 \cdot 10^6$	
SiD-Arg	37	$1.5 \cdot 10^6$	4.2
	21	$1.1 \cdot 10^6$	
	4	$0.5 \cdot 10^6$	

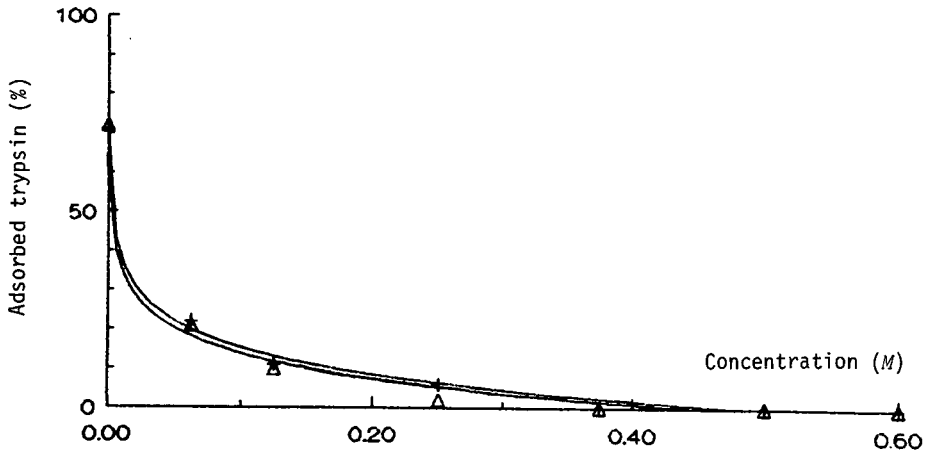


Fig. 4. Elution of bovine trypsin on SiD-pABA support by arginine (+) and guanidine (Δ) in HPLAC. Elution conditions: column, 12.5×0.4 cm; 0.05 M phosphate buffer, 0.1 M NaCl (pH 7.5) containing the competing substance at various concentrations; flow-rate, 1 ml/min.

Influence of ionic strength. Elutions of trypsin adsorbed on SiD-pABA and Si-pABA supports with solutions of sodium chloride at different molarities are presented in Fig. 5. Trypsin is adsorbed at low ionic strength and cannot be desorbed by increasing the ionic strength of the eluent. This observation is valid for these two supports. This result demonstrates that the interactions between trypsin and the supports functionalized with pABA are complex and are not only due to the ionic interactions taking place between the positively charged amidine function fixed on the support and the negatively charged carboxylic function of the aspartic acid 189 residue of the trypsin primary binding site. We must suppose the existence of different

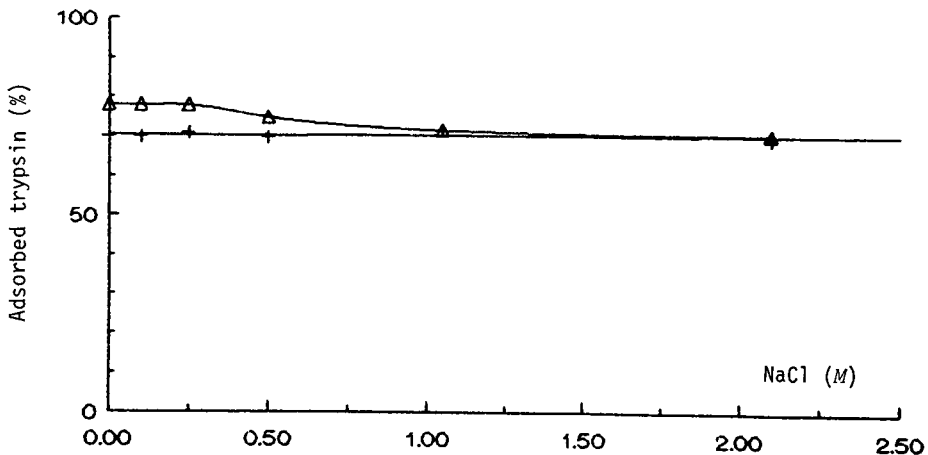


Fig. 5. HPLAC elution of bovine trypsin adsorbed on SiD-pABA (+) and Si-pABA (Δ) supports by sodium chloride. Elution conditions: column, 12.5×0.4 cm; 0.05 M phosphate buffer containing NaCl at various concentrations (pH 7.5); flow-rate, 1 ml/min.

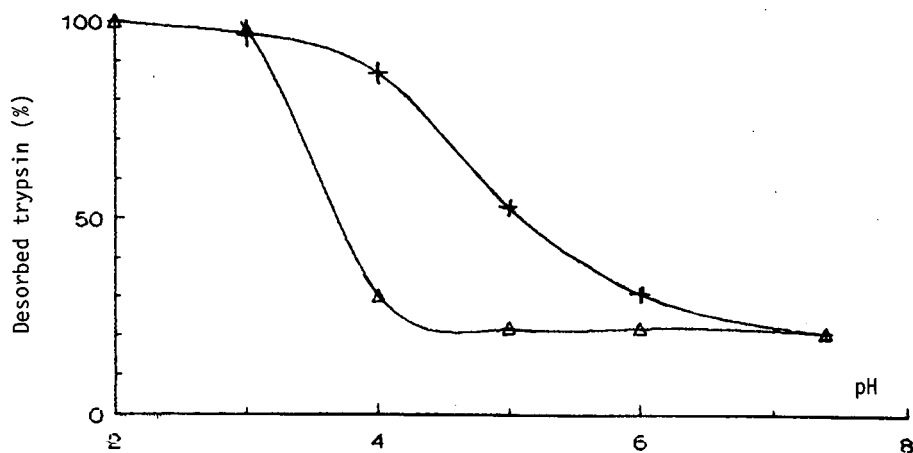


Fig. 6. Elution of bovine trypsin on SiD-pABA (+) and Si-pABA (Δ) supports by pH at 21°C in HPLAC. Elution conditions: column, 12.5 \times 0.4 cm; 0.05 M phosphate buffer, 0.1 M NaCl; pH, from 7.5 to 2; flow-rate, 1 ml/min.

types of interactions, in particular hydrophobic interactions between the aromatic ring of pABA and the enzyme. At low salt concentrations on the commercial Si-pABA support, the amount of trypsin adsorbed is higher than in the case of SiD-pABA support. This may be due to the presence of non-specific interactions between the commercial support and the enzyme. Higher salt concentrations allowed the desorption of trypsin adsorbed in a non-specific manner. This result again demonstrates the importance of the passivation of the native silica obtained by coating with modified polysaccharides.

Influence of pH. The results of the chromatographic elution of trypsin with solutions at different pH values are presented in Fig. 6. The maximum adsorption of

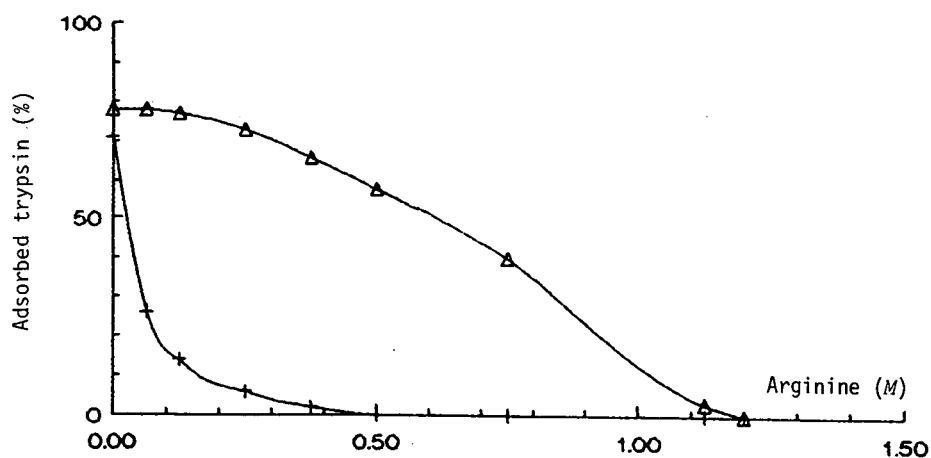


Fig. 7. HPLAC elution of bovine trypsin adsorbed on SiD-pABA (+) and Si-pABA (Δ) supports by arginine. The elution conditions are the same as in Fig. 4.

the enzyme is observed in the pH range 7–8. Desorption of the enzyme occurs when the pH of the eluent decreases. The breakdown of the interaction between trypsin and the support can be explained by the fact that at acidic pH the carboxylic function of the aspartic acid of the primary binding site, which possesses a pK_a of 2.3, is protonated and cannot interact with the amidine function. Desorption is obtained between pH 6 and 3 in the case of SiD–pABA support and between pH 4 and 3 in the commercial support. This result seems to indicate that the commercial support has a better resolution than SiD–pABA, probably related to the smaller granules and the better-defined porosity of the starting silica phase used for the commercial support.

Fig. 7 shows the trypsin elution by arginine in solution at different concentrations on the two supports. On the SiD–pABA support, trypsin elution is obtained by eluting the column with a 0.5 *M* arginine solution, but on the commercial Si–pABA support, this elution is obtained at higher arginine concentration (1.1 *M*). This indicates that the interactions taking place between trypsin and the ligand fixed on these two supports are stronger in the case of the commercial support but this result is inconsistent with the affinity constant values (Table I), which are the same for these two supports. The trypsin desorption differences on these two supports may be explained by the fact that the adsorbed trypsin is rapidly eluted by arginine according to a complex mechanism in the case of SiD–pABA and is slowly eluted from the commercial support. This observation demonstrates the improvement due to the better passivation obtained by polysaccharide coating of the silica beads. On this support, because of the passivation, the adsorption process is essentially the complex formation between the amidine residue and the binding site of the enzyme.

CONCLUSIONS

Amidine derivatives display a selective affinity for serine proteases, in particular for trypsin. These amidine derivatives are easily coupled on silica beads passivated with DEAE–dextran using conventional coupling reagents. Because of their mechanical properties, these phases are excellent supports for high-performance affinity chromatography. These active supports exhibit minimum non-specific ionic interactions with proteins in solution but a strong affinity for bovine trypsin. Affinity constant values are similar for all these supports. Among the synthesized supports, SiD–pABA presents a higher binding capacity in batch procedures and constitutes a good stationary phase in HPLAC for studying the interactions between trypsin and the specific site of the solid support. On this support, trypsin elutions obtained by competition with arginine and guanidine are similar, indicating that the same interactions probably occur between trypsin and these two competing substances. Comparison of the elution profiles of trypsin adsorbed on SiD–pABA or on the commercial Si–pABA support shows that in all cases the profiles are different, demonstrating that the trypsin interactions with pABA fixed on these two supports are different, complex, and depend on the nature of the support. On these two supports, the increase in ionic strength is unable to desorb the trypsin, indicating that the ionic interactions between trypsin and amidine do not prevail in this affinity reaction. The excellent resistance to hydrostatic pressure and high resolution of these two supports means that they can be used in HPLAC to separate and understand the serine protease interaction mechanism. Finally, the decrease in non-specific interactions obtained by coating the silica

beads with the modified polysaccharide enhances the importance of the specific affinity of amidine residues in the affinity process.

REFERENCES

- 1 M. Mares-Guia and E. Shaw, *J. Biol. Chem.*, 240 (1965) 1579.
- 2 H. F. Hixon and A. H. Nishikawa, *Arch. Biochem. Biophys.*, 154 (1973) 501.
- 3 G. W. Jameson and D. T. Elmore, *Biochem. J.*, 141 (1974) 555.
- 4 J. H. Northrop and M. Kunitz, *Science (Washington, D.C.)*, 73 (1931) 262.
- 5 M. Kunitz and J. H. Northrop, *J. Gen. Phys.*, 19 (1936) 991.
- 6 B. Hartley, *Phil. Trans. R. Soc. London*, B257, (1970) 77.
- 7 D. L. Kaufmann, *J. Mol. Biol.*, 12 (1965) 929.
- 8 D. M. Blow, J. J. Birktoft and B. S. Hartley, *Nature (London)*, 221 (1969) 337.
- 9 A. Warshel, G. Naray-Szabo, F. Sussman and J.-K. Hwang, *Biochemistry*, 28 (1989) 3629.
- 10 R. L. Smith and E. Shaw, *J. Biol. Chem.*, 244 (1969) 4704.
- 11 X. Santarelli, D. Muller and J. Jozefonvicz, *J. Chromatogr.*, 443 (1988) 55.
- 12 S. Khamlichi, D. Muller, R. Fuks and J. Jozefonvicz, *J. Chromatogr.*, 510 (1990) 123.
- 13 A. Kanamori, N. Seno and I. Matsumoto, *Chem. Pharm. Bull.*, 35 (1987) 3777.
- 14 F. L. Zhou, D. Muller, X. Santarelli and J. Jozefonvicz, *J. Chromatogr.*, 476 (1989) 195.
- 15 S. J. Thomson and G. Weeb, *Heterogeneous Catalysis*, Wiley, New York, 1968, pp. 22–27.

CHROMSYMP. 2241

Multi-column preparative reversed-phase sample displacement chromatography of peptides

ROBERT S. HODGES*, T. W. LORNE BURKE and COLIN T. MANT

Department of Biochemistry and the Medical Research Council of Canada Group in Protein Structure and Function, University of Alberta, Edmonton, Alberta T6G 2H7 (Canada)

ABSTRACT

Preparative reversed-phase sample displacement chromatography (SDC) of peptides was examined utilizing a multi-column approach. The effects of various SDC run parameters (flow-rate, run time and sample load) on the distribution of a single purified peptide and a mixture of three synthetic peptides was examined. The peptides in the mixture were closely related in hydrophobicity and mixed in a 1:4:1 ratio designed to mimic a typical preparative separation problem frequently encountered in crude synthetic peptide mixtures, that is, where there exist both hydrophobic and hydrophilic synthetic impurities close to the product of interest.

Based on the results of these model systems, a SDC protocol was applied to the preparative purification of a crude synthetic peptide. The multi-column SDC approach provides rapid separations that are easy to employ because isocratic elution is utilized both in the separation process and in elution of the column segments. There is minimal fraction analysis, minimal use of organic solvents and increased utilization of the stationary phase such that the method involves considerably lower costs than traditional gradient-elution chromatography.

INTRODUCTION

The most common analytical method employed for reversed-phase chromatography (RPC) of peptides involves linear gradient elution (gradient-rate of 1% eluent B/min at a flow-rate of 1 ml/min), where eluent A is 0.05–0.1% (v/v) aqueous trifluoroacetic acid (TFA) and eluent B is 0.05–0.1% (v/v) TFA in acetonitrile [1,2]. The elution mode of RPC, however, is handicapped by relatively poor utilization of the stationary and mobile phases [3]. Thus, in order to obtain satisfactory yields and purities of peptides which are closely related in hydrophobicity, large-scale gradient-elution separations of peptides often require large, costly columns.

With the growing use of synthetic peptides in biochemistry, immunology and in the pharmaceutical and biotechnology industries, there is a need for easier and more reliable methods for purification of peptides. We report here a novel preparative method for preparative-scale reversed-phase purification of peptides on analytical columns termed sample displacement chromatography (SDC), which is characterized by the major separation process taking place in the absence of an organic modifier. SDC separations use the well-established general principles of displacement chromatography [3,4] without using a displacer [5–7].

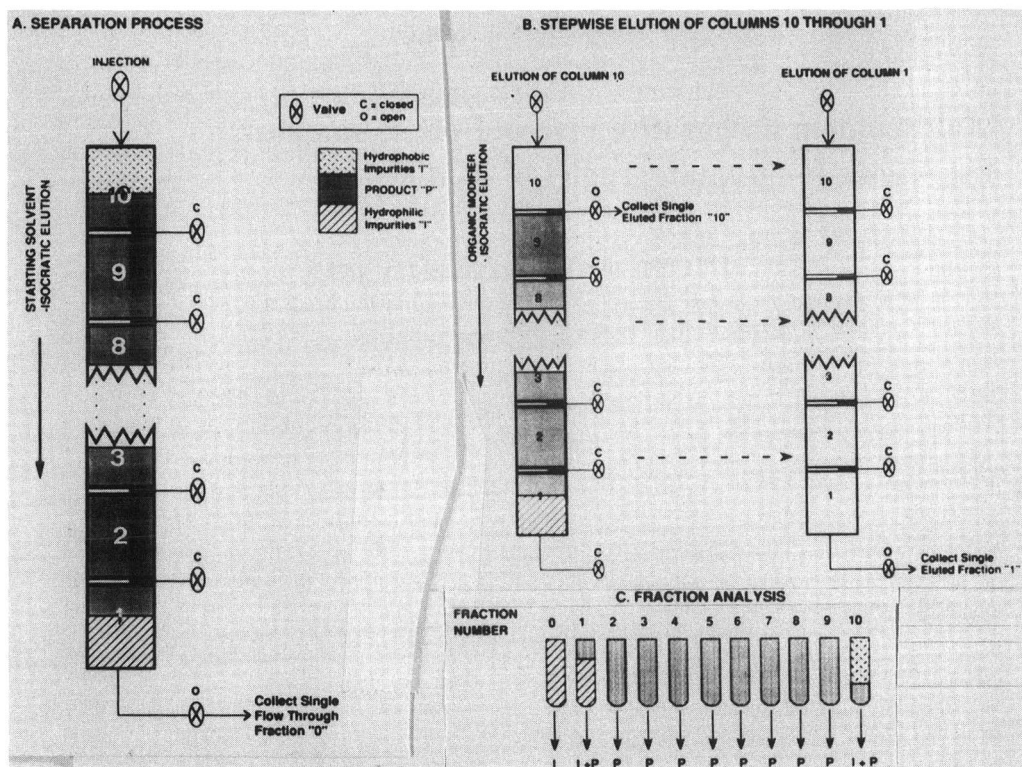


Fig. 1. Schematic representation of multi-column SDC. *Step A (separation process)*: small reversed-phase column segments (ten in this case, numbered 1–10) have been connected in series. Column 1 is closest to the detector and column 10 closest to the injector. The sample mixture, containing the desired peptide product (*P*) as well as hydrophilic and hydrophobic impurities (*I*) is introduced by isocratic elution in the starting eluent. Isocratic elution in this eluent is then continued at a specified flow-rate and run time to complete the separation. Step A shows a representation of sample loading and the subsequent isocratic elution of a typical distribution of peptide components through the total column length following SDC. Purified peptide product (*P*) can be found in columns 2–9; hydrophobic impurities remain in column 10 and hydrophilic impurities in column 1. Hydrophilic impurities may also be displaced from the column into the breakthrough fraction 0. *Step B (stepwise elution of column segments)*: each individual column segment is eluted to remove retained solute(s). This may be achieved either by isolating each column segment via a valve system (as shown) or by disconnecting all column segments prior to individual elution. The retained peptide components are removed from each column segment by an isocratic wash with an aqueous solution of organic modifier. The left schematic in step B represents the situation where only column 10 has been eluted to produce fraction 10; the right schematic represents the situation where all the columns have been individually eluted to produce fractions 1–10. Each column represents a fraction. Thus, for 10 column segments, there is a maximum of 11 fractions (10 columns plus the breakthrough fraction 0). *Step C (fraction analysis)*: each tube number (1–10) corresponds to a fraction eluted from each column segment. Fraction 0 represents the breakthrough fraction containing only hydrophilic impurities displaced from the columns during SDC. The amounts of hydrophilic impurities/product (fraction 1), pure product (fractions 2–9) and hydrophobic impurities/product (fraction 10), represent the peptide components eluted from columns 1–10 (schematic in step A).

This paper aims to develop our understanding of the sample displacement process by examining the effect of various run parameters (flow-rate, sample load, run time) on the retention behaviour of peptides during SDC, and to introduce a multi-column approach to SDC, which promises to increase further the ease and efficiency of an already promising preparative approach to the separation of peptides (Fig. 1).

Principles of SDC utilizing a multi-column approach.

(1) The reversed-phase column consists of small column segments connected in series.

(2) The sample mixture containing the desired peptide product as well as hydrophobic and hydrophilic impurities is dissolved in the starting eluent (in this case, a 100% aqueous mobile phase, 0.05–0.1% aq. TFA), injected onto the column, and eluted isocratically at a specific flow-rate and run time to complete the separation. At high sample load, there is competition by the sample components for the adsorption sites on the hydrophobic stationary phase. The sample components act as their own displacers, with the more hydrophobic peptide components displacing the more hydrophilic components. Thus, the separation process can take place in the absence of organic modifier.

(3) At the end of the separation, the components are distributed on the column according to their relative hydrophobicities: the most hydrophilic near the column outlet and the most hydrophobic near the column inlet. The retained peptide components are removed quickly and efficiently from each column segment by an isocratic wash with an aqueous solution of organic modifier. The concentration of organic modifier need only be just above that required to elute the component of interest (gauged from an analytical gradient-elution run of the original sample mixture).

(4) This methodology is very simplistic, since no gradient elution is involved and the number of fractions for analysis is minimized, since each column represents a fraction. The method, unlike traditional gradient elution, maximizes sample load by making very efficient use of column capacity. In addition, the sample displacement process has high resolving power, leading to increased yields.

EXPERIMENTAL

Materials

High-performance liquid chromatographic (HPLC)-grade water and acetonitrile were obtained from J. T. Baker (Phillipsburg, NJ, USA). HPLC-grade TFA was obtained from Pierce (Rockford, IL, USA).

Peptides were synthesized either on an Applied Biosystems (Foster City, CA, USA) Model 430A peptide synthesizer, using the general procedure for solid-phase peptide synthesis described by Parker and Hodges [8] and Hodges *et al.* [9]. All three peptides used in this study were based on the sequence Ac-Arg-Gly-X-Y-Gly-Leu-Gly-Leu-Gly-Lys-amide, where positions X-Y were substituted with Ala-Gly (peptide S3), Val-Gly (peptide S4) or Val-Val (peptide S5). All peptides contained an N^α-acetylated N-terminal and a C-terminal amide.

Apparatus

The HPLC instrument consisted of a Varian Vista Series 5000 liquid chromatograph (Varian, Walnut Creek, CA, USA) coupled to an Hewlett-Packard (Avon-

dale, PA, USA) HP1040A detection system, HP9000 Series 300 computer, HP9133 disc drive, HP2225A Thinkjet printer and HP7440A plotter.

Column packings

Separations were carried out on two reversed-phase column packings: either (A) Rainin C₈ (11–12 μm particle size, 330 Å pore size; Rainin Instrument Company, Berkeley, CA, USA); or (B) Aquapore RP-300 C₈ (7 μm, 300 Å; Brownlee Labs., Santa Clara, CA, USA).

Run conditions

Preparative separations were carried out with 0.1% (v/v) aq. TFA as the mobile phase eluent.

Analytical separations were carried out by linear AB gradient elution, where eluent A was 0.1% (v/v) aq. TFA and eluent B was 0.1% TFA (v/v) in acetonitrile.

The absorbance of the peptides was detected at 210 nm.

RESULTS AND DISCUSSION

Unless stated otherwise, all of the preparative data presented here were produced on a multi-column setup, consisting of six 3 cm × 4.6 mm I.D. Rainin C₈ column segments (columns 1–6) in series. The numbering of the columns (or fractions) starts at the column segment closest to the detector. Thus, column 1 (fraction 1) is at the multi-column outlet, while column 6 (fraction 6) is at the inlet. The fraction marked 0 is the breakthrough fraction, consisting of components not retained by, or displaced from, the column.

Column equilibration, sample loading and the SDC runs were all carried out in 0.1% (v/v) aq. TFA.

Following each run, the individual column segments were eluted with 25% (v/v) aq. acetonitrile containing 0.1% (v/v) TFA and the resulting peptide solutions subjected to analysis using standard gradient elution (1% B/min at 1 ml/min) on the multi-column setup. It should be stressed that each column segment is a fraction, *i.e.*, for this six column setup, there is a maximum of seven fractions (six column segments plus the breakthrough fraction).

Multi-column SDC of a single peptide component

Before applying the multi-column SDC approach to peptide mixtures, the retention behaviour of a single peptide component under varying run parameters was investigated. SDC was applied under various flow-rates, sample loads and run times to a single synthetic decapeptide (S5).

As the flow-rate was increased, the peptide moved further down the total column length (Table I) indicating that flow-rate affects column capacity. A ten-fold decrease in flow-rate increased the sample capacity of the total column packing by about a third [six column segments at 2 ml/min (columns 1–6) to four column segments at 0.2 ml/min (columns 3–6)].

As run time was increased, there was a slight increase in the distance that the peptide moved down the total column length (Table I) [a four-fold increase in run time (36 min to 144 min) resulted in the peptide moving by one further column

TABLE I

EFFECT OF VARYING RUN PARAMETERS ON MULTI-COLUMN SDC OF A SINGLE DECA-PEPTIDE

Results are presented as amount of peptide (mg) recovered from each fraction following SDC. Column: six 3 cm × 4.6 mm I.D. Rainin C₈ column segments (columns 1–6) in series. The numbering of the columns (or fractions) starts at the column segment closest to the detector. Thus, column 1 (fraction 1) is at the multi-column outlet, while column 6 (fraction 6) is at the inlet. The fraction marked 0 is the breakthrough fraction. Conditions: column equilibration, sample loading and the SDC runs were all carried out in 0.1% (v/v) aq. TFA. Fraction analysis: individual column segments were eluted with 25% (v/v) aq. acetonitrile containing 0.1% (v/v) TFA and samples of the resulting peptide solutions were subjected to linear AB gradient elution (1% B/min at 1 ml/min) on the multi-column setup. Absorbance at 210 nm. Effect of flow-rate: run time and sample load were 36 min and 25 mg, respectively. Effect of run time: flow-rate and sample load were 0.2 ml/min and 25 mg, respectively. Effect of sample load: flow-rate and run time were 0.2 ml/min and 36 min, respectively. The sequence of the synthetic peptide (S5) is shown in Experimental.

Fraction number	Effect of flow-rate (ml/min)			Effect of run time (min)			Effect of load (mg)		
	2	0.5	0.2	36	72	144	50	25	10
0	0	0	0	0	0	0	3.2	0	0
1	1.8	0	0	0	0	0	7.0	0	0
2	5.3	1.7	0	0	3.8	7.3	7.5	0	0
3	5.1	6.0	3.7	3.7	5.7	6.4	7.3	3.7	0
4	5.0	6.4	7.6	7.6	5.3	4.7	7.9	7.6	0
5	4.4	5.9	7.6	7.6	6.3	4.3	8.0	7.6	5.0
6	3.3	5.1	6.1	6.1	4.0	2.3	9.1	6.1	5.0

segment (column 3 to column 2)]. Thus, run time did not substantially affect column capacity.

The total column capacity was between 25 mg and 50 mg (Table I), since 25 mg did not exceed column capacity; whereas with a 50-mg load, there was peptide in the breakthrough fraction (3.2 mg in fraction 0 with the 50-mg load).

Multi-column SDC of a multiple-component mixture

An examination was carried out on the distribution of three peptide components through the length of the column packing, following multi-column SDC under varying run parameters of flow-rate, sample load and run time.

Fig. 2 shows an analytical run of the model three-decapeptide mixture (S3, S4 and S5) on the six-column C₈ setup.

The ratio of the peaks is approximately 1:4:1 (S3:S4:S5). The main component (S4) represents the desired product from a peptide synthesis. The smaller peaks represent more hydrophilic (earlier eluted, S3) and hydrophobic (later eluted, S5) peptide impurities. The peptide mixture was subjected to SDC as shown in Figs. 3–5 and Table II.

Effect of flow-rate. All three peptides moved further down the total column length with increasing flow-rate. At 2 ml/min (Table II), all of S3 has been displaced into the breakthrough fraction (fraction 0) and a significant portion ($\approx 40\%$) of S4, in addition to S3, has also been displaced from the column. Thus, at 2 ml/min, a sample load of 24 mg overloaded the column.

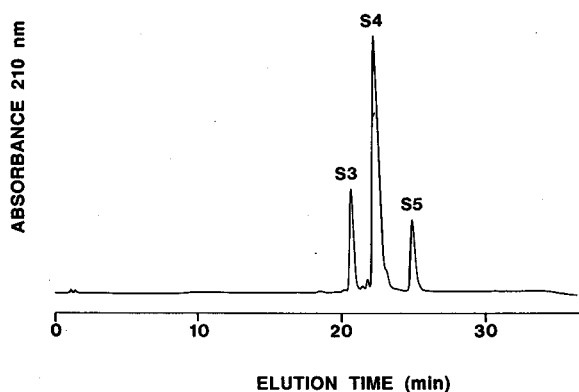


Fig. 2. Analytical RPC of a model three-decapeptide mixture. Column: six 3 cm \times 4.6 mm I.D. Rainin C₈ column segments in series. Conditions: linear AB gradient (1% B/min) at a flow-rate of 1 ml/min, where eluent A is 0.1% aq. TFA and eluent B is 0.1% TFA in acetonitrile. The ratio of the peaks is approximately 1:4:1 (S3:S4:S5). The main component (S4) represents the desired product. The smaller peaks represent more hydrophilic (S3) and hydrophobic (S5) peptide impurities. Multi-column SDC of this mixture provided the preparative data presented in Figs. 3-6. The sequences of synthetic peptides S3, S4 and S5 are shown in Experimental.

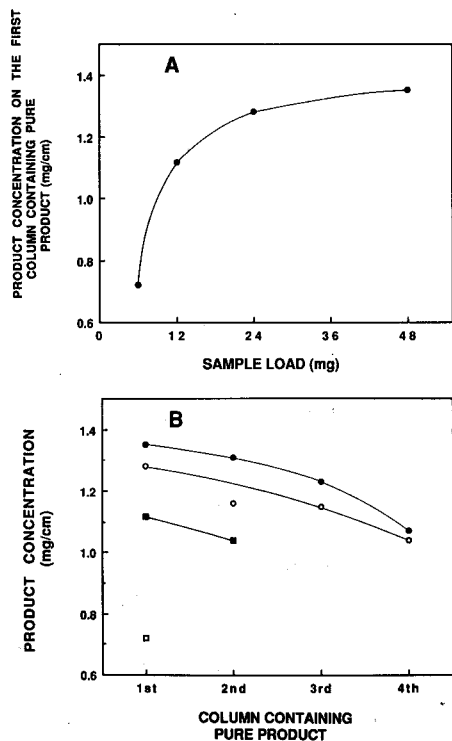


Fig. 3. Effect of sample load on distribution of peptide product, S4, from a three-decapeptide mixture (see Fig. 2) following multi-column SDC. These data are derived from results presented in Table II, with an additional sample load of 6 mg. (A) Relation between product (S4) concentration (mg/cm column) on the first column segment containing product only and the sample load; (B) relation between product (S4) concentration (mg/cm column) on each column segment containing product only and sample load. The first column to contain product only is nearest to the multi-column outlet; the fourth column is closest to the multi-column inlet. Symbols in (B): ● = 48; ○ = 24; ■ = 12; □ = 6 mg.

S4 was separated from S3 and S5 in four fractions at either flow-rate. The amount of pure S4 recovered in each of fractions 1–4 at 2 ml/min was less than that recovered from each of fractions 2–5 at 0.2 ml/min, *i.e.*, there was a dilution effect at the higher flow-rate, resulting in less product bound per individual column segment. The total pure S4 recovered at 2 ml/min was 8.6 mg; in contrast, at 0.2 ml/min, the total pure S4 recovered was 13.8 mg.

Effect of sample load. The 24-mg sample load was found to be optimal (Table II), with four fractions (2–5) containing pure S4 (a total of 13.8 mg). Although the 48-mg sample load also resulted in four pure fractions (1–4) of S4 (a total of 14.8 mg), about 50% of this peptide (16 mg) has been displaced into the breakthrough fraction, *i.e.*, the column was overloaded.

From Fig. 3A, the concentration (mg/cm of column) of peptide in the first column containing pure S4 increased with increasing sample load. From a rapid rise between sample loads of 6 mg and 24 mg, there was a levelling off of product concentration between 24 mg and 48 mg as the maximum column capacity was reached and exceeded.

From Fig. 3B, the concentration (mg/cm of column) of peptide in columns containing only S4 decreased with increasing column (fraction) number, *i.e.*, there was a general decreasing gradient of pure S4 in the direction of the column inlet (compare first and fourth column). Only one and two columns (out of six) contained pure S4 in the 6-mg and 12-mg sample loads, respectively; four out of six columns contained pure S4 in the 24-mg and 48-mg sample loads.

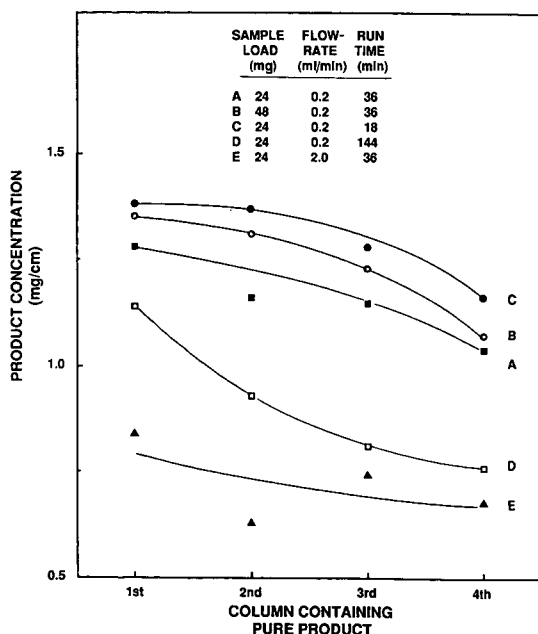


Fig. 4. Summary of effect of run parameters on distribution of pure peptide product, S4, following multi-column SDC of a three-decapeptide mixture (see Fig. 2). These data are derived from results presented in Table II and Fig. 3. The first column segment containing pure S4 is closest to the multi-column outlet; the fourth column is closest to the multi-column inlet.

Effect of run time. There was a general shift of peptide components down the total column length as run time increased (Table II). In addition, there was a dilution effect on the amount of S4 peptide recovered from each fraction containing pure S4 as run time increased.

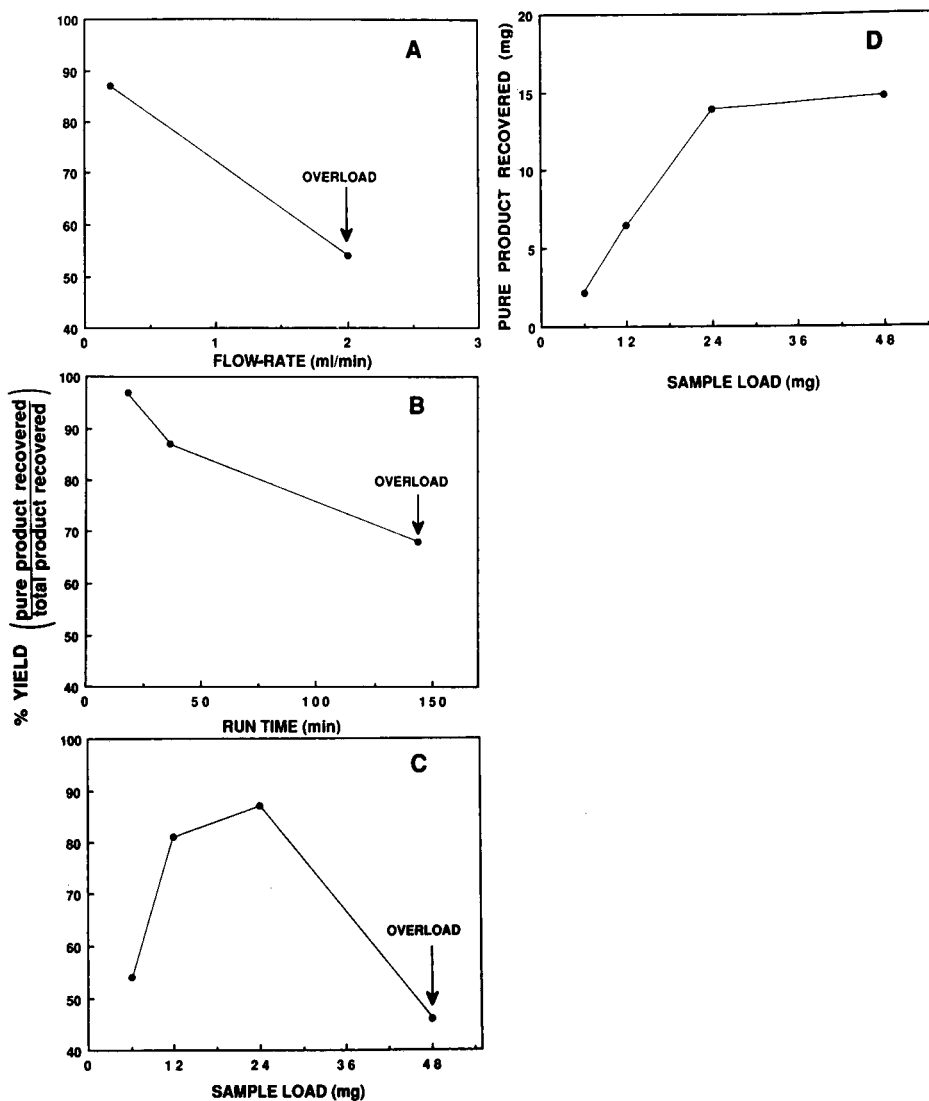


Fig. 5. Effect of varying run parameters on yield of pure peptide product, S4, following multi-column SDC of a three-decapeptide mixture (see Fig. 2). (A) Effect of flow-rate on yield of pure S4; (B) effect of run time on yield of pure S4; (C) effect of sample load on yield of pure S4. Overload conditions are defined as run conditions resulting in the desired peptide product being displaced from the column into the breakthrough fraction. (D) Amount of pure S4 recovered with increasing sample load.

TABLE II

EFFECT OF VARYING RUN PARAMETERS ON MULTI-COLUMN SDC OF A THREE-DECA-PEPTIDE MIXTURE

Results are presented as amount of each peptide recovered (mg) from each fraction following SDC of the peptide mixture. An analytical profile of the mixture is shown in Fig. 2. Column, conditions and fraction analysis: see Table I. Effect of flow-rate: sample load and run time were 24 mg and 36 min, respectively. Effect of sample load: flow-rate and run time were 0.2 ml/min and 36 min, respectively. Effect of run time: flow-rate and sample load were 0.2 ml/min and 24 mg, respectively. The sequences of synthetic decapeptides S3, S4 and S5 are shown in Experimental.

Fraction number	Effect of flow-rate			Effect of load			Effect of run time		
	S3	S4	S5	S3	S4	S5	S3	S4	S5
	<i>0.2 ml/min</i>			<i>12 mg</i>			<i>18 min</i>		
0	2.3	0	0	0	0	0	0	0	0
1	1.7	1.8	0	0	0	0	4.0	0	0
2	0	3.8	0	0	0	0	0	4.1	0
3	0	3.5	0	2.0	0.3	0	0	4.1	0
4	0	3.4	0	0	3.4	0	0	3.8	0
5	0	3.1	0	0	3.1	0	0	3.5	0
6	0	0.3	4.0	0	1.2	2.0	0	0.5	4.0
	<i>2 ml/min</i>			<i>24 mg</i>			<i>36 min</i>		
0	4.0	6.2	0	2.3	0	0	2.3	0	0
1	0	2.5	0	1.7	1.8	0	1.7	1.8	0
2	0	1.9	0	0	3.8	0	0	3.8	0
3	0	2.2	0	0	3.5	0	0	3.5	0
4	0	2.0	0	0	3.4	0	0	3.4	0
5	0	1.2	1.0	0	3.1	0	0	3.1	0
6	0	0	3.0	0	0.3	4.0	0	0.3	4.0
				<i>48 mg</i>			<i>144 min</i>		
0		—		8.0	16.0	0	4.0	3.4	0
1		—		0	4.0	0	0	3.4	0
2		—		0	3.9	0	0	2.8	0
3		—		0	3.7	0	0	2.4	0
4		—		0	3.2	0	0	2.3	0
5		—		0	1.1	3.6	0	1.7	0.4
6		—		0	0	4.4	0	0	3.6

The shortest run time (18 min) was most efficient, with >90% of S4 loaded being recovered as pure peptide (a total of 15.5 mg from columns 2–5). The 144-min run time was the least efficient. The column was overloaded under these conditions with S4 in the breakthrough fraction (3.4 mg).

At each run time, four fractions contained S4 only. However, as shown in Table II, there was a general decrease in the amount of peptide recovered from each fraction containing pure S4 as run time increased (a total of 15.5 mg and 10.9 mg was recovered from the 18-min and 144-min runs, respectively).

Fig. 4 is a summary of the effect of varying SDC run parameters on distribution of pure peptide product, S4.

There was a general decrease in concentration (mg/cm column) of pure product with each successive column from the column outlet containing pure S4. Thus, comparing runs A and B, there was an increase in product concentration with increasing

sample load on each column containing pure S4; comparing runs A and C, there was an increase in product concentration with decreasing run time on each column containing pure S4; comparing runs A and D, there was a significant decrease in product concentration with a large increase in run time (four-fold) on each column containing pure S4; and, finally, comparing runs A and E, there was a significant decrease in product concentration with a large increase in flow-rate (ten-fold) on each column containing pure S4.

From Fig. 4, it is clear that SDC runs of low flow-rates and short run times at appropriate sample loads provided the highest concentration of pure product.

Effect of varying SDC run parameters on peptide yield. Fig. 5 shows the effect of various run parameters on yield of pure peptide product, S4, following multi-column SDC.

From Fig. 5A, it can be seen that there was a significant decrease in overall yield of pure S4 as the flow-rate was increased ten-fold (from 0.2 to 2 ml/min). This was due mainly to the fact that, at the higher flow-rate, SDC was being run under overload conditions (Table II).

From Fig. 5B, it is clear that there was a general decrease in yield of pure S4 as run time was increased. This effect is most apparent at the 144-min run time, where SDC capacity was exceeded (Table II), with S4 being displaced into the breakthrough fraction.

From Fig. 5C, it can be seen that there was an increase in yield of pure S4 as sample load was increased up to 24 mg, reflecting more efficient use of total column capacity with increasing peptide load. The sharp drop in yield of S4 at a sample load of 48 mg was due to the SDC capacity being exceeded (Table II), with S4 being displaced into the breakthrough fraction.

From Fig. 5D, it is apparent that there was an increase of pure S4 recovered with increasing sample load, up to 24 mg. At higher loads, there was no further increase in pure peptide recovered. From Table II, it can be seen that the 24-mg load was optimal in terms of both essentially saturating the individual columns and in the number of columns containing pure product. As the sample load was raised to 48 mg, all or most of the additional S4 loaded was lost to the breakthrough fraction (Table II). This result also reflected the flexibility of sample load during SDC. Thus, even under overload conditions, the same amount of pure product was recovered as in an ideal run, where sample load was just enough to reach total column capacity.

Based on the results presented in Figs. 3–5 and Table II, Fig. 6 represents the optimum SDC run for the three-decapeptide mixture (S3, S4 and S5), in terms of both efficient use of total column capacity and yield of purified S4.

In Fig. 6, the top elution profile shows the analytical preparation of the peptide mixture, carried out on the multi-column setup. Peptide S4 is the desired component. Following SDC, column 1 contained S3 only, while column 6 contained all of the S5 and a small amount of S4. Columns 2–5 contained the vast majority of the desired peptide component, S4, with no S3 or S5 present. It should be noted that, under these run conditions, all of the peptide sample was retained by the multi-column setup, *i.e.*, no peptide was found in the breakthrough peak.

Multi-column SDC of a synthetic peptide crude mixture

In order to examine the effectiveness of multi-column SDC in purifying a crude

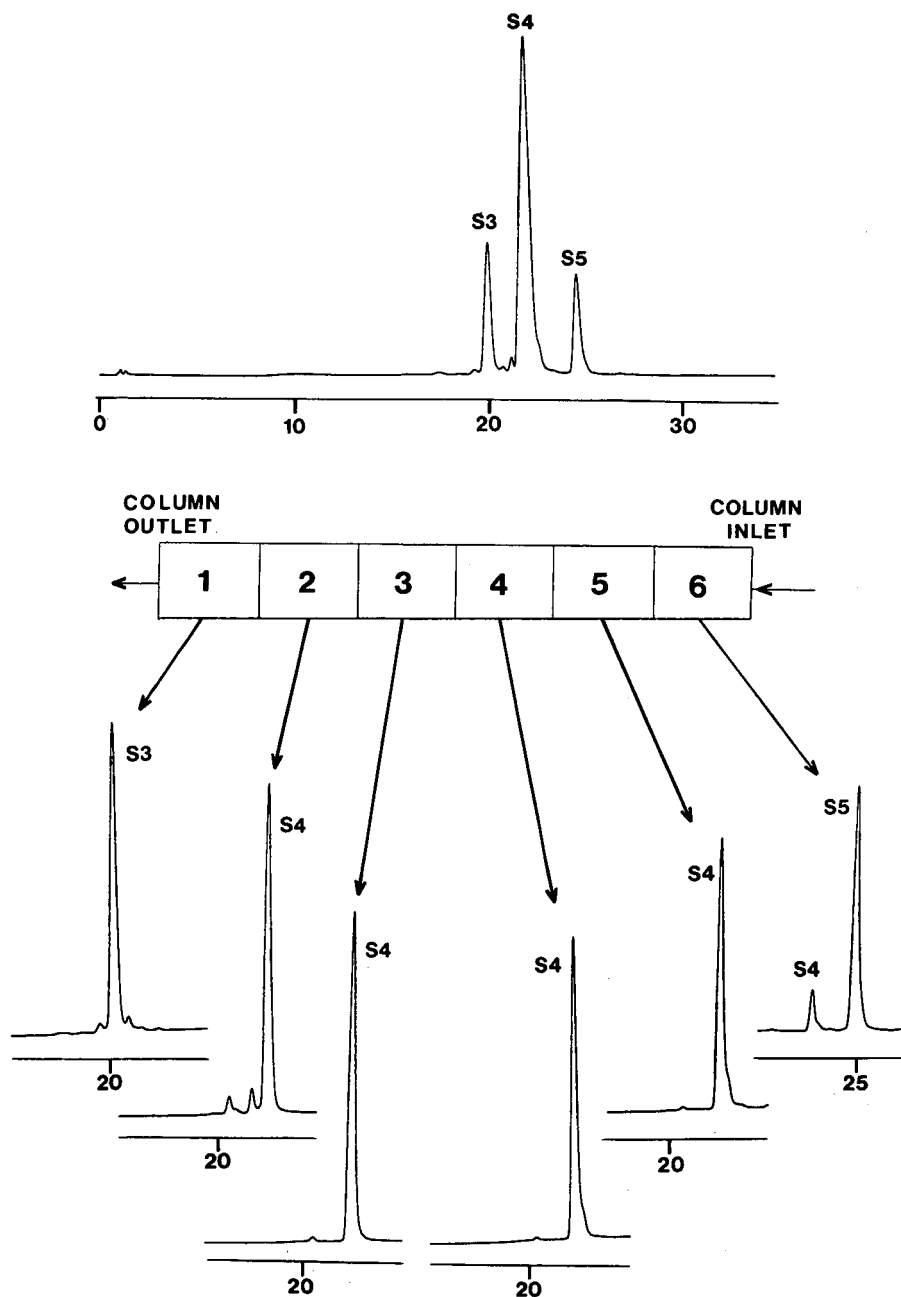


Fig. 6. Multi-column SDC of a model synthetic decapeptide mixture. Column, conditions and fraction analysis: see Table I. Flow-rate = 0.2 ml/min; run time = 18 min; sample load = 24 mg. The top elution profile shows the analytical separation of the mixture [linear AB gradient (1% B/min at 1 ml/min), where eluent A is 0.1% aq. TFA and eluent B is 0.1% TFA in acetonitrile]. The analytical elution profiles at the bottom show the peptide components retained on each individual column segment (columns 1-6) following the SDC run in 0.1% aq. TFA. The peaks are all correctly proportioned. The sequences of synthetic peptides S3, S4 (the desired product) and S5 are shown in Experimental.

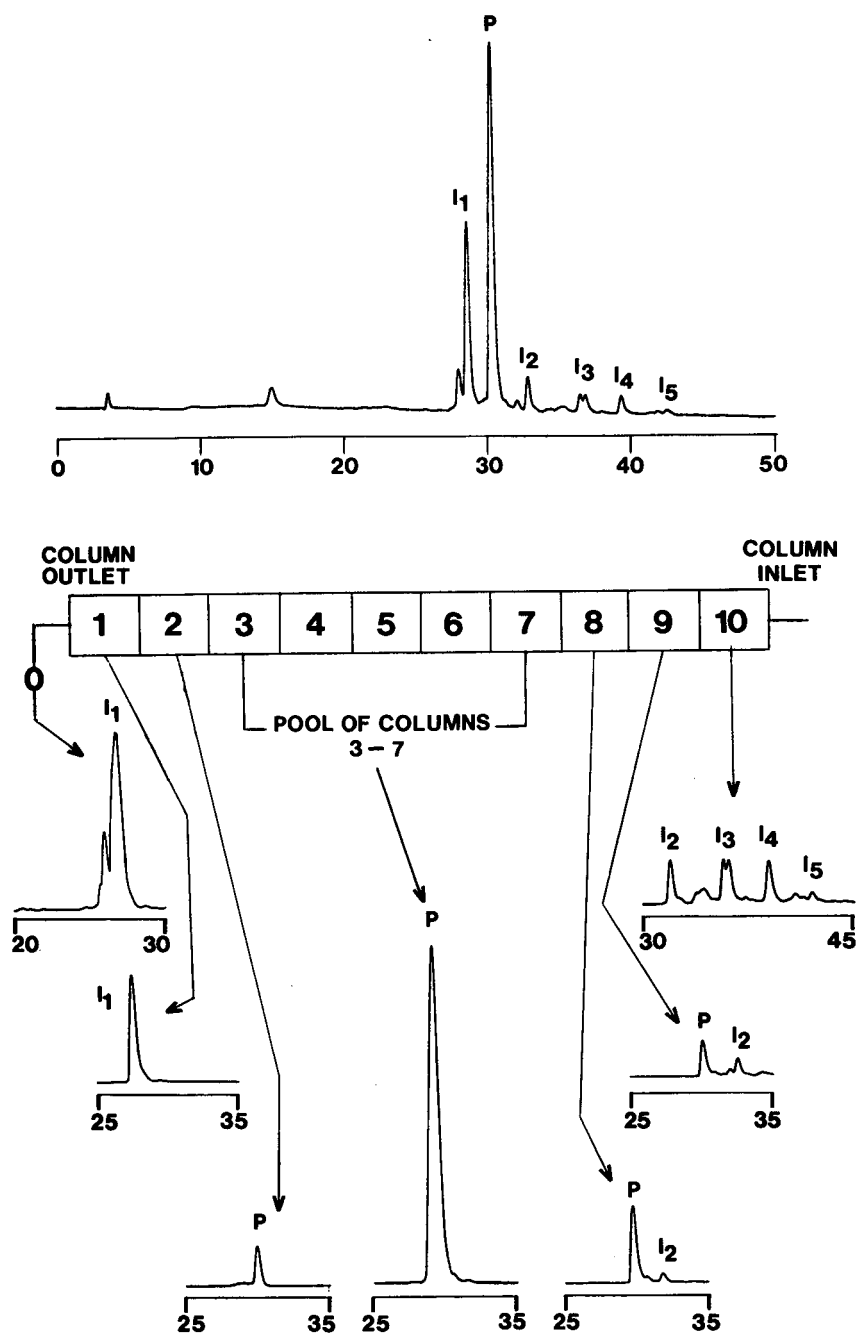


Fig. 7. Multi-column SDC of a synthetic decapeptide crude mixture. Column: ten 3 cm \times 4.6 mm I.D. Aquapore RP300 C_8 column segments in series. Conditions and fraction analyses: as Fig. 6. Flow-rate = 0.5 ml/min; run time = 50 min; sample load = 100 mg. The top elution profile shows the analytical separation of the peptide mixture [linear AB gradient (1% B/min and 1 ml/min), where eluent A is 0.1% aq. TFA and eluent B is 0.1% TFA in acetonitrile]. The analytical elution profiles at the bottom show the peptide components retained on each individual column segment (columns 1-10) following the SDC run in 0.1% aq. TFA. The peaks are all correctly proportioned. P is the desired product; the other peaks are hydrophilic (I_1) and hydrophobic (I_2 - I_5) impurities.

peptide mixture, as opposed to a model system, this technique was applied to the preparative separation of a synthetic decapeptide crude mixture.

In Fig. 7, 100 mg of a crude peptide sample has been applied to a multi-column setup, consisting of ten 3 cm × 4.6 mm I.D. Aquapore RP-300 C₈ column segments (columns 1–10) in series. The increase in the number of column segments (ten) compared to that employed previously (Figs. 3–6 and Table II) enabled the application of this substantial sample load.

The top elution profile shows the analytical separation of the crude synthetic peptide mixture. The large peak, *P*, is the desired peptide component; the smaller peaks are hydrophilic (*I*₁) and hydrophobic (*I*₂, *I*₃, *I*₄ and *I*₅) impurities.

Following SDC, the distribution of sample components through the ten column segments was determined. The breakthrough fraction (0) and column 1 contained only hydrophilic impurities (*I*₁). Column 10 contained only hydrophobic impurities (*I*₂–*I*₅) while columns 8 and 9 contained a small amount of peptide product contaminated with hydrophobic impurity *I*₂.

Columns 2–7 contained essentially pure product, the great majority of which was in columns 3–7. Of the total amount of desired peptide product loaded onto the column, 90% was recovered, with 81% of the peptide product isolated as pure peptide.

Very efficient use of the column capacity had been made during this SDC separation, which demonstrated well both the resolving power of this preparative process as well as the ease of fraction analysis.

CONCLUSION

In summary, this work describes an extension of a novel procedure for preparative reversed-phase separation of peptide mixtures, first reported by our laboratory [5–7]. Multi-column SDC enables the application of sample loads at least ten-fold greater than in comparable gradient elution experiments. Other advantages include minimal use of organic solvents and minimal fraction analyses. In addition, since the sample components act as their own displacers, no added displacer is required, unlike traditional displacement chromatography. Finally, rapid separations are achievable with multi-column SDC at a much lower cost (in terms of solvents, packings and machine use) than is typical for preparative gradient-elution separations. The potential of this technique is considerable (it is routinely used in the authors' laboratory) and should prove of great value to those involved in the purification of synthetic peptides.

ACKNOWLEDGEMENTS

This work was supported by the Medical Research Council of Canada and equipment grants from the Alberta Heritage Foundation for Medical Research. We thank Dr. Jeff Wheatley and Rainin Instrument Co. for providing the Rainin packing material and columns utilized in this study.

REFERENCES

- 1 C. T. Mant and R. S. Hodges, in K. M. Gooding and F. E. Regnier (Editors), *HPLC of Biological Macromolecules: Methods and Applications*, Marcel Dekker, New York, 1990, pp. 301–332.
- 2 C. T. Mant, N. E. Zhou and R. S. Hodges, in E. Heftmann (Editor), *Chromatography*, Part B, Elsevier Science Publishers, Amsterdam, 5th ed., 1991, in press.
- 3 Cs. Horváth, A. Nahum and J. H. Frenz, *J. Chromatogr.*, 218 (1981) 365.
- 4 S. M. Cramer and Cs. Horváth, *Prep. Chromatogr.*, 1 (1988) 29.
- 5 T. W. L. Burke, C. T. Mant and R. S. Hodges, *J. Liq. Chromatogr.*, 11 (1988) 1229.
- 6 R. S. Hodges, T. W. L. Burke and C. T. Mant, *J. Chromatogr.*, 444 (1988) 349.
- 7 R. S. Hodges, T. W. L. Burke and C. T. Mant, in G. R. Marshall (Editor), *Peptides: Chemistry and Biology—Proceedings of the 10th American Peptide Symposium*, Escom Science Publishers, Leiden, 1988, pp. 226–228.
- 8 J. M. R. Parker and R. S. Hodges, *J. Prot. Chem.*, 3 (1985) 465.
- 9 R. S. Hodges, R. J. Heaton, J. M. R. Parker, L. Molday and R. S. Molday, *J. Biol. Chem.*, 263 (1988) 11768.

CHROMSYMP. 2225

Analysis and purification of DNA restriction fragments by high-performance liquid chromatography

P. L. MAURI

Istituto Tecnologie Biomediche Avanzate, CNR, Via Ampere 56, 20131 Milan (Italy)

and

P. G. PIETTA* and M. PACE

Dipartimento di Scienze e Tecnologie Biomediche, Sezione Chimica Organica, Via Celoria 2, 20133 Milan (Italy)

ABSTRACT

The purification and analysis of restriction fragments play a very important role in molecular biology but the traditional assay methods of DNA fragments, based on gel electrophoresis and caesium chloride gradient centrifugation, are time-consuming and difficult to quantify. High-performance liquid chromatography provides an alternative method which allows the direct quantitation of picogram amounts of eluents in short times. In the present work we report the separation of different restriction fragments, the purification of some fragments and the relationship between the length of double-stranded DNA fragments and peak areas.

INTRODUCTION

DNA restriction fragments are the products of digestion of larger DNA with restriction endonucleases that cleave phosphodiester bonds of specific nucleotide sequences. The analysis and purification of these fragments are very important in molecular biology and several conventional methods based on centrifugation and gel electrophoresis are known [1]. However, in recent years high-performance liquid chromatography (HPLC) has been shown to be a useful alternative [2–5]. In comparison with gel electrophoresis, HPLC provides shorter separation times (within 30 min), nearly quantitative recovery, detection in the picogram range, direct quantitation of eluates and the possibility of automizing the overall procedure.

As a part of our interest in the application of HPLC in the study of a wide variety of biological molecules, we extended the use of an anion-exchange column [6] (Gen-Pak FAX) in resolving fragments obtained from double-stranded plasmid 11.3, Φ x174, after digestion with restriction endonucleases (*Pst*I, *Eco*RI and *Hae*III), and a 1-kilobase (kb) ladder DNA.

In the course of the investigation a direct relationship between peak areas and molecular size of the fragments was established.

EXPERIMENTAL

Materials

Plasmid 11.3 [6.0 kilobase pairs (kbp)], coding for a poly A binding protein, its fragments generated by digestion with *Pst*I (f1 = 0.6 kb, f2 = 1.4 kb and f3 = 4.0 kb) and with *Eco*RI (f4 = 2.9 kb and f5 = 3.1 kb) were obtained from P. Vezzoni (Istituto Tecnologie Biomediche Avanzate, CNR, Milan, Italy).

Φ x174 DNA, digested with *Hae*III, and the 1-kb DNA ladder were supplied by J. Malyszko (Farmitalia, Milan, Italy). T4 DNA ligase was from Boehringer Mannheim Biochemica (Mannheim, Germany).

Apparatus

The HPLC system consisted of an automated gradient controller, two Model 510 pumps, equipped with a Model U6K universal injector (Waters Assoc., Milford, MA, USA). For detection of the peaks a Model Lambda Max 480 UV detector (Waters) connected to a CR3A integrator (Shimadzu, Kyoto, Japan) or an HP 1040A photodiode array detector (Hewlett-Packard, Waldbronn, Germany) was used. Peak collection and reinjection was done by means of a Model 232 automatic sample processor and injector with a Model 401 dilutor (Gilson Medical Electronics, Villiers le Bel, France) equipped with a Rheodyne 7010 injector.

Chromatographic conditions

All HPLC runs were performed on Waters Gen-Pak FAX columns (100 × 4.6 mm I.D.). Eluent A was 25 mM sodium phosphate (pH 7.0) and eluent B was the same buffer containing 1 M sodium chloride. Phosphate buffer was made using the monobasic salt and the pH was adjusted using sodium hydroxide. Eluents were filtered through a 0.45- μ m membrane. The gradient profile was 40 to 70% eluent B in 20 min (curve 5). Flow-rate was 0.8 ml/min. The peaks were detected at 260 nm or by means a photodiode array detector.

Electrophoresis

Gel electrophoresis was carried out on 0.7% agarose [7] using 0.08 M Tris-phosphate, pH 8.0, 2 mM EDTA. Capillary electrophoresis was performed using an Applied Biosystems Model 270A and SeptraGene 500 buffer in the laboratory of Dr. G. Sabbatini (Applied Biosystems, Milan, Italy) according to the manufacturer's protocol.

Calibration graphs

Fragments f1, f2 and f3 were collected by means of a Model 232 automatic collector and increasing amounts of each fragment (0.1–2.5 μ g) were injected.

RESULTS AND DISCUSSION

The Gen-Pak FAX column is a DEAE anion-exchange column on methacrylate matrix of 2.5 μ m particle size optimized for DNA restriction fragment separation. Using this column it is possible to separate the 0.6-, 1.4- and 4.0-kb fragments generated by digestion of the 11.3 plasmid with *Pst*I endonuclease (Fig. 1). Baseline

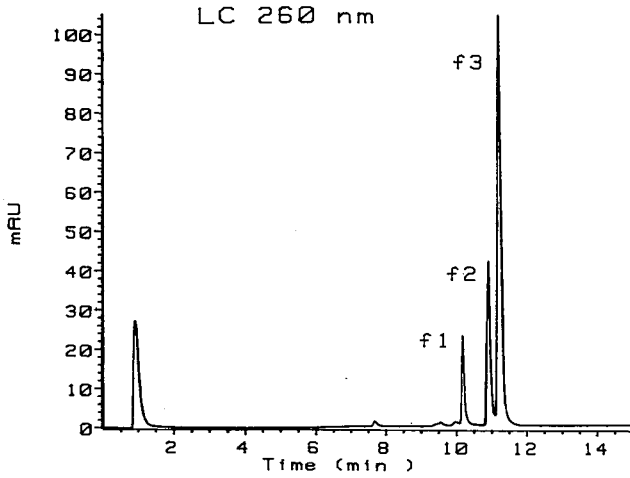


Fig. 1. Typical chromatogram of plasmid 11.3 ($0.5 \mu\text{g}$) digested with *Pst*I endonuclease. See text for chromatographic conditions.

resolution of these relatively small restriction fragments (1.2 and 2.6 kb difference) was achieved. The purity of the collected fractions was checked by HPLC and gel electrophoresis. As shown in Fig. 2, exact coincidence between the UV spectra of the fragments was confirmed, as may be expected. Amounts of up to $15 \mu\text{g}$ of plasmid were fractionated in a single run with 85% recovery. This means that the approach has an important semi-preparative value. Moreover, the three fragments have been recombined by means of T4 DNA ligase to yield the original plasmid, shown on gel

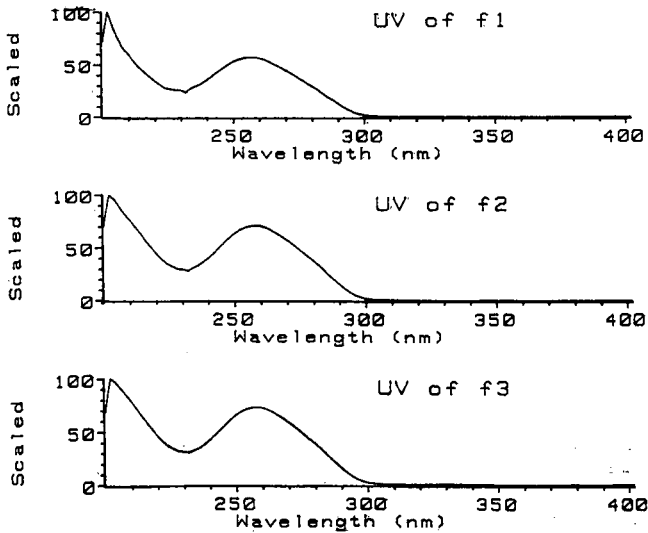


Fig. 2. UV spectra of restriction fragments f1, f2 and f3.

TABLE I

COMPARISON BETWEEN GEL ELECTROPHORESIS AND HPLC KILOBASEPAIR VALUES

Fragment	Electrophoresis (kbp)	HPLC (kbp)	Difference (%)
f1	0.6	0.62	+ 3.3
f2	1.4	1.41	+ 0.9
f3	4.0	3.97	- 0.8

electrophoresis and HPLC analysis, thus indicating that the chromatographic procedure is valuable for the preparation of intact fragments.

Rectilinear responses between peak areas and amounts injected were obtained from four replicate injections of f1, f2 and f3 in the range 0.1–2.5 μg , as indicated by

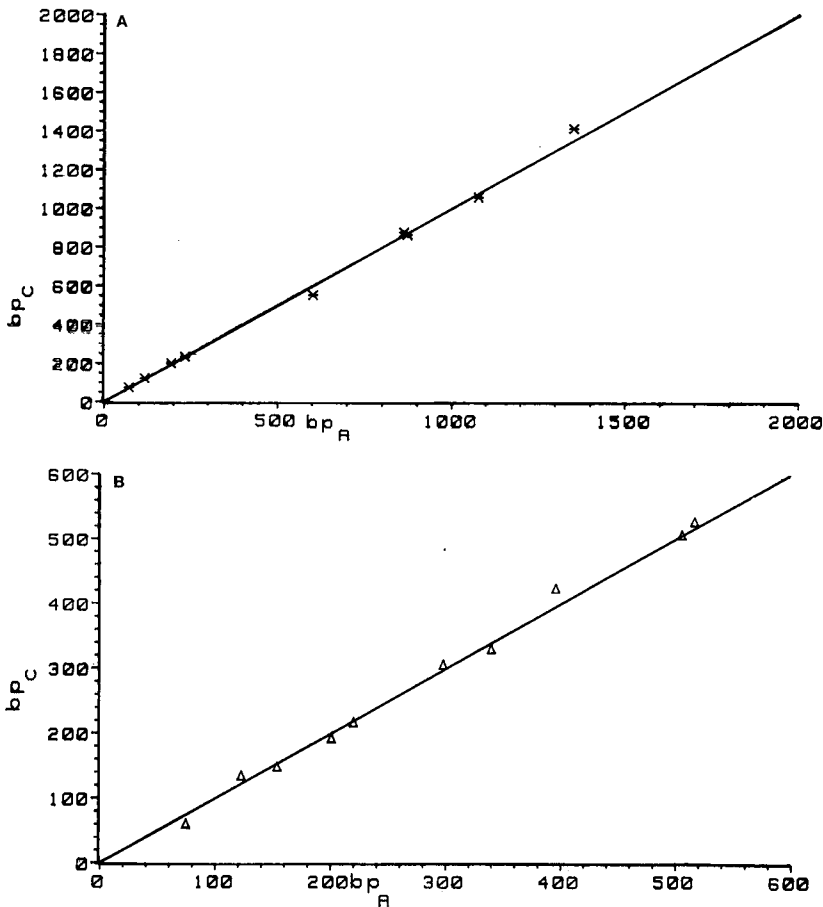


Fig. 3. Comparison between the number of actual (bp_A) and HPLC calculated (bp_C) basepairs for $\Phi\text{x}174$ DNA digested with *Hae*III (A) and the 1-kb DNA ladder previously isolated by HPLC (fragments from 75 to 517 bp) (B). (A) $\text{bp}_C = 1.03 \text{ bp}_A + 4.3$; $r = 0.997$. (B) $\text{bp}_C = 0.98 \text{ bp}_A + 3.2$; $r = 0.998$.

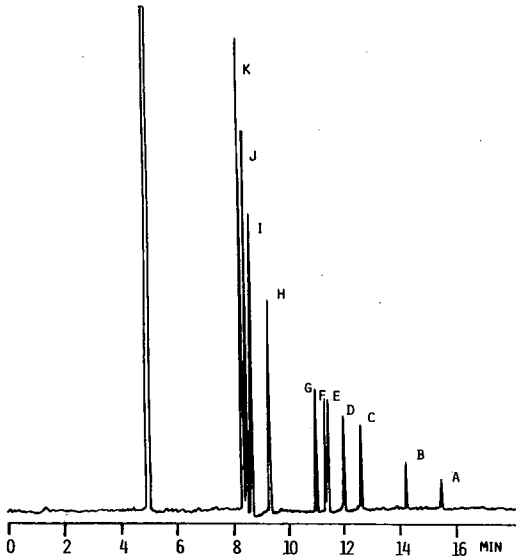


Fig. 4. Typical capillary electropherogram of Φ x174 digested with *Hae*III endonuclease (fragments A-K); detection, 260 nm.

the equation $y = 1388x + 11.2$ ($r = 0.995$), where y represents the peak area and x the amount injected.

Since exhaustive restriction digestion of the 11.3 plasmid yielded equimolar mixture of f1, f2 and f3, these were present in the same molar concentration. Thus, the mass of the fragment in each peak was proportional to the length of the fragment in that peak. This means that the size of each fragment can be obtained by the equation: $x + ax + bx = K$; where x is the kb number of f1, a is (peak area of f2)/(peak area of

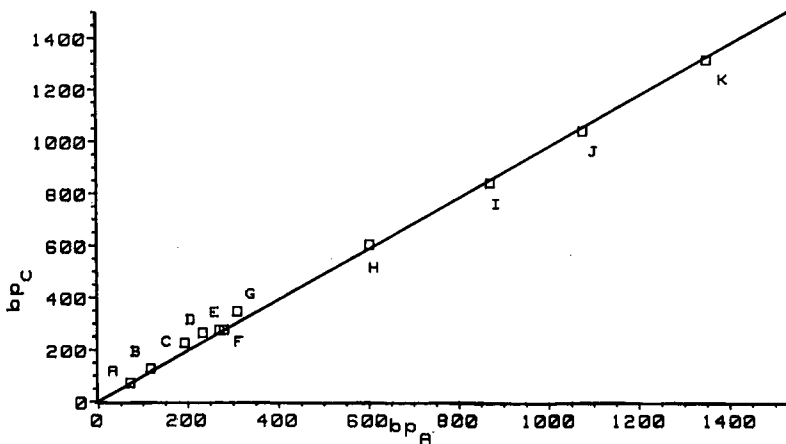


Fig. 5. Comparison between the number of actual and capillary electropherogram calculated basepairs for *Hae*III restriction fragments of Φ x174 (fragments: A-K). $bp_C = 1.02 bp_A + 2.1$; $r = 0.996$.

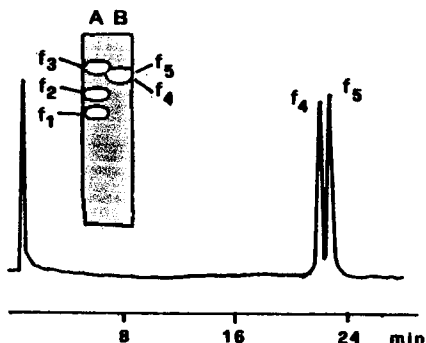


Fig. 6. Comparison of HPLC and slab gel electrophoresis (B) of restriction fragments f4 (2.9 kb) and f5 (3.1 kb) from plasmid 11.3 digested with *EcoRI*. In (A) the electrophoretic separation of restriction fragments f1, f2 and f3 (see Fig. 1) is also shown. See text for HPLC and electrophoresis conditions.

f1); b is (peak area of f3)/(peak area of f1) and K is the length of plasmid 11.3 (6.0 kbp).

Chromatographic data yielded the values of a and b that made it possible to calculate the kilobases of fragments f1 (x), f2 (ax) and f3 (bx). The values of kilobase pairs obtained by this procedure were compared with those from the conventional electrophoretic approach, as shown in Table I.

To verify the validity of this approach, Φ x174 DNA (5386 bp), after digestion with *HaeIII*, and the 1-kb DNA ladder were chromatographed and the lengths of the fragments evaluated as above. The results shown in Fig. 3A and B indicate that the discrepancy between the actual and the calculated basepair values is less than 3%.

Using this approach the length of restriction fragments can also be determined from capillary electrophoresis data, as confirmed by the analysis of the fragments from Φ x174 digested with *HaeIII*. In comparison with the described HPLC procedure, capillary electrophoresis [8] yielded a better peak separation (Fig. 4). Moreover, the difference between the calculated and actual number of bases is comparable to that found by the HPLC method (Fig. 5).

Finally, as further evidence of the ability of the Gen-Pak FAX column in resolving DNA fragments, plasmid 11.3 was digested with *EcoRI* endonuclease to yield two fragments (2.9 and 3.1 kb), which cannot be separated by electrophoresis (Fig. 6). HPLC allowed their preparative separation, as well as the evaluation of their length and purity.

In conclusion, the described procedure allows the semipreparative isolation of intact DNA fragments suitable for yielding the original plasmid and for eventual automated DNA sequencing after a single dialysis step. Furthermore, the proposed method for determination of the length of the restriction fragments represents an innovative alternative that can be applied both to HPLC and capillary electrophoresis data.

ACKNOWLEDGEMENTS

The authors wish to express their gratitude to Dr. I. Biunno (Istituto Tec-

nologie Biomediche Avanzate, CNR, Milan, Italy) and Dr. A. Michael Chin (Applied Biosystems, San Jose, CA, USA) for their advice.

REFERENCES

- 1 J. A. Thompson, *Biochromatography*, 1 (1986) 162.
- 2 P. Steffens, *Bioengineering*, 3 (1987) 40.
- 3 J. P. Liautard, S. Colote, C. Ferraz and J. Sri-Widade, *BioScience*, 6 (1987) 126.
- 4 Y. Kato, Y. Yamasaki, A. Onaka, T. Kitamura, T. Hashimoto, T. Murotsu, S. Fukushige and K. Matsubara, *J. Chromatogr.*, 478 (1989) 212.
- 5 E. D. Katz, L. A. Haff and R. Eksteen, *J. Chromatogr.*, 512 (1990) 433.
- 6 D. J. Stowers, J. M. B. Keim, F. S. Paul, Y. S. Lyoo, M. Merion and R. M. Benbow, *J. Chromatogr.*, 44 (1988) 47.
- 7 T. Maniatis, E. F. Fritsch and J. Sambrook (Editors), *Molecular Cloning: A Laboratory Manual*, Cold Spring Harbor Laboratory, Cold Spring Harbor, NY, 1982.
- 8 *Research News*, No. 2, Applied Biosystems, San Jose, CA, Summer 1990.

CHROMSYMP. 2301

High-performance liquid chromatographic purification of antiviral components in Neuramide

SILVIA GIACOBBE, NICCOLÒ MIRAGLIA and BRUNO RINDONE*

Dipartimento di Chimica Organica e Industriale, Università di Milano, Via Venezian 21, I-20133 Milan (Italy)

GIANCARLO FOLCHITTO

DIBE-Consortio Ricerca, Via della Cancelliera 60, Ariccia (Italy)

and

GUIDO ANTONELLI

Istituto di Virologia, Università di Roma, Via di Porta Tiburtina 28, I-00185 Rome (Italy)

ABSTRACT

Neuramide (NMD), a tissue extract having antiviral action against influenza A virus, was analysed by preparative size-exclusion high-performance liquid chromatography followed by solvent extraction and reversed-phase high-performance liquid chromatography. Some small peptides responsible for the antiviral action were isolated and their amino-acid content was determined.

INTRODUCTION

Neuramide (NMD) is a viral inhibitor that is present in crude preparations of tissue extracts. It is active against herpes viruses [1]. Ultrafiltration experiments have shown that the anti-influenza virus activity is concentrated in the material of molecular weight below 500 dalton [2].

In a previous paper [3] we reported the use of a sequence of chromatographic steps for the enrichment of antiviral and immunostimulant components in NMD. Here we report the preparative high-performance liquid chromatographic (HPLC) multi-step separation of the antiviral fraction in NMD.

EXPERIMENTAL

NMD preparations were obtained from Difa Cooper (Caronno Pertusella, Italy).

HPLC analyses

Preparative size-exclusion HPLC (HPSEC) and tests of antiviral activity were performed as reported previously [3]. Analytical reversed-phase HPLC (RP-HPLC) of the antiviral fraction from HPSEC was performed after methylene chloride extrac-

tion. Methanol solutions were injected through a 20- μ l loop (50 μ g per injection). The instrument was a Varian (Palo Alto, CA, USA) Model 5000 system equipped with a LichroCART 100 RP-18 (5 μ m) RP column (25 cm \times 4.6 mm I.D.) (Merck, Darmstadt, Germany) eluted with methanol at a flow-rate of 1 ml/min. The detector was a Hewlett-Packard (Palo Alto, CA, USA) Model 1040 diode array.

Preparative RP-HPLC purification of the antiviral fraction from HPSEC was performed after methylene chloride extraction. Solutions in water-acetonitrile (2:8) were injected through a 100- μ l loop. The Varian 5000 system was used, equipped with a Waters Assoc. (Milford, MA, USA) μ Bondapak-NH₂ column (30 cm \times 3.9 mm I.D.) eluted with water-acetonitrile (2:8) at a flow-rate of 4 ml/min. The Hewlett-Packard Model 1040 diode-array detector was used.

Extraction of antiviral components with methylene chloride

An aliquot of 1.9 g of the mixture obtained by elution with 0.1 M sodium chloride in eight runs of the sequence ultrafiltration-HPSEC and shown to have antiviral activity was dissolved in 50 ml of water and extracted three times with 50-ml portions of methylene chloride. The organic extracts were collected, dried over sodium sulphate and the solvent was evaporated under reduced pressure to give 7.9 mg of mixture. Antiviral activity was present in both the methylene chloride extract and the aqueous phase.

RESULTS AND DISCUSSION

The HPSEC procedure reported in previously [3] was performed sixteen times, in order to obtain sufficient material for further purification procedures. The antiviral material was eluted with sodium chloride solution and further purification was required to separate the organic material from sodium chloride. This was performed by methylene chloride extraction. Part of the antiviral activity was thus transferred into the organic phase, and was freed from sodium chloride.

The organic extract was then analysed by C₁₈ RP-HPLC (RP-HPLC-C₁₈), eluting with methanol and monitoring at 220 nm (Fig. 1). Two peaks were obtained.

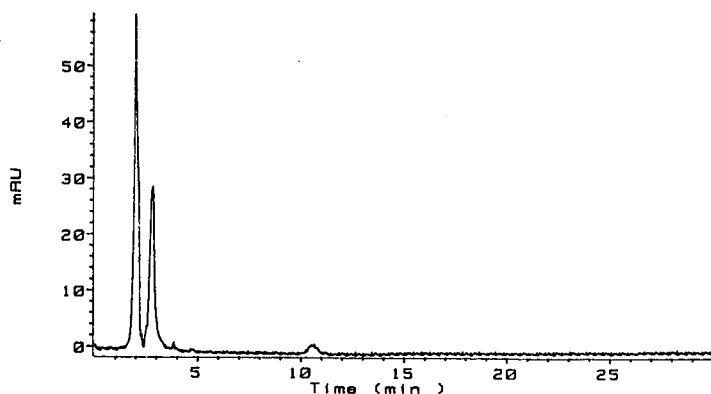


Fig. 1. RP-HPLC-C₁₈ analysis of NMD after HPSEC and solvent extraction.

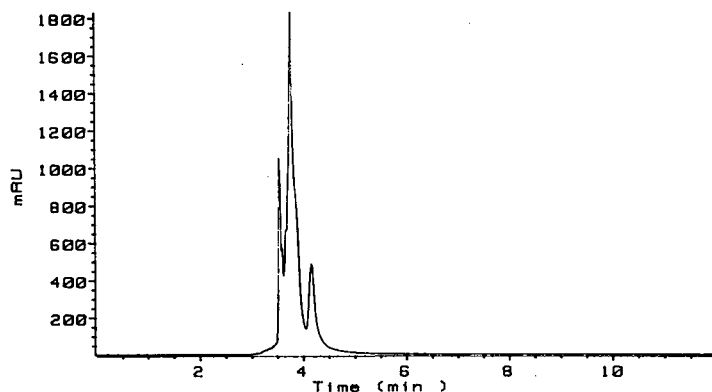


Fig. 2. RP-HPLC-NH₂ analysis of NMD after HPSEC and solvent extraction.

This procedure is unsuitable for scaling-up of the purification as injection of a large amount of material resulted in loss of resolution.

A second RP-HPLC procedure was then performed using an amino RP-HPLC column (RP-HPLC-NH₂) eluted with water-acetonitrile (2:8). An elution profile typical of very polar material was again obtained by monitoring at 220 nm. The result is shown in Fig. 2. At least three components were present, and the separation efficiency allowed the chromatography to be scaled up.

Four runs allowed sufficient material to be collected to perform the biological test which confirmed the antiviral activity of this mixture of components.

The amino acidic nature of the antiviral mixture was demonstrated by the analysis of its amino acid content. This analysis showed the presence of glycine, serine, threonine, glutamic acid and aspartic acid.

ACKNOWLEDGEMENTS

We thank Professor Castagnola, Catholic University of Rome, for the amino acid analysis and our student Miss Simona Mariani. This work was supported by a CNR grant.

REFERENCES

- 1 T. B. Albrecht, N. Cole, D. Speelman, F. Dianzani and S. Baron, *Chemioterapia*, 2 (1983) 255.
- 2 G. Antonelli, F. Dianzani, D. H. Copenhagen, S. Baron, P. Calandra and G. Folchitto, *Antimicrob. Agents Chemother.*, 29 (1986) 49.
- 3 N. Miraglia, B. Rindone, G. Folchitto, P. Amicucci, G. Antonelli, A. Lanfranchi and M. Massa, *J. Chromatogr.*, 512 (1990) 123.

Glycosylation of extracellular superoxide dismutase studied by high-performance liquid chromatography and mass spectrometry

MATS STRÖMQVIST*

Symbicom AB, P.O. Box 1451, S-901 24 Umeå (Sweden)

and

JAN HOLGERSSON and BO SAMUELSSON

Department of Medical Biochemistry, University of Gothenburg, P.O. Box 33031, S-400 33 Gothenburg (Sweden)

ABSTRACT

Extracellular superoxide dismutase, EC-SOD, the main superoxide dismutase in biological fluids, is known from its lectin binding to be a glycoprotein. We have characterized the glycosylation of recombinant EC-SOD. A tryptic digest of the protein contained only one glycosylated peptide. This peptide was specifically bound to lectins and stained by periodic acid–Schiff stain. Although appearing very large on size-exclusion chromatography, it was shown to be glycosylated at only one site, asparagine-89, by specific cleavage with glycanases followed by mass spectrometry of the resulting peptide. Based on the binding properties of the peptide to concanavalin A and lentil lectin and the elution profile of N-glycanase-treated glycopeptide on ion-exchange chromatography, the carbohydrate appears to be of the complex biantennary type with a core fucose.

INTRODUCTION

Extracellular superoxide dismutase, EC-SOD (EC 1.15.1.1), is the major SOD isoenzyme in extracellular fluid. The enzyme was first described by Marklund *et al.* [1] and has been found to consist of four identical subunits and has an apparent molecular weight of 135 000 [2]. The cDNA clone from human placenta coding for the protein has been isolated and characterized [3]. According to this, the subunit consists of 222 amino acids corresponding to a molecular weight of 24 200. The middle part of the protein shows strong homologies with the C-terminal portion of CuZn-SOD. The C-terminal portion of EC-SOD consists of a great number of charged amino acids and is also responsible for its heparin affinity [3]. Each subunit of EC-SOD binds one copper and one zinc atom [4]. EC-SOD bound to concanavalin A, lentil lectin and wheat germ lectin indicating that EC-SOD is glycosylated at least at the possible asparagine site [4]. The difference between the apparent molecular weight and that expected from the amino acid sequence indicates a large carbohydrate moiety.

In the present paper we have further characterized the glycosylation by isolat-

ing the glycosylated, nineteen-amino acid-long, tryptic peptide followed by enzymatic release of the carbohydrate portion. The resulting peptide was characterized by mass spectrometry and the released carbohydrate was studied by high-performance anion-exchange chromatography at high pH. From the results we conclude that each subunit of recombinant human EC-SOD has one single carbohydrate moiety attached to asparagine-89. Based on the binding to lectins and the elution profile on anion-exchange chromatography we suggest that the carbohydrate moiety is of the complex biantennary type having a core fucose.

EXPERIMENTAL

Protein purification

Human recombinant EC-SOD produced in Chinese hamster ovary cells was purified to at least 98% purity [according to reversed-phase chromatography and sodium dodecylsulphate polyacrylamide gel electrophoresis (SDS-PAGE)] by a three-step purification scheme at Symbicom AB, (Umeå, Sweden). The purified EC-SOD was stored at -70°C in 50 mM sodium phosphate buffer, pH 7.4.

Carboxymethylation of EC-SOD

EC-SOD (5 mg) in 200 μl of sodium phosphate buffer, pH 7.4, was mixed with 1.5 ml of 0.5 mM ammonium acetate, 6 M guanidine hydrochloride, pH 8.0, and flushed with nitrogen. The protein was thereafter reduced with 15 μl of 1 M dithiothreitol, flushed with nitrogen, and incubated for 1 h at room temperature. Iodoacetic acid (30 μl) was added and the sample was flushed with nitrogen and incubated in the dark for 2 h. Finally, the reaction was terminated by addition of 30 μl of 2-mercaptoethanol and 525 μl of glacial acetic acid.

Trypsin cleavage

Carboxymethylated EC-SOD was dialysed against 0.1 M NH_4HCO_3 , pH 7.8, and mixed with trypsin (EC 3.4.21.4, Boehringer-Mannheim) at a mass ratio of 50:1. The mixture was then incubated overnight (16–20 h) at room temperature. Cleavage was terminated by addition of 1 mM phenylmethylsulphonyl fluoride (PMSF).

Lectin chromatography

The tryptic digest of EC-SOD was applied to concanavalin A-Sepharose 4B or lentil lectin-Sepharose 4B (Pharmacia, Uppsala) equilibrated with 5 mM sodium acetate, pH 6.9, 1 M NaCl, 1 mM MnCl_2 , 1 mM CaCl_2 and 1 mM MgCl_2 . After the column was thoroughly washed, it was eluted with the same buffer containing 0.5 M α -methylmannoside. Bound and unbound material were collected as single fractions. Both glycopeptide and undigested EC-SOD could be eluted at 0.15 M α -methylmannoside but to keep the volume of the pooled, bound material low, the batch elution was made at higher molarity.

Glycopeptide isolation

The glycopeptide was isolated by reversed-phase chromatography on a Beckman System Gold liquid chromatography system using an Ultrapore C_8 (250 \times 4.6 mm, Beckman Instruments). The glycopeptide was eluted at approximately 30%

acetonitrile in 0.1% trifluoroacetic acid at 38°C. Prior to glycanase cleavage, it was further purified by gel filtration on TSK-3000SW, 375 × 7.6 mm, equilibrated with 10 mM sodium phosphate, pH 7.4 and 0.25 M NaCl.

Enzymatic cleavage of glycopeptide

For cleavage of asparagine-linked carbohydrate, 50 nmol of glycopeptide in 0.25 M sodium phosphate buffer were mixed with 2 U of *N*-glycanase [peptide-N⁴-(*N*-acetyl- β -glucosaminyl)asparagine amidase; EC 3.5.1.52, Genzyme, Boston, MA, USA] and incubated at 37°C. Samples were withdrawn at distinct times for reversed-phase liquid chromatographic (RP-LC) analysis. The reaction was terminated by immersing the samples in boiling water or by immediate RP-LC. For cleavage of serine/threonine-linked carbohydrate the peptide was first subjected to hydrolysis of sialic acid residues by incubation at 80°C for 1 h in 0.05 M sulphuric acid. The peptide was thereafter cleaved with O-glycanase (endo- α -*N*-acetylgalactosaminidase, EC 3.2.1.97, Genzyme) at several enzyme/peptide ratios ranging well above the recommended values in 20 mM sodium cacodylate, 10 mM calcium acetate, pH 6.5. Samples were then analyzed by RP-LC.

Amino acid analysis

For the amino acid analysis we used the Waters (Bedford) Pico-Tag system. Samples were hydrolyzed and derivatized with phenyl isothiocyanate according to the instructions supplied. The following exceptions were made. The chromatographic system was Beckman System Gold and instead of the supplied column we used a Beckman Ultrasphere C₁₈ (150 × 4.6 mm) with an elution program starting at 3% Pico-Tag eluent B, 3–15% B curve 4 (concave) in 6 min, 15–28% B in 1 min, 28–33% B in 5.5 min, 33–40% B in 1.5 min, 40–100% B 1 min, 100% B for 5.5 min and then re-equilibration to 3% B in 1 min. The flow-rate started at 1 ml/min, increased to 1.5 ml/min in 0.5 min at 14 min and decreased to 1 ml/min in 0.5 min at 24 min. The cycle of the program was 24.5 min and all amino acids were well separated and eluted within 17 min.

Periodic acid-Schiff (PAS) staining of blotting matrices

Immobilon-P, polyvinyl difluoride transfer membranes (Waters) were stained with Schiff's reagent (Sigma, St. Louis, MO, USA) using a modification [5] of the method of Glossmann and Neville [6].

Mass spectrometry

A ZAB HF 2F mass spectrometer connected to a VG Analytical 11/250 computer system and equipped with a Xenon FAB gun was used for peptide analysis. Samples were dissolved in distilled water and thioglycerol was used as matrix. The instrument was scanned from high to low masses, m/z 2600–90, 15 s per decade. Acceleration voltage was 8 kV and the target was bombarded with xenon at 8 keV. A cesium iodide spectrum was used for calibration.

High-performance anion-exchange chromatography

The *N*-glycanase-cleaved glycopeptide was analyzed at high pH on a Dionex (Sunnyvale, CA, USA) CarboPac PA-1 column (250 × 4.6 mm) using a Dionex Bio

LC gradient pump and a Model PAD 2 detector [7]. A CarboPac PA guard column (25 × 3 mm) was also used. The elution was done by 2 min of isocratic elution with 100 mM NaOH, followed by a linear gradient to 150 mM sodium acetate in 100 mM NaOH during 63 min, and a flow-rate of 1 ml/min. A 300 mM solution of NaOH was added to the column effluent via a mixing tee at a flow-rate of 1 ml/min. Detection was accomplished by triple-pulse amperometry on the PAD detector using a gold working electrode as described [7].

RESULTS

To identify the glycosylation of EC-SOD, the lectin-binding properties of tryptic peptides were studied. When a tryptic digest of EC-SOD was applied to concanavalin A-Sepharose or lentil lectin-Sepharose the bound material contained one heterogeneous main peak according to RP-LC (Fig. 1). The peptide was identified by

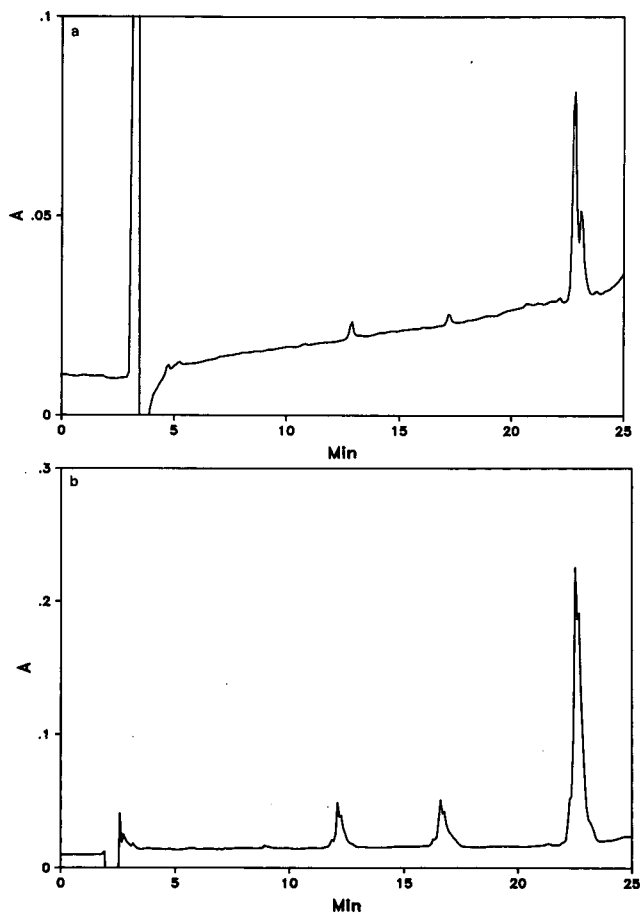


Fig. 1. RP-LC of tryptic fragments of EC-SOD bound to (a) concanavalin-Sepharose 4B and (b) lentil lectin-Sepharose 4B. Conditions as given under Experimental.

TABLE I

THEORETICAL AND OBSERVED AMINO ACID COMPOSITION AND MOLECULAR MASSES OF LECTIN-BOUND MATERIAL, PEPTIDES T8 AND T9, AND THE TWO PEAKS COLLECTED FROM N-GLYCANASE-CLEAVED GLYCOPEPTIDE.

All amino acids not listed in the table had a concentration corresponding to <0.2.

Amino acid	Peptide T8	Peptide T9	Peptide T8 + 9	Lectin-bound		N-glycanase	
				LL ^a	Con A ^b	Peak 1	Peak 2
Asx	0	2	2	2.0	2.2	2.0	2.0
Glx	0	2	2	2.2	1.9	1.9	1.9
Ser	0	3	3	3.5	3.0	2.6	2.6
Gly	0	1	1	1.5	1.9	1.1	1.1
Arg	0	1	1	1.0	1.0	1.1	1.1
Thr	0	1	1	0.9	0.7	1.0	1.0
Ala	1	2	3	2.2	1.7	2.8	2.1
Pro	0	2	2	2.3	2.3	1.8	1.9
Leu	0	2	2	2.1	1.4	2.1	2.1
Phe	0	3	3	2.6	2.4	2.8	2.9
Lys	1	0	1	0.3	0.8	1.0	<0.2
Molecular mass	217	2085	2284	N.D. ^c	N.D. ^c	2279	2084

^a LL = lentil lectin.

^b Con A = concanavalin A.

^c N.D. = not determined.

its mobility on RP-LC and by amino acid analysis (Table I) to be the nineteen-amino acid-long peptide Leu-75-Arg-93 (T9). Small amounts of two other fragments also bound but these were later found by amino acid analysis to be unspecifically cleaved fragments both composed of the main part of T9.

The glycopeptide was purified by collecting peptide T9 from RP-LC of a tryptic digest and by size-exclusion chromatography of the collected fraction (Fig. 2). The carbohydrate-containing peptide was easily separated from its impurities as it migrated as if had a molecular weight between 15 000 and 20 000 (Fig. 2b). The peak was slightly broader than protein peaks of approximately the same apparent molecular weight (myoglobin) probably due to its heterogeneity in the glycosylation.

The peptides separated by RP-LC were also slot-blotted and stained by PAS. Peptide T9 stained strongly and fractions containing the two smaller fragments that bound to lectins also stained but weaker. No other peptides stained, showing that no other parts of EC-SOD contained any carbohydrate stainable with PAS.

The high apparent molecular weight of both the native protein and the glycopeptide raised the question of whether the glycosylation really was restricted only to the single N-glycosylation site of T9 or if some O-linked carbohydrate also existed. To answer this question we tried to cleave the peptide with O-glycanase at several enzyme-to-peptide ratios. However, RP-LC of the cleavage product showed no difference with that of an undigested sample. Secondly, we cleaved the peptide with N-glycanase and separated the cleavage products by RP-LC. In this case the chromatography resulted in the appearance of one major and one minor new peak in the

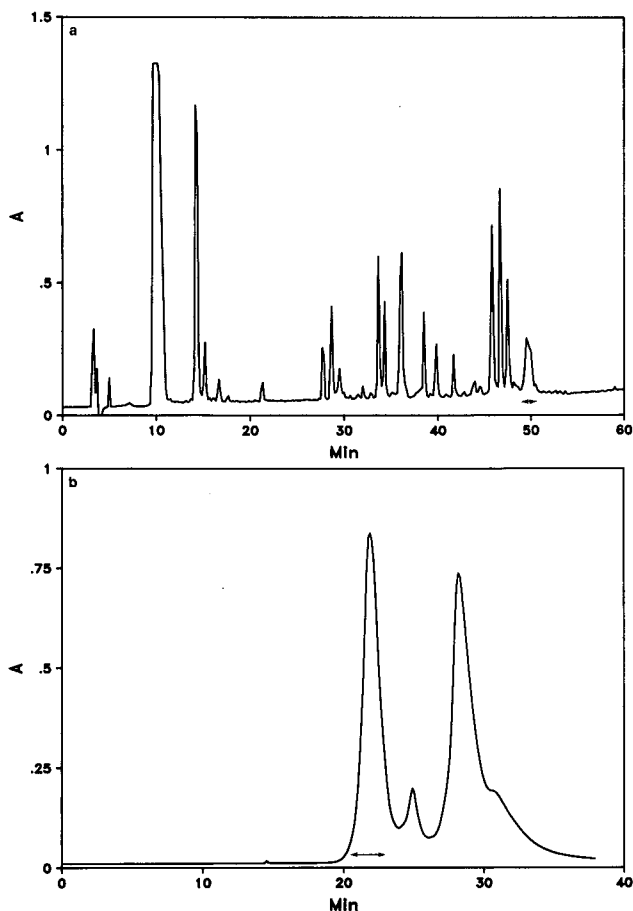


Fig. 2. Purification of the glycosylated peptide. (a) The tryptic peptides of EC-SOD separated on RP-LC. The pooled material is indicated by the arrow. (b) Size-exclusion chromatography of the pooled fraction from RP-LC. The collected fraction is indicated by the arrow.

chromatogram and at the same time the original peak decreased (Fig. 3). The two new peaks were collected and subjected to further analysis. First the amino acid composition was determined and then the molecular weight was established by mass spectrometry.

The results proved that the new peaks were the result of a complete deglycosylation of the peptide. Amino acid analysis showed that the composition of the main peak was the expected for the glycopeptide (Table I). It was very pure, which was not surprising as it now had a completely different mobility from its contaminants. The minor peak was a result of an incomplete tryptic cleavage of EC-SOD by trypsin. It contained, in addition to the amino acids of T9, one alanine and one lysine corresponding to the composition of tryptic fragment T8 (Table I). Apparently T9 and T8 + T9 was not separated by RP-LC when glycosylated due to the dominant carbohydrate portion, but when deglycosylated the difference in hydrophobicity resulted in

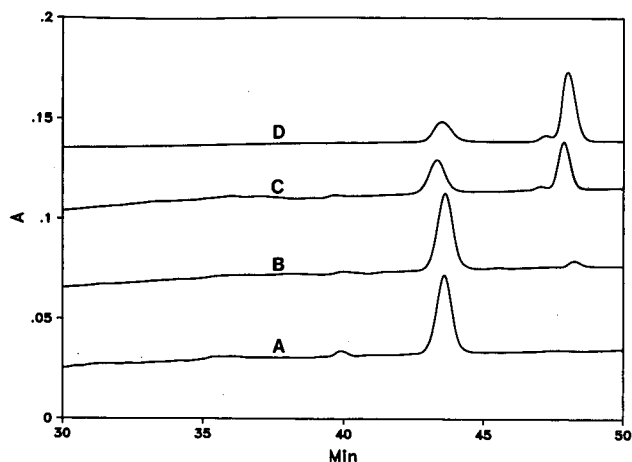


Fig. 3. RP-LC of the N-glycanase-cleaved glycopeptide. The glycopeptide was cleaved as described under Experimental. Samples were withdrawn from the reaction mixture at (A) 0 h, (B) 1 h, (C) 8 h and (D) 18 h.

a separation of the two peptides. The increase in hydrophobicity upon deglycosylation of the two fragments is in accordance with what is expected when the hydrophilic carbohydrate moiety is removed. Mass spectrometry supported these results and gave molecular weights of 2084 and 2279 for the two peaks respectively (Table I).

After N-glycanase cleavage, the glycopeptide was analyzed by anion-exchange chromatography at high pH. As seen in Fig. 4, several peaks were detected. The most retarded peak has a retention time very similar to the reference compound (indicated by an arrow in Fig. 4), the disialylated biantennary structure from human serotransferrin (Fig. 5). Other peaks most probably correspond to peptide and carbohydrate with missing terminal sialic acids. Variations in the grade of sialylation is also supported by inhomogeneity of recombinant EC-SOD upon isoelectric focusing.

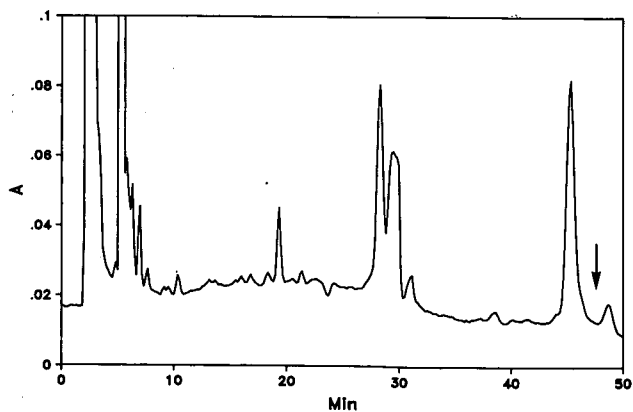


Fig. 4. Ion-exchange chromatography of N-glycanase-cleaved glycopeptide. Conditions as given under Experimental. Retention of the biantennary carbohydrate standard (Fig. 5) is indicated by the arrow.

hydrate moiety by anion-exchange chromatography also supported this proposed structure as the fully glycosylated carbohydrate moiety had a retention time very similar to the disialylated biantennary reference compound from human serotransferrin.

A mutant of the protein with asparagine-89 exchanged to glutamine has a mobility on size-exclusion chromatography that corresponds completely to what is expected (results to be published). One explanation for this behaviour is that the carbohydrate is highly hydrated and thereby interacts with water molecules and orders them into a structure that makes the migrating protein a much larger molecule on SEC. This is not a single phenomenon only restricted to EC-SOD. Several other examples of this behaviour are known and one example is human bile salt-stimulated lipase that migrates on gel filtration as if it had a molecular weight of more than 300 000 but only about 100 000 on SDS-PAGE [10].

ACKNOWLEDGEMENTS

We thank Ms. Helen Gruffman and Mrs. Else-Britt Lundström for excellent technical assistance, Dr. Hasse Karlsson for help with mass spectrometry and Drs. Anders Bergman, Gunnar Skogman and Lena Tibell for valuable discussions. This work was supported by grants from the Swedish Medical Research Council 6521 and 3967 and from the Swedish National Board for Technical Development 87-01842P.

REFERENCES

- 1 S. L. Marklund, E. Holme and L. Hellner, *Clin Chim. Acta*, 126 (1982) 41-51.
- 2 S. L. Marklund, *Proc. Natl. Acad. Sci. USA*, 79 (1982) 7634-7638.
- 3 K. Hjalmarsson, S. L. Marklund, Å. Engström, and T. Edlund, *Proc. Natl. Acad. Sci. USA*, 84, (1987) 6340-6344.
- 4 L. Tibell, K. Hjalmarsson, T. Edlund, G. Skogman, Å. Engström and S. L. Marklund, *Proc. Natl. Acad. Sci. USA*, 84 (1987) 6634-6638.
- 5 M. Strömquist and H. Gruffman, submitted for publication.
- 6 H. Glossmann and D. M. Neville, Jr., *J. Biol. Chem.*, 246 (1971) 6339-6346.
- 7 M. R. Hardy and R. R. Townsend, *Proc. Natl. Acad. Sci. USA*, 85 (1988) 3289-3293.
- 8 K. Karlsson and S. L. Marklund, *Biochem. J.*, 242 (1987) 55-59.
- 9 R. K. Merkle and R. D. Cummings, *Methods Enzymol.*, 138 (1987) 232-259.
- 10 L. Bläckberg and O. Hernell, *FEBS Lett.*, 157 (1983) 337-341.

CHROMSYMP. 2173

Peptide maps at picomolar levels obtained by reversed-phase high-performance liquid chromatography and pre-column derivatization with phenyl isothiocyanate

Microsequencing of phenylthiocarbamyl peptides

FRANCISCO J. COLILLA

Servicio de Endocrinología, Hospital Ramon y Cajal, 28034 Madrid (Spain)

SATYA P. YADAV and KEITH BREW

Department of Biochemistry and Molecular Biology, University of Miami, Miami, FL 33101 (USA)

and

ENRIQUE MENDEZ*

Servicio de Endocrinología, Hospital Ramon y Cajal, 28034 Madrid (Spain)

ABSTRACT

A new reversed-phase high-performance liquid chromatography approach to the production of analytical peptide maps by pre-column derivatization using phenylisothiocyanate is described. Tryptic peptide digests were derivatized with phenyl isothiocyanate to form the phenylthiocarbamyl peptides followed by reversed-phase high-performance liquid chromatographic analysis. The phenylthiocarbamyl peptides were separated by reversed-phase high-performance liquid chromatography with the conventional gradient elution system of water–acetonitrile containing trifluoroacetic acid. The sensitivity of detection of these peptide derivatives was within the range 5–10 pmol with a constant baseline at 254–260 nm. The isolated phenylthiocarbamyl peptides can be subjected to automatic Edman degradation. The effectiveness of this method was exemplified by microsequencing of phenylthiocarbamyl peptides isolated from tryptic digests of three different proteins: α -lactalbumin, β -lactoglobulin and a λ light-chain immunoglobulin.

INTRODUCTION

Phenyl isothiocyanate (PITC) has been the reagent most employed in the structural analysis of proteins since its introduction by Edman 40 years ago [1]. In the conventional Edman procedure for the sequential degradation of peptides or proteins, the free N-terminal amino acid reacts with PITC to form the phenylthiocarbamyl (PTC) derivative [2].

PITC, which reacts readily with amino acids [3], has also been used to quantify them at the picomolar level because it forms the PTC derivatives of the amino acids which can subsequently be identified and quantified by reversed-phase high-performance liquid chromatography (RP-HPLC) [4]. Various pre-column derivatization PTC

systems for amino acid analysis of proteins and peptides [5,6], including one commercial PTC amino acid analyzer [7], as well as a derivatization of two synthetic peptides, dynorphin and leucine-enkephalin, have been reported [8].

The present study describes a new approach, again using the Edman reagent PITC for the pre-column derivatization of peptide mixture digests, the separation of the resulting PTC-peptides by RP-HPLC with a detection sensitivity of the order of picomoles and the microsequence analysis of the isolated PTC-peptides.

EXPERIMENTAL

Acetonitrile was from Scharlau (Barcelona, Spain). Guanidinium chloride, idoacetic acid and dithiothreitol were purchased from Sigma (St. Louis, MO, USA). PITC was from Beckman Instruments (Palo Alto, CA, USA). Triethylamine, methanol, tetrahydrofuran, 1-tosylamino-2-phenylethyl chloromethyl ketone (TPCK)-trypsin, trifluoroacetic acid and other compounds not specified were from Merck (Darmstadt, Germany). Ultrapure water for HPLC, generated by a Milli-RO4-coupled to a Milli-Q water purification system (Millipore, Bedford, MA, USA) was used in the preparation of all buffers.

Proteins

A α -chain (L-chain) immunoglobulin (Ig) was obtained from a human (Escalano, ESC) monoclonal IgM after reduction and alkylation. Bovine α -lactalbumin and β -lactoglobulin were from Sigma.

Reduction and alkylation

Native proteins (3 mg) dissolved in 200 μ l of 2 M Tris-HCl buffer, pH 8.6, containing 0.002 M EDTA and 6 M guanidinium chloride were incubated with 35 mM dithiothreitol for 120 min at 37°C. Alkylation was performed by adding 5.0 mg of idoacetic acid followed by incubation for 15 min at room temperature in the absence of light. The excess reagents were removed by gel filtration on a Sephadex G-25 column.

Trypsin digestion

Reduced and carboxymethylated proteins (500 μ g) were digested with 5 μ g of TPCK-trypsin in 100 μ l of 0.2 M N-methylmorpholine acetate buffer, pH 8.2, for 1 h at 37°C. After digestion the material was freeze-dried.

Manual labeling of peptide mixtures with PITC

Tryptic digests (5–3000 pmol) were dried in Eppendorf tubes and dissolved in 15 μ l of (methanol-water-triethylamine, 2:2:1) at room temperature. This solution was evaporated to dryness by rotary evaporation under high vacuum for 30 min. This step was repeated three times. The dry peptides were dissolved in 20 μ l of methanol-triethylamine-water-PITC (80:10:10:1). After 30 min reaction at room temperature, the solution was evaporated to dryness under high vacuum for 40–50 min. The resulting PTC-peptides were dissolved in 6 M guanidinium hydrochloride containing 0.1% trifluoroacetic acid (TFA) and either injected into the RP-HPLC system or kept in the freezer for 1–10 days prior to being used for subsequent RP-HPLC analysis.

RP-HPLC separation of PTC-peptide mixtures

The chromatograph consisted of two Waters M6000A pumps, a Waters 680 automated gradient controller and a Waters 990 photodiode array detector with a dynamic range from ultraviolet to the visible (UV-VIS) region (190–800 nm), based on an NEC APC III personal computer. All sample injections were made with a Waters U6K universal injector. Separations were made by RP-HPLC on a Nova-Pak column (15 cm I.D. × 3.9 mm) protected by a guard column packed with μ Bondapak C₁₈-Corasil. The column was eluted with acetonitrile gradients containing 0.1% TFA. The column was operated at room temperature at a flow-rate of 0.5 ml/min. The PTC peptides were collected, lyophilized and kept at 4°C before further sequence analysis.

Sequencing procedure

The PTC-peptides were sequenced in a Beckman sequencer (Model 890 D) or in a new Knauer Model 810 modular liquid phase protein sequencer equipped on-line with an Knauer PTH (phenylthiohydantoin)-amino acid analyzer. PTH-amino acids were identified and quantified on an RP-HPLC system based on a C₁₈ column (Knauer, West Berlin, Germany) and gradient elution with 6.5 mM sodium acetate-acetonitrile 1,2-dichloroethane (85:15:0.175) adjusted to pH 4.77 as buffer A and 100% acetonitrile as buffer B. Sequences were performed in the presence of polybrene using the wet-filter technique [9] in a new flow-through reactor [10].

RESULTS AND DISCUSSION

In peptide mapping, a protein is cleaved selectively by enzymes or by chemical digestion, and the resulting peptide mixture is separated by RP-HPLC to yield a peptide map or 'fingerprint'. This technique is one of the most useful applications of RP-HPLC since it provides information concerning expression errors, mutations, location of glycosylation, disulfide linkages, and structural identification of newly discovered or recombinant proteins, as well as being routinely used for the separation of peptides for sequencing analysis.

The sensitivity of detection of peptides in RP-HPLC is mainly limited by the transparency and purity of the mobile phase, and by the characteristic noise and drift of the detector [11]. In the case of analytical columns (3.9 mm I.D.), amounts of peptides in the range 0.5–1.0 nmol are routinely detected with a constant baseline for UV absorption at 220–230 nm, at sensitivities of approximately 2.0–0.05.

However, the ability to detect and manipulate peptides at the picomolar level in RP-HPLC requires the use of appropriate and very sensitive detection systems. A standard way to increase the sensitivity of detection on RP-HPLC is simply by using the scale expansion of the UV detector, but as can be seen in Fig. 1 (top) the increase in the baseline produced by the absorption of the organic solvent (acetonitrile) at 220 nm using three different sensitivities could limit the visualization of peptides in the chromatograms. To resolve the problem we investigated a new approach based on the pre-column derivatization of peptides using the Edman reagent PITC.

One of the advantages of using PITC is that in conventional water-acetonitrile-TFA elution systems in RP-HPLC the PTC derivatives can be detected with a flat, low baseline for UV absorption at 254–260 nm. As can be seen in Fig. 1 (bottom)

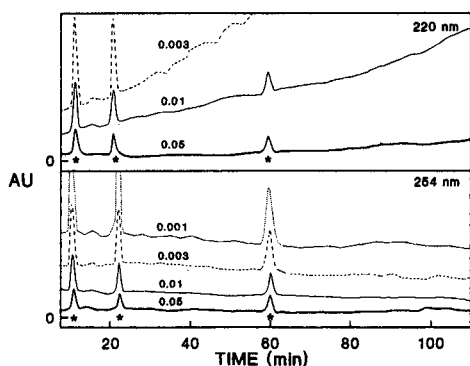


Fig. 1. Elution profile comparisons in the blank gradient produced by the absorption of the organic solvents during gradient elution at different wavelengths and sensitivities. Column: Nova-Pak (15 cm \times 3.9 mm I.D.). The column was run at room temperature, at a flow-rate of 0.5 ml/min with a linear acetonitrile gradient from 20 to 40% containing 0.1% TFA. Sensitivities from 0.05 to 0.001 and absorbance at 220 nm and 254 nm were compared. The peaks corresponding to the derivatizing reagents are marked with an asterisk.

there is no increase in the baseline at 254 nm caused by the absorption of acetonitrile, even at a high sensitivity of detection, in contrast to the large increase in the baseline at 220–230 nm (Fig. 1, top).

Moreover, by using PITC the resulting PTC-peptides are in principle, suitable for Edman degradation, in contrast to other derivatizing reagents which have been described, such as fluorescamine [12], *o*-phthalaldehyde [13,14] or dansyl chloride [14], peptide derivatives of which are blocked at the N-terminal and consequently cannot be used for further sequence analysis.

Another reagent which has been used for pre-column derivatization of peptides at picomolar level, is dimethylaminoazobenzene isothiocyanate (DABITC). However, although the dimethylaminoazobenzene-thiocarbamoyl (DABTC)-peptides are also suitable for Edman degradation, DABITC has the disadvantage that its reaction with peptides is very slow, often incomplete, and several peptide derivatives are obtained from a single peptide [15].

In order to determine the separation and detection of PTC-peptides on RP-HPLC, aliquots of 5, 50 and 200 pmol of a tryptic digest of an L-chain immunoglobulin were derivatized with PITC and then injected into an RP-HPLC system as indicated in Experimental. The chromatographic distribution of the PTC peptide derivatives is shown in Fig. 2 and, as can be seen, a satisfactory resolution was obtained.

Fig. 2 also shows the typical effect of a direct UV detection of three different amounts of PTC-peptides (5, 50 and 200 pmol) monitored at 220 nm and three different scale expansions of the UV detector. Only in the chromatogram of 200 pmol are the PTC-peptides clearly detected either at 254 nm or with a slightly higher sensitivity at 220 nm (Fig. 2, left), while in the chromatogram of 5 and 50 pmol (Fig. 2, right), the increase in the baseline at high sensitivity does not permit the visualization of the PTC peptides at 220 nm and visualization can only be obtained at 254 nm (Fig. 2, right and inset). This technique is very sensitive since it permits the visualization of peptide maps at a level of 5 pmol at 260 nm with still acceptable

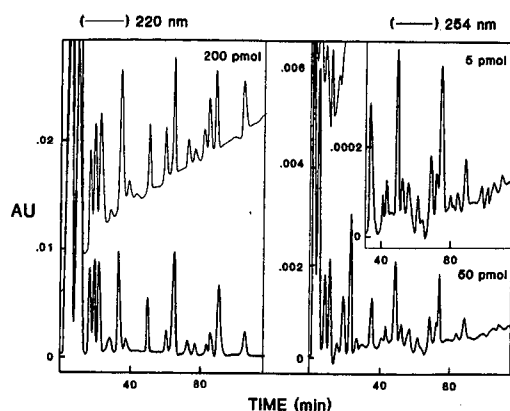


Fig. 2. Detection of different amounts of PTC-derivatized tryptic peptides at 220 and 254 nm at different sensitivities. Samples were 5, 50 or 200 pmol of a tryptic digest of an L-chain immunoglobulin derivatized with PTC. Peptides were eluted at room temperature on a gradient of acetonitrile containing 0.1% TFA as indicated in Fig. 1. The corresponding PTC-peptides identified by amino acid analysis in each chromatogram are numbered. The peaks corresponding to the derivatizing reagents are marked with an asterisk.

baseline using a high sensitivity of detection (Fig. 2). These data demonstrate that the PTC-peptides can be adequately separated at the picomolar level by RP-HPLC.

The elution pattern of PTC-peptides in RP-HPLC (Fig. 2) can be seen to be satisfactory but different from that obtained with underivatized peptides. In general we observed that PTC-peptides in RP-HPLC are eluted at a higher concentration of acetonitrile than underivatized peptides, under the same chromatographic conditions (data not shown).

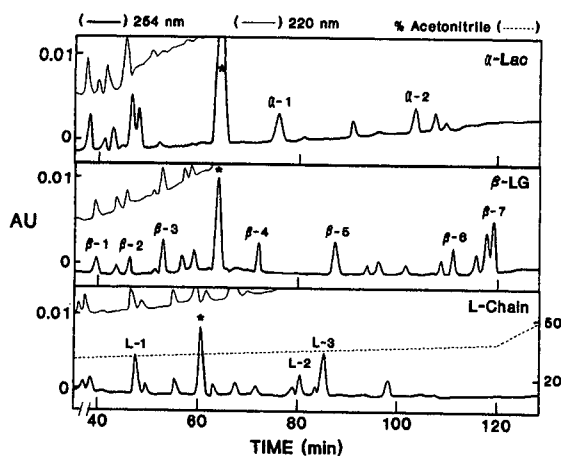


Fig. 3. Fractionation by RP-HPLC of PTC-derivatized tryptic peptides (300 pmol) from α -lactalbumin (α -Lac), β -lactoglobulin (β -LG) and a light-chain (L-chain) immunoglobulin. Peptides were eluted at room temperature on an acetonitrile gradient containing 0.1% TFA as indicated in the figure. Flow-rate: 0.5 ml/min. The peaks corresponding to the derivatizing reagents are marked with an asterisk. All peaks in the chromatograms are PTC-peptides which were identified by amino acid analysis. Only those PTC-peptides which were used for sequence studies have been labelled.

The possibility of subjecting the PTC-peptides isolated from RP-HPLC to Edman degradation analysis was also investigated.

For this purpose aliquots containing 300 pmol of the peptide derivatives of the proteins α -lactalbumin, β -lactoglobulin and L-chain were analyzed by RP-HPLC, and the chromatographic distribution of the corresponding PTC-peptides is shown in Fig. 3. The calculated average yield of the isolated PTC-peptides in the three chromatograms as determined by amino acids analysis, was approximately 80–90% of the applied material. The amino acid composition data indicate that a single PTC derivative of each peptide is obtained, while DABITC gives several derivatives [15].

Aliquots of 250 pmol of the PTC-peptides indicated by numbers in the three peptide maps of Fig. 3 were either subjected to automatic degradation or maintained for 1–30 days in the freezer before being used for sequence analysis. The results of the amino acid sequences obtained from these PTC-peptides are shown in Table I. This also demonstrates that the PTC-peptides are suitable for sequencing analysis and that they are stable for a relatively long period of time if stored frozen (-20°C).

It is noteworthy that in general the yield of the first cycle of these PTC-peptides was always low (Table I) (in comparison with the initial yield of non-derivatized

TABLE I

AMINO ACID SEQUENCE OF TRYPTIC PTC-PEPTIDES FROM α -LACTALBUMIN, β -LACTOGLOBULIN AND L-CHAIN

Residue numbers in parenthesis refer to primary sequence position in α -lactalbumin[16], β -lactoglobulin [17] and (ESC) L-chain (unpublished results). The yield (pmol) of the two PTH-amino acids obtained in the first cycle are indicated below the sequences.

PTC-peptide	Amino acid sequence	Position
α -1	Glu-Gln-Leu-Thr-Lys (22,68)	(1–5)
α -2	Ile-Leu-Asp-Lys (75,225)	(95–98)
β -1	Lys-Ile-Pro-Ala-Val-Phe (99,114)	(77–82)
β -2	Leu-Ser-Phe-Asn-Pro-Thr-Gln-Leu (142,60)	(149–156)
β -3	Tyr-Leu-Leu-Phe-Cys-Met (62,47)	(102–107)
β -4	Leu-Ile-Val-Thr-Gln-Thr-Met-Lys (36,49)	(1–8)
β -5	Ser-Leu-Ala-Met-Ala-Ala-Ser-Asp-Ile-Ser (25,35)	(21–30)
β -6	Thr-Lys-Ile-Pro-Ala-Val (12,33)	(76–81)
β -7	Lys-Val-Ala-Gly-Thr-Trp-Tyr-Ser-Leu-Ala (30,188)	(14–23)
L-1	Tyr-Ala-Ala-Ser-Ser-Tyr-Leu-Ser-Leu-Thr-Pro (15,109)	(173–183)
L-2	Phe-Ser-Gly-Ser-Lys (45,151)	(62–66)
L-3	Ala-Gly-Val-Glu-Thr-Thr-Lys-Pro-Ser-Lys (112,245)	(57–166)

peptides) regularly obtained in our sequencer, however, the yield in the second and subsequent cycles was normal. This is probably because the PTC-amino acid of the first residue undergoes several manipulations, such as manual derivatization, HPLC fractionation and peak collection, which are not done routinely in automatic degradation of non-derivatized peptides. The PTC-peptides can be sequenced using either a regular Edman degradation or a modified one, in which, in the coupling step, the PTC is eliminated from the first cycle, since the PTC-peptide is already formed. In both cases, a single PTH-amino acid is obtained.

A peculiarity observed during the sequencing of PTC-peptides using our wet-filter sequencer was that two different PTH derivatives were obtained in the first cycle, corresponding to the first and second amino acids. This is because, with the program used, prior to initiating the first cycle the PTC-peptide (or sample), containing membrane is gently treated with 100% TFA, and under this acid condition the first PTC-amino acid is liberated from the PTC-peptide. Then, during the coupling step in this first cycle, the PTC reacts with the nascent amino group from the second residue of the peptide, and consequently at the end of this cycle two PTH-amino acids are obtained. Again the yield of the PTH corresponding to the first amino acid is always lower (30–55%) than that of the second amino acid (50–70%) (data not shown). The possibility that the second signal for the first amino acid may be due to the presence of TFA in the RP-HPLC cannot be discounted.

In conclusion, we have shown that the pre-column PTC derivatization procedure described is a simple general procedure which can be used as a very sensitive peptide-mapping method at the picomolar level (5–10 pmol).

As stressed above, in comparison with other reagents, including DABITC, the advantage of using PTC is that the reaction with peptides is complete, reproducible and the peptide derivatives are stable for weeks. In addition the PTC-peptides can be properly fractionated and purified by RP-HPLC with a high degree of resolution. The recovery of the PTC-peptides isolated appears to be quantitative, and the PTC-peptides are suitable for microsequence analysis.

One of the disadvantages of this precolumn derivatization system using PTC is the presence in the chromatograms of several artefacts (Figs. 1–3), resulting from by products of the reagents which can coelute with some PTC-peptides. Several extraction procedures to remove these byproducts have been tried, with unsuccessful results (data not shown).

Nevertheless, this precolumn derivatization procedure can be used as a valid alternative to generate peptide maps at the picomolar level to obtain internal sequence information (either of proteins or of blocked proteins of which the direct primary structure cannot be determined by automatic sequencing) for gene identification or to generate oligonucleotides which can be used to clone genes.

ACKNOWLEDGEMENTS

This work was supported by Grants CICIT (PM89-0102) and F.I.S. We thank Dr. Luis Lamas for his critical evaluation and F. Soriano for his skillful technical assistance.

REFERENCES

- 1 P. Edman, *Acta Chem. Scand.*, 4 (1950) 277.
- 2 P. Edman and G. Begg, *Eur. J. Biochem.*, 1 (1967) 89.
- 3 D. Isle and P. Edman, *Aust. J. Chem.*, 16 (1962) 411.
- 4 R. L. Heinrikson and S. C. Meredith, *Anal. Biochem.*, 136 (1984) 65.
- 5 D. R. Koop, E. T. Morgan, G. E. Tarr, and M. J. Coon, *J. Biol. Chem.*, 257 (1982) 8472.
- 6 B. N. Jones, A. P. Consalvo, L. LeSeur, S. Lovato, S. D. Young, J. A. Koehn and J. P. Gilligan, in J. J. L'Italien (Editor), *Protein Structure and Function*, Plenum Press, New York, 1987, p. 197.
- 7 B. A. Bidlingmeyer, S. A. Coen and T. L. Tarvin, *J. Chromatogr.*, 336 (1984) 93.
- 8 S. Lemaire and S. Nolet, in J. J. L'Italien (Editor), *Protein Structure and Function*, Plenum Press, New York, 1987, p. 53.
- 9 B. Wittmann-Liebold, *J. Protein Chem.*, 7 (1988) 304.
- 10 S. Fisher, F. Reiman and B. Wittmann-Liebold, in B. Wittmann-Liebold (Editor), *Methods in Protein Sequence Analysis*, Springer, Berlin, Heidelberg, New York, 1989, p. 98.
- 11 K. L. Stone, M. B. LoPresti and K. R. Williams, in C. Fini (Editor), *Focus on Laboratory Methodology in Biochemistry*, CRC Press, Boca Raton, FL, 1989, in press.
- 12 S. Stein, P. Bohlen, J. Stone, W. Dairman and S. Udenfrien, *Arch. Biochem. Biophys.*, 155 (1975) 202.
- 13 J. Benson and P. Hare, *Proc. Natl. Acad. Sci., USA*, 72 (1974) 619.
- 14 E. Mendez, R. Matas and F. Soriano, *J. Chromatogr.*, 323 (1985) 373.
- 15 J. Y. Chang, *Biochem. J.*, 199 (1981) 537.
- 16 S. Pervaiz and K. Brew, *Science*, 228 (1985) 335.
- 17 J. G. Shewale, S. K. Sinha and K. Brew, *J. Biol. Chem.*, 259 (1984) 4947.

CHROMSYMP. 2281

Fingerprinting of molecular components in individual human cerebrospinal fluid samples with a new micropurification system

FRED NYBERG*

Department of Pharmacology, University of Uppsala, P.O. Box 591, S-751 24 Uppsala (Sweden)

SVEN LYRENÄS

Department of Gynaecology, University Hospital Uppsala, S-751 85 Uppsala (Sweden)

and

ÅKE DANIELSSON

Pharmacia LKB Biotechnology AB, S-751 82 Uppsala (Sweden)

ABSTRACT

This paper reports a rapid and sensitive microtechnique for fingerprinting as little as 20 μ l of cerebrospinal fluid (CSF) from individual humans. Different molecular components were also isolated from the fluid. The SMART system, a new system optimized for high-recovery micropurification, was used for this purpose. The CSF sample, obtained by lumbar puncture, was applied directly into the system, and the patterns recorded for different individuals under various physiological conditions were compared. The results indicate that the procedure provides a powerful tool for the identification or recovery of CSF components and may also be of importance for diagnostic use.

INTRODUCTION

The access of highly efficient procedures for the separation and analysis of bioactive molecules is of fundamental importance in many areas of biomedical research. A particular need concerns research focussed on bioactive compounds present in the central nervous system (CNS). Substances of interest in the CNS are those involved in neurotransmission or neuromodulation, such as neuropeptides and monoamines. These compounds are present in the tissues of the CNS at relatively low concentration and highly sensitive techniques are necessary for their detection. A procedure in frequent use for the analysis and separation of neuroactive peptide is reversed-phase high-performance liquid chromatography (RP-HPLC). This technique has been successfully used to purify a number of neuropeptides present in the CNS and also in peripheral tissues (*e.g.* refs. 1–5) because of its high resolution power and comparatively short time of analysis.

In previous studies, we have used RP-HPLC to study opioid peptides in the cerebrospinal fluid (CSF) [6–10]. In this fluid, most peptides are present at very low

concentrations and it was therefore necessary to combine the HPLC analyses with radioreceptor or radioimmunoassays. Furthermore, prior to HPLC the CSF sample requires concentration. In RP-HPLC analysis of other non-opioid peptides present in CSF it is possible to use spectrophotometrical methods for their detection [11]. However, a concentration step is also required in this case.

In this paper, we describe the use of the SMART system for the analysis of molecular constituents in human CSF. This new system is optimized for micropurification and microanalysis of biomolecules in samples of different origins. It may, therefore, provide new possibilities for the analysis and recovery of minute amount of peptides from crude tissue extracts or various body fluids. Here, the SMART system was used for the development of a procedure for fingerprint analysis of molecular components in individual human CSF samples.

EXPERIMENTAL

Chemicals and peptides

Standard peptides used in this study were purchased from Bachem (Bubendorf, Switzerland). The monoamines and their derivatives or metabolites were from Sigma (St. Louis, MO, USA). All other chemicals and solvents were of analytical grade from commercial sources.

Cerebrospinal fluid material

Lumbar CSF was obtained from women who volunteered for a study of CSF endorphins during pregnancy and in the puerperium [12]. Samples were frozen immediately following collection and stored at -70°C .

Chromatography

CSF samples (20–200 μl) from different individuals were analyzed by the SMART system (Pharmacia LKB Biotechnology, Uppsala, Sweden). The computer-controlled micropreparative chromatography system was equipped with a dual titanium cylinder syringe pump, a temperature-controlled (4°C to room temperature) separation unit containing a dual chamber dynamic mixer (30 + 30 μl), a six-port injection valve, a column holder, in-built detector cells for UV and conductivity measurement, and a fraction collector [13]. The UV monitor was UV-MII with 214-nm optics. Conductivity was measured using the in-built gradient monitor. The conductivity scale was set by calibration with eluent A (100%) and eluent B (0%); A, 0.14% trifluoroacetic acid (TFA); B, 0.12% TFA in 60% acetonitrile. Control of the system and evaluation of results was done with SMART Manager software. The column was $\mu\text{RPC C}_2/\text{C}_{18}$, PC 3.2/3 (particle size 3 μm , 120 \AA ; 30×3.2 mm I.D.). Elution was achieved with a linear gradient of acetonitrile (0–60%) containing TFA at a flow-rate of 240 $\mu\text{l}/\text{min}$.

RESULTS

Fig. 1 illustrates the UV pattern recorded from chromatographic analysis of a CSF sample (20 μl) collected from a woman in late pregnancy. It is obvious from the figure that the present technique provides an efficient separation of a number of

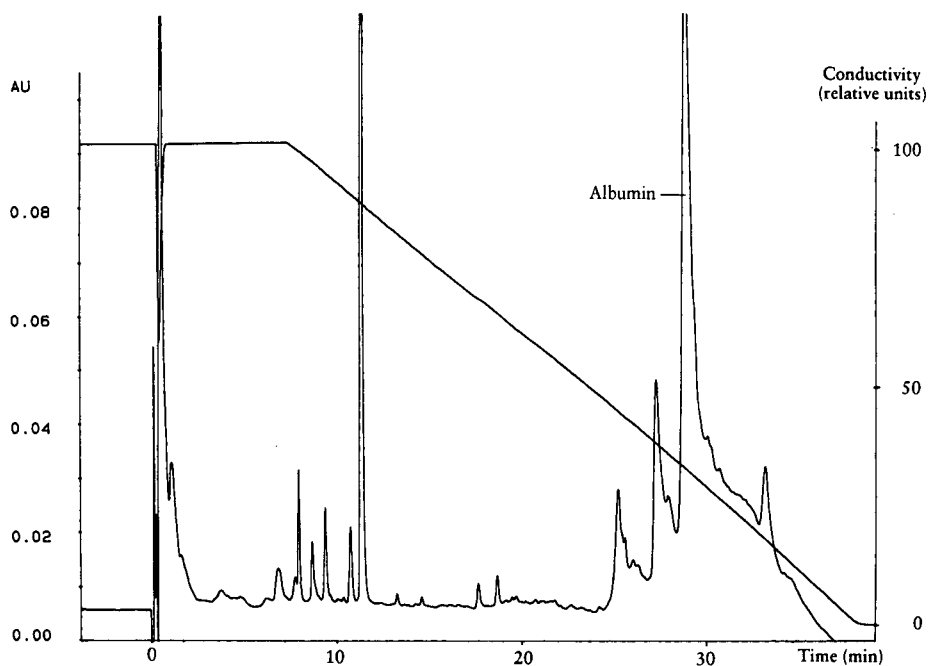


Fig. 1. Reversed-phase separation with the SMART system of human CSF (20 μ l) collected from a woman at late pregnancy. The UV profile was recorded at 214 nm and the true gradient (descending solid line) was monitored by on-line conductivity measurement in the system. The main peak was identified electrophoretically as albumin and the adjacent (earlier-eluting) peak as α -microglobulin. Eluent A: 0.14% trifluoroacetic acid (TFA). Eluent B: 0.12% TFA in 60% acetonitrile. For further details, see text.

TABLE I

RETENTION TIMES RECORDED FOR VARIOUS NEUROPEPTIDES, MONOAMINES AND THEIR METABOLITES

Substance ^a	Retention time (min)
Dopamine	2.5
MOPEG	5.7
Serotonin	7.4
5-HIAA	10.6
HVA	11.4
SP (1-7)	13.4
Met-enkephalin	16.6
Dynorphin B	18.8
SP	20.1

^a MOPEG = MHPG = 3-methoxy-4-hydroxyphenylglycol (noradrenaline metabolite); 5-HIAA = 5-hydroxyindoleacetic acid (serotonin metabolite); HVA = homovanillic acid (dopamine metabolite); SP = substance P (Arg-Pro-Lys-Pro-Gln-Gln-Phe-Phe-Gly-Leu-Met-NH₂); Met-enkephalin = Tyr-Gly-Gly-Phe-Met; dynorphin B = Tyr-Gly-Gly-Phe-Leu-Arg-Arg-Gln-Phe-Lys-Val-Val-Thr.

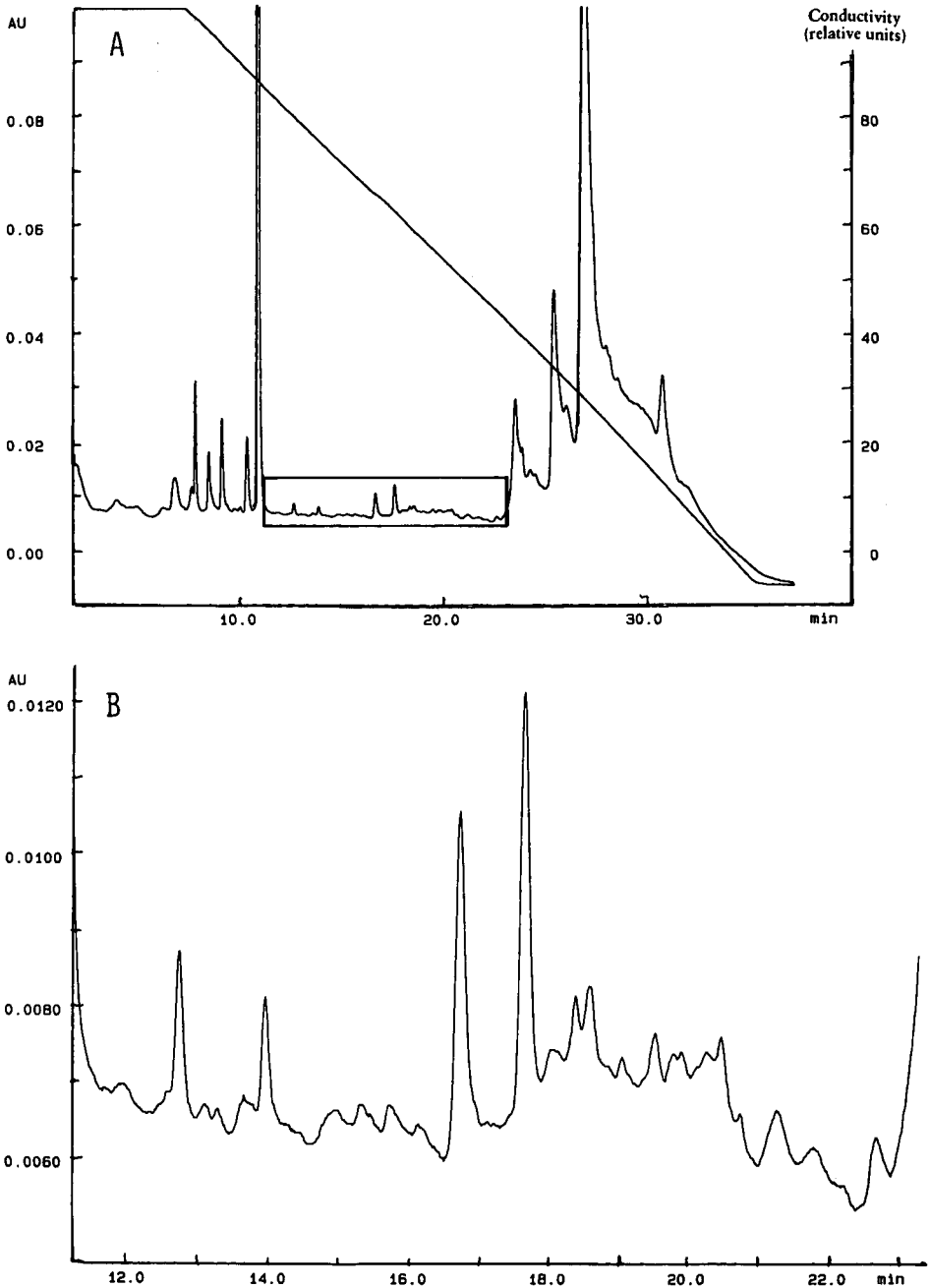


Fig. 2. (A) Analysis of human CSF ($20 \mu\text{l}$), collected from a woman at late pregnancy, by the SMART system using conditions for reversed-phase separation. The UV profile was recorded at 214 nm and the true gradient (descending solid line) was monitored as before. (B) Computer-enhanced enlargement of the boxed area seen in the upper panel. For separation conditions, see text and the legend to Fig. 1.

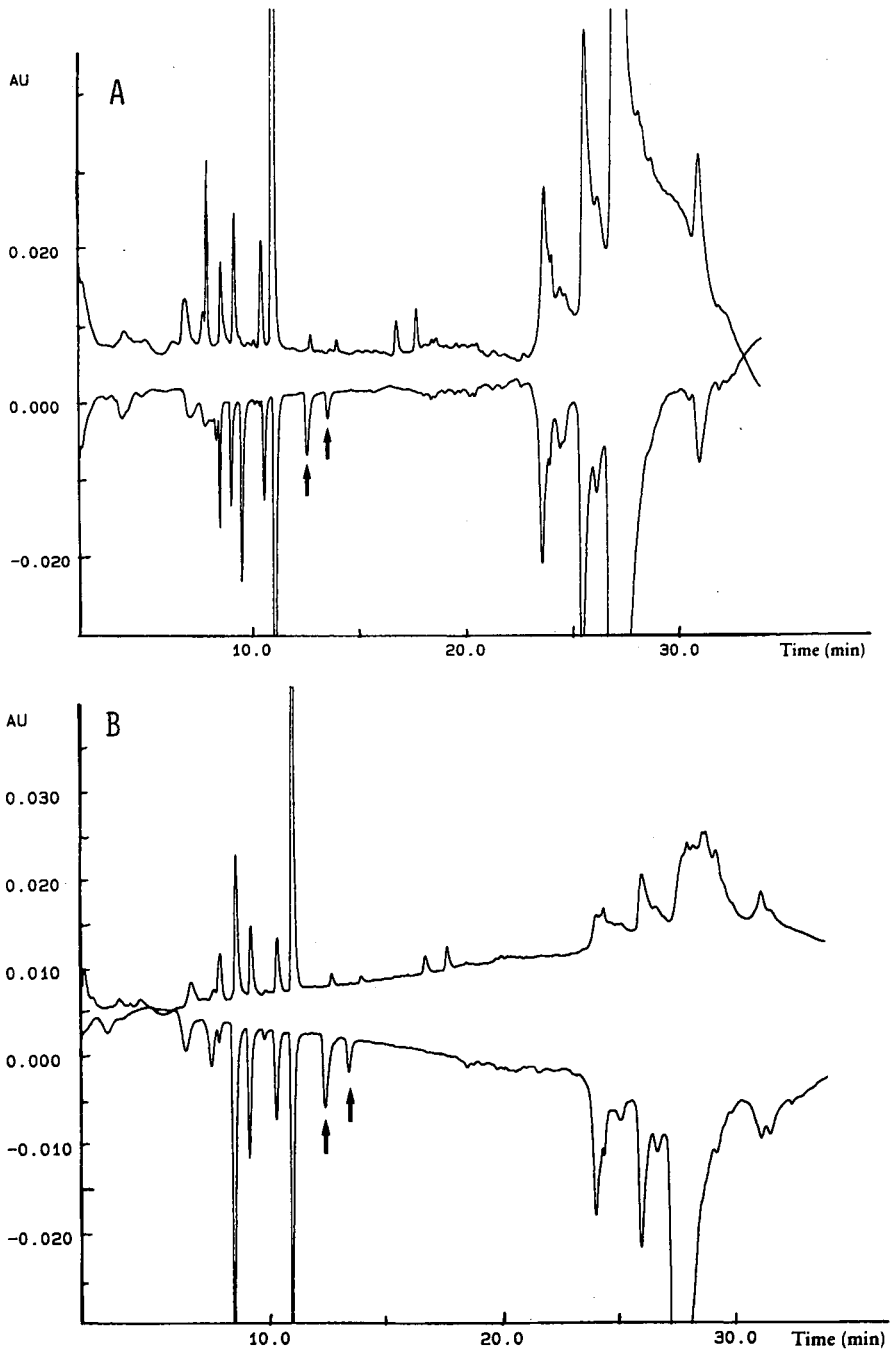


Fig. 3. Fingerprinting of molecular components in CSF obtained from two separate women (A and B), during late pregnancy and the lactation period. The upper curve in each chromatogram is CSF obtained during late pregnancy, whereas the lower curve represents CSF collected during lactation. The mirror images (lower curve) were done with the "shift amplitude" function in SMART Manager. Other conditions were identical to those given in the legend to Fig. 1.

UV-absorbing components present in the fluid. A major component was electrophoretically identified as human serum albumin, whereas a second peak eluting before but adjacent to albumin was identified as α -microglobulin. Several distinct components emerged from the column at retention times between 5 and 15 min. At least two of these components coincided with the monoamine metabolites 5-hydroxyindoleacetic acid (5-HIAA) and homovanillic acid (HVA), as listed in Table I. By the addition of synthetic HVA to the CSF sample, the peak eluting at 11.4 min was significantly increased. Both 5-HIAA and HVA are known to be present in CSF and their levels are the subject of great interest in research on various CNS diseases. Only minor UV peaks are observable in the retention time area corresponding to neuropeptides (*cf.* Fig. 1 and Table I). However, because the instrument allows computer-enhanced enlargement of selected regions in the chromatogram, it was also possible to visualize several UV peaks in this area (Fig. 2). None of these peaks, however, are likely to represent any of those peptides listed in Table I, due to their extremely low levels in the CSF compartment [14]. Runs of standard peptides (Table I) indicated that the procedure allowed UV detection of these synthetic compounds at levels of 10–15 ng. The detection limit for the monoamine and monoamine metabolites used in this study was about ten times lower.

Analysis of samples collected from one woman at term pregnancy and during lactation indicated that the recorded UV pattern remained essentially the same (Fig.

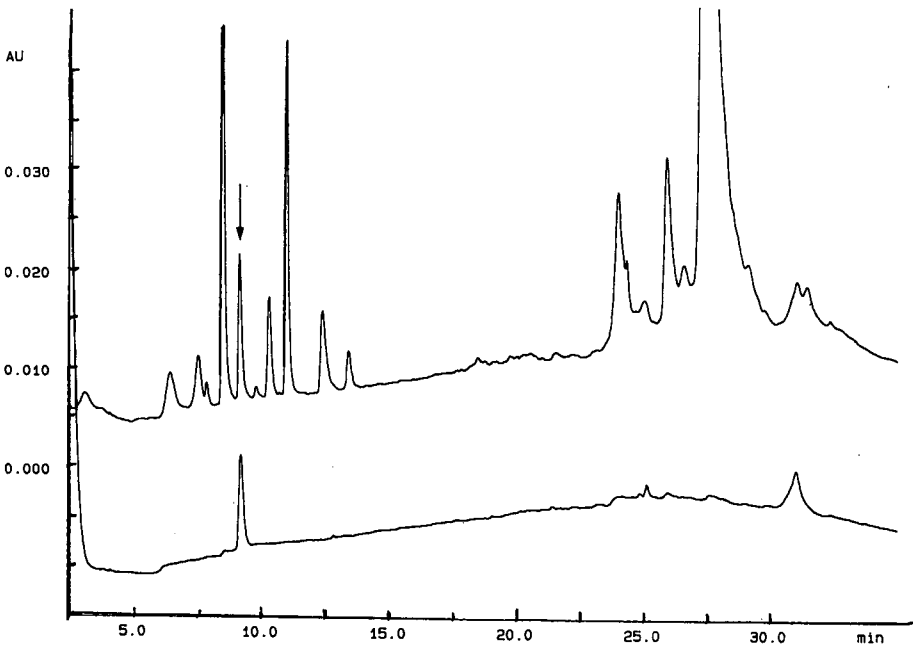


Fig. 4. Isolation and recovery of an unknown component in CSF. The material in the peak marked with an arrow was collected and diluted with eluent A. It was then reinjected onto the same column. The recovery was 78%, as calculated by a comparison of the integrated peak areas (done with SMART Manager). The sample was 20 μ l CSF collected from a lactating woman. Other conditions were identical to those used for the experiment shown in Fig. 1.

3). However, it was possible to distinguish additional peaks that were present in CSF at term pregnancy but not during lactation. Most of these peaks were observed at retention times expected for neuropeptide structures (*cf.* Fig. 3 and Table I). Furthermore, at least two UV-absorbing components (indicated by arrows in the figure) were recorded in samples from women in the lactation period but were not observed in the fluid collected at their term pregnancy (Fig. 3). Other differences in the chromatograms were also observed. The patterns shown in Fig. 3 are also typical for two other women who volunteered for the study (not shown). In samples from the fifth woman in the group of healthy volunteers the additional peaks during lactation were less pronounced. Data also indicated some minor inter-individual differences between the recorded profiles, thus indicating that the pattern is unique for each individual. Apart from the additional peaks discussed above, the inter-relationships between the different components in a single subject seemed to remain over a longer period of time (Fig. 3).

In order to check the recovery of the present technique, individual components present in the CSF were re-analyzed. In the experiment shown in Fig. 4, a CSF component recovered from a 20- μ l sample at a retention time of 9 min was re-chromatographed. Based on peak areas, a recovery of 78% was calculated. In studies of nanogram amounts of synthetic peptides a recovery of 80–90% was found. Furthermore, repetitive runs of individual CSF samples indicated a very high reproducibility for the system.

DISCUSSION

In this work, we have used the SMART system to develop a reversed-phase chromatography technique for the analysis and separation of components in human CSF. As the CSF is in constant exchange with the extracellular fluid of the brain and spinal cord, it represents a source of substances that derive from the CNS. Biochemical changes in the CNS, which may occur in chronic pain, psychiatric diseases or in neurologic disorders, may thus be traceable by CSF analysis. For ethical reasons, however, the volume of CSF that can be drawn from patients is limited. The present procedure allows detection and analysis of molecular constituents in the CSF with as little as 20 μ l of the fluid. In previous studies, we have used around 2 ml of CSF to screen the peptide pattern by RP-HPLC [11].

In the present study, we have used a new system to analyze UV-absorbing components in human CSF. Several of these components are likely to represent proteins (*e.g.* albumin and α -microglobulin) or smaller peptides, whereas other may be due to molecules of non-peptide structure. The chromatographic patterns shown in, for example, Fig. 3 reveal a characteristic profile typical for the samples analyzed in this study. Predominating components are seen both in the area close to the void volume and in the region of the albumin peak. Attempts to recover and determine the structure of these components are in progress. The structures of the "additional" components seen at term pregnancy and during lactation are of particular interest. In a preliminary experiment, the largest component in the group of peaks eluting early in the gradient (see Fig. 1) was recovered in microgram amounts and was subjected to amino acid analysis. No amino acids above background levels were detected in this material, indicating that this component is not a peptide or protein. Structure identifi-

cation of this non-peptide compound may, therefore, require other techniques such as NMR and mass spectrometry. For that purpose, additional amounts of this component are necessary, and in on-going work the SMART system will be used for its recovery from considerable larger volumes of CSF.

The characteristic patterns recorded for individual CSF samples also suggest that the present procedure may be useful for the identification of unique substances that may be characteristic for certain physiological or pathophysiological conditions. For instance, in degenerative CNS disorders such as Alzheimers disease, an abnormal function of some peptide systems have been hypothesized (*e.g.* refs. 15 and 16). Similarly, the generation of abnormal peptides has been suggested to occur in certain psychiatric diseases, *e.g.* schizophrenia [17] and post-partum psychosis [18]. It is therefore tempting to speculate that it might be possible to identify certain CSF peptides that are characteristic for each of these particular disorders using the present technique. Furthermore, as a consequence of this possibility, the system might also be of importance as a diagnostic tool. In this context, the technique may not only be useful for analysis of peptides or peptide products but also for the analysis of other structures including monoamines and their metabolites.

ACKNOWLEDGEMENTS

This study was supported by Göran Gustavssons Stiftelse and the Swedish Medical Research Council (Grant 03X-9459).

REFERENCES

- 1 R. V. Lewis, S. Stein and S. Udenfriend, *Int. J. Pept. Protein Res.*, 13 (1979) 493.
- 2 T. M. Muller and K. Unsicker, *J. Neurosci. Methods*, 4 (1981) 39.
- 3 T. M. Davis, H. Schoemaker, A. Chen and H. I. Yamamura, *Life Sci.*, 30 (1982) 971.
- 4 S. Mousa and D. Couri, *J. Chromatogr.*, 267 (1983) 191.
- 5 G. J. Moore, *Life Sci.*, 30 (1982) 995.
- 6 F. Nyberg, A. Wahlström, B. Sjölund and L. Terenius, *Brain Res.*, 259 (1983) 267.
- 7 F. Nyberg and L. Terenius, *Neuropeptides*, 5 (1985) 537.
- 8 F. Nyberg, I. Nylander and L. Terenius, *Brain Res.*, 371 (1986) 278.
- 9 F. Nyberg and I. Nylander, *Regul. Pept.*, 17 (1987) 159.
- 10 S. Lyrenäs, F. Nyberg, R. Folkesson, B. Lindberg and L. Terenius, *NIDA Res. Monogr.*, 75 (1986) 430.
- 11 J. Silberring, S. Lyrenäs and F. Nyberg, *Biomed. Chromatogr.*, 3 (1989) 203.
- 12 S. Lyrenäs, F. Nyberg, H. Lutsch, B. Lindberg and L. Terenius, *Acta Endocrinol.*, 115 (1987) 253.
- 13 Y. Hareland, in J. Villafranca (Editor), *Techniques in Protein Chemistry II*, Academic Press, New York, 1991, pp. 31-36.
- 14 F. Nyberg, I. Nylander and L. Terenius, *Handb. Exp. Pharm.*, 82 (1987) 227.
- 15 D. L. Price, E. H. Koo and A. Unterbeck, *BioEssays*, 10 (1989) 69.
- 16 H. Zhang, N. H. Sternberger, L. J. Rubinstein, M. M. Herman, L. I. Binder and L. A. Sternberger, *Proc. Natl. Acad. Sci. U.S.A.*, 86 (1989) 8045.
- 17 L. Terenius and F. Nyberg, in J. M. van Ree and S. Matthyse (Editors), *Progress in Brain Research*, Vol. 65, Elsevier, Amsterdam, 1985, p. 205.
- 18 F. Nyberg, L. Lindström and L. Terenius, *Biol. Psychiatr.*, 23 (1988) 115.

CHROMSYMP. 2151

High-performance liquid chromatographic determination of peptides in biological fluids by automated pre-column fluorescence derivatization with fluorescamine

VENKATA K. BOPPANA*, CYNTHIA MILLER-STEIN, JAMES F. POLITOWSKI and GERALD R. RHODES

Department of Drug Metabolism, SmithKline Beecham Pharmaceuticals, P.O. Box 1539, King of Prussia, PA 19406-0939 (USA)

ABSTRACT

Peptides containing a free α - or ϵ -amino group react with fluorescamine under mild alkaline conditions to generate a highly fluorescent but unstable reaction product and, consequently, practical high-performance liquid chromatographic (HPLC) approaches to analysis have typically involved the use of postcolumn derivatization. An automated precolumn approach is reported in which peptides are reacted with fluorescamine just prior to HPLC analysis by a commercially available autoinjector with derivatization capabilities. The autoinjector added base and fluorescamine reagent solutions to a sample vial containing peptide analytes, and the derivatization reaction was allowed to proceed for 5 min at room temperature prior to injection into the HPLC system. The derivatized peptides were analyzed by reversed-phase HPLC with fluorescence detection (excitation at 390 nm; emission 470-nm cut-off filter) on an octylsilica column. Optimization of the precolumn reaction conditions and the use of narrower HPLC columns (2 mm I.D.) resulted in a typical on-column detection limit of 30–50 fmol of peptide, which was substantially lower than that in previously reported post-column methods. This approach was applied to the HPLC of several naturally occurring and synthetic peptides containing α - and ϵ -amino groups. In combination with solid-phase extraction, prior to automated precolumn fluorescence derivatization and chromatographic analysis, the methodology was used for the determination of a synthetic growth hormone-releasing peptide in plasma samples.

INTRODUCTION

The development of novel peptide analogues as therapeutic agents has recently been of increasing interest in drug development. As many synthetic peptide analogues are extremely potent, and often administered at a low dosage, the development of highly sensitive and specific analytical methodology to support pharmacokinetic and disposition studies is a challenging problem for this class of molecules. This is especially true for high-performance liquid chromatographic (HPLC) assays, as many synthetic peptide analogues lack an appropriate chromophoric or fluorescent group which would allow detection of these peptides at the sub-picomole level. Enhancing the detectability of such peptides by chemical modification is one possible solution, and for peptides containing a free α - or ϵ -amino group, selective derivatization (pre-

or postcolumn) can be achieved with several fluorescent reagents to allow HPLC measurement at high sensitivity.

Although fluorescamine was discovered two decades ago [1–5] as a derivatization reagent for the fluorescence detection of primary amines, peptides and proteins, its use for postcolumn reaction detection [6–8] in HPLC has been limited owing to the high cost of reagent. The use of fluorescamine in precolumn derivatization methods for HPLC has also been restricted owing to the limited stability of the fluorescent product formed [9]. Owing to these, and other, practical limitations, previously reported methods for the HPLC of peptides with fluorescence detection following pre- and postcolumn derivatization with fluorescamine have suffered from a lack of routine applicability and/or sensitivity.

This paper describes the development of HPLC methodology for the determination, in plasma samples, of synthetic peptides containing a free α - or ϵ -amino group by automated reaction with fluorescamine using a commercially available autoinjector with sophisticated precolumn derivatization capabilities. The approach involved preliminary isolation of the peptide from plasma prior to automated reaction with fluorescamine and subsequent HPLC. The derivatized peptides were separated by reversed-phase HPLC and detected with a spectrofluorimeter. The use of narrower HPLC columns and optimization of the precolumn derivatization conditions resulted in an on-column detection limit in the range 30–50 fmol (signal-to-noise ratio = 3). Although we developed this methodology primarily to study a series of synthetic lysine-containing peptides which release growth hormone in several species, the method, owing to its high sensitivity, has general applicability in the detection of several naturally occurring peptides such as bradykinin and the angiotensins.

EXPERIMENTAL

Chemicals and materials

The synthetic lysine-containing peptides (Fig. 1), known to release growth hormone in several species, were supplied by Drug Substances and Products, SmithKline Beecham Pharmaceuticals (Swedeland, PA, USA). Naturally occurring peptides, such as bradykinin and angiotensins, were purchased from Sigma (St. Louis, MO, USA). HPLC-grade water (Millipore, Bedford, MA, USA) was used in the mobile phases and in the preparation of buffers and standard solutions. Fluorescamine and trifluoroacetic acid (TFA, 99%) were obtained from Pierce (Rockford, IL, USA). HPLC-grade methanol and acetonitrile were obtained from J. T. Baker (Phillipsburg, NJ, USA). All other chemicals were of analytical-reagent grade and obtained from local sources. Weak cation-exchange (CBA) solid-phase extraction cartridges (1 ml) and a Vac-Elut manifold were purchased from Analytichem International (Harbor City, CA, USA).

PEPTIDE	SK&F	STRUCTURE
I	110679	$\text{NH}_2\text{-L-HIS-D-TRP-L-ALA-L-TRP-D-PHE-L-LYS-NH}_2$
II	110910	$\text{NH}_2\text{-HIS-D-PHE-ALA-PHE-D-PHE-LYS-NH}_2$

Fig. 1. Structures of synthetic lysine-containing peptides.

Tris buffer, 10 mM (pH 7.0), was prepared by dissolving tris(hydroxymethyl) aminomethane (1.21 g) and triethylamine (2.8 ml) in 1 l of HPLC-grade water adjusting the pH to 7.0 with phosphoric acid.

Standard solutions

Stock standard solutions of peptide analytes were prepared by dissolving the appropriate amount of the compounds in methanol to obtain a 1 mg/ml solution. Working standard solutions were prepared by diluting a portion of the stock standards solutions with 0.1 M citrate buffer (pH 4.0) to give a final solution with concentrations ranging from 0.1 to 10 $\mu\text{g}/\text{ml}$. The working standard solutions were used in the generation of chromatographic data and calibration graphs. The stock and working standard solutions were stored at 4°C for not more than 2 weeks.

Extraction of synthetic lysine-containing peptides from plasma

An aliquot of plasma (0.5 ml) containing the synthetic peptide as a standard or as an unknown was mixed with 50 μl of an internal standard solution (1 $\mu\text{g}/\text{ml}$) in a 75 \times 12 mm I.D. borosilicate tube. A CBA solid-phase extraction column was conditioned by successive washings with 1 ml of methanol and 1 ml of water. Following application of the plasma sample to this cartridge, the sample tube was rinsed with 1 ml of water, which was applied to the column also. The CBA columns was then washed successively with 1 ml of 1% TFA in water, 3 ml of water and 1 ml of 50% methanol. The peptide was then eluted from the column with 2 ml of 2% (w/v) ammonium acetate in methanol and collected in a 75 \times 12 mm I.D. borosilicate tube. The methanol was evaporated under a gentle stream of nitrogen and the residue was reconstituted in 100 μl of 0.1 M citrate buffer (pH 4.0)–acetonitrile (75:25, v/v). The sample was then subjected to automated precolumn derivatization and HPLC.

Automated precolumn derivatization

A portion (20 μl) of the reconstituted plasma extract or standard solution was transferred to a limited-volume vial and loaded on the autoinjector. A 20- μl volume of potassium phosphate buffer was added to the sample vial by the autosampler followed by 30 μl of fluorescamine solution. The resulting solution was mixed by purging air into the sample vial and the reaction was allowed to proceed at room temperature. A portion of the reaction mixture (10–50 μl) was then injected for HPLC analysis.

High-performance liquid chromatography

The HPLC system consisted of a Hitachi 665A-12 high-pressure gradient semi-micro solvent-delivery system (EM Science, Cherry Hill, NJ, USA), a Hitachi F-1000 fluorescence detector (EM Science) and an Varian (Sunnyvale, CA, USA) autoinjector with precolumn reagent addition and mixing capabilities (Model 9090). Chromatographic separations were carried out on a 25 cm \times 2.0 mm I.D. Ultrasphere 5- μm octylsilica column (Beckman Instruments, Palo Alto, CA, USA), maintained at 50°C, at a flow-rate of 300 $\mu\text{l}/\text{min}$. The gradient mobile phase eluents utilized were Tris buffer (pH 7.0) and methanol. The specific gradient conditions that were employed for the chromatographic separation of various peptide analytes are described in detail under Results and Discussion. Mobile phase eluents were filtered through a 0.2- μm

nylon 66 filter and degassed before use. Detection was accomplished by excitation at 390 nm while monitoring the fluorescence emission using a 470-nm cut-off filter. An automated laboratory system (Access Chrom, PE/Nelson, Cupertino, CA, USA) was used for data acquisition and processing. Chromatographic peak-height data were collected and used for the generation of calibration graphs.

RESULTS AND DISCUSSION

The need to measure endogenous bioactive peptides and their synthetic analogues in biological fluids requires highly sensitive and specific analytical methods. The application of HPLC to such a problem typically requires derivatization in order to improve the native detectability of the peptide analyte. For many peptide analytes containing a free α - or ϵ -amino group, derivatization with one of the many fluorescence reagents available for primary amines is an attractive approach to high-sensitivity detection by HPLC. Of the reagents available, *o*-phthaldialdehyde and fluorescamine are most commonly used owing to their commercial availability in pure form, ease of handling and high fluorescence quantum yields. Fluorescamine has several advantages in routine use, including a higher rate of reactivity with primary amines, including amino acids, peptides and proteins [3]. Moreover, fluorescamine itself is non-fluorescent, as are the hydrolysis products formed during aqueous reaction, and this provides an extremely low background interference level for both pre- and postcolumn derivatization applications in HPLC.

Previous HPLC approaches using fluorescamine for the analysis of peptides have typically employed either postcolumn or manual precolumn derivatization. In general, precolumn derivatization is often preferred over postcolumn reaction methods in HPLC because a higher sensitivity can be achieved owing to elimination of baseline flow noise, band broadening and dilution effects resulting from the postcolumn addition of reagent solutions. Moreover, the cost of fluorescamine can make its use for postcolumn reaction detection in HPLC prohibitive. However, aside from the need to control the reaction conditions precisely to ensure reproducibility, precolumn derivatization methods using fluorescamine also suffer from the limited stability of the peptide derivatives in the alkaline reaction medium following formation. The use of the Varian 9090 autoinjector for automation and precise control of derivatization, followed by chromatographic injection immediately after reaction, resolves the issues associated with the use of fluorescamine in precolumn derivatization for the HPLC of peptides with fluorescence detection.

Optimization of precolumn reaction conditions

Optimization of the precolumn derivatization conditions was achieved using gradient elution HPLC of the model synthetic peptides I and II. The HPLC conditions used an initial mobile phase composition of Tris Buffer (pH 7.0)–methanol (50:50, v/v) and, following injection, the methanol concentration was increased to 65% over 10 min, held for 7 min and then cycled to the initial conditions in 2 min. Using these HPLC conditions, the precolumn reaction parameters were systematically varied, as described below, during repetitive injections of a standard solution of peptide, and the resulting chromatographic peak height observed was used as a measure of fluorescence response for optimization purposes.

The effect of fluorescamine concentration on precolumn derivatization was examined by varying the concentration from 1 to 5 mg/ml. The results indicated that a fluorescamine concentration ≥ 2 mg/ml gave the maximum fluorescence intensity for these model peptides. In order to minimize chromatographic difficulties associated with excess of reagent, a fluorescamine concentration of 2 mg/ml was adopted. The effect of pH on the reaction was examined by varying the pH of the phosphate buffer from 7.0 to 10.0. The results indicated that maximum fluorescence intensity was observed at pH 9.0 using phosphate buffer. The effect of ionic strength of the buffer was also studied by varying its molarity from 0.1 to 2, while maintaining the fluorescamine concentration at 2 mg/ml and the pH of the buffer at 9.0. The results demonstrated that a buffer molarity of 0.5 was necessary to maintain the reaction medium at the optimum pH of 9.0. The optimum conditions reported here may vary slightly with different peptides and buffers [3].

Using the reagent conditions established above, the effect of reaction time was examined by allowing the derivatization to proceed for times ranging from 1 to 30 min. The results showed that maximum fluorescence intensity was observed at a reaction time of between 1 and 5 min. Longer reaction times provided no increase in fluorescence signal owing to apparent instability of the peptide derivatives, which resulted in the appearance of additional chromatographic signals. A reaction time of 5 min was therefore adopted. Hence the optimum phosphate buffer and fluorescamine concentrations and reaction time were 0.5 M, 2 mg/ml and 5 min, respectively, and these conditions were used in all subsequent work.

The precision of the automated fluorescamine derivatization method described here was examined by repetitive derivatization of 23 pmol of peptide I and 25 pmol of peptide II and injecting 10 μ l of reaction mixture into the HPLC system. The method displayed suitable chromatographic peak-height reproducibility for the routine determination of peptides, yielding a relative standard deviation (R.S.D.) of 7.8% for I and 5.3% for II (Table I).

Detection of synthetic lysine-containing peptides

Fig. 2 shows the results obtained from HPLC of synthetic lysine-containing peptides using the automated precolumn fluorescamine derivatization approach described here. These peptides have been demonstrated *in vivo* to cause the release of growth hormone in several species following intravenous administration. Chromatographic analysis was accomplished using gradient elution on a 2 mm I.D. octylsilica column followed by fluorescence detection. The initial mobile phase composition used was Tris buffer (pH 7.0)–methanol (50:50, v/v). Following injection, the methanol concentration was increased to 65% over a period of 10 min. The peptides were well separated despite only minor structural differences. Although peptides I and II contain both an α - and an ϵ -amino group, which provide two potential sites for derivatization, no evidence for multiple derivative formation was observed. The synthetic peptides examined provided a single reproducible chromatographic peak for analysis. Under these conditions, the limit of detection for these synthetic peptides ranged from 30 to 50 fmol injected on-column.

Application of this methodology to the determination a synthetic lysine-containing peptide was exemplified by an HPLC assay developed to determine the concentration of SK&F 110679 (I) in plasma samples. SK&F 110910 (II) was used as an

TABLE I

CHROMATOGRAPHIC REPRODUCIBILITY OF AUTOMATED PRECOLUMN DERIVATIZATION

Injection ^a	Fluorescence intensity ^b	
	I	II
1	33 352.0	31 119.0
2	29 549.0	30 281.0
3	30 977.0	32 089.0
4	28 060.0	28 457.0
5	24 439.0	28 011.0
6	28 241.0	29 868.0
7	29 582.0	30 103.0
8	29 385.0	33 439.0
9	28 636.0	29 947.0
10	28 286.0	29 698.0
Mean	29 050.7	30 301.2
S.D.	2273.4	1601.2
R.S.D. (%)	7.8	5.3

^a An aliquot (20 μ l) of standard solution containing 23 pmol of peptide I and 25 pmol of peptide II was repetitively analysed using the methods described in the text.

^b Fluorescence intensity as measured by chromatographic peak height (μ V).

internal standard. The assay involved solid-phase extraction of the peptide from plasma, as a preliminary isolation step, followed by quantitative gradient HPLC with the methodology described here. Typical chromatograms of a drug-free plasma sam-

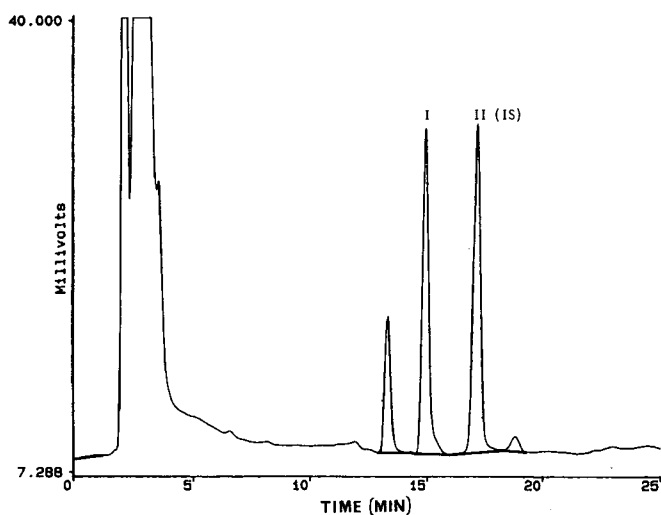


Fig. 2. Chromatogram of an aqueous standard solution of lysine-containing synthetic peptides. A solution containing 20 ng of each peptide was derivatized as described under Experimental and 3 ng were injected onto the column. See text for chromatographic conditions and peak identification.

ple and a plasma sample with 57 pmol of SK&F 110679 added (*ca.* 8 pmol injected on-column) are shown in Fig. 3. The initial mobile phase composition was Tris buffer (pH 7.0)–methanol (55:45, v/v). After injection, the methanol concentration was increased to 65% in 10 min and held for 7 min. The retention times of I and the internal standard (II) were 16.4 and 18.2 min, respectively. No interferences from endogenous compounds were observed and the drug and internal standard were well separated. The mean recovery of I from plasma samples was >90%. Plasma concentrations as low as 5 pmol/ml of I, which corresponded to an injected amount of *ca.* 0.7 pmol, have been determined using this approach. The assay was linear over the plasma

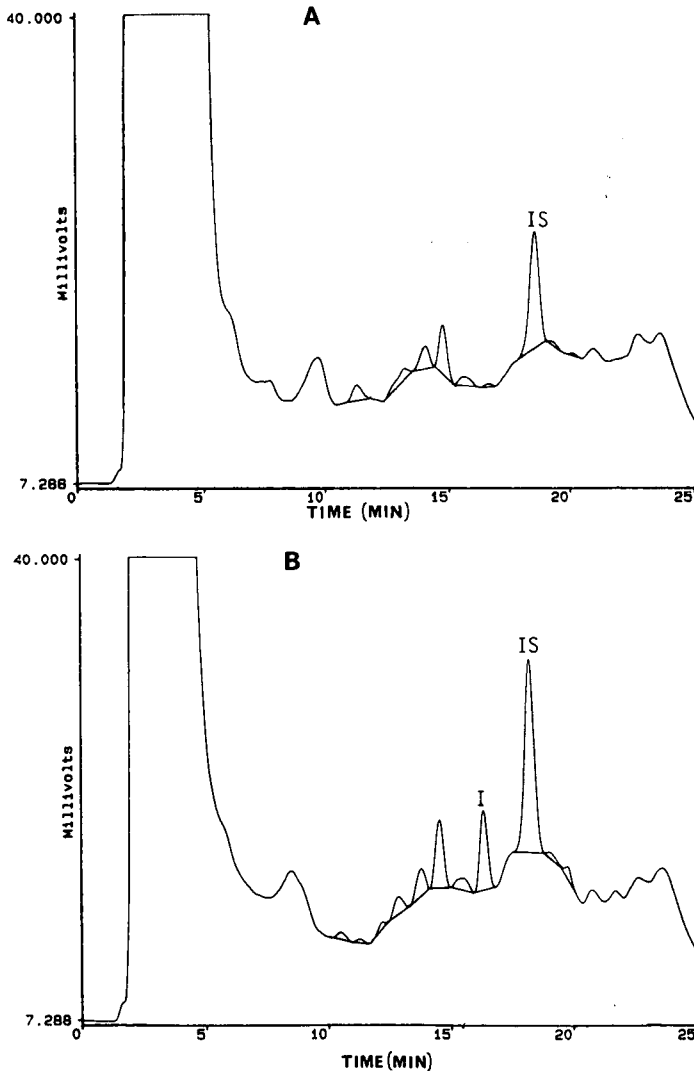


Fig. 3. Chromatograms of extracts of (A) drug-free plasma and (B) a plasma sample containing 57 pmol/ml of peptide I. See text for chromatographic conditions.

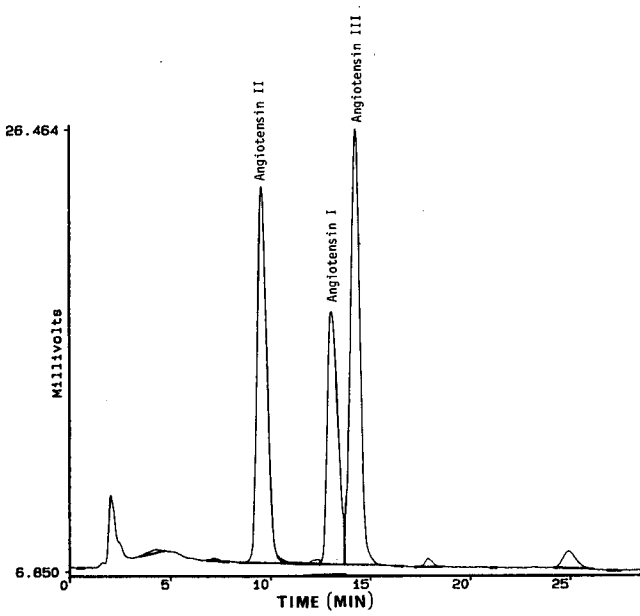


Fig. 4. Chromatogram of an aqueous standard solution of angiotensin I, II and III. The concentration of each peptide injected onto the column was 3 ng. See text for chromatographic conditions.

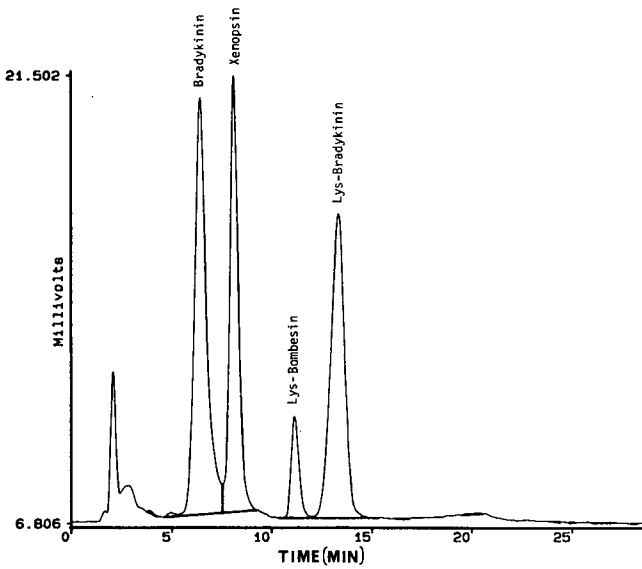


Fig. 5. Chromatogram of an aqueous standard solution of bradykinin, Lys-bradykinin, xenopsin and Lys-bombesin. The concentration of each peptide injected onto the column was 3 ng. See text for chromatographic conditions.

concentration range 5–500 pmol/ml. Correlation coefficients for plasma calibration graphs were typically >0.99 .

Application to naturally occurring peptides

The methodology reported here has also been applied to the HPLC detection of naturally occurring peptides containing free α - and ϵ -amino groups. Fig. 4 shows a gradient HPLC separation of angiotensins I, II and III on a 2 mm I.D. octylsilica column. The initial mobile phase was Tris buffer (pH 7.0)–methanol (60:40, v/v). Following injection, the methanol concentration was increased to 65% over a period of 10 min and held for 10 min. The detection limit for these peptides was in the range 30–50 fmol injected on-column. Fig. 5 shows the gradient elution of bradykinin, Lys-bradykinin, xenopsin and Lys-bombesin on a 2 mm I.D. octylsilica column. The initial mobile phase was Tris buffer (pH 7.0)–methanol (50:50, v/v), then the methanol concentration was raised to 65% over 10 min and held for 10 min. Xenopsin and Lys-bombesin have a blocked N-terminal amino group but contain a lysine residue in the peptide chain. Bradykinin and the angiotensins, on the other hand, do not contain a lysine residue, but have a free N-terminal amino group.

In conclusion, the HPLC methodology described here permitted the specific and highly sensitive detection of the peptides examined. Injection of a variety of other peptides that did not contain either a free α - or ϵ -amino group resulted in a lack of fluorescence response. The molecules examined demonstrated that the method is capable of detecting peptides with either or both a free α - or ϵ -amino group. The detection limits reported here are substantially lower than those described in previous reports for fluorescamine postcolumn detection of similar peptides. The sensitivity of the method allowed its successful application to the determination of synthetic peptides in plasma samples.

REFERENCES

- 1 M. Weigle, J. F. Blount, J. P. Teng, R. C. Czajkowski and W. Leimgruber, *J. Am. Chem. Soc.*, 94 (1972) 4052.
- 2 M. Weigle, S. L. DeBernardo, J. P. Teng and W. Leimgruber, *J. Am. Chem. Soc.*, 94 (1972) 5927.
- 3 S. Udenfriend, S. Stein, P. Bohlen and W. Dairman, *Science*, 178 (1972) 871.
- 4 S. Udenfriend, S. Stein, P. Bohlen and W. Dairman, in M. Johanes (Editor) *Proceedings of Third American Peptide Symposium*, Ann Arbor Sci. Publ., Ann Arbor, MI, 1972, p. 655.
- 5 N. Nakai, C. Y. Lai and B. L. Horecker, *Anal. Biochem.*, 58 (1974) 563.
- 6 S. Stein, P. Bohlen, J. Stone, W. Dairman and S. Udenfriend, *Arch. Biochem. Biophys.*, 155 (1973) 202.
- 7 P. Kucera and H. Umagat, *J. Chromatogr.*, 255 (1983) 563.
- 8 T. D. Schlabach, *J. Chromatogr.*, 266 (1983) 427.
- 9 T. K. Narayanan and L. M. Greenbaum, *J. Chromatogr.*, 306 (1984) 109.

Separation of acidic peptides by reversed-phase ion-pair chromatography

Analytical application to a series of acidic substrates of casein kinases

A. CALDERAN*, P. RUZZA, O. MARIN, M. SECCHIERI, G. BORIN and F. MARCHIORI

Biopolymer Research Centre of C.N.R., Department of Organic Chemistry of University of Padova, Via Marzolo 1, 35131 Padova (Italy)

ABSTRACT

A series of small peptides including clusters of glutamyl residues, synthesized to study the site specificity of rat liver (L-CK2) and yeast (Y-CK2) casein kinase-2, are analytically characterized by ion-pair high-performance liquid chromatography using tetrabutylammonium as counter-ion and acetonitrile as modifier of the aqueous phase. Under these conditions peptides of slightly different acidity can be separated and the elution order parallels the hydrophobicity of the ion-pair-peptide complexes, which increases with the number of the acidic functions present in the sequence.

INTRODUCTION

Synthetic peptides are largely employed as models to study various biochemical properties of protein kinases, in particular the mechanism by which these enzymes discriminate between different substrates and different potential phosphorylation sites. By varying the sequence of amino acid surrounding the target phosphorylated residue, it is in fact possible to detect the primary structure determinants that characterize the phosphorylation sites for a number of specific kinases. Such peptides can also be used in detecting and quantifying the activity of specific kinases in the presence of multiple kinases activities and in developing schemes for the isolation and characterization of these enzymes.

This approach was used in our laboratory to study the site specificity of two different casein kinases: the yeast casein kinase-2 (Y-CK2) and the rat liver casein kinase-2 (L-CK2). These enzymes catalyze the phosphorylation of a few specific seryl and threonyl residues in several proteins like casein. The phosphorylation sites in these proteins are always characterized by the presence of clusters of acidic amino acids on the C-terminal side of the target residue [1,2]. For this reason we have prepared, by the classical method in solution, a series of small peptides, including

clusters of glutamyl residues [3]. The structures of some of these peptides are given in Table I. They differ in the number and relative position of the acidic residues in the clusters, as well as in the nature of the target phosphorylatable residue.

In this paper a convenient method for the analytical separation of these peptides by high-performance liquid chromatography (HPLC) is reported.

EXPERIMENTAL

Synthetic peptides

The peptides used in this work are listed in Table I. The fragment condensation strategy in solution, which allows the utilization of several common intermediates for the preparation of the final peptides, was adopted. The standard procedures for peptide synthesis [4] have been employed, generally using the classical combination benzyloxycarbonyl and *tert.*-butyl groups for selective protection at the α -amino and γ -carboxyl functions, respectively. The methyl or ethyl esters, from which the corresponding hydrazides are readily obtained, were used to mask the α -carboxyl function in the intermediate peptides. The Rudinger modified azide procedure in the presence of N-hydroxysuccinimide as catalyst was therefore employed for fragment condensations, while mixed anhydrides (isobutyl chloroformate) or active esters (*p*-nitrophenyl of N-hydroxysuccinimido esters) were used for the preparation of the fragments.

After application of convenient deprotection procedures (catalytic hydrogenolysis in the presence of 10% palladized charcoal and/or exposure to 98% aqueous trifluoroacetic acid) the final peptides, when heterogeneous, were purified by chromatographic procedures (ionic exchange and gel filtration), then converted into hydrochloride salts by lyophilization with 5% HCl. The homogeneity of the final products was evaluated by thin-layer chromatography on cellulose plates and the correct composition of the peptides was checked by determining the amino acid ratios of the acid hydrolysates (6 M HCl, 110°C, 22 h) as previously reported [3].

TABLE I
AMINO ACID SEQUENCES OF THE SYNTHETIC PEPTIDES

Peptide	Amino acid sequence
1	H-Ser-Glu-Glu-Glu-Glu-Glu-OH
2	H-Ser-Glu-Glu-Ala-Ala-Ala-OH
3	H-Ser-Ala-Ala-Glu-Glu-Glu-OH
4	H-Ser-Ala-Glu-Glu-Glu-Glu-OH
5	H-Ser-Glu-Ala-Glu-Glu-Glu-OH
6	H-Ser-Glu-Glu-Ala-Glu-Glu-OH
7	H-Ser-Glu-Glu-Glu-Ala-Glu-OH
8	H-Ser-Glu-Glu-Glu-Glu-Ala-OH
9	H-Thr-Glu-Glu-Glu-Glu-Glu-OH
10	H-Tyr-Glu-Glu-Glu-Glu-Glu-OH
11	H-Glu-Glu-Glu-Glu-Glu-Ser-NH ₂
12	H-Glu-Ser-Glu-Glu-Glu-Glu-Glu-OH
13	H-Ser-Ala-Glu-Glu-Glu-Glu-OH
14	H-Glu-Glu-Glu-Glu-Glu-OH

Chemicals

All separations were performed using a linear A–B gradient elution technique, where A is $2 \cdot 10^{-2}$ M sodium phosphate buffer pH 5.6– $2 \cdot 10^{-3}$ M tetrabutylammonium hydrogensulfate. B is acetonitrile– $2 \cdot 10^{-3}$ M tetrabutylammonium hydrogensulfate. The solvent gradient was from 5 to 25% B in 35 min. HPLC-grade water was obtained from a Millipore Milli-Q apparatus (Millipore, Bedford, MA, USA); HPLC-grade acetonitrile was obtained from Farmitalia-Carlo Erba (Milan, Italy); tetrabutylammonium hydrogensulfate and sodium dihydrogenphosphate dihydrate were obtained from Fluka (Buchs, Switzerland) and were of analytical grade.

Equipment

The liquid chromatographic system consisted of two LKB 2150 solvent delivery units (Pharmacia LKB Biotechnology, Uppsala, Sweden), a LKB 2152 solvent programmer and a 7125 Rheodyne injector (Rheodyne, Cotati, CA, USA) coupled to a LKB 2158 UV monitor. The detection wavelength was 206 nm. In a typical experiment, approximately 10 nmol of each peptide, dissolved in 15 μ l of water containing 0.05% 1 M NaOH, was injected. The separation column was a ROSil C₁₈, 3 μ m (100 \times 4.6 mm I.D.), always preceded by a short pre-column (Alltech Assoc., Deerfield, IL, USA). The separations were run at a nominal flow-rate of 1 ml/min at room temperature (22°C) and the pH measurements were performed at the same temperature.

RESULTS AND DISCUSSION

The analytical separation of slightly different peptides requires often difficult and time-consuming procedures. With our synthetic glutamic acid-containing peptides (Table I), the presence of one or more acid groups can generally be exploited for separation by ion-exchange chromatography, but acceptable results are obtained only with a long elution times. On the other hand, very good separations are possible using another chromatographic approach: the generation of hydrophobic ion-pairs of these peptides [5]. In this procedure, the acidic peptides are associated with a hydrophobic cation in the eluent leading to less polar complexes [6,7]. Obviously the hydrophobicity of these ion-pair complexes and consequently their retention times on a reversed-phase column increase with the number of acidic functions. As described in Experimental section, the ion-pairing reagent used with success in the water–acetonitrile mobile phase is the hydrophobic tetrabutylammonium ion. The corresponding separation patterns are shown in Figs. 1, 2 and 3.

Fig. 1 shows the separation of the amino- and carboxy-terminal free peptides 2, 3, 4, 13 and 12. From a structural point of view they can be considered sufficiently similar, but possess an increasing number of glutamyl residues: two, three, four, five and six, respectively. In agreement with the prediction, the elution patterns evidence that in the presence of tetrabutylammonium hydrogensulfate the hydrophobicity of the ion-pair complexes increases with the number of acidic groups. In particular, the resulting differences in retention time are considerable and give a clear indication of the usefulness of this chromatographic system.

In Fig. 2 the separation patterns of the six peptides (1, 9, 10, 11, 13 and 14) containing five glutamic acid residues are shown. The similarity in the retention times of compounds 1, 9, 10 and 14, which differ only in the side-chain of the N-terminal

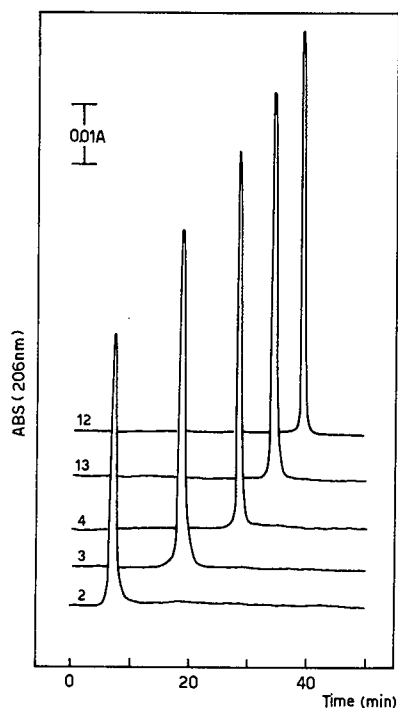


Fig. 1. Elution profiles of five peptides with an increasing number (2–6) of glutamyl residues. The amino acid sequences (one-letter codes) and the corresponding retention times are : 2 = SEAAAA (6.5 min); 3 = SAAEEEE (17.5 min); 4 = SAEEEE (27.0 min); 13 = SAEEEE (33.0 min); 12 = ESEEEEE (37.0 min). Experimental conditions as reported in *Chemicals* and in *Equipment*.

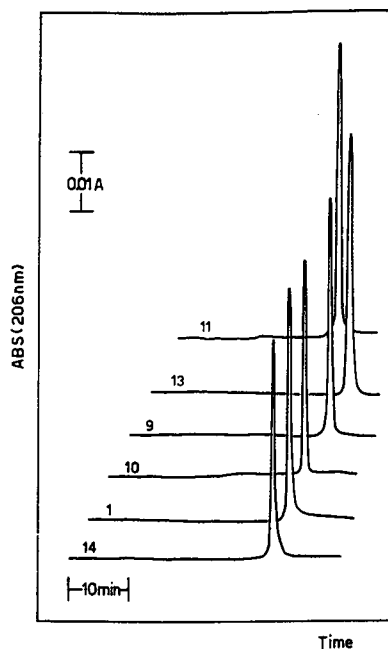


Fig. 2. Elution profiles of six peptides all containing five glutamic acid residues. The amino acid sequences and the corresponding retention times are: 14 = EEEEE (34.0 min); 1 = SEEEEE (33.5 min); 10 = YEEEE (33.0 min); 9 = TEEEE (33.5 min); 13 = SAEEEE (33.0 min); 11 = EEEEEES-amide (27.5 min). Experimental conditions as reported in *Chemicals* and in *Equipment*.

residue (serine, threonine, tyrosine or absent, respectively) indicates that a difference in the hydrophobicity of only one residue does not induce a substantial change in the elution profile of the ion-pair complexes. One additional residue, alanine, causes little change in the chromatographic behaviour of the five glutamyl residues containing peptides, *e.g.* compare compounds 13 and 1. Considering the results of Fig. 1 also, we can conclude that the influence of a change of the nature of residue(s) in the backbone seems to be very limited, especially in the presence of a high number of acidic functions. A direct comparison of the influence of the presence of a seryl residue in the N- or C-terminal position between compounds 1 and 11 is obviously impossible due to the amidation of the C-terminal carboxylic function in compound 11. Notwithstanding this, the corresponding consistent drop in the retention time of the ion-pair complex of 11 even if predicted, again confirms the high sensitivity of this chromatographic system.

In addition, Fig. 3 demonstrates the limited influence of the order in which the amino acid residues are arranged in the sequence. In fact the retention times reported

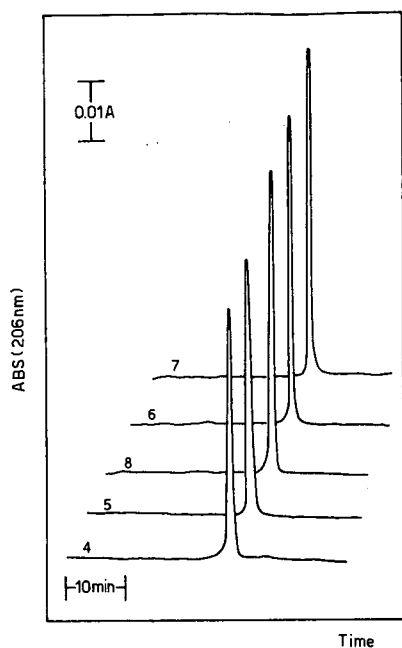


Fig. 3. Elution profiles of five hexapeptides all with the identical amino acid ratios $\text{Ser}_1\text{Glu}_4\text{Ala}_1$. The amino acid sequences and the corresponding retention times are: 4 = SAEEEE (27.0 min); 5 = SEAESE (26.5 min); 8 = SEEEEA (27.5 min); 6 = SEEAEE (26.5 min); 7 = SEEEAE (26.5 min). Experimental conditions as reported in *Chemicals* and in *Equipment*.

in this figure for the five hexapeptides 4, 5, 6, 7 and 8, all having identical amino acid ratios ($\text{Ser}_1\text{Glu}_4\text{Ala}_1$) but different sequential arrangement, are almost coincident. Specifically, no effect on the chromatographic behaviour is detectable for peptides containing acidic clusters of different length if the total number of acidic functions is the same.

CONCLUSIONS

The goal of this paper is to demonstrate that reversed-phase HPLC using ion-pairing reagents previously applied to the analysis of basic hydrophilic peptides [8,9] can also be usefully employed in the analytical characterization of acidic hydrophilic peptides. In fact, using a reversed-phase support to which the tetrabutylammonium ion-pair-peptide complexes are strongly bound, it is possible to separate ion-pair-peptide complexes differing in the number of the acidic functions. The differences in the retention times are sufficient to allow the separation of peptides differing in only one acidic function. On the contrary, the high hydrophobicity induced by the tetrabutylammonium ion in the ion-pair-peptide complexes may mask the variations in the amino acid sequence, particularly when a high number of acidic functions is present.

ACKNOWLEDGEMENTS

This work was supported by grants from the Italian 'Ministero della Pubblica Istruzione' and 'Consiglio Nazionale delle Ricerche' (Progetto Finalizzato 'Chimica Fine e Secondaria'). The amino acid analyses were carried out by Ugo Anselmi and Ernesto De Menego. The skilful technical assistance of Luca Bani in the synthesis of compounds is gratefully acknowledged.

REFERENCES

- 1 F. Meggio, A. P. Boulton, F. Marchiori, G. Borin, D. P. W. Lennon, A. Calderan and L. A. Pinna, *Eur. J. Biochem.*, 177 (1988) 281–284; and references cited therein.
- 2 F. Marchiori, F. Meggio, O. Marin, G. Borin, A. Calderan, P. Ruzza and L. A. Pinna, *Biochim. Biophys. Acta*, 971 (1988) 332–338; and references cited therein.
- 3 O. Marin, A. Calderan, P. Ruzza, G. Borin, F. Meggio, N. Grankowsky and F. Marchiori, *Int. J. Pept. Prot. Res.*, 36 (1990) 374–380.
- 4 E. Wünsch, in E. Wünsch (Editor), *Houben-Weyl, Methoden der Organischen Chemie*, Vol. 15, Georg-Thieme Verlag, Stuttgart, 1974.
- 5 E. Tomlinson, T. M. Jefferies and C. M. Riley, *J. Chromatogr.*, 159 (1978) 315–358.
- 6 W. S. Hancock, C. A. Bishop, J. E. Battersby, D. R. K. Harding and M. T. W. Hearn, *J. Chromatogr.*, 168 (1979) 377–384.
- 7 D. Guo, C. T. Mant and R. S. Hodges, *J. Chromatogr.*, 386 (1987) 205–222.
- 8 B. Fransson, U. Ragnarsson and Ö. Zetterqvist, *J. Chromatogr.*, 240 (1982) 165–171.
- 9 B. Fransson, U. Ragnarsson and Ö. Zetterqvist, *Anal. Biochem.*, 126 (1982) 174–178.

CHROMSYMP. 2198

Animal test or chromatography?

Validated high-performance liquid chromatographic assay as an alternative to the biological assay for ornipressin

R. H. BUCK*, M. CHOLEWINSKI and F. MAXL

Analytical Research and Development and Quality Assurance, Sandoz Pharma Ltd., CH-4002 Basle (Switzerland)

ABSTRACT

Ornipressin is a peptide drug which is usually assayed by a test on live rats. In order to reduce the animal experiments an alternative method was developed which uses gradient high-performance liquid chromatography (HPLC) on reversed-phase. The HPLC method was validated and shown to be selective and precise. Correlation studies were performed on samples of different dosage strengths and on thermally degraded samples, showing good correlation with the results obtained by the biological assay. The HPLC method was applied on various batches of ornipressin in bulk and in pharmaceutical preparations. HPLC is a rapid and inexpensive method which can replace the animal assay. A new quality control concept is proposed which uses HPLC for the analysis of ornipressin in bulk and in pharmaceutical preparations. With this concept animal testing can be reduced by 90%.

INTRODUCTION

Ornipressin is a polypeptide drug which exhibits a vasopressor effect when injected. It is used, *e.g.*, in the case of minor surgery to produce a local ischaemia. The drug is presently assayed by a biological assay which is performed on live rats. In this test, drug solutions are injected into the animals and the blood pressure is monitored. The resulting change in blood pressure is compared with the change produced by a standard preparation. The potency of the drug is expressed in terms of I.U. (approximately 2.4 μg of peptide corresponds to 1 I.U.). The bioassay is very time-consuming and expensive, and shows an assay variation which is higher than that of physico-chemical assays. Such assay variations are often inadequate for potency estimations of bulk substance as any analytical inaccuracy on the bulk material automatically leads to a systematic deviation in the final product.

In order to improve the assay precision and to reduce the animal experiments alternative assay methods were evaluated. Reversed-phase high-performance liquid chromatography (HPLC) is a technique which is nowadays predominant in the field of peptide analysis [1-11], so this methodology was applied for the quantitative analysis of ornipressin in bulk material and pharmaceutical preparations.

EXPERIMENTAL

Chemicals and equipment

Ornipressin and the other nonapeptides were produced by Sandoz Pharma (Basle, Switzerland). The concentrations of the solutions ranged from approximately 2 to 10 I.U./ml. The peptides were about 95% pure. Acetonitrile and water were of HPLC grade, all other chemicals were of analytical grade. An HPLC system was used equipped for automated sample injection, gradient elution, column thermostatisation, UV detection and automated peak integration.

HPLC assay for ornipressin

Gradient chromatography was used for the separation and quantification of ornipressin [11]. Mobile phase A consisted of a 0.02 M solution of tetramethylammonium hydroxide in water, mobile phase B was a 0.02 M solution of tetramethylammonium hydroxide in a mixture of water-acetonitrile (50:50, v/v). The pH of both mobile phases were adjusted to pH 2.5 with concentrated orthophosphoric acid. The mobile phases were degassed prior to use.

As stationary phase, columns of 125 × 4.6 mm or 100 × 4.6 mm filled with octadecylsilanised silica gel of 5 µm mean particle size were used, e.g. Shandon Hypersil ODS or Spheri 5 from Brownlee Labs. (Santa Clara, CA, USA). Injection volume was 100 µl, flow-rate was 1.0 ml/min, a linear gradient was run from 10 to 60% of mobile phase B in 25 min. Column temperature was set to 60°C if not stated otherwise. Detection was by UV at 220 nm.

Biological assay for ornipressin

The biological assays for ornipressin were done in analogy to the biological assay for lyspressin described in The British Pharmacopoeia [12]. As reference, an internal reference standard of ornipressin was used which had previously been standardised against the first international standard for lysine-vasopressin.

Collaborative study

A collaborative study was performed to compare and to validate the two methods with respect to accuracy, precision and laboratory-to-laboratory reproducibility. The study involved three different laboratories on the biological assay and three different laboratories on the HPLC assay. Each laboratory analysed each sample in duplicate or triplicate.

Solutions of ornipressin in the dose range 2.75–8.25 I.U./ml were used for a linearity test. The solutions were prepared in aqueous buffer of pH 4, sterilised by filtration and sealed in ampoules. For a degradation test ampoules of 5 I.U./ml were taken and artificially degraded by exposure to a temperature of 50°C for up to 2 months.

Internal reference standard

Ampoules containing injection material from a pharmaceutical production batch were used for this purpose. The reference standard was calibrated against the first international standard for lysine-vasopressin by means of biological assays in three different laboratories. The mean of the assay results was taken as the potency

for the internal reference standard. This standard was used for all further calibrations by HPLC and bioassay.

RESULTS AND DISCUSSION

Reversed-phase HPLC of ornipressin and some structure-related peptides

The selectivity of the separation system was investigated by studying the retention behavior of ornipressin and four other nonapeptides. The nonapeptides all had structures very similar to that of ornipressin and most of them differ in one amino acid only. The sequences are given in Table I. The samples also contained methyl 4-hydroxybenzoate and chlorobutanol which served as preservatives in the bulk solutions.

TABLE I
STRUCTURES OF THE PEPTIDES INVESTIGATED

Peptide	Structure
Demoxytocin	<u>Mps-Tyr-Ile-Gln-Asn-Cys</u> -Pro-Leu-Gly-NH ₂
Oxytocin	H-Cys-Tyr-Ile-Gln-Asn-Cys-Pro-Leu-Gly-NH ₂
Lypressin	H-Cys-Tyr-Phe-Gln-Asn-Cys-Pro-Lys-Gly-NH ₂
Ornipressin	H-Cys-Tyr-Phe-Gln-Asn-Cys-Pro-Orn-Gly-NH ₂
Felypressin	H-Cys-Phe-Phe-Gln-Asn-Cys-Pro-Lys-Gly-NH ₂

With a mobile phase pH of 2.5 and a temperature of 80°C three of the five nonapeptides are baseline-separated, the peptide pair lypressin/ornipressin being separated with a resolution of $R_s = 0.9$. A chromatogram of the nonapeptide separation is shown in Fig. 1. A very important parameter for selectivity was found to be the temperature. At room temperature the peptide pairs lypressin/ornipressin and felypressin/oxytocin are not separated. Separation improves with increasing temperature and at 80°C a resolution of $R_s = 7.0$ is achieved for the felypressin/oxytocin pair and the lypressin/ornipressin pair is partially separated. Separation is also influenced by the pH of the mobile phase. The critical peptide pair lypressin/ornipressin can only be resolved at very low pH or at high pH: $R_s = 0.9$ at pH 2 and $R_s = 1.4$ at pH 9.

The HPLC method was validated for quantitative determination of ornipressin in bulk and in pharmaceutical preparations. Precision, accuracy, linearity and sample stability were studied. A good linearity was found in the tested range 2–10 I.U./ml: the slope of the linear regression line was 0.94 ± 0.04 , the intercept was 0.15 ± 0.24 . The correlation coefficient was calculated as $r = 0.9997$. The 95% confidence interval

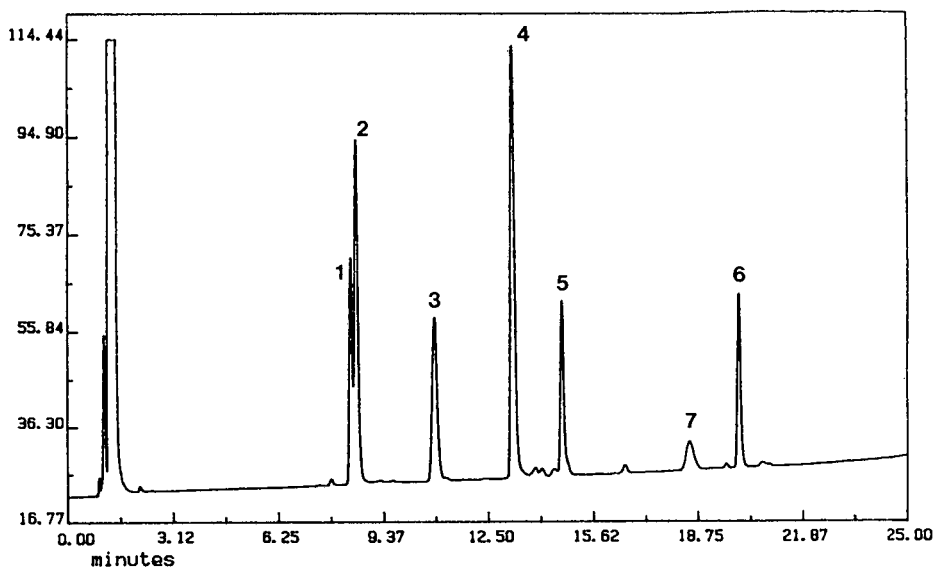


Fig. 1. Separation of various nonapeptides on reversed-phase HPLC. Peaks: 1 = lypressin; 2 = ornipressin; 3 = methyl 4-hydroxybenzoate (preservative); 4 = felypressin; 5 = oxytocin; 6 = demoxytocin; 7 = chlorobutanol (preservative). Chromatographic conditions: stationary phase, Spheri 5 ODS-MP 5 μm , 100 \times 4.6 mm from Brownlee Labs; mobile phase A: 0.02 M tetramethylammonium hydroxide in water, adjusted to pH 2.5 with orthophosphoric acid; mobile phase B: 0.02 M tetramethylammonium hydroxide in a mixture of water-acetonitrile (50:50, v/v), adjusted to pH 2.5 with orthophosphoric acid; gradient programme: 10–60% B in 25 min; flow-rate 1.0 ml/min; injection volume: 20 μl ; column temperature: 80°C; detection: UV at 220 nm; concentration of nonapeptides: 2–5 I.U./ml each.

of the linear regression calculation includes the origin, thus proving the accuracy of the method. The assay precision was tested with seven consecutive assays in one laboratory and was found to be $S_{\text{rel}} = 0.48\%$. Sample stability was tested over a period of 24 h in order to validate the method for use with autosampling systems. Sample solutions were found to be stable at room temperature over the whole testing period and thus samples can be analysed in overnight runs.

Correlation between HPLC and biological assay

The correlation between the two methods was established in a collaborative study where a number of samples were analysed in various laboratories by both techniques. In one experiment, termed the linearity test, samples of various dosages were analysed to compare the two methods with respect to precision and accuracy in a certain dosage range. The results found are given in Table II. A linear regression equation and 95% confidence limits were calculated to compare the two methods. The slope of the regression line was found to be 0.99 ± 0.04 which includes the theoretical value of 1.00; the intercept was found to be -0.11 ± 0.20 , which includes the theoretical value of zero. The correlation coefficient was 0.9998, which is close to the theoretical value of 1.0000. All these parameters of the regression equation prove that the HPLC results are in good agreement with the biological results. Consequent-

TABLE II
LINEARITY TEST

Samples of different dosage strengths (2.75, 4.40, 5.50, 6.60 and 8.25 I.U./ml) were analysed with both assay methods in a collaborative study.

Laboratory	Found (I.U./ml)				
	2.75	4.40	5.50	6.60	8.25
HPLC laboratory 1	2.76	4.35	5.46	6.54	8.11
HPLC laboratory 2	2.68	4.18	5.38	6.40	7.80
HPLC laboratory 3	2.75	4.21	5.35	6.22	7.73
HPLC mean	2.73	4.25	5.40	6.39	7.88
Bioassay laboratory 4	2.65	4.04	5.26	6.20	7.61
Bioassay laboratory 5	2.53	4.04	5.07	6.17	7.80
Bioassay laboratory 6	2.64	4.20	5.16	6.31	7.67
Bioassay mean	2.61	4.09	5.16	6.23	7.69
Standard deviation (%)					
HPLC S_{rel}	1.60	2.14	1.05	2.51	2.75
Bioassay S_{rel}	2.55	2.26	1.84	1.18	1.26

ly HPLC can be used as alternative to the bioassay for the estimation of potency of ornipressin.

In a second experiment, termed the degradation test, we tested whether both methods also correlate when thermally degraded samples are analyzed. This is a prerequisite if the HPLC is to be used for stability testing. The results of this experiment are given in Table III. Two of the three laboratories, No. 4 and No. 5, showed a

TABLE III
DEGRADATION TEST

Thermally degraded samples (without heat treatment and with heat treatment at 50°C for 7, 14, 30 and 60 days) were analysed with both assay methods in a collaborative study.

Laboratory	Found (I.U./ml)				
	None	7	14	30	60
HPLC laboratory 1	5.37	5.07	4.86	4.48	3.90
HPLC laboratory 2	5.33	5.14	5.02	4.57	3.90
HPLC laboratory 3	5.39	5.25	5.03	4.63	3.92
HPLC mean	5.36	5.15	4.97	4.56	3.91
Bioassay laboratory 4	4.90	4.91	5.26	5.00	4.38
Bioassay laboratory 5	5.25	5.23	5.18	4.98	3.97
Bioassay laboratory 6	5.30	4.99	4.71	4.41	3.65
Bioassay mean	5.15	5.04	5.05	4.80	4.00
Standard deviation (%)					
HPLC S_{rel}	0.56	1.76	1.98	1.60	0.37
Bioassay S_{rel}	4.23	3.32	5.94	7.05	9.15

trend to higher values for samples which had been heat-treated for 2 weeks or longer, whereas laboratory 6 obtained results below those of the HPLC laboratories. A reason for these differences could not be found and it is presumed that it is caused by the normal scatter of the biological assay. Calculation of the linear regression and the 95% confidence limits resulted in a slope of 0.78 ± 0.41 , an intercept of 1.06 ± 1.96 and a correlation coefficient of 0.9621. The confidence limits for slope and intercept include the theoretical values of 1.00 and of zero, respectively. There is no statistically significant difference between the two assay methods. However, HPLC seems to be more precise in analysing thermally degraded samples and, as a consequence, HPLC would be the preferred technique for stability testing of ornipressin.

The data in the Tables II and III also show the laboratory-to-laboratory variation of the two methods. Standard deviations for HPLC are up to 2.75%, those for the bioassay are up to approximately 9%. HPLC is more reproducible and easier to transfer to other laboratories.

With respect to method correlation it should be noted that only samples of highly purified ornipressin were used for the study. If there were further compounds with a vasopressor effect present in the test solution, *e.g.* active by-products from the synthesis, the biological assay would reflect the overall activity of the sample without distinguishing between the activity of ornipressin and the activity of the by-products and in this case a correlation between HPLC and biological assay would not longer be given.

TABLE IV

RESULTS OF ORNIPRESSIN BULK SOLUTIONS AND ORNIPRESSIN INJECTIONS ANALYSED BY BIOASSAY AND BY HPLC

Results given as a percentage of the declared activity.

Sample	Bioassay result (%)		HPLC result (%)
	Laboratory 1	Laboratory 2	
Bulk solution (150 I.U./ml)			
Batch 12	107.1	91.7	93.3
Batch 13	105.4	105.1	106.2
Batch 14	108.2	99.1	105.0
Injections (5 I.U./ml)			
Batch 114	100.3	105.4	105.1
Batch 115	—	104.1	105.1
Batch 116	100.1	—	104.4
Batch 117	—	99.8	101.0
Batch 118	103.3	100.3	101.4
Batch 119	100.9	102.1	101.1
Batch 120	104.2	—	105.4
Batch 121	—	101.9	106.8
Batch 122	—	101.0	102.2
Batch 123	—	103.7	102.6

Experience with HPLC in the routine quality control of ornipressin

Experience was gained with the use of HPLC in the routine analysis of ornipressin in bulk solution and in the pharmaceutical preparation. A number of batches were analysed by both methods, with the internal reference standard being used for calibration. The results are given in Table IV. The data from both methods are in good agreement, which confirms that both methods can equally be applied for the quantitation of ornipressin in bulk solutions and in pharmaceutical preparations.

CONCLUSIONS

The present study shows that HPLC can successfully be used for the quantitation of ornipressin in bulk material and in pharmaceutical preparations. HPLC is a quick and inexpensive method which can easily be applied on automated analysis. It shows good selectivity and the results obtained are identical to those of the biological assay within the normal variation of the methods. From this it can be concluded that reliable potency estimations can be performed by HPLC in future and that the blood pressure test in rats, which has been applied so far, is no longer required.

Based upon these findings Sandoz Pharma plans to reduce the animal tests for ornipressin and to use HPLC instead. In detail, the following quality control concept is foreseen: ornipressin bulk material will be analysed by HPLC and by bioassay. HPLC is used for the precise potency determination, while the biological assay serves as an identification test which assures that the product exhibits the required vasopressor effect. The ornipressin formulations will be analysed by HPLC only, not by the biological assay. Biological identification of the final product is no longer seen as necessary as the drug potency has already been proven on the bulk material.

The proposed concept allows a reduction in animal assays for ornipressin by 90%. This is a significant contribution in minimizing animal experiments in the pharmaceutical industry and it is expected that the health authorities will agree to this new control concept.

REFERENCES

- 1 K. Krummen and R. W. Frei, *J. Chromatogr.*, 132 (1977) 27.
- 2 K. Krummen and R. W. Frei, *J. Chromatogr.*, 132 (1977) 429.
- 3 D. H. Calam, *J. Chromatogr.*, 11 (1978) 55.
- 4 F. Maxl and K. Krummen, *Pharm. Acta Helv.*, 53 (1978) 207.
- 5 K. Krummen, F. Maxl and F. Nachtmann, *Pharm. Tech. Int.*, 2 (1979) 37.
- 6 R. A. Pask-Huges, P. H. Corran and D. H. Calam, *J. Chromatogr.*, 214 (1981) 307.
- 7 B. S. Welinder, S. Linde and B. Hansen, *J. Chromatogr.*, 384 (1985) 347.
- 8 M. Ohta, F. Fukuda, T. Kimura and A. Tanaka, *J. Chromatogr.*, 402 (1987) 392.
- 9 D. S. Brown and D. R. Jenke, *J. Chromatogr.*, 410 (1987) 157.
- 10 F. Maxl and W. Siehr, *J. Pharm. Biomed. Anal.*, 7 (1989) 211.
- 11 R. H. Buck and F. Maxl, *J. Pharm. Biomed. Anal.*, 8 (1990) 761.
- 12 The British Pharmacopoeia, H. M. Stationary Office, London, 1988, p. A173.

Non-radioactive detection of MHC class II–peptide antigen complexes in the sub-picomole range by high-performance size-exclusion chromatography with fluorescence detection

HUBERT KALBACHER and HARALD KROPSHOFER*

Medizinisch-naturwissenschaftliches Forschungszentrum der Universität Tübingen, Ob dem Himmelreich 7, 7400 Tübingen (Germany)

ABSTRACT

In order to avoid chemical or structural modification of T-cell epitopes by labelling, a high-performance size-exclusion chromatographic fluorescence binding assay was developed, based on the intrinsic Trp fluorescence of major histocompatibility complex (MHC) proteins. The increase in Trp fluorescence intensity of the isolated human MHC product HLA-DR 1 on complex formation with unlabelled influenza matrix peptide[18–29] (IM[18–29]) was examined. Binding of IM[18–29] to the heterodimeric form of HLA-DR 1 ($K_d=4.8$ mM) and to the disassembled α - and β -subunits ($K_d=9.2$ mM) could be demonstrated. In addition, the assay showed the peptide-induced formation of a dimeric conformer of HLA-DR 1, the nature of which is still undefined. Detection of HLA-DR 1 subunit–peptide complexes was possible in amounts of 25 ng in 10 μ l (80 fmol/ μ l). The technique proved to be reproducible and less time consuming than common methods that need fluorescence or radioactive labelling.

INTRODUCTION

Human lymphocyte antigens DR (HLA-DR) are products of the human major histocompatibility complex (MHC) class II and consist of two non-covalently linked glycoprotein subunits: α (34 kilodalton) and β (29 kilodalton) [1]. The N-terminal domains of each subunit constitute the antigen binding site. According to the hypothetical model of class II proteins [2], deduced from the X-ray crystallographic analysis of the class I molecule HLA-A2, the binding groove is characterized by two lateral α -helices lying on a floor formed by β -pleated sheets [3,4]. Polymorphic positions, which explain the peptide binding specificities of different HLA subtypes, accumulate significantly in this region. Non-immunogenic self-peptides, originating from the endogenous degradation of self-proteins [5,6], and immunogenic foreign peptides are assumed to compete for the same binding site [7]. However, only the latter are successfully presented to a corresponding T-cell receptor leading to an immune response [8]. Self-peptides co-eluting and co-crystallizing with HLA isolates [2,9], are the reason why only a small fraction (1–15%) of the HLA molecules is available for binding exogenous peptides. Previous binding studies using immunogenic peptides and solubilized or native MHC molecules in cellular systems have shown this [5,10].

In order to work out the rules that make HLA proteins potent peptide receptors with a very broad binding specificity, short synthetic peptides are systematically tested for their HLA affinities [11–13]. Influenza matrix peptide[18–29] (IM[18–29]) is one of the T-cell epitopes of influenza matrix protein. IM[18–29] is HLA-DR 1-restricted, direct binding to living Epstein–Barr virus transformed B-cell lines being shown with the radiolabelled peptide [10,14]. In addition to radioiodination of peptides, often extra-tyrosylation, as in the case above, or coupling of bulky fluorophores is necessary to obtain sufficient signal intensities. Our idea was to establish a binding assay without modifying the sequence of the T-cell epitopes. Leaving IM[18–29] and the purified HLA-DR 1 molecule in their natural state, we co-incubated them and investigated the change in intrinsic Trp fluorescence on formation of the bimolecular complexes. The amount and the nature of the so-formed HLA-DR 1–IM[18–29] complexes were analysed by high-performance six-exclusion chromatography (HPSEC) using fluorescence detection.

EXPERIMENTAL

Chemicals and reagents

High-performance liquid chromatographic (HPLC)-grade water and 3-[3-(cholamidopropyl)dimethylamino]-1-propanesulphonate (CHAPS) were obtained from E. Merck (Darmstadt, Germany). All buffers were filtered through 0.45- μ m filters (Millipore, Eschborn, Germany) and degassed with helium.

Chromatography

The chromatographic system consisted of an L 6200 HPLC intelligent pump (Merck–Hitachi, Darmstadt, Germany) connected to a Merck–Hitachi F 1050 spectrofluorimeter operating at an excitation wavelength of 285 nm and an emission wavelength of 335 nm. The integrator was a Model D2500 from Merck–Hitachi. Separation was achieved on a Superose 12 HR 10/30 column (Pharmacia, Freiburg, Germany) using 0.1 M sodium phosphate buffer (pH 7.0) containing 0.025% (w/v) CHAPS (HPSEC buffer). The column was operated at a flow-rate of 0.6 ml/min and a pressure of 200 p.s.i. For peptide purification, the HPLC system was connected to an L-4000 UV detector (Merck–Hitachi).

Peptide synthesis and purification

Peptides were synthesized by continuous-flow solid-phase peptide synthesis using a MilliGen 9050 peptide synthesizer based on Fmoc strategy. All peptides were purified by HPLC using a Nucleosil C₁₈ column (250 × 10 mm I.D., 7 μ m particle size) (Macherey, Nagel & Co., Düren, Germany). The mobile phase contained (A) 0.1% trifluoroacetic acid (TFA) and (B) acetonitrile–0.1% TFA (80:20, v/v) and elution was performed by a gradient starting from 20% B to 100% B in 30 min. The flow-rate was 2.5 ml/min. All separations were monitored at 214 nm. After lyophilization, peptides were analysed by amino acid analysis and by sequencing using an Applied Biosystems (Foster City, CA, USA) 477 A sequencer.

Preparation of biological samples

HLA-DR 1 was purified by immunoaffinity chromatography essentially as de-

scribed by Gorga *et al.* [15] using the Epstein-Barr virus-transformed B-cell line WT-100 (BIS), which is homozygous at the DR locus. Change of buffer and detergent was carried out by ultrafiltration through membranes of Microsep microconcentrators, size exclusion 100 kilodalton (Filtron, Karlstein, Germany). The new buffer contained 100 mM sodium phosphate (pH 8.0) and 0.025% (w/v) CHAPS and was used to adjust the final protein concentration to 0.2 $\mu\text{g}/\mu\text{l}$. Protein content was evaluated by the Bradford protein assay. Purified HLA-DR 1 was kept in a stock solution at 4°C for 1 month prior to use in the HPSEC assay.

The integrity of all HLA-DR 1 samples was routinely tested by sodium dodecyl sulphate polyacrylamide gel electrophoresis, (SDS-PAGE) immunoblotting and HPSEC analysis.

Binding assay

Aliquots of 2 μl of the stock solution of HLA-DR 1 were co-incubated with various doses of synthetic influenza matrix peptide [18–29], using a peptide stock solution of 10 $\mu\text{g}/\mu\text{l}$. The stock solution was prepared by dissolving the lyophilized peptide in HPSEC buffer. The peptide concentrations ranged from 0.1 to 5 mM, the final assay volume being adjusted to 40 μl with HPSEC buffer. The samples were incubated for 50–120 h at room temperature. Aliquots of 10 μl were used for HPSEC analysis.

Release assay

After a 120-h incubation at 20- μl aliquot of the binding assay was adjusted to pH 2.0 with 1 M HCl. After 10 min the sample was readjusted to pH 7.0 with 2 M NaOH and analysed by HPSEC.

Scatchard plot analysis

The dissociation constant, K_d , in the binding assays was calculated using the following Scatchard equation [16]:

$$F_{335}/c(\text{HLA-DR 1})c(\text{peptide}) = 1/K_d - F_{335}/c(\text{HLA-DR 1}) K_d$$
 where F_{335} is the measured fluorescence (proportional to the concentration of bound peptide), $c(\text{HLA-DR 1})$ and $c(\text{peptide})$ are the concentrations of HLA-DR 1 and IM[18–29], respectively. K_d can be obtained from the slope of the Scatchard plot of $F_{335}/c(\text{HLA-DR 1})c(\text{peptide})$ vs. $F_{335}/c(\text{HLA-DR 1})$.

RESULTS AND DISCUSSION

Purified heterodimeric HLA-DR 1 partially dissociates into the α - and β -subunits in dilutions ≤ 0.2 mg/ml. The extent of dissociation of the isolates used in our study was calculated by comparing the peak areas of the dimer (a) and the monomer peaks (b) in the HPSEC analysis (Fig. 1). Detecting Trp fluorescence, the relationship was dimers : monomers = 22:78. The same result was obtained with UV detection (not shown). The resolution in SEC is not high enough to distinguish the subunits, the latter therefore co-eluting with peak b. Peak a disappears quantitatively in favour of peak b on acidification of the sample (see Fig. 4). This was assumed to happen because under these conditions self-peptides can be released from the MHC molecule, destabilizing the heterodimer [7]. In contrast, fresh samples in dilutions > 0.5 mg/ml

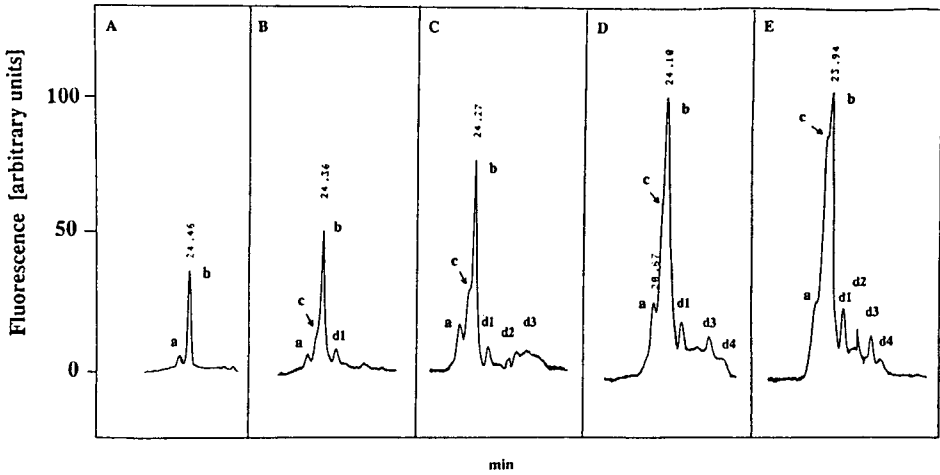


Fig. 1. HPSEC of purified HLA-DR 1 (250 nM) after 120-h co-incubation with various doses of influenza matrix peptide[18–29]. Fluorescence detection, attenuation 32. Peptide concentrations: (A) 0; (B) 2; (C) 3; (D) 4; (E) 5 mM. Peaks: a=HLA-DR 1 heterodimers (floppy conformer); b=HLA-DR 1 subunits; c=HLA-DR 1 dimers (compact conformer); d₁–d₄=endogenous peptides.

show a predominant peak a, representing 90% of the total fluorescence (not shown). Hence it is certain that it is the subunits eluting with peak b.

The basis for the peptide-binding assay is the fact that two Trp residues, Trp-9 and Trp-61 of the β -subunit, being part of the peptide-binding groove of HLA-DR 1, increase their fluorescence intensities on interaction with a peptide [17]. Using this principle, the peptide-binding assay reveals four significant tendencies, three of which have never been reported in comparable chromatographic assays with MHC class II molecules (Fig. 1): (1) peak a, denoting the heterodimer, increases with increasing peptide concentration, reaching its maximum at 4 mM IM[18–29]; (2) peak b, denoting the HLA-DR 1 subunits, shows the same characteristics; (3) addition of peptide leads to the appearance of a new species (peak c), located between the heterodimer and the monomer peaks, with an apparent molecular weight of 50–55 kilodalton; peak c, in contrast to peaks a and b, is still growing at the highest peptide concentration tested; (4) fluorescent low-molecular-weight material elutes (peaks d₁–d₄), the maxima at 4 mM IM[18–29] coinciding with the maximum of peaks a and b, respectively, albeit added IM[18–29] shows no fluorescence signal.

The results confirm the data we obtained with FITC- and biotin-labelled influenza matrix peptide [17] and two observations made previously with isolated MHC class II molecules analysed by SDS-PAGE: under non-reducing conditions bimolecular complexes of T-cell epitopes and the α - or β -subunit are stable [18,19]. The second fact was the appearance of a 55 kilodalton band originating from HLA-DR heterodimers [15,18]. This band was ascribed to a compact dimeric conformer which is distinct from the floppy conformer, with a band of 64 kilodalton. Peak c in our binding assay (Fig. 1) seems to be the chromatographic equivalent of the compact conformer, its formation being induced by IM[18–29]. As this requires a trimolecular association, this process is bound to proceed more slowly than the formation of the

bimolecular complexes. This explains the result of the binding kinetics shown in Fig. 2: the intensity of the monomer peak has nearly doubled after a 50-h incubation, whereas the signal of the compact conformer cannot be identified. We have to postulate that IM[18–29] is capable of cross-linking disassembled α - and β -subunits. We cannot rule out the formation of $\alpha\alpha$ - and/or $\beta\beta$ -homodimers under the influence of connecting peptides. Interestingly, peptides functioning as chaperonins *in vivo* have already been documented with MHC class I molecules [20]. It seems that the rules for building up a quaternary structure are the same for both class I and class II molecules.

The dissociation constants characterizing the affinity of IM[18–29] to the monomeric and dimeric HLA-DR 1 were calculated according to Scatchard (Fig. 3). The slopes of the Scatchard plots indicate that binding to the heterodimer ($K_d = 4.8$ mM) is greater than that to the subunits ($K_d = 8.5$ mM). The data can be explained by the fact that the heterodimer possesses all the elements constituting the peptide-binding groove whereas each individual monomer does not. A comparison of K_d (heterodimer) = 4.9 mM with the few values available for other T-cell epitopes, ranging from 2 to 10 μ M, suggests that IM[18–29] belongs to a class of low-affinity peptides. K_d calculations with the original influenza matrix peptide [17–31] have not been done. Data of Ceppellini *et al.* suggest that IM[17–29] has a high affinity to HLA-DR 1 [10]. The lack of N-terminal serine might be the reason for the high K_d value of IM[28–29]. Another reason could be that binding of exogenous peptides to HLA molecules is a two-step phenomenon: using low peptide-concentrations (≤ 1 mM) only binding to

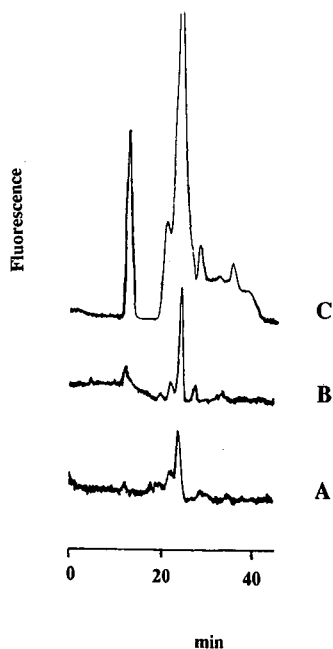


Fig. 2. HPSEC in a kinetic study using HLA-DR 1 (250 nM) and IM[18–29] (3 mM). Incubation time: (A) 0; (B) 50; (C) 120 h.

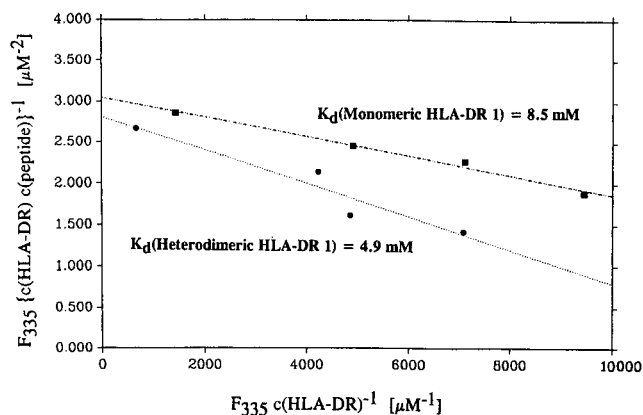


Fig. 3. Scatchard plot. The data originate from the HPSEC binding assay using changes in the intrinsic Trp fluorescence on binding IM[18–29]. $K_d(\text{monomeric HLA-DR}) = 8.5 \text{ mM}$; $K_d(\text{heterodimeric HLA-DR 1}) = 4.9 \text{ mM}$.

the fraction of empty HLA molecules is detectable, proceeding with $K_d \approx 2\text{--}10 \mu\text{M}$. Co-incubation with a high peptide excess ($> 1 \text{ mM}$) leads to competitive displacement of endogenous peptides with the remaining 90% of HLA molecules, either dimeric or monomeric, proceeding with $K_d \approx 5\text{--}10 \text{ mM}$. Evidence for the accuracy of the displacement idea is given by the low-molecular-weight fraction (peaks $d_1\text{--}d_4$), eluting with increasing proportions of bound IM[18–29] (Fig. 1). The fluorescence of the low-molecular-weight material must be ascribed to Trp-containing endogenous peptides, as there is no further increase on addition of IM[18–29] at a concentration of 5 mM. Additional proof of the relevance of the endogenous peptide fraction (EPF) is given by the fact that readdition of EPF to released HLA-DR 1 restores the initial fluorescence intensity [21].

In order to test whether bound IM[18–29] can be released from HLA-DR 1 under the same conditions as endogenous peptides, we acidified HLA-DR 1-IM[18–29] complexes after a 125h-incubation. The result is depicted in Fig. 4: pH 2.0 treatment for 10 min leads to a decline of peaks a, b and c to the starting intensities (*cf.* Fig. 1D), leaving constant the total intensities of peaks d_1 and d_2 . Obviously, the bi- and trimolecular complexes dissociated nearly completely. Because no extra fluorescence appeared in the low-molecular-weight range, probably all self-peptides had been previously displaced by IM[18–29]. The increase in the signal of the void volume (800 kilodalton) could be explained by acid-induced additional high-molecular-weight micelles containing trapped HLA-DR 1-IM[18–29] complexes that are not able to dissociate because of dense packing. The formation of high-molecular-weight micelles is also found with high protein and peptide concentrations (*cf.* Figs. 1 and 4), but can be neglected as the relationship of HLA-DR 1 species is unbiased (not shown).

Considering the sensitivity of this peptide-binding assay, in standard measurements 2.5 pmol of purified HLA-DR 1 per HPSEC run were sufficient to obtain the signal shown above, using a signal attenuation of 32. With a signal attenuation of 4, we were able to detect 800 fmol of HLA-DR 1-peptide complexes, in significant

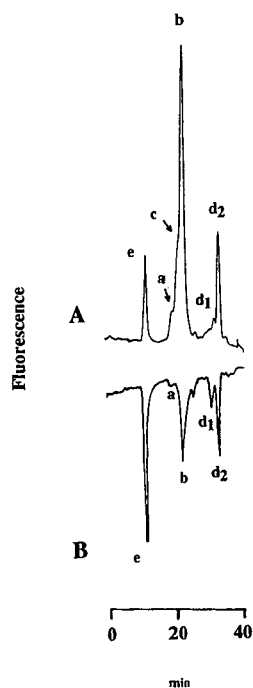


Fig. 4. HPSEC of purified HLA-DR 1 (200 mM) after 120-h incubation with IM[18–29] (4 mM). Fluorescence detection, attenuation 32. (A) Before acid treatment; (B) after acid release (pH 2.0, 10 min) of endogenous peptides. Peaks: a = HLA-DR 1 heterodimers (floppy conformer); b = HLA-DR 1 subunits; c = HLA-DR 1 dimers (compact conformer); d_1 – d_4 = endogenous peptides; e = oligomeric HLA-DR 1.

contrast to the background fluorescence (not shown). Therefore, the assay has a sensitivity comparable to those of standard assays using fluorescence or radioactively labelled peptides. Advantages of the Trp fluorescence assay are that there is no need to label the peptides and the HPSEC system requires less than 1 h per analytical run. In addition, for the first time different molecular weight species of HLA-DR-peptide complexes could be distinguished by a chromatographic system.

ACKNOWLEDGEMENTS

We thank M. Stöhr for the synthesis and purification of the peptides. We are grateful to I. Böhlinger and H. Max for helpful discussions. This work was supported by the Sonderforschungsbereich 120.

REFERENCES

- 1 J. F. Kaufman and J. L. Strominger, *Proc. Natl. Acad. Sci. USA*, 76 (1979) 6304.
- 2 H. J. Brown, T. Jardetzky, M. A. Saper, B. Samraoui, P. Bjorkman and D. C. Wiley, *Nature (London)*, 332 (1988) 845.
- 3 P. Bjorkman, M. A. Saper, B. Samraoui, W. S. Bennett, J. L. Strominger and D. C. Wiley, *Nature (London)*, 329 (1987) 506.

- 4 P. Bjorkman, M. A. Saper, B. Samroui, W. S. Bennett, J. L. Strominger and D. C. Wiley, *Nature (London)*, 329 (1987) 512.
- 5 B. P. Chen and P. Parham, *Nature (London)*, 37 (1989) 743.
- 6 P. Parham, *Immunol. Today*, 9 (1988) 65.
- 7 S. Buus, A. Sette, S. M. Colon and H. M. Grey, *Science*, 242 (1988) 1045.
- 8 B. P. Babbitt, P. M. Allen, G. Matsueda, E. Haber and E. R. Unanue, *Nature (London)*, 317 (1985) 359.
- 9 T. P. J. Garrett, M. A. Saper, P. J. Bjorkman, J. L. Strominger and D. C. Wiley, *Nature (London)*, 342 (1989) 692.
- 10 R. Ceppellini, G. Frumento, G. B. Ferrara, R. Tosi, A. Chersi and B. Pernis, *Nature (London)*, 339 (1989) 392.
- 11 T. S. Jardetzky, J. C. Gorga, R. Bush, J. Rothbard, J. L. Strominger and D. C. Wiley, *EMBO J.*, 9 (1990) 1797.
- 12 P. M. Allen, G. R. Matsueda, R. J. Evans, J. B. Dunbar, Jr., G. R. Marshall and E. R. Unanue, *Nature (London)*, 327 (1987) 713.
- 13 S. Buus, A. Sette, S. M. Colon, D. M. Jenis and H. M. Grey, *Cell*, 47 (1986) 1071.
- 14 J. B. Rothbard, R. I. Lechler, K. Howland, V. Bal, D. D. Eckels, R. Sekaly, E. Lang, W. R. Taylor and J. Lamb, *Cell*, 52 (1988) 512.
- 15 J. C. Gorga, V. Horejsi, D. R. Johnson, R. Raghupathy and J. L. Strominger, *J. Biol. Chem.*, 262 (1987) 16087.
- 16 G. Scatchard, *Ann. N.Y. Acad. Sci.*, 51 (1949) 660.
- 17 H. Kropshofer, C. Müller and H. Kalbacher in E. Giraldo (Editor), *Proceedings of the 21st European Peptide Symposium*, Escom Sc. Publ. Leiden, 1990, p. 892.
- 18 M. Viguier, K. Dornmaier, B. R. Clark and H. McConnell, *Proc. Natl. Acad. Sci. USA*, 87 (1990) 7170.
- 19 K. Dornmaier, B. Rothenhäusler and H. M. McConnell, *Cold Spring Harbour Symp. Quant. Biol.*, 54 (1989) 409.
- 20 A. Townsend, C. Öhlen, L. Foster, J. Bastin, H.-G. Ljunggren and K. Kärre, *Cold Spring Harbour Symp. Quant. Biol.*, 54 (1989) 299.
- 21 H. Kropshofer, I. Bohlinger, H. Max and H. Kalbacher, *Biochemistry*, submitted for publication.

CHROMSYMP. 2309

High-performance liquid chromatographic separation of modified and native melittin following transglutaminase-mediated derivatization with a dansyl fluorescent probe

ENRIQUE PEREZ-PAYA, LORENZO BRACO and CONCEPCION ABAD*

Departamento de Bioquímica y Biología Molecular, Universidad de Valencia, Burjassot, E-46100 Valencia (Spain)

and

JEAN DUFOURCQ

Centre de Recherche Paul Pascal, CNRS, Château Brivazac, F-33600 Pessac (France)

ABSTRACT

The 26-amino acid linear, amphiphilic peptide melittin was enzymatically modified with the fluorescent probe monodansylcadaverine using guinea pig liver transglutaminase and a fluorescent derivative of stoichiometry 1:1 was obtained. Reversed-phase and size-exclusion high-performance liquid chromatographic modes were tested in order to resolve the labelled peptide and native species. The influence of several operational variables was analysed and the elution conditions were optimized so that a satisfactory resolution could be achieved in both instances in a rapid, easy manner. Both chromatographic modes offer the possibility of accurate monitoring of the time course of the enzyme-mediated conversion and, more interestingly, can be applied to the semi-preparative purification of the labelled peptide.

INTRODUCTION

We have been involved in the past in the investigation of protein–lipid interactions using hydrophobic or amphiphilic peptides [1–7]. Among other goals, our interest has recently been directed to the selective covalent modification of the cytolytic toxin melittin with dansyl fluorescent probes. This amphiphilic, 26-amino acid linear peptide has the sequence: Gly–Ile–Gly–Ala–Val–Leu–Lys–Val–Leu–Thr–Thr–Gly–Leu–Pro–Ala–Leu–Ile–Ser–Trp–Ile–Lys–Arg–Lys–Arg–Gln–Gln–CO–NH₂. Dansyl-labelled melittin can undoubtedly be regarded as a valuable tool for studies on the detailed mechanism of membrane lysis at a molecular level, on the basis of both its dramatically enhanced sensitivity to fluorimetric detection and its distinctive emission features relative to native membrane proteins.

In order to achieve a rational, selective modification of the peptide, conventional chemical procedures should in principle be disregarded, owing to their frequent lack of selectivity, if one needs to introduce a probe at a selected single position in the sequence. In contrast, the use of enzyme-mediated modification, in particular with

transglutaminases, provides a unique strategy for the specific modification of glutamine residues in peptides [8,9] and proteins [10–12]. Transglutaminases (TGase; R-glutaminy-peptide: amine γ -glutamyltransferase, E.C. 2.3.2.13) catalyse acyl transfer reactions in which the γ -carboxamide groups of glutamine residues act as acyl donors and primary amino groups from specific amines as acyl acceptors [13]. Evidence in this field has shown that the *in vitro* transglutaminase-mediated covalent modification of proteins and peptides generally leads to the incorporation of a single probe molecule per molecule of biopolymer [8,10]. However, as this exquisite selectivity minimizes the structural and chemical differences between modified and native species, it often becomes a source of difficulties in any separation and purification attempt.

Recently, using guinea pig liver transglutaminase, we have carried out a facile, selective modification of melittin in its C-terminal end with the probe monodansylcadaverine (DNC), yielding a derivative with a 1:1 stoichiometry [14]. This paper reports on the development of high-performance liquid chromatographic (HPLC) methods allowing a complete separation of DNC-melittin from the native peptide. It will be shown that both species can be successfully resolved by using either size-exclusion (SE) or reversed-phase (RP) supports. In both chromatographic modes several experimental factors were tested in order to optimize peptide separation. Note that this separation is particularly complicated owing to the amphiphilic nature of melittin, which exhibits a highly positively charged C-terminal end and an amphipathic helical organization for the remainder of the molecule [15]. Finally, the advantages of each HPLC mode for the determination and semi-preparative isolation of labelled melittin are discussed.

EXPERIMENTAL

Materials

Melittin and monodansylcadaverine [N-(5-aminopentyl)-5-dimethylamino-1-naphthalenesulphonamide] were obtained from Serva (Heidelberg, Germany), guinea pig liver transglutaminase from Sigma (St. Louis, MO, USA) and dithiothreitol (DTT) and HPLC-grade solvents from Merck (Darmstadt, Germany). Doubly distilled water was purified by passing it through a Milli-Q purification system (Millipore, Bedford, MA, USA). All salts used were of analytical-reagent grade from Merck. The eluents were always filtered and degassed through a 0.45- μ m regenerated cellulose filter (Micro Filtration System, Dublin, CA, USA) prior to use. Fluorescence spectroscopy-grade methanol from Merck was used in fluorimetric measurements.

TGase-mediated modification of melittin by monodansylcadaverine

The procedure was basically similar to that described for the TGase-mediated modification of small peptides such as substance P [8] or β -endorphin [9] by polyamines. Briefly, melittin (100 μ g) was incubated at 37°C for 3 h with 2 μ M TGase in 50 mM Tris-HCl buffer (pH 8.0) containing 20 mM DTT, 20 mM CaCl₂ and 700 μ M DNC (final volume 100 μ l). The reaction was stopped by heating at 60°C for 5 min [16].

Apparatus

The HPLC instrumentation consisted of M-510 solvent-delivery systems, an

automated gradient controller, a U6K universal injector and an M-418 multi-wavelength detector, all from Waters Assoc. (Milford, MA, USA). Fluorescence of the effluent was monitored ($\lambda_{\text{ex}} = 330 \text{ nm}$, $\lambda_{\text{em}} = 520 \text{ nm}$) with an F-1050 fluorescence detector from Merck. Peak areas were digitized using an SP-4290 integrator (Spectra-Physics, San Jose, CA, USA).

Reversed-phase experiments were carried out using a μ Bondapak C_{18} column (30 cm \times 0.78 cm I.D.) from Waters Assoc. A Guard-PAK (μ Bondapak C_{18}) pre-column, from Waters Assoc., was placed between the pump and the injector to protect the analytical column from mobile phase contaminants. When the system was operated under gradient conditions, the binary eluent consisted of 0.1% aqueous TFA (solvent A) and acetonitrile (solvent B).

For size-exclusion experiments, a Waters Assoc. Ultrahydrogel column (30 cm \times 0.78 cm I.D.) packed with hydroxylated polymethacrylate-based gel of 120 Å nominal pore size (Ultrahydrogel-120) was used. This chromatographic support has been reported to bear some residual carboxyl groups, to be stable over a broad pH range (from 2 to 12) and to be compatible with mobile phases containing a high percentage of organic solvents [17]. All chromatographic measurements were conducted at room temperature. The flow-rate in all experiments under isocratic conditions was 1.0 ml/min. The injection volume was in the range 5–25 μl and up to 150 μl for analytical and semi-preparative purposes respectively, without any decrease in resolution. Good run-to-run reproducibility was observed in all instances and the recovery was always higher than 90%.

Corrected fluorescence spectra were obtained at 25°C on a Perkin-Elmer (Beaconsfield, UK) LS-5B spectrofluorimeter coupled to a Model 3700 data station using a 2.5-nm slit width.

RESULTS AND DISCUSSION

Reversed-phase chromatography

We first examined the ability of RP-HPLC to resolve modified and unmodified melittin, because this is by far the most widely used mode of HPLC of peptides [18]. The reaction products derived from TGase assay after 3-h incubation at a DNC:melittin ratio of 2 were analysed directly, without any sample pretreatment, on a μ Bondapak C_{18} column using either isocratic or gradient conditions. As illustrated in Fig. 1A, when elution was performed under isocratic conditions with a mobile phase containing 0.1% aqueous TFA–acetonitrile (55:45, v/v) four peaks were detected by UV detection at 283 nm, corresponding to DTT (2.9 min), free DNC (3.3 min), melittin (5.77 min) and DNC-melittin (10.1 min). Moreover, simultaneous fluorescence detection using excitation and emission wavelengths specific for the dansyl group showed only two peaks at retention times of 3.3 and 10.1 min (not shown). In fact, verification of the identity of the labelled melittin peak was carried out after collection, neutralization and lyophilization of the corresponding fraction, by using absorption or fluorescence spectroscopy, as described below for the SEC mode. The resolution between melittin and DNC-melittin was excellent, although under these conditions the separation was poor for DTT and free DNC.

When the volume fraction of acetonitrile in the eluent, ϕ , was varied from 0.44 to 0.50 at constant flow-rate under isocratic conditions, a plot of $\log k'$ (k' = capacity

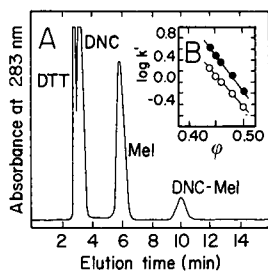


Fig. 1. Reversed-phase separation of melittin and DNC-melittin under isocratic conditions. (A) Elution profile obtained after direct injection, without any sample pretreatment, of an aliquot from the TGase reaction mixture incubated for 3 h. Column, μ Bondapak C18; mobile phase, 0.1% aqueous TFA-acetonitrile (55:45, v/v); flow-rate, 1.0 ml/min; detection, UV at 283 nm. (B) Effect of volume fraction of acetonitrile in the eluent, ϕ , on the retention of (○) melittin and (●) DNC-melittin.

factor) vs. ϕ was obtained as shown in Fig. 1B. The good linearity observed for both melittin and DNC-melittin demonstrates that the column is operating mainly through a reversed-phase mechanism. Moreover, the similarity between the slopes indicates that the perturbation introduced by the probe does not significantly alter the chromatographic behaviour of labelled melittin relative to its native species. Suitable selectivities (α = ratio of capacity factors) and reasonable analysis times were obtained for ϕ values in the range 0.44–0.50. On the other hand, the addition of 0.1% of TFA to acetonitrile in the mobile phase did not improve the resolution. Volatile buffers such as 0.1 M (pH 4.4) or 0.2 M (pH 3.0) ammonium acetate, which have often proved to be suitable for the separation of specific peptide mixtures [19,20], resulted in peak broadening and longer retention times in the present system.

A better resolution for all the components of the TGase reaction mixture was obtained when gradient elution conditions were used. In this instance, the effect of several operating factors on the retention behaviours of melittin and DNC-melittin was examined. For example, Fig. 2A shows resolution, R_s , as a function of the flow-rate at different gradient rates (for a constant range of ϕ from 0.3 to 0.7). R_s is defined as the ratio of the distance between the maxima of two adjacent peaks to the arithmetic mean of their base widths. As expected, R_s increases in all instances as the gradient rate decreases, whereas the influence of flow-rate is relatively small under the gradient conditions applied. Fig. 2B depicts the relationship between R_s and the average solute

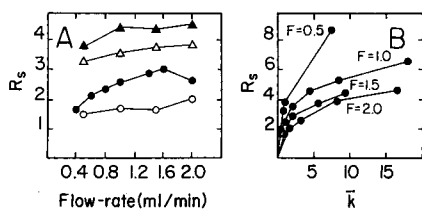


Fig. 2. Dependence of the resolution, R_s , between melittin and DNC-melittin under gradient conditions on the flow-rate, F , at different gradient rates: (▲) 0.5, (△) 1.0, (●) 2.0 and (○) 5.0% acetonitrile/min. (B) Plot showing the variation of R_s with \bar{k} using different flow-rates. Column, μ Bondapak C₁₈.

capacity factor under gradient conditions for labelled melittin, \bar{k} , at different flow-rates, F ; \bar{k} is defined as [21]

$$\bar{k} = t_G(F)/1.15 (\Delta\varphi) V_m S$$

where t_G is the gradient time, φ the fraction of organic solvent in the mobile phase, $\Delta\varphi$ the change in φ during the gradient, V_m the column void volume and S a solute parameter (slope of $\log k'$ vs. φ).

The interpretation of the data in Fig. 2B may not be immediately obvious and some comments are deserved. The figure is aimed at illustrating the different possibilities of variation of experimental conditions that can be used to obtain a given R_s value. For a given flow-rate, a given \bar{k} value can be obtained by varying either t_G or $\Delta\varphi$. Note also that the pronounced variation of R_s with F does not contradict the data in Fig. 2A, because in this instance $\Delta\varphi$ was not always maintained constant. Thus, all the points in Fig. 2B correspond to points in Fig. 2A (for which $\Delta\varphi = 0.4$) except for the two R_s values higher than 6, for which $\Delta\varphi$ was 0.14 instead of 0.4. Although the highest value of R_s in the plot is achieved at $F = 0.5$ ml/min (for $\bar{k} = 7.4$), the long analysis time required (> 200 min) is clearly not desirable and, therefore, for the best compromise between separation time and resolution the following elution conditions can be recommended: $F = 1.0$ ml/min and a 20-min linear gradient from 0.1% TFA-acetonitrile (70:30, v/v) to a final composition of 30:70 (v/v), which implies a total running time, including column recycling, of about 45 min.

Fig. 3 illustrates the elution profile corresponding to the same TGase reaction mixture as in Fig. 1 using the chromatographic gradient conditions recommended above. Note that in this instance the separation between DTT and DNC is improved relative to isocratic conditions (Fig. 1A), whereas the good resolution between native and modified peptide is maintained.

The above results show not only that both isocratic and gradient RP modes allow an excellent separation between melittin and DNC-melittin, but also that easy, accurate monitoring of the progress of the enzymatic labelling can be achieved, especially taking into account that the reported reaction times for transglutaminase-mediated conversions are long, from 1 to 24 h [10,11]. In fact, we have observed that as

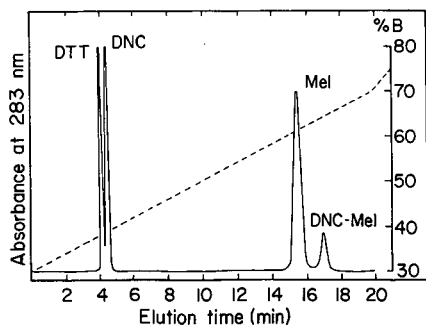


Fig. 3. Reversed-phase separation of melittin and DNC-melittin under optimized gradient conditions (see text), corresponding to the same sample as in Fig. 1A. Column, μ Bondapak C_{18} ; flow-rate, 1.0 ml/min; solvent A, 0.1% aqueous TFA; solvent B, acetonitrile.

reaction takes place a gradual increase in the DNC-melittin peak area occurs at the expense of a concomitant decrease in the melittin and DNC peaks (results not shown).

Size-exclusion chromatography

The effectiveness of the Ultrahydrogel-120 column for melittin analysis was next investigated using 0.1 M sodium acetate buffer (pH 4.4) as eluent, on the basis of our recent optimization study on the elution of polyanions and polycations on Ultrahydrogel supports [22]. When melittin was injected under these conditions a strong retention was observed, much longer than the total permeation volume of the column ($V_t = 11.0$ ml), as shown in Fig. 4A. This anomalous behavior is not surprising if the amphiphilic nature of melittin is taken into account. In fact, the peptide hydrophobic (residues 1–20) and highly positively charged (residues 21–26) moieties are likely to be responsible for the superimposition of hydrophobic and electrostatic secondary effects, causing a dramatic deviation from ideality. The electrostatic interactions between melittin and the matrix residual carboxyl groups may have relatively little importance because at this eluent pH poly-L-lysine standards are not significantly retained [22]. Therefore, if hydrophobic interaction is indeed predominant, addition of a miscible organic modifier to the eluent should diminish the retention of melittin. This is demonstrated in Fig. 4A, where it is shown that a gradual increase in the acetonitrile content of the mobile phase caused a drastic reduction of the peptide elution volume concomitant with pronounced peak sharpening. A similar behaviour has been reported by Mant *et al.* [23] for the elution of a polymer series of synthetic peptides when using a similar range of acetonitrile concentrations in the eluent. Note that even for the highest acetonitrile proportion applied (20%, v/v) the melittin elution volume does not strictly correspond to that expected from its molecular weight (*ca.* 2840). This implies that even under these conditions elution does not occur through a pure size-exclusion mechanism. Anyway, a linear relationship was observed between peak area and injected sample concentration, as shown in Fig. 4B. Higher organic modifier compositions were not tested according to manufacturer's directions.

Fig. 5 shows a typical elution profile of the TGase reaction mixture after incubation for 3 h under the same experimental conditions as in Fig. 1A using 0.1 M

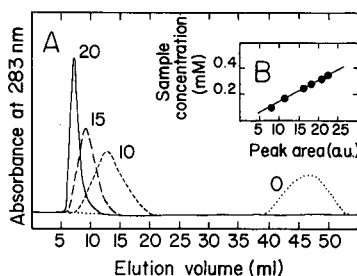


Fig. 4. (A) Elution profiles of melittin on Ultrahydrogel-120 as a function of the percentage of acetonitrile in the eluent (as indicated). Flow-rate, 1.0 ml/min. (B) Correlation between injected melittin concentration and peak area using 0.1 M acetate buffer (pH 4.4) containing 20% of acetonitrile as eluent.

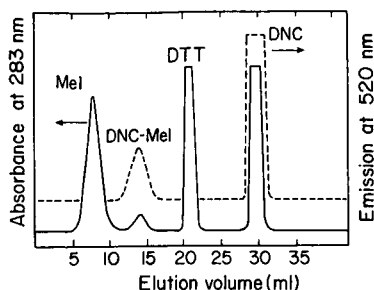


Fig. 5. Separation of melittin and DNC-melittin on Ultrahydrogel-120. Eluent, 0.1 *M* acetate buffer (pH 4.4) containing 20% of acetonitrile; flow-rate, 1.0 ml/min. Simultaneous detection by UV at 283 nm and fluorescence emission at 520 nm on excitation at 330 nm.

acetate buffer (pH 4.4) containing 20% of acetonitrile as mobile phase. Four well resolved peaks were obtained by UV detection at 283 nm at 7.6, 12.8, 21.0 and 30.7 ml, corresponding to melittin, DNC-melittin, DTT and free DNC, respectively. As expected, only the two peaks corresponding to DNC-melittin and free DNC were detected on monitoring the effluent fluorescence emission at 520 nm. As with melittin, labelled melittin and also DNC and DTT exhibited non-ideal behaviour, all eluting beyond the total permeation volume of the column. Note that this non-ideal behaviour was particularly advantageous for our purposes, and that otherwise a satisfactory separation between modified and native peptide based only on molecular weight differences would probably have been impossible. It is worth emphasizing in this regard that, as has been described previously [18,23], the non-ideal properties of size-exclusion columns, rather than being a limitation, may in many instances become a useful analytical tool.

The identity of the peak eluting at 12.8 ml (putative DNC-melittin) was checked by both absorption and fluorescence spectroscopy after peak collection, desalting and lyophilization of this fraction. Fig. 6 shows the UV absorption spectrum of the powder after dissolution in methanol. This spectrum differed markedly from that corresponding to a single tryptophan (native melittin), as a result of the attached fluorescent probe. In fact, the spectrum was similar to that obtained for a 1:1 mixture of melittin and free DNC or for the model peptide dansyl-Gly-Trp (see Fig. 6). Moreover, from the molar absorptivities of melittin and DNC in methanol [ϵ_{280} (melittin) = 5900 l mol⁻¹ cm⁻¹; ϵ_{332} (DNC) = 3860 l mol⁻¹ cm⁻¹], a 1:1 stoichiometry was deduced for the DNC-melittin derivative. In addition, Fig. 6 also shows the fluorescence emission spectra in methanol upon excitation at 280 and 350 nm. As expected, emission bands were obtained corresponding to Trp (maximum at 340 nm) and dansyl (maximum at 530 nm) groups. The position of the emission maxima was coincident with that deduced using a 1:1 melittin-DNC mixture or dansyl-Gly-Trp under the same experimental conditions. Further, the labelled melittin yielded a single peak at 12.8 ml when rechromatographed on Ultrahydrogel-120. All the above observations demonstrate that this peak indeed corresponds to a 1:1 monodansylcadaverine-melittin covalent derivative. The same conclusions were drawn after a similar analysis of the modified melittin peak emerging from the reversed-phase support.

Finally, volatile buffers such as 0.1 *M* ammonium acetate (pH 4.4), were also

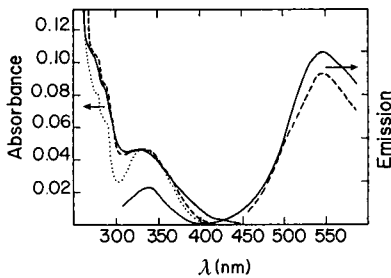


Fig. 6. Left-hand axis: absorption spectra in methanol of (solid line) DNC-melittin obtained from the corresponding fraction in the Ultrahydrogel-120 effluent (see text), (dashed line) an equimolar mixture of native melittin and free DNC and (dotted line) the model dipeptide dansyl-Gly-Trp. Right-hand axis: fluorescence emission spectra in methanol of DNC-melittin on excitation at (solid line) 280 and (dashed line) 350 nm. Peptide concentration: $11 \mu\text{M}$.

tried as mobile phases in the SEC mode and a similar resolution was obtained as with the above-mentioned conditions. Hence these buffers can be used for semi-preparative purposes avoiding the need for desalting of the collected sample.

CONCLUSIONS

The amphiphilic peptide melittin was enzymatically modified with the fluorescent probe monodansylcadaverine using guinea pig liver transglutaminase and a fluorophoric derivative of stoichiometry 1:1 was obtained. It has been shown that reversed-phase and size-exclusion HPLC modes can be successfully used for the complete separation, directly from the reaction mixture, of the labelled peptide and its native species. When operating under isocratic conditions both modes provide an easy, rapid, convenient means of accurately monitoring the time course of the enzymatic reaction and of isolating the labelled product for semi-preparative purposes.

A good resolution of all the components of the TGase enzymatic assay was achieved in both size-exclusion and gradient reversed-phase modes, the former being more appropriate in the present case based on its simpler operation and especially its shorter time of analysis. However, if larger peptides or even proteins were labelled in a similar manner with a dansyl-containing probe, reversed-phase gradient conditions might be the method of choice owing to the greater versatility of operation.

Finally, the behaviour observed for both melittin and dansyl-labelled melittin on Ultrahydrogel-120 is a clear example of how a non-ideal SEC mechanism can turn out to be advantageous for an *a priori* compromised separation.

ACKNOWLEDGEMENTS

E.P.P. was the recipient of a long-term postgraduate fellowship from the Generalitat Valenciana (Spain). This work was supported by grant No. PB87-0996 from DGICYT (Spain).

REFERENCES

- 1 L. Braco, C. Abad, A. Campos and J. E. Figueruelo, *J. Chromatogr.*, 35 (1986) 181.
- 2 L. Braco, M. C. Bañó, F. Chillarón and C. Abad, *J. Liq. Chromatogr.*, 10 (1987) 3463.
- 3 M. C. Bañó, L. Braco and C. Abad, *J. Chromatogr.*, 458 (1988) 105.
- 4 M. C. Bañó, L. Braco and C. Abad, *FEBS Lett.*, 250 (1989) 67.
- 5 M. C. Bañó, L. Braco and C. Abad, *Biochemistry*, 30 (1991) 886.
- 6 M. Lafleur, J. F. Faucon, J. Dufourcq and M. Pézolet, *Biochim. Biophys. Acta*, 980 (1989) 85.
- 7 J. E. Alouf, J. Dufourcq O. Siffert, E. Thiaudiere and C. Geoffroy, *Eur. J. Biochem.*, 183 (1989) 381.
- 8 R. Porta, C. Esposito, S. Metafora, P. Pucci, A. Malorni and G. Marino, *Anal. Biochem.*, 172 (1988) 499.
- 9 P. Pucci, A. Malorni, G. Marino, S. Metafora, C. Esposito and R. Porta, *Biochem. Biophys. Res. Commun.*, 154 (1988) 735.
- 10 R. Takashi, *Biochemistry*, 27 (1988) 938.
- 11 D. C. Sane, T. L. Moser, A. M. M. Pippen, C. J. Parker, K. E. Achyuthan and C. S. Greenberg, *Biochem. Biophys. Res. Commun.*, 157 (1988) 115.
- 12 Y. Ando, S. Imamura, Y. Yamagata, T. Kikuchi, T. Murachi and R. Kannagi, *J. Biochem.*, 101 (1987) 1331.
- 13 J. E. Folk, *Annu. Rev. Biochem.*, 49 (1980) 517.
- 14 E. Pérez-Payá, E. Thiaudière, C. Abad and J. Dufourcq, *FEBS Lett.*, 268 (1991) 51.
- 15 A. W. Bernheimer and B. Rudy, *Biochim. Biophys. Acta*, 864 (1986) 123.
- 16 S. Nury, J. C. Meunier and A. Mouranche, *Eur. J. Biochem.*, 161 (1989) 161.
- 17 Waters Chromatography Division, Millipore, *Polym. Notes*, 2, No. 1, July (1987).
- 18 C. T. Mant and R. S. Hodges, in K. M. Gooding and F. E. Regnier (Editors) *HPLC of Biological Macromolecules. Methods and Applications*, (Chromatographic Science Series, Vol. 51), Marcel Dekker, New York, Basle, 1990, pp. 301–332.
- 19 W. S. Hancock and J. T. Sparrow, *J. Chromatogr.*, 206 (1981) 71.
- 20 H. Gaertner and A. Puigserver, *J. Chromatogr.*, 350 (1985) 279.
- 21 L. R. Snyder and M. A. Stadalius, in Cs. Horváth (Editor), *High Performance Liquid Chromatography—Advances and Perspectives*, Vol. 4, Academic Press, New York, 1986, pp. 195–309.
- 22 E. Pérez-Payá, L. Braco, A. Campos, V. Soria and C. Abad, *J. Chromatogr.*, 461 (1989) 229.
- 23 C. T. Mant, J. M. R. Parker and R. S. Hodges, *J. Chromatogr.*, 397 (1987) 99.

Phenotyping of bovine milk proteins by reversed-phase high-performance liquid chromatography

SERVAAS VISSER*, CHARLES J. SLANGEN and HARRY S. ROLLEMA

Department of Biophysical Chemistry, Netherlands Institute for Dairy Research (NIZO), P.O. Box 20, 6710 BA Ede (Netherlands)

ABSTRACT

A reversed-phase high-performance liquid chromatographic method for the separation of the most common and some less common genetic variants of the bovine caseins is described. When the method is used for analysing clarified skim milk, simultaneous identification of casein variants and major whey protein variants can be effected in a single run. The potential of the method for quantitative application is discussed.

INTRODUCTION

About 80% of the bovine milk proteins consists of caseins, a heterogeneous fraction which is insoluble at its isoelectric pH (pH 4.6). The casein fraction can be subdivided into the α_{s1} -, α_{s2} -, β - and κ -casein components (α_{s1} CN, α_{s2} CN, β CN and κ CN), which in milk occur as a micellar complex in the approximate proportions 4:1:4:1, respectively. The remaining 20% of the milk protein fraction is formed by the whey proteins (soluble at pH 4.6), of which β -lactoglobulin (β Lg) and α -lactalbumin (α La) are the main components (ratio *ca.* 3:1). During the classical cheesemaking process it is the casein fraction which constitutes the cheese curd after the enzyme-triggered milk coagulation step.

The caseins and the major whey proteins have been found to show genetic polymorphism [1]. In western breeds certain genetic variants occur exclusively or are strongly predominant.

During the last decade studies on milk protein polymorphism have gained renewed interest, because the occurrence of certain milk protein genetic variants is correlated with the composition of milk and also with some milk processing parameters. For instance, the genotype κ CN-BB has been reported to be associated with enhanced rennetability of the milk [2–6], casein content [4], cheese curd firmness [2,5], curd syneresis [7–9] and overall cheese yield [5,7,9]. It has also been found that the κ CN-BB genotype is accompanied by a relatively high Ca^{2+} activity [10] and low citrate concentration [3] in the milk, but the difference between the effects of the κ CN A and B variants on the renneting properties can be eliminated by addition of calcium

chloride [2,10]. The latter facts may provide a more direct explanation for the observed relationship between κ CN genotype and rennetability of milk. The B variant of β Lg is also associated with some of the above-mentioned favourable technological properties [3,6,10,11]. Consequently, the combined occurrence of κ CN-BB and β Lg-BB genotypes could be of particular importance for obtaining improved cheese technological parameters [12,13]. Other properties reported to be influenced by milk protein genetic polymorphism are total milk production [12,14,15], heat stability of milk [16–19], water sorption of the casein fraction [18] and fat content of cheese [9,15,20]. Conclusions in reports concerning the relationship between protein genotype and various technological properties are not always consistent [5,20]; the influence of the season should also be considered [18].

From the above it follows that for the optimum selection of milk for further processing, a reliable method for the qualitative and quantitative determination of milk protein genetic variants should be available. Reported procedures for the identification of genetic milk protein variants are classical gel electrophoresis [16,17,21–23], isoelectric focusing [24–28] and, in the case of β Lg, high-performance liquid chromatography (HPLC) [29–33]. Recently, for κ CN genotypes, identification at the DNA level has been reported [34–36].

In this paper we describe a reversed-phase (RP) HPLC method by which the most common and also some less common casein variants can be separated. The method permits the simultaneous identification of various casein variants and the whey proteins α La-B, β Lg-A and β Lg-B in a single chromatographic run. Furthermore, attention is paid to the quantitative aspects of the method.

EXPERIMENTAL

Materials

Whole casein was isolated from skimmed bulk milk or from skim milk from individual cows by isoelectric precipitation at pH 4.6; the soluble fraction contained the whey proteins. Purified casein components were gifts from Dr. D. G. Schmidt. *para*- κ CN (the 1–105 fragment of κ CN) and the κ CN glycomacropeptides (GMP-A and GMP-B, both representing non- and differently glycosylated 106–169 fragments) were obtained by splitting κ CN-A and κ CN-B with chymosin at pH 6.5, which results in a precipitate (*para*- κ CN) and a soluble fraction (GMP-A and GMP-B, respectively).

Analysis

The HPLC equipment consisted of two M 6000A pumps (Waters Assoc.), an ISS-100 automatic sample injector (Perkin-Elmer), a Kratos Model 783G UV detector and a Waters Type 680 automated gradient controller. The equipment was linked to a data acquisition and processing system (Waters Maxima 820). A 250 mm \times 4.6 mm I.D. HiPore RP-318 column (Bio-Rad Labs.) was used with a C₁₈ cartridge (Bio-Rad Labs.) as a guard column. Solvent A was acetonitrile–water–trifluoroacetic acid (100:900:1 v/v/v) and solvent B was the same mixture with the proportions 900:100:0.7 (v/v/v). The solvent gradient reported for casein separation [37] was adapted for genetic casein variants and whey proteins: starting from 26% of solvent B (equilibration buffer) a gradient was generated immediately after injection by in-

creasing this proportion at 0.60% min⁻¹ (15 min), 0% min⁻¹ (7 min), 0.67% min⁻¹ (3 min), 0% min⁻¹ (12 min), 0.44% min⁻¹ (18 min), 12.5% min⁻¹ (2 min) and 0% min⁻¹ (5 min) subsequently, before returning to starting conditions in 5 min. After re-equilibration, the next analysis was carried out under the same conditions. If only casein variants were to be separated, the last three steps of the gradient were replaced by 6.6% min⁻¹ (5 min) and 0% min⁻¹ (5 min), subsequently, before returning to the starting conditions in 5 min. The column temperature was 30°C and peak detection was at 220 nm. The flow-rate was 0.8 ml min⁻¹, except in the determination of response curves for the caseins, when it was 1.0 ml min⁻¹. The system pressure was 1500 p.s.i.

Freeze-dried samples were dissolved in 0.02 M 1,3-bis[tris(hydroxymethyl)-methylamino]propane (Bis-Tris) buffer (pH 7) containing 4 M urea and 0.3% of 2-mercaptoethanol (ME). After standing at room temperature for 1 h, the samples were diluted (at least four-fold) with solvent A containing 6 M urea. The final sample concentration was about 2 mg ml⁻¹ for whole casein and 0.5 mg ml⁻¹ for casein components and whey proteins; 50- μ l amounts were applied to the column.

Clarified milk samples were obtained by mixing skim milk with a buffer (1:1, v/v) containing 0.1 M Bis-Tris, 8 M urea, 0.3% ME and 1.3% trisodium citrate dihydrate (pH 7); in some experiments ME was omitted from the buffer. After standing at room temperature for 1 h, the mixture was diluted with solvent A containing 6 M urea as above. Whole casein and whey protein fractions were isolated from the same skim milk and prepared for HPLC analysis, the whey protein solution (pH 4.6) being directly diluted with solvent A containing 6 M urea.

For the determination of response curves for the various milk proteins, use was made of freeze-dried, purified components of known protein content.

RESULTS AND DISCUSSION

For the main κ CN variants, *i.e.*, types A and B, we examined the influence of various glycosylation states on the RP-HPLC pattern. In Fig. 1 patterns for carbohydrate-free fractions and fractions with different levels of glycosylation [38] are depicted. It appears that the first-eluting protein peak of whole casein from bulk milk (reference) represents a mixture of carbohydrate-rich κ CN A and B. The carbohydrate-free κ CN A and B subcomponents are eluted at different positions and can therefore be distinguished from each other. Minor peaks at intermediate positions originate from partly glycosylated κ CN A or B. The small peak(s) immediately following those of carbohydrate-free κ CN A and B (also seen in the pattern of whole κ CN-B; Fig. 1B, trace *d*) should probably be attributed to remaining non-reduced κ CN or to a complex between κ CN and α_{s2} CN, formed by intermolecular S-S linkages.

We also established the retention times of the fragments *para*- κ CN and GMP formed after specific cleavage of κ CN A and B by chymosin during the first step of the milk-clotting process. The two genetically determined amino acid substitutions in these variants are both located in the GMP part [39], so that in the cheese whey from bulk milk essentially two GMP fractions (GMP-A and GMP-B) can be expected; the *para*- κ CN fraction is entrapped in the cheese curd. As seen in Fig. 2, *para*- κ CN elutes just prior to the carbohydrate-free κ CN-A variant, whereas the GMP A and B variants elute at quite different positions ahead of all the casein components.

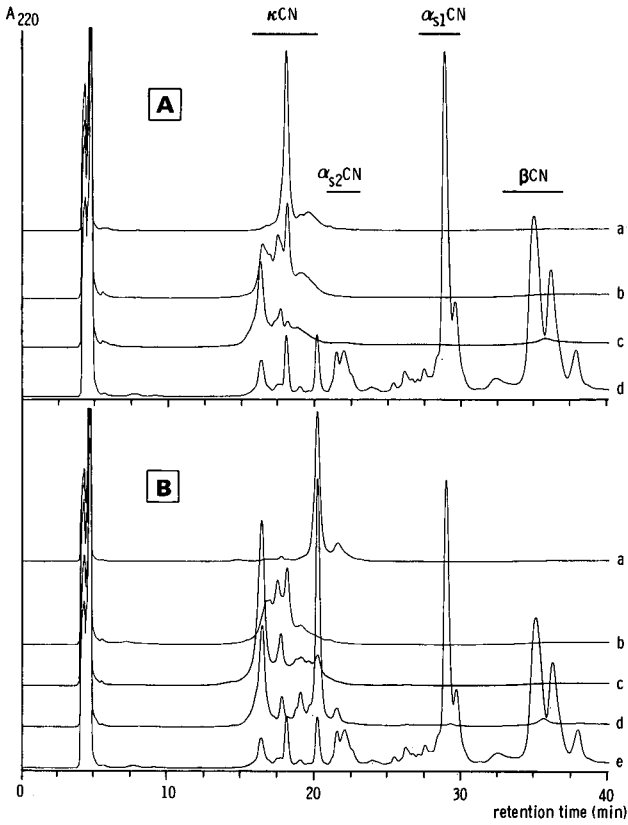


Fig. 1. Effect of degree of glycosylation on the retention of κ CN fractions during RP-HPLC. (A) (a) Carbohydrate-free κ CN-A; (b) partly glycosylated κ CN-A; (c) carbohydrate-rich κ CN-A; (d) whole casein from bulk milk (reference). (B) (a) Carbohydrate-free κ CN-B; (b) partly glycosylated κ CN-B; (c) carbohydrate-rich κ CN-B; (d) whole κ CN-B (reference); (e) whole casein from bulk milk (reference).

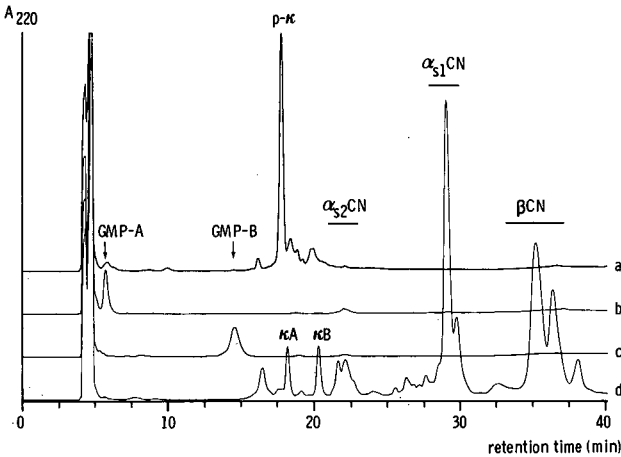


Fig. 2. RP-HPLC patterns of chymosin-generated breakdown products of κ CN A and B; carbohydrate-free κ CN indicated as κ A and κ B. (a) *para*- κ CN (p- κ); (b) GMP-A; (c) GMP-B; (d) whole casein from bulk milk (reference).

TABLE I

LOCATION OF DIFFERENCES IN THE PRIMARY STRUCTURE OF SOME GENETIC VARIANTS OF THE MAJOR BOVINE MILK PROTEINS [40]

Protein	Variant	Position in amino acid sequence				
α_{s1} CN (199 residues)		14-26	53	192		
	A	Deleted	Ala	Glu		
	B	Present	Ala	Glu		
	C	Present	Ala	Gly		
	D	Present	ThrP	Glu		
β CN (209 residues)		35	37	67	106	122
	A ¹	SerP	Glu	His	His	Ser
	A ²	SerP	Glu	Pro	His	Ser
	A ³	SerP	Glu	Pro	Gln	Ser
	B	SerP	Glu	His	His	Arg
	C	Ser	Lys	His	His	Ser
κ CN (169 residues)		136	148			
	A	Thr	Asp			
	B	Ile	Ala			
β Lg (162 residues)		64	118			
	A	Asp	Val			
	B	Gly	Ala			

The two relatively polar amino acid substitutions in κ CN-A as compared with κ CN-B (Table I) are in agreement with the earlier elution of the A-variant (including GMP-A compared with GMP-B) from the reversed-phase column.

In Fig. 3 RP-HPLC patterns of whole caseins obtained from milks of single cows are compared. Also, the patterns of two purified (less common) casein variants have been added. The genotypes of the casein components (including that of α_{s2} CN, which occurs predominantly as the A variant in European cattle) had been established by gel electrophoresis [16] or by isoelectric focusing [28]. As was already shown in Fig. 1, the κ CN A and B variants can be identified by the positions of their carbohydrate-free subcomponents. As far as α_{s1} CN is concerned, a distinction could be made between the A variant (missing a 13-residue fragment in its primary structure, see Table I), the B/C and the D variant. No separation could be achieved between the B and C variants (Glu \leftrightarrow Gly at position 192, Table I), both of which give rise to a double peak, due to a difference in the degree of post-translational phosphorylation (an extra phosphate group at position 41 [40]). The α_{s1} CN-B variant and to a much lesser extent the C variant are predominant in western cattle. β CN mainly occurs as its A¹, A² and/or, at a much lower frequency, as its B variant (for structural differences see Table I). These forms could be completely separated using the present RP-HPLC programme. In addition, the less common β CN-A³ is also separately seen in the elution pattern; it elutes just after β CN-A² from the column, owing to a His \rightarrow Gln replacement at position 106 (Table I). On the other hand, the rare β CN-C co-elutes with the β CN-A¹ variant. The minor component β X, which in the reference whole casein appears as the last-eluting peak (just after the position of β CN-A³), was isolated and shown to be also a β CN, as judged by sodium dodecyl sulphate-po-

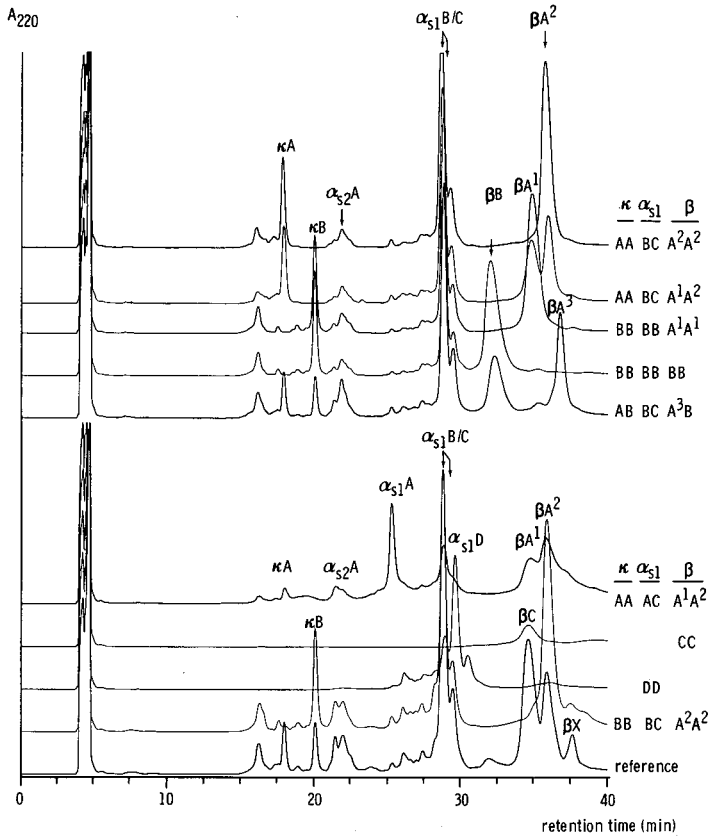


Fig. 3. RP-HPLC patterns of whole caseins and some casein components from milks from single cows. The α_{s2} CN is present as the A type throughout. The other genotypes are indicated. Whole casein from bulk milk is added as a reference; the unknown component βX herein is referred to in the text.

lyacrylamide gel electrophoresis and amino acid analysis (results not shown). We found this component in several whole caseins from bulk milk, although in different amounts. Re-chromatography of the isolated component under the same conditions (see Experimental) showed a single peak at its original position, so that its designation as some aggregated form of β CN can be excluded. It could be a still unidentified β CN variant [41].

The RP-HPLC separation of α La-B, β Lg-A and β Lg-B is well documented [29,32,33]. It generally concerns purified whey proteins or total whey protein preparations. However, identification and phenotyping of these proteins in combination with the caseins directly in milk could be desirable. We have achieved this by analysing samples of skim milk clarified in a buffer containing urea, ME and sodium citrate (for details see Experimental). The RP-HPLC pattern of a total milk protein fraction is shown in Fig. 4. It also shows the patterns of the casein and whey protein fractions isolated from the same milk, together with a pattern of cheese whey, in which the main whey proteins and also GMP-A and GMP-B can be observed. In the total milk

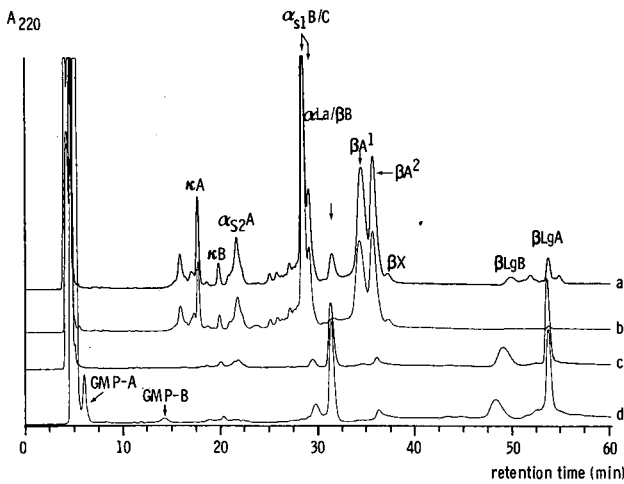


Fig. 4. RP-HPLC patterns of (a) a clarified skim milk sample and of (b) whole casein and (c) acid whey prepared from the same milk. A pattern of a cheese whey has also been added (d).

protein pattern the casein variants can be clearly distinguished from the whey proteins except β CN-B, which is largely obscured by α La-B, the latter being the only α La variant found in milk from western cattle [40]. The buffer used to clarify the milk sample contained ME to obtain an optimum separation in the κ CN and α_{s2} CN region of the RP-HPLC pattern. However, this ME-containing clarification buffer tends to deform the β Lg peaks in the RP-HPLC pattern, giving rise to small peaks between those of the A and B variants (see Fig. 4, trace *a*). The minor component immediately following the β Lg-A peak appears exclusively in the presence of urea in the reaction mixture at pH 7 and could be avoided by using deionized urea (not done in this study). In the whey protein fractions not treated with ME/urea at pH 7 (Fig. 4, traces *c* and *d*) such additional peaks are absent. The α La-B component seems to be much less subject to deformation by mild ME treatment, probably because of its more compact globular character. Altogether, this means that proper quantification of separate β Lg A and B variants from patterns as shown in Fig. 4, trace *a*, is difficult as it is unknown to which of the variants, if both are present, the intermediate peaks should be assigned. The peak of β Lg-B can be sharpened by shortening the "hold" period of 12 min in the gradient programme (see Experimental). In that case, however, ME-generated peaks between the A and B variants remain largely hidden.

In principle, the RP-HPLC method lends itself better to quantification of milk protein genetic variants than do electrophoretic methods, because when using the latter procedures problems with quantitative staining may arise. On the other hand, with electrophoretic methods many samples can be handled simultaneously. Therefore, RP-HPLC and electrophoresis or isoelectric focusing may be used as complementary techniques. In Fig. 5 the relationships between RP-HPLC peak areas and concentrations of various isolated casein components (A) and whey proteins (B) are shown. For caseins reasonable linearity was obtained in the concentration range investigated (Fig. 5A). However, the linear α_{s2} CN curve did not pass through the origin (result not shown), owing to a "memory effect" observed with α_{s2} CN on the

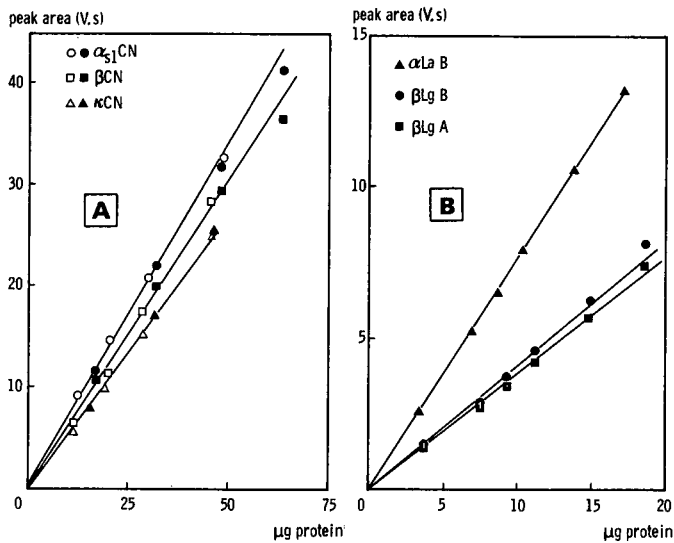


Fig. 5. Relationship between RP-HPLC peak area(s) and amount of milk protein samples injected. (A) Casein components (open and closed symbols represent two independent experiments); (B) whey proteins.

column used. Of the whey proteins, both β Lg and α La show satisfactory linearity with a significantly higher slope observed for α La (Fig. 5B). To minimize experimental variations, proper standards should be included in each series of analyses. Quantification of RP-HPLC patterns of skim milks after clarification gave problems with β Lg, owing to the effect of ME described above; in that case an additional run with a clarified, non-reduced milk sample should provide the analytical data for β Lg. The quantitative aspects of the method are being investigated further.

CONCLUSIONS

With the RP-HPLC method described, separation can be achieved between (in order of increasing retention time) carbohydrate-rich κ CN-A + -B, carbohydrate-free κ CN-A, carbohydrate-free κ CN-B, α_{s2} CN-A, α_{s1} CN-A, α_{s1} CN-B/C, α_{s1} CN-D, β CN-B, β CN-C/A¹, β CN-A² and β CN-A³. In addition, the products of κ CN cleavage by the milk-clotting enzyme chymosin (*i.e.*, GMP-A, GMP-B and *para*- κ CN) can be distinguished from each other and from the above-mentioned casein components. When the whey proteins α La and β Lg are also included in the mixture (for instance, by injecting diluted, clarified skim milk), the β Lg A and B variants can be observed separately from the caseins, whereas α La-B co-elutes with the less common B variant of β CN.

Except for α_{s2} CN, quantification should be possible provided that precautions are taken, such as inclusion of standards in each series of analyses and standardization of the experimental conditions.

ACKNOWLEDGEMENTS

We are grateful to Drs. P. J. de Koning and D. G. Schmidt of this Institute and to Ir. H. Bovenhuis (Wageningen Agricultural University) for helpful discussions and gifts of protein and milk samples.

REFERENCES

- 1 M. P. Thompson and H. M. Farrell, in B. L. Larson and V. R. Smith (Editors), *Lactation, a Comprehensive Treatise*, Vol. III, Academic Press, New York, 1974, pp. 109–134.
- 2 J. Schaar, *J. Dairy Res.*, 51 (1984) 397–406.
- 3 J. Schaar, B. Hansson and H.-E. Pettersson, *J. Dairy Res.*, 52 (1985) 429–437.
- 4 E. Jakob and Z. Puhán, *Dtsch. Molk.-Ztg.*, 107 (1986) 833–834.
- 5 D. M. McLean, *Anim. Genet.*, 18, Suppl. 1 (1987) 100–102.
- 6 C. Corradini, P. Vecchia and G. Rossi, *Sci. Tec. Latt. Cas.*, 39 (1988) 423–430.
- 7 P. Mariani, G. Losi, V. Russo, G. B. Castagnetti, L. Grazia, D. Morini and E. Fossa, *Sci. Tec. Latt. Cas.*, 27 (1976) 208–227.
- 8 D. M. McLean and J. Schaar, *J. Dairy Res.*, 56 (1989) 297–301.
- 9 D. Morini, G. Losi, G. B. Castagnetti and P. Mariani, *Sci. Tec. Latt. Cas.*, 30 (1979) 243–262.
- 10 G. van den Berg, P. J. de Koning, J. T. M. Escher and H. Bovenhuis, *Voedingsmiddelen Tec.*, 23, No. 20 (1990) 13–15, 17.
- 11 D. Morini, G. B. Castagnetti, C. Chiavari, L. Grazia, G. Losi, R. Davoli and P. Bosi, *Sci. Tec. Latt. Cas.*, 33 (1982) 475–492.
- 12 P. J. de Koning, *Voedingsmiddelen Tec.*, 21, No. 11 (1990) 22–25.
- 13 K. F. Ng Kwai Hang, *Mod. Dairy*, 69, No. 1 (1990) 14–15.
- 14 K. F. Ng Kwai Hang, J. F. Hayes, J. E. Moxley and H. Monardes, *J. Dairy Sci.*, 67 (1984) 835–840.
- 15 A.-M. Bech and K. R. Kristiansen, *J. Dairy Res.*, 57 (1990) 53–62.
- 16 D. G. Schmidt and J. Koops, *Neth. Milk Dairy J.*, 19 (1965) 63–68.
- 17 D. G. Schmidt, in *Proceedings of XVIIth International Dairy Congress (Munich)*, Vol. A, Verlag Th. Mann, Hildesheim, 1966, pp. 259–262.
- 18 O. Kirchmeier, A. Mehana, R. Graml, J. Buchberger and F. Pirchner, *Milchwissenschaft*, 38 (1983) 589–591.
- 19 D. M. McLean, E. R. B. Graham, R. W. Ponzoni and H. A. McKenzie, *J. Dairy Res.*, 54 (1987) 219–235.
- 20 R. Aleandri, L. G. Buttazzoni, J. C. Schneider, A. Caroli and R. Davoli, *J. Dairy Sci.*, 73 (1990) 241–255.
- 21 C. A. Kiddy, J. O. Johnston and M. P. Thompson, *J. Dairy Sci.*, 47 (1964) 147–151.
- 22 M. P. Thompson, C. A. Kiddy, J. O. Johnston and R. M. Weinberg, *J. Dairy Sci.*, 47 (1964) 378–381.
- 23 R. Aschaffenburg and M. Thymann, *J. Dairy Sci.*, 48 (1965) 1524–1526.
- 24 F. Addeo, L. Chianese, A. Di Luccia, P. Petrilli, R. Mauriello and G. Anelli, *Milchwissenschaft*, 38 (1983) 586–588.
- 25 B. Seibert, G. Erhardt and B. Senft, *Anim. Genet.*, 18 (1987) 269–272.
- 26 A.-M. Bech and K. S. Munk, *Milchwissenschaft*, 43 (1988) 230–232.
- 27 G. E. Vegarud, T. S. Molland, M. J. Brovold, T. G. Devold, P. Alestrøm, T. Steine, S. Rogne and T. Langsrud, *Milchwissenschaft*, 44 (1989) 689–691.
- 28 H. Bovenhuis and A. J. M. Verstege, *Neth. Milk Dairy J.*, 43 (1989) 447–451.
- 29 R. J. Pearce, *Aust. J. Dairy Tec.*, 38 (1983) 114–117.
- 30 R. S. Humphrey and L. J. Newsome, *N. Z. J. Dairy Sci. Tec.*, 19 (1984) 197–204.
- 31 A. T. Andrews, M. D. Taylor and A. J. Owen, *J. Chromatogr.*, 348 (1985) 177–185.
- 32 C. Olieman, *Voedingsmiddelen Tec.*, 22, No. 23 (1989) 26–28.
- 33 B. G. Venter, L. van Rensburg and D. J. de Lange, *S. Afr. J. Dairy Sci.*, 21 (1989) 41–44.
- 34 A. Rondo, P. Di Gregorio and P. Masina, *Anim. Genet.*, 19 (1988) 51–54.
- 35 S. Rogne, S. Lien, G. Vegarud, T. Steine, T. Langsrud and P. Alestrøm, *Anim. Genet.*, 20 (1989) 317–321.
- 36 J. F. Medrano and E. Aguilar-Cordova, *Bio/Technology*, 8 (1990) 144–146.

- 37 S. Visser, K. J. Slangen and H. S. Rollema, *Milchwissenschaft*, 41 (1986) 559–562.
- 38 H. J. Vreeman, S. Visser, K. J. Slangen and J. A. M. van Riel, *Biochem. J.*, 240 (1986) 87–97.
- 39 P. J. De Koning, *Neth. Milk Dairy J.*, 22 (1968) 121–124.
- 40 W. N. Eigel, J. E. Butler, C. A. Ernstrøm, H. M. Farrell, V. R. Harwalkar, R. Jenness and R. McL. Whitney, *J. Dairy Sci.*, 67 (1984) 1599–1631.
- 41 C. Carles, *J. Dairy Res.*, 53 (1986) 35–41.

CHROMSYMP. 2195

Separation and quantitation of serum proinsulin and proinsulin intermediates in humans

SUSANNE LINDE*

Hagedorn Research Laboratory, Niels Steensens Vej 6, DK-2820 Gentofte (Denmark)

MICHAEL E. RØDER, SVEND G. HARTLING and CHRISTIAN BINDER

Steno Memorial and Hvidøre Hospital, DK-2820 Gentofte (Denmark)

and

BENNY S. WELINDER

Hagedorn Research Laboratory, Niels Steensens Vej 6, DK-2820 Gentofte (Denmark)

ABSTRACT

Two reversed-phase high-performance liquid chromatographic (RP-HPLC) systems were developed for the separation of human insulin, proinsulin and the major proinsulin intermediates. The individual components were quantified using two enzyme-linked immunosorbent assays for insulin and proinsulin immunoreactive material (PIM) after (passive) evaporation of the organic modifier. Serum samples from normal subjects and patients with non-insulin-dependent diabetes mellitus were immunopurified and analysed in one of the RP-HPLC systems. The proportion of PIM relative to insulin immunoreactive material was higher in the diabetic patient compared with that in the normal subject. In both, PIM was heterogeneous, consisting of intact proinsulin and des-proinsulin intermediates.

INTRODUCTION

The insulin precursor proinsulin is converted by specific enzymes in the β -cell secretory granules to insulin via several intermediate forms [1]: two trypsin-like enzymes cleave next to the paired basic amino acids in positions 31–32 and 64–65, respectively [2], followed by removal of the basic residues by carboxypeptidase H [3].

Elevated amounts of proinsulin immunoreactive material (PIM) in serum have been described in various conditions and diseases [4–7], including non-insulin-dependent diabetes mellitus (NIDDM) [8–10], and could be an indication of altered β -cell function. The extent to which the proinsulin intermediate forms exist together with intact proinsulin in serum is not known.

In order to determine the composition of PIM in serum samples, a method for the specific determination of proinsulin and all the individual conversion intermediates is required. As it is difficult to develop site-specific immunoassays that can distinguish between the small structural differences in the various proinsulin conversion products (Fig. 1), the aim of this study was to develop reversed-phase high-performance liquid chromatographic (RP-HPLC) methods capable of separating insulin,

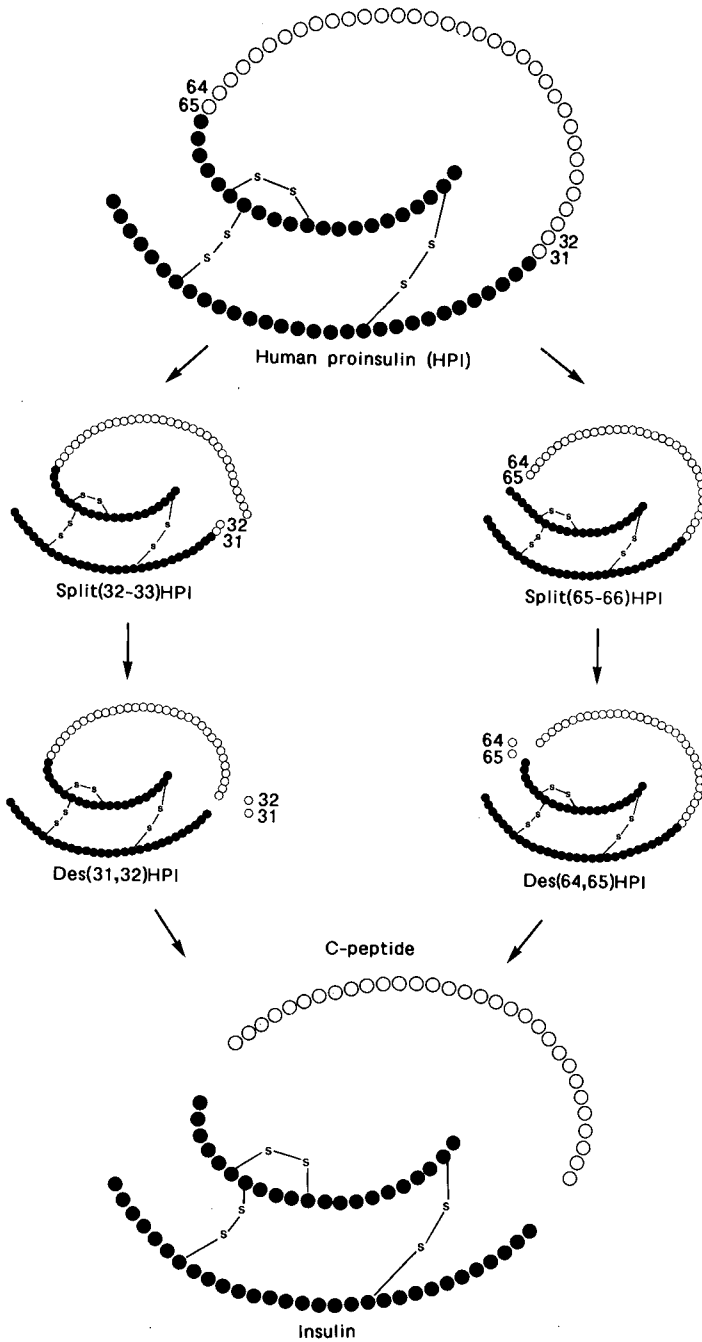


Fig. 1. Conversion of human proinsulin to (●) insulin and (○) C-peptide via split- and des-proinsulin intermediates. Amino acids 31, 32 and 65 are arginine and 64 is lysine.

proinsulin and the four major proinsulin intermediates. The individual fractions obtained after RP-HPLC were analysed in two enzyme-linked immunosorbent assays (ELISAs) for the determination of insulin [11] and PIM [12], and this paper reports such analyses of serum samples from normal subjects and NIDDM patients using one of the optimized RP-HPLC systems.

EXPERIMENTAL

Reagents

Trifluoroacetic acid (TFA) (peptide synthesis grade) was obtained from Applied Biosystems, phosphoric acid (analytical-reagent grade) from Merck, ammonium sulphate (Aristar) from BDH, triethylamine (99%) from Janssen Chimica and acetonitrile (HPLC grade S) from Rathburn Chemicals. All other chemicals were of analytical-reagent grade. Distilled water was obtained from a Millipore Milli-Q system, and all buffers were filtered (0.45 μm , Millipore) and vacuum/ultrasound degassed before use.

HPLC equipment

The HPLC system consisted of two Waters Assoc. Model M510 pumps, a Model 660 solvent programmer, a Model U6K injector, a Linear UVIS 200 detector and an LKB Model 2210 one-channel recorder.

HPLC columns

Nucleosil 100-5C₁₈ (5 μm), 250 \times 4.0 mm I.D., and 300-5C₄ (5 μm), 250 \times 4.0 mm I.D. and 30 \times 4.0 mm I.D., columns were obtained from Macherey-Nagel & Co., a LiChrosorb RP-18 (5 μm), 250 \times 4.0 mm I.D., column from Merck and a Zorbax Protein Plus (6 μm), 250 \times 4.6 mm I.D., column from DuPont.

HPLC conditions

The following mobile phases were used: 0.1% TFA (pH 2.0), 0.125 M triethylammonium phosphate (TEAP) (pH 4.0) and 0.125 M ammonium sulphate (AS) (pH 4.0), all in acetonitrile (ACN). The columns were eluted at ambient temperature at 1.0 ml/min with shallow linear acetonitrile gradients ranging from 1.2% to 6% during 60 min. The column eluate was monitored at 210 nm and collected in 0.5-min fractions in a FRAC 300 fraction collector (Pharmacia).

ELISA analyses

To avoid non-specific adsorption to the tubes, 50 μl of 0.04 M sodium phosphate (pH 7.4) containing 6% of human serum albumin (HSA) and 0.1% Tween 20 were added to each tube prior to the collection of fractions. After (passive) evaporation of acetonitrile overnight at room temperature, the fractions were compatible with the ELISA assays performed as described [11,12]. The standard operating range was 0–400 pmol/l for insulin and 0–80 pmol/l for proinsulin. Detection limits were 2.5 and 1.2 pmol/l, respectively.

Standards

Human proinsulin (Lot A18-TS9-16) and the four major proinsulin intermedi-

ate standards, des(31,32)HPI (Lot A18-7W8-1), des(64,65)HPI (Lot A18-7W8-2), split(32-33)HPI (Lot A18-JC5-96) and split(65-66)HPI (Lot A18-JC5-92), were kindly donated by B. H. Frank (Lilly Research Labs.). Human insulin was obtained from Novo Nordisk. The standards were dissolved to give 0.1 mg/ml concentrations in 3 M acetic acid containing 0.1% HSA before the RP-HPLC analyses. Mono-[¹²⁵I-(TyrA14)]-porcine insulin obtained from Novo Nordisk and [³H-Leu]proinsulin (rat) prepared as described [13] were used for recovery determinations.

Serum sample preparation

Owing to the low PIM concentration in serum, the samples (10 ml) from fasting normal humans (control) and fasting NIDDM patients were transferred to empty 10 × 1.5 cm I.D. siliconized Econo-Columns (Bio-Rad Labs.) followed by 200 μl of a guinea-pig anti-insulin immunobead slurry containing excess immunobinding capacity in relation to the sample. The columns were closed and rotated overnight at 4°C. The serum was then drained off, the immunobeads were washed with distilled water and subsequently insulin, proinsulin and intermediates were recovered after addition of 400 μl of 1 M acetic acid-30% ACN (15 min at 4°C), this procedure being repeated twice. The combined acetic acid-ACN solutions were lyophilized, redissolved in 200 μl of 3 M acetic acid-0.1% HSA and centrifuged prior to RP-HPLC analysis (corresponding to a 50-fold concentration).

RESULTS

A sample containing human insulin, proinsulin and the four major proinsulin intermediates (see Fig. 1) was analysed using different stationary-mobile phase combinations in order to obtain a satisfactory (baseline) separation of all the components. As mobile phases, TFA-ACN and also TEAP and AS in ACN, previously shown to be excellent for insulin-proinsulin separations [14], were applied. The results are summarized in Table I, from which it can be seen that only two systems were able to fulfil this demand. Representative chromatograms using LiChrosorb RP-18-AS-ACN and Nucleosil 300-5C4-TFA-ACN are shown in Figs. 2 and 3, respectively.

The ELISA determinations and the UV trace for the RP-HPLC-separated components in a sample containing 1 μg of insulin, proinsulin and each of the four intermediates using the Nucleosil-TFA-ACN system are shown in Fig. 4. Insulin ELISA was performed on fractions 1-45 and proinsulin ELISA on fractions 46-120.

The Nucleosil-TFA-ACN system was chosen for the separation of insulin and PIM in serum samples because guard columns packed with the same stationary phase are available and probably necessary in order to protect the separation column from harsh serum constituents and thus extend the column lifetime. Further, the deleterious effect of the corrosive salt used in the alternative system was avoided.

Examples of the application of this RP-HPLC analysis to serum samples from a normal subject (control) and a NIDDM patient are shown in Fig. 5. In Fig. 6 the proinsulin ELISA values are shown from a selected range of fractions with an extended concentration scale in order to reveal minor peaks.

To avoid cross-contamination from sample to sample and also from standards run between samples to verify the positions of the individual components by the UV signal, the Hamilton syringe used for injection of the sample was rinsed at least three

TABLE I

RP-HPLC SEPARATIONS OF INSULIN, PROINSULIN AND THE FOUR PROINSULIN INTERMEDIATES

Stationary phase	Mobile phase		
	0.1% TFA-ACN (pH 2.0)	0.125 M TEAP (pH 4.0)-ACN	0.125 M AS (pH 4.0)-ACN
LiChrosorb RP-18	Irreversible binding of insulin and proinsulin	One intermediate eluted with proinsulin	Baseline separation of all components
Nucleosil 100-5C ₁₈	Irreversible binding of insulin and proinsulin	Two intermediates eluted with proinsulin	
Nucleosil 300-5C ₄	Baseline separation of all components		
Zorbax Protein Plus	One des-proinsulin eluted with proinsulin		

times with 3 M acetic acid-0.1% HSA before each injection. ELISA of the fractions collected after injection of 200 μ l of 3 M acetic acid-0.1% HSA after such a rinsing procedure showed no content of insulin and PIM.

As HSA and other hydrophobic proteins from the serum samples will bind to the stationary phase with the optimized shallow acetonitrile gradient used in this separation (maximum 32% acetonitrile), the column was eluted for 15 min with 60% acetonitrile after each analysis.

In order to confirm the retention times of the serum PIM, a standard containing insulin and HPI was analysed before and after each serum sample. Further, a mixture of the four intermediates was analysed within each batch of column and mobile phase.

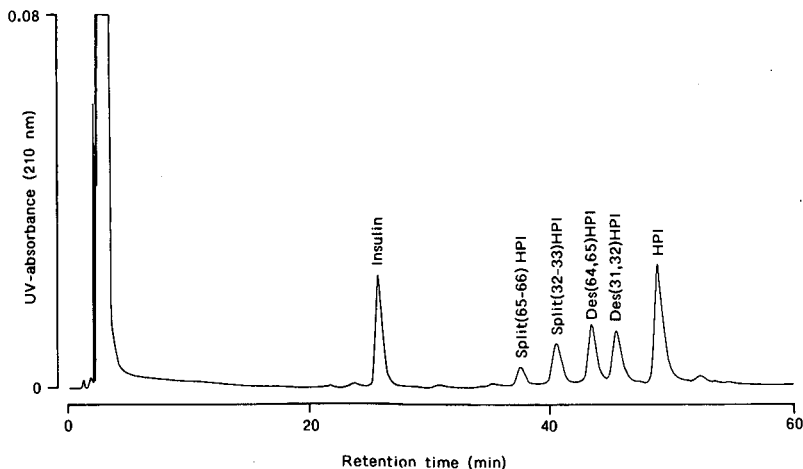


Fig. 2. RP-HPLC separation of human insulin (ca. 1 μ g), proinsulin (HPI, ca. 2 μ g) and the four proinsulin intermediates (ca. 1 μ g of each) using a LiChrosorb RP-18 column eluted at 1.0 ml/min with a linear acetonitrile gradient (29.4 to 33.6%) in 0.125 M ammonium sulphate (AS) (pH 4.0) during 60 min.

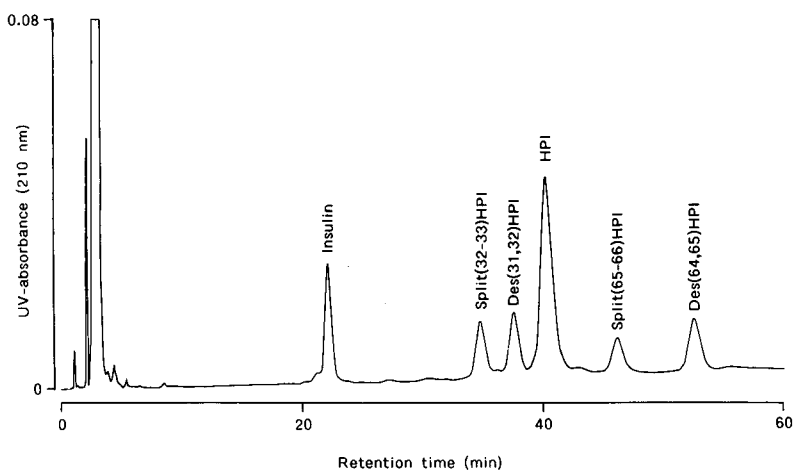


Fig. 3. RP-HPLC separation of human insulin (*ca.* 1 μg), proinsulin (*ca.* 3 μg) and the four proinsulin intermediates (*ca.* 1 μg of each) using a Nucleosil 300-5C₄ column eluted at 1.0 ml/min with a linear acetonitrile gradient (29.4 to 30.6%) in 0.1% TFA during 60 min.

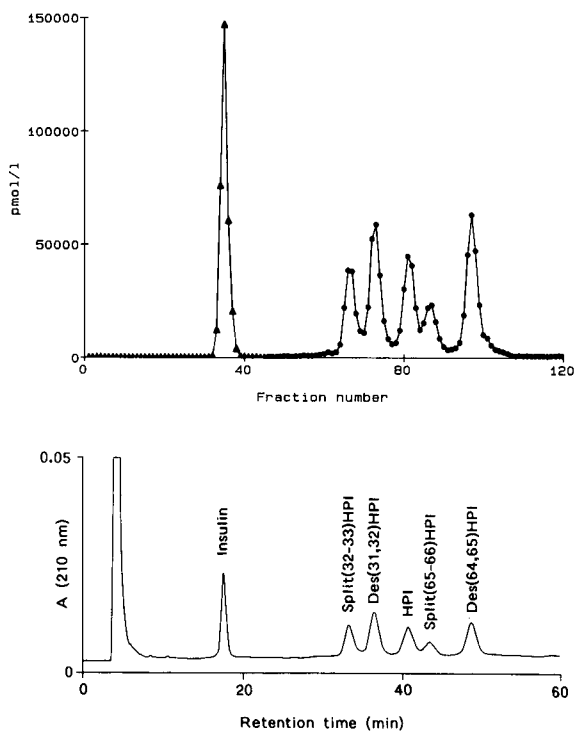


Fig. 4. RP-HPLC separation of human insulin, proinsulin and the four proinsulin intermediates (1 μg of each) essentially as in Fig. 3, but using another batch of Nucleosil stationary phase protected by a guard column. 0.5-min fractions were collected followed by (\blacktriangle) insulin ELISA of fractions 1–45 and (\bullet) proinsulin ELISA of fractions 46–120.

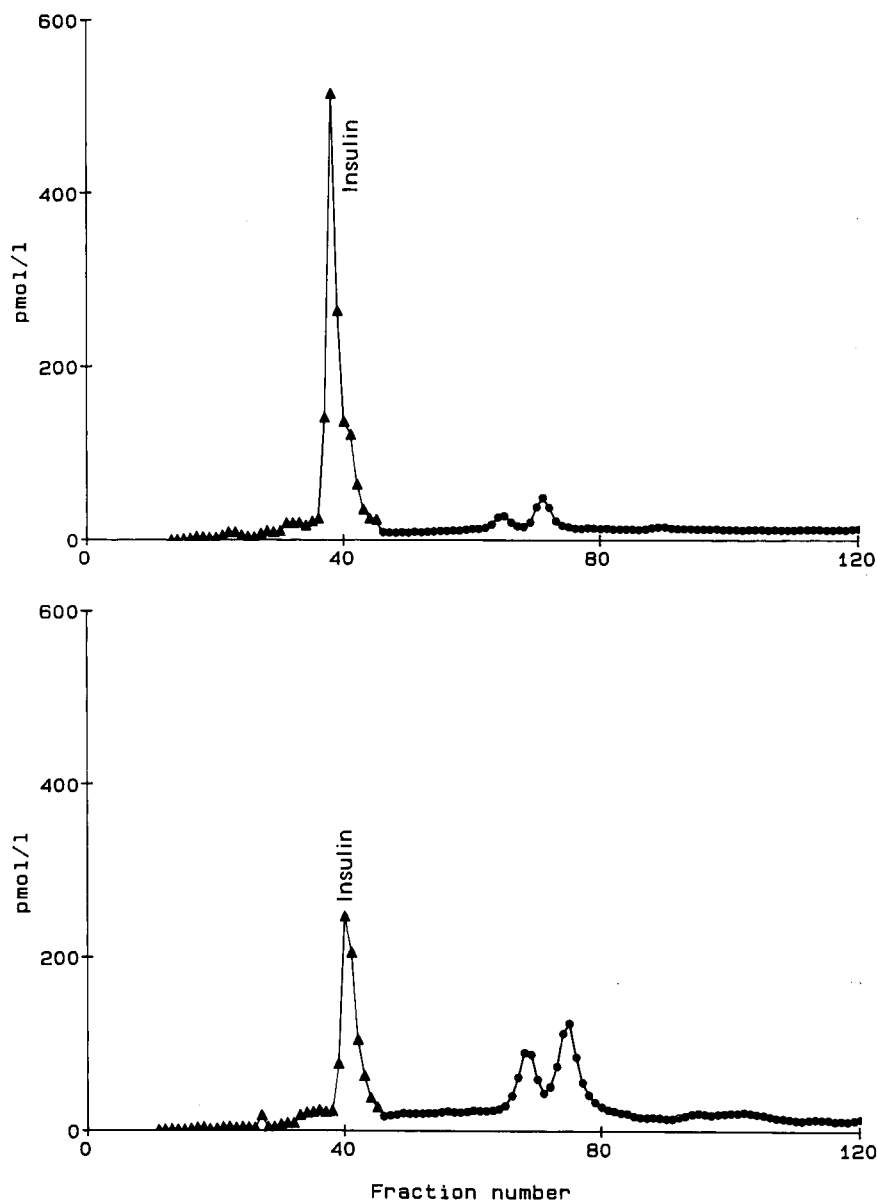


Fig. 5. RP-HPLC of immunoaffinity-purified serum from a normal human (control) and a NIDDM patient (upper and lower curve, respectively) using a Nucleosil 300-5C₄ column as described in Fig. 3. Insulin and proinsulin ELISA as in Fig. 4. The proinsulin ELISA results for fractions 46-100 are shown with an extended scale in Fig. 6.

The recovery of insulin and proinsulin after RP-HPLC of picogram to nanogram amounts was evaluated using radioactively labelled insulin (mono-[¹²⁵I-(TyrA14)-insulin) and proinsulin ([³H-Leu]proinsulin) as samples. The recoveries (amount of radioactivity collected relative to the radioactivity injected) were found to be in the range 99-105%.

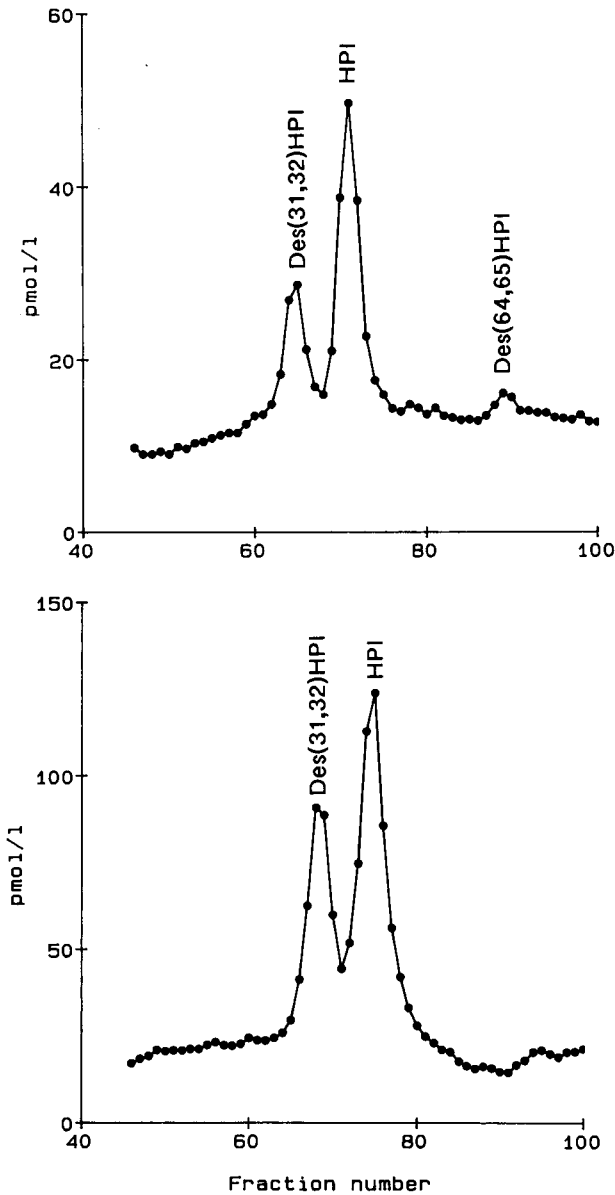


Fig. 6. Proinsulin ELISA of fractions 46–100 (see Fig. 5) corresponding to serum samples from a normal human (control) (upper curve) and a NIDDM patient (lower curve).

DISCUSSION

There have been few reports of RP-HPLC separations of insulin, proinsulin and proinsulin intermediates [3,15], whereas several immunological methods for the determination of proinsulin and proinsulin intermediates in plasma and serum have

been published [10,16–19]. Various degrees of cross-reactivity confuse these results and all individual intermediates have never been determined directly.

We evaluated the use of several stationary–mobile phase combinations in order to obtain the desired separation. From Table I it can be concluded that TFA–ACN in combination with a Nucleosil C₄ column was able to separate all six components (Fig. 3). The two C₁₈ columns showed irreversible binding of insulin and proinsulin with this mobile phase (as previously described in ref. 20) and were thus unsuitable. Neither of the two C₁₈ stationary phases eluted with TEAP–ACN was able to separate all the components, whereas one of these columns gave a baseline separation of all six components when AS–ACN was used as the mobile phase (Fig. 2).

By comparison of the separation patterns shown in Figs. 2 and 3, it can be concluded that the selectivities of the two stationary–mobile phase combinations were very different, resulting in altered elution orders of the proinsulin and proinsulin intermediates. A change in selectivity was also observed using the same stationary phase (LiChrosorb RP-18) with AS–ACN at different pH values. At pH 4.0 all components were baseline separated, whereas the two split-proinsulins were found to co-elute and des(64,65)HPI eluted later than proinsulin at pH 3.0 (data not shown).

Further differences from the elution orders shown in Figs. 2 and 3 were found when an Ultrasphere C₁₈ column was eluted with 100 mM phosphoric acid–12 mM triethylamine–50 mM sodium perchlorate (pH 3.0) in shallow acetonitrile gradients during 100 min [15] and when a LiChrosorb RP-18 column was eluted with 50 mM phosphoric acid–100 mM sodium perchlorate–10 mM heptanesulphonic acid (pH 3.0) in a shallow acetonitrile gradient [3]. These results clearly show the versatility of RP-HPLC and the need for careful optimization of both the stationary and mobile phases.

The insulin and proinsulin ELISA determinations in the fractions collected from the separation of a mixture of insulin, proinsulin and proinsulin intermediates using the preferred RP-HPLC system, Nucleosil–TFA–ACN, were comparable to the UV trace as shown in Fig. 4 (the UV trace in Fig. 3 was obtained with a different batch of Nucleosil stationary phase, showing that batch-to-batch variations might occur).

The system was subsequently used to measure the content of insulin and PIM in serum from controls and NIDDM patients. Representative examples are shown in Figs. 5 and 6. Compared with a control (Fig. 5, upper curve), the NIDDM serum (Fig. 5, lower curve) showed a higher proportion of PIM (the minor peaks eluted around fractions 60–80) relative to insulin immunoreactive material. The PIM was shown to be heterogeneous (Fig. 6) in both categories, consisting of intact proinsulin and des-proinsulin intermediates. Their identities were deduced by comparison with the retention times of insulin, HPI and the four intermediates, as analysed before and after the actual serum sample.

Proinsulin in human serum has previously been reported to be heterogeneous [16–19], although intact proinsulin infused intravenously in diabetic subjects reveals less than 1% proteolytic degradation and when infused subcutaneously revealed 4–11% processing [15], the main product being des(31,32)HPI. The primarily detected proinsulin intermediate in human serum is reported to be the split(32–33)HPI [10,19,21]. This does not necessarily conflict with our finding of the des-HPI forms in serum, as the immunological methods do not distinguish between the split- and des-

forms. The RP-HPLC analyses of the individual split-HPI standards showed no transformation to the corresponding des-HPI forms during chromatography (data not shown). Further investigations on this aspect are in progress.

The recovery of insulin and proinsulin after RP-HPLC was found to be quantitative. As radiolabelled proinsulin intermediates were not available, their recoveries could not be determined as such; however, as their hydrophobicities and molecular weights are very similar to those of proinsulin, their recoveries would be expected to be similar. The recovery in the immunoaffinity purification step has yet to be evaluated.

In conclusion, we have developed two rapid (60 min) RP-HPLC methods for the baseline separation of insulin, proinsulin and the four major proinsulin intermediates. One of the methods (with Nucleosil-TFA-ACN) will be used for future evaluations of the insulin and PIM composition in serum from different patient categories in order to obtain information on possible changes in β -cell function.

ACKNOWLEDGEMENTS

We thank Ingelise Fabrin, Marianne Munck and Susanne Kjellberg for excellent technical assistance.

REFERENCES

- 1 W. Kemmler, J. D. Peterson and D. F. Steiner, *J. Biol. Chem.*, 246 (1974) 6786.
- 2 H. W. Davidson, C. J. Rhodes and J. C. Hutton, *Nature (London)*, 333 (1988) 93.
- 3 H. W. Davidson and J. C. Hutton, *Biochem. J.*, 245 (1987) 575.
- 4 P. Gordon, C. M. Hendricks and J. Roth, *Diabetologia*, 10 (1974) 469.
- 5 J. Ludvigsson and L. G. Heding, *Acta Diabet. Lat.*, 19 (1982) 351.
- 6 S. G. Hartling, F. Lindgren, G. Dahlquist, B. Persson and C. Binder, *Diabetes*, 38 (1989) 1271.
- 7 D. A. Heaton, B. A. Millward, P. Gray, Y. Tun, C. N. Hales, D. A. Pyke and R. D. G. Leslie, *Biochem. Med. J.*, 294 (1987) 145.
- 8 M. E. Mako, J. I. Starr and A. H. Rubenstein, *Am. J. Med.*, 33 (1977) 865.
- 9 B. Glaser, G. Leibowich, R. Nesher, S. G. Hartling, C. Binder and E. Cerasi, *Acta Endocrinol. (Copenhagen)*, 118 (1988) 365.
- 10 R. C. Temple, C. A. Carrington, S. D. Luzio, D. R. Owens, A. E. Schneider, W. J. Sobey and C. N. Hales, *Lancet*, i (1989) 293.
- 11 M. E. Røder, H. Cheng, S. G. Hartling, C. Binder, H. Worsaa and B. Dinesen, to be published.
- 12 S. G. Hartling, B. Dinesen, A.-M. Kappelgård, O. K. Faber and C. Binder, *Clin. Chim. Acta*, 156 (1986) 289.
- 13 S. Linde and B. S. Welinder, *J. Chromatogr.*, 548 (1991) 195.
- 14 B. S. Welinder, H. H. Sørensen and B. Hansen, *J. Chromatogr.*, 361 (1986) 357.
- 15 B. D. Given, R. M. Cohen, S. E. Shoelson, B. H. Frank, A. H. Rubenstein and H. S. Tager, *J. Clin. Invest.*, 76 (1985) 1398.
- 16 R. M. Cohen, B. D. Given, J. Licinio-Paixao, S. A. Provow, P. A. Rue, B. H. Frank, M. A. Root, K. S. Polonsky, H. S. Tager and A. H. Rubenstein, *Metabolism*, 35 (1986) 1137.
- 17 P. Gray, K. Siddle, B. H. Frank and C. N. Hales, *Diabetes*, 36 (1987) 684.
- 18 T. R. Zilker, S. J. Rainbow, C. N. Hales, S. von Saldern and I. P. Gray, *Horm. Metab. Res.*, 18 (1988) 48.
- 19 W. J. Sobey, S. F. Beer, C. A. Carrington, P. M. S. Clark, B. H. Frank, P. Gray, S. D. Luzio, D. R. Owens, A. E. Schneider, K. Siddle, R. C. Temple and C. N. Hales, *Biochem. J.*, 260 (1989) 535.
- 20 S. Linde and B. S. Welinder, *J. Chromatogr.*, 536 (1991) 43.
- 21 D. K. Nagi, T. J. Hendra, A. J. Ryle, T. M. Cooper, R. C. Temple, P. M. S. Clark, A. E. Schneider, C. N. Hales and J. S. Yudkin, *Diabetologia*, 33 (1990) 532.

CHROMSYMP. 2207

Structure–stability relationship of Immobiline chemicals for isoelectric focusing as monitored by capillary zone electrophoresis

MARCELLA CHIARI and CLAUDIA ETTORI

Chair of Biochemistry and Department of Biomedical Sciences and Technologies, University of Milan, Via Celoria 2, Milan 20133 (Italy)

ADA MANZOCCHI

Dipartimento di Chimica e Biochimica Medica, Università di Milano, Via Saldini 50, Milan 20133 (Italy)
and

PIER GIORGIO RIGHETTI*

Chairs of Biochemistry and Department of Biomedical Sciences and Technologies, University of Milan, Via Celoria 2, Milan 20133 (Italy)

ABSTRACT

An acrylamido buffer for isoelectric focusing in immobilized pH gradients, 1-acryloyl-4-methylpiperazine ($pK = 6.85$ at 25°C), was synthesized. As it is a disubstituted amide, it was thought that it would be much more resistant to alkaline hydrolysis. In reality, it degraded rapidly in 0.1 M sodium hydroxide solution at 70°C (86% in 6 h). Therefore, the stability of Immobiline buffers of pK 9.3, 8.5, 7.0 and 6.2 was investigated. Under the same hydrolysis conditions, the degradation was 11%, 22%, 26% and 34%, in order of decreasing pK values. The kinetics of degradation were monitored by capillary zone electrophoresis in 0.1 M borate buffer ($\text{pH } 9$). The decrease of the main Immobiline peak and the appearance of its hydrolytic products, acrylic acid and a diamine, could be easily measured. The following general rules were derived: when the nitrogen engaged in the amido bond is inserted into a cyclic structure (e.g., 1-acryloyl-4-methylpiperazine) there is very little protection against hydrolysis; and conversely, when this nitrogen carries flexible, fairly long substituents (4–5 atoms long) much stronger shielding and protection of the amido bond can be obtained. These findings helped in designing new acrylamido derivatives strongly resistant to chemical degradation.

INTRODUCTION

Isoelectric focusing (IEF) in immobilized pH gradients (IPGs) represents perhaps the most powerful development in electrokinetic separations, with an unrivalled resolving power and a very high load ability in preparative runs [1]. The power and precision of IPG rely on the quality of the buffers used to generate and maintain the pH gradient in the electric field. Unlike conventional IEF, where the pH gradient is obtained by electrophoretic sorting of a large number of soluble amphoteric buffers, called carrier ampholytes [2], the IPG technique uses a set of a few, well defined chemicals available commercially as crystalline powders or liquids. We have recently

decoded the structures and given the formulae of acidic [3] and basic [4] Immobiline chemicals. In addition, we have proposed over the years a number of additional compounds for expanding the fractionation ability of IPGs: both more acidic [5,6] and more alkaline [7] compounds have been produced in our laboratory. We have also synthesized analogues of the weakest Immobiline bases (the morpholine derivatives, with pK values of 6.2 and 7.0): by introducing a thiomorpholino ring, the pK values of these compounds were increased to 6.6 and 7.4, respectively, thus offering additional species buffering around neutrality, *i.e.*, in a region which normally lacks suitable buffering groups and where the bulk water conductivity reaches a minimum [8]. A new hydrophilic Immobiline with a pK of 8.05 has also been synthesized recently, in order to close the gap in the pH 7.0–8.5 region [9]. Hence, the family of acrylamide buffers is expanding: we have now described fourteen monoprotic compounds and there is a report on a biprotic species, itaconic acid [10]. Nevertheless, we have continued the search for new chemicals, especially for compounds buffering around neutrality, so as to increase the versatility and flexibility of the IPG technique.

We report here the synthesis of a new weakly basic acrylamide buffer, 1-acryloyl-4-methylpiperazine (AMPip), with $pK = 6.85$ (at 25°C). This compound was chosen because it has a disubstituted amido group, in the hope that it would show a high stability against alkaline hydrolysis. These expectations, although in line with current chemical understanding, proved to be fallacious: AMPip turned out to be the most unstable of all alkaline Immobiline chemicals synthesized so far. In an attempt to understand this phenomenon, we reinvestigated the hydrolysis kinetics of the most common Immobiline species available, *i.e.*, those with $pK = 9.3, 8.5, 7.0$ and 6.2. The results contributed to the understanding of the mechanism of their degradation and to the formulation of future, highly stable chemicals.

EXPERIMENTAL

Commercial Immobilines, Repel- and Bind-silane, Gel Bond PAG, the Multiphor II chamber, Multitemp thermostat, the Macrodrive power supply and Pharmalyte carrier ampholytes (pH 7–9) were purchased from Pharmacia–LKB Biotechnology (Bromma, Sweden). Non-commercial acrylamido weak acids and bases were synthesized as reported [5–9]. Acrylamide, N,N' -methylenebisacrylamide (Bis), TEMED, ammonium persulphate and Coomassie Brilliant Blue were obtained from Bio-Rad Labs. (Richmond, CA, USA). 1-Acryloyl-4-methylpiperazine (AMPip) and acryloylmorpholine (AMorph) were a gift from Dr. M. C. Tanzi (Institute of Organic Chemistry, School of Engineering, Milan, Italy). Acrylic acid was from Fluka and was distilled just prior to use. AMPip was synthesized and purified as described [11]; the synthesis of AMorph has been reported by Artoni *et al.* [12]. Horse heart myoglobin was purchased from Sigma (St. Louis, MO, USA) and haemoglobin mutants were a gift from Dr. A. Mosca (University of Milan, Milan, Italy). Mandelic acid, used as an internal standard in capillary zone electrophoresis (CZE) runs, was purchased from Aldrich (Steinheim, Germany).

Alkaline hydrolysis

All acrylamide derivatives and Immobiline buffers were dissolved (10 mM each) in 0.1 M sodium hydroxide solution and incubated at 70°C, under a nitrogen atmo-

sphere, for up to 6 h. At hourly intervals aliquots were collected and diluted in 0.1 *M* borate buffer (pH 9.0) to 2.5 mM. Mandelic acid (2.50 mM) was then added, followed by CZE analysis.

Capillary zone electrophoresis

CZE was performed in a Beckman (Palo Alto, CA, USA) instrument (P/ACE System 2000) equipped with a 50 cm × 75 μm I.D. capillary. All runs were performed at 25°C in a thermostated environment in 0.1 *M* borate (pH 9.0). In all instances the migration direction was toward the negative electrode, which means that the acidic species (acrylic and mandelic acid) are transported there by electroosmosis, as they migrate electrophoretically toward the positive electrode. The sample was injected in the capillary by pressure, usually for 10 s. The calibration graph for each acrylamido derivative analysed was constructed with the Beckman Gold integration system, with the concentration points 0.25, 0.50, 1.00, 1.25, 2.00, 2.50 and 3.50 mM. In each run mandelic acid (2.50 mM) was used as an internal standard.

Thin-layer chromatography (TLC)

TLC was performed on silica gel 60F₂₅₄ plates from Merck using chloroform-methanol (7:3, v/v) as eluent. The spots were revealed either with 3.5% molybdophosphoric acid in ethanol or with ninhydrin. The reaction products formed during alkaline hydrolysis were analysed every 2 h and after prior extraction in chloroform.

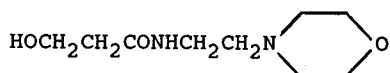
Column chromatography

As all monosubstituted acrylamide buffers revealed, after hydrolysis, in addition to two major components (acrylic acid and diamine) a small, unidentified peak, preparative purification of this unknown compound was attempted. A 1-g amount of p*K* 6.2 Immobiline (2-morpholinoethylacrylamide, as a representative compound) was hydrolysed at 70°C for 6 h and then extracted with chloroform. The 400 mg recovered were purified on a silica gel column (Merck 60, 230–400 mesh) with a ratio 1:80 (w/w) of product to silica gel [elution system chloroform-methanol-water (15:10:2, v/v/v)]. A 40-mg amount of the unknown product (see spot 3 in Fig. 3) was recovered and analysed by NMR and IR spectrometry.

NMR spectrometry

The unknown degradation product of the p*K* 6.2 Immobiline (see spot 3 in Fig. 3) was purified and subjected to NMR spectrometry. NMR analyses were carried out for solutions in [²H]chloroform, C²HCl₃ using tetramethylsilane (TMS) as internal standard, with a Model AM-500 (at 500 MHz, for ¹H) and an AC-200 (at 50.3 MHz, for ¹³C) NMR spectrometer (Bruker, Rheinstetter, Germany). The ¹H and ¹³C NMR spectra lacked signals for olefinic function. The presence of the CONH function was shown in an IR spectrum (a band at 1670 cm⁻¹), in an ¹³C NMR spectrum (δ 170 ppm for CO) and in a ¹H spectrum, due to the presence of a quartet at δ = 3.345 ppm; the value of δ was as expected for a methylene group linked to an amide function (in the diamine precursor the corresponding signal was at δ = 2.7 ppm). After exchange of mobile NH hydrogen with deuterium oxide, the signal was transformed to a triplet (J = 6.4 Hz, due to the vicinal coupling with a CH₂). The ¹H NMR spectrum (with exclusion of 2 mobile hydrogens) showed only three groups of

signals: the first at δ 3.75–3.65 ppm (6H), the second at 3.345 (2H) and a third at 2.5–2.42 ppm (8H). A two-dimensional ^1H homonuclear shift correlation experiment (COSY) showed that the CH_2NHCO signal at $\delta = 3.345$ ppm is coupled with a signal in the third group (centred at 2.48 ppm) and that the two parts of the first group of signals (centred at 3.73 and 3.68 ppm) are coupled with signals in the third group (centred at 2.48 ppm). These findings suggest the following structure, due to a nucleophilic addition of water to the conjugated double bond of the acrylamide moiety:



The first group ($\delta = 3.75\text{--}3.65$ ppm) is due to the primary alcoholic methylene and the morpholino $\text{CH}_2\text{--O--CH}_2$ groups, whereas the third group is due to the three methylenes of the tertiary amine function and to the CH_2CO group.

Isoelectric focusing in immobilized pH gradients

IEF in IPGs was performed in a T4%, C4% polyacrylamide gel^a in the pH range 6.5–8.5. The recipe for this IPG interval, utilizing the commercially available Immobilines, was as given by Gianazza *et al.* [13], whereas the corresponding recipe for the same pH interval utilizing the new acrylamide buffer (pK 6.85) instead of the pK 7.0 Immobiline was as follows (in μl of 0.2 M Immobiline solutions per 15 ml of gel):

pH 6.5	pK	pH 8.5
380 μl	3.6	94 μl
138 μl	6.2	76 μl
92 μl	6.85	139 μl
269 μl	8.5	181 μl

The gel, after polymerization, washing and drying [1], was reswollen in 0.5% Pharmalyte (pH 6–8). Protein samples (20 μg each) were applied at the anodic gel side. The run was for 2 h at 400 V, followed by 4 h at 2000 V, 10°C. The gels were stained with Coomassie Brilliant Blue R-250 in Cu^{2+}

Synthesis of 1-acryloyl-4-methylpiperazine (AMPip)

AMPip was synthesized according to Barbucci *et al.* [11], modified as follows: 5 g (0.05 mol, 5.5 ml) of N-methylpiperazine were dissolved in anhydrous toluene and added dropwise to an acryloyl chloride solution (5.6 mol, 0.07 M) in 40 ml of the same solvent, at 0°C. A white precipitate was recovered by filtration. After suspending the precipitate in chloroform, 6.8 g (0.05 mol) of K_2CO_3 were added with stirring for 20 min. After eliminating precipitated salts by filtration and solvent evaporation, 2.0 g of product were recovered. This material was purified on a silica gel column (1:30 ratio of product to silica) and eluted with chloroform–methanol (9:1, v/v). The yield of purified product was 30% (1.5 g).

^a C = g Bis/%T; T = g acrylamide + g Bis per 100 ml of solution.

Potentiometric titration

The new acrylamide buffer (AMPip) was titrated manually under nitrogen at 25°C. A 10-ml volume of a 10 mM AMPip solution was titrated with 10 ml of 10 mM hydrochloric acid. The pK value was independently assessed also by measuring the pH of a 2:1 molar solution of AMPip-titrant, which, by definition, should correspond to its pK value. The pK value was found to vary as a function of temperature as follows: 25, 20, 15 and 10°C, pK = 6.85, 6.88, 6.90 and 6.93, respectively.

RESULTS

Fig. 1 shows the titration curve for the synthesized weakly basic acrylamide buffer: it has a pK of 6.85 at 25°C, which is very close to that of the commercial Immobiline of pK 7.0 (3-morpholinopropylacrylamide). When this new compound was substituted, in an IPG pH 6.5–8.5 interval, for the pK 7.0 species, the two gels exhibited essentially identical protein patterns (Fig. 2), indicating that the two weakly basic acrylamide buffers are interchangeable. The reason why we synthesized this new compound, however, was in the hope of obtaining a highly stable derivative, resistant to alkaline hydrolysis, as AMPip is a disubstituted amide. It is well known that hydrolytic stability increases in the order acrylamide < methacrylamide < N-substituted acrylamide < N-substituted methacrylamide < N,N-disubstituted acrylamide [14]. In addition, we had previously reported the hydrolysis kinetics of alkaline Immobiline buffers and found them to be unstable [15] (they are all monosubstituted amides). Much to our surprise, however, when we performed some preliminary hydrolysis experiments, we found that AMPip degraded rapidly.

We therefore decided to study the degradation kinetics of all alkaline Immobiline buffers (pK 9.3, N,N-dimethylaminopropylacrylamide; pK 8.5, N,N-dimethylaminoethylacrylamide; pK 7.0, 3-morpholinopropylacrylamide; and pK 6.2, 2-morpholinoethylacrylamide) and of a neutral monomer (4-acryloylmorpholine), in the hope of elucidating the mechanism of their proneness or resistance to hydrolysis.

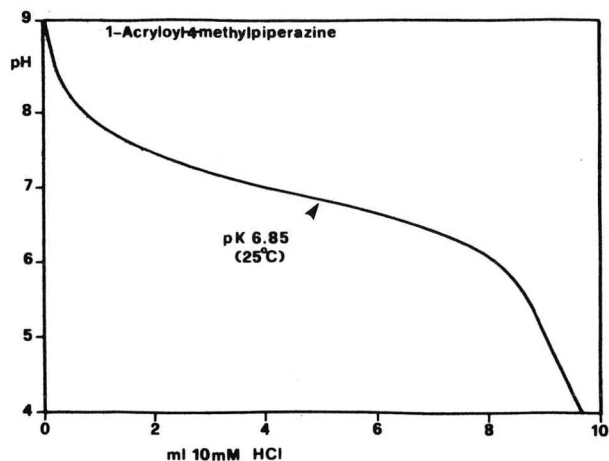


Fig. 1. Titration curve of 1-acryloyl-4-methylpiperazine. A 10-ml aliquot of a 10 mM solution of AMPip was titrated with 10 ml of 10 mM HCl at 25°C under a nitrogen atmosphere. The pK value was determined to be 6.85.

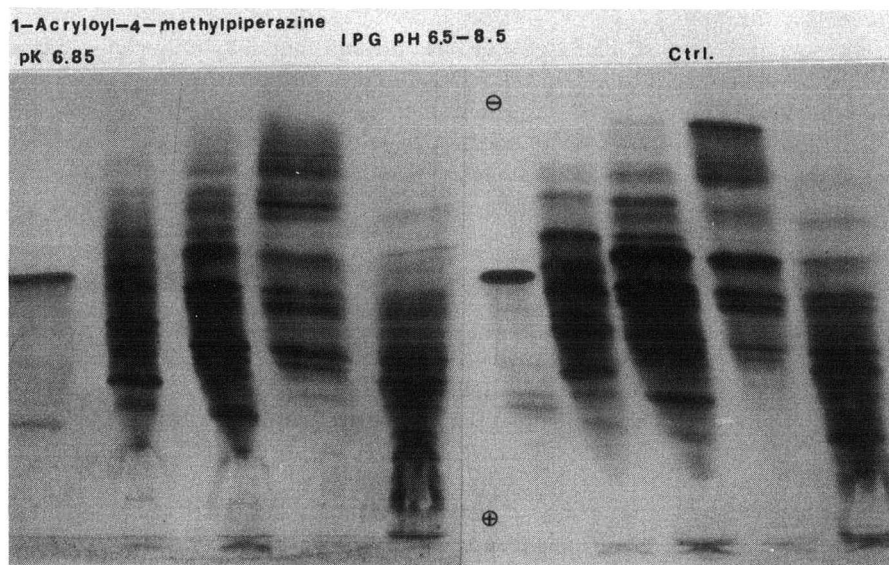


Fig. 2. Analytical IEF gel in the IPG pH 6.5–8.5 interval. The gel was a T4%, C4% polyacrylamide matrix, reswollen in 0.5% Pharmalyte (pH 6–8). Left, formulation containing the pK 6.85 chemical; right, recipe with the pK 7.0 Immobiline buffer (control, Ctrl.). Samples: 1 = horse myoglobin; 2 = haemoglobin A/S; 3 = hemoglobin A/lepore; 4 = hemoglobin A/C; 5 = hemoglobin A/S Paris. All samples loaded in a 20- μ g amount at the anodic gel side. Run: 2 h at 400 V followed by 4 h at 2000 V. Stain: Coomassie Brilliant Blue R-250 in Cu^{2+} .

As an example of what happens to these chemicals on alkaline attack, Fig. 3 shows the TLC pattern of the pK 6.2 Immobiline before and after extended hydrolysis. The two main hydrolytic products are spots 1 (the diamine) and 2 (acrylic acid), *i.e.*, the two precursors used to synthesize the acrylamide derivative. There was a third, unidentified spot (No. 3), which we purified on a preparative scale and subjected to NMR analysis. The results of structural investigation suggested this to be the pK 6.2 species non-hydrolysed, but with a molecule of water added to the double bond (see Discussion). This latter compound represents a small percentage of the total hydrolytic products, so this degradation pathway is decidedly a minor one. All of the acrylamido buffers analysed showed the formation of the same type of degradation products.

CZE was instrumental in assessing the identity of the hydrolytic products and quantifying them. Fig. 4 shows a representative CZE run of (A) a control and (B) an extensively hydrolysed sample of 4-acryloylmorpholine, a neutral acrylamide monomer possessing a disubstituted amido group. It is seen that no acrylic acid is present in the control; at the end of the 6-h hydrolysis period, the monomer peak has greatly diminished and a large peak of acrylic acid has appeared. In all runs, mandelic acid (2.5 mM) was added to each sample as an internal standard for quantification purposes. The CZE pattern is representative of all the runs performed with all the chemicals investigated. After analysing all samples in CZE, we could construct curves representing the degradation kinetics of each species.

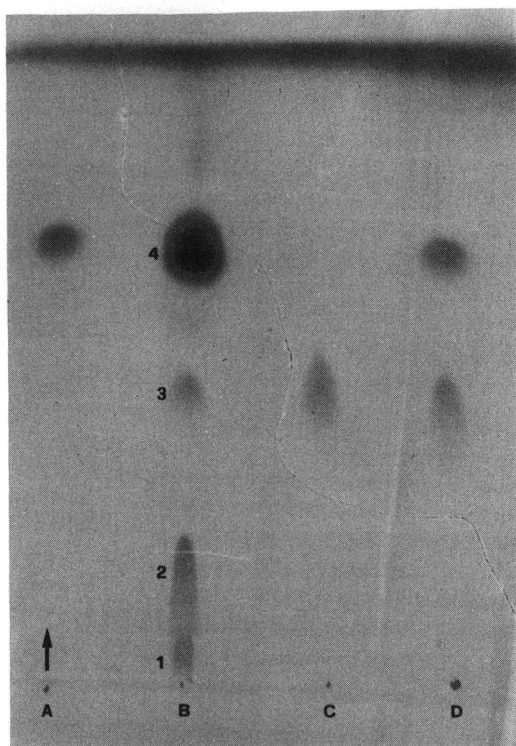


Fig. 3. TLC of the pK 6.2 Immobiline before and after degradation. TLC was performed on silica gel 60F₂₅₄ plates using chloroform-methanol (7:3, v/v) as eluent. Samples (from left to right): A = control, undegraded pK 6.2; B = pK 6.2 after 6-h hydrolysis (at 70°C in 0.1 M NaOH); C and D = purified spot No. 3 (in two different degrees of purification). Spots: 1 = diamine; 2 = acrylic acid; 3 = unidentified product; 4 = undegraded pK 6.2 Immobiline. The vertical arrow indicates the migration direction of the eluent.

Fig. 5 shows the destruction rate of two such species, the neutral monomer 4-acryloylmorpholine and the charged species 1-acryloyl-4-methylpiperazine. Even though they both contain a disubstituted amide, they were found to degrade extensively (86%). Conversely, when the pK 9.3 and 8.5 Immobilines were subjected to the same hydrolysis conditions (70°C, 0.1 M NaOH, up to 6 h), much reduced degradation rates were observed (Fig. 6): only 11% for the pK 9.3 Immobiline and 22% for the pK 8.5 Immobiline. The last two compounds investigated, the pK 7.0 and 6.2 Immobilines (both containing a morpholino ring at different distances from the amide bond), were found to have intermediate degradation kinetics with degradations of 26% and 34%, respectively (Fig. 7).

The data on the degradation kinetics of all the species investigated (five charged and one neutral monomer) are shown in the bar graph in Fig. 8, expressed as a percentage of undegraded compound remaining at the end of a 6-h hydrolysis time. It is interesting that the four commercial Immobilines have degradation kinetics inversely proportional to the pK value.

DISCUSSION

We have previously performed an extensive investigation on the stability of the Immobiline buffers used for IEF in IPGs [15], and reported that indeed the alkaline species would degrade rapidly as a function of pH and temperature. On hydrolysis, free acrylic acid is produced, which is incorporated into the polyacrylamide gel instead of the original basic compound, resulting in totally offset pH gradients. The situation became so problematic that an Immobiline II generation was proposed [16], by which the alkaline Immobilines were stabilized by dissolving them in *n*-propanol, while the acidic species were prepared as 0.2 M solutions in water containing traces of inhibitor. Simultaneously, we found other degradation pathways, namely autopolymerization on storage to oligomers and *n*-mers [17] and oxidation during the polymerization process by persulphate to produce N-oxides [18]. All of these problems, connected with the alkaline Immobiline buffers, spurred us to search for suitable acrylamido weak bases, resistant to hydrolysis. Disubstituted amides were deemed to be suitable compounds, as it is amply documented [14] that such compounds are stable, probably because the two substituents on the nitrogen engaged in the amido bond sterically protect the latter against reactants approaching the plane of the

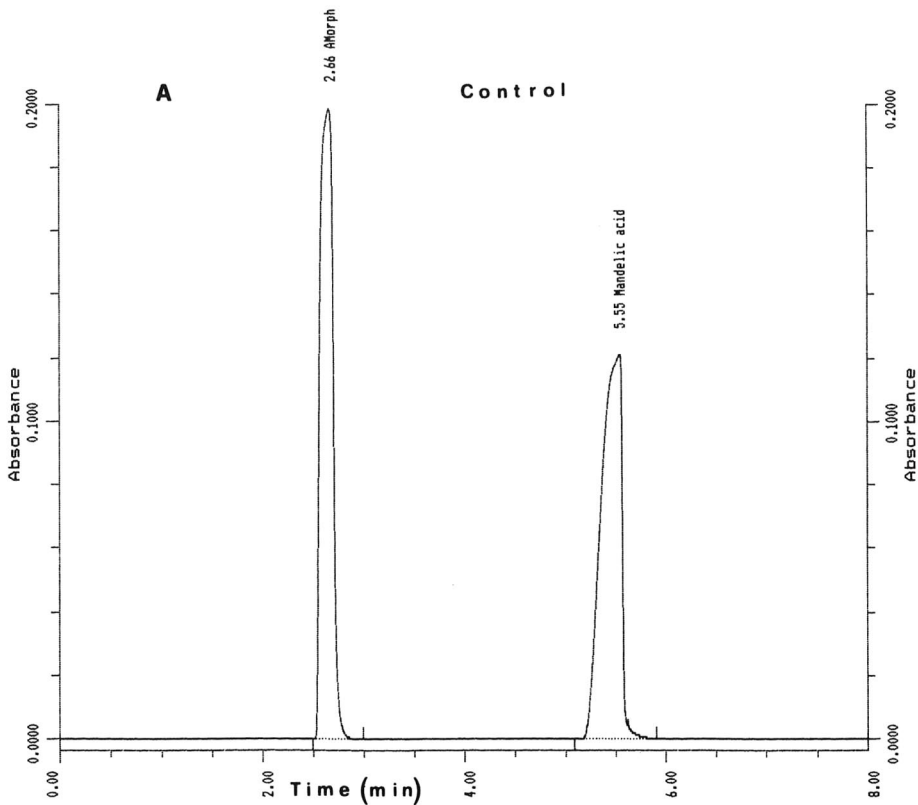


Fig. 4.

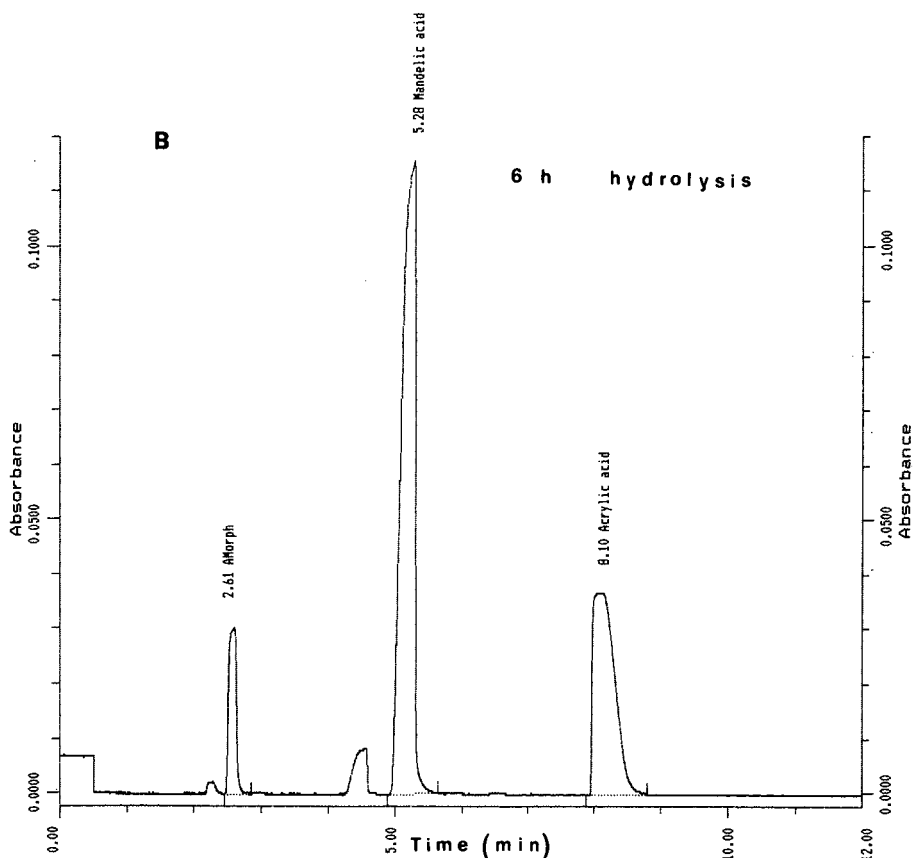


Fig. 4. Representative CZE run for analysis of Immobiline hydrolytic products. CZE run in a Beckmann P/ACE 2000 with a 50 cm \times 75 μ m I.D. capillary. Run at 15 kV, 25°C in 0.1 M borate buffer (pH 9). All migrations toward the cathode. Detection at 214 nm. Mandelic acid (2.5 mM) was used in all runs as an internal standard. (A) Control; (B) after 6 h of hydrolysis. Sample injected: 4-acryloylmorpholine.

amide. As it turned out from our data, the only two disubstituted amides we had available (AMorph and AMPip) were, on the contrary, extensively degraded, in fact almost completely destroyed in a 6-h period at 70°C in 0.1 M NaOH. Conversely, all other acrylamide buffers (with pK values of 9.3, 8.5, 7.0 and 6.2) showed only moderate to medium degradation, even though they are all monosubstituted amides.

While we agree with the general knowledge on the stability of disubstituted amides, it is clear from our results that there are other, more subtle mechanisms governing such stability. On the basis of our data, and of the known structures of the acrylamide derivatives, we derived the following rules:

(a) to afford protection of the amide bond, the most important parameter is not the degree of substitution in the nitrogen engaged in the amido plane (primary secondary or tertiary) but the type of substituent;

(b) in particular, rigid ring structures (as in AMorph and AMPip) are complete-

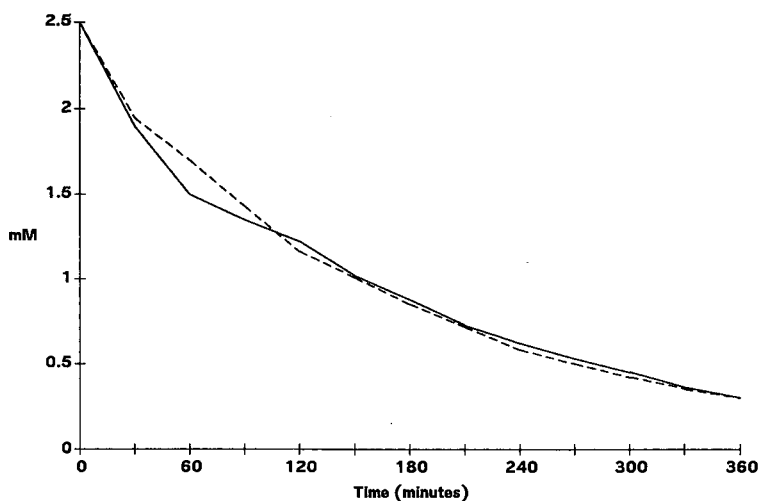


Fig. 5. Degradation kinetics of 4-acryloylmorpholine (----) and of 1-acryloyl-4-methylpiperazine (—). The quantitative data were obtained from analytical CZE runs as exemplified in Fig. 4. All integrations done with the Beckman Gold system. Note that here the molarity scale goes from 0 to 2.5 mM; note also the almost complete destruction of the two chemicals under the hydrolysis conditions (70°C, 0.1 M NaOH).

ly inefficient in protecting the adjacent amide bond, as their rigidity prevents them from oscillating in the surrounding space and thus shielding the amido plane;

(c) flexible chains bound to the nitrogen of the amido bond are efficient in protecting the amido plane, as they can oscillate in the surrounding space and shield the amido group;

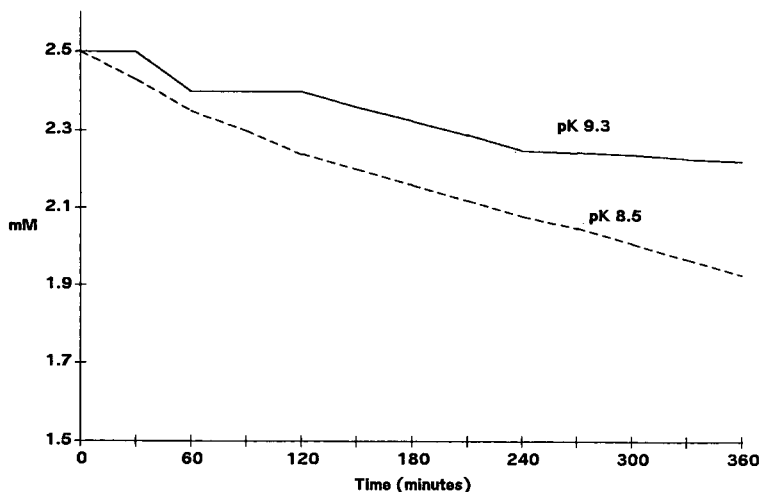


Fig. 6. Degradation kinetics of the pK 9.3 and 8.5 Immobilines. The quantitative data were obtained from analytical CZE runs as exemplified in Fig. 4. All integrations were done with the Beckman Gold system. Note that here the molarity scale goes from 1.5 to 2.5 mM (as opposed to 0 to 2.5 mM in Fig. 5); note also the very modest destruction of these two chemicals under the hydrolysis conditions used (70°C, 0.1 M NaOH).

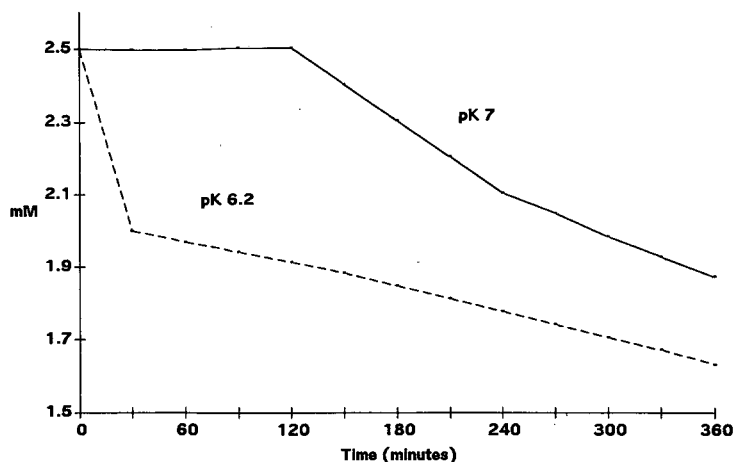


Fig. 7. Degradation kinetics of the pK 7.0 and 6.2 Immobilines. The quantitative data were obtained from analytical CZE runs as exemplified in Fig. 4. All integrations were done with the Beckman Gold system. Note that here the molarity scale goes from 1.5 to 2.5 mM (as opposed to 0 to 2.5 mM in Fig. 5); note also the more extensive destruction of these two chemicals under the hydrolysis conditions used (70°C, 0.1 M NaOH) compared with those of Fig. 6.

(d) if rigid structures are present in the nitrogen substituents, they should be removed from the plane of the amido bond: this is why the pK 7.0 Immobiline (3-morpholinopropylacrylamide) degrades substantially less than the pK 6.2 (2-morpholinoethylacrylamide);

(e) if a simple, flexible chain is present as a substituent on the nitrogen of the amido bond, greater protection of the latter is afforded by a longer chain; this is why the pK 9.3 Immobiline (N,N-dimethylaminoethylacrylamide) is more resistant than the pK 8.5 (N,N-dimethylaminoethylacrylamide) derivative.

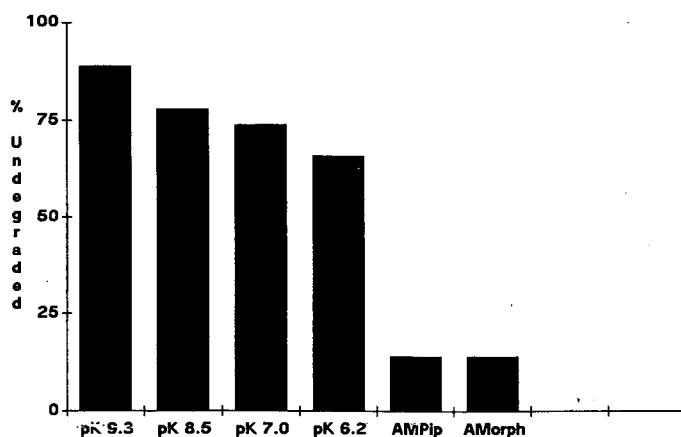


Fig. 8. Summary of the degradation kinetics of the five acrylamido bases and the neutral monomer studied. The vertical bars represent the amount of undegraded product remaining after 6 h of hydrolysis at 70°C in 0.1 M NaOH. AMorph = 4-acryloylmorpholine; AMPIP = 1-acryloyl-4-methylpiperazine.

These general findings have helped us in designing a general strategy for the synthesis of new monomers that are extremely resistant to chemical attack (their synthesis will be reported elsewhere). Another finding of great interest is the unknown reaction product found in all acrylamido derivatives tested (and exemplified in Fig. 3, spot 3, in the case of the pK 6.2 derivative). After preparative purification and NMR analysis, it was found to be the product derived from the addition of water to the acrylic double bond. Given the relatively mild hydrolysis conditions (6 h at 70°C in 0.1 M NaOH) this was unexpected. However, on a literature search, we were able to locate a few examples of such reaction (nucleophilic attack of water on the carbon-carbon double bond); *e.g.*, one way of preparing β -hydroxypropionic acid is by the action of alkali on acrylic acid [19]. Although the extent of conversion is minute, it opens up new perspectives in the chemistry of acrylamide, certainly the most popular monomer in the field of biochemical separations.

ACKNOWLEDGEMENTS

This work was supported in part by grants from Progetto Finalizzato Chimica Fine II, CNR (Rome) and by the Ministero della Pubblica Istruzione. We are greatly indebted to Drs. R. Montini and S. Di Biase of Beckman Italia for the kind loan of the instrument and for their advice on CZE.

REFERENCES

- 1 P. G. Righetti, *Immobilized pH Gradients: Theory and Methodology*, Elsevier, Amsterdam, 1990.
- 2 P. G. Righetti, *Isoelectric Focusing: Theory, Methodology and Applications*, Elsevier, Amsterdam, 1983.
- 3 M. Chiari, E. Casale, E. Santaniello and P. G. Righetti, *Appl. Theor. Electrophoresis*, 1 (1989) 99–102.
- 4 M. Chiari, E. Casale, E. Santaniello and P. G. Righetti, *Appl. Theor. Electrophoresis*, 1 (1989) 103–107.
- 5 E. Gianazza, F. Celentano, G. Dossi, B. Bjellqvist and P. G. Righetti, *Electrophoresis*, 5 (1984) 88–97.
- 6 P. G. Righetti, M. Chiari, P. K. Sinha and E. Santaniello, *J. Biochem. Biophys. Methods*, 16 (1988) 185–192.
- 7 C. Gelfi, M. L. Bossi, B. Bjellqvist and P. G. Righetti, *J. Biochem. Biophys. Methods*, 15 (1987) 41–48.
- 8 M. Chiari, P. G. Righetti, P. Ferraboschi, T. Jain and R. Shorr, *Electrophoresis*, 11 (1990) 617–620.
- 9 M. Chiari, L. Pagani, P. G. Righetti, T. Jain, R. Shorr and T. Rabilloud, *J. Biochem. Biophys. Methods*, 21 (1990) 165–172.
- 10 R. Charlionet, R. Sesboué and C. Davrinche, *Electrophoresis* 5 (1984) 176–178.
- 11 R. Barbucci, M. Casolaro, P. Ferruti, M. C. Tanzi, L. Grassi and C. Barozzi, *Makromol. Chem.*, 185 (1984) 1525–1533.
- 12 G. Artoni, E. Gianazza, M. Zaroni, C. Gelfi, M. C. Tanzi, C. Barozzi, P. Ferruti and P. G. Righetti, *Anal. Biochem.*, 137 (1984) 420–428.
- 13 E. Gianazza, F. Celentano, G. Dossi, B. Bjellqvist and P. G. Righetti, *Electrophoresis*, 5 (1984) 88–97.
- 14 V. Kudela, in H. F. Mark, N. M. Bikales, C. G. Overberger and G. Menges (Editors), *Encyclopedia of Polymer Science and Engineering*, Wiley-Interscience, New York, 1987, pp. 783–807.
- 15 P. G. Pietta, E. Pocaterra, A. Fiorino, E. Gianazza and P. G. Righetti, *Electrophoresis*, 6 (1985) 419–422.
- 16 B. M. Gäveby, P. Petterson, J. Andrasko, L. Ineva-Flygare, U. Johannesson, A. Görg, W. Postel, A. Domscheit, P. L. Mauri, P. Pietta, E. Gianazza and P. G. Righetti, *J. Biochem. Biophys. Methods*, 16 (1988) 141–164.
- 17 T. Rabilloud, C. Gelfi, M. L. Bossi and P. G. Righetti, *Electrophoresis*, 8 (1987) 305–312.
- 18 P. G. Righetti, M. Chiari, E. Casale and C. Chiesa, *Appl. Theor. Electrophoresis*, 1 (1989) 115–121.
- 19 S. Patai and Z. Rappoport, in S. Patai (Editor), *The Chemistry of Alkenes*, Wiley-Interscience, New York, 1964, Ch. 8, pp. 469–584.

CHROMSYMP. 2140

Effects of temperature, carrier composition and sample load in asymmetrical flow field-flow fractionation

ANNE LITZÉN^a

Department of Analytical Pharmaceutical Chemistry, University of Uppsala Biomedical Center, P.O. Box 574, S-751 23 Uppsala (Sweden)

and

KARL-GUSTAV WAHLUND*

Department of Technical Analytical Chemistry, Chemical Center, University of Lund, P.O. Box 124, S-221 00 Lund (Sweden)

ABSTRACT

The use of asymmetrical flow field-flow fractionation for accurate sample characterization requires good control of side effects which can adversely influence sample retention. Some of these factors are identified and means to avoid or minimize them are given. The behaviour of a model protein and virus was investigated. Bad reproducibility of the retention times and peak deformations were traced to incomplete temperature control and adsorption to the accumulation wall membrane. Good thermostatic control gave constant retention times because it eliminated temperature variations caused by friction heat produced in the carrier stream. Rinsing of the channel removed adsorbed species. The mechanism involved in the adsorption is unknown but the pH of the carrier liquid appears to have an influence. Exceeding the sample load limit leads to a complex behaviour of peak deformations. This behaviour as well as the load limit is governed by the choice of buffer and ionic strength of the carrier liquid.

INTRODUCTION

Field-flow fractionation (FFF) is a family of fractionation techniques designed for macromolecular and particle separation and characterization [1]. The common characteristic for all of the FFF sub-techniques is the parabolic flow profile which is created by a carrier liquid being pumped through the open, thin flat channels. Retention is effected by a field applied perpendicular across the channel. A number of different fields such as sedimentation, thermal gradient, electrical and crossflow can be used [2].

Asymmetrical flow FFF is a variant of FFF utilizing a crossflow field [3]. The crossflow is created as the carrier liquid, that is pumped through the channel, exits through the porous accumulation wall as well as through the channel outlet. The

^a Present address: Department of Technical Analytical Chemistry, Chemical Center, University of Lund, P.O. Box 124, S-221 00 Lund, Sweden.

accumulation wall is made up of an ultrafiltration membrane making it possible for the carrier liquid to permeate the wall while the sample molecules are retained. The separations obtained are basically size fractionations since they depend on differences in the diffusion coefficients.

Previous papers [4–6] have reported on improvements in the asymmetrical flow FFF technique leading to faster and more efficient separations. The improvements include a downstream central injection technique, thinner channels and a new trapezoidal channel geometry.

While the construction and design of channels has advanced there is still very limited knowledge of the behaviour of samples under varying conditions for the elution. An accurate characterization of a sample, *e.g.*, by its diffusion coefficient, or after transformation, by its molecular weight or its distribution, requires that sample retention conforms to retention theory in a predictable way under all conditions used.

Experience gained during the development of the method has indicated a number of potential error sources such as variations in the retention time and band broadening during an extended sequence of repeated fractionations. The objective of the present paper is therefore to describe these problems, identify their origin and possibly find means to avoid or minimize them. Careful studies revealed that the problems mentioned often originate in unsuitable experimental conditions which therefore should be corrected. Without such knowledge attempts to run flow FFF may result in failures.

The factors studied are temperature effects, adsorption to the accumulation wall membrane, the reproducibility of measured diffusion coefficients and the influence of the carrier liquid composition on sample loadability. Some general guidelines for the optimization of the system will also be given.

Since the diffusion coefficient directly governs the retention time it must be important to perform separations under constant temperature. This is necessary in order to keep the diffusion coefficients constant so as to obtain good accuracy and reproducibility in sample retention and characterization. An increase in temperature will increase the diffusion coefficient. Repeated sample fractionations performed with no thermostatic control will be shown to cause gradually decreasing retention times. This effect will be traced to an increasing channel temperature originating in frictional heat produced within the system. Good thermostatic control of the equipment is therefore necessary, at least when using high flow-rates.

One property of the FFF techniques that is often brought forward as an advantage is the non-existence of a stationary phase. It has been assumed that difficulties such as surface interactions often associated with the stationary phase in chromatography may therefore be avoided in FFF. There are, however, numerous opportunities for the solutes to interact with the channel walls, particularly the accumulation wall, and this has to be considered. This is becoming increasingly important as the channel thickness is reduced in order to shorten elution times and to improve efficiency. Such conditions will drive the solutes into more concentrated layers and closer to the accumulation wall. Thus the possibilities of undesired interactions with the wall, and also within the concentrated solute zone, are enhanced. Extended use of a channel will be shown to affect the retention time and peak symmetry, presumably by adsorption. A rinsing procedure is suggested.

Problems associated with sample mass overloading of FFF channels is one of the

major drawbacks of the FFF techniques. The effects have been shown to vary with sample components and carrier liquid composition. In sedimentation FFF colloidal particles in solutions of ionic strength $10^{-3} M$ or lower have been reported to be eluted earlier than predicted with a tailing peak shape [7]. For polymers in organic solvents the opposite effect has been reported, *i.e.*, the overloaded peaks were fronting, emerging from the channel later than predicted [8]. In asymmetrical flow FFF a buffer of ionic strength $0.1 M$ resulted in plasmids and plasmid fragments being eluted with a fronting peak symmetry or with completely distorted peaks when the channel was overloaded [4]. At the same ionic strength water-soluble polymers were observed to emerge later than predicted when the load limit was exceeded [5]. All of the above-mentioned effects were observed in this study, *i.e.*, sample overloading can lead to either retained symmetry, fronting or tailing of the peaks accompanied by increased zone broadening, and increased or decreased retention times.

THEORY

The theory has been described in detail elsewhere [3,6] and only the more important equations will be defined below.

The retention ratio, R , is calculated from the ratio of the void time, t_0 , to the retention time, t_R , or from the ratio of the sample zone velocity, V , to the channel flow velocity, $\langle v \rangle$ [3]

$$R = \frac{t_0}{t_R} = \frac{V}{\langle v \rangle} \quad (1)$$

The void time is calculated from [6]

$$t_0 = \frac{V^0}{\dot{V}_c} \ln \left[1 + \frac{\dot{V}_c}{\dot{V}_{out}} \left(1 - \frac{w\{b_0 z' - [(b_0 - b_L)/2L]z'^2 - y\}}{V^0} \right) \right] \quad (2)$$

where V^0 is the void volume, \dot{V}_c is the crossflow-rate, \dot{V}_{out} is the channel outlet flow-rate, z' is the distance from the inlet to the focusing point, and L is the channel length. b_0 and b_L are the breadths of the channel at the inlet and outlet, respectively, when the tapered ends are not considered, and y is the area cut off by the tapered inlet end (see Fig. 1). The void time equation is valid for $z' \geq z''$ where z'' is the length of the tapered end.

The retention ratio can be expressed in terms of the transversal distribution of the sample zone, *i.e.*, by λ , which is a dimensionless measure of the distance of a sample zone from the accumulation wall. λ is defined by the ratio l/w where l is the average distance of the zone from the wall and w is the channel thickness. The retention ratio is a complex function of λ [3] and a calculation of λ from experimental retention ratios requires numerical integration. However, at high retention levels the retention equation can be approximated by [3]

$$R \approx 6 \lambda \quad (3)$$

and it is a simple matter to calculate λ from R values. The diffusion coefficient, D , of a sample can be calculated from the λ value

$$D = \frac{\lambda \dot{V}_c w^2}{V^0} \quad (4)$$

Alternatively, of course, if the flow conditions and the diffusion coefficient are known, the retention time can be predicted from

$$t_R = \frac{t_0 \dot{V}_c w^2}{6 D V^0} \quad (5)$$

The diffusion coefficient for a spherical particle with radius r can be calculated from Stokes' equation:

$$D = \frac{k T}{6 \pi \eta r} \quad (6)$$

where k is the Boltzmann constant, T the temperature and η the viscosity coefficient.

EXPERIMENTAL

Two different channels were used. The design was basically the same as described previously [3–6]. However, one of the channels was modified to allow for thermostatic control.

The channels differ only in the material and design of the upper wall. In one it was a glass plate and in the other it was made of Lucite. Both walls had a length of 36 cm and a breadth of 6 cm. The thickness was 1 cm for the glass wall and 2 cm for the Lucite wall. The latter was equipped with an internal channel to permit the passage of thermostated water. During operation thermostated water was continuously pumped through the wall to help control the temperature of the channel. In both walls PTFE tubing for the carrier inlet and outlet flows were positioned 28.5 cm apart. The injection inlet was positioned 2.0 cm downstream from the carrier flow inlet. The channel with the glass wall was only used for the initial studies documenting the temperature changes occurring and is referred to as the "non-thermostated channel". In all other studies the thermostated channel with the Lucite wall was used.

The ultrafiltration membrane was a cellulosic DDS membrane type RC70PP with a nominal cut-off of 10 000 dalton (De danske suckerfabrikker DDS RO-division, Nakskov, Denmark).

A PTFE spacer (fluorinated ethylene propylene, FEP) of thickness 0.013 cm was used to define the channel thickness. The channel geometry was trapezoidal (Fig. 1). The length was 28.5 cm, the breadth at the inlet, b_0 , was 2.12 cm, and the breadth at the outlet, b_L , was 0.47 cm. The length of the tapered end at the inlet was 2.0 cm and at the outlet 0.5 cm. The area, y , cut off at the inlet, was 2.12 cm². The geometrical void volume of the channel was 0.45 ml.

Two pumps were used. A Beckman 114 M solvent delivery system (Beckman

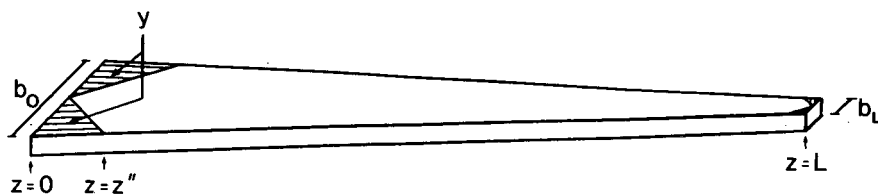


Fig. 1. Geometry of the trapezoidal channel.

Instruments, Berkeley, CA, USA) delivered the carrier flow, and the injection flow was delivered by an LKB 2150 HPLC pump (Pharmacia LKB Biotechnology, Bromma, Sweden). An LDC SpectroMonitor III spectrophotometric detector (LDC, Riviera Beach, FL, USA) set at 280 nm was used for the detection. A Rheodyne 9125 syringe injector (Cotati, CA, USA) was used with a sample loop of 20 μl . The system was designed according to a previous procedure [5] and the same valves were used. One additional three-way valve was inserted between the pressure gauge valve and the inlet. This valve was used during the backwards flushing and the rinsing procedures.

Temperature control was conducted by a Haake type F water-bath (Haake, Berlin, Germany). The water was pumped through a mantled carrier reservoir and the upper wall. The temperature was kept at 24.0°C. For the temperature study the entire channel was placed in a thermostated water bath (Heto, Birkeröd, Denmark).

Ferritin was obtained from a gel filtration calibration kit (Pharmacia, Uppsala, Sweden). Human serum albumin (HSA) Fraction V was from Sigma (St. Louis, MO, USA). The Cow Pea Mosaic Virus (CPMV) was a generous gift from Dr. P. Oxelfeldt at the Agricultural University (Uppsala, Sweden).

The retention times were measured from the peak apices and the void times were determined from eqn. 2. Calculations of the λ values from the retention ratios were made on a personal computer by numerical integration using Simpson's rule. To measure the asymmetry factor (asf) at 10% of the peak height, a perpendicular was drawn from the apex. The back part of the peak divided by the front part of the peak, both measured at 10% of the peak height, gives the asf.

The operation of the system followed previous procedures [3,5,6]. The relaxation/focusing procedure was carried out for 45 s using a pump flow-rate of 3 ml/min. The focusing point, z' , was adjusted to 2.5 cm. Sample injection was made with a flow-rate of 0.1 ml/min for 30 s. The sample loop had a volume of 20 μl .

Channel rinsing between runs was effected by flushing backwards for 1–2 min. During the back flush the three-way valve at the inlet was switched to direct the liquid from the channel to waste. A more thorough cleaning of the membrane was obtained if the channel was filled with air before the back flush. In this case air was introduced into the channel from a Luer syringe attached to the additional three-way valve at the channel inlet. At the same time the channel outlet tubing was disconnected from the detector. The channel was then flushed with carrier liquid using the same Luer syringe. A very high flow-rate was obtained and this easily removed the air from the channel. This was done after fractionation of highly retained materials.

RESULTS AND DISCUSSION

The retention characteristics of the proteins albumin and ferritin, and the spherical virus CPMV were studied under different experimental conditions in a number of different carriers (Table I). The molecular weights of albumin, ferritin and CPMV are 67 000, 440 000 and $5.5 \cdot 10^6$, respectively. The isoelectric point for albumin is 4.7–4.9 [9], for ferritin 4.1–4.6 and for CPMV 3.7–4.5 [10].

Temperature effects

According to Stokes' equation the diffusivity of molecules will depend upon the temperature in two ways (eqn. 6). One is due to the increase in kinetic energy (kT) along with an increase in temperature. This effect is of relatively small magnitude for modest temperature changes. The other, and more important in this case, is due to the decrease in the viscosity of water which occurs at increasing temperatures. Calculations based on the known viscosity of pure water [11] show that an increase of the temperature by 1°C will increase the diffusion coefficient by almost 3% at the temperature levels used in this study. It is thus clear that good temperature control is mandatory in order to obtain consistent and reproducible retention data.

A good temperature control is even more important in the present apparatus when it is used for rapid separations requiring high flow-rates. Somewhat surprisingly it was found that in a non-thermostated channel having an upper glass wall the temperature increased by several tenths of a degree centigrade as soon as the relaxation flow was turned on. This was measured by a thermometer in contact with the glass wall and positioned next to the outlet tubing in the bore drilled through the upper Lucite block. The bore contained some water which improved the contact between the tip of the thermometer and the glass wall. During a day of operation a continuously increasing channel temperature was observed. Thus repeated fractionations of a sample led to shorter and shorter retention times caused by the increasing diffusion coefficients of the sample molecules. The temperature increase was apparently caused by frictional heat produced in the tubing.

Manipulation of the temperature can be made to an advantage. An increase in temperature will increase the diffusion coefficient. For ultra-high-molecular-weight materials, which, due the low levels of their diffusion coefficients, tend to give high zone broadening, a temperature increase may help in obtaining more efficient separations.

TABLE I
LIST OF CARRIER LIQUIDS USED FOR THE FRACTIONATIONS

Carrier liquid	pH	Ionic strength (M)
(I) 0.02% NaN_3	6.9	0.003
(II) 0.02% NaN_3 , Tris- HNO_3 buffer	7.5	0.008
(III) 0.02% NaN_3 , Tris- HNO_3 buffer, 1 mM glutamic acid	6.3	0.009
(IV) 0.02% NaN_3 , Tris- HNO_3 buffer	7.5	0.1
(V) 0.02% NaN_3 , 0.1 M NaCl	6.5	0.1
(VI) 0.02% NaN_3 , citrate buffer	4.8	0.008

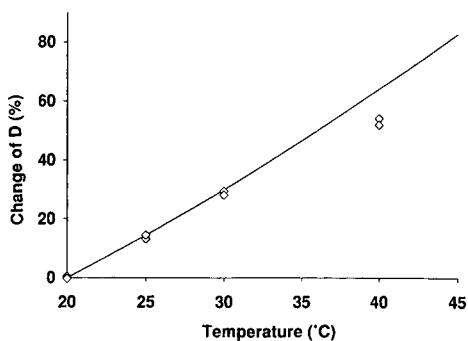


Fig. 2. Percentage increase of the diffusion coefficient, D , relative to D at 20°C. — = Prediction according to eqn. 6; \diamond = experimental determination. Sample: CPMV, 0.7 μg in 20 μl . Elution: $\dot{V}_{\text{in}} = 5.9$ ml/min, $\dot{V}_c = 5.50\text{--}5.90$ ml/min, $\dot{V}_{\text{out}} = 1.00\text{--}1.40$ ml/min, where \dot{V}_{in} is the channel inlet flow-rate. Carrier II.

A test of the effect of temperature on the experimentally determined diffusion coefficient of the virus CPMV was done in the temperature range 20–40°C. The relative increase in the diffusion coefficient was compared to that predicted by Stokes' equation, assuming that the viscosity of the carrier liquid varies with temperature as in pure water. During this study the channel was kept in thermostatically controlled water bath, since it is not sufficient to thermostat only the upper wall when working at elevated temperatures.

Fig. 2 shows that in the temperature interval from 20 to 30°C the increase in the experimentally determined diffusion coefficient agrees well with that predicted by Stokes' equation. The diffusion coefficient at 40°C was, however, somewhat lower than expected. In this case the temperature of the water bath was at 40°C but the temperature measured on the upper wall by the outlet tubing was only 37°C. Therefore the temperature within the channel was probably somewhere between 37 and 40°C, which might explain part of the deviation.

Membrane effects

Practical experience shows that the retention times gradually increase and the peak efficiencies decrease, followed by tailing, when the channel is used without any rinsing procedures. So far this applies to all channels that have been tested, and to all of the carrier liquids in Table I. In order to study this effect the virus CPMV was injected repeatedly at conditions of very high retention without using the rinsing procedure between each run. At very high retentions the relative concentration by the accumulation wall is high and thus the possibility of interactions with the wall is enhanced. Fig. 3 shows that the retention times increases, as expressed by the decrease in the observed diffusion coefficient, at the same time as the peak efficiency decreases for each consecutive sample injection. After using the rinsing procedure, *i.e.*, the channel is first flushed with air and then with the carrier liquid, the performance of the first injection could be reproduced (Fig. 3). The peak efficiency was expressed by the plate number defined in the usual way according to

$$N = \frac{t_R^2}{\tau^2} \quad (7)$$

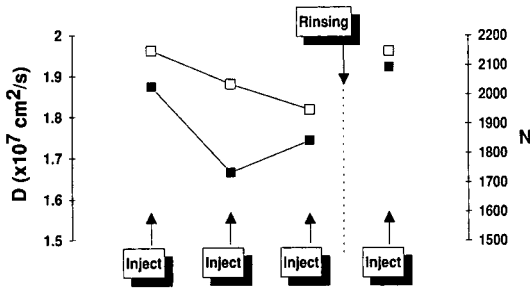


Fig. 3. Influence of channel rinsing on high retention fractionations. Sample: CPMV, $0.35 \mu\text{g}$ in $20 \mu\text{l}$. Elution: $\dot{V}_{\text{in}} = 9.0 \text{ ml/min}$, $\dot{V}_{\text{c}} = 7.80\text{--}8.00 \text{ ml/min}$, $\dot{V}_{\text{out}} = 1.10\text{--}1.40 \text{ ml/min}$, $t_0 = 0.11 \text{ min}$, $R = 0.02$. Carrier IV. After the third injection the rinsing procedure was applied. \square = Observed diffusion coefficient (D); \blacksquare = efficiency (N).

where τ is the standard deviation of the peak in time units. Fig. 4 shows a CPMV peak obtained after the channel had been subjected to the rinsing procedure. The peak is symmetrical with no indication of tailing.

A simpler rinsing procedure, involving only a backwards flushing with the carrier liquid while the crossflow was shut off, did not give complete recovery of channel performance. Apparently the introduction of air in the channel is vital in order to obtain complete rinsing. Observations during the rinsing procedure revealed that after the air was pumped into the channel, so that the latter is emptied from carrier liquid, the carrier liquid penetrates the membrane from below and re-enters the channel when the excess pressure disappears. This may suggest that a backwards flushing of the membrane by reversing the crossflow could help in rinsing the membrane. Such a procedure was, however, impossible to perform because it displaced the membrane from the support causing it to contact the upper wall so that the flow was interrupted. It may well be possible that the introduction of air is the key step in

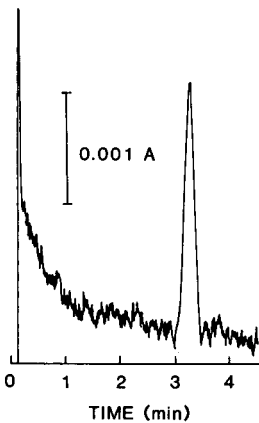


Fig. 4. Elution of CPMV. Load $0.28 \mu\text{g}$ in $20 \mu\text{l}$. Relaxation/focusing: $\dot{V}'_{\text{c}} = 3 \text{ ml/min}$ for 30 s and 7 ml/min for 15 s. Elution: $\dot{V}_{\text{c}} = 7.60 \text{ ml/min}$, $\dot{V}_{\text{out}} = 2.18 \text{ ml/min}$, $t_0 = 0.085 \text{ min}$. Carrier IV.

recovering the membrane properties, perhaps by somehow changing the interaction between the solute and the membrane.

There are several possible causes for the peak distortion and excess retardation found in all carrier liquids when the channel is not rinsed regularly. First, the sample can be physically entrapped in the pores. This may potentially lead to increased flow resistance across the membrane. This is, however, contradicted by the fact that there are indications that the permeability of the membrane is increased by the presence of a sample in the channel. During a series of sample injections, without intermediate washing, the ratio \dot{V}_c/\dot{V}_{out} continuously increases. Because the flow-rates \dot{V}_c and \dot{V}_{out} are controlled by the ratio of the restriction to flow in each flow-line [3] this effect can be interpreted as being due to an increased permeability of the membrane leading to an increase of \dot{V}_c at the cost of \dot{V}_{out} . Second, higher-molecular-weight compounds of unknown origin may be left in the channel, interacting with the samples in the next injection. This is, however, unlikely because then it should be sufficient to flush the channel while the crossflow is shut off. The last statement suggests rather that the need

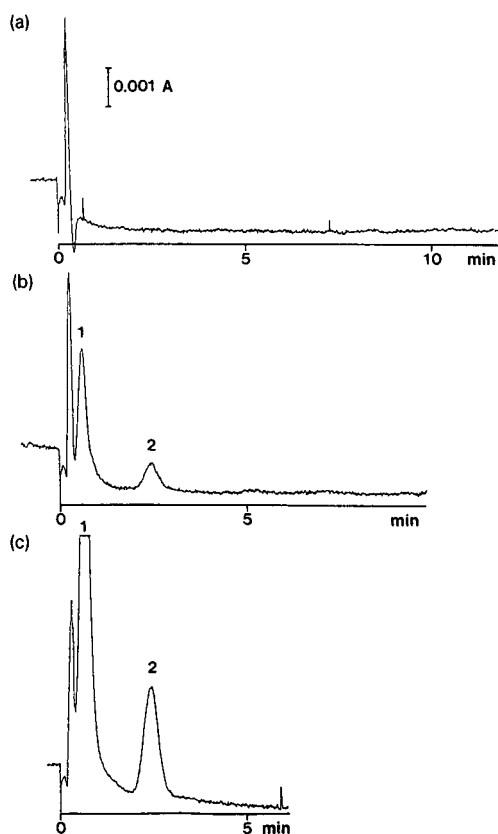


Fig. 5. Behaviour of CPMV and albumin in the citric acid buffer. (a) Sample: CPMV, 0.35 μg in 20 μl . (b) Sample: HSA, 5 μg in 20 μl . Peaks: 1 = HSA; 2 = CPMV. (c) Sample: HSA, 10 μg and CPMV, 0.7 μg in 20 μl . Peaks: 1 = HSA; 2 = CPMV. Elution: $\dot{V}_c = 4.7$ ml/min, $\dot{V}_{out} = 1.2$ ml/min, $t_0 = 0.23$ min. Carrier VI.

for the channel to be rinsed is caused by adsorption of solute to the accumulation wall membrane, and this third cause is indeed the more likely one. Adsorption may also explain the increase in membrane permeability discussed above. It may be a result of a change of a property such as the wettability of the membrane. Nevertheless, the washing procedure, which is easy to manage, eliminates most of the above-mentioned problems.

The suspicion that some solutes adsorb to the membrane was further confirmed when the behaviour of CPMV, ferritin and albumin was studied in a carrier liquid buffered by citric acid to a pH of 4.8 (carrier VI, Table I). In this carrier the performance of all three compounds changed for the worse as compared to the other carriers. The protein peaks were tailing also at loads well below the loads that gave symmetrical peaks in the other carriers. The virus sample did not elute at all, it remained within the channel during the entire elution, which was maintained for 11 min (Fig. 5a). After this sample albumin (HSA) was injected. This run not only gave an albumin peak, but also caused elution of the CPMV which had remained in the channel from the previous injection (Fig. 5b). The CPMV peak was symmetrical and was eluted at the retention time predicted from the results in the other carrier liquids. The narrow peak and the retention time indicate that the virus must have been retained at the focusing point. If it were distributed along a large portion of the channel one would have expected a broader peak eluted earlier. The introduction of albumin obviously released CPMV, apparently from the membrane. This was further confirmed by injection of CPMV in a mixture with albumin. The result was two peaks, both at the expected retention times for albumin and CPMV, respectively (Fig. 5c). Once albumin had been present in the channel a subsequent injection of CPMV caused a peak at the expected retention time for CPMV, although a further injection of albumin released yet more CPMV along with the elution of albumin.

The results from the citric acid buffer pH 4.8 may be caused by adsorption to the membrane. The pH of the buffer was close to the isoelectric points of the samples and several authors (*cf.*, refs. 12 and 13) have reported on an enhanced adsorptivity of proteins at pH values around their isoelectric point on several different materials. A similar situation may exist in the flow FFF channel. The elution of CPMV in the presence of albumin indicates that some kind of competitive adsorption takes place between these two samples.

Influence of ionic strength on sample loadability

Fig. 6a and b show the observed diffusion coefficients, calculated from the retention time measured at the peak maximum, as a function of the sample load of CPMV and ferritin, respectively. The data were obtained using carrier liquids differing in their component types and ionic strengths according to Table I. Even if only a limited range of composition types were tested it appears that the ionic strength has a strong influence on the retention behaviour. Carriers II and IV, containing identical component types but having different ionic strengths, result in opposing effects on the observed diffusion coefficient at increasing sample loads. At a low ionic strength, 0.008 *M* (carrier II), an increase in sample load causes an increase of the diffusion coefficient, *i.e.*, a decrease in the retention time. At high ionic strength, 0.1 *M* (carrier IV), the opposite result is obtained. The same tendencies are observed for ferritin and CPMV.

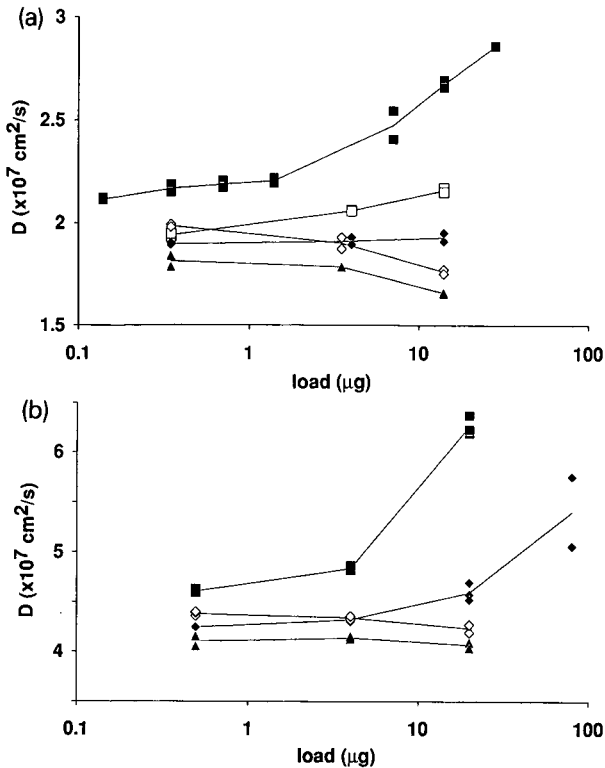


Fig. 6. Effects of sample load on observed diffusion coefficients, D , in different carriers. Carriers (see Table I): ■ = I; □ = II; ◆ = III; ◇ = IV; ▲ = V. (a) Sample: CPMV, 0.14–0.28 μg in 20 μl . Elution: $\dot{V}_{\text{in}} = 6.4 \text{ ml/min}$, $\dot{V}_{\text{c}} = 5.00\text{--}5.70 \text{ ml/min}$, $\dot{V}_{\text{out}} = 0.70\text{--}1.50 \text{ ml/min}$. (b) Sample: ferritin, 0.5–80 μg in 20 μl . Elution: $\dot{V}_{\text{in}} = 9.1 \text{ ml/min}$, $\dot{V}_{\text{c}} = 7.40\text{--}8.20 \text{ ml/min}$, $\dot{V}_{\text{out}} = 0.90\text{--}1.60 \text{ ml/min}$.

The change in retention time with increasing sample load is accompanied by a change in peak symmetry. This is demonstrated in Fig. 7a and b where the peak asymmetry factors, measured at 10% of the peak height, are given. Again, as with the data in Fig. 6, the ionic strength appears as an important factor. At low ionic strength increased sample loads causes peak tailing ($\text{asf} > 1$). On the contrary, at high ionic strength large sample loads cause fronting ($\text{asf} < 1$) and for the highest loads even a peak distortion. The appearances of the overloaded peaks in carriers II and IV are shown in Fig. 8. In carrier III neither fronting nor tailing was observed. Yet, the loadability was limited because there was a gradual increase in the peak width. This carrier differs from carrier II only by its content of 1 mM glutamic acid. Glutamic acid is known to reduce the adsorption of proteins to glass [14] and was therefore added as an attempt to affect the particle wall interactions.

Other authors [7,8] who have investigated overloading phenomena have reported on one or the other of the two effects discussed above. The origin of the phenomena is in both cases thought to be caused by too high a concentration in the migrating sample zone. In the case of colloidal particles in an aqueous buffer (ionic strength below 10^{-3} M) the overloading was reported to originate in effective

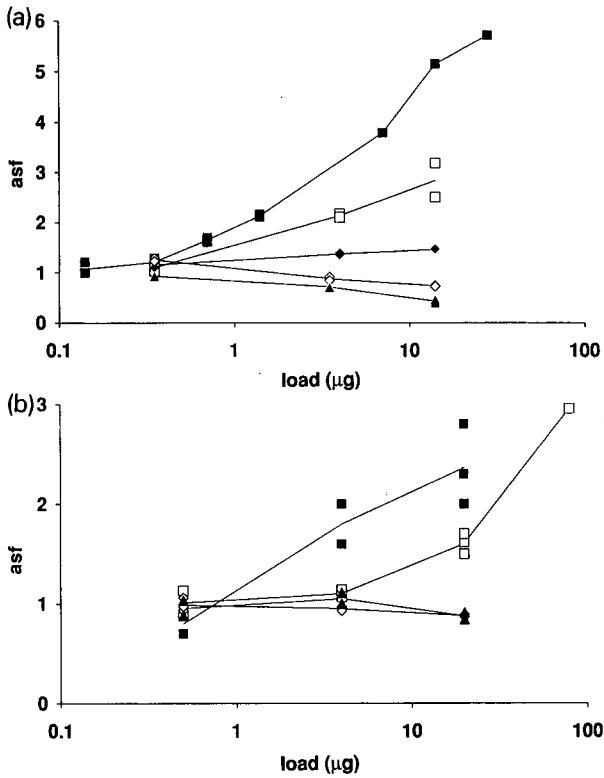


Fig. 7. Effects of sample load on asymmetry factors (asf) in different carriers. (a) Sample: CPMV. (b) Sample: ferritin. Conditions as in Fig. 6.

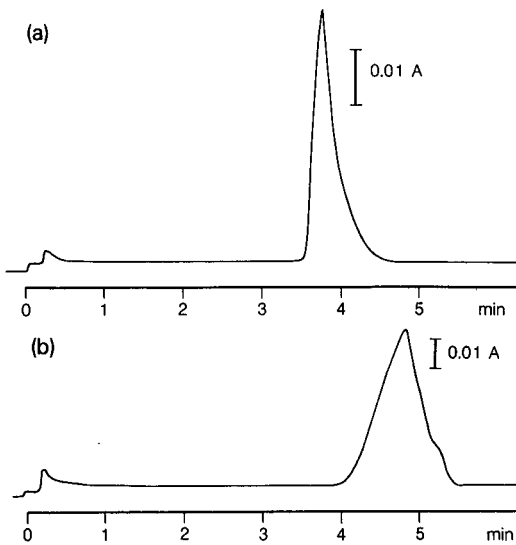


Fig. 8. Appearance of overloaded peaks in different carriers. Sample: CPMV, $14 \mu\text{g}$ in $20 \mu\text{l}$. (a) Carrier II: $\dot{V}_c = 5.36 \text{ ml/min}$, $\dot{V}_{\text{out}} = 1.09 \text{ ml/min}$. (b) Carrier IV: $\dot{V}_c = 5.47 \text{ ml/min}$, $\dot{V}_{\text{out}} = 0.96 \text{ ml/min}$.

repulsion between particles caused by volume exclusion as well as other repulsive effects [7]. This effected the exponential distribution of the particles by the wall causing them to migrate at a larger distance from the accumulation wall than they would at low loads. Therefore the retention time decreased with increasing sample loads [7].

The different behaviour shown by CPMV and ferritin is probably related to the fact that these two samples are polyelectrolytes. This can lead to quite complex solution behaviour as a function of the electrolyte composition of the carrier. Also, a wider range of ionic strengths was studied than in the other reports. Yet in the buffers having the lowest ionic strengths the behaviour was very similar to that previously mentioned [7] and it is reasonable to assume that similar mechanisms are involved. In carrier I the ionic strength was only 0.003 *M* leading to a modest screening of the charged groups. Therefore the intermolecular interaction may be mainly repulsive. This will effect the particle distribution so that the samples migrate further away from the wall. When the ionic strength is increased the screening of the charged groups will increase and the net interaction may instead be attractive, thus explaining the change in behaviour. More studies are necessary to evaluate these effects in detail.

Guidelines for the choice of experimental conditions

It is clear that the choice of experimental conditions such as membrane material, type of carrier and temperature control are vital to obtain efficient, reproducible and accurate data. If fractionations are performed at very high retentions, where the possibilities for interactions between the solutes and the membrane are enhanced, the channel should be flushed with air and carrier liquid between each run. For proteinaceous samples it may be necessary to chose a pH outside the range of the isoelectric point in order to avoid adsorption tendencies.

To avoid conditions where concentration-dependent retention data are obtained it seems recommendable that the sample load be kept below the maximum load (defined as the highest load for which the diffusion coefficient is still constant and the peak shape symmetrical) which is obtained at conditions which give the highest retention level to be used (equal to the highest crossflow-rate to be used). Then, concentration dependencies should not be observed in experiments done at lower retention levels.

The flow-rate for the relaxation-focusing procedure can be chosen rather arbitrarily. Ideally the crossflow-rate during the relaxation should be set to the same value as the crossflow to be used during the elution. This is the prerequisite for the sample zones to form the correct steady-state distributions. It has, however, been found that the performance is not significantly effected even if the crossflow-rate during the relaxation is kept much lower than during the elution. When such a situation exists a secondary relaxation will occur once the elution is started [15]. Since this process is very rapid its contribution to the overall bandbroadening may be negligible.

In Table II results are shown from runs with CPMV using the same flow conditions during the elution but different conditions for the relaxation. The crossflow-rate during the elution was kept at 7.4 ml/min, corresponding to a λ value of 0.004. In case 1 the relaxation crossflow-rate was kept at 3 ml/min for 45 s. Thus the sample zone was subjected to less than half the force field acting upon the particles during the elution. In the second case the flow-rate was increased to 7.4 ml/min for the

TABLE II

INFLUENCE OF RELAXATION CONDITIONS ON THE ELUTION PERFORMANCE

Sample: CPMV, 0.35 μg in 20 μl . Elution: $\dot{V}_c = 7.8\text{--}7.9$ ml/min; $\dot{V}_{\text{out}} = 1.3$ ml/min. Carrier I.

Relaxation crossflow-rate (ml/min)	Duration (s)	Diffusion coefficient (cm^2/s)
3	45	$2.1 \cdot 10^7$
3 + 7.4	30 + 15	$2.1 \cdot 10^7$

last 15 s of the relaxation in order to allow for the molecules to adjust to the field strength that would act upon them during the elution. Even though the particles in the first run were subjected to a secondary relaxation after the initiation of the elution the agreement between the calculated diffusion coefficients was good.

For practical reasons it is preferable to use the same relaxation flows for most of the applications. It is also thought to be an advantage to keep the duration of the relaxation and the relaxation flow-rate as low as possible in order to minimize the opportunity for the sample to interact with the membrane. Experience shows that with the downstream central injection technique a relaxation time of 1 min at a flow-rate of 3 ml/min is usually sufficient to assure a complete relaxation.

ACKNOWLEDGEMENTS

We gratefully acknowledge the Swedish Natural Science Research Council for financial support. We also thank Pharmacia Biotechnology for supporting us with some instrumental parts and the proteins, and Dr. Per Oxelfeldt at the Agricultural University of Uppsala for the gift of CPMV.

REFERENCES

- 1 J. C. Giddings, *Sep. Sci.*, 1 (1966) 123.
- 2 J. C. Giddings, *Sep. Sci. Technol.*, 19 (1984–1985) 831.
- 3 K.-G. Wahlund and J. C. Giddings, *Anal. Chem.*, 59 (1987) 1332.
- 4 A. Litzén and K.-G. Wahlund, *J. Chromatogr.*, 476 (1989) 413.
- 5 K.-G. Wahlund and A. Litzén, *J. Chromatogr.*, 461 (1989) 73.
- 6 A. Litzén and K.-G. Wahlund, *Anal. Chem.*, (1991) in press.
- 7 M. E. Hansen, J. C. Giddings and R. Beckett, *J. Colloid Interface Sci.*, 132 (1989) 300.
- 8 K. D. Caldwell, S. L. Brimhall, Y. Gao and J. C. Giddings, *J. Appl. Polym. Sci.*, 36 (1988) 703.
- 9 E. G. Young, in M. Florkin and E. H. Stotz (Editors), *Comprehensive Biochemistry*, Vol. 7, Elsevier, New York, 1963, p. 25.
- 10 A. van Kammen and C. P. de Jager, *CMI/AAB Description of Plant Viruses*, No. 197, Commonwealth Agricultural Bureaux and the Association of Applied Biologists, Aberystwyth, August, 1978.
- 11 R. C. Weast (Editor), *CRC Handbook of Chemistry and Physics*, CRC Press, Boca Raton, FL, 70th ed., 1989–1990, p. F-40.
- 12 P. van Dulm, W. Norde and J. Lyklema, *J. Colloid Interface Sci.*, 82 (1981) 77.
- 13 T. Suzawa and T. Murakami, *J. Colloid Interface Sci.*, 78 (1980) 266.
- 14 T. Mizutani, *J. Colloid Interface Sci.*, 82 (1981) 162.
- 15 J. C. Giddings, *Anal. Chem.*, 58 (1986) 735.

Author Index

- Abad, C., see Perez-Paya, E. 548(1991)93
Abad, C., see Perez-Paya, E. 548(1991)351
Abouelezz, M., see Dunn, L. 548(1991)165
Aguilar, M. I., see Hearn, M. T. W.
548(1991)117
Aguilar, M. I., see Wilce, M. C. J. 548(1991)105
Antonelli, G., see Giacobbe, S. 548(1991)289
Binder, C., see Linde, S. 548(1991)371
Bloemhoff, W., see Welling, G. W. 548(1991)235
Bolzacchini, E., Di Gennaro, P., Di Gregorio, G.,
Rindone, B., Falagiani, P., Mistrello, G. and
Sondergaard, I.
Purification of *Phleum pratense* pollen
extract by immunoaffinity chromatography
and high-performance ion-exchange
chromatography 548(1991)229
Boppana, V. K., Miller-Stein, C., Politowski, J.
F. and Rhodes, G. R.
High-performance liquid chromatographic
determination of peptides in biological fluids
by automated pre-column fluorescence
derivatization with fluorescamine
548(1991)319
Borin, G., see Calderan, A. 548(1991)329
Boulkanz, L., see Vidal-Madjar, C. 548(1991)81
Braco, L., see Perez-Paya, E. 548(1991)93
Braco, L., see Perez-Paya, E. 548(1991)351
Brew, K., see Colilla, F. J. 548(1991)303
Buck, R. H., Cholewinski, M. and Maxl, F.
Animal test or chromatography?. Validated
high-performance liquid chromatographic
assay as an alternative to the biological
assay for orniopressin 548(1991)335
Calderan, A., Ruzza, P., Marin, O., Secchieri, M.,
Borin, G. and Marchiori, F.
Separation of acidic peptides by reversed-
phase ion-pair chromatography. Analytical
application to a series of acidic substrates of
casein kinases 548(1991)329
Campos, A., see Perez-Paya, E. 548(1991)93
Chaufer, B., Rollin, M. and Sébille, B.
High-performance liquid chromatography
and ultrafiltration of whey proteins with
inorganic porous materials coated with
polyvinylimidazole derivatives 548(1991)215
Chiari, M., Etori, C., Manzocchi, A. and
Righetti, P. G.
Structure-stability relationship of
Immobiline chemicals for isoelectric focusing
as monitored by capillary zone
electrophoresis 548(1991)381
Cholewinski, M., see Buck, R. H. 548(1991)335
Colilla, F. J., Yadav, S. P., Brew, K. and
Mendez, E.
Peptide maps at picomolar levels obtained
by reversed-phase high-performance liquid
chromatography and pre-column
derivatization with phenyl isothiocyanate.
Microsequencing of phenylthiocarbamyl
peptides 548(1991)303
Cummings, L., see Dunn, L. 548(1991)165
Cysewski, P., Jaulmes, A., Lemque, R., Sébille,
B., Vidal-Madjar, C. and Jilge, G.
Multivalent ion-exchange model of
biopolymer chromatography for mass
overload conditions 548(1991)61
Damhof, R. A., see Welling, G. W.
548(1991)235
Danielsson, Å., see Nyberg, F. 548(1991)311
Davankov, V. A., see Kurganov, A. A.
548(1991)207
Di Gennaro, P., see Bolzacchini, E.
548(1991)229
Di Gregorio, G., see Bolzacchini, E.
548(1991)229
Drijfhout, J. W., see Welling, G. W.
548(1991)235
Dufourcq, J., see Perez-Paya, E. 548(1991)351
Dunn, L., Abouelezz, M., Cummings, L.,
Navvab, M., Ordunez, C., Siebert, C. J. and
Talmadge, K. W.
Characterization of synthetic macroporous
ion-exchange resins in low-pressure
cartridges and columns. Evaluation of the
performance of Macro-Prep 50 S resin in the
purification of anti-Klenow antibodies from
goat serum 548(1991)165
Elling, L., see Kula, M.-R. 548(1991)3
Ellouali, M., Khamlichi, S., Jozefonvicz, J. and
Muller, D.
Affinity of trypsin for amidine derivatives
immobilized on dextran-coated silica
supports 548(1991)255
Etori, C., see Chiari, M. 548(1991)381
Falagiani, P., see Bolzacchini, E. 548(1991)229
Fang, F. W., see Hearn, M. T. W. 548(1991)117
Folchitto, G., see Giacobbe, S. 548(1991)289
Giacobbe, S., Miraglia, N., Rindone, B.,
Folchitto, G. and Antonelli, G.
High-performance liquid chromatographic
purification of antiviral components in
Neuramide 548(1991)289

- Hartling, S. G., see Linde, S. 548(1991)371
- Hearn, M. T. W., Hodder, A. N., Fang, F. W. and Aguilar, M. I.
High-performance liquid chromatography of amino acids, peptides and proteins. CXI.
Retention behaviour of proteins with macroporous tentacle-type anion exchangers 548(1991)117
- Hearn, M. T. W., see Johnston, A. 548(1991)127
- Hearn, M. T. W., see Mao, Q. M. 548(1991)147
- Hearn, M. T. W., see Wilce, M. C. J. 548(1991)105
- Hodder, A. N., see Hearn, M. T. W. 548(1991)117
- Hodges, R. S., Lorne Burke, T. W. and Mant, C. T.
Multi-column preparative reversed-phase sample displacement chromatography of peptides 548(1991)267
- Hodges, R. S., see Zhou, N. E. 548(1991)179
- Hodges, R. S., see Zhu, B.-Y. 548(1991)13
- Holgersson, J., see Strömqvist, M. 548(1991)293
- Jaulmes, A., see Cysewski, P. 548(1991)61
- Jaulmes, A., see Vidal-Madjar, C. 548(1991)81
- Jilge, G., see Cysewski, P. 548(1991)61
- Johnston, A., Mao, Q. M. and Hearn, M. T. W.
High-performance liquid chromatography of amino acids, peptides and proteins. CXII.
Analysis of operating parameters affecting the breakthrough curves in fixed-bed chromatography of proteins using several mathematical models 548(1991)127
- Johnston, A., see Mao, Q. M. 548(1991)147
- Jozefonvicz, J., see Ellouali, M. 548(1991)255
- Kalbacher, H. and Kropshofer, H.
Non-radioactive detection of MHC class II-peptide antigen complexes in the sub-picomole range by high-performance size-exclusion chromatography with fluorescence detection 548(1991)343
- Khamlichi, S., see Ellouali, M. 548(1991)255
- Kirkland, J. J., see Zhou, N. E. 548(1991)179
- Kotarski, S. F., see Barsuhn, K. 546(1991)273
- Kropshofer, H., see Kalbacher, H. 548(1991)343
- Kula, M.-R., Eling, L. and Walsdorf, A.
Investigations of liquid-liquid partition chromatography of proteins 548(1991)3
- Kurganov, A. A., Davankov, V. A. and Unger, K. K.
Ion-exchange high-performance liquid chromatography of nucleotides and polypeptides on new types of ion-exchange sorbents, based on polystyrene-coated silicas 548(1991)207
- Lemque, R., see Cysewski, P. 548(1991)61
- Liapis, A. I., see McCoy, M. A. 546(1991)25
- Linde, S., Röder, M. E., Hartling, S. G., Binder, C. and Welinder, B. S.
Separation and quantitation of serum proinsulin and proinsulin intermediates in humans 548(1991)371
- Linde, S. and Welinder, B. S.
Silica *versus* polymer-based stationary phases for reversed-phase high-performance liquid chromatographic analyses of rat insulin biosynthesis. A comparison of resolution and recovery 548(1991)195
- Litzén, A. and Wahlund, K.-G.
Effects of temperature, carrier composition and sample load in asymmetrical flow field-flow fractionation 548(1991)393
- Lorne Burke, T. W., see Hodges, R. S. 548(1991)267
- Lyrenäs, S., see Nyberg, F. 548(1991)311
- Mant, C. T., see Hodges, R. S. 548(1991)267
- Mant, C. T., see Zhou, N. E. 548(1991)179
- Mant, C. T., see Zhu, B.-Y. 548(1991)13
- Manzocchi, A., see Chiari, M. 548(1991)381
- Mao, Q. M., Johnston, A., Prince, I. G. and Hearn, M. T. W.
High-performance liquid chromatography of amino acids, peptides and proteins. CXIII.
Predicting the performance of non-porous particles in affinity chromatography of proteins 548(1991)147
- Mao, Q. M., see Johnston, A. 548(1991)127
- Marchiori, F., see Calderan, A. 548(1991)329
- Marin, O., see Calderan, A. 548(1991)329
- Mauri, P. L., Pietta, P. G. and Pace, M.
Analysis and purification of DNA restriction fragments by high-performance liquid chromatography 548(1991)281
- Maxl, F., see Buck, R. H. 548(1991)335
- McCoy, M. A. and Liapis, A. I.
Evaluation of kinetic models for biospecific adsorption and its implications for finite bath and column performance 548(1991)25
- Mendez, E., see Colilla, F. J. 548(1991)303
- Miller-Stein, C., see Boppana, V. K. 548(1991)319
- Miraglia, N., see Giacobbe, S. 548(1991)289
- Mistrello, G., see Bolzacchini, E. 548(1991)229
- Muller, D., see Ellouali, M. 548(1991)255
- Navvab, M., see Dunn, L. 548(1991)165
- Nyberg, F., Lyrenäs, S. and Danielsson, Å.
Fingerprinting of molecular components in individual human cerebrospinal fluid samples with a new micropurification system 548(1991)311
- Ordunez, C., see Dunn, L. 548(1991)165
- Pace, M., see Mauri, P. L. 548(1991)281

- Perez-Paya, E., Braco, L., Abad, C. and Dufourcq, J.
High-performance liquid chromatographic separation of modified and native melittin following transglutaminase-mediated derivatization with a dansyl fluorescent probe 548(1991)351
- Perez-Paya, E., Braco, L., Abad, C., Soria, V. and Campos, A.
Solution properties of polyelectrolytes. VII. Non-ideal mechanisms in size-exclusion chromatography of synthetic polyions, peptides and proteins 548(1991)93
- Pietta, P. G., see Mauri, P. L. 548(1991)281
- Place, H., see Vidal-Madjar, C. 548(1991)81
- Politowski, J. F., see Boppana, V. K. 548(1991)319
- Prince, I. G., see Mao, Q. M. 548(1991)147
- Rhodes, G. R., see Boppana, V. K. 548(1991)319
- Righetti, P. G., see Chiari, M. 548(1991)381
- Rindone, B., see Bolzacchini, E. 548(1991)229
- Rindone, B., see Giacobbe, S. 548(1991)289
- Røder, M. E., see Linde, S. 548(1991)371
- Rollema, H. S., see Visser, S. 548(1991)361
- Rollin, M., see Chaufer, B. 458(1991)215
- Ruzza, P., see Calderan, A. 548(1991)329
- Samuelsson, B., see Strömqvist, M. 548(1991)293
- Sébille, B., see Chaufer, B. 458(1991)215
- Sébille, B., see Cysewski, P. 548(1991)61
- Secchieri, M., see Calderan, A. 548(1991)329
- Siebert, C. J., see Dunn, L. 548(1991)165
- Slangen, C. J., see Visser, S. 548(1991)361
- Sondergaard, I., see Bolzacchini, E. 548(1991)229
- Soria, V., see Perez-Paya, E. 548(1991)93
- Strömqvist, M., Holgersson, J. and Samuelsson, B.
Glycosylation of extracellular superoxide dismutase studied by high-performance liquid chromatography and mass spectrometry 548(1991)293
- Talmadge, K. W., see Dunn, L. 548(1991)165
- Unger, K. K., see Kurganov, A. A. 548(1991)207
- Van Gorkum, J., see Welling, G. W. 548(1991)235
- Vidal-Madjar, C., Place, H., Boukantz, L. and Jaulmes, A.
Application of the split-peak effect to study the adsorption kinetics of human serum albumin on a reversed-phase support 548(1991)81
- Vidal-Madjar, C., see Cysewski, P. 548(1991)61
- Visser, S., Slangen, C. J. and Rollema, H. S.
Phenotyping of bovine milk proteins by reversed-phase high-performance liquid chromatography 548(1991)361
- Wahlund, K.-G., see Litzén, A. 548(1991)393
- Walsdorf, A., see Kula, M.-R. 548(1991)3
- Welinder, B. S., see Linde, S. 548(1991)195
- Welinder, B. S., see Linde, S. 548(1991)371
- Welling, G. W., Van Gorkum, J., Damhof, R. A., Drijfhout, J. W., Bloemhoff, W. and Welling-Wester, S.
A ten-residue fragment of an antibody (mini-antibody) directed against lysozyme as ligand in immunoaffinity chromatography 548(1991)235
- Welling-Wester, S., see Welling, G. W. 548(1991)235
- Wheatley, J. B.
Effect of antigen size on optimal ligand density of immobilized antibodies for a high-performance liquid chromatographic support 548(1991)243
- Wilce, M. C. J., Aguilar, M. I. and Hearn, M. T. W.
High-performance liquid chromatography of amino acids, peptides and proteins. CX. Principal component analysis of four sets of group retention coefficients derived from reversed-phase high-performance liquid chromatography of peptides 548(1991)105
- Yadav, S. P., see Colilla, F. J. 548(1991)303
- Zhou, N. E., Mant, C. T., Kirkland, J. J. and Hodges, R. S.
Comparison of silica-based cyanopropyl and octyl reversed-phase packings for the separation of peptides and proteins 548(1991)179
- Zhu, B.-Y., Mant, C. T. and Hodges, R. S.
Hydrophilic-interaction chromatography of peptides on hydrophilic and strong cation-exchange columns 548(1991)13

PUBLICATION SCHEDULE FOR 1991

Journal of Chromatography and Journal of Chromatography, Biomedical Applications

MONTH	D 1990- F 1991	M	A	M	J	J	A	S	This publication schedule for further issues will be published later.
Journal of Chromatography	Vols. 535-539	540/1 + 2 541/1 + 2 542/1	542/2 543/1	543/2 544/1 + 2 545/1	545/2 546/1 + 2 547/1 + 2	548/1 + 2 549/1 + 2 550/1 + 2	552/1 + 2 553/1 + 2 554/1 + 2 555/1 + 2	556/1 + 2	
Cumulative Indexes, Vols. 501-550							551/1 + 2		
Bibliography Section		560/1			560/2			561/1	
Biomedical Applications	Vols. 562, 563	564/1	564/2 565/1 + 2	566/1 566/2	567/1	567/2 568/1	568/2	569/1 + 2	

INFORMATION FOR AUTHORS

(Detailed *Instructions to Authors* were published in Vol. 522, pp. 351-354. A free reprint can be obtained by application to the publisher, Elsevier Science Publishers B.V., P.O. Box 330, 1000 AH Amsterdam, The Netherlands.)

Types of Contributions. The following types of papers are published in the *Journal of Chromatography* and the section on *Biomedical Applications*: Regular research papers (Full-length papers), Review articles and Short Communications. Short Communications are usually descriptions of short investigations, or they can report minor technical improvements of previously published procedures; they reflect the same quality of research as Full-length papers, but should preferably not exceed six printed pages. For Review articles, see inside front cover under Submission of Papers.

Submission. Every paper must be accompanied by a letter from the senior author, stating that he/she is submitting the paper for publication in the *Journal of Chromatography*.

Manuscripts. Manuscripts should be typed in double spacing on consecutively numbered pages of uniform size. The manuscript should be preceded by a sheet of manuscript paper carrying the title of the paper and the name and full postal address of the person to whom the proofs are to be sent. As a rule, papers should be divided into sections, headed by a caption (*e.g.*, Abstract, Introduction, Experimental, Results, Discussion, etc.). All illustrations, photographs, tables, etc., should be on separate sheets.

Introduction. Every paper must have a concise introduction mentioning what has been done before on the topic described, and stating clearly what is new in the paper now submitted.

Abstract. All articles should have an abstract of 50-100 words which clearly and briefly indicates what is new, different and significant.

Illustrations. The figures should be submitted in a form suitable for reproduction, drawn in Indian ink on drawing or tracing paper. Each illustration should have a legend, all the legends being typed (with double spacing) together on a separate sheet. If structures are given in the text, the original drawings should be supplied. Coloured illustrations are reproduced at the author's expense, the cost being determined by the number of pages and by the number of colours needed. The written permission of the author and publisher must be obtained for the use of any figure already published. Its source must be indicated in the legend.

References. References should be numbered in the order in which they are cited in the text, and listed in numerical sequence on a separate sheet at the end of the article. Please check a recent issue for the layout of the reference list. Abbreviations for the titles of journals should follow the system used by *Chemical Abstracts*. Articles not yet published should be given as "in press" (journal should be specified), "submitted for publication" (journal should be specified), "in preparation" or "personal communication".

Dispatch. Before sending the manuscript to the Editor please check that the envelope contains four copies of the paper complete with references, legends and figures. One of the sets of figures must be the originals suitable for direct reproduction. Please also ensure that permission to publish has been obtained from your institute.

Proofs. One set of proofs will be sent to the author to be carefully checked for printer's errors. Corrections must be restricted to instances in which the proof is at variance with the manuscript. "Extra corrections" will be inserted at the author's expense.

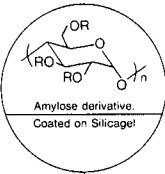
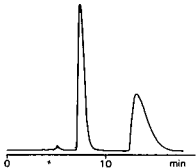
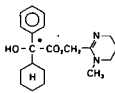
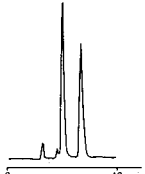
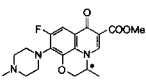
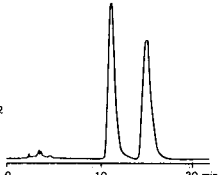
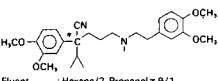
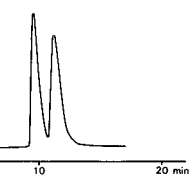
Reprints. Fifty reprints of Full-length papers and Short Communications will be supplied free of charge. Additional reprints can be ordered by the authors. An order form containing price quotations will be sent to the authors together with the proofs of their article.

Advertisements. Advertisement rates are available from the publisher on request. The Editors of the journal accept no responsibility for the contents of the advertisements.

For Superior Chiral Separation From Analytical To Preparative.

The finest from DAICEL.....

Why look beyond DAICEL? We have developed the finest CHIRALCEL, CHIRALPAK and CROWNPAK with up to 17 types of HPLC columns, all providing superior resolution of racemic compounds.

NEW CHIRALPAK AS	NEW CHIRALPAK AD	
<p>● CHIRALPAK AS</p> $R: -\overset{\text{O}}{\parallel}{\text{C}}-\text{N}-\overset{\text{H}}{\text{C}}-\overset{\text{H}}{\text{C}}^*-\text{C}_6\text{H}_4-\overset{\text{CH}_3}{\text{C}}^*$ <p>for β-Lactam antibiotics</p>	 <p>Amylose derivative. Coated on Silicagel</p>	<p>● CHIRALPAK AD</p> $R: -\overset{\text{O}}{\parallel}{\text{C}}-\text{N}-\overset{\text{H}}{\text{C}}-\text{C}_6\text{H}_3(\text{CH}_3)_2$
4-Acetoxy-2-azetidine	Oxyphencyclimine	
 <p>Eluent : Hexane/Ethanol = 8/2 Flow rate : 1.0 ml/min Temperature : r.t. Detection : UV254 nm</p> 	 <p>Eluent : Hexane/2-Propanol = 9/1 Flow rate : 1.0 ml/min Temperature : r.t. Detection : UV254 nm</p> 	
Ofloxacin methyl ester	Verapamil	
 <p>Eluent : Hexane/EtOH = 8/2 Flow rate : 1.2 ml/min Temperature : 40°C Detection : UV254 nm</p> 	 <p>Eluent : Hexane/2-Propanol = 9/1 Flow rate : 1.0 ml/min Temperature : r.t. Detection : UV254 nm</p> 	

Analytical column 0.46cm x 25cm(10 μ m)

CHIRALCEL OA
OB
OC
OD
OJ
OF
OG
OK
CHIRALPAK AS
AD



Normal Phase



Semi-preparative column 2cm x 25cm(10 μ m)

You can have
Pure enantiomer
quickly!!

■ Separation Service

- A pure enantiomer separation in the amount of 100g~10kg is now available.
- Please contact us for additional information regarding the manner of use and application of our chiral columns and how to procure our separation service.



DAICEL CHEMICAL INDUSTRIES, LTD.

chiral chemicals division.

8-1, Kasumigaseki 3-chome, Chiyoda-ku, Tokyo 100, Japan Phone: 03 (507) 3151 FAX: 03 (507) 3193

DAICEL(U.S.A.) INC.

Fort Lee Executive Park
Two Executive Drive, Fort Lee,
New Jersey 07024
Phone: (201) 461-4466
FAX: (201) 461-2776

DAICEL(U.S.A.) INC.

23456 Hawthorne Blvd.
Bldg. 5, Suit 130
Torrance, CA 90505
Phone: (213) 791-2030
FAX: (213) 791-2031

DAICEL(EUROPA) GmbH

Oststr. 22
4000 Düsseldorf 1, F.R. Germany
Phone: (211) 369848
Telex: (41) 8588042 DCEL D
FAX: (211) 364429

DAICEL CHEMICAL(ASIA) PTE. LTD.

65 Chulia Street #40-07
OCBC Centre, Singapore 0104
Phone: 5332511
FAX: 5326454